AD-780 596

MATERIALS RESEARCH IN SUPPORT OF SUPERCONDUCTING MACHINERY

NATIONAL BUREAU OF STANDARDS

PREPARED FOR
ADVANCED RESEARCH PROJECTS AGENCY

MARCH 1974

NBS - ARPA

MATERIALS RESEARCH for SUPERCONDUCTING MACHINERY

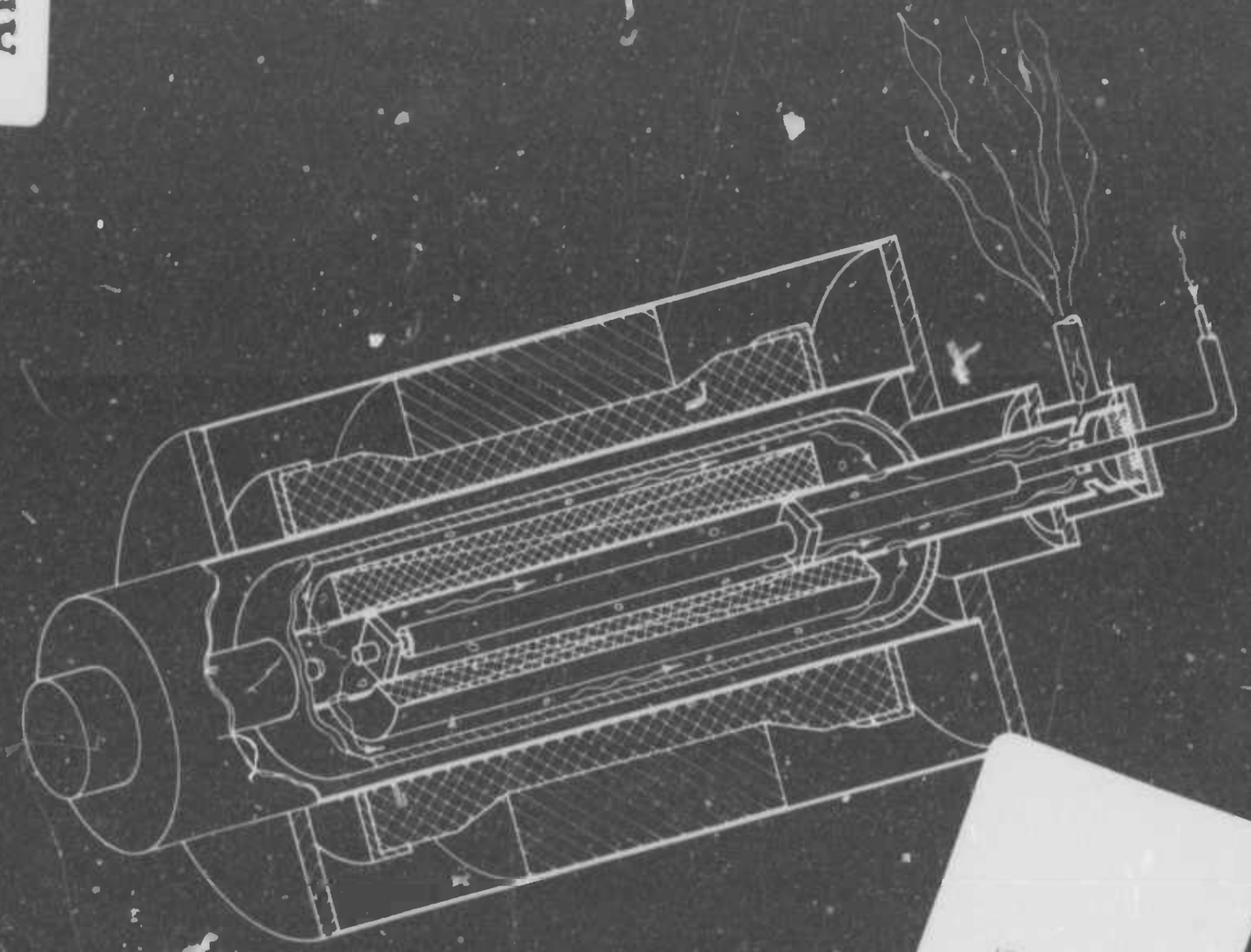

Semi Annual Technical Reports

March 1974

NBS-114A REV. 7-73)

U.S. DEPT. OF COMM. BIBLIOGRAPHIC DATA SHEET	1. PUBLICATION OR REPORT NO. NBSIR 74-359	2. Gov't Accession No.	3. Recipient's Accession No. AD-780596

4. TITLE AND SUBTITLE

Semi-Annual Report on Materials Research in Support of Superconducting Machinery

5. Publication Date March 1974

6. Performing Organization Code

7. AUTHOR(S) Sparks, Fickett, Hust, Ledbetter, Kasen, Tobler, Mikesell, Fowlkes, Durcholz, Reed, Giarratano, Naimon, and Weston

8. Performing Organ. Report No.

9. PERFORMING ORGANIZATION NAME AND ADDRESS

NATIONAL BUREAU OF STANDARDS, Boulder Labs.
DEPARTMENT OF COMMERCE
Boulder, Colorado 80302

10. Project/Task/Work Unit No.

11. Contract/Grant No. ARPA Order #2569

12. Sponsoring Organization Name and Complete Address (Street, City, State, ZIP)

Advanced Research Projects Agency
Department of Defense
Washington, D. C.

13. Type of Report & Period Covered

14. Sponsoring Agency Code ARPA

15. SUPPLEMENTARY NOTES

16. ABSTRACT *(A 200-word or less factual summary of most significant information. If document includes a significant bibliography or literature survey, mention it here.)*

Results of six months research are reported to the sponsor, the Advanced Research Projects Agency of the Department of Defense. Subjects include magneto-thermal conductivity, thermal conductivity, composites, elastic properties, fracture toughness, fatigue, and tensile. All measurements include the temperature range 4 to 300 K. Materials examined are those either presently being used in superconducting machinery or considered for use in future prototypes. Material classes include stainless steels, inconels, titanium alloys, and composites.

Special results include: the thermal conductivity in a magnetic field is considerably lower than would be predicted; a comprehensive review of glass-reinforced composite behavior at low temperatures is included; the elastic moduli of 12 engineering alloys from 4 to 300 K are reported; and fracture toughness and fatigue crack growth rate data on AISI 304, AISI 316, A286, Ti-5Al-4V and Ti-6Al-2.5 Sn at 4, 76 and 300 K have been measured.

At the beginning of each individual report a Summary is provided to highlight the project results.

17. KEY WORDS *(six to twelve entries; alphabetical order; capitalize only the first letter of the first key word unless a proper name; separated by semicolons)*

Composites; fracture; liquid helium; mechanical properties; structural materials; superconducting machinery; thermal conductivity.

18. AVAILABILITY ☐ Unlimited	19. SECURITY CLASS (THIS REPORT) UNCLASSIFIED	21. NO. OF PAGES 567
☐ Order From Sup. of Doc., U.S. Government Printing Office Washington, D.C. 20402, SD Cat. No. C13	20. SECURITY CLASS (THIS PAGE) UNCLASSIFIED	22. Price $10.75
☐ Order From National Technical Information Service (NTIS) Springfield, Virginia 22151		

USCOMM-OC 29042-P74

SEMI-ANNUAL TECHNICAL REPORTS ON MATERIALS

RESEARCH IN SUPPORT OF SUPERCONDUCTING MACHINERY

FOR

1 September 1973 to 1 March 1974

Sponsored by

Advanced Research Projects Agency
1400 Wilson Boulevard, Arlington, VA 22209
ARPA Order No. 2569 - Program Code 4D10

Contracted for 10 August 1973

by

Cryogenics Division, Institute for Basic Standards
National Bureau of Standards, Boulder, CO 80302

ARPA Program Director -	Edward C. van Reuth	202-694-4750
NBS Program Manager -	Richard P. Reed	303-499-1000 x3870
NBS Contracts Monitor -	Alan F. Clark	303-499-1000 x3253

Subcontracts to:

Argonne National Laboratory
Battelle, Columbus Laboratories
General Electric Research & Development Center
Martin Marietta Aerospace, Denver Division
National Bureau of Standards, Cryogenics Division
Westinghouse Electric Research and Development Center

DISCLAIMER

The views and conclusions contained in this document are those of the authors and should not be interpreted as necessarily representing the official policies, either expressed or implied, of the Advanced Research Projects Agency or the U. S. Government.

SUMMARY

The first semi-annual technical reports are collected from six subcontractors on an ARPA sponsored program on the very low temperature properties of structural materials in support of superconducting machinery. The program is outlined and initial progress reported. Low temperature data are presented for the fatigue and fracture properties, thermal expansion, specific heat, and elastic properties of structural alloys. Initial results of data compilations on these alloys and composites are described.

TABLE OF CONTENTS

GENERAL ELECTRIC COMPANY

Composite Structural Materials Investigation at Cryogenic Temperatures
Hillig, W. B.
McLoughlin, J. R.

MARTIN MARIETTA AEROSPACE, DENVER DIVISION

Study of Fracture Behavior of Metals for Superconducting Applications
Schwartzberg, F. R.

NATIONAL BUREAU OF STANDARDS

Magnetothermal Conductivity
Sparks, L. L.
Fickett, F. R.

Thermal Conductivity
Hust, J. G.
Giarratano, P. J.

Elastic Properties/Engineering Alloys at Cryogenic Temperatures
Ledbetter, H. M.
Naimon, E. R.
Weston, W. F.

Advanced Composites
Kasen, M. B.

Fatigue and Fracture Toughness Testing at Cryogenic Temperatures
Tobler, R. L.
Mikesell, R. P.
Durcholz, R. L.
Fowlkes, C. W.
Reed, R. P.

WESTINGHOUSE RESEARCH LABORATORIES

Structural Materials for Cryogenic Applications
Lessmann, G. G.
Logsdon, W. A.
Kossowsky, R.
Mathur, M. P.
Wells, J. M.

INTRODUCTION

Bound together in this report are the initial results of a widespread program designed to fulfill the need for materials properties data to assist the design and development of superconducting machinery. The program was conceived and developed jointly by the staffs of the Materials Sciences - Advanced Research Projects Agency and the Cryogenics Division - National Bureau of Standards. This ARPA - sponsored program on "Low Temperature Properties of Structural Materials in Support of Superconducting Machinery" is managed by NBS, with subcontracts to five other laboratories.

PROGRAM DESCRIPTION

The program's objectives are: 1) to evaluate candidate structural materials for use in superconducting electrical machinery by determining their mechanical and physical properties between 4 and 300 K and the effects on these properties of processing and joining, 2) to explore new materials, such as composites, for potential innovative design applications by performing screening tests on their low temperature properties, and 3) to assist the information transfer of the available low temperature properties data into design use by compiling and publishing what literature data are available and assessing what properties need further study.

The first year's program plan to meet these objectives is shown in Table 1. It outlines the efforts at the six research laboratories with a brief

description of each program. The organizational contacts for each research laboratory are shown in Table 2. It can be easily seen from the first year's program plan that the major thrust has been to initiate fatigue and fracture measurements at low temperatures where virtually no data have previously existed. Exploration of high potential new materials has also begun.

Table 1

ARPA - Low Temperature Properties of Structural Materials

First Year Program (FY 74)

Program Area	Organization	Program Description
Mechanical Properties		
1. Fracture and Fatigue		
a. Materials Group a)	NBS-Cryogenics	Fracture toughness, fatigue crack growth rate, fatigue, sustained load crack growth rate tests from 4-300 K on structural alloys.
b. Materials Group b)	Westinghouse	Mechanical, magnetic, electrical loss characterization of alloys currently in use by Westinghouse in DOD sponsored programs. Mechanical tests include tensile, fracture toughness, fatigue.
c. High Load-Large Specimens	Martin-Denver	Fracture toughness, fatigue crack growth rate data on very selected tough alloys requiring loads in excess of 30,000 lbs. to fracture.
2. Effects		
a. Processing	Westinghouse	Identification of effects of fabrication and processing techniques on mechanical properties of selected alloys. Variables include industrial melting practices, powder metallurgy techniques, and cold working.
b. Joining	Westinghouse	Mechanical properties of fabricated metal joints, including welding (GTAW, EB, GMAW) brazing, and soldering from 4-300 K. Properties include tensile, notched tensile, fracture toughness, and fatigue crack growth rate.
3. Elastic Moduli, Tensile	NBS-Cryogenics	Tensile and dynamic elastic (Young's, shear, bulk moduli) measurements on structural alloys from 4-300 K.

Table 1 (continued)

Program Area	Organization	Program Description
Thermal Properties		
4. Thermal Expansion, Specific Heat	Battelle	Thermal expansion and specific heat measurements on selected insulations and structural alloys.
5. Thermal-Magnetothermal Conductivity	NBS-Cryogenics	Thermal conductivity and thermal conductivity in magnetic fields up to 50 kilogauss from 4-300 K of structural alloys.
Composites		
6. Evaluation of Advanced Composites	NBS-Cryogenics	Screening tests (tensile, fatigue at 4 K) on selected candidate metal and non-metal base composites, including B-epoxy, C-epoxy and polyimide, PRD 49-epoxy, borsic-Al, Steel-Al.
7. Screening for Shield Materials	General Electric	Screening study of composites for torque tube and electromagnetic shield applications.
Data Compilation and Evaluation		
8. Handbook	Battelle	Publication of Handbook containing recommended best value data and complete set of references for 39 selected materials (structural alloys, superconductors). Data presented in graphical and tabular formats; mechanical, thermal, magnetic properties from 0-300 K.
Specialized Structures		
9. Effects on Magnet Materials	Argonne	Characterization of change of electrical and mechanical properties of magnet materials as a function of fatigue and temperature.

Table 2

ARPA - Low Temperature Properties of Structural Materials

Organizational Contacts

Advanced Research Projects Agency, 1400 Wilson Blvd., Arlington, Virginia 22209

Program Director	Edward C. van Reuth	202-694-4750	

National Bureau of Standards, Cryogenics Division, Boulder, Colorado 80302

Program Manager	Richard P. Reed	303-499-1000	Ext. 3870
Contract Monitor	Alan F. Clark	303-499-1000	Ext. 3253
Fracture	Ralph L. Tobler	303-499-1000	Ext. 4447
Elastic Moduli	Hassell M. Ledbetter	303-499-1000	Ext. 3232
Thermal Conductivity	Jerome G. Hust	303-499-1000	Ext. 3733
Magnetothermal Conductivity	Frederick R. Fickett	303-499-1000	Ext. 3785
Composites	Maurice B. Kasen	303-499-1000	Ext. 3558

Argonne National Laboratory, 9700 South Cass Avenue, Argonne, Illinois 60439

Program Coordinator	Joseph B. Darby	312-739-2225	
Principal Investigators	Edward S. Fisher	312-739-3415	
	Ronald Linz		

Battelle, Columbus Laboratories, 505 King Avenue, Columbus, Ohio 43201

Program Manager	James E. Campbell	614-295-8045	Ext. 2829
Mechanical Properties Data	James E. Campbell	614-295-8045	Ext. 2829
Thermal Properties Data	Edward A. Eldridge	614-295-8045	Ext. 2572
Magnetic Properties Data	J. Ken Thompson	614-295-8045	Ext. 2612
Physical Properties Meas't.	Frank Jelinek	614-295-8045	Ext. 1735

General Electric Company, Research and Development Center, P.O. Box 8, Schenectady, N.Y. 11506

Program Manager	William B. Hillig	518-346-8771	Ext. 6139
Principal Investigator	J. Bob McLoughlin	518-346-8771	Ext. 6398

Martin Marietta Aerospace, Denver Division, P.O. Box 179, Denver, Colorado 80201

Program Manager	Fred Schwartzberg	303-794-5211	Ext. 2516
Principal Investigator	Emory Beck	303-794-5211	Ext. 3438

Westinghouse Electric Corporation, Research & Development Center, Beulah Road, Pittsburgh, Pennsylvania 15235

Program Manager	G. G. Lessmann	412-256-7000	Ext. 3412
Joining & Processing	Joseph M. Wells	412-256-7000	Ext. 3633
Fracture Mechanics	William A. Logsdon	412-256-7000	Ext. 3652
Magnetic Measurements	M. P. Mathur	412-256-7000	Ext. 3289
Metallurgy-Fractography	R. Kossowsky	412-256-7000	Ext. 3684

RESULTS HIGHLIGHTS

The best way, of course, to grasp the extent of this reporting period's results is to read the technical summary of each report. However, we will briefly summarize some of the more important highlights during this contract period in some of the contract areas. Specific materials which have been measured are listed by property and laboratory in Table 3; to find the data refer to the report from the indicated laboratory.

Of major importance is the generation of fracture toughness and crack growth rate data for several alloys at 4 K, the first ever produced. Use of new elastic-plastic J integral test techniques have allowed estimation of quantitative fracture toughness values in alloys which are quite tough. The measurements of elastic moduli from 4 to 300 K of engineering alloys are also a first. Another surprising, but perhaps not totally unexpected result, was that both the elastic moduli and magnetic susceptibility measurements indicate that Inconel 750 may be ferromagnetic at 4 K. An extensive review of the low temperature behavior of composites is highlighted, providing rare and valuable guidance in the selection of design properties from a great variety of composite materials.

Another highlight of this reporting period was the workshop meeting held in Estes Park, Colorado on 10 January 1974. It was attended by representatives of the three services of the Department of Defense, the primary users of the program's output. The meeting agenda and a list of attendees

are shown in Tables 4 and 5. The contractor representatives outlined research plans and preliminary results and the service representatives described their superconducting machinery programs and needs. The rapport and interchange were excellent and fruitful, and the need for more exchange was expressed by many. Several people initiated specimen and data sharing at the meeting. A second workshop is tentatively scheduled for early October 1974.

Table 3

Project Summary of Materials Properties Measurements for First Half Year

	Argonne	Battelle	G.E.	Martin	NBS	Westinghouse
Thermal Expansion	-	Inc 750, Kro 58, OFHC, AISI 310S Ti-Nb	-	-	-	-
Thermal Conductivity	-	-	-	-	*	-
Magneto-thermal Conductivity	-	-	-	-	Inc 718	-
Specific Heat	-	Inc 750, Kro 58, AISI 310S	-	-	-	-
Fracture Toughness	-	-	-	*	AISI 304, 316; Ti-5Al-2.5 Sn Ti-6Al-4V, A286	Inc 750, AISI 310S
Fatigue Crack Growth	-	-	-	-	AISI 304, 316; Ti-SAl-2.5Sn, Ti-6Al-4V, A286	Inc 750, AISI 310S
Tensile	-	-	-	-	AISI 304, 316; Ti-5Al-2.5Sn, Ti-6Al-4V, A286	Inc 750, AISI 310S, OFHC
Fatigue	*	-	-	-	-	-
Elastic Modull	-	-	-	-	Tl-6 Al-4V, Ti-5 Al-2.5Sn, Inc 600 and 750, A286, AISI 304, 310, 316, Al 1100, 5083, 7005, 7075, Invar	-
Flexure	-	-	S-glass, PRD-49, Modmor II with Empol resins	-	-	-
Welds, brazes	-	-	-	-	-	Inc 750, AISI 310S

* For some projects elther equipment assembly for testing at 4K or llmlted contract obligations precluded materlal testing for this 6-month perlod.

Table 4

AGENDA

NBS-ARPA WORKSHOP

on

Low Temperature Properties of Materials
in support of
Superconducting Machinery

9:00 a.m.	ARPA Objectives		E. C. van Reuth
9:05 a.m.	Program Overview		R. P. Reed
9:15 - 12:00	Contractor Research Programs		
	Westinghouse	(~ 30 min.)	
	Battelle	(~ 20 min.)	
	General Electric	(~ 15 min.)	
	Martin	(~ 15 min.)	
	Argonne	(~ 15 min.)	
	NBS	(~ 30 min.)	
12:00 -	Lunch		
1:30	Large Scale Applications of Superconductivity		
	The World Picture		F. R. Fickett
2:00	The Service Research Programs		
	Army	(~ 30 min.)	
	Navy	(~ 30 min.)	
	Air Force	(~ 30 min.)	
3:30 - 4:00	Discussion and Wrap-up		

Table 5

ARPA - Low Temperature Properties of Structural Materials

Final List of Attendees

1. Emory Beck
Martin Marietta Aerospace
Denver Division
P.O. Box 179
Denver, Colorado 80201
Phone: 303-794-5211 Ext. 3438

2. James E. Campbell
Battelle-Columbus Laboratories
505 King Avenue
Columbus, Ohio 43201
Phone: 614-299-3151 Ext. 2829

3. Alan F. Clark
National Bureau of Standards
Cryogenics Division
Boulder, Colorado 80302
Phone: 303-499-1000 Ext. 3253

4. E. W. Collings
Battelle-Columbus Laboratories
505 King Avenue
Columbus, Ohio 43201
Phone: 614-299-3151

5. Joseph B. Darby, Jr.
Argonne National Laboratory
9700 South Cass Avenue
Argonne, Illinois 60439
Phone: 312-739-7711 Ext. 2255

6. Edward A. Eldridge
Battelle-Columbus Laboratories
505 King Avenue
Columbus, Ohio 43201
Phone: 614-299-3151 Ext. 2572

7. Frederick R. Fickett
National Bureau of Standards
Cryogenics Division
Boulder, Colorado 80302
Phone: 303-499-1000 Ext. 3785

8. Carl J. Heise
MERDC
Ft. Belvoir, Virginia
Phone: 703-664-5724

9. William B. Hillig
General Electric Company
Research & Development Center
P.O. Box 8
Schenectady, New York 11506
Phone: 518-346-8771 Ext. 6139

10. Frank J. Jelinek
Battelle-Columbus Laboratories
505 King Avenue
Columbus, Ohio 43201
Phone: 614-299-3151

11. Maurice B. Kasen
National Bureau of Standards
Cryogenics Division
Boulder, Colorado 80302
Phone: 303-499-1000 Ext. 3558

12. Ted Kiefer
Martin Marietta Aerospace
Denver Division
P.O. Box 179
Denver, Colorado 80201
Phone: 303-794-5211

13. Richard H. Kropschot
National Bureau of Standards
Cryogenics Division
Boulder, Colorado 80302
Phone: 303-499-1000 Ext. 3252

14. G. G. Lessmann
Westinghouse Electric Corporation
Research & Development Center
Beulah Road
Pittsburgh, Pennsylvania 15235
Phone: 412-256-3412

15. W. J. Levedahl
NSRDC
Annapolis, Maryland 21402
Phone: 301-267-2663

16. Ronald Linz
Argonne National Laboratory
9700 South Cass Avenue
Argonne, Illinois 60439
Phone: 312-739-7711 Ext. 3418

17. Donald W. McGrath
AIRESEARCH MFG. CO.
Division of Garrett Corp.
9851 Sepulveda Boulevard
Los Angeles, California 90009
Phone: 213-323-9500 Ext. 3579

18. J. R. McLoughlin
General Electric Company
Research and Development Center
P.O. Box 8
Schenectady, New York 11506
Phone: 518-346-8771 Ext. 6398

19. Charles Oberly
AFAPL/POD-1
Wright-Patterson AFB
Dayton, Ohio 45433
Phone: 513-255-6244

20. Fred R. Schwartzberg
Martin Marietta Aerospace
Denver Division
P.O. Box 179
Denver, Colorado 80201
Phone: 303-794-5211 Ext. 3438

21. Howard O. Stevens
NSRDC (Code 2791)
Annapolis, Maryland 21402
Phone: 301-267-2150

22. Clyde E. Taylor
Lawrence Livermore Laboratory
Livermore, California
Phone: 415-447-1100 Ext. 7501

23. Richard P. Reed
National Bureau of Standards
Cryogenics Division
Boulder, Colorado 80302
Phone: 303-499-1000 Ext. 3870

24. E. C. van Reuth
Advanced Research Projects Agency
1400 Wilson Boulevard
Arlington, Virginia 22209
Phone: 202-694-4750

25. E. T. Wessel
Westinghouse Electric Corporation
Research & Development Center
Beulah Road
Pittsburgh, Pennsylvania 15235
Phone: 412-256-3544

March 1974

SEMI-ANNUAL TECHNICAL REPORT

EFFECTS OF CYCLIC LOADING ON ELECTRICAL CONDUCTIVITY OF SUPERCONDUCTING COMPOSITES

by

ARGONNE NATIONAL LABORATORY
9700 South Cass Avenue
Argonne, Illinois 60439

Principle Investigators:	E. S. Fisher	312/739-3415
	R. J. Linz	312/739-3418
Program Manager:	J. B Darby	312/739-2255
Contract Monitor:	Cryogenics Division National Bureau of Standards Boulder, Colorado 80302	
Program Code Number:	4D10	
Purchase Order Number:	40821-4	
Effective Date of Contract:	9/1/73 - 8/31/74	
Contract Expiration Date:	8/31/74	
Amount of Contract:	$40,000	

Sponsored by
Advanced Research Project Agency
ARPA Order No. 2569

SUMMARY

The objective of the present project is to obtain reliable data on the influence of cyclic-stress loading on the low-temperature electrical and thermal conductivities of metals. The initial effort will be to provide information that will be used in the design of superconducting devices that will be subjected to cyclic magnetic fields and mechanically and/or thermally induced cyclic-stress loading.

Fatigue damage introduces point defects into the crystal lattice of a metal. Point defects are extremely effective scatterers of electrons and can significantly reduce the low-temperature thermal and electrical conductivities in high-conductivity metals. Because they do not anneal out at temperatures below $\gtrsim$ 30°K, point defects accumulate during successive stress cycles. Fatigue damage can lead to severe degradation of the transport properties of a metal at a small fraction of the ultimate mechanical fatigue life.

The optimum design of low-temperature machinery depends on the ability to predict the minimum values of electrical and thermal conductivities of a metal that are likely to be encountered. The data required to make such predictions accurately are not available and the effort of the project will be to provide such data.

The effort during the past six months has been directed toward establishing the required experimental facilities, which are now operational. A brief description of the apparatus follows.

Sample fatigue is accomplished with an Instron machine capable of operating in the cyclic compression-tension mode. The sample is mechanically coupled directly to the Instron machine and is contained in a liquid-helium cryostat mounted on the movable beam of the Instron. A strain-gauge resistance bridge, mounted on extensometer clamps, measures the strain amplitude and the degree of buckling of the sample. Brass knife edges, attached to the tips of the extensometer clamps. serve as voltage probes for the resistivity measurements. Changes in the electrical resistivity of the sample are monitored between incremental cyclic loading by means of standard, four-terminal dc current-voltage techniques. The voltage measurements incorporate a voltage-frequency conversion that requires an appreciable counting time; therefore, cycling must be stopped during the voltage measurements. The resolution of the voltage-measuring circuit is $\pm$ 2 nv, which is the noise limit of the preamplifier.

Fatigue samples have been prepared from 99.999+% pure copper and oxygen-free high conductivity (OFHC) copper. Samples of aluminum are being prepared from bulk material with residual-resistivity ratios between 500 and 10,000.

The experimental facilities are completely functional and preliminary experiments to calibrate the instrumentation have been completed. The acquisition of experimental data on copper will begin immediately. The initial experiments will determine the increase in electrical resistivity, at 4.2°K, as a function of the number of strain cycles and cyclic frequency

for strain amplitudes up to 0.3%. Metallurgical variables will include the degree of cold work after annealing and the sample purity.

INTRODUCTION

Some components of low-temperature machinery may be subjected to cyclic plastic strains during normal operation. The plastic deformation encountered during low-cycle fatigue introduces point defects in the metallic components. The thermal energies required to spontaneously anneal out point defects are not available below $\sim$ 30°K. The point defects can accumulate to a relatively high concentration as a result of successive fatigue cycling at cryogenic temperatures. Point defects are extremely effective scatterers of electrons and, in sufficient quantity, can substantially reduce the low-temperature electrical and thermal conductivities of relatively pure metals. No reliable data are available that indicate the rate or the magnitude of the degradation of the transport properties as a function of fatigue parameters. Hence, the design criteria for low-temperature machinery may be excessive, which would result in increased cost, size, and weight.

A specific example of the immediate need for such transport data is found in the design of superconducting magnets. The design of large superconducting magnets relies almost entirely on the superior transport properties of the pure copper or aluminum stabilizer material for safe operation of the magnet. The stabilizing material ensures that local nonsuperconducting regions in the superconductor do not propagate and

lead to catastropic failure. The design must allow for the reductions in the thermal and electrical conductivities of the stabilizing material as a result of mechanical deformation during construction and operation of the magnet. The reductions must be compensated for during design by specifying either an increase in the quantity of the stabilizer used or a reduction in the maximum allowable current density in the superconductor.

The purpose of the present investigation is to provide reliable design data that indicates the rate and extent of degradation of the thermal and electrical conductivities for typical materials used in low-temperature machinery, as a function of various fatigue parameters. The parameters include pure tensile and compressive strain amplitudes and number and frequency of cycles.

EXPERIMENTAL PROGRESS

The accomplishments during the initial phase of the program include the acquisition and construction of appropriate experimental facilities for applying cyclic stresses, the acquisition and calibration of electronic equipment to accurately measure the electrical resistivity of fatigue specimens in situ, and the acquisition of low-temperature facilities. Preliminary experiments on the integrated facility, including electrical resistivity measurements, have been completed. Fatigue specimens of 99.999+% pure copper and OFHC copper have been prepared. Experiments on OFHC copper are in progress. A detailed description of the experimental facilities and instrumentation follows.

1. Fatigue Facility

The fatigue apparatus consists of an Instron machine, Model TT-CM-L, with crosshead speeds from 0.03 to 5.0 cm/min and a load capability to 10,000 kg. The Instron machine operates in the push-pull mode to produce the fatigue conditions. A cryostat has been attached directly to the movable crosshead beam of the Instron. Specimen fatigue occurs at liquid-helium temperatures ($\approx$ 4.2°K). The strain gauges that monitor strain amplitude and the voltage probes that measure the changes in electrical resistivity during the fatigue cycle are attached to extensometer clamps mounted directly on the sample. At the present time, strain versus cycling time is continuously monitored during fatigue. Figure 1 is a schematic of the complete fatigue apparatus, and Fig. 2 is a photograph of the apparatus. Figure 3 is a cross-sectional view (drawn to scale) of the fatigue assembly showing complete design details. Figure 4 is a photograph of the portion of the fatigue assembly that is immersed in the liquid-helium cryostat. Superconducting wires are employed as current leads to the fatigue specimen (see bottom of Fig. 4).

2. Fatigue Grips

The fatigue specimens are attached to the fatigue assembly by means of split stainless steel grips shown in Fig. 5(a). One set of grips is mounted on each end of the specimen, and the specimen-grip nut, shown in Fig. 5(b), fits firmly over the grips to bolt the specimen in place, as shown in Fig. 5(c). Figure 5(d) shows the specimen with the grips and the extensometer clamps in place.

3. Strain Gauge and Voltage Probes

Figure 6 shows the typical experimental configuration for measuring the specimen strain and the voltage differences during fatigue. Two "U"-shape extensometer clamps are spring mounted to a specimen. The springs are enclosed in Teflon sleeves for electrical isolation from the specimen. Brass knife edges that serve as voltage probes are attached to, but electrically isolated from, the extensometer clamps. Only one set of probes is electrically active. The distance between the probes is 2 cm. Two strain-gauge resistors are glued to the closed end of the "U"-clamp, with one resistor on each face of the clamp. The two "U"-clamps are oriented 180° from each other; the resistance bridge constructed in this configuration simultaneously determines the strain amplitude and whether the specimen is buckling.

4. Specimen Preparation

Fatigue specimens have been prepared from American Smelting and Refining Company 99.999+% copper and from OFHC copper. The copper specimens were annealed at 400°C for 3 hr in a helium atmosphere. Pure aluminum specimens are being prepared; the residual electrical-resistivity ratios of these specimens will be between 500 and 10,000.

Figure 7 shows the specimen configuration used in this work. The specimens have an overall length of 2-1/2 in., and the diameter of the gauge section is either 1/4 or 3/8 of an inch.

5. Electrical-resistivity Instrumentation

The electrical resistivity of the specimen is obtained by means of the standard four-probe dc technique. Direct currents of up to 60 A are available. Voltage differences across the specimen are determined by means of a low-noise voltage-frequency conversion apparatus. At the present time, the resolution of this apparatus is $\pm$ 2 nv, which is the noise limit imposed by a Keithley preamplifier. The resolution is sufficient for the initial experiments on OFHC copper. It is anticipated that ultimate resolutions on the order of 10^{-10} to 10^{-11} V will be necessary, and the appropriate instrumentation will be acquired.

Figure 8 is a block diagram of the instrumentation used to measure electrical resistivity and stress-strain characteristics of the specimen during fatigue. The differential amplifier, the phase-sensitive detector, and the gating and logic circuitry used in the voltage-detection circuit were designed and constructed at Argonne.

LIST OF FIGURES

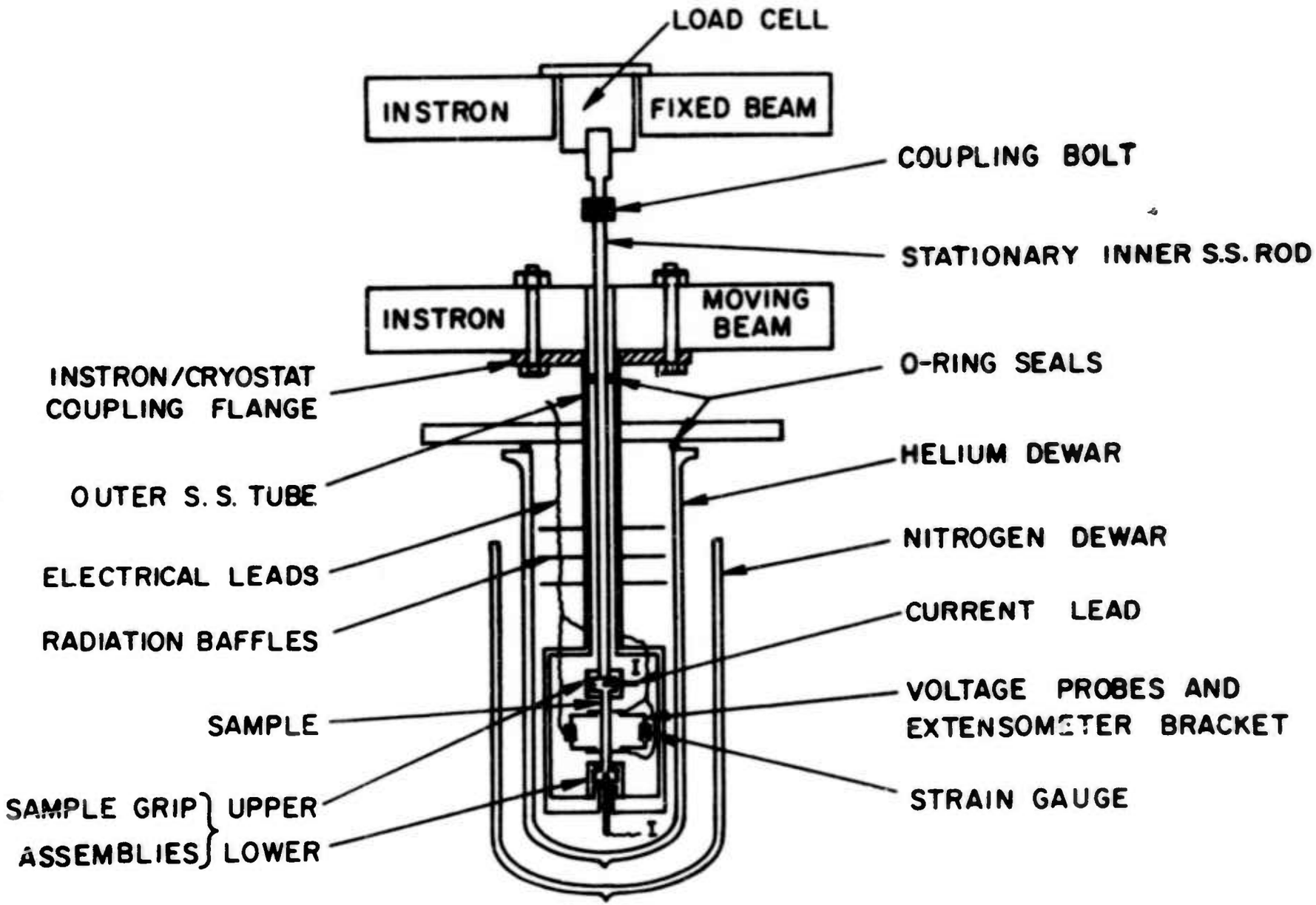
LOAD CELL
INSTRON
FIXED BEAM
COUPLING BOLT
STATIONARY INNER S.S. ROD
INSTRON
MOVING BEAM
INSTRON/CRYOSTAT COUPLING FLANGE
O-RING SEALS
HELIUM DEWAR
OUTER S. S. TUBE
NITROGEN DEWAR
ELECTRICAL LEADS
CURRENT LEAD
RADIATION BAFFLES
VOLTAGE PROBES AND EXTENSOMETER BRACKET
SAMPLE
STRAIN GAUGE
SAMPLE GRIP ASSEMBLIES
UPPER
LOWER

Fig. 1

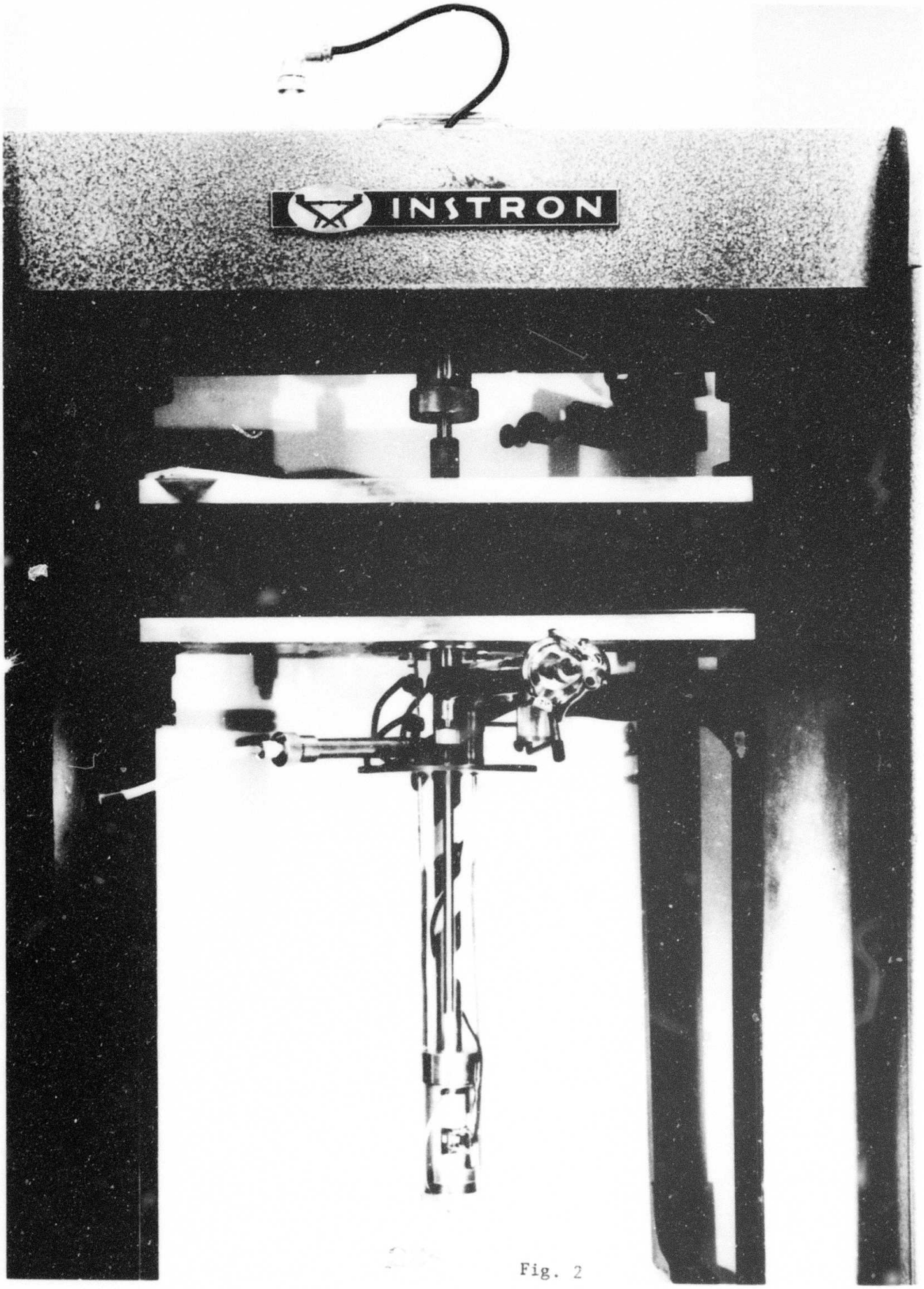

Fig. 2

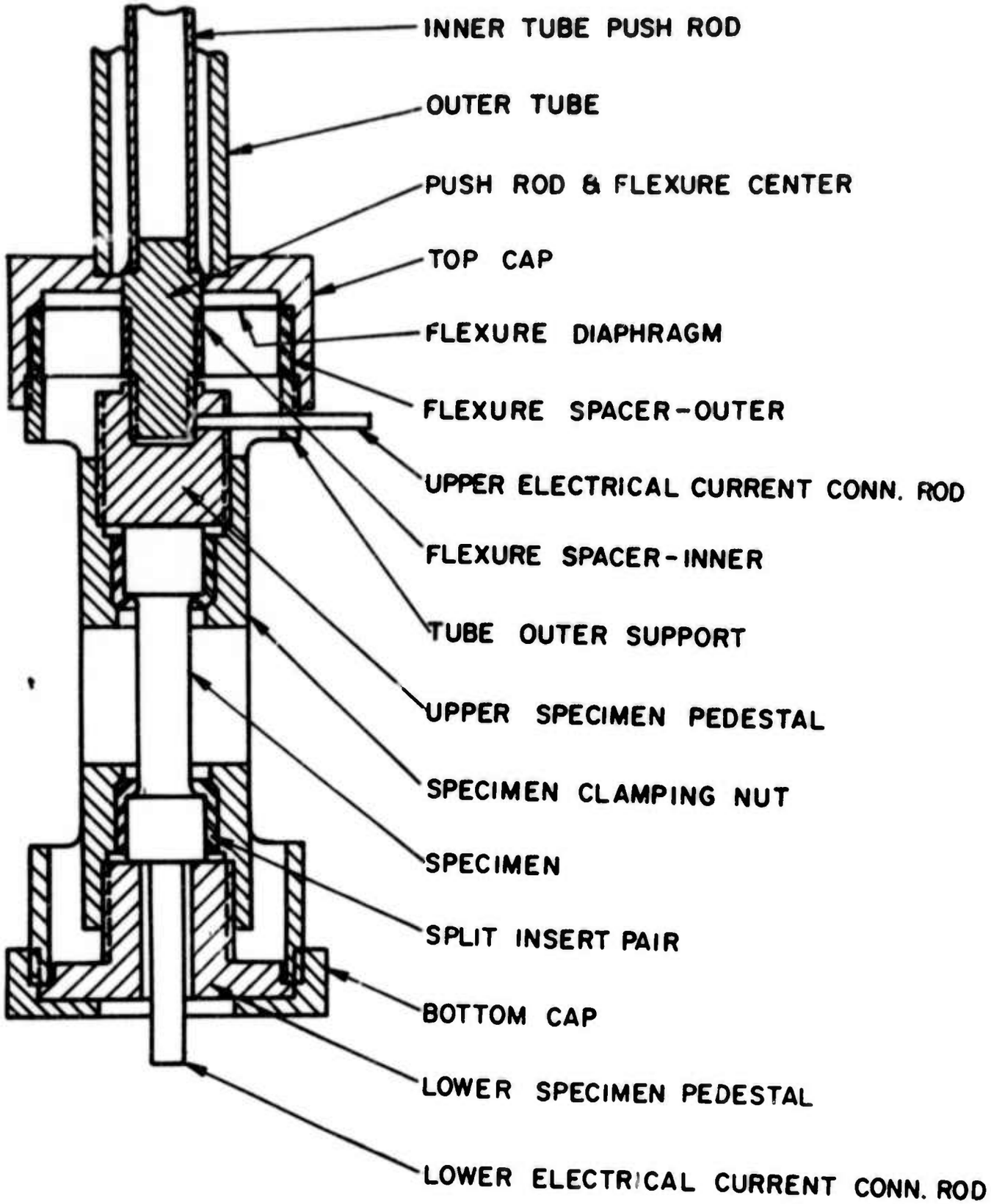
INNER TUBE PUSH ROD
OUTER TUBE
PUSH ROD & FLEXURE CENTER
TOP CAP
FLEXURE DIAPHRAGM
FLEXURE SPACER-OUTER
UPPER ELECTRICAL CURRENT CONN. ROD
FLEXURE SPACER-INNER
TUBE OUTER SUPPORT
UPPER SPECIMEN PEDESTAL
SPECIMEN CLAMPING NUT
SPECIMEN
SPLIT INSERT PAIR
BOTTOM CAP
LOWER SPECIMEN PEDESTAL
LOWER ELECTRICAL CURRENT CONN. ROD

Fig. 3

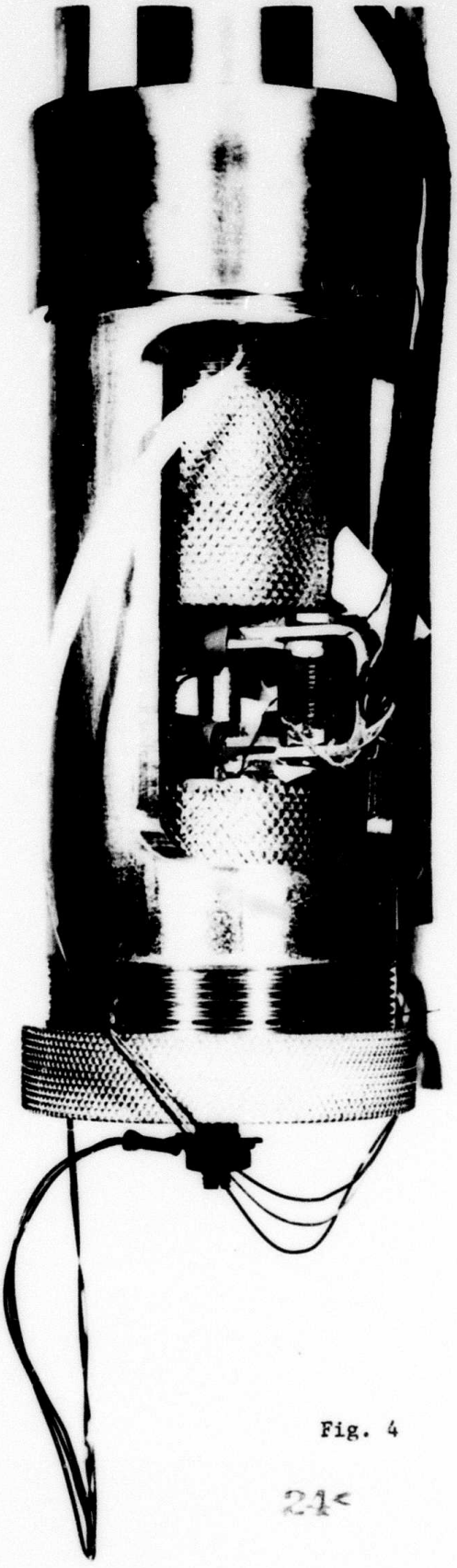

Fig. 4

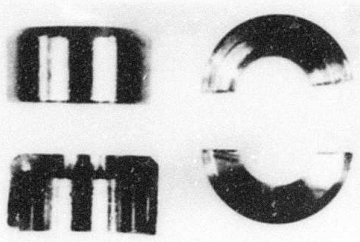

(a)

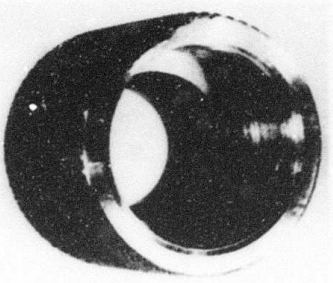

(b)

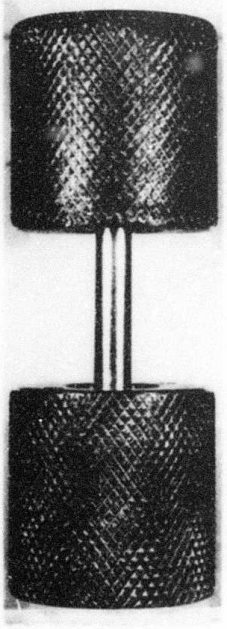

(c)

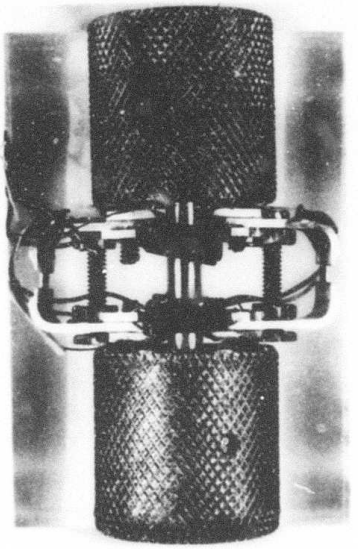

(d)

Fig. 5

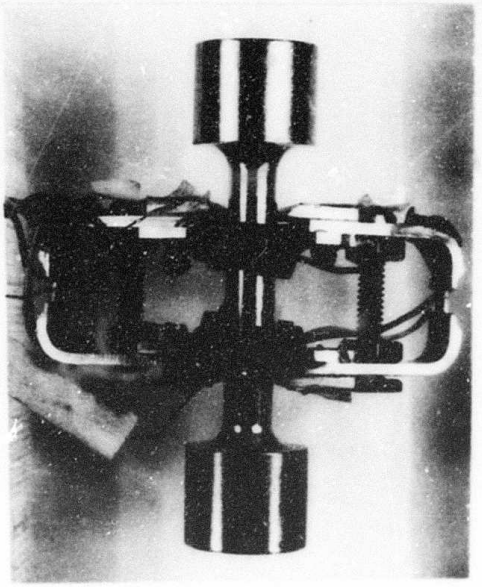

Fig. 6

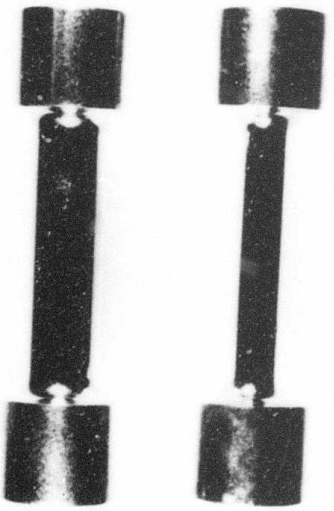

Fig. 7

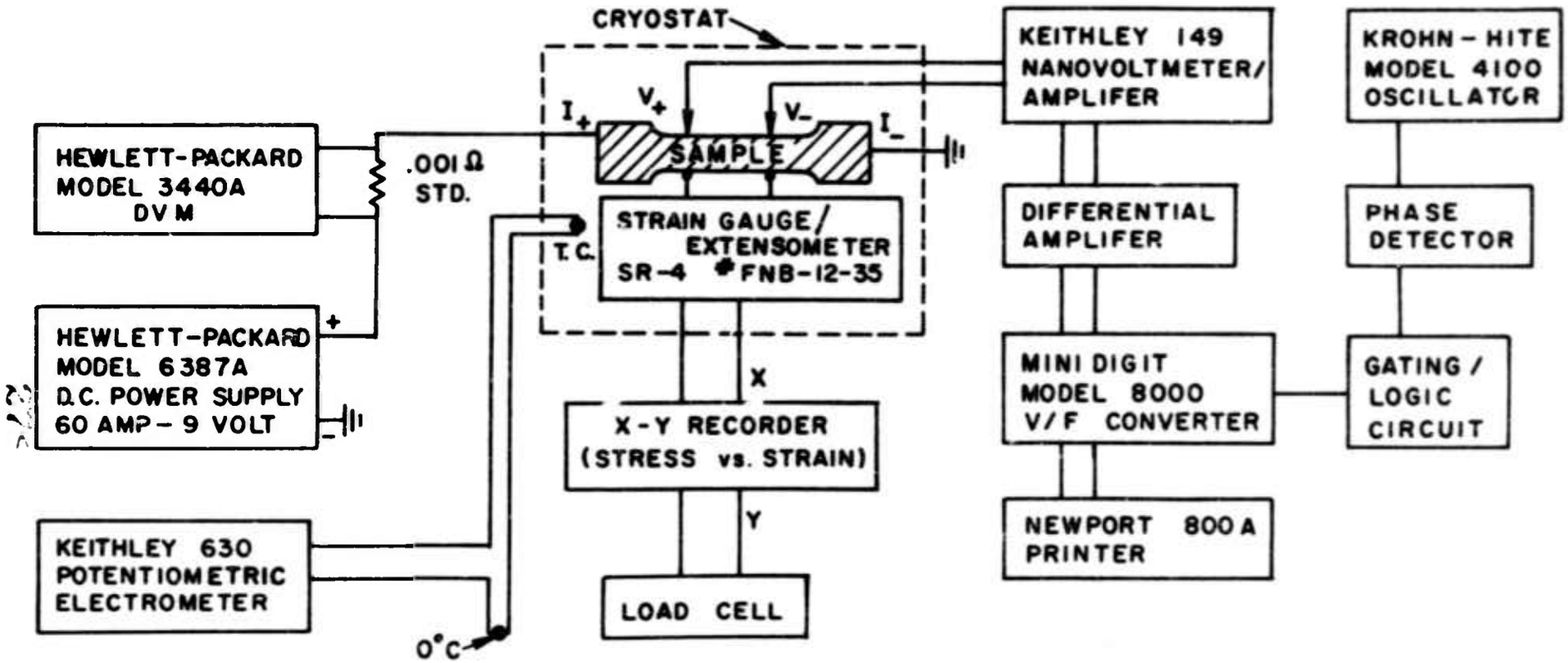
CRYOSTAT
KEITHLEY 149
NANOVOLTMETER/
AMPLIFER
KROHN-HITE
MODEL 4100
OSCILLATOR
I+
V+
V-
I-
SAMPLE
HEWLETT-PACKARD
MODEL 3440A
DVM
.001 Ω
STD.
STRAIN GAUGE/
EXTENSOMETER
SR-4 * FNB-12-35
T.C.
DIFFERENTIAL
AMPLIFER
PHASE
DETECTOR
HEWLETT-PACKARD
MODEL 6387A
D.C. POWER SUPPLY
60 AMP - 9 VOLT
+
-
X
MINI DIGIT
MODEL 8000
V/F CONVERTER
GATING /
LOGIC
CIRCUIT
X-Y RECORDER
(STRESS vs. STRAIN)
KEITHLEY 630
POTENTIOMETRIC
ELECTROMETER
Y
NEWPORT 800A
PRINTER
LOAD CELL
0°C

Fig. 8

SEMIANNUAL TECHNICAL REPORT

on

PREPARATION OF A HANDBOOK ON MECHANICAL, THERMAL, AND MAGNETIC PROPERTIES OF MATERIALS FOR SUPERCONDUCTING MACHINERY

Sponsored by
Advanced Research Projects Agency
ARPA Order No. 2569
Program Code 4D10
Contract No. CST-8303

Contract Monitor
Cryogenics Division
National Bureau of Standards
Boulder, Colorado 80302

March 1, 1974

METALS AND CERAMICS INFORMATION CENTER
A Department of Defense Information Analysis Center
BATTELLE
Columbus Laboratories
505 King Avenue
Columbus, Ohio 43201
Telephone (614) 299-3151

TABLE OF CONTENTS

FOREWORD

This research was supported by the Advanced Research Projects Agency of the Department of Defense and was monitored by the Cryogenics Division, National Bureau of Standards under Contract No. CST-8303 with Dr. Richard P. Reed as Program Manager and Dr. Alan F. Clark as Contract Monitor.

The research was carried out under ARPA Order No. 2569 and Program Code 4D10 by the Metals and Ceramics Information Center (MCIC) with J. E. Campbell (614, 299-3151, Extension 2829) as Program Manager, and E. A. Eldridge (614, 299-3151, Extension 2572), and J. K. Thompson (614, 299-3151, Extension 2612) as Principal Investigators. Contract No. CST-8303 includes two tasks. Task I provides for a compilation (handbook) of low-temperature property data on selected materials for structural application in superconducting machinery. Task II provides for determination of thermal expansion and specific heat values at cryogenic temperature for selected structural alloys. The Semiannual Technical Report on the latter program is presented under separate cover. Overall contract funding was $100,000 with $50,000 for the handbook program and $50,000 for the laboratory study. The effective date of the contract was September 10, 1973, and the contract expiration date is September 10, 1974.

DISCLAIMER

PREPARATION OF A HANDBOOK ON MECHANICAL, THERMAL, AND MAGNETIC PROPERTIES OF MATERIALS FOR SUPERCONDUCTING MACHINERY

INTRODUCTION

Recent advancements in the field of superconductivity have demonstrated the advantages of superconducting generators, motors, transmission lines, and other electrical equipment. Because of the marked improvement in efficiency and the reduction in size of such equipment, there is considerable incentive to develop superconducting systems for certain military applications. New ship propulsion systems which are being developed by the Navy represent major developments in superconducting generators and motors. These developments represent considerable new design technology in environments that may expose the components to cryogenic temperatures as low as 4K. Exposure of structural materials to such low temperatures affects the mechanical and physical properties of the materials. The purpcse of the Handbook is to provide a ready reference for designers on the effects of low temperature on the properties of the materials that will be considered in developing new designs for superconducting machinery.

SUMMARY

This report describes the results of the first six months effort in compiling recommended best-value data for mechanical, thermal, and magnetic properties of 42 selected metals and alloys in the range 0 to 300 K. Most of the metals represent structural alloys that might be considered for construction of superconducting machinery. Some of the metals and alloys also are conductor or superconductor materials. Recommended formats are presented for summarizing the results of the compilations in both tabular and graphical presentations of the best-value data. These

formats have been planned for ready reference by designers who may need information on the properties of materials at low temperatures in designing superconducting machinery.

Data for these compilations is being collected from the files of the Metals and Ceramics Information Center and from searches of the accessions of the Defense Documentation Center and the Cryogenic Data Center. Additional data for the Handbook are being generated on a number of other ARPA contracts being monitored by the Cryogenics Division of the National Bureau of Standards. The Handbook will be published in a loose leaf binder which will allow for adding new data sheets and updating the old data sheets as new data become available.

METALS AND ALLOYS

The selected metals and alloys for which available data are being compiled are listed in Table 1. In this series, there are nine aluminums and aluminum alloys, nine coppers and copper alloys, six nickel alloys, two alloy steels, eight stainless steels, a c.p. titanium and two titanium alloys, and five superconducting niobium-base materials including a composite. The two major factors that were considered in selecting these alloys were (1) is the alloy suitable for certain cryogenic components, and (2) are property data available on the alloy at cryogenic temperatures? Although many other alloys are available that qualify for inclusion on the list, those in Table 1 are judged to be the most important for the first year's program.

Additional alloys and also a number of types of composites, including reinforced polymers, will be considered for data compilation for the second year of the program.

DATA COMPILATIONS

The compilation of best-value data on the mechanical, thermal, and magnetic properties of selected metals is based on a collection of test data from various sources, and specific guidelines for selecting the

TABLE 1. ALLOYS FOR FIRST EDITION OF HANDBOOK ON MATERIALS FOR SUPERCONDUCTING MACHINERY

Aluminum and Aluminum Alloys

99.99 Al
EC
1050
1100
2014-T6, T62
2219-T81, T87
5083-0, H113, H38
6061-T6, T651
7039-T6

Copper and Copper Alloys

99.96Cu, ann. (101)
Electrolytic tough pitch, ann. (110)
OFHC Cu, ann. (102)
Phosphorized Cu, ann. (122)
80CU-20Zn, ann. (240)
70Cu-30Zn, ann. (260)
65Cu-35Zn, ann. (270)
90Cu-10Ni, ann. (706)
Cu-Be, AT (170, 172)

Nickel Alloys

Inconel 600, ann.
Inconel X-750, STA
K Monel (K-500), STA
Inconel Alloy 718, STA
Invar, ann.
Ni-Span C, STA

Alloy Steels

9Ni, NNT (ASTM A553)
18Ni (180-200) maraging, STA

Stainless Steels

301, ann., CW
304, ann.
304 ELC, ann.
310, ann.
316, ann.
321, ann.
A-286, STA
Kromark 58

Titanium and Titanium Alloys

Ti, comm. pure
Ti-5Al-2.5Sn (ELI), ann.
Ti-6Al-4V (ELI), ann.

Special Metals and Alloys

Nb, ann.
Nb_3Sn, as received
Nb-Zr, heat treated (various Nb-Zr ratios)
Nb-Ti, heat treated (various Nb-Ti ratios)
Nb-Ti + Cu composite, as received

available data. If data were obtained at testing temperatures of 77 K (-320 F) or lower, such data were retained including all data obtained at room temperature and below. In general, no data were retained that were reported prior to 1950. One less obvious reason for this cut-off date is that over the years procedures for producing alloys change and may cause minor changes in certain properties. If the data compilations are to represent modern production procedures, some limitation in earliest date for data generation should be established, i.e., within the past 25 years. This will not eliminate variations in properties based on current production procedures for any of the alloys, especially titanium alloys, but it should eliminate variations from earlier practices.

Another selection requirement is that the test data be obtained by standard or by accepted test methods. Although some judgement may be required to accept or reject data because of irregularities in testing methods, such judgement is made by program personnel based on their extensive experience in obtaining similar data. For all data selected thus far, the test methods employed were either described or indicated by reference.

Sources of Data

In order to obtain as broad a data base as possible within the funding limitations of the program, searches were made of the accessions of the Metals and Ceramics Information Center (MCIC), the Defense Documentation Center (DDC), and the Cryogenic Information Center (CIC). Many of the documents referenced were in the MCIC files. Documents identified as having useful input for the program but not originally available, either have been obtained or will be ordered.

All documents that are identified as having some direct or indirect input for the program are being collected and listed with an identifying code number in an annotated accessions list. Notations with each entry indicate the alloys and properties that are discussed in the document. These documents are then circulated to or requested by the appropriate investigators for extraction of the appropriate data. As of March 1, 1974, over 400 documents have been added to the accessions list excluding those from the Cryogenics Data Center.

Data Presentations

Since the data to be presented in the Handbook will represent summaries of best-value data for various parameters, the original source data must be compiled in a permanent collection. This has been done by copying data sheets from the original reports and retaining them along with pertinent information on the materials, specimen dimensions, testing procedure, etc., in loose leaf binders indexed for specific alloys. Data from the original data sheets are then entered in master compilation tables from which the recommended best values or average values are calculated. New data may be added to the master tables, and new best-values can be computed with a minimum of confusion by this method. All data and data sheets are coded with a reference number so the information can be traced to its original source.

The primary system of units for the tabulated data and graphical presentations will be SI units. Data based on English units also will be included as a secondary system of units. All data in English units will be enclosed in parenthesis. In the tables, best-value or average data will be printed in bold-face type. The minimum value from a series will be in light-face type. Information also will be presented on the number of specimens and the number of heats from which data were obtained to arrive at the best values that are reported. Procedures used in analyzing the available data will be discussed in detail in the Handbook and all abbreviations and coding systems will be explained.

Data presented in tabular formats will be supplemented by showing the same data in graphical presentations to illustrate trends in the data versus testing temperature and to permit interpolation of the data for intermediate temperatures. Where certain mathematical expressions can be used to produce least squares best fit curves for the plotted data points, this method will be used to produce the curves. Otherwise, the curves will be fitted to the data points by eye.

Mechanical Properties

The mechanical property data being compiled for the Handbook represents information that is most frequently required in designing

components for heavy machinery. Such data include tension, compression, shear, impact, fracture toughness, and fatigue properties.

The Handbook data will be presented in formats as shown in Tables 2, 3, and 4. This general type of format is somewhat similar to that developed for Military Handbook 5 which is a standard reference for aircraft designers. The first sheet of each tabulation will be reserved for tensile property data as in Table 2 (for A-286 stainless steel sheet). Separate tables will be prepared for each product form (sheet, plate, forgings, extrusions, etc.) and for limited ranges of thickness if sufficient data are available. More tensile property data are available at cryogenic temperatures than data from other types of tests.

Available information on compression, shear, impact, fracture toughness, and fatigue properties is very limited for any of the selected alloys at cryogenic temperatures. However, available data on these properties will be reported in the formats shown in Figures 3 and 4.

Mechanical properties data have been obtained from 107 references.

Thermal Properties

The objective of this phase of the program is to collect and organize low-temperature data (in the 0 to 300 K range) on the thermal conductivity, thermal expansion, specific heat, and electrical resistivity of the materials identified in Table 1.

Of the references collected, approximately 125 individual sets of thermal property data have been evaluated. In general, there are extensive areas for which data on these materials do not exist, or have not been published for the cryogenic temperature range. With regard to the data examined thus far, several summary statements are appropriate:

(1) There are considerable thermal conductivity data on the high purity coppers (OFHC, electrolytic tough pitch, etc.). However, data on the alloy systems are very scarce.

(2) Thermal expansion data are available for most of the metals and alloys.

(3) Most of the available specific heat data relate to pure metals aluminum, copper, titanium, and

TABLE 2.

Alloy Designation: A 286 Stainless Steel

Specification:
Form: Sheet
Thickness, cm (in.): 0.041 (0.016)
Condition: 1255 K (1800 F) 30 min. WQ, 985 K (1325 F) 16 hr, AC

Testing Temperature, K (F)		297 (75)	194 (-109)	77 (-320)	20 (-423)	4.2 (-452)
Tensile, Longitudinal						
Ftu, MN/m^2 (ksi)	Avg	1034 (150.0)		1400 (203.0)	1603 (232.5)	
	Min	1028 (149.1)		1397 (202.6)	1588 (230.3)	
Fty, MN/m^2 (ksi)	Avg	663 (96.9)		839 (121.7)	956 (133.7)	
	Min	658 (95.5)		795 (115.3)	945 (137.0)	
e, percent	Avg	14.5		22.3	17.7	
	Min	13.5		21.0	17.0	
RA, percent	Avg					
	Min					
No. of Spec. (No. of Heats		3 (1)		3 (1)	3 (1)	
E, 10^3 MN/m^2 (10^6 psi)	Avg					
	Min					
No. of Spec. (No. of Heats)						
Ftun, MN/m^2 (ksi)	Avg	1050 (152.3)		1241 (180.0)		
K_t = 3.2	Min	1047 (151.9)		1197 (173.6)		
No. of Spec. (No. of Heats)		3 (1)		3 (1)		
Ftun, MN/m^2 (ksi)	Avg	1015 (147.2)		1228 (178.1)	1401 (203.2)	
K_t = 6.3	Min	1014 (147.0)		1211 (175.6)	1393 (202.0)	
No. of Spec. (No. of heats)		2 (1)		3 (1)	3 (1)	
Tensile, Transverse						
Ftu, MN/m^2 (ksi)	Avg	1042 (151.2)		1382 (200.4)		
	Min	1036 (150.3)		1362 (197.6)		
Fty, MN/m^2 (ksi)	Avg	729 (105.7)		889 (128.9)		
	Min	720 (104.5)		878 (127.3)		
e, percent	Avg	19.3		27.0		
	Min	19.0		26.0		
RA, percent	Avg					
	Min					
No. of Spec. (No. of heats)		2 (1)		2 (1)		
E, 10^3 MN/m^2 (10^6 psi)	Avg					
	Min					
No. of Spec. (No. of heats)						
Ftun, MN/m^2 (ksi)	Avg	1031 (150.8)		1319 (191.3)		
K_t = 3.2	Min					
No. of Spec. (No. of heats)		1		1		
Ftun, MN/m^2 (ksi)	Avg	1093 (158.5)		1296 (187.9)		
K_t = 6.3	Min					
No. of Spec. (No. of heats)		1		1		
References NBS-427,						

TABLE 2. (Continued)

Alloy Designation: A-286 Stainless Steel

Specification:
Form: Sheet
Thickness, cm (in.): 0.160 (0.063)
Condition: 1255 K (1800 F) 30 min, WQ, 1005 K (1325 F) 16 hr, AC

Testing Temperature, K (F)		297 (75)	194 (-109)	77 (-320)	20 (-423)	4.2 (-452)
Tensile, Longitudinal						
Ftu, MN/m^2 (ksi)	Avg	1101 (159.7)		1426 (206.9)	1552 (225.1)	
	Min	1092 (158.7)		1417 (205.5)	1522 (220.8)	
Fty, MN/m^2 (ksi)	Avg	733 (106.3)		854 (123.8)	933 (136.1)	
	Min	720 (104.4)		844 (122.4)	924 (134.0)	
e, percent	Avg	17.7		22.4	16.2	
	Min	17.0		20.0	14.0	
RA, percent	Avg					
	Min					
No. of Spec. (No. of heats)		3 (1)		3 (1)	3 (1)	
E, 10^3 MN/m^2 (10^6 psi)	Avg					
	Min					
No. of Spec. (No. of heats)						
Ftun, MN/m^2 (ksi)	Avg	1119 (162.3)		1344 (195.0)	1485 (215.4)	
K_t = 3.2	Min	1100 (159.6)		1316 (190.8)	1459 (211.6)	
No. of Spec. (No. of heats)		3 (1)		3 (1)	3 (1)	
Ftun, MN/m^2 (ksi)	Avg	1169 (169.6)		1396 (202.4)	1567 (227.3)	
K_t = 6.3	Min	1167 (169.2)		1383 (200.6)	1531 (222.0)	
No. of Spec. (No. of heats)		3 (1)		3 (1)	3 (1)	
Tensile, Transverse						
Ftu, MN/m^2 (ksi)	Avg	1076 (156.1)		1360 (197.3)		
	Min	1071 (155.3)		1352 (196.1)		
Fty, MN/m^2 (ksi)	Avg	738 (107.1)		852 (123.5)		
	Min	732 (106.2)		829 (120.2)		
e, percent	Avg	22.8		21.0		
	Min	21.5		20.0		
RA, percent	Avg					
	Min					
No. of Spec. (No. of heats)		3 (1)		3 (1)		
E, 10^3 MN/m^2 (10^6 psi)	Avg					
	Min					
No. of Spec. (No. of heats)						
Ftun, MN/m^2 (ksi)	Avg	1167 (169.2)		1377 (199.7)		
K_t = 3.2	Min	1164 (168.8)		1372 (199.0)		
No. of Spec. (No. of heats)		3 (1)		3 (1)		
Ftun, MN/m^2 (ksi)	Avg	1180 (171.2)		1408 (204.2)		
K_t = 6.3	Min	1176 (170.5)		1397 (202.6)		
No. of Spec. (No. of heats)		3 (1)		3 (1)		

References NBS-427

TABLE 2. (Continued)

Alloy Designation: A-286 Stainless Steel

Specification:
Form: Sheet
Thickness, cm (in.): 0.241-0.254 (0.095-0.100)
Condition: 1255 K (1800 F) 30 min, WQ, 985-1005 K (1325-1350 F) 16 hr, AC

Testing Temperature, K (F)		297 (75)		200 (-100)		144 (-200)		77 (-320)		20 (-423)	
Tensile, Longitudinal											
Ftu, MN/m^2 (ksi)	Avg	994	(144.1)	1054	(152.9)	1116	(161.9)	1326	(192.4)	1495	(216.8)
	Min	969	(140.5)						(191.2)	1452	(210.6)
Fty, MN/m^2 (ksi)	Avg	655	(95.4)	696	(101.0)	760	(110.3)	820	(119.0)	909	(131.9)
	Min	645	(93.6)					780	(113.1)	862	(125.0)
e, percent	Avg	21.8		25.7		28.2		36.9		27.8	
	Min	20.5						32.5		26.5	
RA, percent	Avg										
	Min										
No. of Spec. (No. of heats)		6	(2)	3	(1)	3	(1)	6	(2)	6	(2)
E, 10^3 MN/m^2 (10^6 psi)	Avg										
	Min										
No. of Spec. (No. of heats)											
Ftun, MN/m^2 (ksi)	Avg	1102	(159.9)					1348	(195.5)	1454	(210.9)
K_t = 3.2	Min	1101	(159.8)					1342	(194.7)	1452	(210.6)
No. of Spec. (No. of heats)		3	(1)					3	(1)	3	(1)
Ftun, MN/m^2 (ksi)	Avg	1102	(159.9)					1361	(197.4)	1429	(207.3)
K_t = 6.3	Min	1096	(158.9)					1355	(196.5)	1404	(203.6)
No. of Spec. (No. of heats)		3	(1)					3	(1)	3	(1)
Ftun, MN/m^2 (ksi)	Avg	910	(132)	967	(140.3)	1005	(145.7)	1080	(156.6)	1246	(180.7)
K_t = 10	Min										
No. of Spec. (No. of heats)		3	(1)	3	(1)	3	(1)	3	(1)	3	(1)
Tensile, Transverse											
Ftu, MN/m^2 (ksi)	Avg	1029	(149.3)	1122	(162.7)	1185	(171.9)	1344	(195.0)	1526	(221.4)
	Min	1022	(148.2)					1327	(192.5)	1520	(220.5)
Fty, MN/m^2 (ksi)	Avg	716	(103.8)	783	(113.6)	839	(121.7)	837	(121.4)	932	(135.2)
	Min	676	(98.1)					760	(110.3)	848	(123.0)
e, percent	Avg	23.6		27.3		27.3		38.8		34.8	
	Min	22.0						35.0		31.5	
RA, percent	Avg										
	Min										
No. of Spec. (No. of heats)		6	(2)	3	(1)	3	(1)	6	(2)	6	(2)
E, 10^3 MN/m^2 (10^6 psi)	Avg										
	Min										
No. of Spec. (No. of heats)											
Ftun, MN/m^2 (ksi)	Avg	1102	(159.9)					1338	(194.1)	1444	(209.4)
K_t = 3.2	Min	1090	(158.1)					1325	(192.2)	1431	(207.6)
No. of Spec. (No. of heats)		3	(1)					3	(1)	3	(1)
Ftun, MN/m^2 (ksi)	Avg	1087	(157.6)					1327	(192.4)	1446	(209.8)
K_t = 6.3	Min	1035	(157.4)					1318	(191.2)	1441	(209.0)
No. of Spec. (No. of heats)		3	(1)					3	(1)	3	(1)

References: NBS-120, NBS-177, NBS-427

TABLE 3

Alloy Designation:

Specification:
Form:
Thickness, cm (in.):
Condition:

Testing Temperature, K (F)		297 (75)	194 (-109)	77 (-320)	20 (-423)	4.2 (-452)
Compression, Longitudinal						
Cys, MN/m^2 (ksi)	Avg					
	Min					
No. of Spec. (No. of heats)						
Ec, 10^3 MN/m^2(10^6 psi)	Avg					
	Min					
No. of Spec. (No. of heats)						
Compression, Transverse						
Cys, MN/m^2 (ksi)	Avg					
	Min					
No. of Spec. (No. of heats)						
Ec, 10^3 MN/m^2 (10^6 psi)	Avg					
	Min					
No. of Spec. (No. of heats)						
Shear[a]						
Fsu, MN/m^2 (ksi)	Avg					
	Min					
No. of Spec. (No. of heats)						
G, 10^3/MN/m^2(10^6 psi)	Avg					
	Min					
No. of Spec. (No. of heats)						
Impact, Charpy V						
Long., Nm(ft-lb)	Avg					
	Min					
No. of Spec. (No. of heats)						
Trans., Nm(ft-lb)	Avg					
	Min					
No. of Spec. (No. of heats)						
Fracture Toughness						
K_{Ic}(·)[b] $MN/m^{3/2}$(ksi$\sqrt{in.}$)	Avg					
	Min					
No. of Spec. (No. of heats)						
K_{IE}(·), $MN/m^{3/2}$(ksi$\sqrt{in.}$)	Avg					
(From PTSC specimens)	Min					
No. of Spec. (No. of heats)						

References

(a) Indicate specimen design and orientation for shear specimens:
(b) Indicate specimen design for K_{Ic} data:

TABLE 4

Alloy Designation:

Specification:
Form:
Thickness, cm (in.):
Condition:

Testing Temperature, K (F)	297 (75)	194 (-109)	77 (-320)	20 (-423)	4.2 (-452)
Fatigue, Longitudinal					
S_N at 10^6 cycles, MN/m^2(ksi) for axial loading at Hz with R = and K_t = No. of SN curves (No. of heats)					
S_N at 10^7 cycles, MN/m^2(ksi) for axial loading at Hz with R = and K_t = No. of SN curves (No. of heats)					
Fatigue, Transverse					
S_N at 10^6 cycles, MN/m^2(ksi) for axial loading at Hz with R = and K_t = No. of SN curves (No. of heats)					
S_N at 10^7 cycles, MN/m^2(ksi) for axial loading at Hz with R = and K_t = No. of SN curves (No. of heats)					
References					

niobium. There are very few data on the alloy systems.

(4) Considerable electrical resistivity property data seem to be available, but again primarily for the pure metals aluminum, copper, and titanium. Although some data are available for the aluminum alloys, stainless steels, Inconel 718, and titanium alloys, there are no data available for the alloy steels and very few for the copper alloys.

To illustrate how data on the thermal properties will be presented in the Handbook, this report includes several figures which are plots of typical data for copper. Figure 1 gives thermal conductivity, Figure 2, thermal expansion, Figures 3 and 4, specific heat, and Figures 5 and 6, electrical resistivity. These curves represent visual fits to reported data which have been evaluated to date; the final curves might vary somewhat depending on additional data, and on a more precise computer fit of the curves to the data.

Table 5 is an example of how tabulated data will be presented in the Handbook; these values were read from "best-fit" curves, and Table 6 is a list of conversion factors, that will be included in the Handbook for convenience.

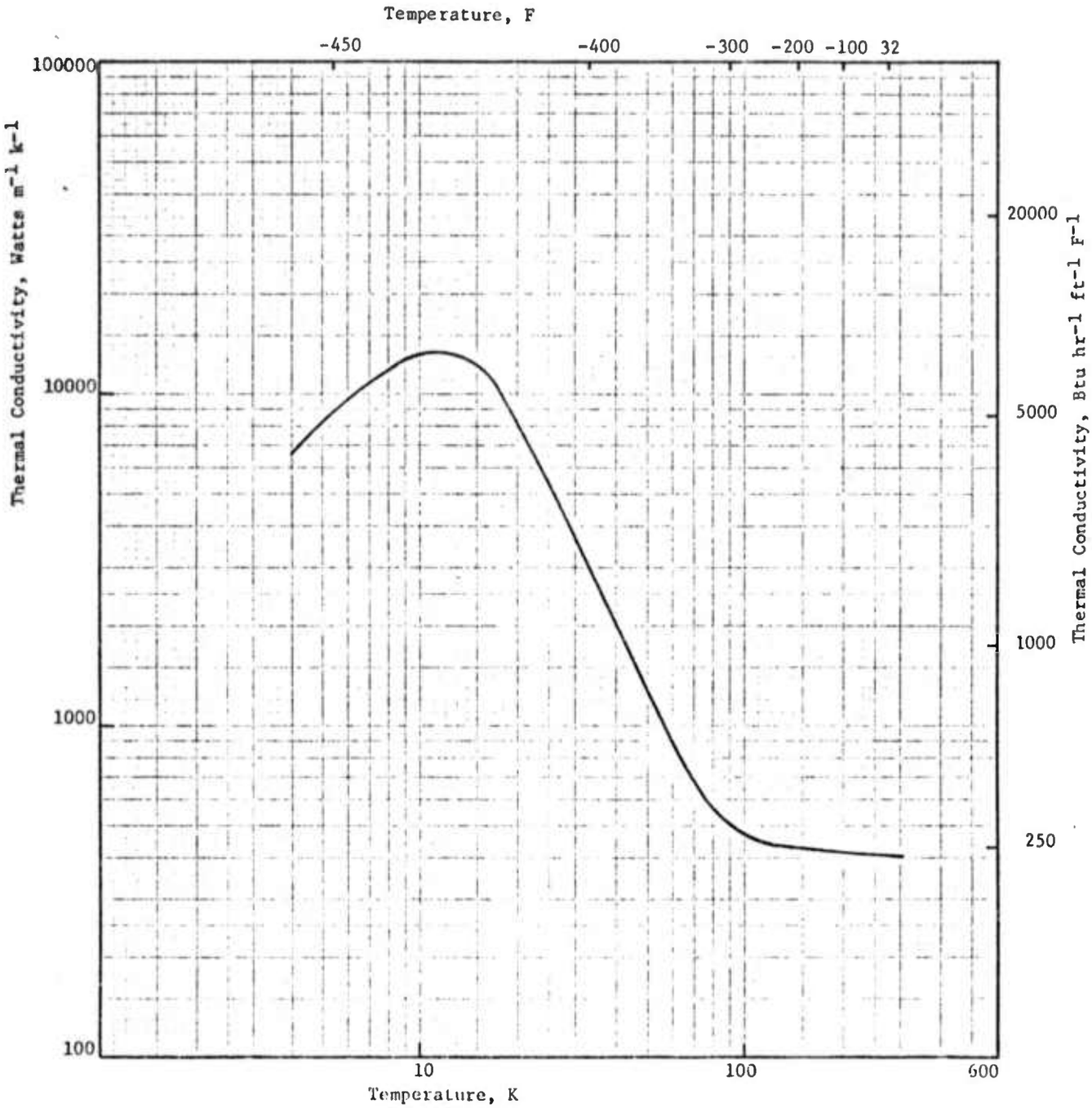

FIGURE 1. THERMAL CONDUCTIVITY VERSUS TEMPERATURE FOR COPPER

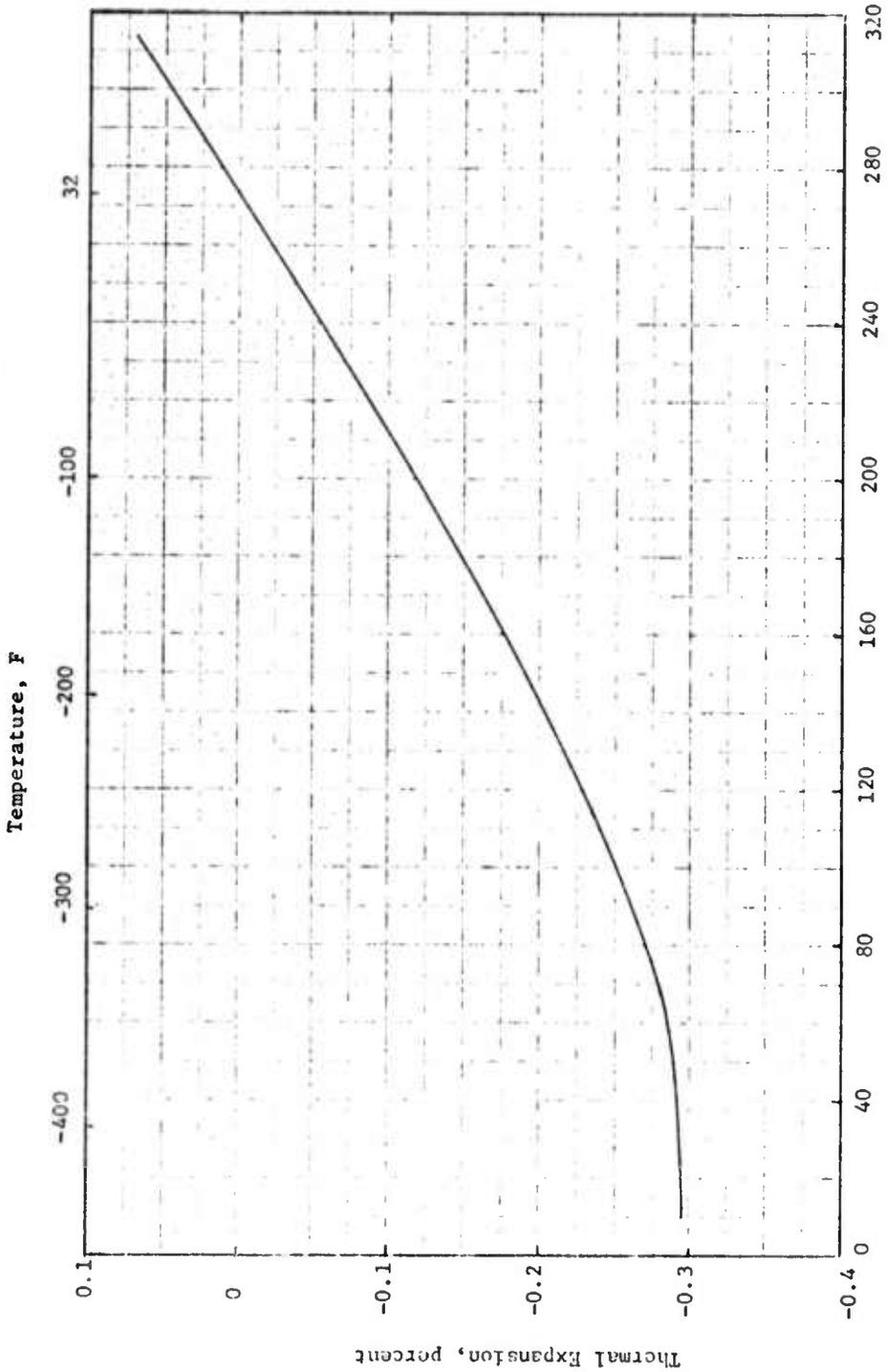

FIGURE 2. THERMAL EXPANSION VERSUS TEMPERATURE FOR COPPER

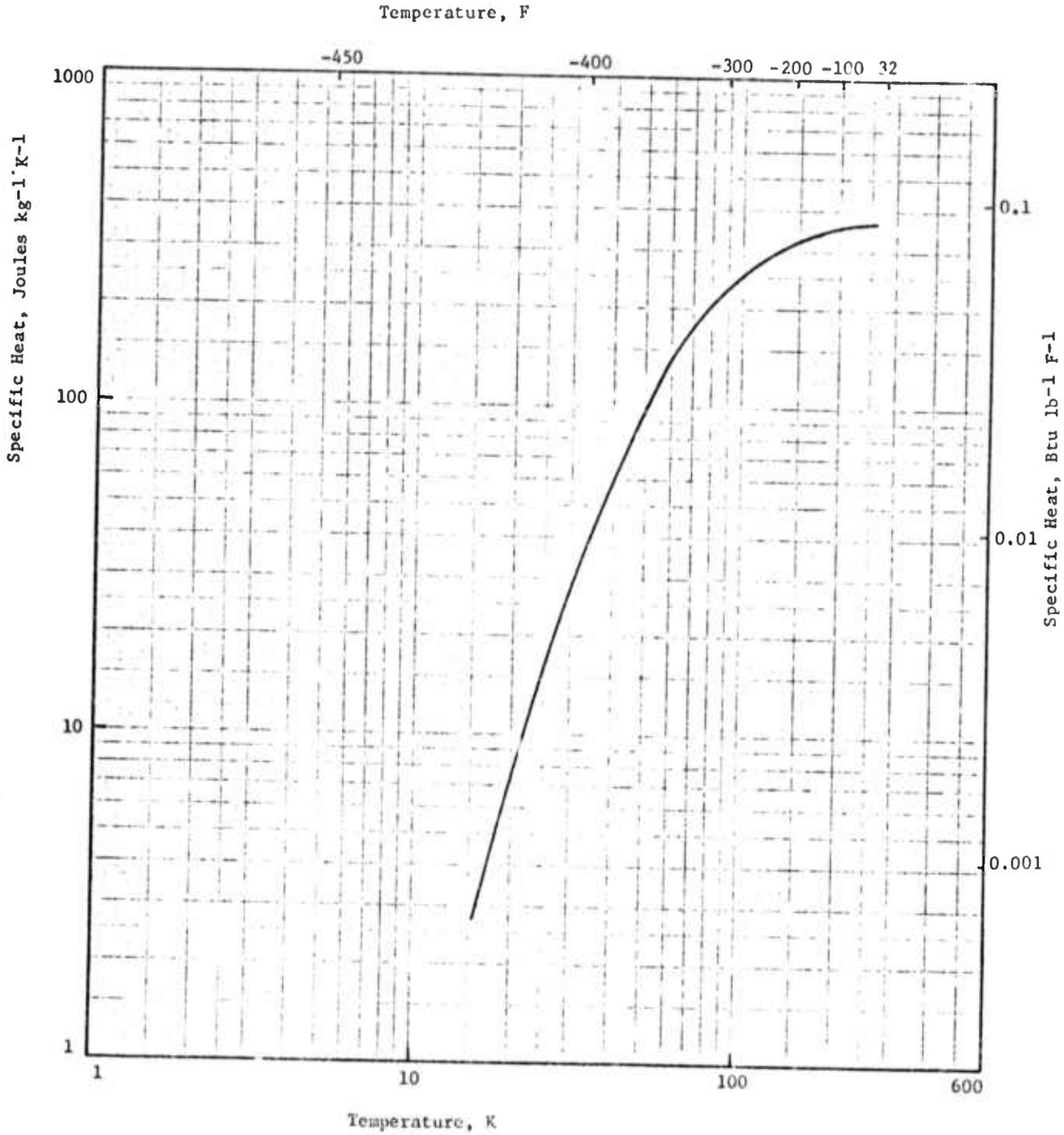

FIGURE 3. SPECIFIC HEAT VERSUS TEMPERATURE FOR COPPER

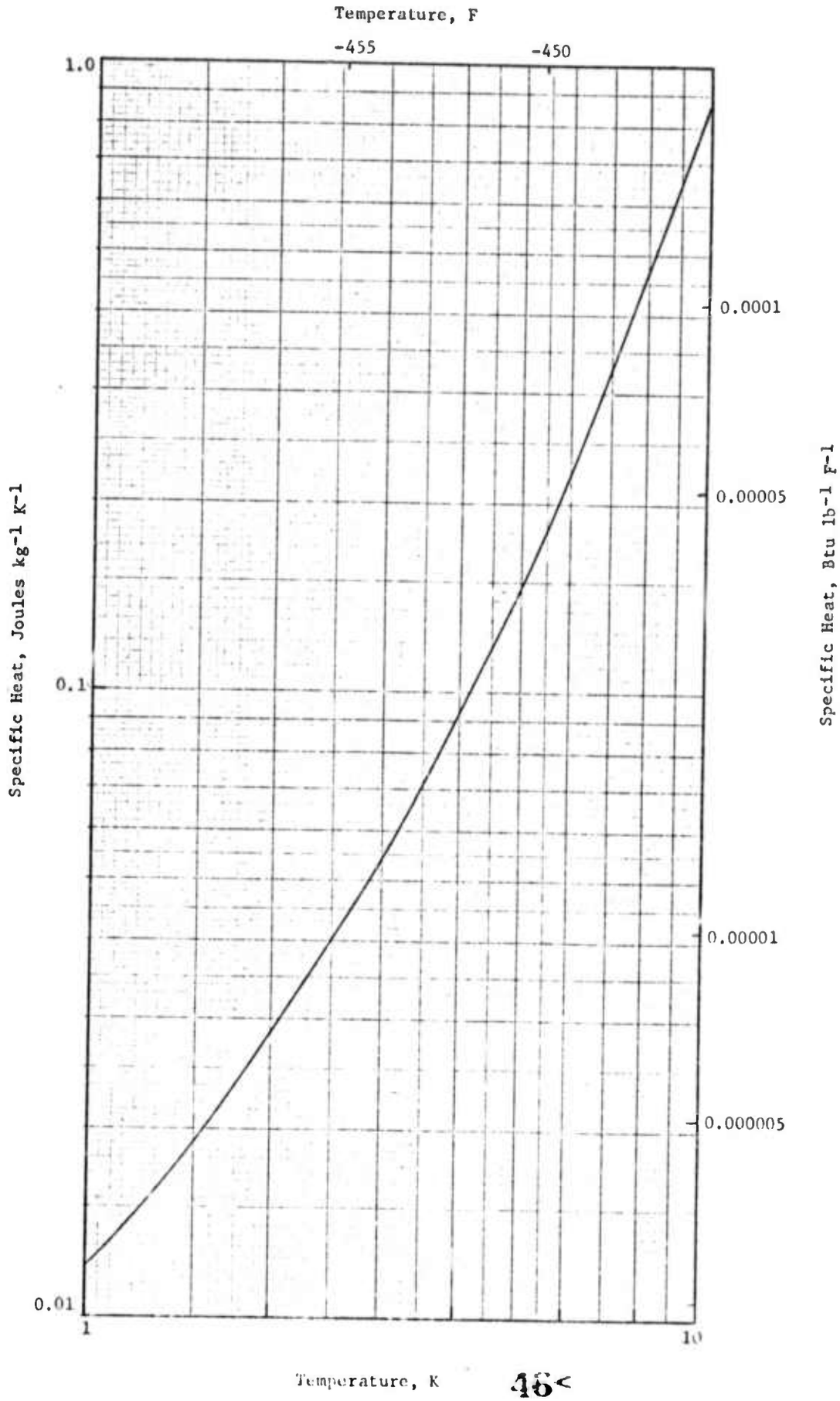

46<

FIGURE 4. SPECIFIC HEAT VERSUS TEMPERATURE FOR COPPER

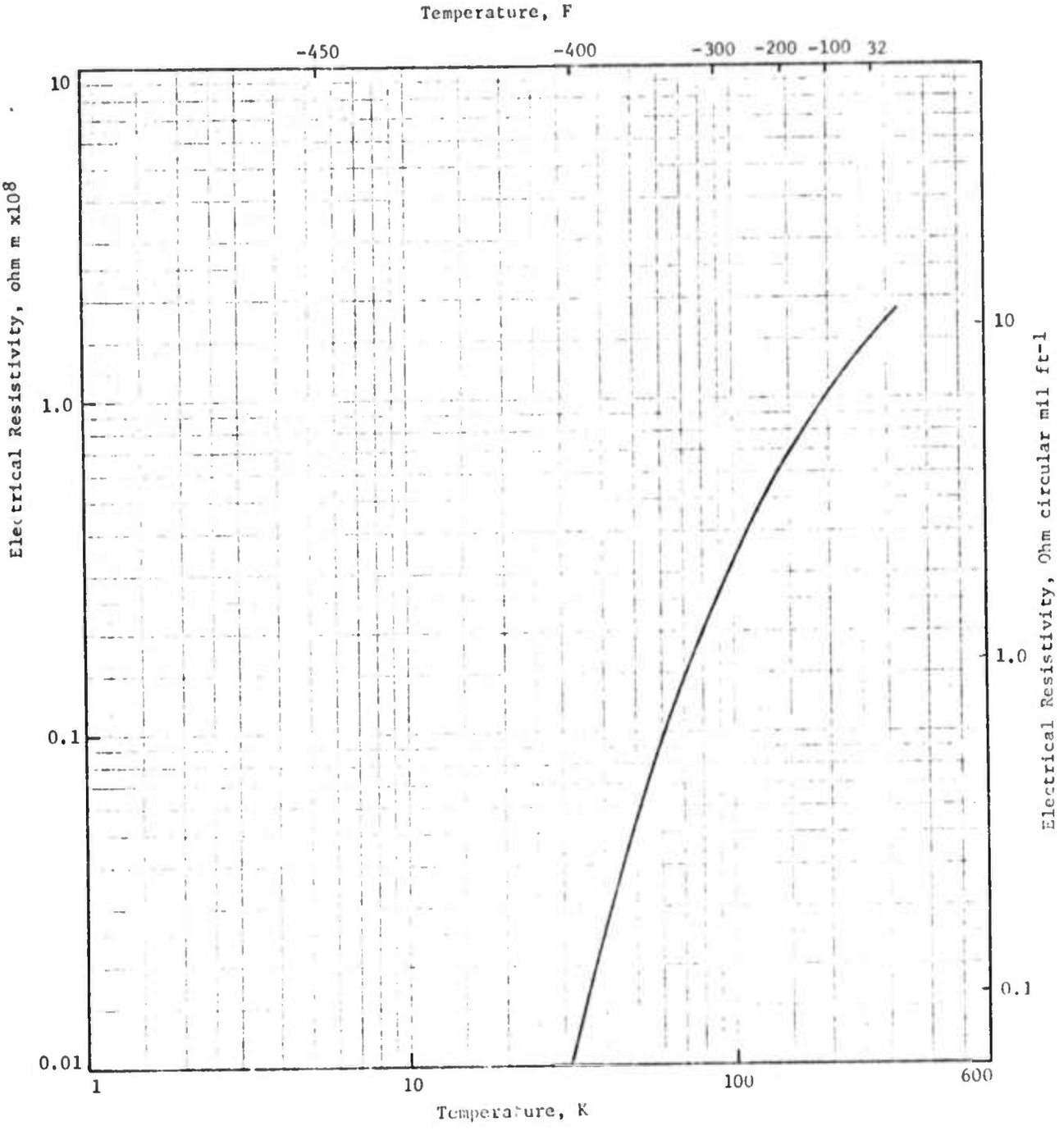

FIGURE 5. ELECTRICAL RESISTIVITY VERSUS TEMPERATURE FOR COPPER

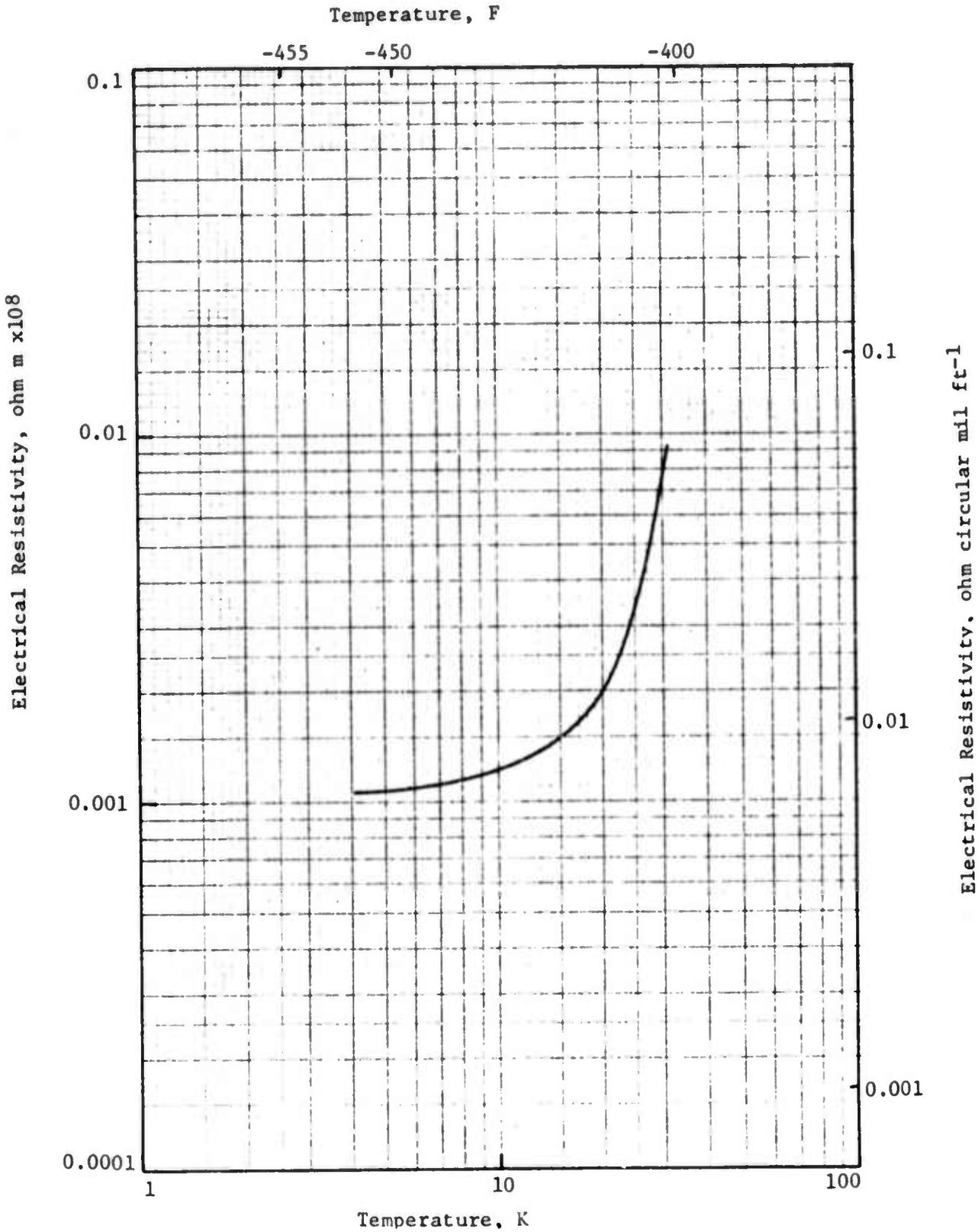

FIGURE 6. ELECTRICAL RESISTIVITY VERSUS TEMPERATURE FOR COPPER

TABLE 5.

Alloy Designation: Copper

Specification:
Form:
Dimension:
Condition: Annealed

Testing Temperature K (F)	273 (32)	100 (-280)	50 (-370)	25 (-415)	10 (-442)	4 (-452)
Thermal Conductivity						
Watts m^{-1} K^{-1}	410	470	1270	5350	13000	6600
Btu hr^{-1} ft^{-1} F^{-1}	(237)	(272)	(734)	(3093)	(7517)	(3816)
No. of Spec. (No. of heats)	1	2	2	2	2	2
References: 87, 282						
Thermal Expansion (T_{273} to T) Longitudinal						
Percent	0	-0.251	-0.289	-0.295	-0.294	
No. of Spec. (No. of heats)	4	4	4	1	4	
References: 116, 282, 371, 396						
Thermal Expansion (T_{273} to T) Transverse						
Percent						
No. of Spec. (No. of heats)						
References:						
Specific Heat						
Joules kg^{-1} K^{-1}	370	250	97	16	0.86	0.093
Btu lb^{-1} F^{-1}	(0.0884)	(0.0598)	(0.0282)	(0.00382)	(0.00021)	(0.000022)
No. of Spec. (No. of heats)	2	2	2	2	2	2
References: 160, 282						
Electrical Resistivity						
Ohm m	1.55×10^{-8}	0.132×10^{-8}	0.054×10^{-8}	0.0033×10^{-8}	0.00122×10^{-8}	0.00108×10^{-8}
Ohm circular mil ft^{-1}	(9.32)	(0.794)	(0.325)	(0.020)	(0.0073)	(0.0065)
No. of Spec. (No. of heats)	7	9	8	8	6	6
References: 87, 385						

TABLE 6

Conversion Factors

Temperature (IPTS)

$°F = 9/5\ °C + 32$
$= 9/5\ (°K - 273.15) + 32$
$= °R - 459.67$

$°K = 5/9\ (°F + 459.67)$
$= °C + 273.15$
$= 5/9\ °R$

To Convert To	From	Multiply By
Thermal Conductivity (Thermochemical Units)		
*Watts m^{-1} K^{-1}	Btu hr^{-1} ft^{-1} F^{-1}	1.730
	Btu in. hr^{-1} ft^{-2} F^{-1}	1.441×10^{-1}
	Cal sec^{-1} cm^{-1} C^{-1}	4.184×10^{2}
	Watts cm^{-1} C^{-1}	1×10^{2}
Btu hr^{-1} ft^{-1} F^{-1}	*Watts m^{-1} K^{-1}	5.782×10^{-1}
	Watts cm^{-1} C^{-1}	57.82
	Cal sec^{-1} cm^{-1} C^{-1}	2.419×10^{2}
	Btu in. hr^{-1} ft^{-2} F^{-1}	8.333×10^{-2}
Specific Heat (Thermochemical Units)		
*Joules kg^{-1} K^{-1}	Btu lb^{-1} F^{-1}	4.184×10^{3}
	Cal g^{-1} C^{-1}	4.184×10^{3}
Btu lb^{-1} F^{-1}	*Joules kg^{-1} K^{-1}	2.390×10^{-4}
	Cal g^{-1} C^{-1}	1
Thermal Expansion		
Percent	*m m^{-1}	1×10^{2}
	in. $in.^{-1}$	1×10^{2}
	cm cm^{-1}	1×10^{2}
Electrical Resistivity		
*Ohm m	Ohm circular mil ft^{-1}	1.662×10^{-9}
	Ohm cm	1×10^{-2}
Ohm circular mil ft^{-1}	*Ohm m	6.015×10^{8}
	Ohm cm	6.015×10^{6}

* SI Units

Magnetic Properties

Structural Materials

An extensive literature search has turned up only a limited amount of usable data on the magnetic susceptibility or permeability of structural materials having potential for use in cryogenic electrical machinery. This situation might be expected since most of these materials are generally considered to be nonmagnetic -- or at most, paramagnetic -- and therefore there has been little reason to investigate their actual permeability. Much of the low-temperature magnetic data in the literature on these materials merely represents magnetization (M) determination under conditions of research interest.

However, some useful data on susceptibility or permeability at cryogenic temperatures has been collected, particularly for the austenitic stainless steels and some forms of nickel and pertinent nickel alloys. It is intended to make an attempt to supplement these data, especially for other materials of specific interest, by contacting selected material suppliers and electrical manufacturers.

An example of the proposed data presentation format for use in the Handbook is shown in Table 7. For materials having determined anisotropy of magnetic properties, the format shown in Table 8 is proposed. Most of the useable magnetic property data obtained to date on the cryogenic structural materials has been reported in the literature in terms of magnetic susceptibility, and therefore both the reported values and the values converted to permeability are planned to be presented in the Handbook tables. Best values will be used if sufficient data are available to permit their determination.

Superconductive Materials

A relatively large amount of superconductor magnetic property data have been acquired to date for the superconductive materials of initial interest. This published material is being reviewed in order to obtain a better understanding of the exact nature of the data at hand and

TABLE 7

Alloy Designation: Type 304 Stainless Steel (N)

Specification:
Form: Rods
Diameter, cm(in.): 0.4 (0.157)
Condition: Annealed (1348 K (1075 C) 30 min. WQ)

Testing Temperature, K(F)	297 (75)	77 (-320)	4.2 (-452)
Magnetic Properties			
Susceptibility, k x 10^4	1.99	4.15	5.68
Permeability, u x 10^4	26.0	53.2	72.4

TABLE 8

Alloy Designation:

Specification:
Form:
Dimension:
Condition:

Testing Temperature, K(F)			
Magnetic Susceptibility,	(as	reported)	
Longitudinal, k x 10^4			
Number of tests (heats)			
Transverse, k x 10^4			
Number of tests (heats)			
Magnetic Permeability, u			
Longitudinal			
Number of tests (heats)			
Transverse			
Number of tests (heats)			

to identify information gaps. Some data have been gathered for all of the materials of primary interest, with the majority pertaining to Nb-Ti alloys.

Initial data correlation is being concentrated on Nb-Ti alloys. A conclusion has not yet been reached as to the most desirable or practical way to present the magnetic property data in the Handbook. In the meeting at BCL on October 16, 1973, it was indicated that, from the designer's standpoint, the preferred presentations would show critical field versus temperature and critical current versus temperature. While a great amount of data are available on critical field versus temperature, as typified by plots such as that shown in Figure 7, relatively little data are available concerning critical current versus temperature. The latter could perhaps be derived by conversion of data on critical current versus critical field, given for various temperatures. The practicality of such an approach needs further investigation. Since superconductivity is considered to be a structure-sensitive property, this aspect will be appropriately treated in presentation of data in the Handbook. As an additional aid to the designer, it is suggested that a table listing the maximum critical values for each of the superconductive materials of interest be included. Suggestions and recommendations regarding presentation of superconductivity data in the Handbook will be appreciated.

HANDBOOK ORGANIZATION

The Handbook will consist of text, data sheets, and graphs in a loose leaf binder. The numbering system for the tables and graphs will be designed to permit updating of the data sheets and adding new data sheets while retaining the continuity of the contents.

The general organization of the Handbook will be as follows:

Title Page
Foreward
Table of Contents
Section 1.0 Introduction
Section 2.0 Methods of Data Collection
Section 3.0 Materials and Compositions

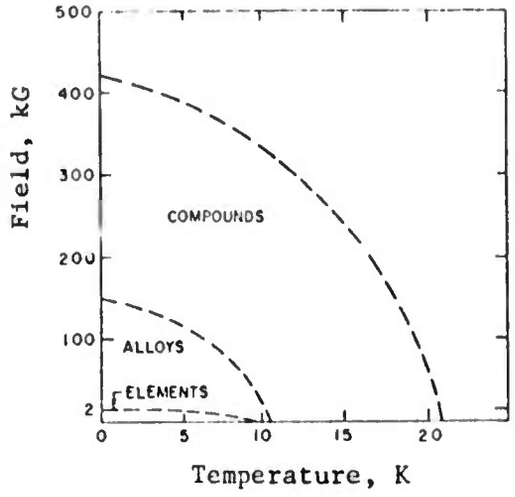

FIGURE 7. TEMPERATURE VERSUS FIFLD ENVELOPES FOR THREE TYPES OF SUPERCONDUCTOR

Section 4.0 Aluminum and Aluminum Alloys
Section 5.0 Copper and Copper Alloys
Section 6.0 Nickel Alloys
Section 7.0 Alloy Steels
Section 8.0 Stainless Steels
Section 9.0 Titanium and Titanium Alloys
Section 10.0 Special Metals and Alloys
References
Appendix, Comparison of Materials Properties

Sections 4 through 10 will be divided into subsections with each alloy in Table 1 represented by one subsection. Thus 99.99 Al will be in Subsection 4.1, EC (electrical conductor) aluminum will be in Subsection 4.2, etc. For each specific alloy, the data sheets and graphs will be presented in the following sequence according to the formats discussed above:

Mechancial Properties

Tension
Compression, shear, impact, fracture toughness
Fatigue

Thermal Properties

Thermal conductivity, thermal expansion, specific heat, electrical resistivity

Magnetic Properties

Magnetic susceptibility, magnetic permeability

Each page will contain the publication date. Each of the major sections will be identified with a tab divider and each page will indicate alloy type and section number to facilitate quick referencing of the data.

New sections (Section 11, Section 12, etc.) may be added later for glass reinforced plastics, other types of composites, and other types of materials when the scope of the Handbook is expanded to include these other materials.

FUTURE WORK

The effort to collect information on the mechanical, thermal, and magnetic properties of the selected metals will be continued. However, increasing emphasis will be placed on compiling the available data in master tables which will be used in computing the best-value data for presentation in the Handbook. Other details of the Handbook preparation that will receive our attention in the near future will include designing the cover for the binders and ordering the binders, preparation of the text material, preparation of the list of references, and compiling information on comparison of alloy properties.

We shall include as much of the property data that are being obtained on current ARPA programs at Westinghouse, Martin-Marietta, and Battelle as become available before the end of the contract period.

SEMIANNUAL TECHNICAL REPORT

on

LOW TEMPERATURE THERMAL EXPANSION AND SPECIFIC HEAT PROPERTIES OF STRUCTURAL MATERIALS

Sponsored by

ADVANCED RESEARCH PROJECTS AGENCY

ARPA Order No. 2569

Program Code 4D10

Contract No. CST-8303

Contract Monitor

CRYOGENICS DIVISION
NATIONAL BUREAU OF STANDARDS
Boulder, Colorado 80302

March 1, 1974

BATTELLE
Columbus Laboratories
505 King Avenue
Columbus, Ohio 43201

FOREWORD

This research was supported by the Advanced Research Projects Agency of the Department of Defense and was monitored by the Cryogenics Division, National Bureau of Standards under Contract No. CST-8303. Dr. Richard P. Reed was Program Manager, and Dr. Alan F. Clark was Contract Monitor.

The research was carried out under ARPA Order No. 2569 and Program Code 4D10 by the Materials Technology and Metal Science Sections of BCL with F. J. Jelinek (614-299-3151, Extension 1735) and E. W. Collings (614-299-3151, Extension 1664) as Principal Investigators. Contract CST-8303, under the overall management of J. E. Campbell, covers both the handbook program and the property measurement program reported here. The semiannual handbook program report has been presented under separate cover. Overall contract funding was $100,000 with $50,000 for the laboratory study reported here. Effective date of the contract was September 10, 1973, and the contract expiration date is September 10, 1974.

DISCLAIMER

TECHNICAL REPORT SUMMARY

The development of superconducting electrical machinery requires the suitable engineering property characterization of all candidate materials at cryogenic temperatures. This program involves the determination of thermal expansion and specific heat for several structural materials in the cryogenic temperature region (4.2 to 300 K).

The materials selected for the first phase of this program were supplied, for the most part, through the cooperation of Westinghouse R&D. These materials have been utilized for superconducting generator development work at Westinghouse.

Thermal expansion measurements were performed utilizing a fused silica dilatometer with a linear differential transducer as the dilatometer head. The accuracy of the measurement is 1 percent. Specific heat at low temperatures is measured to 1 percent by adiabatic calorimetry from a method developed by Nernst. In this method, small increments of heat are supplied to a thermally insulated sample, and the accompanying temperature increase is measured.

In this reporting period, thermal expansion characteristics of 15 alloy specimens were determined in the temperature range 77 to 300 K. In addition, 7 specific heat specimens were evaluated in the temperature range 4.2 to 20 K. These results are shown in the accompanying text of this report. It can be seen that the thermal expansion and specific heat evaluations were done in the nitrogen and helium temperature regions, respectively. This arrangement was used to improve liquid helium consumption efficiency. The second half of the FY 74 program will be used to complete

the expansion measurements at liquid helium temperatures and the specific heat measurements at higher temperatures. In addition, new materials (e.g., structural insulators) will be added to the second half of the program as a result of interactions with other contracting groups.

EXPERIMENTAL METHODS

Low-Temperature Heat Capacity

(a) Description of the Equipment

Specific heat at low temperatures is measured by adiabatic calorimetry (the Nernst method). In this method, small increments of heat are supplied to a thermally insulated sample, and the accompanying temperature increase is measured. Heat capacity is calculated using the relationship

$$C_p = \frac{dQ}{dT} \cong \frac{\Delta Q}{\Delta T} \quad ,$$

$$= \frac{i^2 R \Delta t}{\Delta T} \quad ,$$

where current i is supplied for a time-interval Δt to a heater winding of resistance R in thermal contact with the sample; and ΔT is its resultant rise in temperature. The experiment is of course carried out at constant pressure, hence the subscript p. However, in the temperature range of interest the difference between C_p and C_v ($= \alpha^2$ TV/K, where α is the coefficient of volume thermal expansion, V the molar volume, T the absolute temperature, and K is the isothermal compressibility) is negligible.

Figure 1 and the accompanying photograph shows the general arrangement of the apparatus. The calorimeter can is immersed in liquid helium during the course of the experiment, and thermal insulation of the sample is achieved with the aid of a "diffusion vacuum". By pumping on the helium dewar with a large capacity rotary oil pump, the temperature of the helium bath may be lowered to about 1.6K.

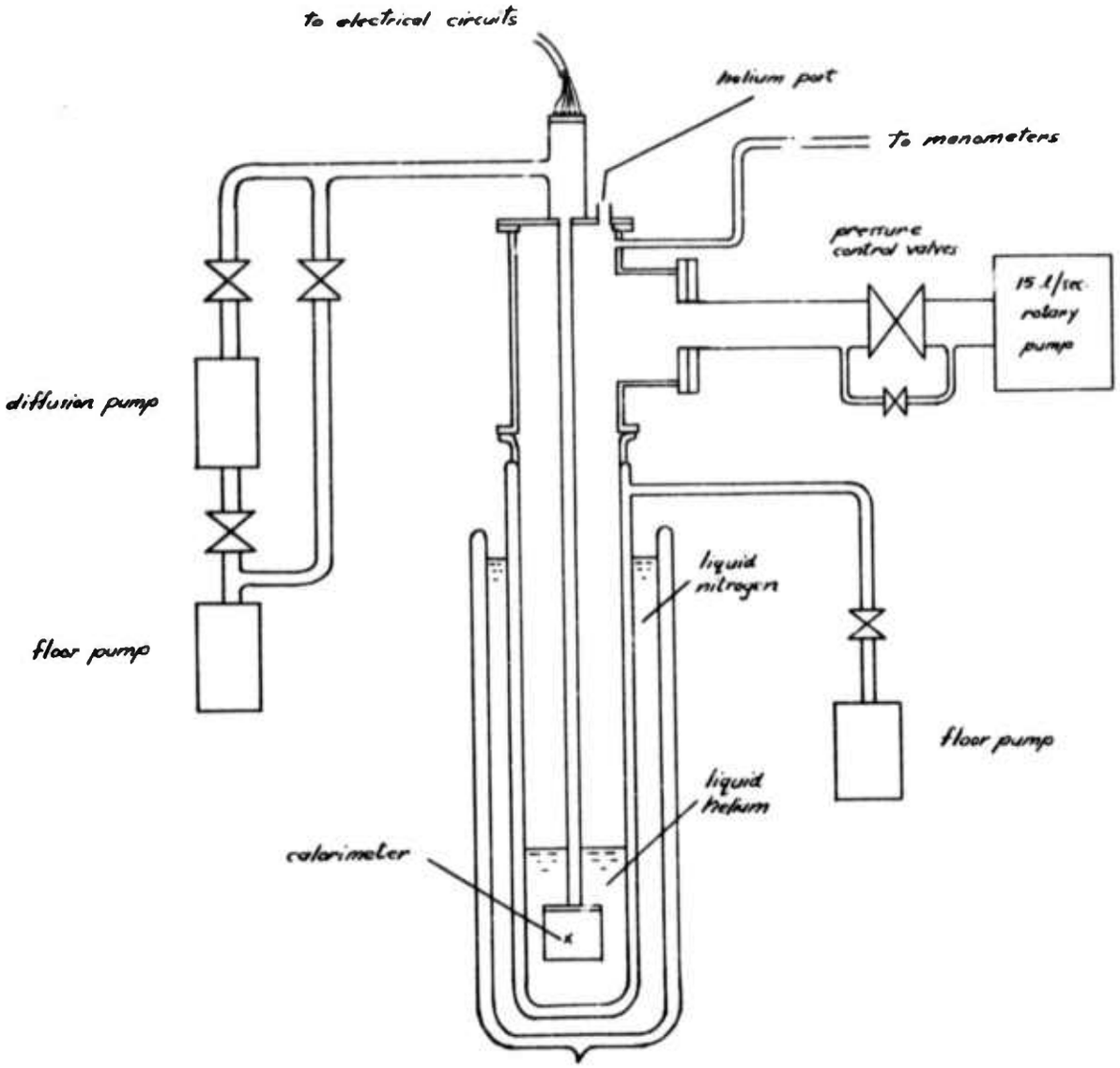

FIGURE 1. SCHEMATIC OF THE LOW-TEMPERATURE SPECIFIC HEAT APPARATUS

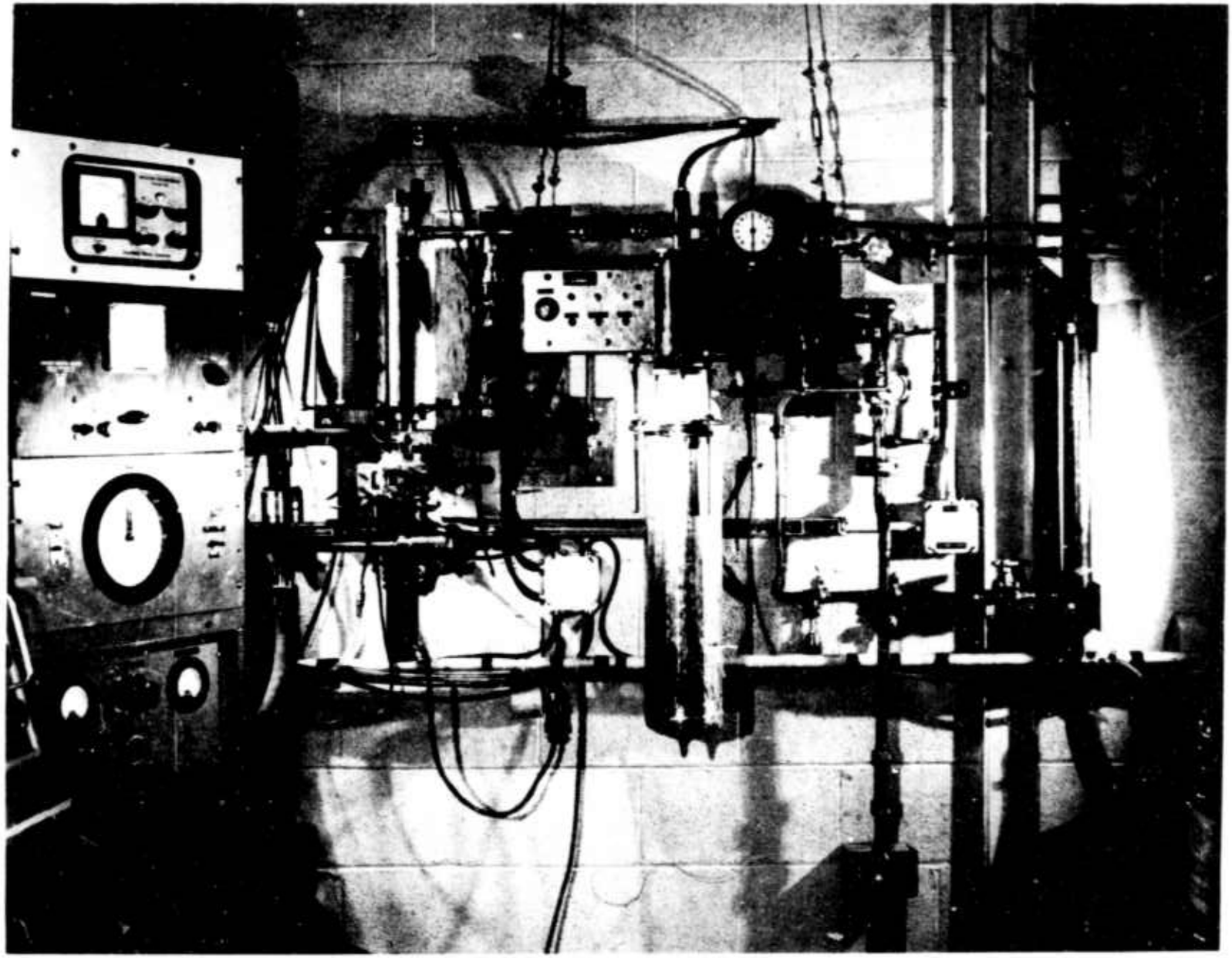

LOW-TEMPERATURE SPECIFIC HEAT APPARATUS

Figure 2 shows the method of mounting the sample (typical weight, 30g) inside the calorimeter can. Using a weighed amount of copper wire, the sample is secured to a copper block which carries a manganin heater (1900 ohms) and a calibrated germanium resistance thermometer. The two leads from the heater, and the four from the thermometer are of fine manganin wire, and are thermally anchored to the can before being connected to a bundled copper wires which pass out of the cryostat through a thin-wall stainless-steel tube.

Figure 3 is a schematic diagram of the electrical circuitry. The calibrated germanium resistance thermometer (Cryocal Inc.) is useful in the temperature range 1.5 to 50-70K. At higher temperatures a metallic resistance thermometer or thermocouple are more suitable. In performing a measurement, a switch is depressed allowing a current of some 5 to 20 μA to pass through the heater coil. The duration of the heat pulse is some 6 to 60 seconds, as measured (to an accuracy of 0.2 m sec) by a clock also actuated by the current switch.

If, as is usually the case, the sample temperature is above 4.2K, it will tend to decrease gradually with time due to heat leakage of various kinds. With reference to Figure 4, heat is applied at time t_1 when the sample temperature is T_1. Heater current is kept on for time $\Delta t = t_2 - t_1$ during which the sample temperature rises to T_2. On switching off the heater current, the temperature of the sample again gradually decreases due to the omnipresent heat leakage. As indicated in Figure 4(a), the leakage-corrected increase in the sample temperature due to the passage of heater current is obtained by extrapolating the cooling curves to time $\frac{t_1 + t_2}{2}$.

All current values and resistances are measured with the aid of a Leeds-Northrup K3 potentiometer. This is associated with a chart recorder

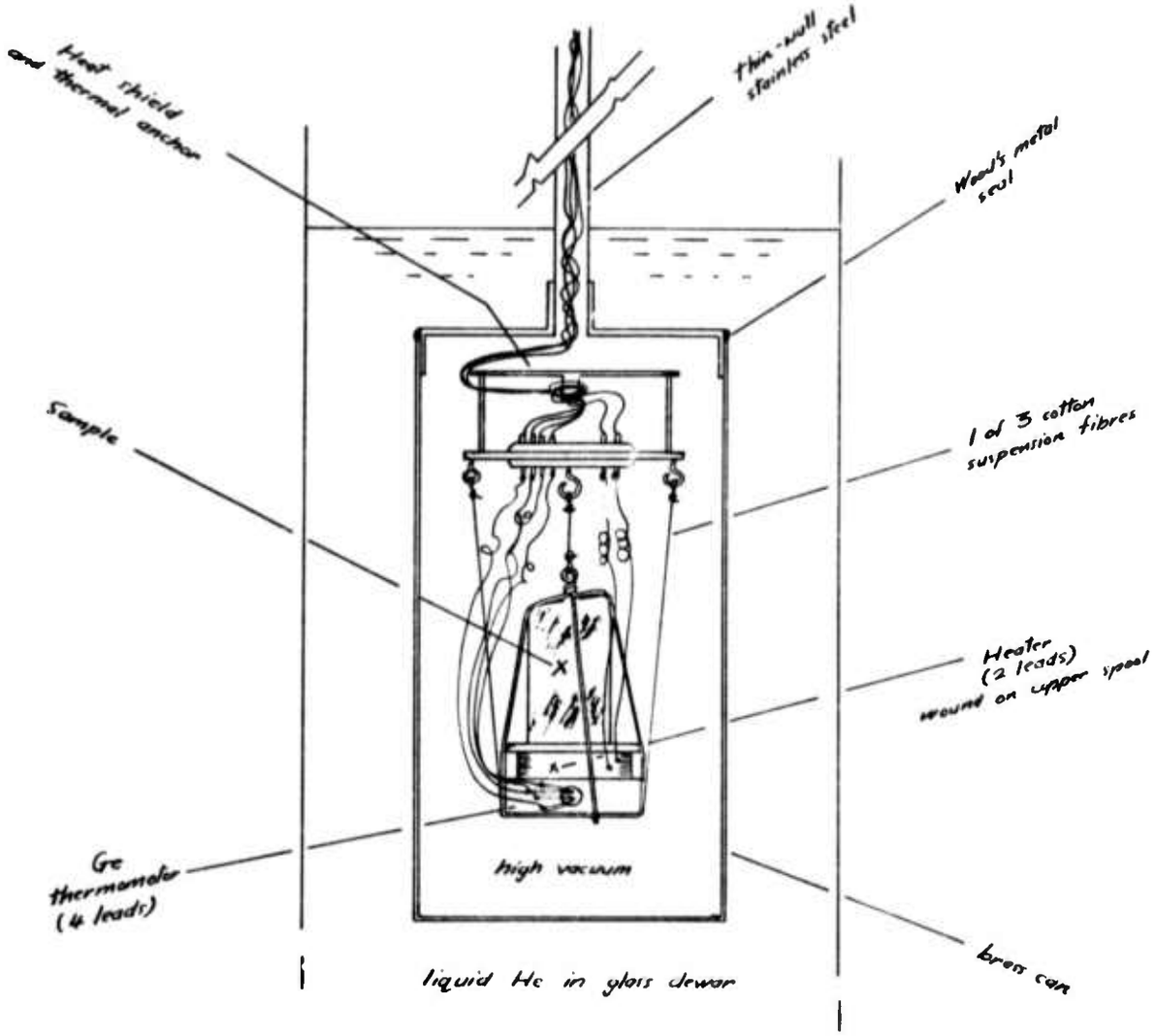

FIGURE 2. SPECIMENS MOUNTED IN THE CALORIMETER CAN

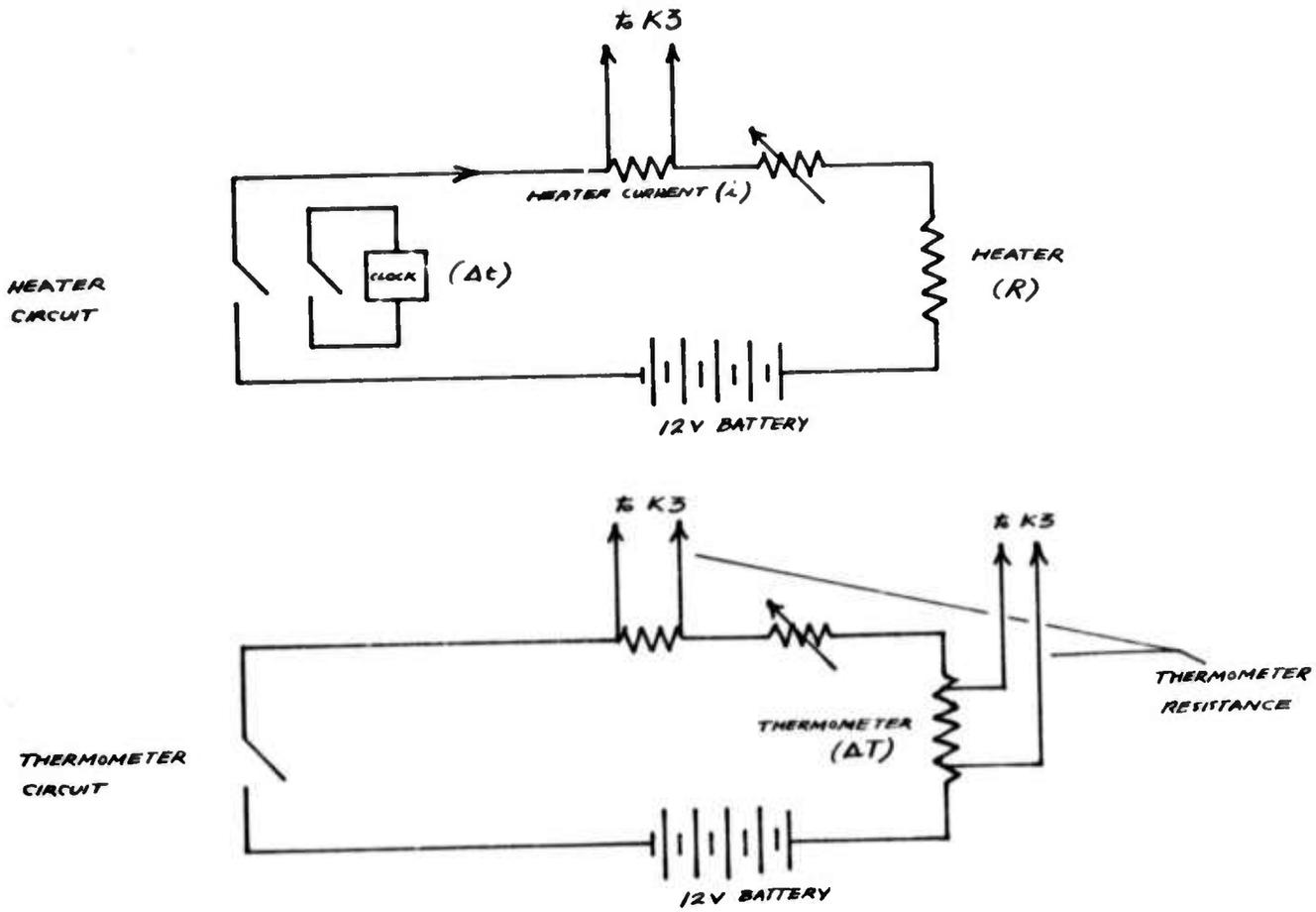

$$i^2 R \Delta t = C_p \Delta T$$

$$\boxed{C_p = \frac{i^2 R \Delta t}{\Delta T}}$$

FIGURE 3. SCHEMATIC DIAGRAM OF THE ELECTRICAL CIRCUITRY

(a)

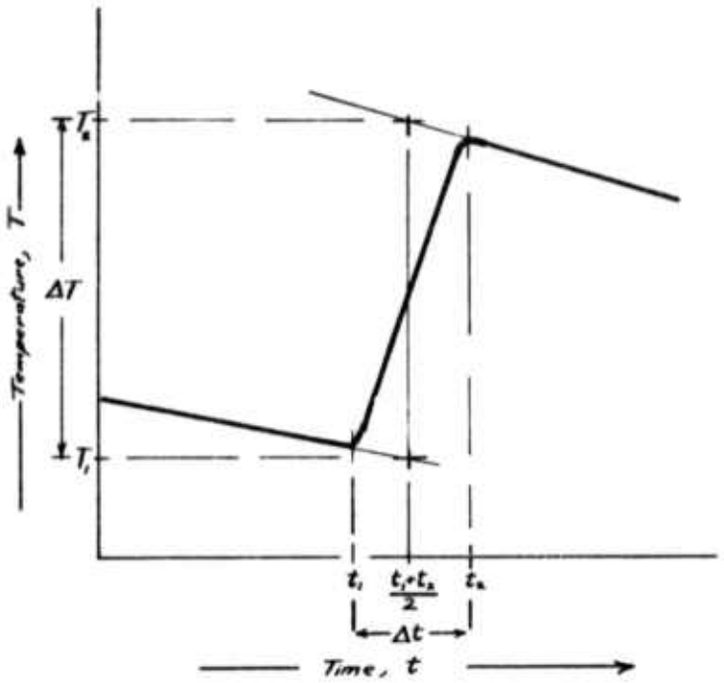

(b)

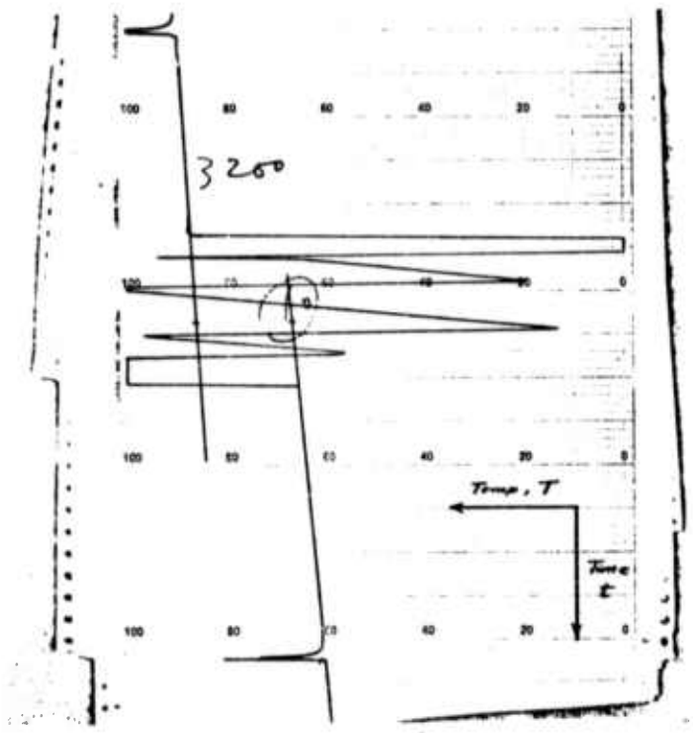

FIGURE 4a. METHOD OF APPLYING A COOLING CORRECTION

FIGURE 4b. EXAMPLE OF A TYPICAL CHART RECORD, WITH APPLIED COOLING CORRECTION

when following the temperature drift of the sample prior to and after the application of a heat pulse, as illustrated in Figure 4(b). In that figure, the excursions of the pen between t_1 and t_2 occur on switching the K3 voltage settings.

(b) Analysis of the Data

The low-temperature heat capacities of normal non-magnetic metals are found to fit an equation of the type

$$C = \gamma T + \beta T^3 \quad , \tag{1}$$

where γT is the conduction-electron heat capacity at temperature T; and βT^3, that of the lattice. Rewriting Equation (1):

$$C/T = \gamma + \beta T^2 \quad , \tag{2}$$

enabling γ and β to be obtained as the intercept and slope, respectively, of a plot of C/T versus T^2. Once γ and β have been obtained for a given metal, as a result of measurements at several temperatures, the heat capacity at any temperature in the "T^3" region can be calculated.

Furthermore a Debye temperature, Θ_D, can be extracted from the coefficient β, since in the appropriate units (mJ, mole, deg K):

$$\Theta_D = \left(\frac{1.94 \times 10^6}{\beta}\right) \quad . \tag{3}$$

Admittedly this is a low-temperature value for Θ_D, which can be expected to differ slightly from higher temperature values depending on the form of the phonan density-of-states. However, by using the Θ_D so obtained, heat capacities up to temperatures in excess of Θ_D (i.e., 300 - 400K) can be easily calculated by assuming the validity of Debye's universal $C_v(T/\theta_D)$ relationship.

(c) Performance of the Equipment

In a test of performance, a specimen of high-purity copper was measured yielding $\gamma = 7.07$ mJ/mole - deg^2 and $\Theta_D = 338$K. These values agree reasonably well with those reported in the literature. The accuracy of the heat-capacity results are estimated to be ± 1 percent in γ and ± 3 percent in Θ_D.

Low-Temperature Thermal Expansion

Linear thermal expansion is measured utilizing a fused-silica dilatometer with a linear differential transducer as the dilatometer head. Care was taken to insure that the fused silica pushrod and the sample tube were of the same material (i.e., same manufacturer, heat treatment, etc). The LVDT was calibrated periodically to insure linearity and a run was made with no specimen present to check the integrity of all mechanical couplings, etc, over the entire temperature range.

The sample tube and pushrod were housed in a liquid helium throttling dewar. This dewar is capable of attaining and controlling specimen temperature in the range 1.3 to 300 K. Thermocouples were mounted directly on the specimen and at regular intervals along the length and radius of the sample tube. A constant temperature region of about 25 centimeters along the length of the tube is achievable at any given throttle setting. Measurements were also taken to insure that the pushrod and sample tube temperatures were the same at any position along the length of the assembly.

Specimen length required is generally 50.8 mm, however, specimens as small as 5 mm have been successfully measured. Specimen diameter can be as high as 13 mm. The accuracy of a measurement on a 50-mm specimen is better than 1 percent. This is based on measurements of standard materials

such as copper and nickel. The reproducibility of a given experiment over the entire range is about 15-25 x 10^{-8} metre. The minimum detectable length change is 10^{-7} cm/cm.

The results reported in this work are shown as percent contraction versus temperature (K) with all data normalized at the ice point (273 K).

RESULTS

Specific Heat

Experimental Materials

Experimental materials were very generously supplied in heat-treated form by the Westinghouse Electric Corporation, Research and Development Center; and we specially acknowledge the help and cooperation of Drs. G. G. Lessmann and J. M. Wells. Low-temperature specific heat, in the temperature range 4.2 - 20 K, has been measured on the specimens listed in Table 1.

Experimental Data

The computer numerical results of the calorimetric experiments performed on the seven specimens listed in Table 1 are presented in Tables 2 through 8; and in the format C/T versus T^2 are displayed in Figures 5 and 6.

Discussion of the Results

Had the data fitted the equation $C = \gamma T + \beta T^3$, a linear fit would have been applied, γ and β tabulated, and θ_D computed. Finally it had been

TABLE 1. LIST OF SPECIFIC HEAT SPECIMENS MEASURED

	Processing and Treatment
Inconel X750	ST
	STDA VIM-VAR
	STDA AAM-VAR
	STDA VIM
Krcmarc 58	STQ
	CW (30%)
310 S Stainless	STFC

ST	Solution treated
STDA	Solution treated double aged
VIM	Vacuum induction melted
VAR	Vacuum arc re-melted
STQ	Solution treated and quenched
STFC	Solution treated and furnace cooled
CW	Cold worked

TABLE 2. SPECIFIC HEAT

Specimen: Inconel X750 ST

Temperature Range: 4-21K

Temperature, K	Specific Heat (J/kg-deg)	Temperature, K	Specific Heat (J/kg-deg)
4.2	1.192	8.3	2.301
4.3	1.220	8.5	2.372
		8.7	2.420
4.3	1.209		
4.4	1.232	8.9	2.297
4.5	1.255	9.2	2.554
		9.5	2.634
4.6	1.280		
4.7	1.307	9.7	2.743
4.8	1.332	9.8	2.714
		10.0	2.813
5.0	1.369		
5.1	1.413	10.2	2.861
5.2	1.431	10.3	2.899
		10.5	2.962
5.4	1.472		
5.5	1.512	10.8	3.058
5.7	1.552	11.2	3.155
		11.6	3.299
5.8	1.602		
6.0	1.642		
6.1	1.706	12.0	3.527
		13.9	4.136
6.2	1.735	14.2	4.345
6.2	1.717		
6.3	1.763	14.9	4.598
		15.6	4.934
6.5	1.820	16.4	5.261
6.8	1.888	17.3	5.752
7.1	1.967	18.3	6.317
7.2	1.994	19.8	7.272
7.6	2.117	21.0	8.151
7.8	2.182		
8.1	2.251		

TABLE 3. SPECIFIC HEAT

Specimen: Inconel X750 STDA VIM-VAR

Temperature Range: 4-15K

Temperature, K	Specific Heat (J/kg-deg)	Temperature, K	Specific Heat (J/kg-deg)
4.2	1.188	7.2	1.984
4.3	1.201	7.5	2.056
4.4	1.221	7.7	2.117
4.4	1.238	8.0	2.207
4.5	1.261	8.2	2.261
4.6	1.276	8.5	2.356
4.7	1.310	8.7	2.443
4.8	1.346	9.0	2.518
5.0	1.383	9.4	2.627
5.1	1.420	9.3	3.425
5.3	1.458	9.5	3.337
5.5	1.523	9.8	2.747
5.7	1.576	9.9	2.748
5.9	1.641	10.0	2.784
6.1	1.697	10.3	2.862
6.3	1.739	10.8	3.042
6.5	1.795	11.4	3.222
6.7	2.692	14.3	4.361
6.8	1.893	15.0	4.722
7.0	1.935		

TABLE 4. SPECIFIC HEAT

Specimen: Inconel X750 STDA AAM-VAR

Temperature Range: 4-15K

Temperature, K	Specific Heat (J/kg-deg)	Temperature, K	Specific Heat (J/kg-deg)
4.3	1.180	6.9	1.860
4.3	2.635	7.2	1.936
4.4	1.210	7.4	2.032
4.5	1.232	7.9	2.152
4.6	1.258	8.4	2.278
4.7	1.266	8.9	2.427
4.8	1.301	9.4	2.545
4.9	1.338	10.0	2.754
5.2	1.395	10.4	2.898
5.4	1.474	11.0	3.064
5.7	1.553	11.7	3.286
5.9	1.619	12.2	3.477
6.1	1.660	13.1	3.808
6.4	1.732	14.0	4.130
6.6	1.782	14.8	4.161
		15.4	4.715

TABLE 5. SPECIFIC HEAT

Specimen: Inconel X750 STDA VIM

Temperature Range: 4-20K

Temperature, K	Specific Heat (J/kg-deg)	Temperature, K	Specific Heat (J/kg-deg)
4.4	1.216	9.5	2.668
4.5	1.240	9.8	2.779
4.6	1.271	10.2	2.895
4.8	1.305	10.4	2.978
4.9	1.353	10.7	3.095
5.1	1.405	11.1	3.189
5.3	1.467	11.4	3.308
5.5	1.526	11.9	3.461
5.7	1.595	12.3	3.609
5.9	1.637	12.7	3.779
6.1	1.687	13.2	3.955
6.3	1.757	13.6	4.127
6.6	1.837	14.1	4.327
6.9	1.889	14.6	4.541
7.1	1.973	15.4	4.899
7.4	2.050	16.4	5.132
7.7	2.081	17.1	5.734
8.0	2.221	17.8	6.293
8.4	2.332	18.8	6.911
8.8	2.445	20.2	8.275
9.1	2.549		

TABLE 6. SPECIFIC HEAT

Specimen: Kromarc 58 STQ

Temperature Range: 4-14K

Temperature, K	Specific Heat (J/kg-deg)	Temperature, K	Specific Heat (J/kg-deg)
4.2	1.697	7.1	2.899
4.2	1.714	7.4	3.034
4.3	1.750	7.8	3.220
4.5	1.802	8.2	3.256
4.6	1.851	8.6	3.603
4.7	1.931	8.8	3.714
4.9	1.958	9.2	3.875
5.0	2.039	9.3	3.919
5.2	2.118	9.9	4.263
5.4	2.207	10.1	4.364
5.6	2.295	10.4	4.467
5.8	2.372	10.8	4.714
6.0	2.442	11.4	6.540
6.2	2.543	11.8	5.212
6.4	2.638	12.3	5.530
6.6	2.708	13.0	5.938
6.8	2.789	14.2	3.378

TABLE 7. SPECIFIC HEAT

Specimen: Kromarc 58 CR (30%)

Temperature Range: 4-15K

Temperature, K	Specific Heat (J/kg-deg)	Temperature, K	Specific Heat (J/kg-deg)
4.1	1.691	6.8	2.795
4.3	1.738	7.2	2.951
4.4	1.783	7.5	3.087
4.5	1.814	7.9	3.240
4.6	1.863	8.3	3.434
4.7	1.924	8.7	3.621
4.8	1.985	9.1	3.813
5.0	2.066	9.6	3.978
5.2	2.155	10.3	4.320
5.4	2.244	10.8	4.565
5.6	2.305	11.6	4.852
5.7	2.362	13.7	6.346
5.9	2.458	14.9	7.022
6.1	2.561		
6.5	2.792		

TABLE 8. SPECIFIC HEAT

Specimen: 310 S Stainless Steel STFC

Temperature Range: 4-17K

Temperature, K	Specific Heat (J/kg-deg)	Temperature, K	Specific Heat (J/kg-deg)
4.2	2.280	7.3	3.732
4.3	2.297	7.5	3.897
4.5	2.406	7.7	3.985
4.6	2.438	8.0	4.091
4.7	2.490	8.2	4.325
4.8	2.560	8.5	4.378
5.0	2.637	8.9	4.544
5.1	2.726	9.3	4.686
5.3	2.824	9.9	4.911
5.5	2.915	10.5	5.282
5.7	3.025	11.0	5.603
5.9	3.099	11.4	5.843
5.9	3.131	12.0	6.134
6.1	3.181	12.5	6.364
6.2	3.249	12.9	6.591
6.3	3.303	13.3	6.755
6.4	3.359	13.8	7.075
6.6	3.435	14.3	7.396
6.8	3.523	15.0	7.755
6.9	3.599	15.8	8.253
7.1	3.659	16.6	8.856
		17.4	9.365

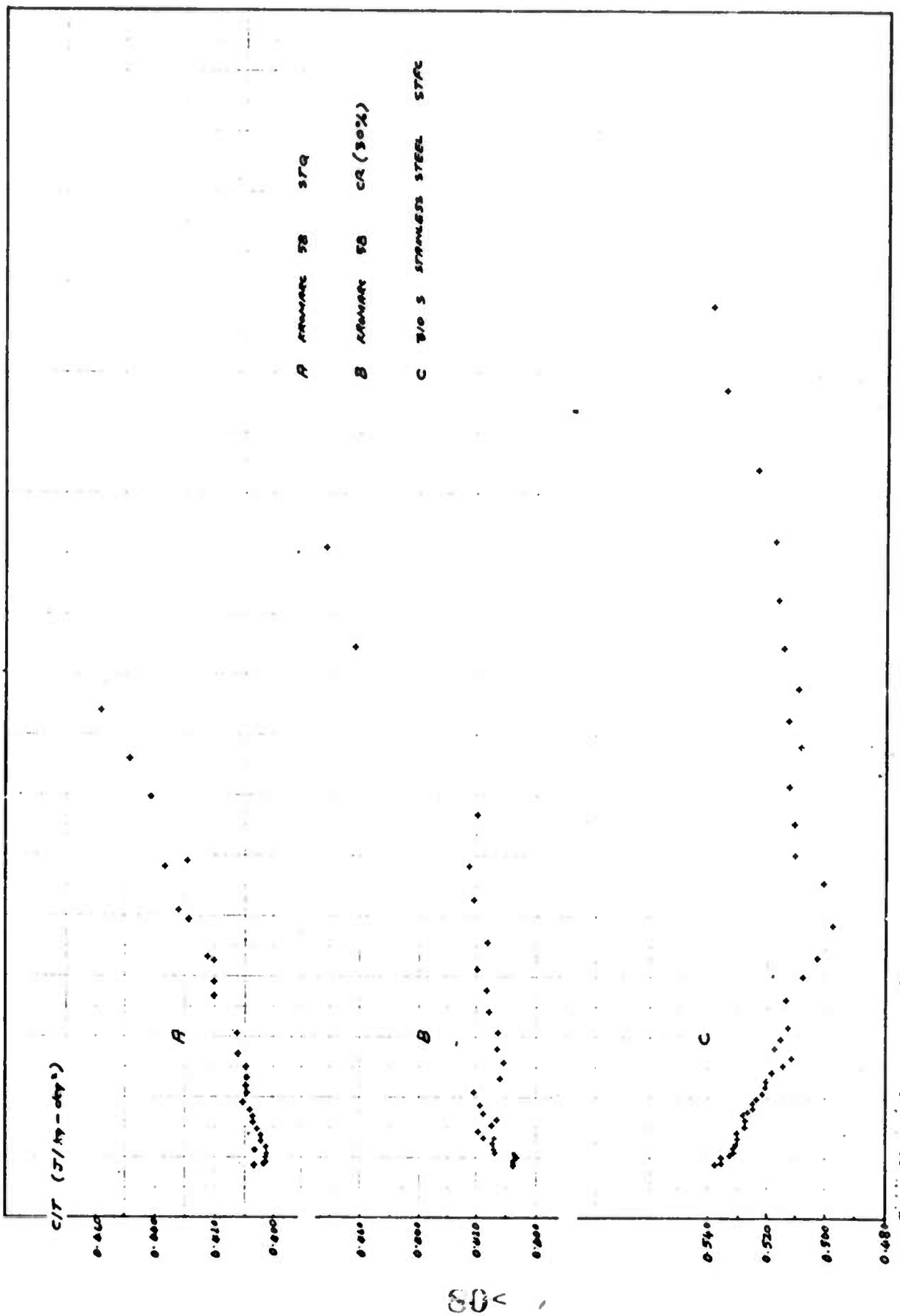

FIGURE 5. C/T VERSUS T^2 REPRESENTATION OF ALLOY DATA

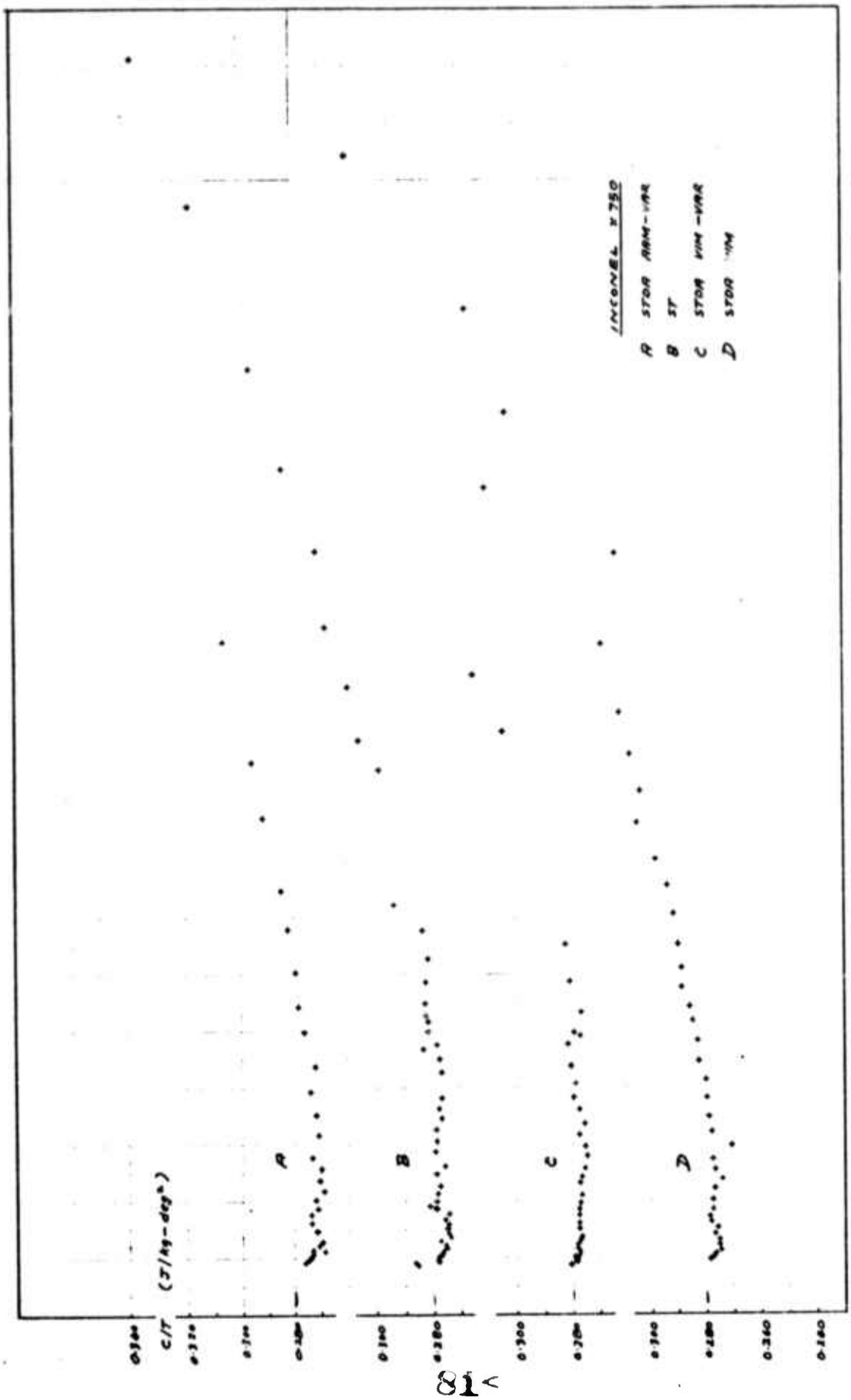

FIGURE 6. C/T VERSUS T^2 REPRESENTATION OF ALLOY DATA

planned to prepare summarizing tablulations of specific heats, derived from the calculated γ and β, at the temperatures 4, 5, 10, 15, and 20 K. But as a glance at Figures 5 and 6 shows, the data do not fit a simple $C/T = \gamma + \beta T^2$ relationship. The form of the C/T temperature dependence, viz, a tendency for an up-turn to develop as the temperature decreases toward the liquid-helium range, suggests the presence of a significant magnetic contribution to the specific heat at low temperatures. Inconel, Kromarc, and stainless-steel are all clustering alloys. The specific-heat data suggest the existence of superparamagnetic clusters. During the second half of this program, we intended to fit the specific heat data to a relationship of the form

$$C/T = A/T + \gamma + \beta T^2 \quad *$$

compute A, γ and β, and complete the summarizing tabulation referred to above.

Thermal Expansion

Experimental Materials

Low-temperature thermal expansion in the temperature range 77 - 300 K has been measured on the specimens listed in Table 9.

Experimental Data

The computed numerical results of the expansion experiments performed on the 15 specimens listed in Table 9 are presented in Tables 10 through 15.

---

* c.f., "Anomalous Low-Temperature Specific Heat of Alloys Near the Critical Concentration for Ferromagnetism", Hahn, A and Wohlfarth, E. P., Helvetia Physica Acta, 41, 857 (1968).

TABLE 9. LIST OF THERMAL EXPANSION SPECIMENS MEASURED

	Processing and Treatment
Inconel X750	ST
	STDA VIM-VAR
	STDA AAM-VAR
	STDA VIM
Kromarc 58	STQ
	CW (30%)
OFHC Copper	AR
	SR
310S Stainless	STQ
	STFC
INCO (LE) Unnamed	STA
Ti-Nb	5 a/o Nb
	10 a/o Nb
	15 a/o Nb
	20 a/o Nb

ST	Solution treated
AR	As received
SR	Stress relieved
STDA	Solution treated double aged
STA	Solution treated aged
STQ	Solution treated and quenched
STFC	Solution treated and furnace cooled
VIM	Vacuum induction melted
VAR	Vacuum arc remelted

TABLE 10. THERMAL EXPANSION BEHAVIOR OF KROMARC 58

T (K)	STQ $-\frac{\Delta L}{L_o}$ (%)	CW (30%) $-\frac{\Delta L}{L_o}$ (%)
300	-0.044	-0.044
290	-0.029	-0.028
280	-0.011	-0.010
273	0	0
260	0.021	0.020
250	0.036	0.036
240	0.052	0.051
230	0.068	0.066
220	0.084	0.081
210	0.100	0.094
200	0.115	0.107
190	0.129	0.122
180	0.144	0.135
170	0.158	0.149
160	0.171	0.161
150	0.183	0.173
140	0.195	0.185
130	0.207	0.196
120	0.218	0.208
110	0.228	0.219
100	0.238	0.229
90	0.247	0.237
80	0.255	0.245
78	0.257	0.247

TABLE 11. THERMAL EXPANSION BEHAVIOR OF INCONEL X750

T (K)	ST $-\frac{\Delta L}{L_o}$ (%)	STDA VIM-VAR $-\frac{\Delta L}{L_o}$ (%)	MP2 STDA AAM-VAR $-\frac{\Delta L}{L_o}$ (%)	MP3 STDA VIM $-\frac{\Delta L}{L_o}$ (%)
300	-0.039	-0.039	-0.037	-0.042
290	-0.026	-0.025	-0.025	--
280	-0.013	-0.013	-0.013	-0.013
270	0	0	0	0
260	0.013	0.011	0.012	0.013
250	0.025	0.023	0.024	0.024
240	0.037	0.036	0.036	0.035
230	0.050	0.048	0.047	0.048
220	0.062	0.061	0.058	0.060
210	0.074	0.073	0.070	0.073
200	0.086	0.084	0.081	0.083
190	0.098	0.096	0.092	0.094
180	0.108	0.108	0.105	0.107
170	0.120	0.120	0.115	0.116
160	0.131	0.129	0.125	0.127
150	0.141	0.140	0.135	0.137
140	--	0.149	0.144	0.147
130	0.160	0.159	0.155	0.156
120	0.169	0.167	0.163	0.164
110	0.178	0.176	0.172	0.171
100	0.186	0.184	0.180	0.178
90	0.193	0.191	0.189	0.184
80	0.200	0.197	0.193	0.190
78	0.201	0.199	0.193	0.191
77			0.194	0.192

TABLE 12. THERMAL EXPANSION BEHAVIOR OF CFHC COPPER

T (K)	AR $-\frac{\Delta L}{L_o}$ (%)	SR $-\frac{\Delta L}{L_o}$ (%)
300	-0.052	-0.045
290	-0.034	-0.029
280	-0.017	-0.014
270	0	0
260	0.017	0.014
250	0.033	0.029
240	0.051	0.043
230	0.067	0.060
220	0.083	0.076
210	0.099	0.091
200	0.114	0.107
190	0.130	0.122
180	0.145	0.137
170	0.161	0.152
160	--	0.168
150	0.191	0.183
140	0.205	0.197
130	0.219	0.210
120	0.233	0.223
110	0.246	0.237
100	0.258	0.249
90	0.269	0.260
80	0.279	0.270
78	0.280	0.272

TABLE 13. THERMAL EXPANSION BEHAVIOR OF 310 STAINLESS STEEL

T (K)	STQ $-\frac{\Delta L}{L_o}$ (%)	STFC $-\frac{\Delta L}{L_o}$ (%)
300	-0.045	-0.035
290	-0.026	-0.026
280	-0.011	-0.009
273	0	0
260	0.020	0.022
250	0.034	0.037
240	0.051	0.052
230	0.066	0.065
220	0.080	0.079
210	0.095	0.093
200	0.112	0.107
190	0.126	0.123
180	0.139	0.138
170	0.153	0.151
160	--	0.162
150	0.177	0.174
140	0.189	0.186
130	0.201	0.196
120	0.213	0.205
110	0.223	0.214
100	0.234	0.221
90	0.244	0.228
80	0.253	0.234
78	0.254	0.234

TABLE 14. THERMAL EXPANSION BEHAVIOR OF INCO LE (UNNAMED)

T (K)	ST-A $-\frac{\Delta L}{L_o}$ (%)
300	-0.010
290	-0.006
280	-0.002
273	0
260	0.003
250	0.006
240	0.012
230	0.015
220	0.018
210	0.022
200	0.027
190	0.031
180	0.036
170	0.041
160	--
150	0.051
140	0.055
130	0.059
120	0.063
110	0.066
100	--
90	0.072
80	0.076
78	0.077

TABLE 15. THERMAL EXPANSION BEHAVIOR OF Ti-Nb ALLOYS

(Data above 200 K are a linear extrapolation)

T (K)	No. 1 Ti-5 a/o Nb $-\frac{\Delta L}{L_o}$ (%)	No. 2 Ti-10 a/o Nb $-\frac{\Delta L}{L_o}$ (%)	No. 3 Ti-15 a/o Nb $-\frac{\Delta L}{L_o}$ (%)	No. 4 Ti-20 a/o Nb $-\frac{\Delta L}{L_o}$ (%)
300	- 0.185	-0.175	-0.165	-0.140
290	- 0.12	-0.11	-0.110	-0.085
280	- 0.05	-0.045	-0.045	-0.035
273	0	0	0	0
260	0.09	0.085	0.075	0.070
250	0.155	0.145	0.135	0.125
240	0.225	0.210	0.195	0.175
230	0.295	0.275	0.255	0.230
220	0.36	0.340	0.315	0.280
210	0.43	0.405	0.375	0.335
200	0.495	0.465	0.435	0.385
190	0.57	0.543	0.502	0.443
180	0.645	0.615	0.570	0.500
170	0.720	0.694	0.629	0.558
160	0.799	0.762	0.683	0.617
150	0.870	0.829	0.743	0.672
140	0.949	0.895	0.804	0.728
130	1.020	0.955	0.864	0.781
120	1.091	1.013	0.927	0.836
110	1.155	1.067	0.991	0.883
100	1.222	1.129	1.054	0.932
90	1.285	1.199	1.130	0.975
80	1.328	1.213	1.162	1.015
78	1.328	1.217	1.161	
77		1.257		

Discussion of the Results

Results of the measurements were quite typical of alloy materials. Aside from generally unavailable engineering data, the most practical benefit of work thus far is the determination of the effects of various heat treatments and alloying on the expansion behavior. In all cases some effect was observed (Tables 10-15), although the magnitude of the effect is not considered serious for design purposes.

FUTURE WORK

Specific Heat

During the second half of the program year we plan to complete the calorimetric investigation of the eleven Westinghouse materials by performing the following tasks:

- Measure low-temperature specific heat of four remaining specimens
- Analyse the eleven sets of low-temperature data by computer-fitting them to the equation
$$C = A + \gamma T + \beta T^3$$
- Prepare summarizing tablies of specific heats listed at the temperatures 4, 5, 10, 15, and 20 K
- Compute low temperature θ_D's
- Measure the specific heats of the eleven Westinghouse specimens at 77 K and room temperature
- Fit the "high-temperature" data (i.e., $\gtrsim$ 20 K) to a universal Debye relationship of the form $C_p\ (T/\theta_D)$ and prepare suitable tabulations.

Thermal Expansion

The following work will be performed in the second six months of the funded program:

- Thermal expansion behavior of the eleven Westinghouse materials will be completed in the temperature range 4.2 - 77 K.
- A minimum of 5 - 7 new materials will be evaluated. These new materials will include structural alloys, structural composites, and various Cu-Sn bronzes. The materials will be either prepared in our facility or obtained from other participants in the program.

COMPOSITE STRUCTURAL MATERIALS INVESTIGATION AT CRYOGENIC TEMPERATURES

Semi-Annual Technical Report
9/1/73 through 2/28/74

W. B. Hillig
Program Manager

J. R. McLoughlin
Principal Investigator

Sponsored by
Advanced Research Projects Agency
ARPA Order No. 2569
Program Code 4D10

This research was supported by the Advanced Research Projects Agency of the Department of Defense and was monitored by the Cryogenics Division, National Bureau of Standards, Boulder, Colorado 80302, under Contract No. CST-8300, 9/1/73 through 8/31/74, $60,000.

General Electric Company
Corporate Research and Development
P. O. Box 8
Schenectady, New York 12301
Phone: (518)346-8771

SUMMARY

Flexural tests and interlaminar shear tests were carried out at 4°K on four fiber reinforced plastics: S-glass/epoxy 828-1031, S-glass/epoxy 828-Empol resin, PRD-49/828-1031, and Modmor II fibers/828-1031. The two S-glass epoxy composites are by far the stronger of this group with flexural strengths on some samples over 600,000 PSI.

Correlation studies run on the collection of data showed that high strength correlated with high density samples. This is not unexpected since high density samples tend to have higher fiber volume % and lower void %.

COMPOSITE STRUCTURAL MATERIALS INVESTIGATION AT CRYOGENIC TEMPERATURES

CRYOGENIC SCREENING OF REINFORCED PLASTICS

The purpose of this phase of the contract is to carry out mechanical evaluation of a number of reinforced plastics at liquid helium temperature to determine what material(s) would be most suitable for more exhaustive testing. For the purposes of this screening phase of the program, it has been agreed that flexural tests and interlaminar shear tests at 4°K will be carried out. All the samples reported on here were made by us by a vacuum molding technique described below under Sample Preparation. Tests were conducted in a double dewar with the inner dewar containing liquid helium and the outer dewar liquid nitrogen. The tester used is described under the section, Test Method.

SAMPLE PREPARATION

Samples were prepared by vacuum molding using two different resins and four fibers. The composition of the first resin was:

828-1031 Resin

Component	Parts by Weight
Epon 828 resin	100
Epon 1031 resin	127
Methyl nadic anhydride	300
Benzyl dimethyl amine	3

The second resin used was a softer formulation made up as follows:

828-Empol 1040 Resin

Component	Parts by Weight
Epon 828 resin	100
Empol 1040 resin	20
Dodecenyl succinic anhydride	117
Benzyl dimethyl amine	1

Dilute solutions in methyl ethyl ketone of these resins were used in impregnating 6" long segments of S-glass 904. The bare glass was ca efully weighed before impregnating with a measured amount of resin solution from a micropipette using enough to make the resin solids about one-half the weight of glass. This provided an excess of resin which was squeezed out during molding. The amount squeezed out depended on what ratio of resin to fiber volume fraction was desired. After impregnation with resin solution, the wet roving was hung in an air oven at 60°C for one minute to evaporate some of the solvent and make it easier to handle. The 6" pieces were then cut into 1.5" long segments which were loaded into a mold 1.5" long by 0.05" wide. This (cold) mold was next transferred to a heated metal cylinder and positioned so that a gasketed piston to which the upper force of the mold is fastened was in position above the mold cavity. The cylinder was then evacuated boiling off the remaining solvent and at the same time removing the air present. This hot evacuation was carried out for 10 minutes for most of the 828-1031 resin samples and for 15 minutes for most of the 828-Empol 1040 samples. (However, some samples from each group were not boiled out in this way to encourage voidness for comparison purposes.) At the end of the boil out and without releasing the vacuum, the piston was lowered dropping

the force into the mold. A dial micrometer recorded the exact position of the force within the mold, and this position was varied to squeeze the desired amount of resin out of the mold thus controlling the ratio of fiber volume and resin volume. Two Teflon polymer gaskets were used, above and below the impregnated roving in the mold, to effectively seal the glass within the mold cavity and prevent it from squeezing out laterally. However, the upper gasket was cut about .02" shorter than the cavity so that excess resin would squeeze out at the ends.

After 10 minutes for the 828-1031 (or 15 minutes for 828-Empol resin) at 125°C with the mold open and under vacuum, the piston was dropped to the desired setting still maintaining the vacuum. Temperature was raised to 150°C and cure was carried out for one hour. The sample was then removed from the mold and postbaked in an air oven for 16 hours at 175°C. After postbaking the bar was deflashed, measured dimensionally, weighed, and its density measured by weighing it in a tiny pycnometer filled with water.

Knowing the weight of the fiber originally going into the mold, one can calculate the resin weight. These weights together with known density of the resin, the fiber and the measured density of the finished bar allows calculation of the void volume which is so important in its affect on properties.

$$\text{Thus: } \frac{\text{Sample Weight}}{\text{Sample Density}} - \frac{\text{Fiber Wt.}}{\text{Fiber Density}} - \frac{\text{Resin Wt.}}{\text{Resin Density}}$$

$$= \text{Void Volume}$$

Using this technique of closing the mold in vacuum after degassing in vacuum, we have been able to make consistently low void samples. In order to obtain the high void samples

reported in the table following, it was necessary to drop the vacuum from the molding step and in some cases to advance the cure of the resin somewhat before closing the mold.

With boron fiber as the reinforcement, it was difficult to get low fiber volume fraction samples due to the large size of the fibers and consequent orderly packing; this resulted in a tendency for most of the resin to be squeezed out unless care was exercised during mold closure.

TEST METHODS

Two types of tests are reported on in this report: flexural testing and interlaminar shear testing. Both were run in a 3-point flexural jig but at different spans. The flexural tests were started at a span-to-thickness ratio of 24, but the S-glass epoxy samples were so strong and flexible that it was necessary to lower the ratio to 16. Accordingly, all the bars were run at this ratio. This made the span 0.83" as the thickness averaged 0.052". Widths varied between .08 and 0.10". The radius of curvature of the end supports was 1/16" while the center loading nose had a radius of curvature of 3/8". In the interlaminar shear tests, the distance between end supports (span) was only six times thickness or 0.3". The short span causes much greater shearing stresses to be exerted at the midplane of the sample compared with the outer fiber tensile and compressive stresses so that the sample failed by delamination rather than in tension or compression.

In both types of test, the rate of deflection of the bar used was 0.02"/min. This was provided by a gear motor which drove a threaded fitting attached to a thin-walled stainless steel tube of 5/8" outside diameter and .02" wall thickness. At the lower end of this tube, down in the liquid helium, was attached the fitting containing the two outside support points of the flexural jig. The thin-walled tube was pushed down by the gear motor forcing

the end loading points down thus bending the sample around the center loading nose which was in the form of a stirrup pulling down against the load cell by means of a 3-foot long stainless rod 1/4" in diameter.

For the purpose of measuring sample stiffness in flexural tests, the measuring equipment was calibrated by deflecting with the deflection in the measurement jig blocked completely. The observed deflection, attributable to deflection of the equipment itself, was plotted for various loads and the correction was applied to observed sample deflections.

DISCUSSION OF RESULTS

The strength of the S-glass reinforced samples was gratifyingly high. Correlations were run between the four dependent variables (flexural strength, modulus of elasticity, % elongation and interlaminar shear) and the three independent variables (fiber volume %, void volume %, and density) for each of the three principal composites tested; these were S-glass/828-1031, S-glass/828-Empol, and PRD-49/828-1031. Not enough samples of Modmor II carbon fiber epoxy have been tested yet to warrant analysis.

In the case of S-glass/828-1031 samples, there was a 55% correlation between flexural strength and density for the 15 samples tested. This means that 55% of the variance in the flexural strengths was explained by density variation. The equation of the best straight line was:

$$F = -687.23 + 663.05 \cdot D$$

where F = flexural strength in thousands of PSI, and D = density in g/ml. Thus an increase in density of 0.1 g/ml corresponds to a flexural strength increase of 66,300 PSI.

For the same material, the modulus of elasticity showed a 40% correlation with fiber volume %. The best line equation was:

$$E = -1.569 + .158 \cdot FV$$

where E is modulus in millions of PSI, and FV is fiber volume %.

For the % elongation, the correlation was 56% with void content. The equation was:

$$L = 7.55 - .155 \cdot V$$

where L = % elongation at break, and V = void content in %.

For interlaminar shear the correlation was 48% with fiber volume % and 78% for a combination of fiber volume % and void content. Thus,

$$S = 119.4 - 1.755\ FV - .745 \cdot V$$

where S = shear strength in thousands of PSI, FV is fiber volume %, and V is void content %.

For the S-glass/Empol resin 828 samples, the correlation between flexural strength and density was 65% and when void content was also included the correlation was 78%. Thus,

$$F = -788.9 + 705.5\ D - 19.9\ V$$

where again F is flexural strength in thousands of PSI, D is density in g/ml, and V is void content %.

The correlation between flexural modulus and density was 93%. Thus,

$$E = -21.0 + 15.5\ D$$

The correlation between flexural elongation and voids was only 36%. The equation was:

$$L = 6.80 - .25\ V$$

The correlation between interlaminar shear and density was 81%.

$$S = -43.15 + 34.4\ D$$

For PRD-49/828-1031 the best correlation between flexural strength and an independent parameter was only 16%, but only six samples were tested. The parameter was void content %, and the

equation is:

$$F = 169.9 - 5.73\ V$$

The correlation is so poor that it is almost meaningless.

For the same material, the best correlation of flexural modulus was only 26%; this was with fiber volume:

$$E = -6.29 + .28\ FV$$

For the same material, the best correlation of % elongation was with fiber volume and it was only 14%:

$$L = 11.77 - .137\ FV$$

For the same material, the best correlation of interlaminar shear was with fiber volume and voids combined, and it was a 56% correlation:

$$S = -666.6 + 8.85\ FV + 3.4\ V$$

It is apparent that both the composites reinforced with S-glass are very strong indeed at liquid helium temperature and endure surprisingly high elongations before failure. In fact if one calculates the strength of the S-glass assuming the validity of the somewhat over-simplified rule of mixtures, the strength of the fiber itself is $1.0 \pm 0.2 \times 10^6$ PSI. This is a most impressive number for a standard engineering material. Furthermore, the interlaminar shear for the S-glass with both resins is very high. This suggests that this combination of material should be given serious consideration for engineering applications at cryogenic temperatures. It may also be noted that failures of the S-glass/epoxy composites are <u>not</u> catastrophic and sudden. The stress falls off a little and, if deflection is continued, the load climbs again, and this goes on several times as more and more fibers break.

PRD-49 is also much stronger at 4° in flexure than at room temperature though not as good as S-glass. Modmor II fibers appear to be fairly strong at 4°K, but there is some decrease in its strength

as compared with room temperature especially in interlaminar shear strength. We obtained values of over 300,000 PSI for similar Modmor II fibers/828-1031 bars at room temperature and shear values averaging over 12,000 PSI.

FURTHER WORK PLANS

Further work will include more data on Modmor II fibers/828-1031, inclusion of S-glass composites made with several other epoxy resins, and the testing of larger samples of the most promising S-glass epoxy. Included in the larger sample testing will be tests on notched samples for the purpose of measuring fracture energy.

ACKNOWLEDGMENT

The authors would like to thank R. W. Bulson for his careful work in sample preparation.

RESULTS OF CRYOGENIC SCREENING TESTS AT 4°K ON REINFORCED PLASTICS

TEST NO.	SAMPLE CHARACTERISTICS FIBER	RESIN	FIBER VOL.,%	VOIDS %	DENSITY G/ML	TEST RESULTS FLEXURAL STRENGTH*	FLEXURAL MODULUS+	ELONG. %	INTERLAM. SHEAR #
10	S-GLASS	828-1031	65.3	.37	2.035	689	9.11	8.1	---
11			54.9	5.27	1.865	832	7.5	8.36	---
21			52.8	1.88	1.88	529	7.39	6.8	---
22			61.3	.2	2.007	815	8.94	7.04	---
23			59.9	.48	1.987	583	6.59	6.52	---
71			52.6	.98	1.89	604	7.1	7.68	---
74			55.8	1.93	1.92	886	8.17	6.65	---
85			52.9	.41	1.9	576	7.27	7.21	25.1
86			52.1	14.9	1.71	347	8.71	5.36	12.7
67			54.7	1.23	1.91	525	7.54	6.98	25.1
88			55.8	1.9	1.92	553	7.52	7.66	24.3
89			53.9	1.79	1.9	581	5.77	8.11	22.7
70			53.3	1.75	1.89	543	8.23	7.44	23.3
72			58	12.7	1.81	507	8.81	4.34	15.5
73			53.4	14.9	1.73	535	8.38	5.81	12
		EMPOL RESIN							
36	S-GLASS	828	63.5	.23	1.977	---	---	---	27
37			63.5	.23	1.977	---	---	---	25.9
38			66.8	1.75	2.003	---	---	---	24.8
39			66.6	1.75	2.003	---	---	---	24.8
36			55	.59	1.85	551	8	7.02	21.4
57			57.1	6.89	1.81	345	7.05	4.91	18.5
58			52.7	1.45	1.81	421	6.56	6.15	20.3
59			55.7	4.72	1.82	480	7.25	6.69	19.6
60			54	1.96	1.82	382	7.05	5.02	19.3
82			57	.35	1.88	512	7.39	7.75	19
83			54.8	2.2	1.83	421	8.97	6.57	18.7
64			56.3	3.59	1.84	437	7.37	5.9	21.8
40			65.2	2.38	1.977	508	9.88	5.11	---
41			65.3	2.57	1.976	519	9.78	5.97	---
		EMPOL RESIN							
42	S-GLASS	828	61.2	3.47	1.909	531	9.06	6.14	---
43			55.7	4.79	1.818	413	7.47	5.96	---
44			65.7	1.02	1.998	546	9.48	5.69	---
45			62.3	.52	1.956	601	9.45	6.61	---
46			62.3	0	2.05	873	10.56	6.65	---
47			83.8	-.44	1.989	899	9.86	7.79	---
61			54.3	.38	1.85	535	7.87	6.64	---
	MODMOR 11								
12	FIBERS	828-1031	70.3	1.38	1.633	198	28.6	1.21	---
13			67.6	1.95	1.611	172	28.1	1.15	---
14			68.8	1.55	1.623	204	23.3	1.39	---
15			67.6	1.95	1.611	---	---	---	4.08
16			67.6	1.95	1.611	---	---	---	4.46
17			70.3	1.38	1.633	---	---	---	15.1
24	PRD-49	828-1031	73.0	1.66	1.375	185	13.8	2.15	---
25			75.6	.87	1.39	155	15.1	1.34	---
28			74.7	.65	1.391	165	14.0	1.77	---
27			73.2	2.48	1.365	148	14.7	1.04	---
28			73.5	3.19	1.357	152	15.1	2.01	---
29			75.5	2.18	1.374	151	15.4	1.4	---
30			75.0	1.83	1.377	---	---	---	2.9
31			75.0	1.83	1.377	---	---	---	3.3
32			75.4	2.17	1.374	---	---	---	8.1
33			75.4	2.17	1.374	---	---	---	7.5
34			75.8	.89	1.391	---	---	---	10.1
35			75.8	.89	1.391	---	---	---	3.8

*Flexural strength in thousands of PSI.

+Flexural modulus in millions of PSI.

#Interlaminar shear in thousands of PSI.

MCR-74-89
Issue 1

STUDY OF FRACTURE BEHAVIOR OF METALS FOR SUPERCONDUCTING APPLICATIONS

Fred R. Schwartzberg
Program Manager
303-794-5211, ext. 3438

SEMI-ANNUAL TECHNICAL REPORT

March 1974

Sponsored by Advanced Research Projects Agency
ARPA Order No. 2569, Program Code 4D10
Contract Monitor: Cryogenics Division,
National Bureau of Standards, Boulder, Colo. 80302
NBS Contract No. CST 8301
Period of Performance: 9/1/73 to 8/31/74
Contract Value: $50,000

MARTIN MARIETTA CORPORATION
P. O. Box 179
Denver, Colorado 80201

FOREWORD

This report describes technical activities conducted during the period 1 September 1973 through 1 March 1974 under NBS Contract CST-8301.

The views and conclusions contained in this document are those of the authors and should not be interpreted as necessarily representing the official policies, either expressed or implied, of the Advanced Research Projects Agency or the U.S. Government.

I. Introduction

The purpose of this program is to establish preliminary characterization of the fracture mechanics properties of three alloy candidates being considered for use in superconducting equipment. The three alloys to be evaluated are:

- 304L Stainless Steel,
- A-286 Stainless Steel,
- X-750 Nickel Alloy.

All alloys will be evaluated using parent metal stock to provide static fracture toughness and cyclic flaw growth behavior at 77, 20, and 4°K.

Fracture testing will be performed using compact tension specimens, as described in ASTM Specification E399 for both static and cyclic conditions. The thicknesses have been selected in an attempt to achieve valid plane strain conditions. However, it is recognized that the materials are sufficiently tough so that the attainment of validity conditions in practical thicknesses is difficult. In order to compensate for the probable inability to test valid thicknesses at 4°K, a study of the effect of thickness on apparent toughness at 77 and 20°K will be performed. Side grooving was considered as a variable in the thickness study in order to simulate thicker stock. However, based on discussion with Westinghouse personnel, it appears that the promise for this effect is limited and probably will be deleted from the program.

In order to achieve the goals of the research, the following two studies will be performed

- Effect of temperature on toughness and cyclic crack growth rate from 77 to 4°K;
- Effect of thickness on toughness at 77 and 20°K.

II. Materials

Stock of each alloy in both 1-inch and 2-inch thicknesses has been obtained. The 304L was obtained in the form of plate material. No certifications or analyses were available for this material. The 1-inch thick A-286 was obtained as 1 in. x 3 in. flat rolled stock. Two-inch A-286 and both gages of X-750 nickel alloy were purchased as forgings (1 in. x 3 in. and 2 in. x 5 in.).

Certified test report data for the A-286 and X-750 materials are given in Table 1.

Table 1. Certified Test Report Data

Material	Thickness (in.)	Heat No.	Condition	Chemical Analysis	Mechanical Properties			
					Tensile Strength (ksi)	Yield Strength (ksi)	Elong. (%)	R.A. (%)
A-286	1	L2397-K11	STA	24.97 Ni, 14.30 Cr, 2.25 Ti, 1.12 Mo, 1.31 Mn, .54 Si, .25 V, .05C	147 (L) 144 (T)	103 (L) 112 (T)	24	45
A-286	2	6870-6	STA	26.66 Ni, 15.30 Cr, 2.16 Ti, 1.36 Mo, 0.74 Mn, .45 Si, .31V, .05C	156	118	24	49
X-750	1 and 2	31C6X8	ST	73.84 Ni, 15.27 Cr, 6.22 Fe, 2.69 Ti, .89 Cb + Ta, 0.05C	184	140	23	37

III. Specimen Preparation

Compact tension specimens of the 1T and 2T design are being used for this work. Machining of all 304L and A-286 stainless steel specimens has been completed. Nickel alloy (X-750) specimens are currently being machined.

Precracking of 304L stainless steel specimens has been completed. The stress selected for this work was 25,000 psi; cracking occurred in approximately 150,000 cycles for the 1-inch specimens and 50,000 cycles for the 2-inch specimens. The 1-inch specimens of A-286 stainless steel were precracked at a stress of 50,000 psi; approximately 30,000 cycles were used to grow the fatigue crack. All precracking was performed at room temperature.

IV. Testing

The liquid helium cryostat required for this program has been designed, fabricated, and is ready for use in the test program. The systems consists of an internal load frame fabricated from filament wound glass-epoxy rods, a titanium base plate, and a liquid nitrogen jacketed dewar (Figure 1). The system is designed to sustain a force of 50,000 pounds. Testing at liquid nitrogen and liquid hydrogen temperatures will be performed in equipment proven through many years of prior testing programs.

All static and cyclic testing will be compliance gage monitored. For this work, a recently developed MTS cryogenic compliance gage will be utilized. Martin Marietta will be service testing this gage for MTS. Delay in receipt of this gage has prevented initiation of the testing effort. The gage is currently in shipment. Testing will be initiated approximately 15 March.

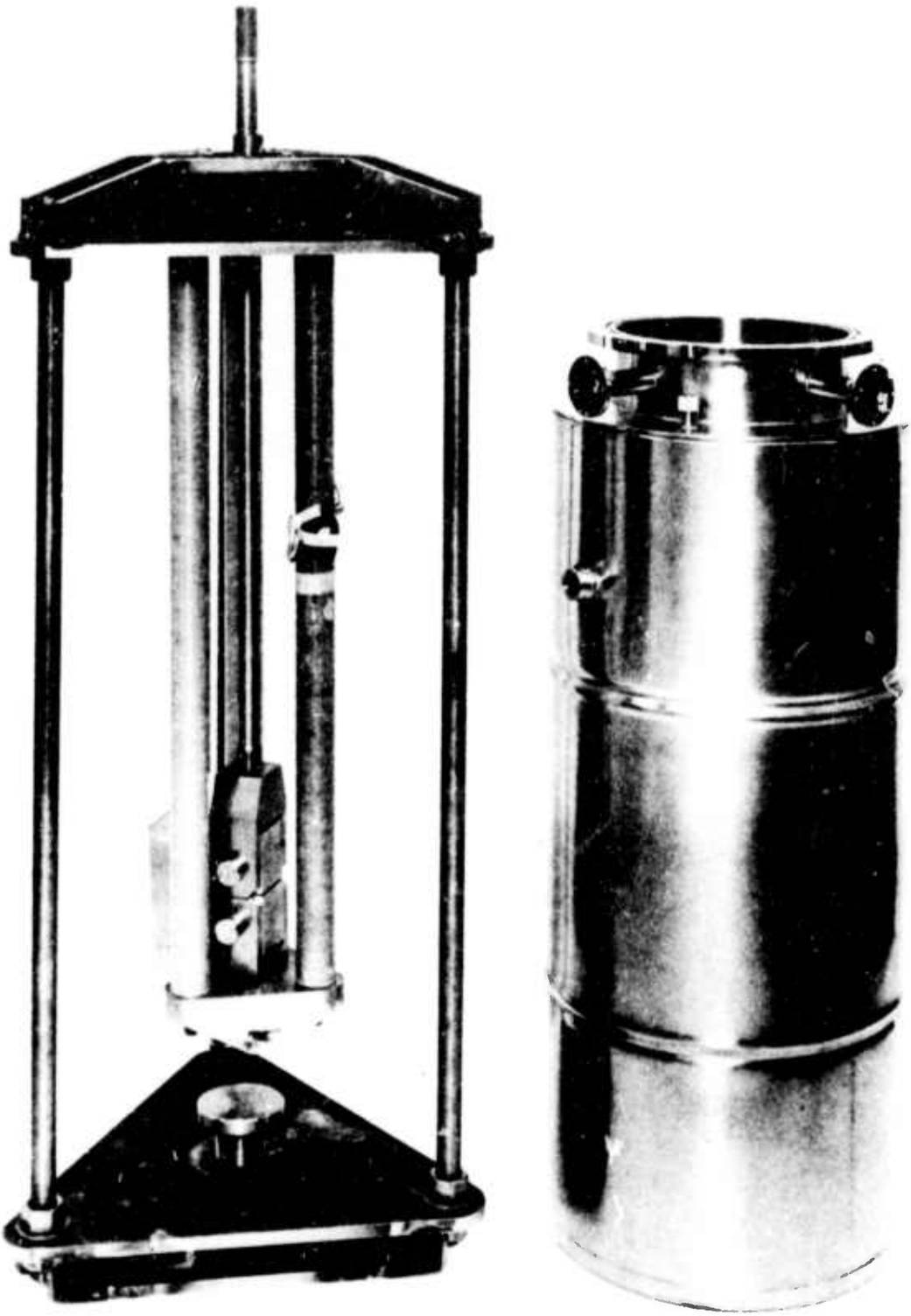

Figure 1 Liquid Helium Cryostat

V. Future Plans

During the second half of the year, emphasis will be given to initiation and completion of all testing. No schedule or cost problems are apparent with respect to completion of the required effort.

111<

NBSIR 74-359

SEMI-ANNUAL REPORT ON MATERIALS RESEARCH IN SUPPORT OF SUPERCONDUCTING MACHINERY

L.L. Sparks, F.R. Fickett, J.G. Hust, P.J. Giarratano, H.M. Ledbetter, E.R. Naimon, W.F. Weston, M.B. Kasen, R.L. Tobler, R.P. Mikesell, R.L. Durcholz, C.W. Fowlkes and R.P. Reed

Cryogenics Division
Institute for Basic Standards
National Bureau of Standards
Boulder, Colorado 80302

March 1974

Prepared for:
Advanced Research Projects Agency
1400 Wilson Boulevard
Arlington, Virginia 22209

U.S. DEPARTMENT OF COMMERCE, Frederick B. Dent, Secretary

NATIONAL BUREAU OF STANDARDS, Richard W. Roberts, Director

SEMI-ANNUAL REPORT ON MATERIALS RESEARCH IN SUPPORT OF SUPERCONDUCTING MACHINERY

Sponsored by
Advanced Research Projects Agency
ARPA Order No. 2529
Program Code 4D10
August 10, 1973 - August 9, 1974

Program Director
Dr. E. C. van Reuth
Materials Sciences
Advanced Research Projects Agency
1400 Wilson Boulevard
Arlington, Virginia 22209

Program Manager
Dr. R. P. Reed
Cryogenics Division
Institute for Basic Standards
National Bureau of Standards
Boulder, Colorado 80302

TABLE OF CONTENTS

ABSTRACT

Results of six months research are reported to the sponsor, the Advanced Research Projects Agency of the Department of Defense. Subjects include magneto-thermal conductivity, composites, elastic properties, fracture toughness, fatigue, and tensile. All measurements include the temperature range 4 to 300 K. Materials examined are those either presently being used in superconducting machinery or considered for use in future prototypes. Material classes include stainless steels, inconels, titanium alloys, and composites.

Special results include: the thermal conductivity in a magnetic field is considerably lower than would be predicted; a comprehensive review of glass-reinforced composite behavior at low temperatures is included; the elastic moduli of 12 engineering alloys from 4 to 300 K are reported; and fracture toughness and fatigue crack growth rate data on AISI 304, AISI 316, A286, Ti-5Al-4V and Ti-6Al-2.5Sn at 4, 76 and 300 K have been measured.

At the beginning of each individual report a Summary is provided to highlight the project results.

DISCLAIMER

Tradenames of equipment and materials are used in this report for clarity and in order to conform with standard usage in the literature. The selection of materials for discussion and examination with regard to application in superconducting machinery is based on properties reported in the literature, and must be regarded as preliminary and tentative. In no case does such selection as the results reported imply recommendation or endorsement by the National Bureau of Standards, nor does it imply that the material or equipment is necessarily the best available for the purpose.

SEMI-ANNUAL REPORT ON MATERIALS RESEARCH IN SUPPORT OF SUPERCONDUCTING MACHINERY

Magnetothermal Conductivity

by

L. L. Sparks and F. R. Fickett

Cryogenics Division
NBS - Institute for Basic Standards
Boulder, Colorado

SUMMARY

The purpose of this study is to determine the thermal conductivity of technically important materials in high magnetic fields at cryogenic temperatures. This information is becoming increasingly important as the use of machinery operating at cryogenic temperatures develops. There has been essentially no previous experimental work on the magnetothermal conductivity of materials which will be used in cryogenic machinery. Appendix A of this report is a bibliography of work in the area of magnetothermal conductivity; this literature deals mostly with high purity materials which are of little use in machine design. It does indicate, however, that the effect of the magnetic field on the thermal resistivity can be large. Our program will determine the extent of this effect on technical alloys and other commercial materials which will be used in actual structures.

The experimental approach utilizes the axial heat flow method of determining thermal conductivity. This method basically introduces a measured, steady heat flow at one end of a cylindrical specimen; the temperature gradient caused by this energy is measured. The temperature gradient, the heat applied, and the specimen dimensions are used to compute the thermal conductivity. Measurements will be made in magnetic fields to 100 kOe. This magnet produces a one inch diameter sphere of homogeneous (1%) field. One of the difficulties of the experiment is the miniaturization needed to keep all critical components within the homogeneous field. A complete description of the experimental system is given in the Procedures section of this report.

118<

Preliminary magnetothermal conductivity results in this report are on Inconel 718. These data are primarily for system evaluation and are very limited in the temperature range examined (~ 4.8 K to 5.8 K). If, however, the results prove to be valid, the magnetic field effect is much larger than expected. The implication is that effects other than those expected from simple theory are being encountered. Additional materials being considered for testing (see Procedures, specimen section) include two coppers and one additional, as yet undetermined material. If the unexpectedly high effect on Inconel 718 is substantiated by further testing, an additional Inconel, stainless steel, or some other near magnetic material will be the fourth specimen.

TABLE OF CONTENTS

LIST OF FIGURES

LIST OF TABLES

120<

INTRODUCTION

Optimum design of machinery operating at cryogenic temperatures requires a detailed knowledge of the thermal and electrical characteristics of the materials at low temperatures. Most applications also involve magnetic fields of 0-10 Tesla, and it is well known that fields of this intensity alter the physical properties of conducting materials, sometimes causing changes of several orders of magnitude in a given property.

The purpose of this study is to determine the behavior of the thermal conductivity of technically important materials in high magnetic fields at cryogenic temperatures. The materials are those actually used for the structural and electrical components of machinery. This class includes, but is not restricted to, alloys such as stainless steels and Inconels, metals used as stabilizing materials (Cu, Al and Ni) and, possibly, composite superconductors. The data generated from this program is needed for optimum machine design, and also it will help us to gain a better understanding of heat transfer in metals and alloys under the influence of high magnetic fields.

The effect of magnetic fields on the thermal resistivity of metals is not known. The world's literature on magnetothermal conductivity is essentially given in Appendix A of this report. Most of these papers deal with very pure metals and single crystals and are of little interest to this program. No literature at all exists on modern technical alloys. The literature on pure metals indicates that large increases in thermal resistivity can occur at high fields. Our program will determine how large this effect is in the various technical alloys and less pure metals used in actual structures.

121<

It is possible in many cases to predict the approximate zero field low temperature thermal conductivity of a given material from the electrical resistivity for the specimen in question and knowledge of the Lorenz ratio for that class of alloys. Lorenz ratio data currently exists only for the zero field case, and in general one would expect the ratio to show a different behavior when a magnetic field is applied. Data from this project will allow us to evaluate the possibility of a "magnetic field" Lorenz number for predicting the thermal conductivity of alloys in a magnetic field from a measurement of the electrical resistivity--inherently a much easier measurement to make than the thermal one.

122<

PROCEDURES

Apparatus

The experimental determination of the magnetothermal conductivity, λ (H), of metals is complicated by the requirement that the specimen be contained in a homogeneous magnetic field. For all but the very largest laboratories, this restriction necessitates small specimen lengths and thus relatively small temperature gradients along the specimens. Furthermore, the precision thermometry required for the measurement is considerably complicated by large, nonlinear magnetic field effects on the thermometers.

The probe described here is designed to be used in a superconducting solenoid with a 1.5 inch bore and a 1 inch homogeneous (1%) field sphere. The maximum available magnetic field is 100 kOe (7.96 MA/m).

Probe Design Figure 1 shows the principal components of the probe with the specimen in the longitudinal position (H parallel to heat flow, $\dot{Q}$). The temperature controlled heat sink (TCHS) is designed to allow a (somewhat shorter) specimen to be installed in a horizontal position for transverse (H - $\dot{Q}$) measurements.

At our operating temperatures of 4-20 K, radiative heat transfer is not important and convective losses from the specimen are prevented by evacuating the copper SPECIMEN CHAMBER,which is usually immersed in a liquid helium bath. The sink (TCHS) temperature is selected by adjusting the power input to a wire heater (Evanohm, 36 AWG, 40.1) wound on the TCHS. Energy is transmitted up to the liquid helium (LHe) bath via the THERMAL LINKS which are three stainless steel (310 ss, 3/16" diam.) rods. Provision is also made for connecting a #18 copper wire in parallel with each of the stainless steel rods in order to give additional heat

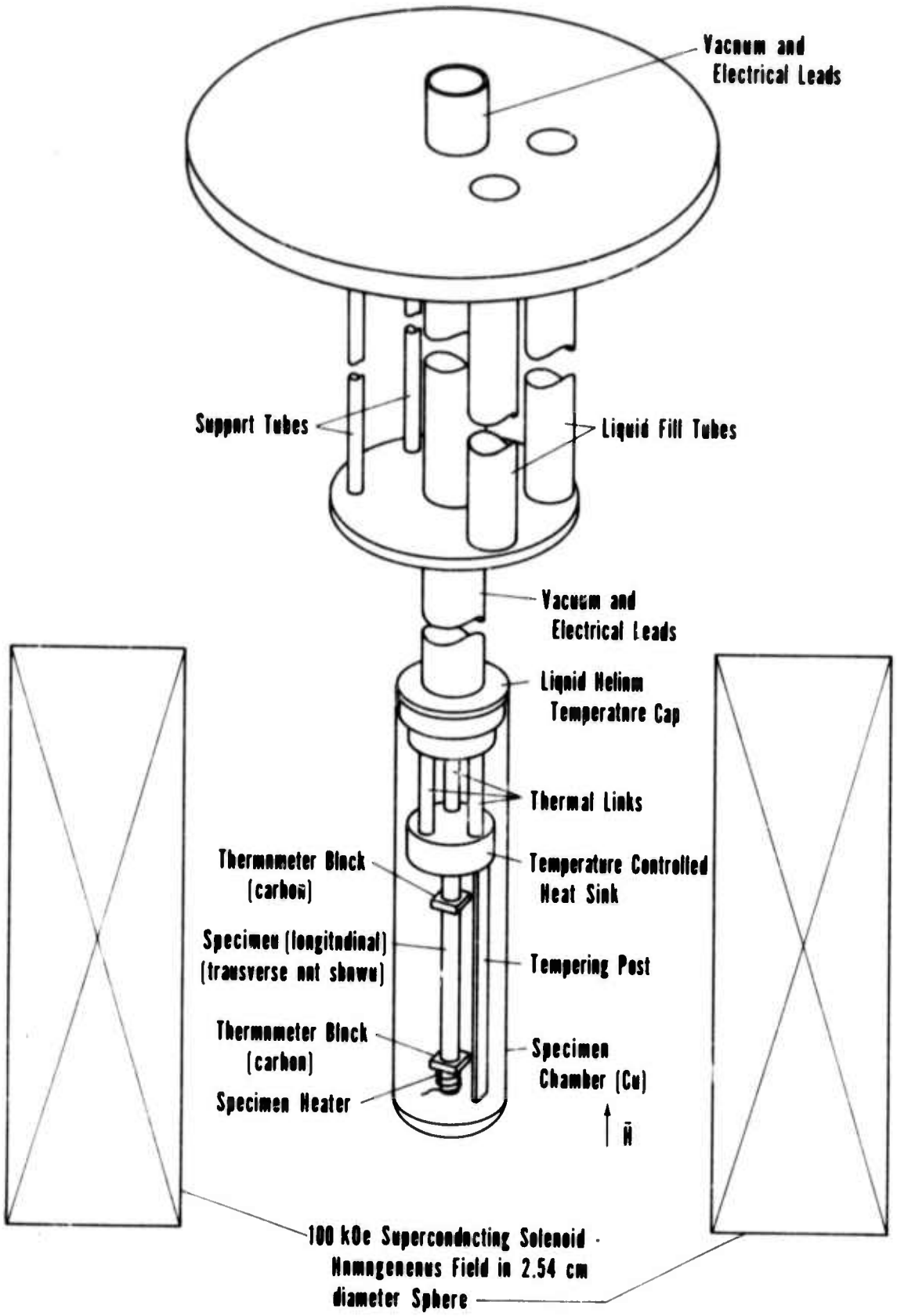

Figure 1. Magnetothermal conductivity probe and magnet.

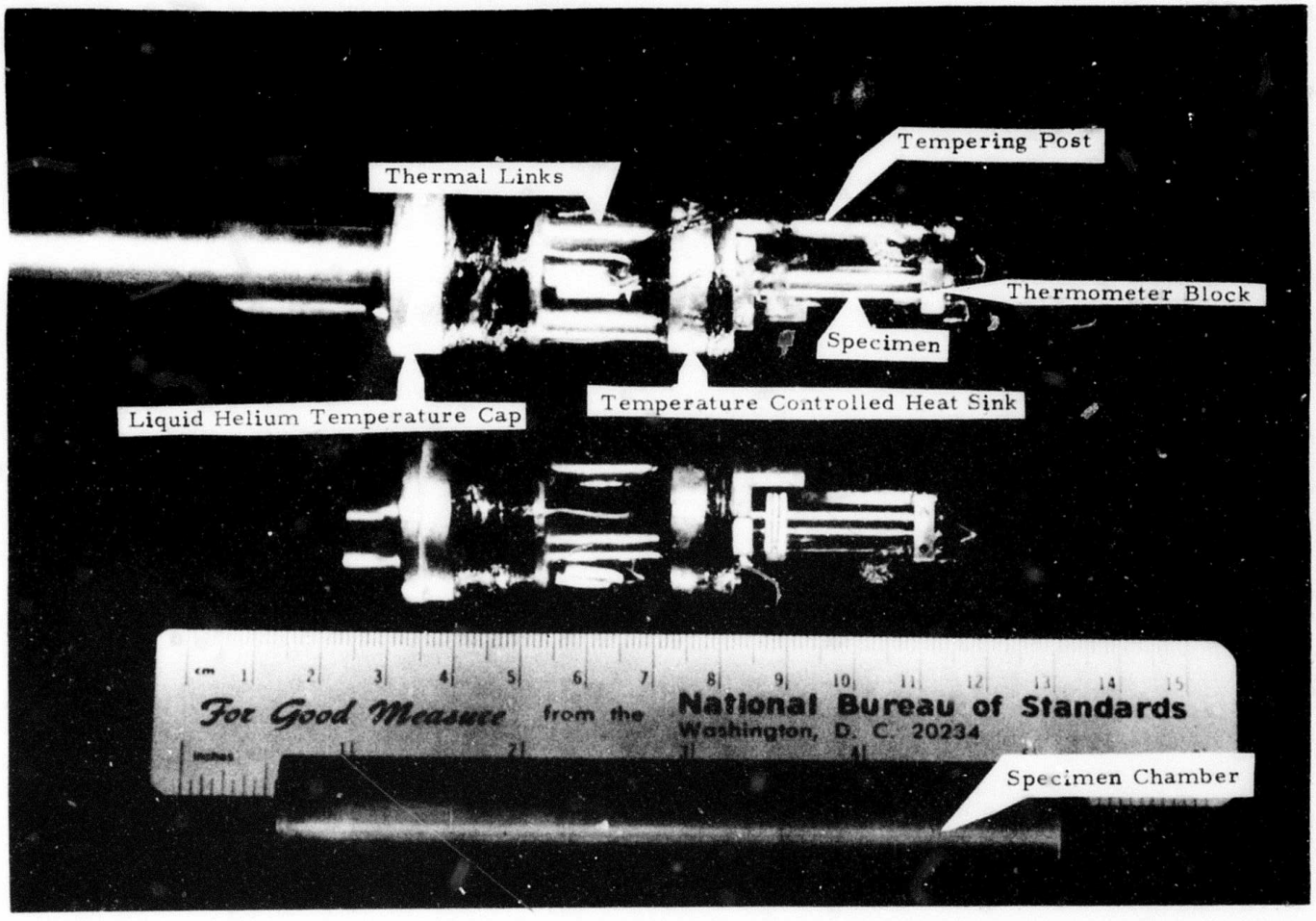

Figure 2. Photograph of completed probe with specimen in place.

transfer to the bath. This added heat leak capacity will be necessary for measurements on high conductivity specimens. Once set, the temperature of the TCHS is controlled automatically. For purposes of temperature measurement and control, the sink is instrumented with a 100Ω, 1/8 W carbon resistance thermometer (CRT) and a germanium resistance thermometer (GRT). The GRT, while very accurate, is useless in a magnetic field, so high field temperature readings are taken on the field-calibrated CRT.

The temperature gradient, Δ T, along the specimen is established by heating the bottom end of the specimen with an electrical heater (Evanohm, 40 AWG wire, 40Ω). The absolute temperature and Δ T are determined by measuring the resistance of CRTs embedded in each of the THERMOMETER BLOCKS mounted on the specimen. The stainless steel (310 ss) TEMPERING POST thermally anchors the wires to the specimen temperature before they actually contact the specimen. This tempering eliminates energy transfer via the wires. The TEMPERING POST is attached to the TCHS at one end and is adjusted to match the specimen temperature by an electrical heater (Evanohm, 40 AWG wire, 40Ω) on the lower end (not shown in Fig. 1). A differential thermocouple (KP vs Au 0.07 at % Fe) is connected between the lower end of the tempering post and the lower thermometer block on the specimen in order to monitor and maintain the necessary zero temperature difference.

A photograph of the completed probe with a specimen mounted in the longitudinal configuration is shown in Fig. 2.

The probe is also instrumented for measurements of electrical resistivity and thermopower - information which is sometimes helpful in interpreting the thermal conductivity data.

Thermometry Carbon resistors (Allen-Bradley, 1/8 watt, 100 Ω) are used to measure both the absolute temperature of the specimen and the temperature difference between the two THERMOMETER BLOCKS. A calibrated GRT is situated in the TCHS for purposes of zero field calibration of the CRTs.

Neuringer and Shapira (1969) found that the relative effect of magnetic fields, $\Delta R/R_o = (R_H - R_o)/R_o$, is very nearly the same for all Allen-Bradley resistors with the same power rating and nominal room temperature resistance. These authors have generously supplied detailed data for $\Delta R/R_o$ as a function of temperature for 100 Ω, 1/8 watt, Allen-Bradley CRTs.

Measurements of CRT resistances are made on an a.c. Wheatstone bridge. Low frequency a.c. power eliminates the need for current reversal when determining the resistance of the CRTs. A lockin amplifier serves as both the detector and the bridge power supply. The bridge system (Fig. 3) is designed to allow direct measurement of the resistance of all of the CRTs as well as the resistance difference measurement between the thermometers in the THERMOMETER BLOCKS.

Equipment The electronics associated with the experiment are shown diagrammatically in Fig. 4. The 100 kOe superconducting magnet system and the electronics associated with it are not shown in the figure. The precision voltage measurement system is indicated by a single box. This system, capable of measurements in the .1-1 nV range, is described in detail by Clark and Fickett (1969).

127<

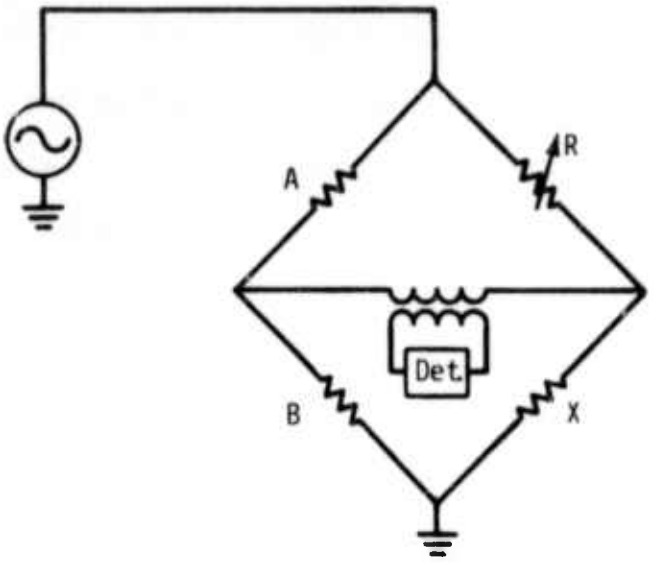

(1) ABSOLUTE TEMPERATURE MEASUREMENT $R \alpha T$

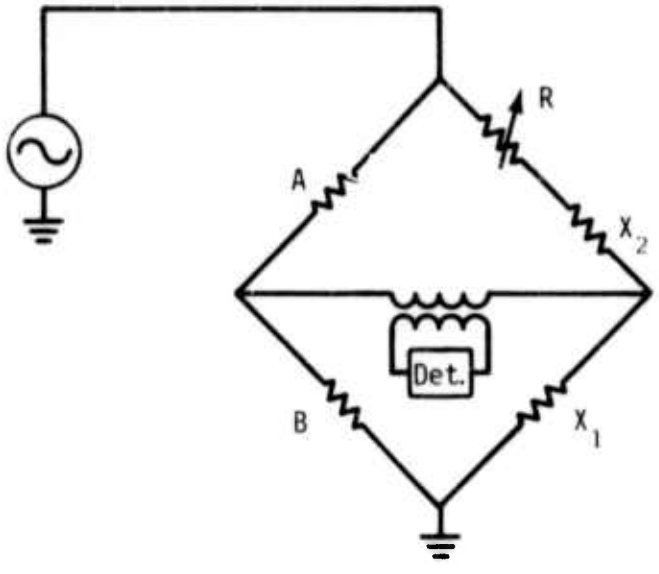

(2) DIFFERENTIAL TEMPERATURE MEASUREMENT $R \alpha \Delta T$

Figure 3. Resistance bridge for measuring carbon resistance thermometers (CRTs). Drive voltage and detection are provided by a lockin amplifier. A and B are 10K Ω, 0.01% resistors. R is a series of precision decade resistors. (1) X is any one of the three CRTs. (2) X_1 and X_2 are the CRTs used to determine the specimen ΔT.

128<

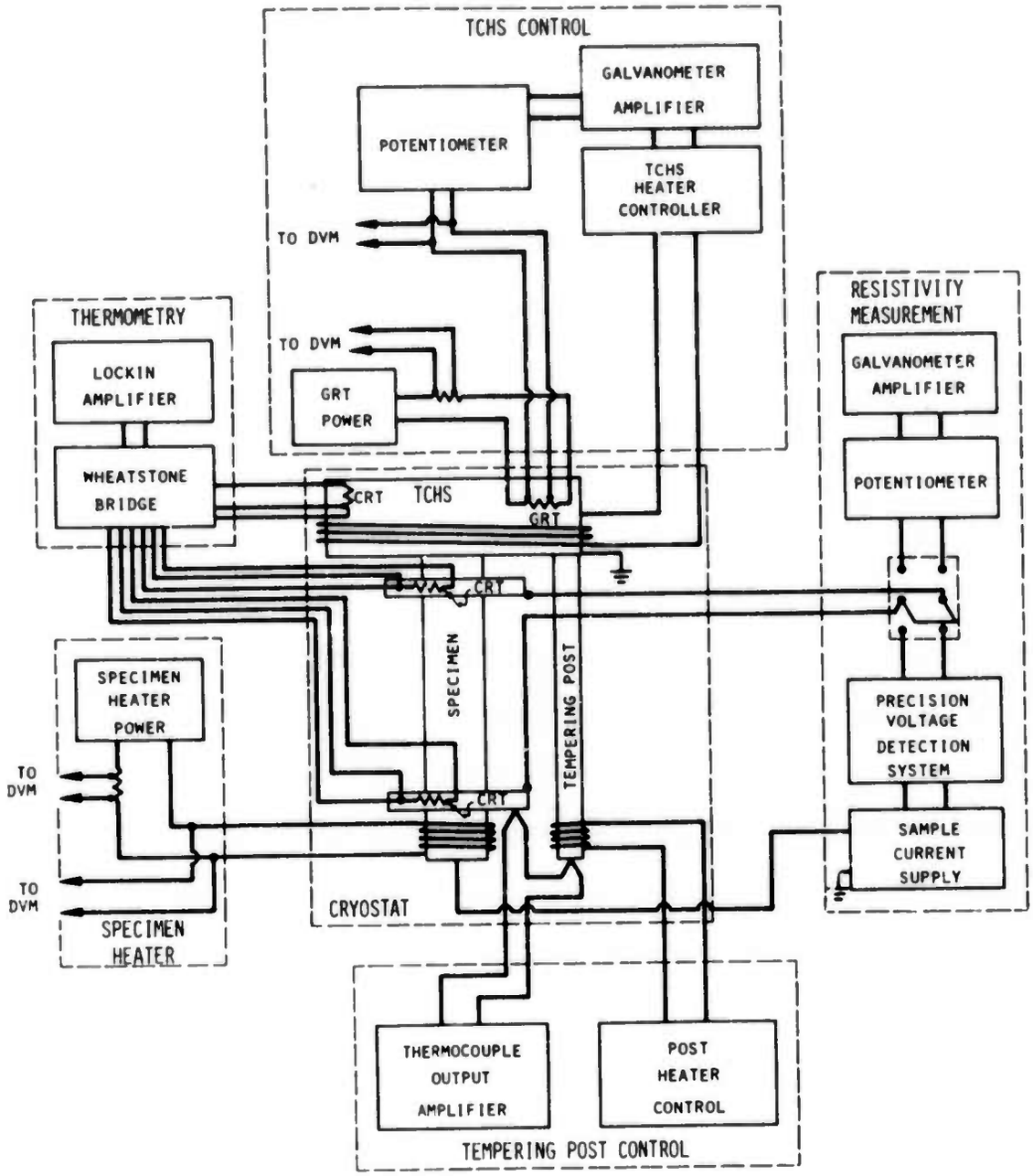

Figure 4. Block diagram of the system electronics.

Experimental Procedures

Two basic procedures are needed in order to acquire the experimental data. The first is calibration of the CRTs and the second is the actual measurement of the magnetothermal conductivity, λ (H), and the electrical resistivity, ρ (H).

As mentioned previously, work on CRTs has shown that $\Delta R/R_o = (R_H - R_o)/R_o$ holds for all similar resistors. Thus, to find T(R,H) all we need is R versus T at zero field. These data are obtained by a series of isothermal measurements -- isothermal in the sense that the TCHS, the specimen, and the THERMOMETER BLOCKS are all at the same temperature. This is done as follows: 1) the evacuated SPECIMEN CHAMBER is immersed in LHe and allowed to reach a stable temperature; 2) the system reaches an equilibrium in less than 5 minutes below 20 K; 3) the equilibrium temperature is determined by the GRT, and the resistances of the three CRTs at this temperature are recorded; 4) a higher equilibrium temperature is achieved by powering the TCHS heater. In this manner the zero field R-T profile is found for each CRT.

A check of the Neuringer and Shapira formula for R(H,T) was made for our CRTs. For this procedure helium gas is introduced into the evacuated SPECIMEN CHAMBER which then serves as a constant volume gas thermometer. The system is cooled by a transfer gas arrangement between the SPECIMEN CHAMBER and the liquid helium surrounding the superconducting magnet. Isothermal data is taken as before at zero field, then at successively higher fields. Constant temperature is maintained by

adjusting the TCHS heater power so as to maintain constant pressure in the SPECIMEN CHAMBER.

The second procedure is the experimental determination of λ (H) and ρ (H). Refrigeration of the SPECIMEN CHAMBER during these tests is either by transfer gas to the magnet LHe or by immersion of the chamber in LHe. In either case the SPECIMEN CHAMBER is evacuated. The thermal conductivity of the specimen at T is calculated from $(H,T) = \frac{Q\Delta\ell}{A\Delta T}$. The parameters are: $\Delta\ell$ ($\equiv$ distance between THERMOMETER BLOCKS), A ($\equiv$ (cross sectional area of specimen), $\dot{Q}$ ($\equiv$ power used to establish the temperature gradient) and ΔT ($\equiv$ temperature difference between the THERMOMETER BLOCKS).

In an actual measurement the temperature of the TCHS is set at some selected temperature. Power to the SPECIMEN HEATER is applied until the desired ΔT is obtained. The heater power is measured by the system shown in Fig. 4. The absolute temperature of the two specimen thermometers is measured, as is the resistance difference between them. A series of these measurements are made as the field is progressively increased. Data are taken over the range from 4-20 K and from 0-100 kOe.

At each gradient and field, the electrical resistivity of the specimen is also measured at $\bar{T} = 1/2\ (T_{HOT} + T_{COLD})$ by a conventional four probe method. A potentiometer is used to measure the voltage drop for high resistivity specimens and the precision detection system for lower resistivity ones.

Specimens

Table 1 lists the initial set of specimens to be tested in the magnetothermal conductivity program. Inconel 718 was the first to be installed and preliminary data taken on this specimen is being used in the system evaluation. The two copper specimens will be tested following

the Inconel. A final decision has not been made as to what material will be used as the fourth specimen. Iron, as listed in table 1, and a different Inconel are being considered.

132<

Table 1

Magnetothermal Conductivity Test Specimens

Material	Specimen Characterization
Inconel 718	Produced by International Nickel Company, HT4675E. Specimen not annealed, hardness B39.
Copper (OFHC)	Swaged to ~ 0.1 inch diameter from 3/16 inch rod stock. Etched (50-50 H_2O-HNO_3) and annealed at 600°C for 1 hour in vacuum several times during swaging process. Final anneal at 850°C for 1 hr. in vacuum.
Copper (STOCK 7)	< 1 ppm of any impurity with possible exception of Fe. Specimen was centerless ground to ~ 0.1 inch diameter. Annealed at 850°C for 1 hr. in vacuum.
Iron (OSRM)	Specimen was centerless ground to ~ 0.1 inch diameter. To be annealed at 400°C for 46 hours in vacuum.

133<

DISCUSSION

In this section we present a very brief explanation of the mathematical basis of our experiment. We also define the terminology commonly used in the literature.

Thermal conductivity, in the absence of a magnetic field, is probably one of the best understood of the transport effects observed in solids. It is however a relatively complex effect because many separate mechanisms are operating simultaneously to transmit energy through the material. The basic quantity of interest is the thermal conductivity, λ, as defined by the heat transfer equation, which, in its simplest one dimensional form, is

$$\dot{Q} = \lambda(T)\, A \frac{dT}{dx},$$

where, conventionally, $\dot{Q}$ is the heat current in watts, A is the cross-sectional area in cm^2, T is in Kelvin and thus λ has the units of watt/cm K. In general the thermal energy in a material is transported both by the lattice vibrations (phonons) and by the conduction electrons. These two modes operate as thermal resistors in parallel, such that the total thermal conductivity is

$$\lambda = \lambda_e + \lambda_g,$$

where the subscript g is the conventional designation for the lattice component. Each of these two contributions are in turn made up of a number of separate components, reflecting the modes by which energy may be lost in transit. These are series additive such that the thermal resistivity, W, of, say, the electronic branch may be written,

$$W_e = \frac{1}{\lambda_e} = W(\text{electron-lattice}) + W(\text{electron-impurity}) + W(\text{electron-defect}).$$

The lattice contribution, λ_g, is small in pure metals but may be significant in alloys, and in nonconductors (where $\lambda_e = 0$) it represents the total contribution. Application of a magnetic field to a thermal conductor results in a change primarily in the electronic component of the conductivity. Theory predicts little effect on the lattice component although no experimental data exist to verify this result. Our experiment will be the first to look at this effect in detail.

As with the electrical (galvanomagnetic) effects three common orientations are possible between the temperature gradient, the magnetic field, and the heat flow:

(1) All three are parallel [H_z, Q_z, dT/dz]. This is the longitudinal magnetothermal resistance.

(2) The temperature gradient and heat flow are parallel and the field is normal to that direction [H_z, Q_x, dT/dx]. This is the transverse magnetothermal resistance also known as the Maggi-Righi-Leduc effect.

(3) All three are at right angles to each other [H_z, Q_x, dT/dy]. This is the thermal Hall effect or the Righi-Leduc effect.

Other effects, such as the behavior of the thermopower under the influence of a magnetic field, can be included in the list, and in fact some have been referenced in the bibliography of Appendix A; but this project is primarily concerned with (1) and (2) above.

As is the case with the electrical magnetoresistance, the thermal resistance is observed to always increase in an applied field. The effect in pure metals can be quite large, the resistivity increasing by more than an order of magnitude at 4 K. One would expect a smaller effect for most alloys, but even a relatively small change can be critical in some applications.

135<

Another parameter of interest is the Lorenz ratio. Because the conduction electrons carry both thermal and electrical energy, it is reasonable to assume that the electronic contribution to the thermal conductivity and the electrical conductivity should be related. The equation expressing this relationship is the Wiedemann-Franz-Lorenz law,

$$\frac{\lambda \rho}{T} = L,$$

where, by simple theory, the Lorenz ratio, L, should be a constant. Sommerfeld calculated the free electron theory value to be $L_o = 2.443 \times 10^{-8}\ V^2/K^2$. Needless to say, L is not altogether constant, but it is the most constant of the trio, λ, ρ, L. In any event, if one knows the L vs T curve for a given alloy group, and the electrical resistivity vs T for a particular alloy, it is quite possible to predict the thermal conductivity at zero field with sufficient accuracy for many applications. We wish to determine whether or not a similar relationship holds in the presence of a magnetic field. Indications are that L is field dependent, at least in pure metals.

RESULTS

Data given below must be considered preliminary and is being used for purposes of system evaluation. The computer programs necessary to compute temperatures for each of the CRTs as a function of resistance and magnetic field are especially needed for accurate analysis of data.

Figure 5 indicates the field sensitivity of one of the three CRTs; note that the field effect is not large even at 4 K. Figure 6 gives the ratio of the thermal conductivity of Inconel 718 in the presence of a magnetic field to the thermal conductivity at the same temperature with zero field. If this preliminary data remains substantially unchanged upon further analysis, the magnetic effect is larger than expected and almost certainly indicates some interaction beyond the electronic effect considered in the simple theory.

136<

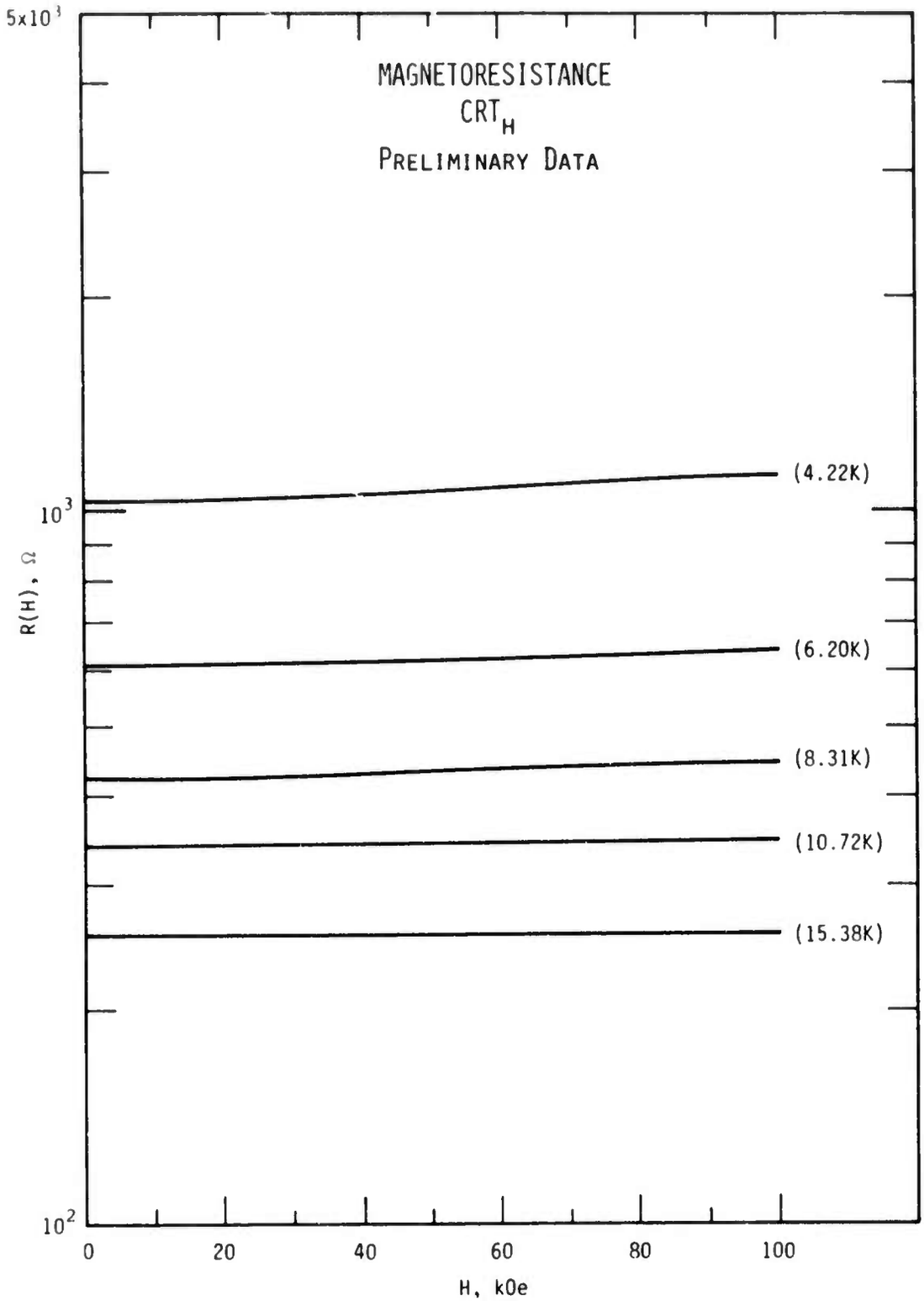

Figure 5. Magnetoresistance of a 100 Ω, 1/8 watt, Allen-Bradley carbon resistor at selected cryogenic temperatures.

137<

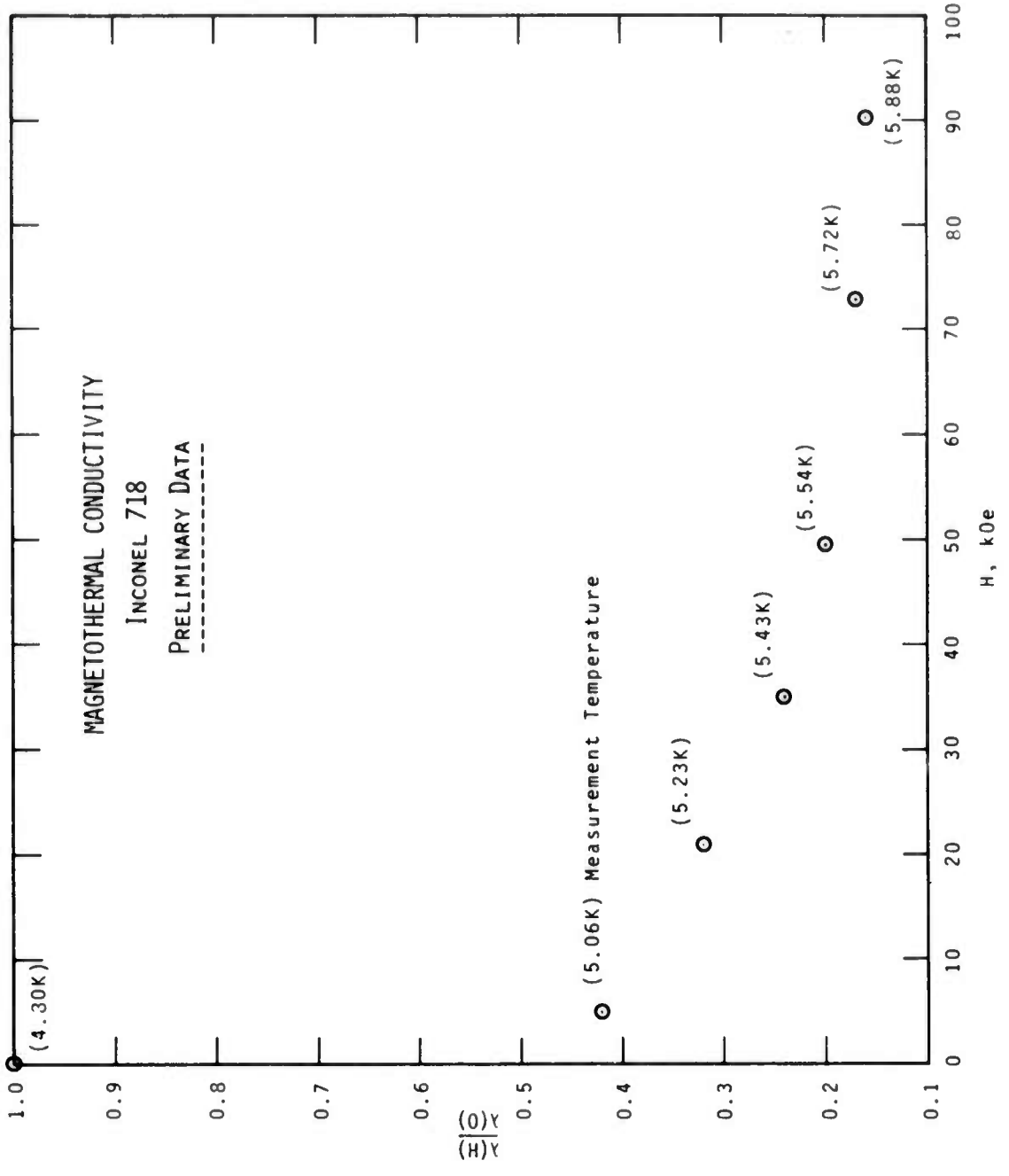

Figure 6. Preliminary data on unannealed Inconel 718 showing $\lambda(H)/\lambda(0)$ as a function of applied magnetic field.

REFERENCES

A. F. Clark and F. R. Fickett, RSI 40, 465 (1969).

L. J. Neuringer and Y. Shapira, RSI 40, 1314 (1969).

139<

APPENDIX A

"Bibliography of Magnetothermal Measurements at Low Temperatures"

1973

T. Amundsen and O. Kverndalen, "A Note on the Anisotropy of the Thermal Magnetoresistance of Aluminum," Phys. Lett. 43A, 9 (1973).

R. S. Averback, C. H. Stephan and J. Bass, "Magnetic Field Dependence of the Thermopower of Dilute Aluminum Alloys," J. Low Temp. Phys. 12, 319 (1973).

A. Fevrier and D. Morize, "The Effect of Magnetic Field on the Thermal Conductivity and Electrical Resistivity of Different Materials," Cryogenics 13, 603 (1973).

M. V. Glushkov and A. I. Markin, "Longitudinal Magnetoresistance of n-Si in Strong Magnetic Fields," Sov. Phys. Solid State 14, 2967 (1973).

1972

R. S. Averback and D. K. Wagner, "Low-Temperature Magnetothermoelectric Power of Aluminum," Solid State Commun. 11, 1109 (1972).

J. M. L. Engels, F. W. Gorter and A. R. Miedema, "Magnetoresistance of Gallium -- A Practical Heat Switch at Liquid Helium Temperatures," Cryogenics 12, 141 (1972).

R. S. Newrock and B. W. Maxfield, "Thermal and Magnetothermal Resistance of Potassium," Bull. Am. Phys. Soc. 17, 256 (1972).

N. N. Sirota, A. A. Drozd and V. I. Gostishchev, "Measurement of Electrical and Thermal Conductivity of Metals in Strong Magnetic Fields," Thermophysical Properties of Substances at Low Temperatures (Proc. 1st all-union meeting) M. P. Orlova ed., Published by All-union Scientific-Research Inst. of Physicotechnical and Radiotechnical Studies (Moscow, 1972) In Russian.

N. N. Sirota, V. I. Gostishchev and A. A. Drozd, "Thermal Conductivity of Aluminum in Strong Magnetic Fields at Low Temperatures," JETP Letters 16, 170 (1972).

N. N. Sirota, V. I. Gostishchev and A. A. Drozd, "Thermoelectric Power of Aluminum in Strong Magnetic Fields at Low Temperatures," JETP Lett. 16, 409 (1972).

H. Van Kempen, H. N. DeLang, J. S. Lass and P. Wyder, "Lattice Conductivity and Thermal Linear Magnetoresistance of Indium Using the Corbino Geometry," Phys. Lett. A. 42, 277 (1972).

C. H. Stephan and B. W. Maxfield, "Righi-Leduc Effect in Indium," Phys. Rev. B 6, 2893 (1972).

D. K. Wagner, "Lattice Thermal Conductivity and High-Field Electrical and Thermal Magnetoconductivities of Tungsten," Phys. Rev. B 5, 336 (1972).

1971

J. R. Long, "Thermal and Electrical Transport in a Tungsten Crystal for Strong Magnetic Fields and Low Temperatures," Phys. Rev. B 3, 1197 (1971).

1970

T. Amundsen and R. P. Sovik, "Measurements of Thermal Magnetoresistance of Aluminum," J. Low Temp. Phys. 2, 121 (1970).

L. J. Challis and R. G. Ward, "Magnetic Field Dependent Phonon Scattering by MN^{3+} ion in Al_2O_3," 9th Conf. on Thermal Cond. (1970), H. R. Shanks ed. [USAEC Conf-69-1002] pp 3-8.

L. Halbo and R. J. Sladek, "Magneto-Thermal Conductivity of n-type Germanium at Low Temperatures," 9th Conf. on Thermal Cond. (1970) H. R. Shanks, ed. [USAEC Conf. 69-1002] p 9. Abstract only.

N. S. Natarajan and M. S. R. Chari, "Thermal Conductivity of Rhodium at Helium Temperatures and in Magnetic Fields," 9th Conf. on Thermal Cond. (1970) H. R. Shanks, ed. [USAEC Conf - 691002] pp. 208-216.

N. S. Natarajan and M. S. R. Chari, "Thermal Conductivity of Dilute Copper-Manganese Alloys at Helium Temperatures and in Magnetic Fields," 9th Conf. on Thermal Cond. (1970) H. R. Shanks, ed. [USAEC Conf - 691002] pp. 169-177.

1969

T. Amundsen, "The Righi-Leduc Effect of Aluminum and Indium," Phil. Mag. 20, 687 (1969).

S. F. Grishin, E. Ya. Grishina and G. A. Milner, "Feasibility of Using a Cadmium Thermal Switch in a Magnetic Refrigerator," Ukranian Physics Journal 13, 969 (1969).

C. H. Stephan and B. W. Maxfield, "High Field Thermal Transport Properties of Indium," Solid State Comm. 7, 1039 (1969).

1968

T. Amundsen, "Size Effects in the Thermal Hall Effect of Aluminum Films," Phil. Mag. 17, 107 (1968).

T. Amundsen, "The Righi-Leduc Effect of Pure Aluminum in High Magnetic Fields," Phil. Mag. 17, 1303 (1968).

F. W. Gorter and A. R. Miedema, "Thermal Magnetoresistance of Gallium and its Use as a Heat Switch," Cryogenics 8, 86 (1968).

1966

J. Laudy and A. Knol, "A Cadmium Heat Switch," Cryogenics 6, 370 (1966).

E. Lerner and J. G. Daunt, "Thermal and Electrical Conductivities of Mo-Re Alloys in the Superconducting and Normal States," Phys. Rev. 142, 251 (1966).

S. G. Lipson, "The Righi-Leduc Effect in Copper at Low Temperatures," Proc. Roy. Soc. A 93, 275 (1966).

1965

T. Amundsen and T. Olsen, "Size-dependent Thermal Conductivity in Aluminum Films," Philosophical Magazine 11, 561 (1965).

S. G. Lipson, "The Thermal Hall Effect in Copper," Proc. 9th Int. Conf. on Low Temp. Phys., Daunt et al., eds. (Plenum Press, 1965) pp. 814-817.

J. R. Long, C. G. Grenier and J. M. Reynolds, "Electron and Lattice Transport Phenomena in an Antimony Crystal at Liquid-He^4 Temperatures," Phys. Rev. 140, A187 (1965).

1963

T. Amundsen and T. Olsen, "Oscillatory Thermal Magnetoresistance in Aluminum," Physics Letters 4, 304 (1963).

C. G. Grenier, J. M. Reynolds and J. R. Sybert, "Electron Transport Phenomena in Bismuth at Liquid-Helium Temperatures," Phys. Rev. 132, 58 (1963).

C. G. Grenier, J. M. Reynolds, N. H. Zebouni, "Electron Transport Phenomena in Zinc at Liquid-Helium Temperatures," Phys. Rev. 129, 1088 (1963).

1962

L. Berger and D. Rivier, "Au Resistivite Electrique et Thermique du Nickel pur et d'un Alliage Fer-Nickel en Champmagnetique aux Basses Temperatures," Helv. Phys. Acta 35, 715 (1962).

J. L. Olsen, Electron Transport in Metals, (Interscience Publishers, 1962) p. 77.

1961

D. Douthett and S. A. Friedberg, "Effects of a Magnetic Field on Heat Conduction in Some Ferrimagnetic Crystals," Phys. Rev. 121, 1662 (1961).

1959

M. S. R. Chari and J. de Nobel, "Thermal Conductivity of Some Dilute Silver Alloys at Low Temperatures and in Magnetic Fields," Physica 25, 60 (1959).

M. S. R. Chari and J. de Nobel, "Thermal Conductivity of Some non-Superconducting Alloys at Low Temperatures," Physica 25, 84 (1959).

1957

J. de Nobel, "Thermal and Electrical Resistivity of Some Tungsten Single Crystals at Low Temperatures and in Strong Magnetic Fields," Physica 23, 261 (1957).

1956

P. B. Alers, "Thermal Magnetoresistance of Zinc at Low Temperatures," Physical Review, 101, 41 (1956).

1953

K. Mendelssohn and H. M. Rosenberg, "The Thermal Conductivity of Metals in High Magnetic Fields at Low Temperatures," Proc. Roy. Soc. A218, 190 (1953).

J. L. Olsen and H. M. Rosenberg, "Thermal Conductivity of Metals at Low Temperatures," Adv. in Physics, 2, 28 (1953).

1951

K. Mendelsohn and H. M. Rosenberg, "Thermal Conductivity of Cadmium in Magnetic Field at Low Temperatures," Proc. Roy. Soc. A64, 1057 (1951).

1950

E. Gruneisen, K. Rausch and K. Weiss, "Conduction of Electricity and Heat in Bismuth Single Crystals in a Transverse Magnetic Field," Ann. Phys. Lpz. 7, 1 (1950).

J. K. Hulm, "Thermal Conductivity of Tin, Mercury, Indium and Tantalum at Liquid Helium Temperatures," Roy. Soc. London (Proc.) 204A, 98 (1950).

143<

1949

J. de Nobel, "The Thermal and Electrical Resistance of Tungsten at Low Temperatures and High Magnetic Fields," Physica 15, 532 (1949).

1947

K. Rausch, "Investigations of Antimony Single Crystals in a Transverse Magnetic Field," Ann. Phys. Lpz. 1, 190 (1947).

1944

S. Shalyt, "Thermal Conductivity of Bismuth at Low Temperatures," J. Physics (USSR) 8, 315 (1944).

1940

E. Gruneisen and H. D. Erfling, "The Electrical and Thermal Resistances of Beryllium Crystals in a Magnetic Field," Ann. Phys. Lpz. 38, 399 (1940).

1938

E. Gruneisen and H. Adenstedt, "The Influence of Transverse Magnetic Fields on the Electrical and Thermal Conductivities of Metals at Low Temperatures," Ann. Phys. Lpz. 31, 714 (1938).

W. J. de Haas and J. de Nobel, "Thermal and Electrical Resistance of a Tungsten Single-Crystal at Low Temperatures and in a Magnetic Field," Physica 5, 449 (1938).

1936

W. J. de Haas, A. N. Gerritsen and W. H. Capel, "Thermal Resistance of Bismuth Single-Crystals at Low Temperatures and in a Magnetic Field," Physica 3, 1143 (1936).

1934

A. Reddemann, "Anderung der thermischen und electrischen Leitfahigkeit eines Bi-Einkristalls im Magnetfeld," Ann. Phys. 20, 441 (1934).

1926

N. C. Little, "Thermagnetic and Galvanothermomagnetic Effects in Arsenic," Phys. Rev. 28, 418 (1926).

SEMI-ANNUAL REPORT ON MATERIALS RESEARCH IN SUPPORT OF SUPERCONDUCTING MACHINERY

Thermal Conductivity

by

J. G. Hust and P. J. Giarrantano

Cryogenics Division
NBS - Institute for Basic Standards
Boulder, Colorado

SUMMARY

Thermal conductivity measurement philosophy is outlined and two apparatus are described. The need for precision measurements, lower accuracy measurements, and predictive methods is outlined. Candidate materials for superconducting machinery are listed and existing data on these materials have been surveyed. Based on this survey, materials have been selected for measurement and specimens in various metallurgical conditions have been obtained. Measurements on OFHC copper have been completed, but data analysis is still in progress; therefore, experimental values of thermal conductivity are presented. An example is presented of a predictive procedure, based on Lorenz ratio and electrical resistivity data. Upon completion of the OFHC copper data analysis, comparisons will be made to indicate the degree of accuracy of the predictive method. A schedule of measurements for this contract year is included.

TABLE OF CONTENTS

LIST OF FIGURES

LIST OF TABLES

147<

INTRODUCTION

Optimum design of superconducting machinery requires a knowledge of thermal properties of technically important materials at low temperatures. But, often, components extend from ambient temperatures to low temperatures, and, therefore, data are needed from 4 K to 300 K. Thermal conductivity of metals is a function of the host metal and its constituent elements and temperature; but it also depends on the microstructure of the material, strain, fatigue, heat treat, and in some cases environmental effects are important (e.g., in the case of superconducting machinery, magnetic field intensities may produce significant changes). Specific thermal conductivity data for particular components are required to limit heat losses and thermal stresses in machines.

With such a myriad of parameters it is difficult (at best) to determine accurately, by experiment, the thermal conductivity of each component. Instead, we often rely on a limited number of measurements on specific types of materials, characterized according to the above parameters, and indicate the degree of variability of these data. This uncertainty is usually limited primarily by material variability, i.e., variations in the material parameters listed above.

It should also be noted that accurate thermal conductivity measurements are much more expensive and time consuming relative to many other properties measurements. The ease with which high accuracy can be obtained is primarily a function of temperature and conductivity itself. The extremes of conductivity (both very high, such as in pure metals, and very low, such as in insulating materials) promote inaccuracies in measurement. Generally, low temperature data (below about 100 K) are more readily obtained with accuracy because of the absence of radiation effects.

For the above reasons, various methods of obtaining thermal conductivity data are used. The method used depends primarily on the accuracy dictated by the application. Usually accuracies of 10% are sufficient; in other cases values accurate to 50% suffice. The present state-of-the-art in thermal conductivity measurements is about 1% accuracy, but seldom is this required except in theoretical or standardization work.

PROCEDURES

In this work, three methods of data determination will be used:

(a) A precision apparatus, capable of measuring at any temperature from 4 to 300 K, with an accuracy of about 2%. This apparatus also simultaneously measures electrical resistivity and thermopower for additional specimen characterization and subsequent predictions of similar materials. This apparatus will be used to measure materials that have not been sufficiently measured and characterized previously and for accurate temperature dependence determinations.

(b) A fixed point apparatus, capable of measuring only near the fixed temperatures of various boiling fluids (such as liquid helium and liquid nitrogen) and melting or subliming solids (such as ice and CO_2). The accuracy of this apparatus is at best about 5%, depending mainly on the conductivity of the specimen.

(c) Predictive methods such as those described by Hust and Clark (1) and Hust and Sparks (2). The latter paper also contains data for many metals and alloys, necessary to carry out such predictions.

These predictive methods work best for pure metals (5% accuracy or better), not as well for intermediate alloys (10-20%), worse for structural materials (20-60%), and are not applicable to non-metals. The figures in parenthesis are to be considered as rough estimates of the validity of these techniques and are strongly dependent on temperature, as explained in the above references. There is evidence that the above techniques will also be reasonably valid for predicting the effects of magnetic field. (Magnetic field effects is a separate area of investigation under this contract and is not discussed here).

The above techniques are listed in order of decreasing cost per measurement and likewise increasing inaccuracies, with occasional exceptions. They will be applied to obtain the most cost effective data consistent with system requirements.

Precision Apparatus

The precision apparatus has been described in detail by Hust et al. (3). It is a longitudinal heat flow apparatus requiring a 23 cm long specimen. The diameter of the specimen is dictated by its approximate thermal conductivity. The largest diameter which can be accommodated is about 3 cm and the smallest is limited only by one's dexterity. Specimens as small as 2 mm diameter have been measured. Figure 1 depicts the cryostat of this apparatus.

The precision apparatus has been in operation for many years; the first model was built in the late 50's. Recently, to correct some faults which have developed during the past ten years and to incorporate a few improvements in thermometry and temperature control, the cryostat

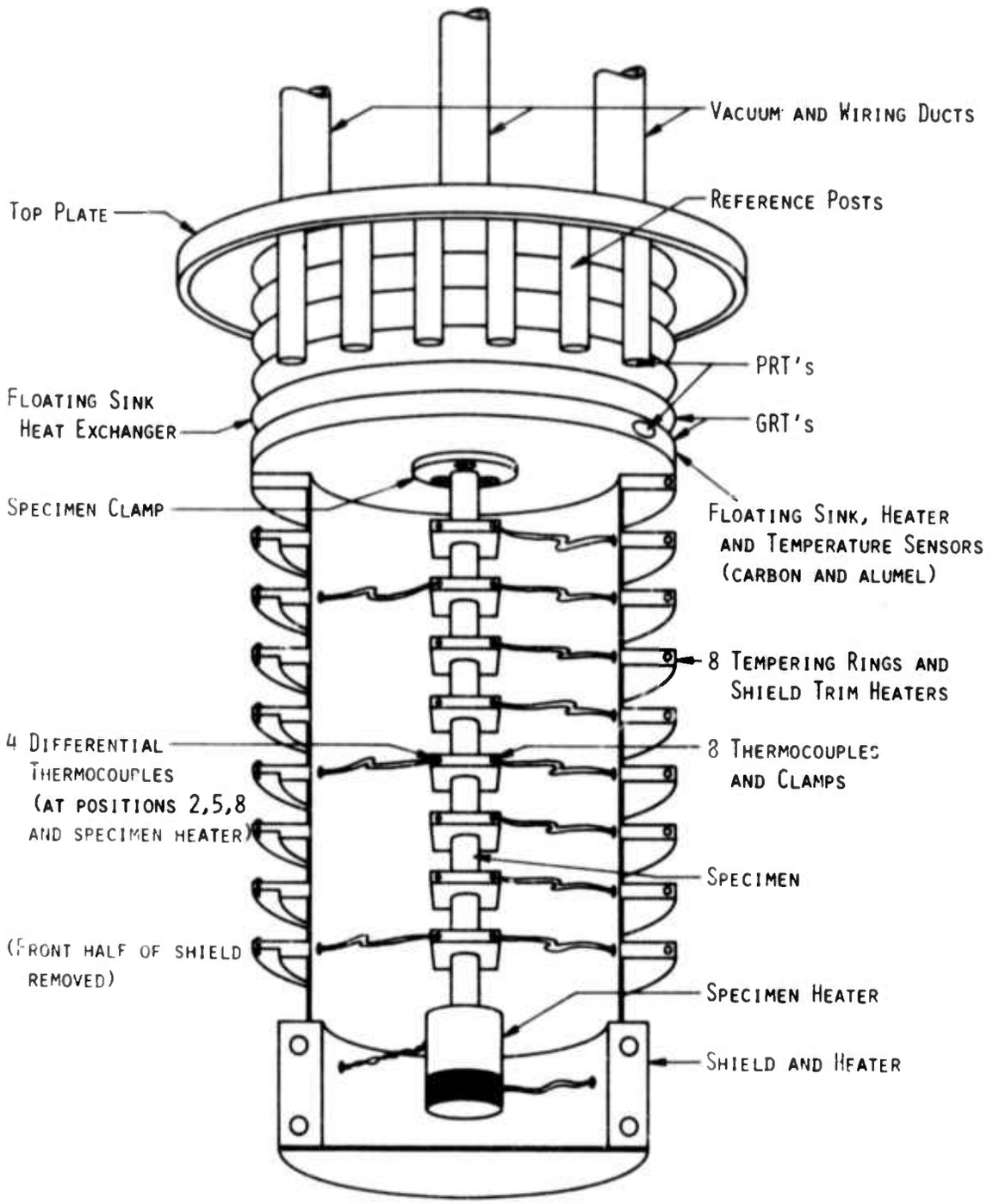

Figure 1. Precision Thermal Conductivity Apparatus

was rebuilt and new wiring was installed. For this reason, the first specimen to be measured was chosen to fulfill several criteria:

(1) It is to be a material of interest to this program which was not previously measured over at least a portion of the range 4 to 300 K,

(2) It is to be a good conductor to facilitate in-place calibration of the new thermocouples, and

(3) It should be a material whose conductivity is predictable over most of the temperature range to check the operation of the system.

OFHC copper was chosen to satisfy these requirements. It is of obvious interest to the program, it was never previously measured in the range 4-20 K, is a good conducting material, and is most predictable based on the previously mentioned Lorenz ratio method.

Fixed Point Apparatus

This apparatus is inherently less accurate than the precision apparatus; it can measure thermal conductivity at only a few temperatures below ambient but requires less time to obtain data and requires only a 2 inch long specimen. It is a new apparatus in this laboratory and its accuracy limitations are not well defined. Its design accuracy for midrange conductors is 10%. A schematic drawing of the cryostat is shown in figure 2.

The principal of operation is as follows. For each bath temperature a series of empty chamber runs are conducted to establish $\dot{Q}_o = f(\Delta T)$ for relatively small ΔT. $\dot{Q}_o$ is the heat input required to establish a given temperature difference ΔT. A specimen is installed and the heat input, $\dot{Q}$, to establish a small ΔT is measured. The increased heat input

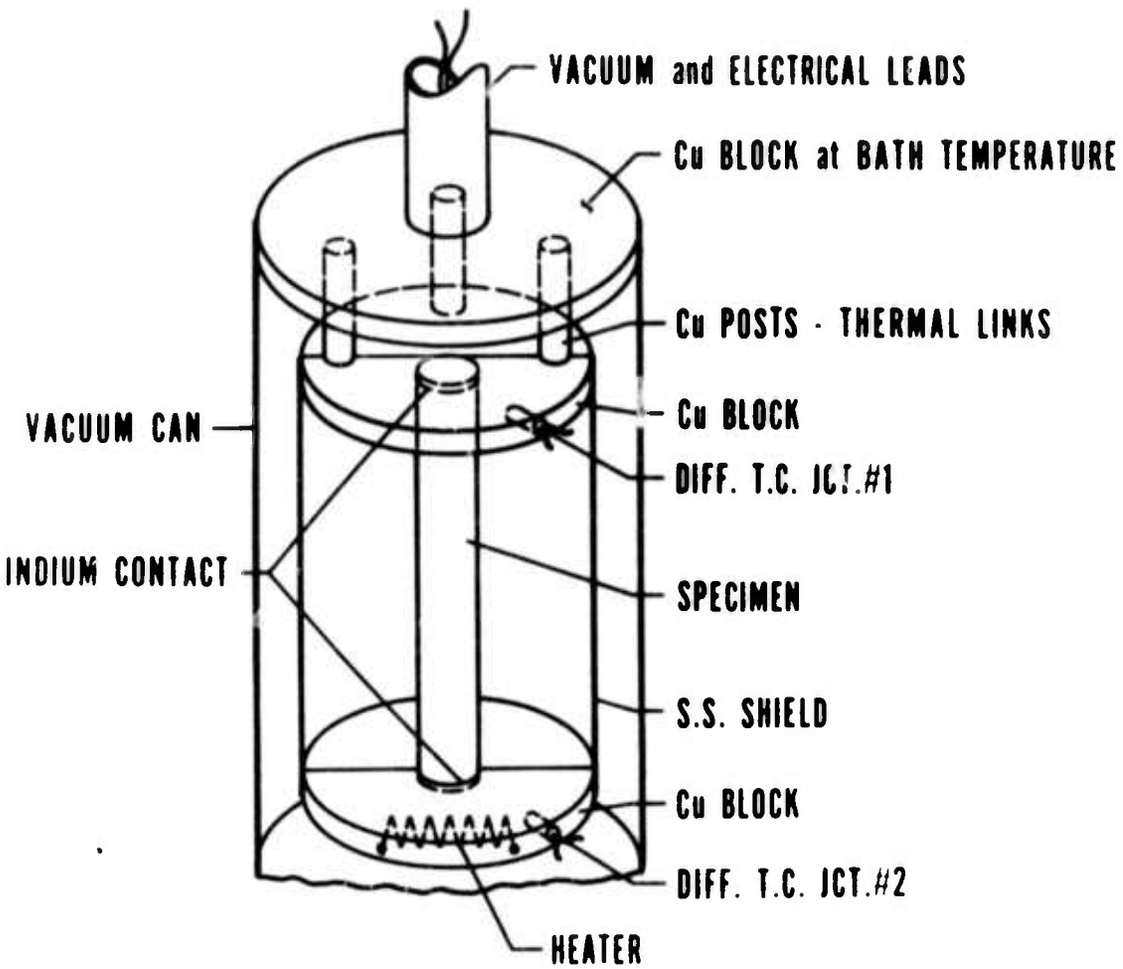

Figure 2. Fixed-Point Thermal Conductivity Apparatus

153<

at this ΔT, $\dot{Q} - \dot{Q}_o$, is determined and λ, thermal conductivity of the specimen, is calculated from

$$\lambda = \frac{(\dot{Q} - \dot{Q}_o)\ell}{A\Delta T} ,$$

where A is the cross-sectional area of the specimen and ℓ is the distance between the copper clamps. The principal source of error with this technique is due to the temperature discontinuity at the interface between the specimen and the copper clamps. Indium is used at this junction to improve the thermal contact. Other sources of error are thermocouple calibration, temperature determination, loss of heat by radiation, non-steady state, and strain caused by differential contraction. For specimens which are small compared to the specimen chamber, radiation losses should be nearly equal in the determination of $\dot{Q}_o$ and $\dot{Q}$ and, therefore, are eliminated by subtraction. Temperature drift and radiation errors are most important when measuring poor conducting, large specimens. The temperature discontinuity errors are largest with small, good conducting specimens. This apparatus is checked, using NBS standard reference materials of thermal conductivity, to determine it's accuracy.

Material Selection and Measurement Criteria

This project is to be conducted as follows:

(1) Select candidate materials of interest to the ARPA superconducting machinery program.

(2) Search existing compilations to determine the candidate materials whose thermal conductivities are not sufficiently defined (including effects of heat treatment, microstructure etc).

(3) Measure these materials in the appropriate apparatus or predict their thermal conductivities based on the Lorenz ratio method and their measured electrical resistivities.

RESULTS

Materials selected for their potential application to the ARPA superconducting machinery program are listed below.

Iron Alloys

AISI-301*, 303*, 304*, 304L*, 310, 316*, 321, and 347*
ARMCO 31-6-9 and 21-13-5*
CARPENTER 20cb-3
KROMARC 58
A-286*
W-545
PYROMET 860
DISCALOY
MARAGING STEELS

Nickel Alloys

Inconel 625, 718*, and X750
Hastelloy C-276
PYROMET 680 and 102
UNITEMP-HX
HAYNES 188
MULTIPHASE MP35N
INCOLOY 903
INCO (low expansion, unnamed)
INVAR

Titanium Alloys

Ti-6Al-4V (ELI)*
Ti-5Al-2.5 Sn (ELI)*

Aluminum Alloys

2014
X2048
2219
5083*

Copper Alloys

OFHC copper*

Those alloys marked with an * have been measured over most of the range 4 to 300 K and would be of interest only from the standpoint of heat treat, strain, and microstructure variation. Any of these of interest would be measured in the fixed-point apparatus or predicted on the basis of electrical resistivity [See also Clark et al (3)], with the exception of OFHC copper. Of the remaining alloys, the iron base alloys generally have well-behaved thermal conductivities, as a function of temperature, and will usually be measured in the fixed point apparatus. Aluminum alloys will be treated similarly. The thermal conductivity curves of nickel alloys tends to be less systematic and the precision apparatus will be used most frequently for these.

The following materials have been selected and several specimens procured for additional study:

AISI 310S
Inconel X750
Kromarc 58
Inco Low expansion alloy (unnamed)
OFHC copper.

Most of the materials have been obtained in various heat treat and strain conditions.

The following measurements are scheduled for this contract year:

Precision Apparatus

OFHC copper
Inco Low Expansion Alloy (unnamed)
Inconel X75(

Fixed Point Apparatus

Iron and Steel, SRM's for apparatus accuracy check
AISI 310S
Kromarc 58.

156<

DISCUSSION

Measurements on OFHC copper are nearly complete and data analysis has been initiated. No measured thermal conductivity data are available; however, this is an excellent opportunity to illustrate the value of the Lorenz ratio prediction method mentioned earlier. Based upon preliminary data from the precision apparatus, the residual electrical resistivity of this specimen of OFHC copper is 7.4 $n\Omega$-cm. Lorenz ratio values, $L = \rho\lambda/T$, for a copper of similar residual resistivity are taken from Hust and Sparks (2) and listed in table 1. Electrical resistivity values are obtained from the intrinsic resistivity of copper, the measured residual resistivity and Mathiessen's rule. These along with calculated values (predicted) of thermal conductivity, $\lambda = TL/\rho$, are tabulated in table 1. Upon completion of the thermal conductivity measurements on this OFHC copper specimen, comparisons will be made to illustrate the degree of agreement.

157<

Table 1. Calculation of thermal conductivity of OFHC copper based upon electrical resistivity and Lorenz ratio data

T,K	L, $V^2/K^2 \times 10^{+8}$	ρ_i, $n\Omega$ cm	ρ, $n\Omega$ cm	$\lambda = \frac{LT}{\rho}$, W/cmK
5	2.4	0.0	7.4	16.2
10	2.0	0.0	7.4	27.0
15	1.8	0.3	7.7	35.1
20	1.5	0.8	8.2	36.6
25	1.2	2.5	9.9	30.3
30	1.2	6.3	13.7	26.3
40	1.2	22	29	16.6
50	1.2	50	57	10.5
70	1.4	153	160	6.12
80	1.5	215	222	5.40
100	1.7	350	357	4.76
150	2.00	700	707	4.24
200	2.16	1060	1070	4.04
250	2.26	1400	1410	4.01
300	2.31	1750	1760	3.94

158<

REFERENCES

1. Hust, J. G. and Clark, A. F., The Lorenz Ratio as a Tool for Predicting the Thermal Conductivity of Metals and Alloys, Materials Research and Standards, 11, No. 8, 22-24 (Aug. 1971).

2. Hust, J. G. and Sparks, L. L., Lorenz Ratios of Technically Important Metals and Alloys, Nat. Bur. Stand. Tech. Note 634, 133 pp. (Feb. 1973).

3. Clark, A. F., Childs, G. E. and Wallace, G. H., Electrical Resistivity of Some Engineering Alloys at Low Temperatures, Cryogenics 10, 295-305, (Aug. 1970).

SEMI-ANNUAL REPORT ON MATERIALS RESEARCH
IN SUPPORT OF SUPERCONDUCTING MACHINERY

Elastic Properties of Engineering Alloys at Cryogenic Temperatures

by

H. M. Ledbetter, E. R. Naimon, and W. F. Weston

Cryogenics Division
NBS - Institute for Basic Standards
Boulder, Colorado

SUMMARY

The problem was to determine the elastic properties of engineering alloys at cryogenic temperatures, 4 - 300 K. These properties include: longitudinal modulus, Young's modulus, shear modulus, bulk modulus, and Poisson's ratio. Such data are vital to areas such as structural design, fracture analysis, and properties of composites. Data have been acquired for thirteen materials: Ti - 6 Al - 4V and Ti - 5 Al - 2.5 Sn; Inconels 600 and X-750; stainless steels A286, 304, 310, and 316; aluminum alloys 1100, 5083, 7005, and 7075; and invar. The hardness, mass density, and (when appropriate) grain size of these materials were measured. Chemical analysis and thermal-mechanical history are also reported. Elastic properties were determined by measuring ultrasonic velocities using pulse-echo and pulse-superposition techniques. In final manuscripts, the few existing data are compared with present results. Originally, fixed-temperature measurements were planned at 300, 195, 77, and 4 K. However, an experimental system was developed capable of semi-continuous measurements between 300 and 4 K, both cooling and warming. Recommendations for further research in the cryogenic elastic properties of engineering alloys include: (1) similar studies on additional materials; (2) effects of mechanical deformation and heat treatment; (3) effects of magnetic fields on ferromagnetic and antiferromagnetic materials; (4) effects of manufacturing and processing variables; and (5) effects of low-temperature phase transformations. The primary problems

in extending this work are: (a) constructing a helium cryostat for measurements in a magnetic field (presently we are limited to room-temperature magnetic measurements); (b) developing a new measurement technique for copper alloys, which highly attenuate ultrasonic waves in the 1-10 MHz region - a composite oscillator technique (10 - 100 kHz) is being studied.

RESULTS

Results from this program are given below and include:

(1) A manuscript "Elastic properties of two titanium alloys at low temperatures," by E. R. Naimon, W. F. Weston, and H. M. Ledbetter. This manuscript has been accepted for publication in Cryogenics.

(2) A manuscript "Dynamic low-temperature elastic properties of two austenitic nickel-chromium-iron alloys," by E. R. Naimon, H. M. Ledbetter, and W. F. Weston. This is to be submitted for publication.

(3) A set of ten figures showing the elastic properties of four stainless steels and four aluminum alloys.

Details concerning experimental procedures are given in items (1) and (2) or in the references cited therein.

Elastic Properties of Two Titanium Alloys at Low Temperatures†

E. R. Naimon*, W. F. Weston*, and H. M. Ledbetter

Cryogenics Division, Institute for Basic Standards,
National Bureau of Standards, Boulder, Colorado 80302

ABSTRACT

Sound velocities and elastic constants were determined semi-continuously for two annealed polycrystalline titanium alloys between 4 and 300K. Results are given for: longitudinal sound velocity, transverse sound velocity, Young's modulus, shear modulus, bulk modulus, Poisson's ratio, and elastic Debye temperature. A pulse-superposition technique was used.

Key words: Bulk modulus; compressibility; Debye temperature; elastic constant; Poisson's ratio; shear modulus; sound velocity; titanium alloys; Young's modulus.

---

*NRC-NBS Postdoctoral Research Associate, 1973-4.

Elastic Properties of Two Titanium Alloys at Low Temperatures

E. R. Naimon*, W. F. Weston*, and H. M. Ledbetter

Cryogenics Division, Institute for Basic Standards
National Bureau of Standards, Boulder, Colorado 80302

Introduction

Despite the fact that titanium alloys Ti-6Al-4V and Ti-5Al-2.5Sn are intended mainly for high-strength high-temperature applications, they also have cryogenic uses. Their important properties include: ease of fabrication, corrosion resistance, high strength-to-density ratios (especially at cryogenic temperatures), and high strength-to-thermal-conductivity ratios.

The low-temperature elastic properties of these alloys are reported here. A pulse-superposition method was used to determine the ultrasonic wave velocities in annealed specimens. From longitudinal and transverse wave velocities, together with the mass density, the elastic constants were calculated: Young's modulus, shear modulus, bulk modulus (reciprocal compressibility), Poisson's ratio, and the elastic Debye temperature. These constants are useful in a wide variety of applications, from engineering design to equations of state for solids.

Experimental Procedures

Alloys were obtained from commercial sources in the form of 3/4-in. (1.9-cm) diameter rods. Cylindrical specimens 5/8-in. (1.6-cm) in diameter

* NRC-NBS Postdoctoral Research Associate, 1973-4.

and 5/8-in. (1.6-cm) long were prepared by grinding. Opposite faces were flat and parallel within 100×10^{-6} in. (2.5 μm). Specimens were annealed at a pressure of 5×10^{-6} torr, or less, and cooled in the furnace. Annealing times and temperatures are given in Table 1, together with chemical compositions (obtained from mill analyses), hardness numbers, microstructures, grain sizes, and mass densities. Hardness, microstructure, and grain size were determined by standard metallurgical methods. Mass density was determined by Archimedes' method using distilled water as a standard.

The specimen holder is shown in Fig. 1. The holder was placed in the ullage of a helium dewar and lowered stepwise to achieve cooling. Temperatures were monitored with a chromel-constantan thermocouple contacting the specimen.

Quartz transducers (10 MHz) were bonded to the specimens with phenyl salicylate for room-temperature measurements and with a stopcock grease for lower temperatures. In a few cases, failure of these bonds at very low temperatures required using a silicone fluid (viscosity = 200.0 cP at 25°C) for bonding.

A pulse-superposition method[1,2] was used to determine the sound-wave velocities over the temperature range 4-300 K. No thermal-contraction corrections were made; for titanium alloys this introduces a maximum error (over a 300 K range) of about 0.2 percent. No bond corrections were made; this error is insignificant for the purposes of the present study. Maximum uncertainties

in the velocity measurements are estimated to be about one percent.

Results

Longitudinal and transverse sound-wave velocity data are shown in Figs. 2 and 3, where the longitudinal modulus is given by

$$C_\ell = \rho v_\ell^2 = B + \frac{4}{3} G \tag{1}$$

and the transverse modulus is given by

$$C_t = \rho v_t^2 = G. \tag{2}$$

Here v_ℓ and v_t are the longitudinal and transverse sound-wave velocities, ρ is the mass density, B is the bulk modulus, and G is the shear modulus.

Temperature dependences of both C_ℓ and C_t were fit to a semi-theoretical relationship suggested by Varshni:[3]

$$C = C^o - s/(e^{t/T} - 1), \tag{3}$$

where C^o, s, and t are adjustable parameters and T is temperature. The value of C at T = 0 K is C^o, and -s/t is the high-temperature limit of the temperature coefficient dC/dT. By invoking an Einstein oscillator model of solids, it can be shown (in the absence of electronic effects) that t is the Einstein characteristic temperature. Parameters C^o, s, and t are given in Table 2. Room-temperature values of the temperature coefficients of the elastic moduli are given in Table 3.

Curves in Figs. 2 and 3 are plots of Eq. (3) determined by an unweighted least-squares fit of the data. Average percentage differences between measured and curve values are 0.03% and 0.07% for the longitudinal and transverse moduli, respectively.

While polycrystalline aggregates (quasi-isotropic solids) have only two independent elastic constants, several constants are commonly used for various applications. The four most common are the bulk modulus B, Young's modulus E, the shear modulus G, and Poisson's ratio ν. The relationships among these are

$$\frac{1}{E} = \frac{1}{3G} + \frac{1}{9B} \tag{4}$$

and

$$\nu = \frac{E}{2G} - 1 . \tag{5}$$

These elastic constants were calculated from the moduli shown in Figs. 2 and 3 by the relationships:

$$E = 3C_t (C_\ell - \frac{4}{3} C_t)/(C_\ell - C_t), \tag{6}$$

$$B = C_\ell - \frac{4}{3} C_t , \tag{7}$$

and

$$\nu = \frac{1}{2} (C_\ell - 2C_t)/(C_\ell - C_t). \tag{8}$$

The constants E, B, and ν are shown in Figs. 4-6.

It is of interest to calculate the elastic Debye temperature θ for the two alloys. This fundamental parameter is important in the lattice properties of solids and is related to the elastic wave velocities by[4]

$$\theta = K \langle v \rangle , \tag{9}$$

where

$$K = \frac{h}{k} \left(\frac{3N\rho}{4\pi A} \right)^{1/3} . \tag{10}$$

Here h is Planck's constant, k is Boltzmann's constant, N is Avogadro's constant, ρ is the mass density, and A is the atomic weight. The average velocity is given by

$$\langle v \rangle = \left(\frac{v_\ell^{-3} + 2v_t^{-3}}{3} \right)^{-1/3} . \tag{11}$$

The Debye temperatures for the two alloys at $T = 0K$, and also for pure titanium, are given in Table 4.

Discussion

The elastic properties of both Ti-6Al-4V and Ti-5Al-2.5Sn behave regularly with respect to temperature. All of the elastic moduli (C_ℓ, $C_t = G$, B, E) decrease with increasing temperature, show a relative flatness at low temperatures, achieve zero slope at $T = 0$, and approach linear behavior at high temperatures. Poisson's ratio also behaves regularly, having a positive temperature coefficient.

Assuming that the specimens studied are representative of the two alloys, then conclusions concerning their relative elastic behavior can be drawn. Not surprisingly, as shown in Figs. 2-6 and Tables 2 and 3, for most practical purposes the two alloys are elastically identical. Thus, whether the second alloying element is vanadium or tin, the elastic properties are essentially the same.

As is well known, titanium undergoes a c.p.h. -to-b.c.c. (α-to-β) crystal-structure transition when heated to 1155 K. Fisher and Renken[5] found a large temperature dependence of the c_{66} shear modulus in titanium: $\frac{1}{c_{66}} \frac{dc_{66}}{dT} = -11.93 \times 10^{-4}\ K^{-1}$. A small value of c_{66} is expected from the shear mechanism of a c.p.h. -to-b.c.c. transition proposed by Burgers[6]. For hexagonal symmetry, the shear modulus G is an approximate average of the two single-crystal shear constants c_{66} and c_{44}. Thus, from the smaller values of $\frac{1}{G} \frac{dG}{dT}$ in Table 3 one can infer that both alloys have higher c.p.h. -to-b.c.c. transition temperatures than pure titanium. That is, the α-titanium phase is stabilized in the alloys. As shown in Hansen and Anderko[7], aluminum is a strong stabilizer of α titanium, while both vanadium and tin are moderate stabilizers of β titanium.

Despite the extensive use of these alloys, very little elastic data exist for them. Most information has appeared in engineering reports and is summarized in references 8-12. For comparison, the room-temperature values of E, G, B, and ν are given in Table 5. Generally good agreement is observed between previous and present results.

The elastic moduli of both alloys are several percent higher than those reported for commercial-grade titanium[12]. But they are lower by several percent than the quasi-isotropic moduli obtained from a Voigt-Reuss-Hill average of the data obtained from zone-refined single crystals[5]. The elastic Debye temperatures of the alloys are also about 2% lower than that calculated

from the single-crystal elastic data of titanium. The relatively low elastic anisotropy of titanium does not allow for a large error in the Voigt-Reuss-Hill averages. Thus, existing data suggest a strong impurity effect on the elastic constants of titanium, perhaps due to interstitial impurities.

Finally, it is emphasized that the data reported here are dynamic (adiabatic) rather than static (isothermal) and apply to rapid, rather than slow, loading. In most cases the differences between adiabatic and isothermal elastic constants are small. Conversion formulas are given in Landau and Lifshitz[13], for example. For titanium at room temperature:

$$(E_S - E_T)/E_S = 0.001, \qquad (B_S - B_T)/B_S = 0.009,$$

$$(\nu_S - \nu_T)/\nu_S = 0.005, \text{ and} \qquad (G_S - G_T)/G_S \equiv 0,$$

where subscripts S and T denote adiabatic and isothermal, respectively.

Acknowledgment

This work was supported in part by the Advanced Research Projects Agency.

170<

References

1. McSkimin, H. J., J. Acoust. Soc. Amer. 33, 12 (1961).
2. McSkimin, H. J. and Andreatch, P., J. Acoust. Soc. Amer. 34, 609 (1962).
3. Varshni, Y. P., Phys. Rev. B2, 3952 (1970).
4. Debye, P., Ann. Phys. (Leipz.) 39, 789 (1912).
5. Fisher, E. S. and Renken, C. J., Phys. Rev. 135, A482 (1964).
6. Burgers, W. G., Physica 1, 561 (1934).
7. Hansen, M. and Anderko, K., Constitution of Binary Alloys (McGraw-Hill, New York, 1958).
8. Metals Handbook, 8th Edition, Vol. 1, Properties and Selection of Metals (Amer. Soc. Metals, Metals Park, Ohio, 1961).
9. Cryogenic Materials Data Handbook, AFML Rep. No. ML-TDR-64-280 (PB 171809, revised) (Aug. 1964).
10. NERVA Program Materials Properties Data Book, Vol. 1, Introduction and Light Metal Alloys (Aerojet Nuclear Systems, Sacramento, Calif., 1970).
11. Hanlein, S. L., Hinckley, W. M., and Stecher, F. P., NOLTR Report 70-141 (1970).
12. Fahey, N. H., WAL Tech. Rep. No. TR 118.1/1 (1960).
13. Landau, L. D. and Lifshitz, E. M., Theory of Elasticity (Pergamon, London, 1959), p. 17.

171<

List of Tables

List of Figures

Table 1. Compositions and properties of alloys

Alloy	Chemical Composition, Mill Analyses (wt. pct.) Ti	Al.	V	Sn	Fe	C	N	H	Hardness (DPH No., 1000 g load)	Grain Size Avg. Dia. (mm)	Mass Density at 294 K (g/cm^3)	Conditions	Microstructure
Ti-6Al-4V	Bal.	6.2	4.0	-	0.1	0.01	0.01	0.01	320	0.005	4.42	Annealed (800°C, 2 h)	Equiaxed alpha grains with intergranular beta
Ti-5Al-2.5Sn	Bal.	5.5	-	2.5	0.2	0.07	-	0.02	330	0.02	4.47	Annealed (816°C, ½ h)	Equiaxed alpha grains in a mottled dark-etching (Kroll's reagent) matrix phase, probably acicular alpha

Table 2. Parameters in equation 3

Alloy	Mode	C° (10^{11} N/m^2)	s (10^{11} N/m^2)	t (K)
Ti-6Al-4V	ρv_ℓ^2	1.688	0.085	213.7
	ρv_t^2	0.467	0.039	183.6
Ti-5Al-2.5Sn	ρv_ℓ^2	1.716	0.085	208.8
	ρv_t^2	0.470	0.051	210.4

Table 3. Temperature derivatives of elastic constants at room temperature ($10^{-4}K^{-1}$)

Alloy	$\frac{1}{B}\frac{dB}{dT}$	$\frac{1}{E}\frac{dE}{dT}$	$\frac{1}{G}\frac{dG}{dT}$	$\frac{1}{\nu}\frac{d\nu}{dT}$
Ti-6Al-4V	-1.01	-4.44	-4.90	1.89
Ti-5Al-2.5Sn	-0.75	-4.99	-5.55	2.26
Pure Ti*	-0.93	-6.63	-7.15	2.80

* Calculated from data in ref. 5 using a Voigt-Reuss-Hill average.

175<

Table 4. Elastic Debye temperatures at T = 0 K

Alloy	θ (K)
Ti-6Al-4V	418.1
Ti-5Al-2.5Sn	416.9
Pure Ti	425.7*

* Ref. 5

Table 5. Comparison of present and previously reported results; room-temperature values; units of 10^{11} N/m^2 except ν (dimensionless)

	Ti-5Al-2.5Sn				Ti-6Al-4V			
Source	E	G	B	ν	E	G	B	ν
Ref. 12	-	-	-	-	1.11	0.421	1.06	0.325
Ref. 8	1.14	-	-	-	-	-	-	-
Ref. 9	0.96-1.17	-	-	-	1.07-1.21	0.421	-	-
Ref. 10	1.07	-	1.07	-	1.10	-	1.13	-
Ref. 11	1.10	-	-	-	1.03	-	-	-
Present	1.11	0.420	1.07	0.327	1.11	0.420	1.05	0.323

177<

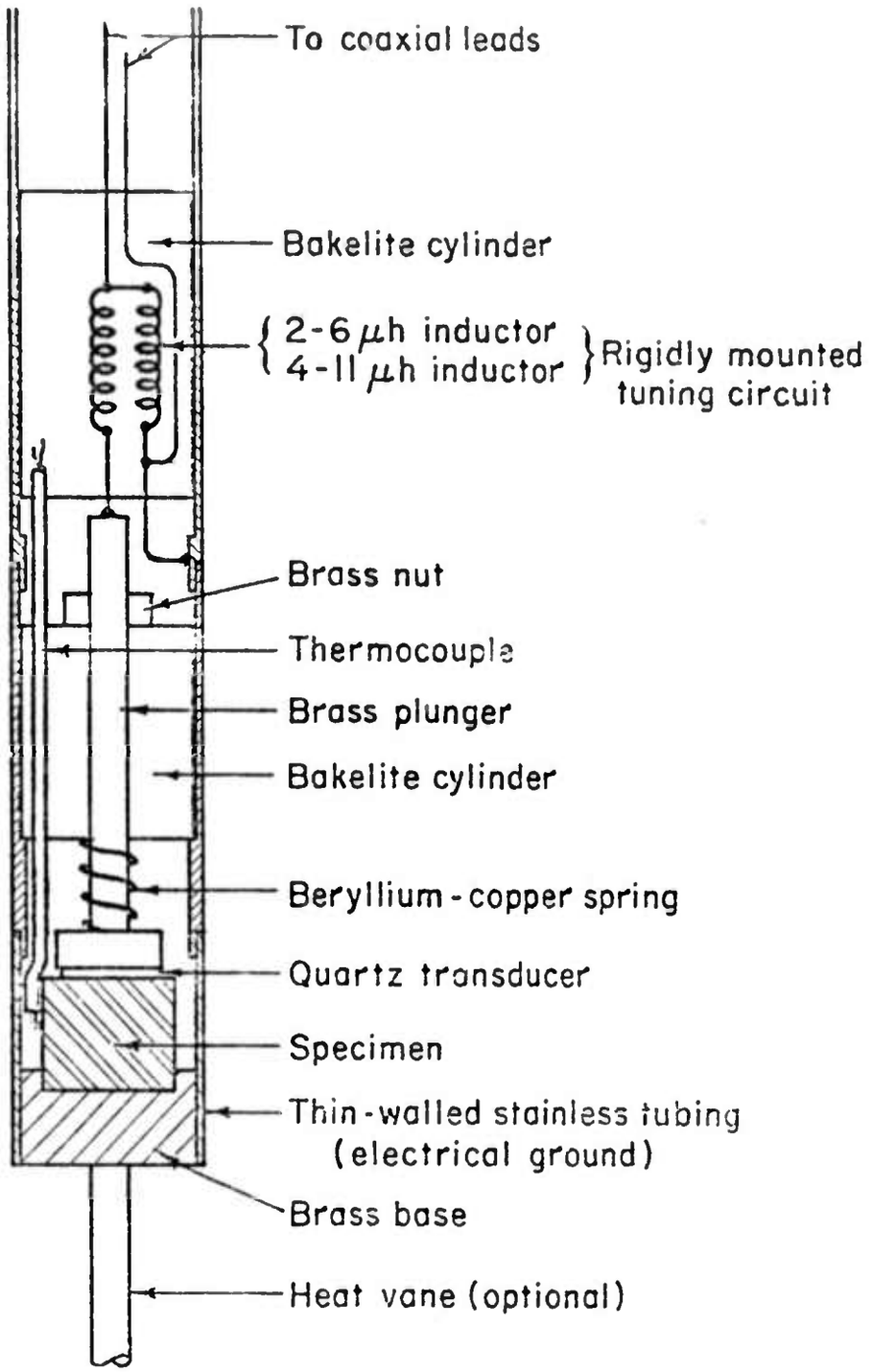

Fig. 1 Specimen holder.

178

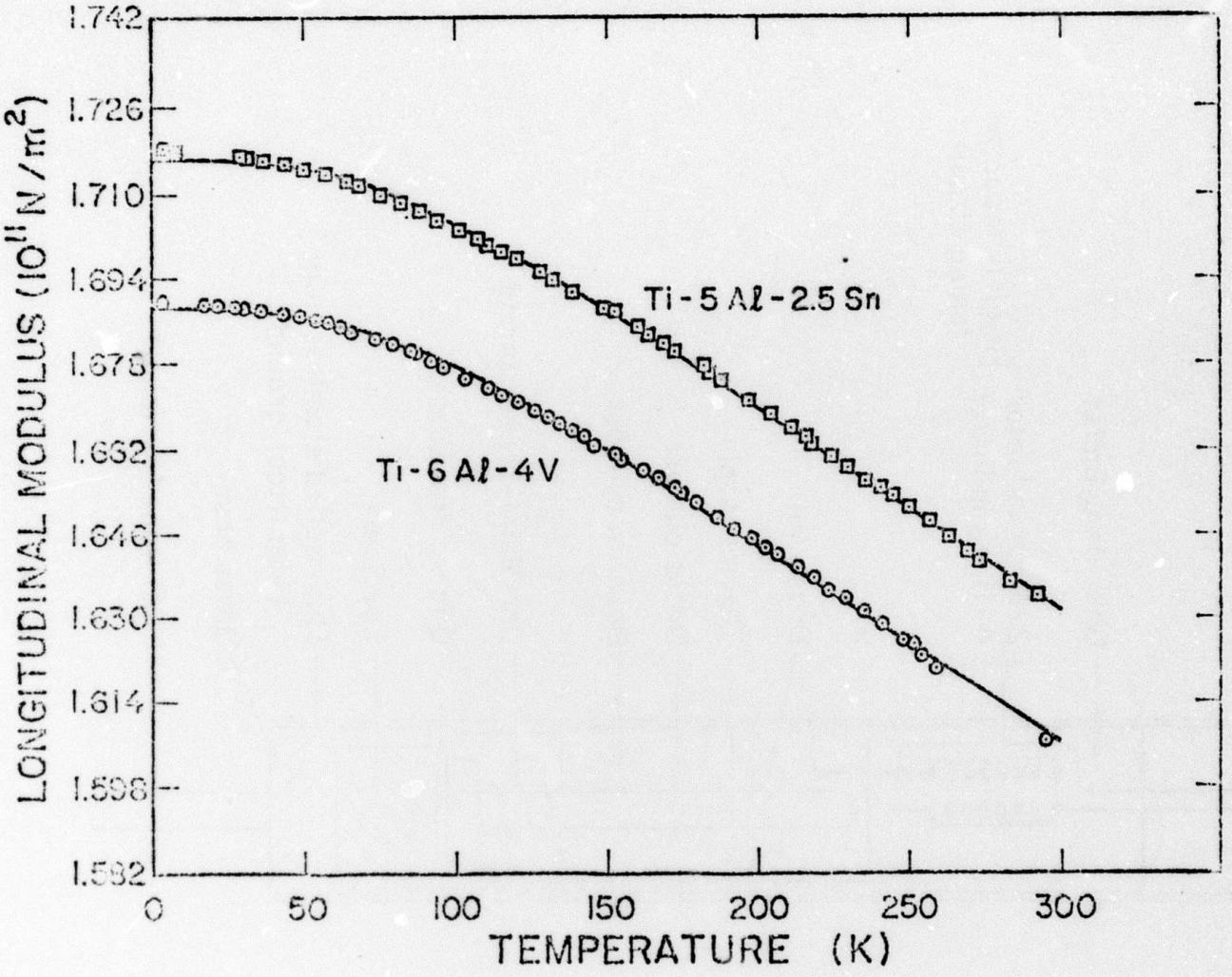

Fig. 2 Longitudinal modulus $C_\ell = \rho v_\ell^2$ of two titanium alloys.

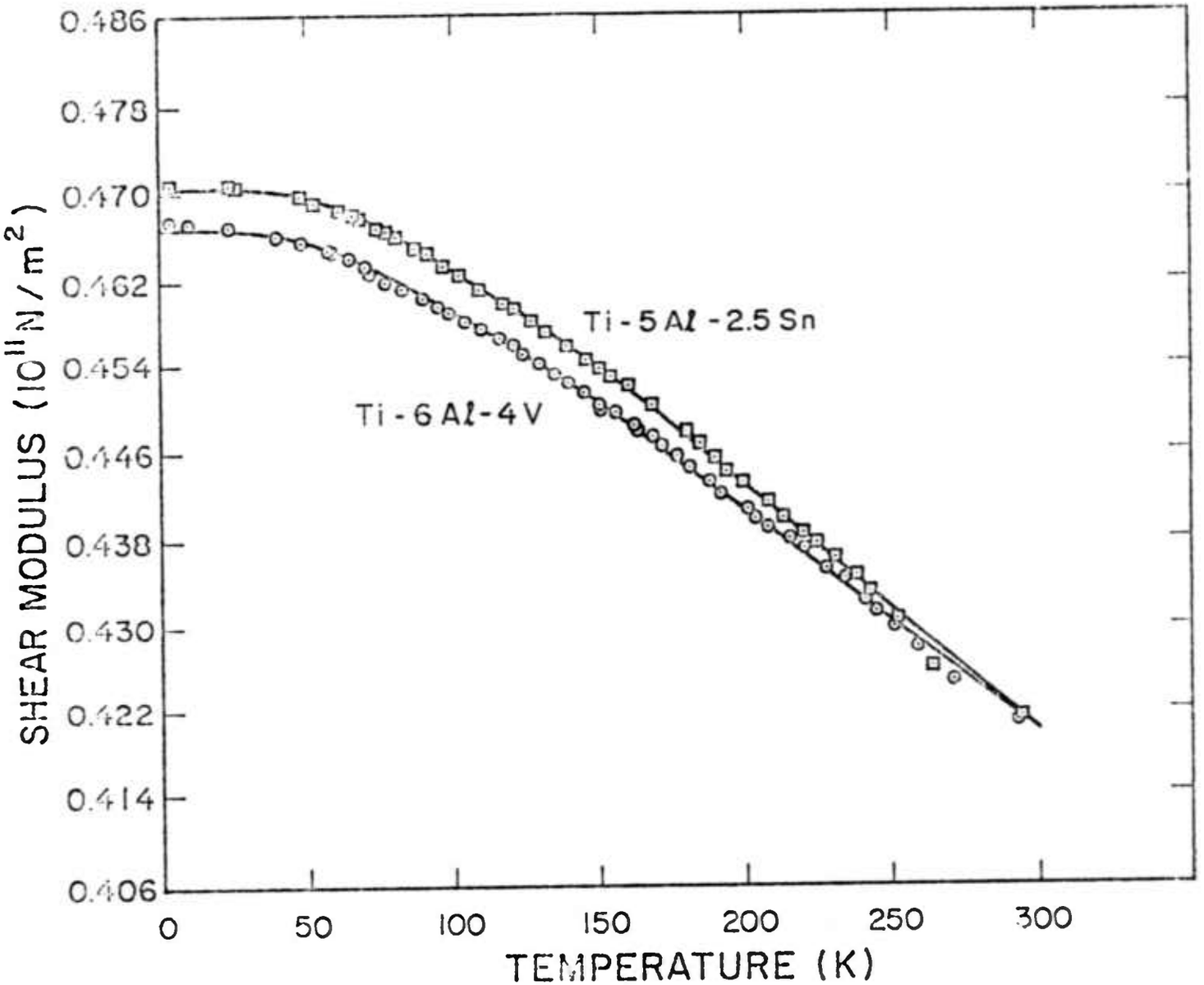

Fig. 3 Transverse or shear modulus $C_t = G = \rho v_t^2$ of two titanium alloys.

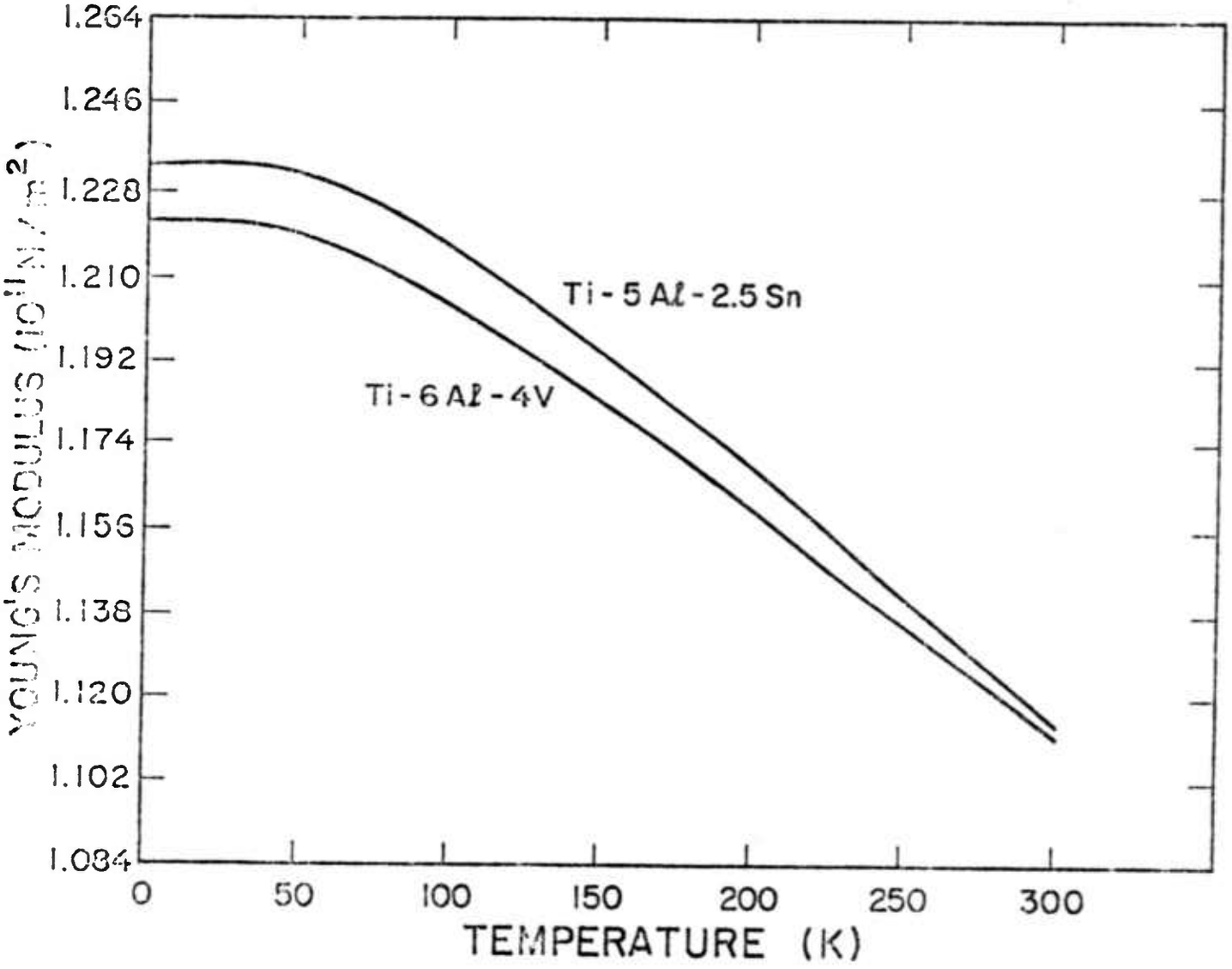

Fig. 4 Young's modulus of two titanium alloys.

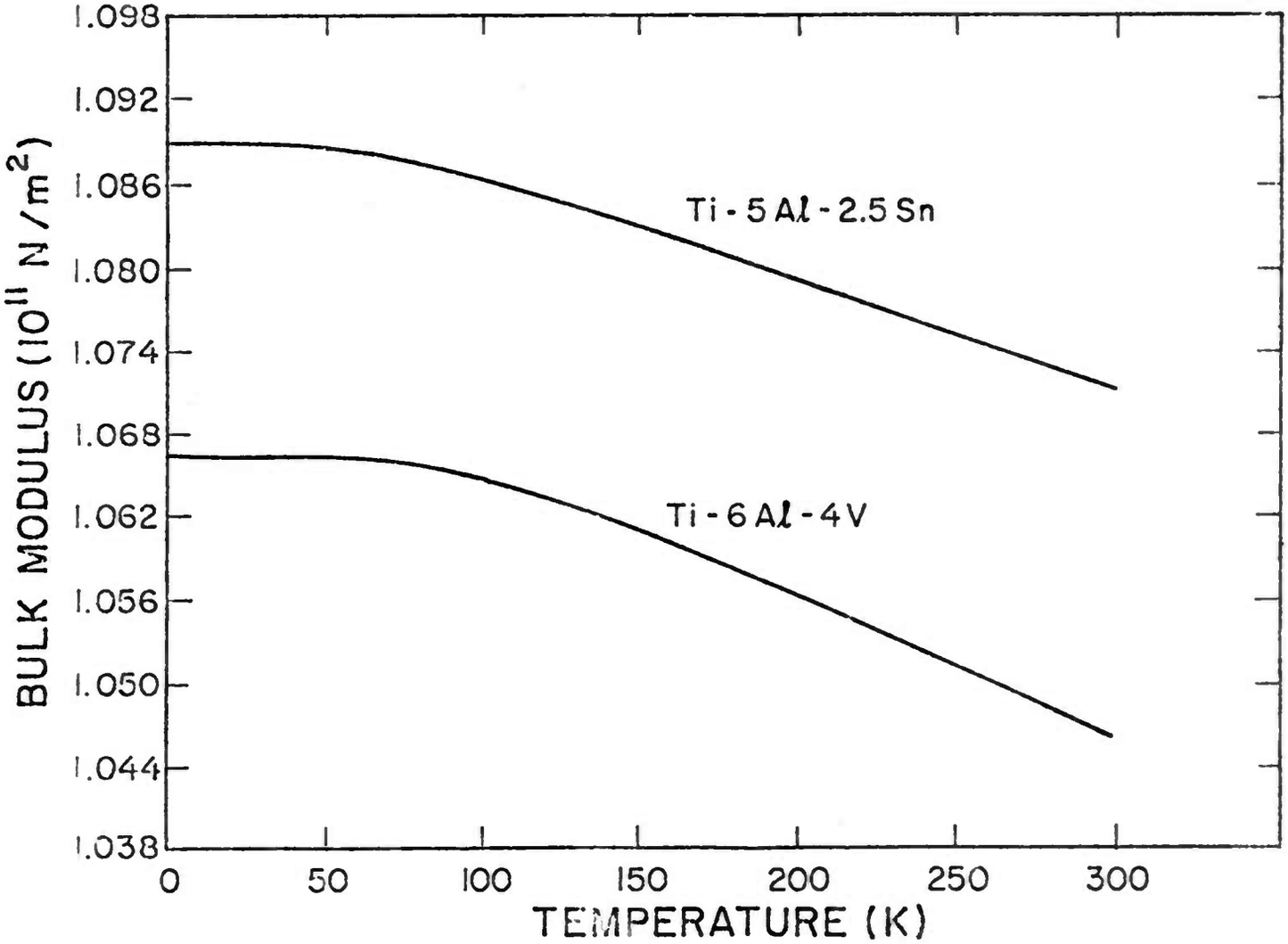

Fig. 5 Bulk modulus (reciprocal compressibility) of two titanium alloys.

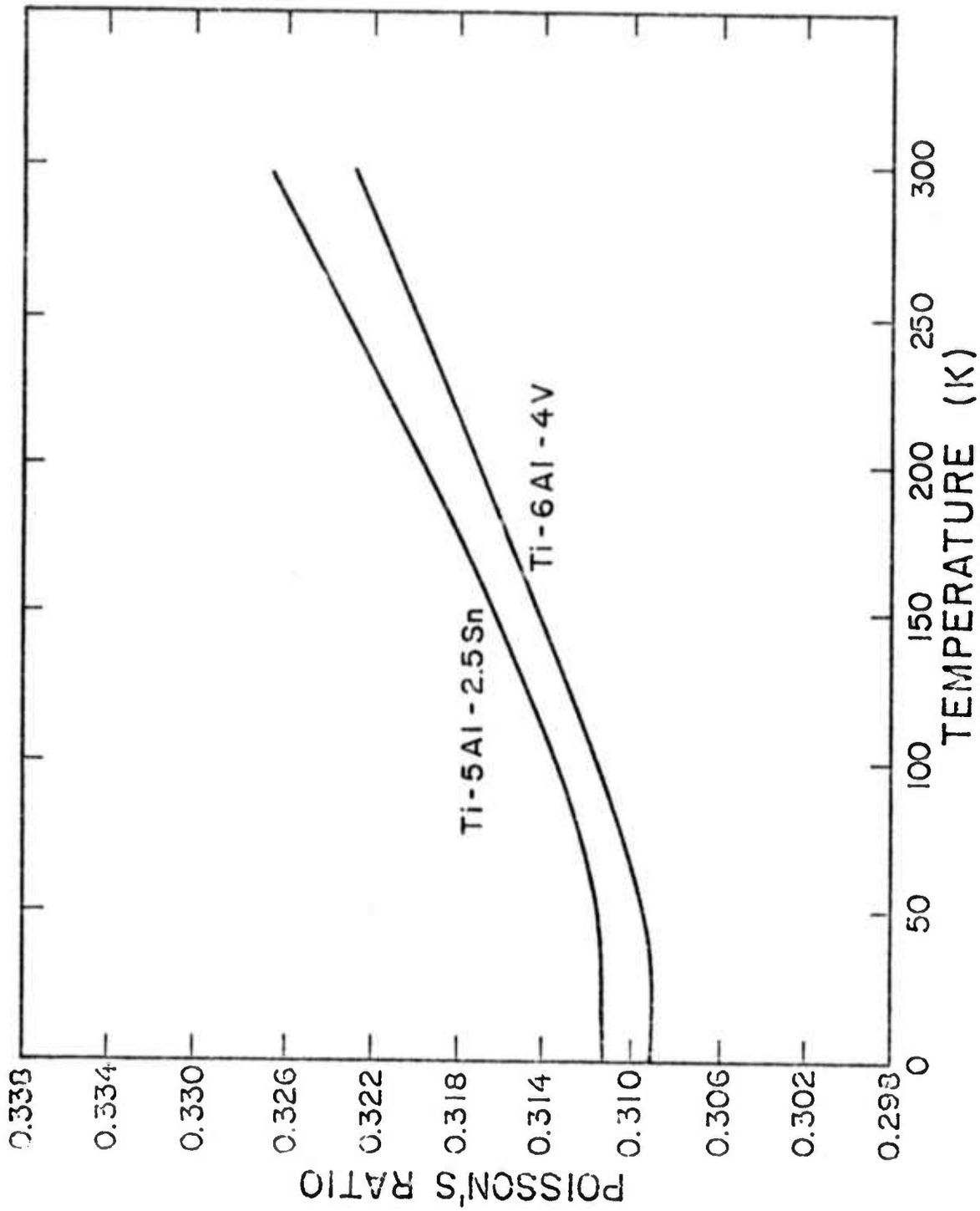

Fig. 6 Poisson's ratio of two titanium alloys.

Dynamic Low-temperature Elastic Properties of Two Austenitic Nickel-Chromium-Iron Alloys*

E. R. Naimon**, H. M. Ledbetter, and W. F. Weston**

Cryogenics Division, Institute for Basic Standards,
National Bureau of Standards, Boulder, Colorado 80302

Abstract

The zero-magnetic-field low-temperature elastic properties of two polycrystalline nickel-chromium-iron alloys were determined ultrasonically between 4 and 300 K. Results are given for: longitudinal and transverse sound velocities, Young's modulus, shear modulus, bulk modulus, Poisson's ratio, and elastic Debye temperature. Effects of alloying are discussed.

Key words: Bulk modulus; compressibility; Debye temperature; elastic constant; nickel-chromium-iron alloys; Poisson's ratio; shear modulus; sound velocity; Young's modulus.

184<

---

* Contribution of NBS, not subject to copyright.

** NRC-NBS Postdoctoral Research Associate, 1973-4.

Introduction

Elastic properties of metals at low temperatures have twofold interest. First, the absence of thermal vibrations permits a determination of intrinsic lattice properties; such information is essential for understanding the basic aspects of mechanical deformation, for example. Second, low-temperature elastic properties are essential design parameters for cryogenic structures.

Austenitic nickel-base alloys containing chromium and iron are standard engineering materials. They have high heat resistance, high corrosion resistance, good high-temperature strength, and can be readily fabricated into structures. Many of these materials also have low-temperature applications. In particular, Inconel* 600 has exceptional cryogenic mechanical properties. Its strength increases with decreasing temperatures, and its ductility and toughness are preserved. Inconel X-750 (formerly Inconel X) is similar to Inconel 600, but it contains small amounts of aluminum, titanium, and niobium. Aluminum and titanium make precipitation hardening possible by forming Ni_3 (Al, Ti) by suitable thermal treatment. (Inconel 600 is usually hardened by low-temperature mechanical deformation.) Niobium further stiffens the matrix and stabilizes the carbides.

The zero-magnetic-field dynamic low-temperature elastic properties of Inconel 600 and Inconel X-750 are reported here. A pulse-superposition method was used to determine ultrasonic wave velocities in specimens prepared from as-received commercial bar stock.

---

* Tradenames are used to characterize materials; they are not NBS endorsements of particular products.

Experimental

Inconel 600 and X-750 alloys were obtained from commercial sources in the form of about 3-in (7.6-cm) and 4-in (10.2-cm) diameter rods, respectively. Specimens 3/8-in (1-cm) long were prepared by grinding. Opposite faces were flat and parallel within 100 x 10^{-6} in. (2.5 μ m). Chemical compositions (obtained from mill analyses), hardness numbers, microstructures, and mass densities are given in Table 1. Hardnesses, microstructures, and grain sizes were determined by standard metallurgical methods. Mass density was determined by Archimedes' method using distilled water as a standard.

A pulse-superposition method[1,2] was used to determine all ultrasonic velocities except the shear mode of Inconel X-750. This particular mode was highly attenuated, and for its measurement the standard pulse-echo technique was used.

Quartz transducers (10 mHz) were bonded to the specimens with phenyl salicylate for room-temperature measurements and with a stopcock grease for lower temperatures. Occasional failure of the bond at very low temperatures resulted in using a silicone fluid (viscosity = 200,000 cP at 25°C) for bonding.

The specimen holder is shown schematically in Fig. 1. The holder was placed in the ullage of a helium dewar and lowered stepwise to achieve cooling. Temperatures were monitored with a chromel-constantan thermocouple contacting the specimen.

No thermal contraction corrections were made for the sound velocities or for the elastic constants; for nickel alloys this introduces a maximum error in the velocity of about 0.2 percent. Bond corrections were not

made; this error is insignificant for the purposes of the present study. Maximum uncertainties in the velocity measurements are estimated to be about one percent.

For Inconel X-750, velocity measurements were made over the range 40-300 K. Below 40 K, the attenuation was too high for both longitudinal and transverse modes. However, little change is expected in the velocities from 40-0 K and theoretical curves fit to the data points (as explained in the next section) should give accurate low-temperature values. For Inconel 600, velocity measurements were made from 4-300 K.

Results

Longitudinal and transverse modulus are shown in Figs. 2 and 3. The longitudinal modulus is given by

$$C_\ell = \rho v_\ell^2 = B + \frac{4}{3} G \qquad (1)$$

and the transverse modulus is given by

$$C_t = \rho v_t^2 = G. \qquad (2)$$

Here v_ℓ and v_t are the longitudinal and transverse sound-wave velocities, ρ is the mass density, B is the bulk modulus, and G is the shear modulus.

Temperature dependences of both C_ℓ and C_t were fit to a semi-theoretical relationship suggested by Varshni[3]:

$$C = C^o - s/(e^{t/T} - 1), \qquad (3)$$

where C^o, s, and t are adjustable parameters and T is temperature. The value of C at T = 0 K is C^o, and -s/t is the high-temperature limit of dC/dT. By invoking an Einstein oscillator model of solids, it can be

shown (in the absence of electronic effects) that t is the Einstein characteristic temperature. Parameters C^o, s, and t for Inconels 600 and X-750 are given in Table 2. Room-temperature values of the temperature coefficients of the elastic moduli are given in Table 3.

Curves in Figs. 2 and 3 are plots of eqn. (3) determined by an unweighted least-squares fit of the data. For Inconel 600, average percentage differences between measured and curve values are 0.05% for both the longitudinal and transverse moduli. For Inconel X-750, the average percentage differences between measured and curve values are 0.04% and 0.18% for the longitudinal and transverse moduli, respectively. The comparatively large error for the transverse modulus of Inconel X-750 was due to a relatively poor echo pattern.

While polycrystalline aggregates (quasi-isotropic solids) have only two independent elastic constants, several constants are commonly used for various applications. The four most common are the bulk modulus B, Young's modulus E, the shear modulus G, and Poisson's ratio ν . The relationships among these are:

$$\frac{1}{E} = \frac{1}{3G} + \frac{1}{9B} \tag{4}$$

and

$$\nu = \frac{E}{2G} - 1. \tag{5}$$

These elastic constants were calculated from the moduli shown in Figs. 2 and 3 by the relationships:

$$E = 3C_t (C_\ell - \tfrac{4}{3} C_t)/(C_\ell - C_t), \tag{6}$$

$$B = C_\ell - \tfrac{4}{3} C_t, \tag{7}$$

and

$$\nu = \frac{1}{2} (C_\ell - 2C_t)/(C_\ell - C_t). \tag{8}$$

The constants E, B, and ν are shown in Figs. 4-6.

It is of interest to calculate the elastic Debye temperature θ for the two alloys. This fundamental parameter is important in the lattice properties of solids and is related to the elastic wave velocities by[4]

$$\theta = K \langle v \rangle, \tag{9}$$

where

$$K = \frac{h}{K} \left(\frac{3N\rho}{4\pi A}\right)^{1/3}. \tag{10}$$

Here h is Planck's constant, k is Boltzmann's constant, N is Avogadro's constant, ρ is the mass density, and A is the atomic weight. The average velocity is given by

$$\langle v \rangle = \left(\frac{v_\ell^{-3} + 2v_t^{-3}}{3}\right)^{-1/3}. \tag{11}$$

The Debye temperature of each alloy at T = 0 K, and also of nickel, is given in Table 4.

Discussion

The elastic properties of both Inconel 600 and Inconel X-750 behave regularly with respect to temperature. The elastic moduli (C_ℓ, C_t = G, B, E) decrease with increasing temperature, show a relative flatness at low temperatures, achieve zero slope at T = 0 K, and approach linear behavior at high temperatures. Poisson's ratio also behaves regularly, having a positive temperature coefficient.

189<

Assuming that the specimens studied are representative of the two alloys, then conclusions concerning their relative elastic behavior can be drawn. Not surprisingly, as shown in Figs. 2-6 and in Tables 2 and 3, for most practical purposes the two alloys are elastically identical. Thus, additions of small amounts of aluminum, titanium, and niobium have little effect on the elastic properties of nickel alloys containing about 15 percent chromium and about 7 percent iron.

Very little elastic data exist for these alloys[5-11], especially Inconel 600. Most information has appeared in engineering reports and is summarized in refs. 7-11. For comparison the room-temperature values of E, G, B, and ν are given in Table 5. Generally good agreement is observed between previous and present results.

The elastic moduli of both alloys range from several percent lower (E, B) than polycrystalline nickel[12] to about the same (G,ν) as polycrystalline nickel. This also holds if the elastic moduli of the two alloys are compared with the quasi-isotropic moduli obtained from a Voigt-Reuss-Hill average of the single-crystal data[13], although there is some discrepancy for the value of G obtained by this method[14]. The elastic Debye temperatures of the alloys are also within 2% of the value calculated from the single-crystal elastic data of nickel.

It is emphasized that the data reported here are dynamic (adiabatic) rather than static (isothermal) and apply to rapid, rather than slow, loading. In most cases the differences between adiabatic and isothermal elastic constants are small. Conversion formulas are given in Landau and Lifshitz[15], for example. For nickel at room temperature:

$$(E_s - E_T)/E_s = 0.003,\ (B_s\ B_T)/B_s = 0.022,$$

$$(\nu_s - \nu_T)/\nu_s = 0.012,\ \text{and}\ (G_s - G_T)/G_s \equiv 0, \qquad (12)$$

where subscripts S and T denote adiabatic and isothermal, respectively.

Acknowledgment

This work was supported in part by the Advanced Research Projects Agency.

191<

References

1. H. J. McSkimin, J. Acoust. Soc. Amer., 33 (1961) 12.

2. H. J. McSkimin, and P. Andreatch, J. Acoust. Soc. Amer., 34, (1962) 609.

3. Y. P. Varshni, Phys. Rev., B2 (1970) 3952.

4. P. Debye, Ann. Phys. (Leipz.), 39 (1912) 789.

5. H. C. Burnett, unpublished results (1956).

6. W. H. Hill, K. O. Shimmin, and B. A. Wilcox, Proc. ASTM, 61 (1961) 890.

7. International Nickel Co., Report on Inconel Alloy 600 (1973).

8. International Nickel Co., Report on Inconel Alloy X-750 (1970).

9. NERVA Program Materials Properties Data Book, Vol. 1A, Nickel Base Alloys (Aerojet Nuclear Systems, Sacramento, Calif., 1970).

10. Cryogenic Materials Data Handbook, AFML Rep. No. ML-TDR-64-280 (PB 171809, revised) (Aug. 1964).

11. Aerospace Structural Metals Handbook, Vol. II, AFML Rep. No. ASD-TDR-63-741 (Mar. 1966).

12. H. M. Ledbetter, and R. P. Reed, J. Phys. Chem. Ref. Data, Vol. 2, No. 3, (1973).

13. S. G. Epstein, and O. N. Carlson, Acta Met., 13 (1965) 487.

14. G. Simmons, and H. Wang, Single Crystal Elastic Constants and Calculated Aggregate Properties: A Handbook, (M.I.T. Press, Cambridge, 1971) pp. 223-227.

15. L. D. Landau, and E. M. Lifshitz, Theory of Elasticity (Pergamon, London, 1959) p. 17.

16. M. Dixon, F. E. Hoare, T. M. Holden, and D. E. Moody, Proc. Roy. Soc. 285 (1965) 561.

192<

List of Tables

List of Figures

193<

Table 1. Compositions and Properties of Alloys

Alloy	Chemical Composition, Mill Analyses (wt. pct.)											Hardness (DPH No., 1 kg load)	Mass Density at 294 K (g/cm^3)	Condition
	Ni	Cr	Mn	Fe	S	Si	Cu	C	Al	Ti	Cb			
Inconel 600	Bal	15.8	0.20	7.20	0.007	0.20	0.10	0.04	-	-		179	8.415	As received; hot rolled annealed
Inconel X-750	Bal	15.4	0.60	7.00	0.01	0.30	-	0.05	0.90	02.50	0.70	330	8.238	As received; hot rolled 1625°F (1158 K) and aged

Table 2. Parameters in Equation 3

Alloy	Mode	C^o (10^{11} N/m^2)	S (10^{11} N/m^2)	t (K)
Inconel 600	ρv_l^2	2.909	0.107	203.1
	ρv_t^2	0.828	0.063	246.0
Inconel X-750	ρv_l^2	2.920	0.105	165.9
	ρv_t^2	0.846	0.120	315.8

195<

Table 3. Logarithmic temperature derivatives of elastic constants at room temperature (10^{-4} K^{-1})

Material	$\frac{1}{B}\frac{dB}{dT}$	$\frac{1}{E}\frac{dE}{dT}$	$\frac{1}{G}\frac{dG}{dT}$	$\frac{1}{\nu}\frac{d\nu}{dT}$
Inconel 600	-1.07	-2.82	-3.08	1.10
Inconel X-750	-0.89	-3.94	-4.40	1.97
Nickel*	-1.56	-4.16	-4.53	1.72

* Ref. 12

196<

Table 4. Elastic Debye temperatures at T = 0 K

Material	θ (K)
Inconel 600	464.9
Inconel X-750	473.5
Nickel*	476.2

* Ref. 16

Table 5. Room-temperature elastic constants of Inconel 600 and Inconel X-750; units of 10^{11} N/m^2 except ν (dimensionless)

Source	Inconel 600				Inconel X-750			
	E	G	B	ν	E	G	B	ν
Present	2.036	0.780	1.760	0.307	2.040	0.784	1.736	0.304
Ref. 5	-	-	-	-	-	0.789	-	-
Ref. 6	-	-	-	-	2.144	-	-	-
Ref. 7-8	2.11	0.75	-	-	2.11	0.75	-	0.29
Ref. 9	-	-	-	-	2.075	0.714	-	0.29
Ref. 10	-	-	-	-	2.041	0.766-0.813	-	-
Ref. 11	2.109	-	-	-	2.109	0.749	-	-

198<

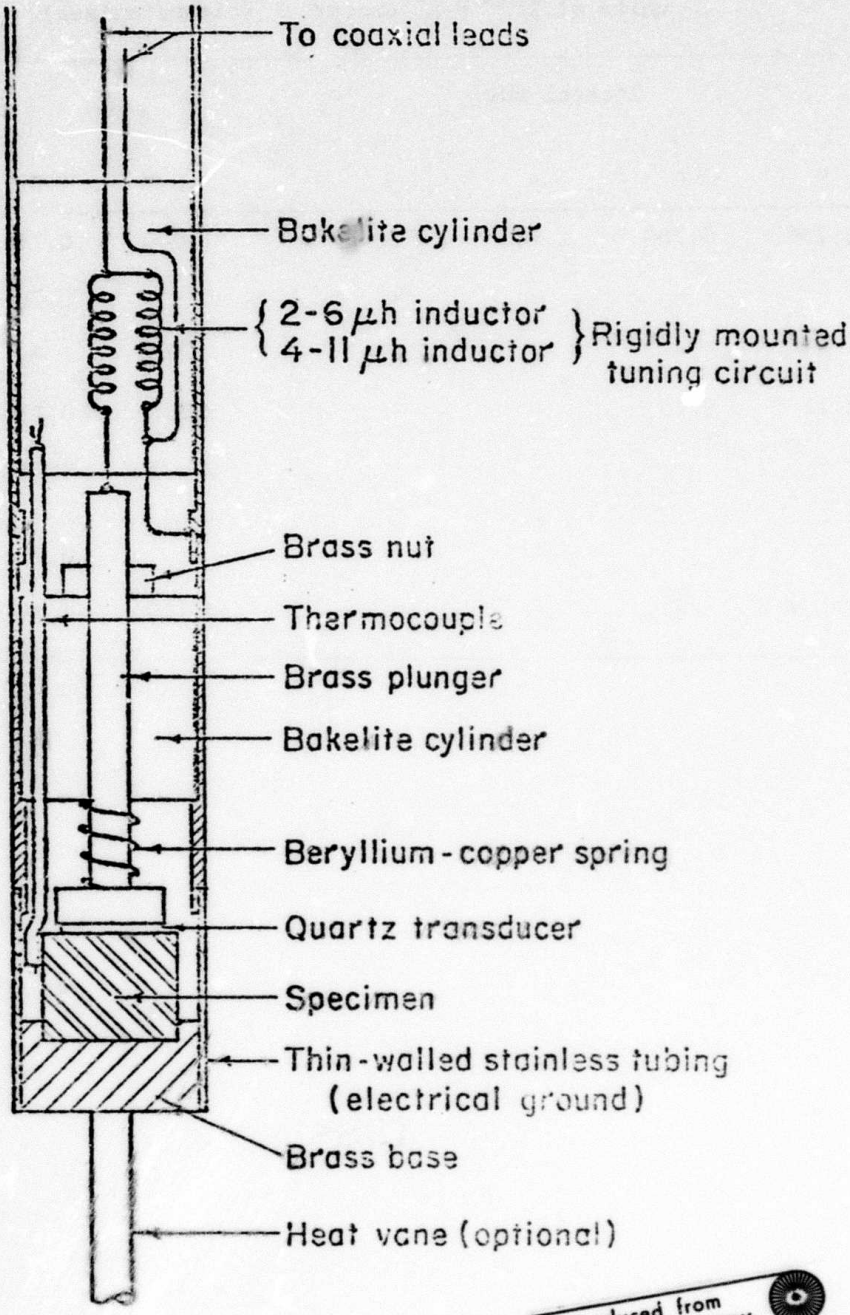

Fig. 1 Specimen holder.

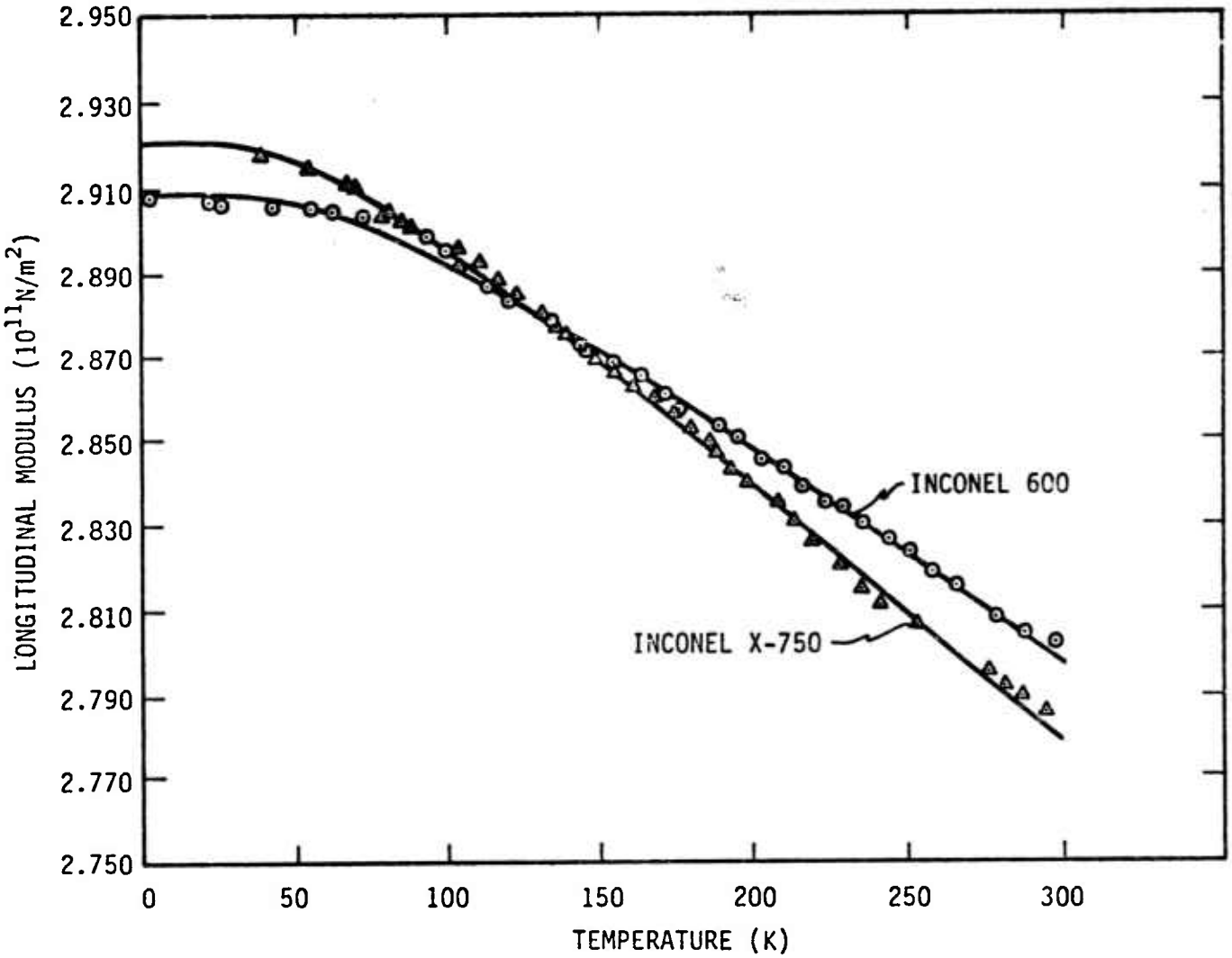

Fig. 2. Longitudinal modulus $C_\ell = \rho v_\ell^2$ of two nickel-chromium-iron alloys.

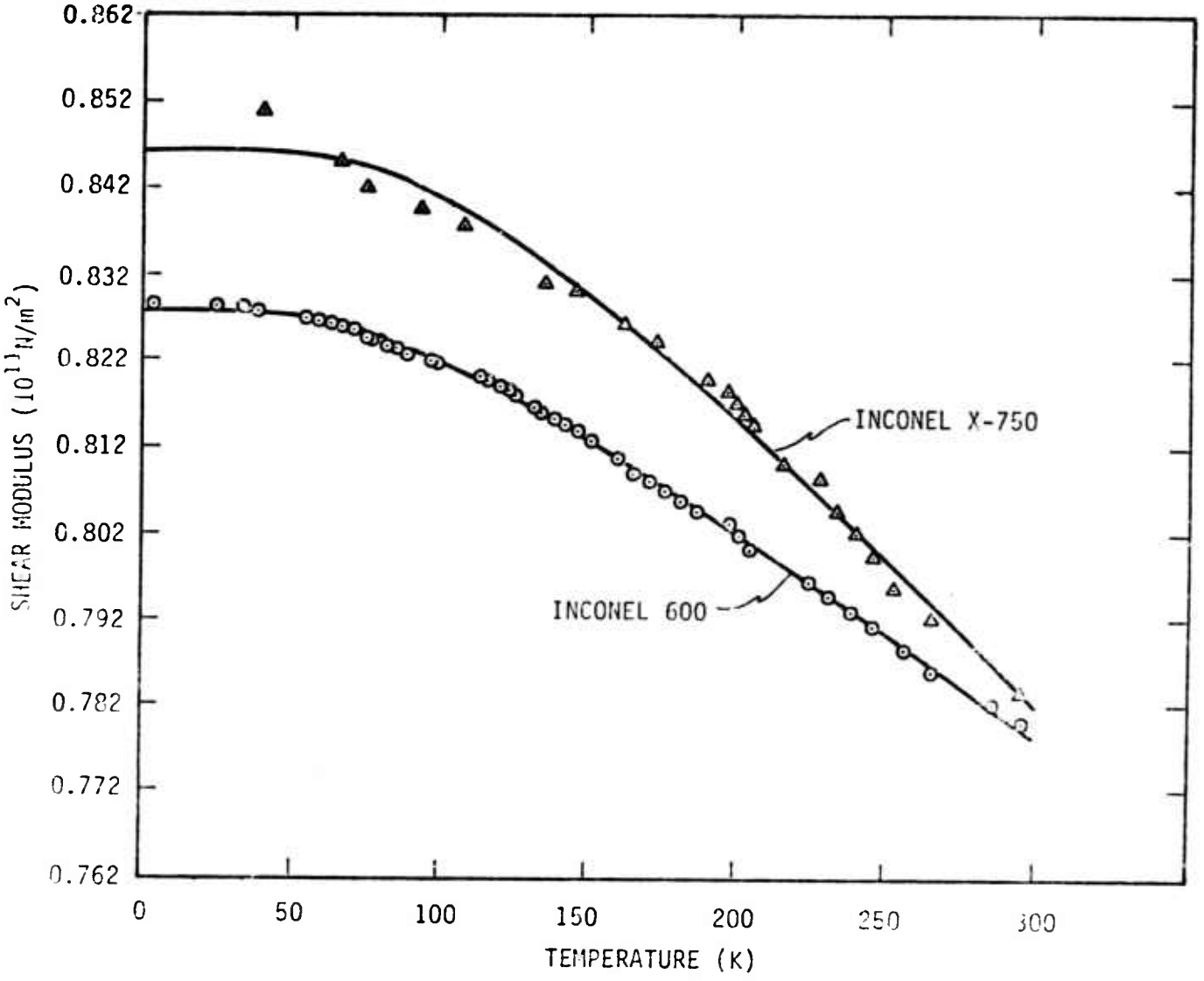

Fig. 3. Transverse or shear modulus $C_t = \rho v_t^2 = G$ of two nickel-chromium-iron alloys.

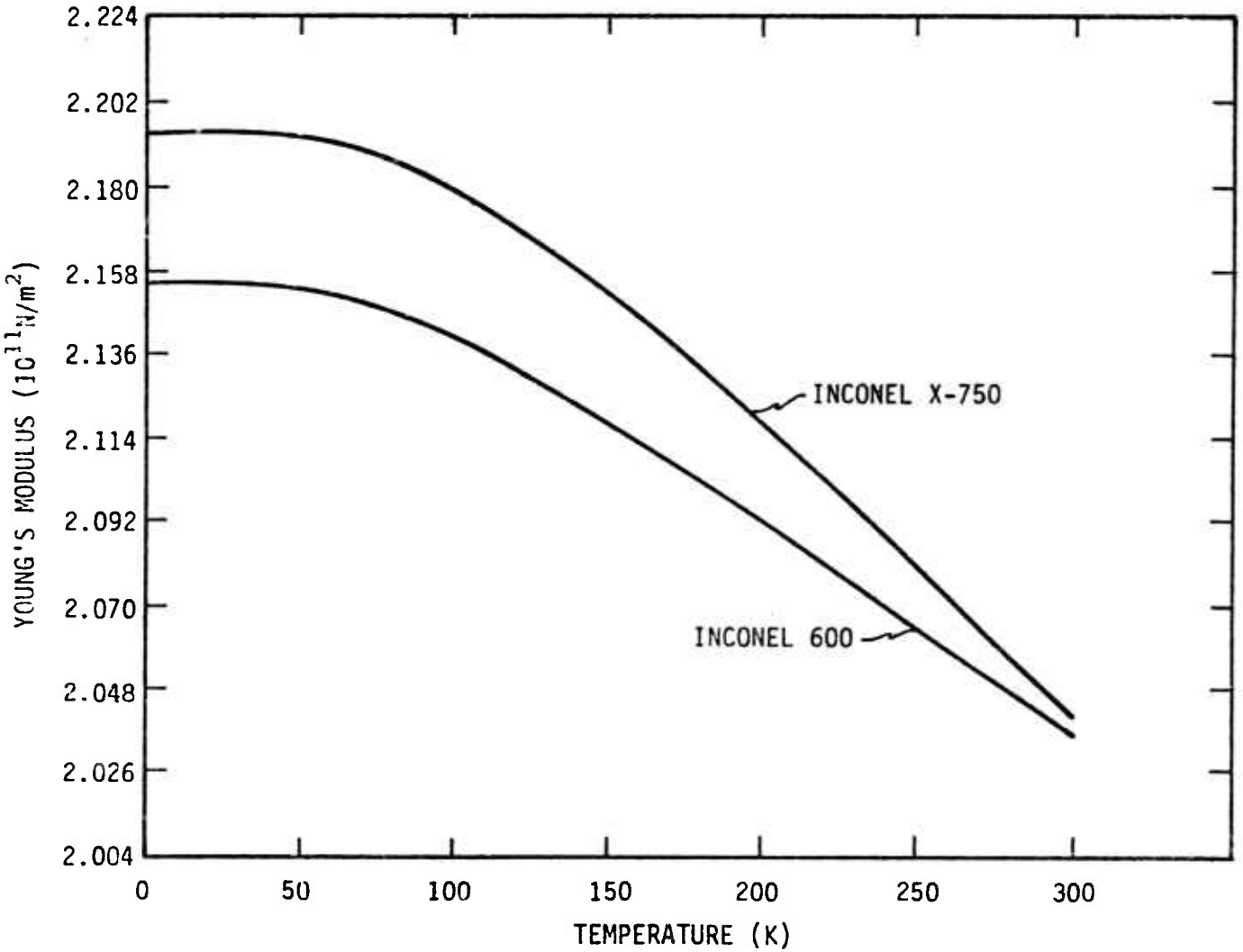

Fig. 4. Young's modulus of two nickel-chromium-iron alloys.

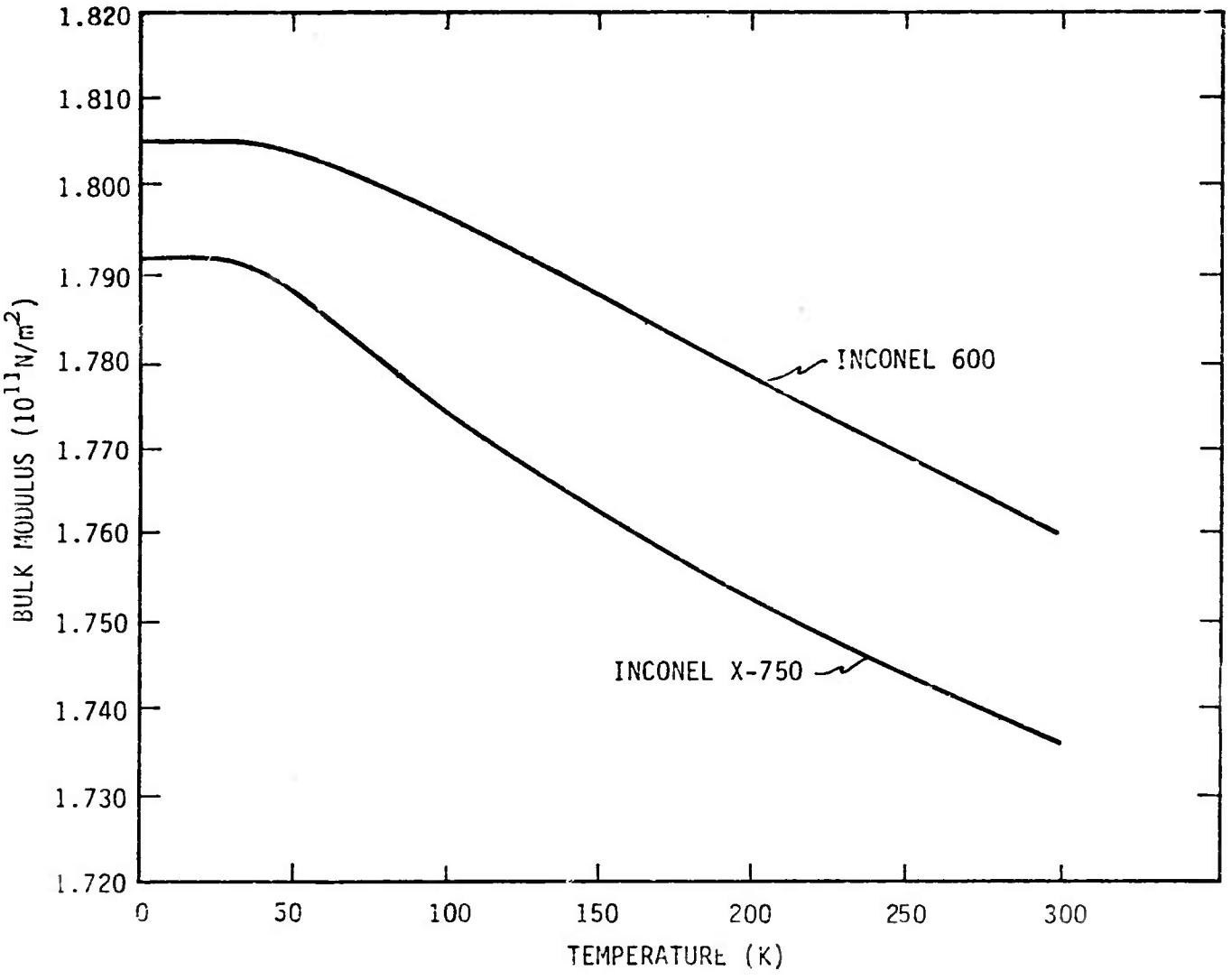

Fig. 5. Bulk modulus (reciprocal compressibility) of two nickel-chromium-iron alloys.

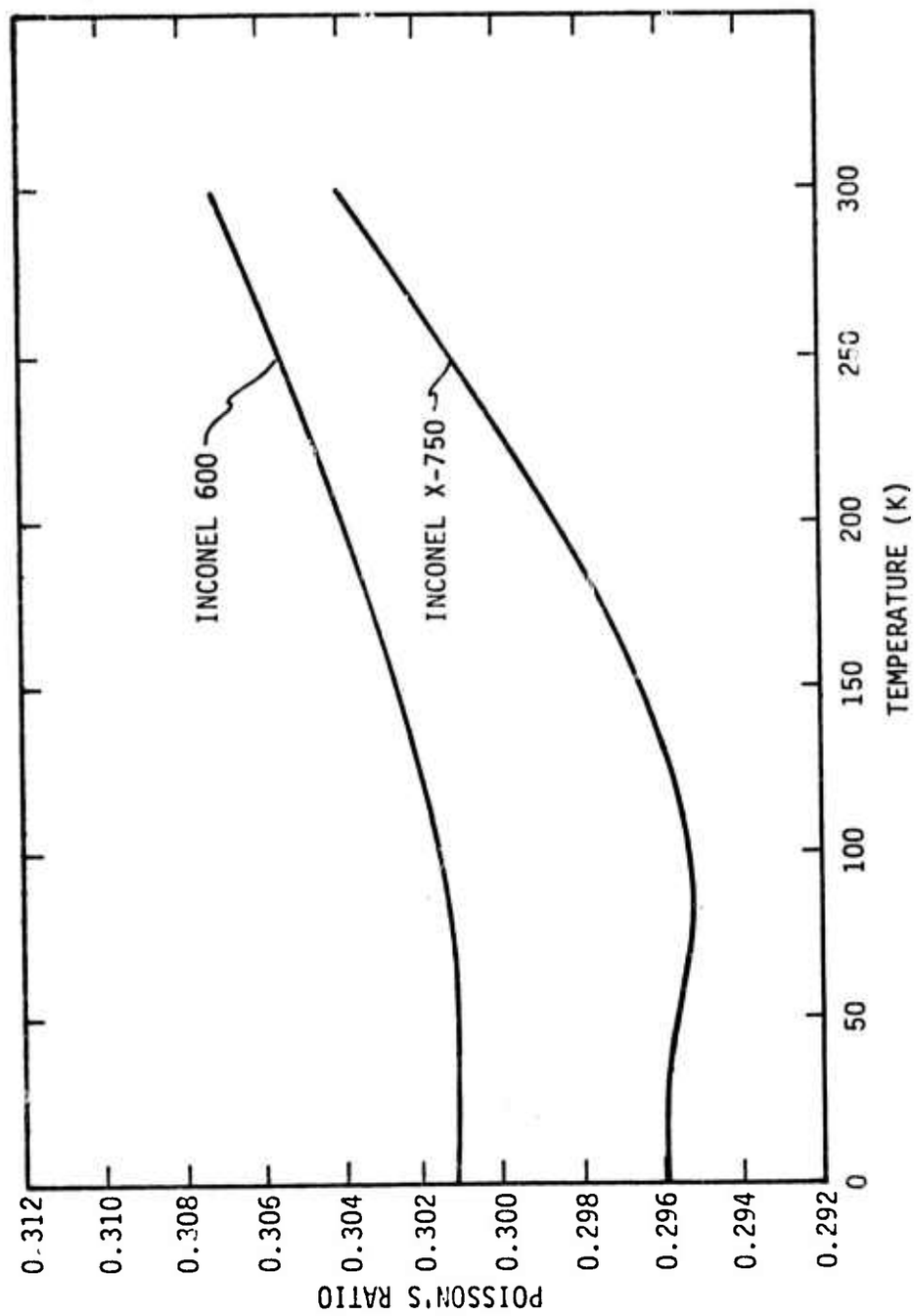

Fig. 6. Poisson's ratio of two nickel-chromium-iron alloys.

Elastic Properties of Four Stainless Steel Alloys

Elastic Properties of Four Aluminum Alloys

The following ten figures are unaccompanied by text and give the elastic constants

Longitudinal modulus

Shear modulus

Young's modulus

Bulk Modulus

Poisson's ratio

for

Stainless steels 304, 310, 316, A286

and

Aluminum alloys 1100, 5083, 7005, and 7006.

The preceding two manuscripts for titanium alloys and nickel-chromium-iron alloys give experimental procedures, etc. that largely apply to the stainless steels and the aluminum alloys.

205<

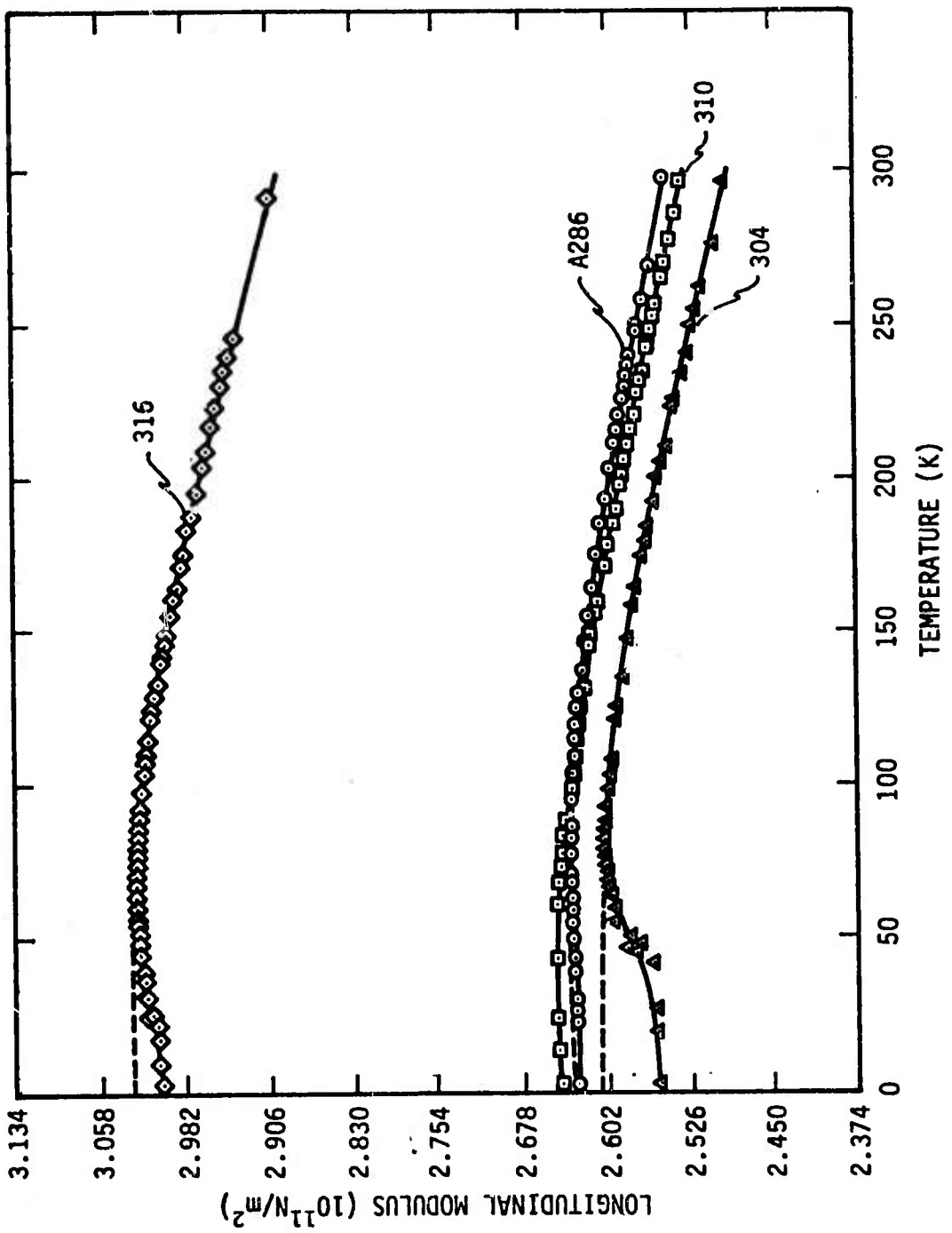
316
A286
310
304
LONGITUDINAL MODULUS ($10^{11}N/m^2$)
TEMPERATURE (K)
3.134
3.058
2.982
2.906
2.830
2.754
2.678
2.602
2.526
2.450
2.374
0
50
100
150
200
250
300

206<

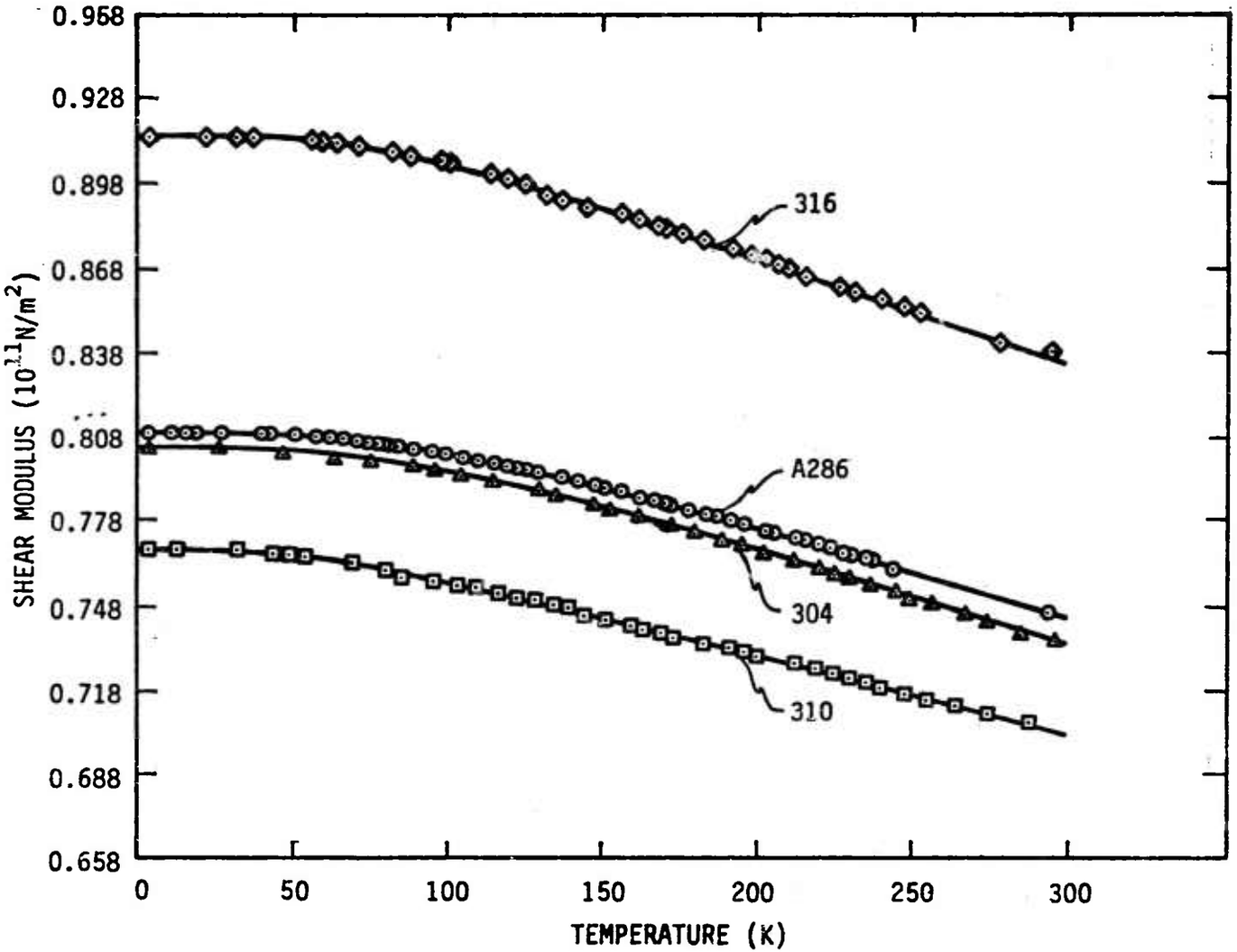
0.968
0.928
0.898
0.868
0.838
0.808
0.778
0.748
0.718
0.688
0.658
SHEAR MODULUS (10^{11}N/m^2)
0
50
100
150
200
250
300
TEMPERATURE (K)
316
A286
304
310

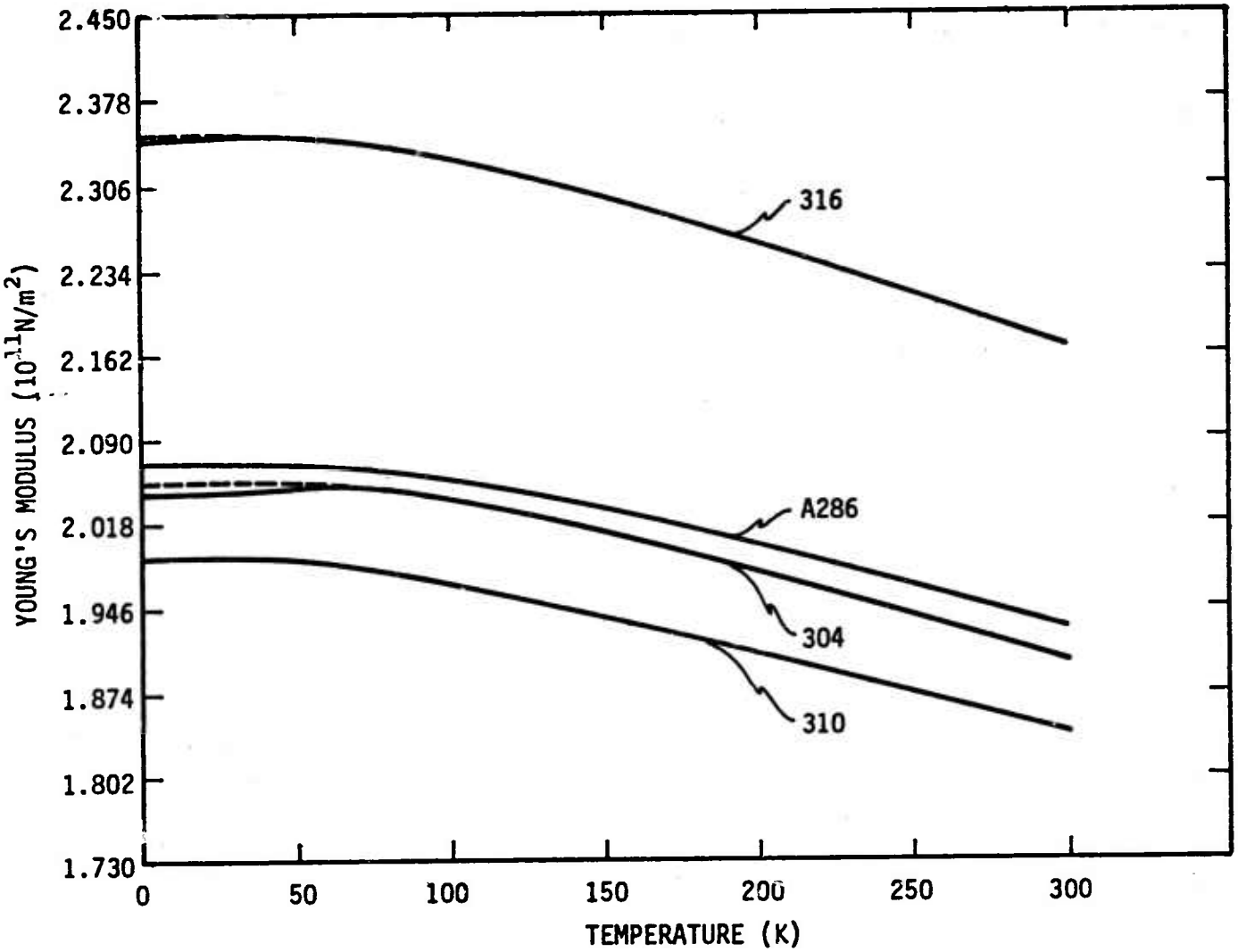
2.450
2.378
2.306
2.234
2.162
2.090
2.018
1.946
1.874
1.802
1.730
YOUNG'S MODULUS (10^{11}N/m^2)
0
50
100
150
200
250
300
TEMPERATURE (K)
316
A286
304
310

208<

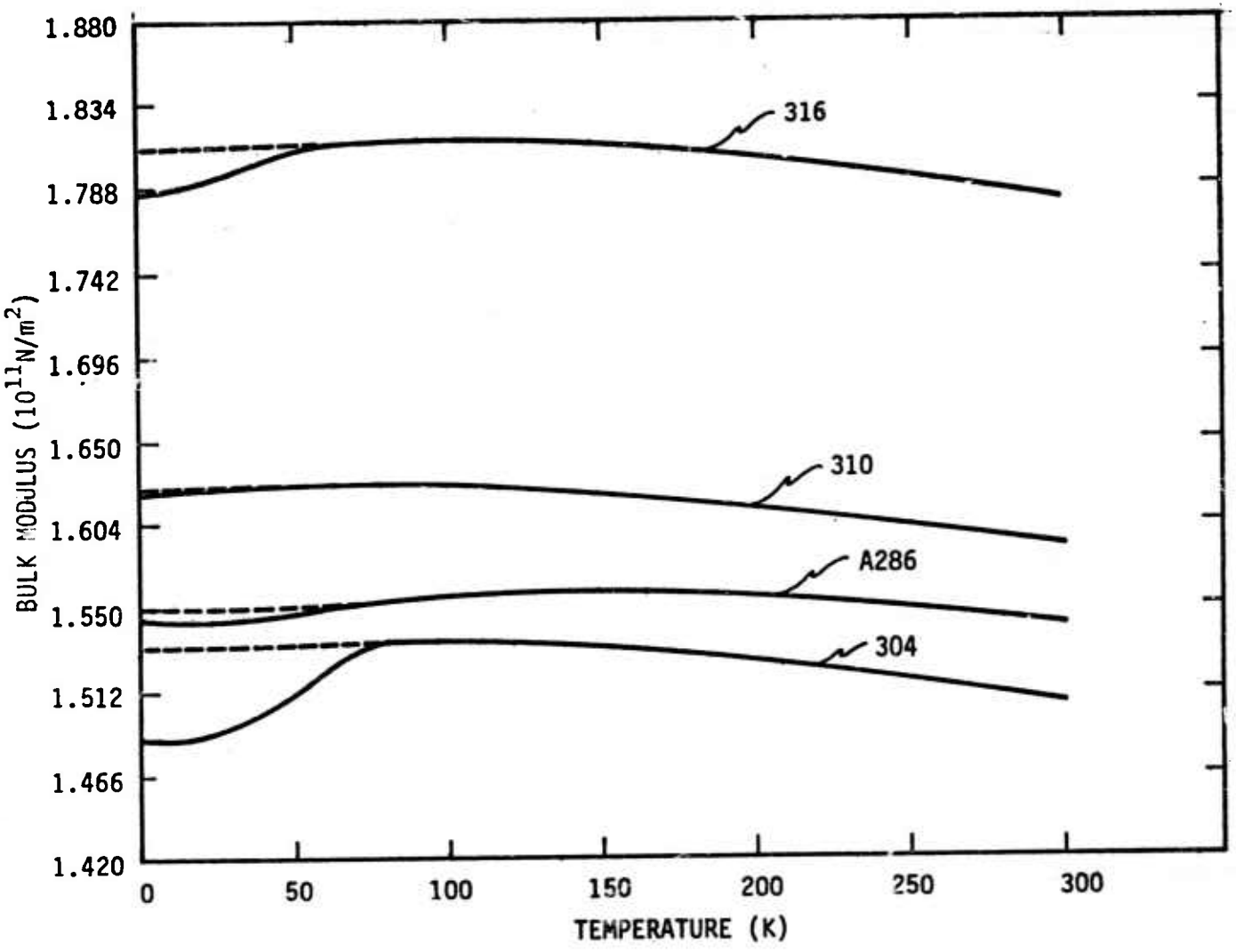
1.880
1.834
1.788
1.742
1.696
1.650
1.604
1.550
1.512
1.466
1.420
BULK MODULUS (10^{11}N/m^2)
316
310
A286
304
0
50
100
150
200
250
300
TEMPERATURE (K)

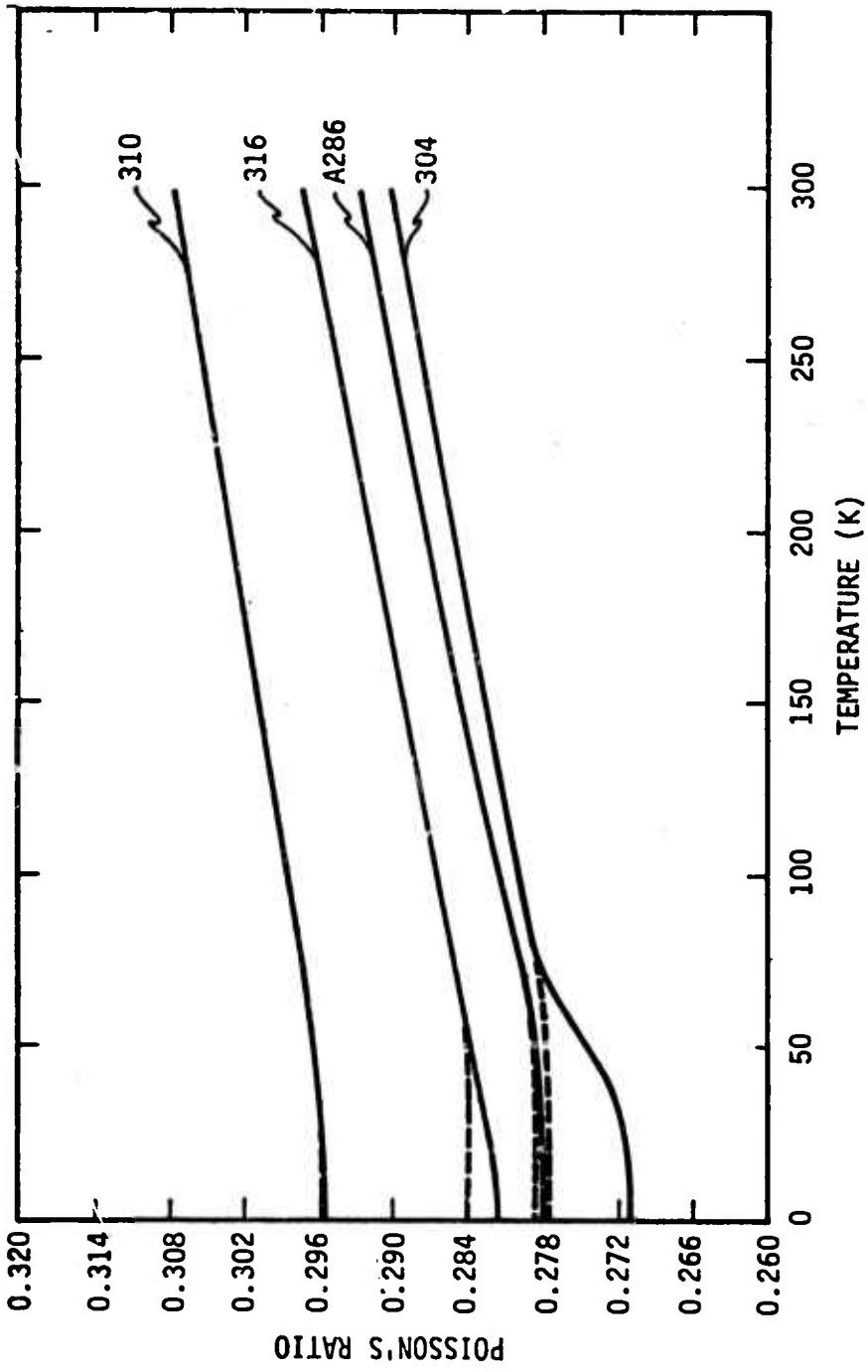
310
316
A286
304
0.320
0.314
0.308
0.302
0.296
0.290
0.284
0.278
0.272
0.266
0.260
POISSON'S RATIO
0
50
100
150
200
250
300
TEMPERATURE (K)

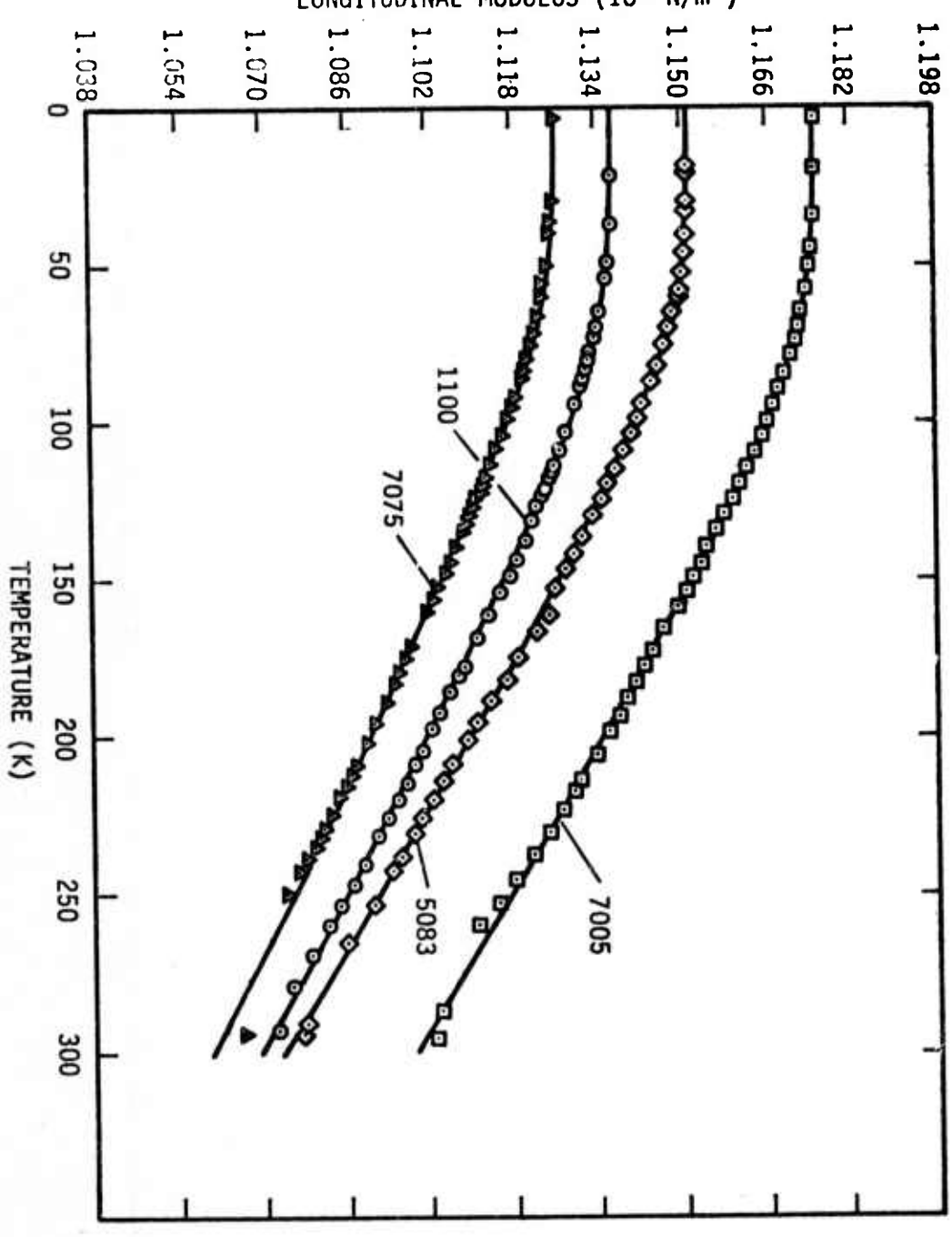
LONGITUDINAL MODULUS (10^{11}N/m^2)
1.038
1.054
1.070
1.086
1.102
1.118
1.134
1.150
1.166
1.182
1.198
0
50
100
150
200
250
300
TEMPERATURE (K)
1100
7075
5083
7005

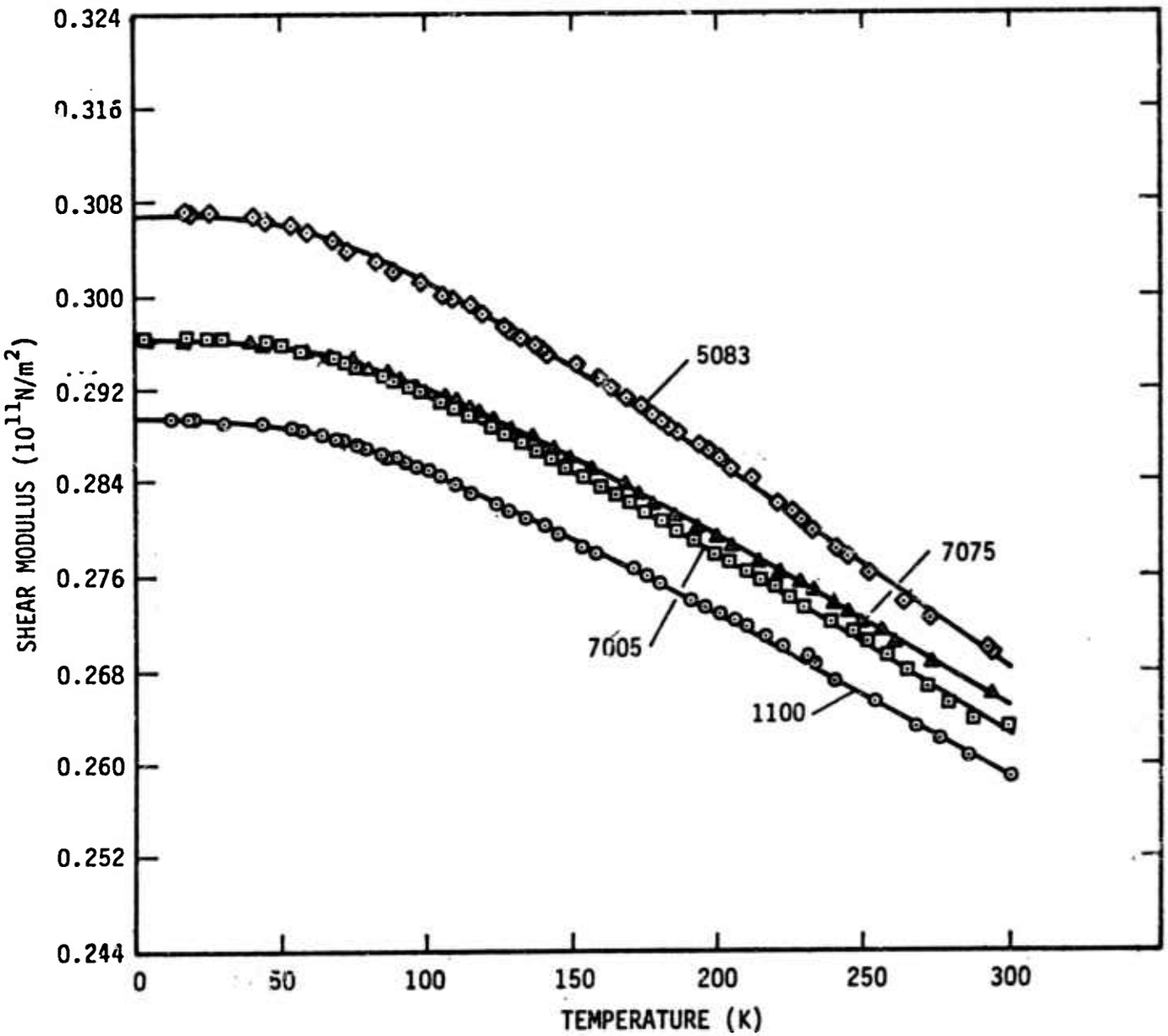
0.324
0.316
0.308
0.300
0.292
0.284
0.276
0.268
0.260
0.252
0.244
SHEAR MODULUS (10^{11}N/m^2)
0
50
100
150
200
250
300
TEMPERATURE (K)
5083
7075
7005
1100

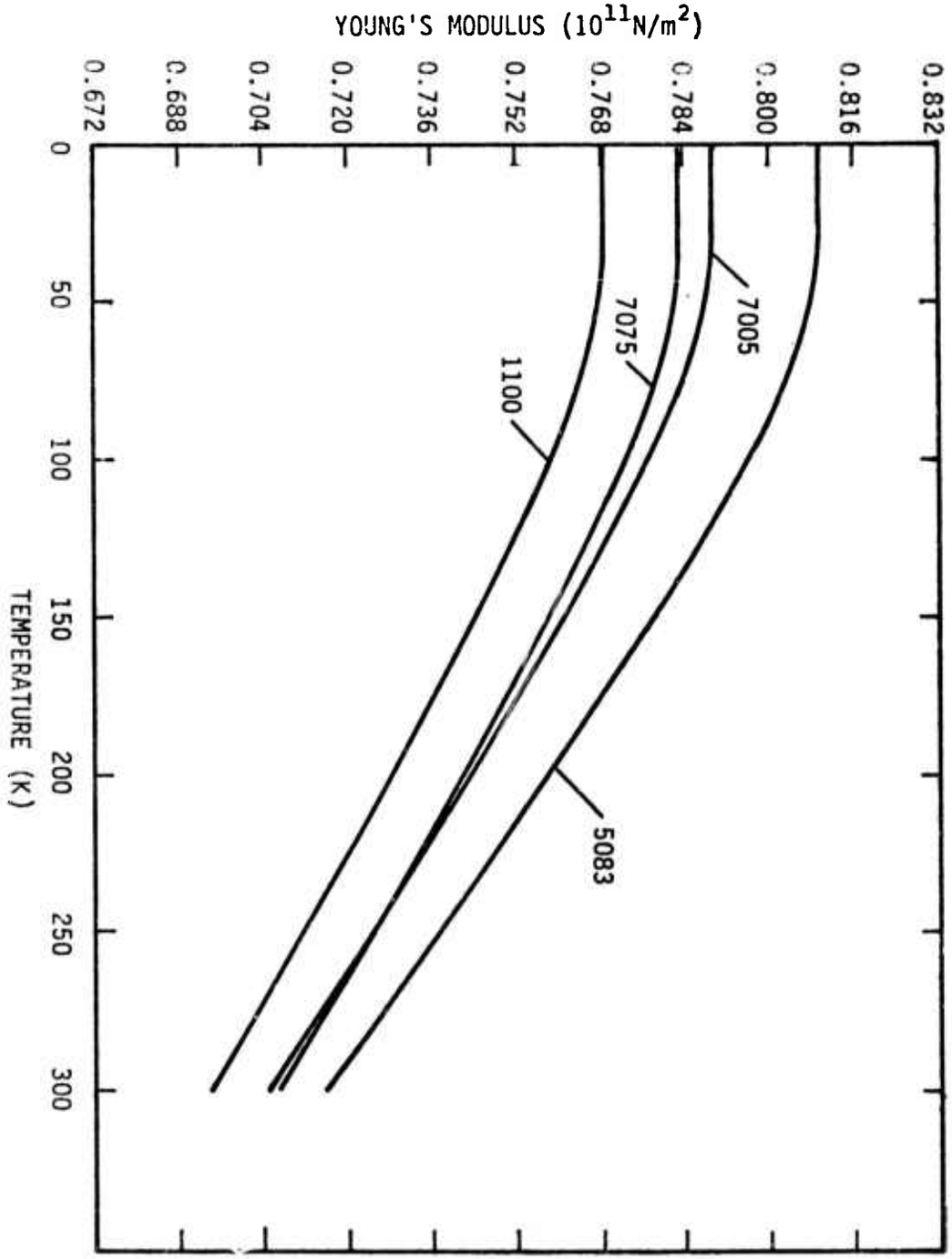
YOUNG'S MODULUS (10^{11}N/m^2)
0.672
0.688
0.704
0.720
0.736
0.752
0.768
0.784
0.800
0.816
0.832
0
50
100
150
200
250
300
TEMPERATURE (K)
1100
7075
7005
5083

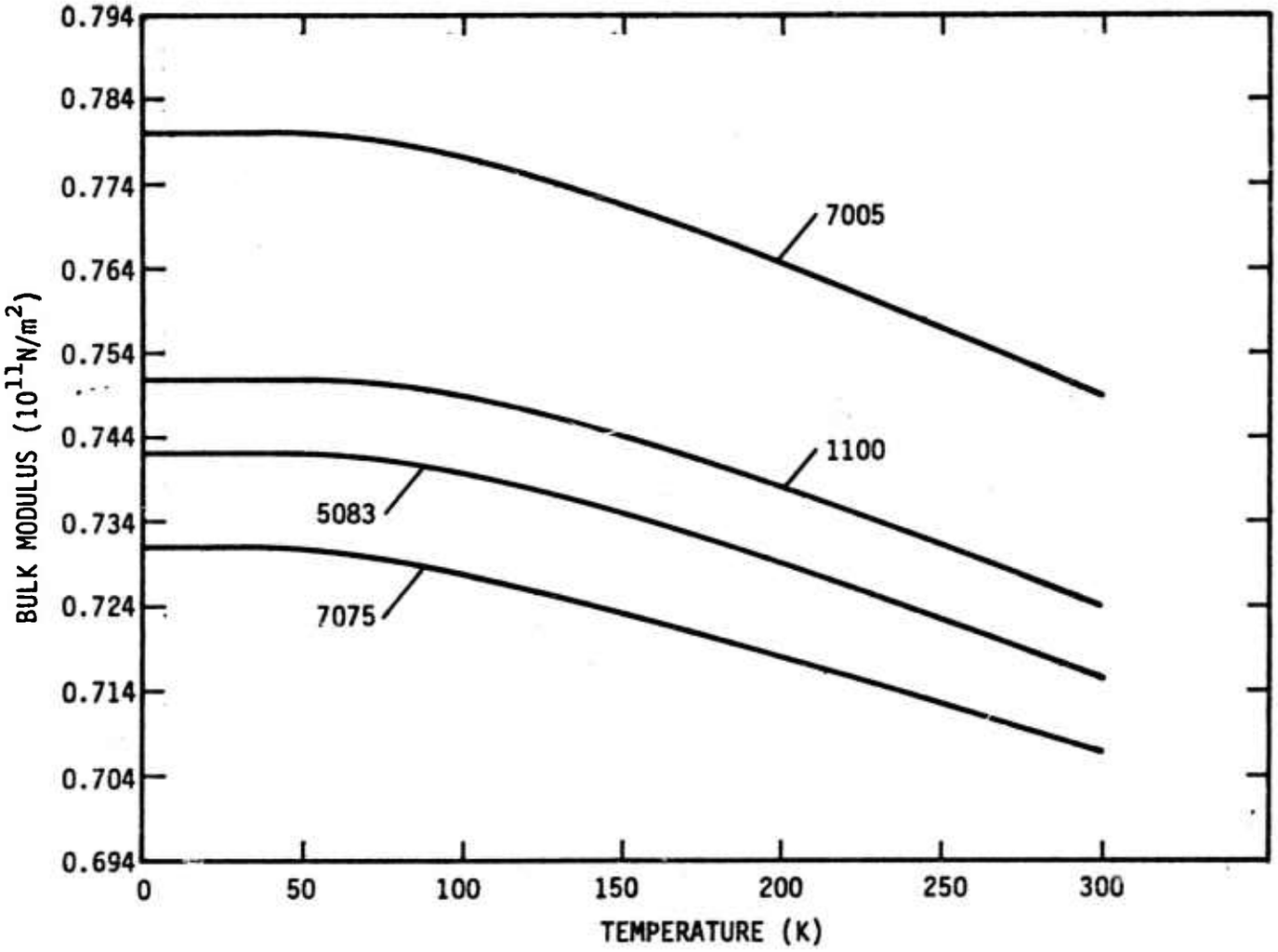
0.794
0.784
0.774
0.764
0.754
0.744
0.734
0.724
0.714
0.704
0.694
BULK MODULUS (10^{11}N/m^2)
7005
1100
5083
7075
0
50
100
150
200
250
300
TEMPERATURE (K)

Fig. 2.14

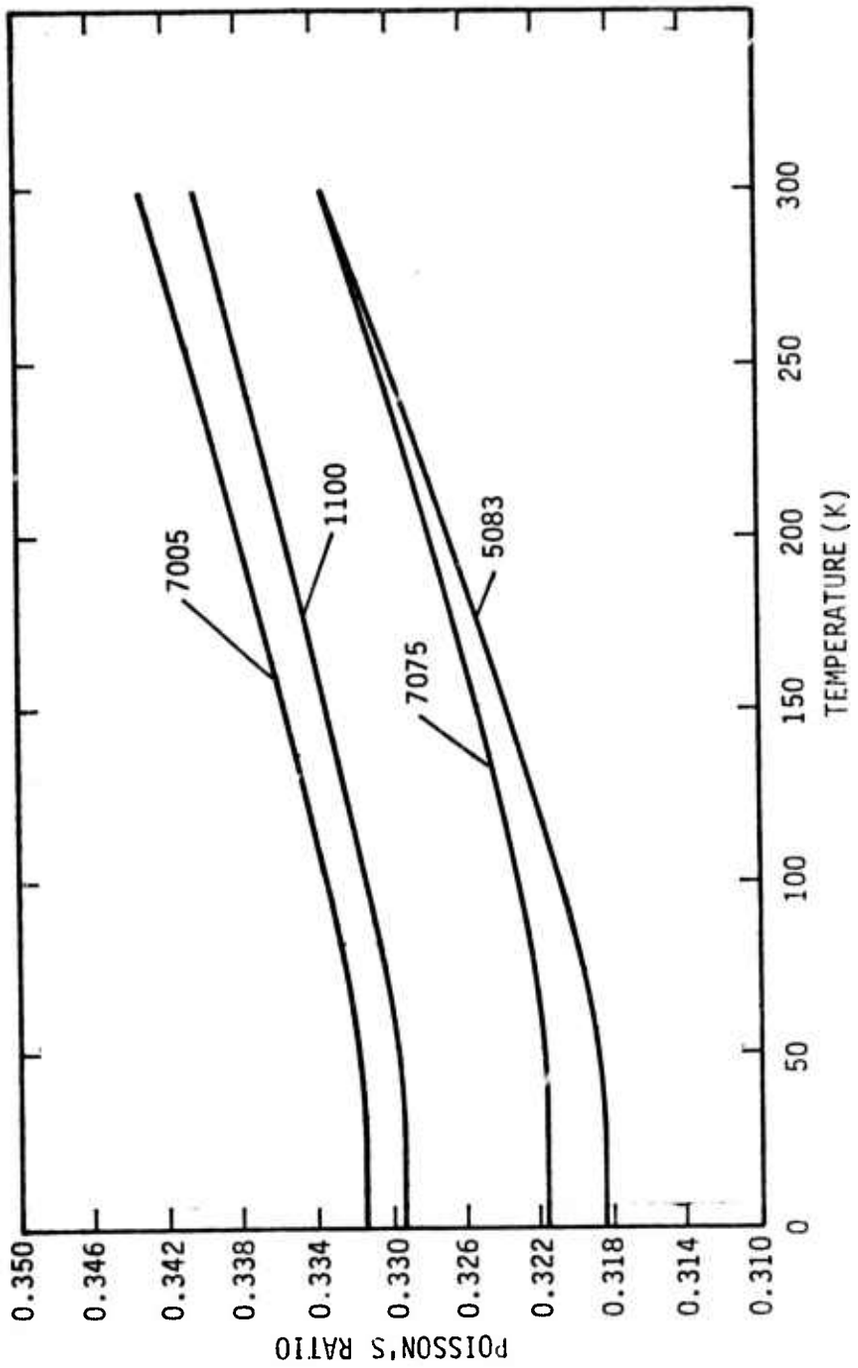
POISSON'S RATIO
0.350
0.346
0.342
0.338
0.334
0.330
0.326
0.322
0.318
0.314
0.310
0
50
100
150
200
250
300
TEMPERATURE (K)
7005
1100
5083
7075

215

SEMI-ANNUAL REPORT ON MATERIALS RESEARCH IN SUPPORT OF SUPERCONDUCTING MACHINERY

Advanced Composites

by

M. B. Kasen

Cryogenics Division
NBS - Institute for Basic Standards
Boulder, Colorado

SUMMARY

A comprehensive review of the literature on the mechanical and thermal properties of glass-filament reinforced structural composites at cryogenic temperatures has been completed. This is Part I of a two-part series, Part II reviewing the literature on advanced composites. The latter review is presently 75% complete.

The review includes tensile, flexural and compressive strengths and moduli, interlaminar shear, ultimate tensile strain, static and dynamic fatigue, fracture properties, thermal contraction, thermal conductivity and specific heat. Uniaxial, crossply and cloth-reinforced epoxies, polyurethanes, phenolics, polyimides, polyesters, silicones, phenyl silanes, teflons and Imidites are included in the review.

The literature indicates that glass-reinforced composites are most useful in cryogenic applications requiring high strength combined with high toughness and low thermal conductivity, but where stiffness is not a major requirement and where cyclic fatigue is not a major problem. There are indications that static fatigue may not be a problem at cryogenic temperatures; however, both static and dynamic fatigue must be studied more thoroughly before glass-reinforced composites are utilized in critical areas of superconducting machinery.

No literature data were available on the thermal fatigue resistance of glass-reinforced composites within the cryogenic range. As elevated temperature thermal fatigue is known to seriously degrade composite properties, this parameter should also be investigated for those composites most likely to be used in superconducting machinery, particularly for any component likely to be subjected to thermal cycling.

At the present time, the composite most widely used for cryogenic applications is S-901 glass in an epoxy matrix composed of Epon 828/DSA/Empol 1040/BDMA in proportions 100/115.9/20/1 by weight. This resin probably represents the current state-of-the-art for cryogenic applications in glass-reinforced systems.

The literature data suggests that, while epoxy matrices probably yield superior overall cryogenic properties, the glass-polybenzimidazole (PBI or Imidite) composites appear to have almost as good static strength properties with superior resistance to cyclic fatigue. The latter type of composite should be more thoroughly investigated.

Recent studies have indicated that the mechanical properties of weakly cross-linked polymers at cryogenic temperature are altered by the activity of the gas or liquid in contact with the specimen surface. The possibility therefore exists that data obtained with polymer-matrix composites at 77K in liquid nitrogen might differ from data obtained at 77K in helium vapor. This phenomenon should be further investigated.

Construction of a tensile cryostat capable of testing composite specimens at temperatures from 295K to 4K has been completed. Initial tests shall be run on state-of-the-art commercial boron-epoxy, boron-aluminum and graphite-epoxy materials. All but the boron-aluminum materials have been received. The testing program is scheduled to begin upon completion of the literature survey (approximately May 1).

TABLE OF CONTENTS

TABLE OF CONTENTS (cont)

220<

LIST OF FIGURES

INTRODUCTION

The primary impetus for structural composite development has arisen from the need to obtain improved long-term mechanical properties at elevated temperatures or to reduce the cost of structures designed for ambient temperature use. Comparatively little effort has been expended on development of composites for use at cryogenic temperatures. A notable exception has been the rather extensive body of work sponsored by NASA during the Apollo Program wherein a series of glass-reinforced plastics were characterized to 20K. The other major field of cryogenic development has been concerned with composite reinforcement of pressure vessels for aerospace use, largely exploiting the continuous-filament method of fabrication. To a large extent, the remaining published data on composite properties at cryogenic temperatures reflects work on which the generation of cryogenic property data was peripheral to the main work objective.

This relative lack of emphasis on cryogenic structural composites is perhaps understandable, as the majority of such structural applications are presently satisfied by readily available and well-characterized metals and alloys. In view of the extensive data base available on metals, it is probable that metals will continue to constitute the main body of structural materials at low temperatures.

Why, then, should one consider composites? The answer lies in the increasingly stringent demands made on materials in advancing cryogenic technology, of which superconducting machinery may serve as an example. Undoubtedly, the first generation of superconducting motors and generators will be dependent almost entirely on metals technology. However, it is highly probable that succeeding generations of such equipment will capitalize on advanced composite technology for reasons of increased reliability, reduced weight and increased efficiency, reflecting the higher specific strengths and moduli of advanced composites coupled with a wider range of thermal and electrical properties than are obtainable with any conventional metal.

The technological problems associated with integration of composites into superconducting machinery are threefold: a) most designers lack a feel for the properties available with composites, b) an adequate data base does not exist for composites at cryogenic temperatures, particularly at 4K, and c) most existing composites are optimized for service at room temperature and above--not for cryogenic service. The current program at NBS has taken aim at these three problem areas.

Our first effort has been to initiate a comprehensive review of what is known about the mechanical and thermal properties of composites at cryogenic temperatures. The objectives of the review are threefold: a) we wish to provide the designer with a feel for the general magnitude of property values which may reasonably be expected from a given category* and class of composites within the cryogenic range, b) we wish to provide him with a feel for the ranking of specific composite classes with regard to a specific property, c) we wish to impart a feel for whether the property of interest is likely to increase, remain unaffected, or to decrease with lowering of temperature, and d) we wish to define those areas in which further data are needed and to define the direction that future work should take in optimizing composites for cryogenic service and for implimenting their use in the construction of superconducting machinery.

The literature review covers 1960 to the present time, as it is within this time span that almost all of the significant work was undertaken. We include only filamentary-reinforced structural composites, and among these, only such composites as are amenable to a general characterization. The review, therefore, excludes cryogenic insulations, superconductor composites,

---

*We define a composite category by the general reinforcement type, e. g., glass-fiber or advanced fiber (graphite, boron, etc.). We define a composite class by the general matrix type, e. g., glass-polyester or graphite-epoxy. We define a composite type by a specific reinforcement/matrix combination, e. g., S-901 glass/E787 epoxy or HT-S graphite/X-904 epoxy.

thin films, honeycomb structures and composite-overwrapped metal. Filled composites (as distinct from filamentary reinforcement) are also excluded. There remains the very large field of composites reinforced by a variety of fibers in a variety of layups in a variety of matrix materials, and it is with this body of data that this review is concerned.

The wide variety of composite formulations and layups are further complicated by lack of standard test procedures. Furthermore, as the field is relatively new, much of the earlier work was performed on relatively poorly characterized composites. We have attempted to cope with this complexity by dividing the review into two major sections: the first treating glass-reinforced composites and the second treating the so-called advanced composites. The rationale for this separation is the distinctly different use of these two composite categories in engineering practice, i. e., glass-reinforced composites are used in applications where stiffness is not a design limitation, while the advanced composites are used where a high modulus material is essential.

Within each of these categories, we present the reader with a series of graphs on which appear the <u>average</u> literature values of each property for each composite class from room temperature into the deep cryogenic range. Admittedly, presenting average data is in danger of being misleading, as each curve has associated with it a considerable scatter band. For this reason, we discuss the range of values associated with each curve, emphasizing those specific composite types for which the highest values were reported. It is of utmost importance, however, that the reader understand that the graphed data appearing in this review are class averages and are not to be used for engineering purposes.

The second basic objective of the present NBS program is to initiate a test program to establish a viable data base for advanced composites potentially useful in superconducting machinery. This program will emphasize advanced composites, as glass-reinforced composites have been rather widely used for cryogenic applications over the past decade, primarily for support structures where the low modulus may be tolerated. Such composites

have also found applications in fiber-overwrapped cryogenic pressure vessels. As a result, the technological base for their application is comparatively well established. Conversely, the cryogenic application of advanced composite technology is relatively new with the potential for exploitation of their unique properties hardly investigated. In terms of the overall scope of the present ARPA program, the present NBS effort interfaces between the basic composite screening studies being undertaken by the General Electric Company and the eventual development of design allowable data required by the design engineer. The screening studies utilize the simple and inexpensive flexural strength test which is valuable in establishing a relative ranking among a large number of experimental composite formulations. However, flexural tests do not generate data which can be directly applied to design allowables, primarily because the state of strain is continually changing throughout the test. The tensile test is more difficult and time consuming; however, it is the least complex test which yields data of use to the design engineer. Furthermore, the tensile test may be used to evaluate the properties of a uniaxial lamella, the "fundamental building block" of composite laminates. Modern composite theory predicts that, having valid data on the ultimate values in tension, compression and shear for such lamella along with the pertinent poissons ratios, the mechanical properties obtainable in the complex crossply layups required in engineering structures may be calculated.

We have chosen to use the tensile test as our primary experimental method, working with unidirectional lamella for the above reasons. This decision was arrived at after extensive survey and consultation in person with a large number of individuals prominent in the composite field. Furthermore, this approach allows us to capitalize on the extensive experience of our laboratory in conducting tensile tests at cryogenic temperatures.

Tensile testing of composite materials is not as easy as with metals, even at room temperature. An extensive survey was also made of those individuals who had worked in this area in order to determine what, if any,

problems remain to be solved. It does appear that some development work will be necessary. The basic problem stems from the extreme anisotropy of composites and of the unidirectional composite in particular. The very high strength of the fibers coupled with a relatively low interlaminar shear strength in the composite frequently results in invalid test data due to specimen failure in shear within the grip area. A relatively high fraction of such failures may be tolerated during room temperature testing; however, the high cost of testing at cryogenic temperatures dictates that every effort must be made to obtain valid data from each specimen under test. Our laboratory can make a significant contribution in this area.

Tensile testing of composites requires the use of a much longer specimen than is normally used for metals; consequently, it has been necessary to construct a tensile cryostat capable of taking specimens up to 11 inches in length. The expense of this unit is being equally shared with another project.

The materials selected for our initial test program represent a selection of the current state-of-the-art commercial production of boron-epoxy, graphite-epoxy, and boron-aluminum composites. The reason for this approach is twofold. First, cost is reduced by working with materials donated by the manufacturer who finds it an advantage to have his materials evaluated for potential cryogenic use. Secondly, the data obtained in this initial phase of the program will provide a reference against which experimental composite formulations optimized for cryogenic service may be compared.

The present report contains that portion of the literature review concerned with glass-reinforced composites and that portion of the experimental program concerned with construction of the tensile cryostat and the acquisition of the test materials.

The following symbol nomenclature is used in this report:

σ^{tu}	- tensile ultimate strength	E^c	- compressive modulus
E_1^t	- initial tensile modulus	σ^{si}	- interlaminar shear strength
E_2^t	- secondary tensile modulus	σ^{by}	- bearing yield strength
ϵ^t	- tensile ultimate strain	σ^I	- impact strength
n^{tu}	- tensile fatigue	λ	- thermal conductivity
σ^{fu}	- flexural ultimate strength	$\Delta L/L$	- thermal contraction
E_1^f	- initial flexural modulus	C_p	- specific heat
E_2^f	- secondary flexural modulus		
σ^{cu}	- compressive ultimate strength		

MECHANICAL AND THERMAL PROPERTIES OF FILAMENTARY-REINFORCED STRUCTURAL COMPOSITES AT CRYOGENIC TEMPERATURES- I: Glass-Reinforced Composites

SCOPE OF THE LITERATURE SURVEY

We initially conducted a subject search using the data bases of the NBS Cryogenic Data Center, DDC and NTIS. Additionally, a subject search was conducted through the volumes of NASA STAR, and the ASM - AIME Metals Review. As the search progressed, a series of contract numbers were identified as being associated with studies of the cryogenic properties of composites. The DDC and NASA data bases were then searched for all reports issued under such contracts. Finally, the DDC data base and that of the Smithsonian Science Information Exchange were searched for current work in progress.

ORGANIZATION OF THE BIBLIOGRAPHY

The appended Bibliography contains 148 references. As the work progressed, it became apparent that a large part of the relevant data had been produced under a relatively few contracts sponsored either by NASA or USAF. Eleven such contracts have been listed at the start of the Bibliography with references to the most pertinent publications issued under each contract.

Only final reports are listed, as they adequately summarize the data which also appeared in numerous interim reports on each project. Journal publications are listed as they often provide a convenient review of the subject matter contained in the comprehensive reports and are generally more readily available to the reader.

The Bibliography also contains a general section, alphabetically arranged by author, listing relevant publications sponsored by other contracts or by corporate in-house funding. A separate part of the Bibliography itemizes handbooks or reviews which will be found useful references but which do not contain original data. Finally, a miscellaneous reference section lists publications which are referenced in the text which do not contain relevant mechanical or thermal property data.

Wherever possible, the pertinent NASA or DDC code number is included to facilitate retrieval of specific publications. Corporate reports not so identified must be obtained from the corporate source.

An extensive cross-reference relating mechanical and physical properties of specific types of composites to specific literature references is included so as to simplify literature retrieval by the reader. The latter includes separate references to filament-wound pressure vessels in recognition of the importance of such applications to cryogenic technology. A separate listing is also provided of reports containing information on the effect of combined cryogenic temperature and nuclear radiation.

GLASS-REINFORCED COMPOSITES

The mechanical and thermal properties of glass-polymeric composites are summarized on Figures 1-16. Where available, data are presented for 295K, 200K, 77K, and 20K (4K data are almost nonexistent). Straight lines connect average values at each temperature. Absence of a data point for a given temperature implies no significant data. An asterisk adjacent to the number identifying a curve indicates that the data for that particular composite type was minimal relative to that available for the other composite types included on the Figure.

In considering the mechanical property data, the reader should be aware that there exists no universally accepted method of determining these properties for composites, although committees of the ASTM are working diligently on the problem of standardization. Furthermore, testing of composites, particularly at cryogenic temperatures, introduces numerous complexities. The problems of tensile testing are primarily those of obtaining fractures within gage lengths in uniaxial longitudinal layups and dealing with misalignment in off-axis layups. The problems in compression testing are column buckling in the high-aspect-ratio specimens normally used for composite testing. The data discussed in the present review were for the most part obtained in the course of comprehensive research programs by reliable investigators who were concerned with obtaining the most valid results possible. Nevertheless, it remains a possibility that some of the scatter in the data reported in the literature, particularly for compression and interlaminar shear, reflects differing test procedures. Where this has become apparent, the data have been separated by test method.

STATIC MECHANICAL PROPERTIES

Tensile Strength and Modulus - Figures 1 and 2

The reason for the widespread use of glass-reinforced composites is evident from the tensile strength data presented on Figure 1. No other type of composite can match the uniaxial tensile strengths of 250-300 KSI provided by the glass-epoxy formulations. Even in the 0°/90° crossply layup, the glass-epoxy strength is almost equal to that of the advanced composites in the uniaxial longitudinal configuration. Unfortunately, the moduli of glass-reinforced composites are quite low, as may be seen in Figure 2. It is this low modulus of glass that has given impetus for development of the advanced composites.

From Figure 1 we see that the tensile strength is reduced about 50% at all temperatures in a 0°/90° configuration as compared to uniaxial, e. g., from about 300 KSI to about 150 KSI for glass-epoxies. This is expected from a 50% decrease in longitudinal fiber content, the crossply fibers contributing nothing to the overall strength when tested parallel to one fiber direction.

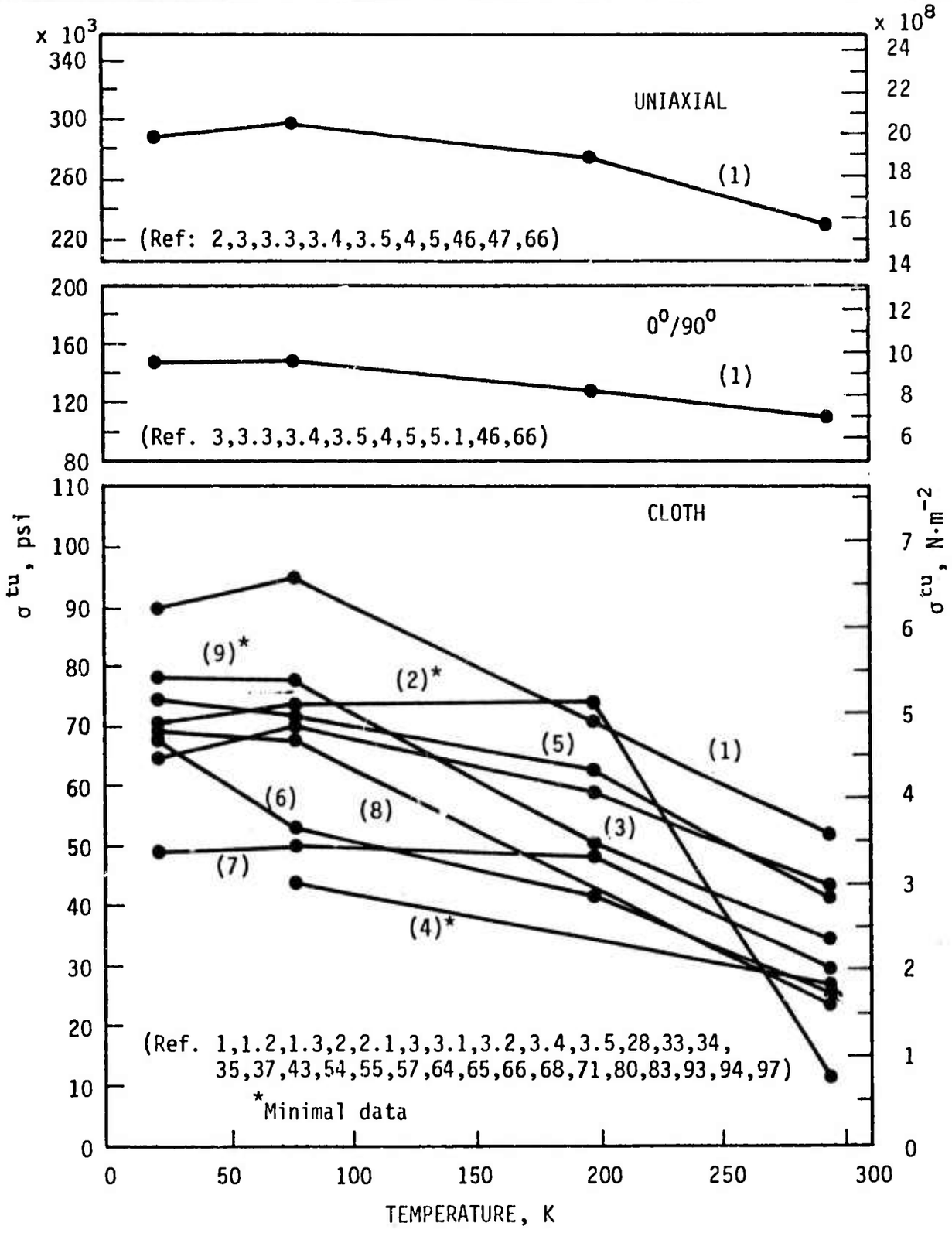

Fig. 1. Ultimate Tensile Strength of Glass-Reinforced Composites.

(1) Epoxy	(4) Polyimide	(7) Phenyl Silane
(2) Polyurethane	(5) Polyester	(8) Teflon
(3) Phenolic	(6) Silicone	(9) Imidite

Approximately another 25% decrease in strength is found upon going to woven cloth reinfo cement of an epoxy matrix, reflecting the decrease in load carrying capacity of fibers which are slightly bent in the weaving process.

Epoxy resins are most widely used as matrices for structural applications where maximum strength is required. This appears justified on the basis of the data of Figure 1 wherein the ultimate tensile strengths of the cloth-epoxy composites are overall higher than those of other cloth-polymeric composites at all temperatures. The polyurethane-, teflon-, phenyl silane polyimide-, and silicone-matrix composites appear to have the poorest strength properties at 295K, with phenolic-, Imidite-*, and polyester-matrix composites being intermediate in strength. At 77K, the polyimide-, silicone-, and phenyl silane-matrix composites continue their relatively poor performance, while the polyurethane-, Imidite-, and teflon-matrix composites have about equalled the phenolics and polyesters.

Among the uniaxial glass-epoxy composites, the highest reported strengths were 360 KSI[46] and 375 KSI[47] during NOL ring test of S-HTS/660 FW and S-901/ERL 2256 glass composites.** This work was directed toward filament-wound pressure vessels, which has been the incentive for much of the cryogenic composite development work. Other authors[3, 66] have also reported strengths of about 330 KSI at 77K for S-901/E-787 and S-HTS/Epon 828 filament-wound uniaxial composites respectively. The overall data range was 213-375 KSI.

---

* The use in this paper of tradenames of specific products is essential to the proper understanding of the work presented. Their use in no way implies approval, endorsement, or recommendations by NBS. Imidite is the Narmco Division, Whittaker Corporation tradename for a polybenzmidazole resin of the polyaromatic family. The generic name rarely appears in the literature, although the abbreviation PBI is sometimes used. The present review follows the literature in using the tradename. Polyimide resins are of the same family, sometimes referred to as PI. In the latter case, the generic name is used in this report, again following the literature convention.

** For present purposes, tensile data obtained from Naval Ordnance Laboratory ring tests has been combined with data obtained from testing of flat tensile specimens in the uniaxial longitudinal direction, even though it is recognized that the NOL test is not strictly a uniaxial test.

Among the 0°/90° data, the best results have been reported for S-901/E-787[3] and S-901/modified Epon 828[5] with tensile strengths ranging from 170-200 KSI. The overall range was 115-200 KSI.

Among the woven cloth composites, the highest strength epoxy-matrix composites were 181/modified Epon 828[2] and 1581/E-787[3] having strengths on the order of 125-145 KSI at 77K tested parallel to the woof or warp. The phenolic-matrix composite data shows quite consistent strengths of 60-70 KSI at 77K except for the work of Levin, et al.,[71] who has reported 100 KSI at 77K in a composite based on a butvar-phenolic adhesive. The polyester-matrix data scatters from 50-80 KSI at 77K except for one report of 100-105 KSI for 181 glass in Hetron 31 or Narmco 527 resin.[2] The teflon-matrix composites ranged from 50-80 KSI at 77K, the highest value being reported for type 116 glass in TFE or FEP.[80] The silicone-matrix data showed relatively large scatter from 25-70 KSI at 77K with the highest values being reported for 181/Trevarno F-131[2] and for 181/Narmco 513.[3] Few data were found for polyurethane-, phenyl silane- and polyimide-matrix composites. About 73 KSI was reported at 77K for 181 glass reinforced with the flexible polyurethane Adiprene L-100 and 60 KSI for the same reinforcement in the phenyl silane Narmco 534.[2] Polyimides are relatively new matrix materials, having been developed primarily for elevated-temperature use, particularly for stability. The one reference reports a value of 43 KSI at 77K for a glass-polyimide composite, a value which is hardly impressive.[68] On the other hand, the Imidite-matrix composites which are of the same family as the polyimides, developed excellent strength at 77K and at 20K, being second only to the epoxies.

All of the above comparisons were made at 77K because, as seen on Figure 1, while the tensile strength in all cases increases between 295K and 77K, further cooling to 20K produces erratic results. This is more clearly illustrated in Figure 5(a) which shows that cooling of glass-epoxy composites from 295K to 77K can produce a strength increase of from 10-140 KSI with

a high probability of an increase on the order of 30-60 KSI , essentially independent of the type of layup. However, on cooling further to 20K, the probability is for a slight decrease in strength for cloth and 0°/90° crossply reinforced epoxies and a reasonably high probability that uniaxial glass-epoxies will suffer a strength degradation which may be as high as 80 KSI. The phenolic-, polyester-, phenyl silane- and polyurethane-matrix composites all showed a similar erratic behavior. An exception appeared to be the silicone-matrix composites which showed consistent moderate increases in strength at 20K.

The behavior at 200K offers few surprises except for the polyurethane-matrix data which indicates an exceptionally large increase from relatively poor room temperature strength in 181/Adiprene L-100.[2]

As with the tensile strength, the initial tensile modulus, Figure 2, shows the expected dependence on fiber orientation. Values range from about 10^7 psi for the uniaxial longitudinal layups to 5-6 x 10^6 psi for the 0°/90° crossply to 2-5 x 10^6 psi for the woven cloth composites. The Imidite-matrix composites developed much higher moduli than any of the other cloth-reinforced materials at cryogenic temperatures. Also, the glass-cloth phenolic composites are found to have, on the average, slightly superior moduli than glass cloth-epoxies, while glass cloth-polyesters appear almost as good as the epoxies. The silicone-, polyurethane-, and teflon-matrix composites displayed the lowest moduli with an indication that phenyl silane-matrix composites are of intermediate modulus.

Again taking 77K as a criterion temperature, the uniaxial glass-epoxies showed a modulus range of about 8-11 x 10^6 psi with the higher values reflecting on variants of S-HTS/Epon 828[66] and on variants of Hi-Stren/Epon 828.[4] The 0°/90° crossply data ranged from 3-7 x 10^6 psi with values of 5.5-7 x 10^6 psi being reported for S-901 glass with a series of epoxy resin formulations.[3] The cloth-reinforced epoxies yielded moduli from 2-5 x 10^6 psi with the highest values being reported for 181 glass/Epon 828 formulations.[2]

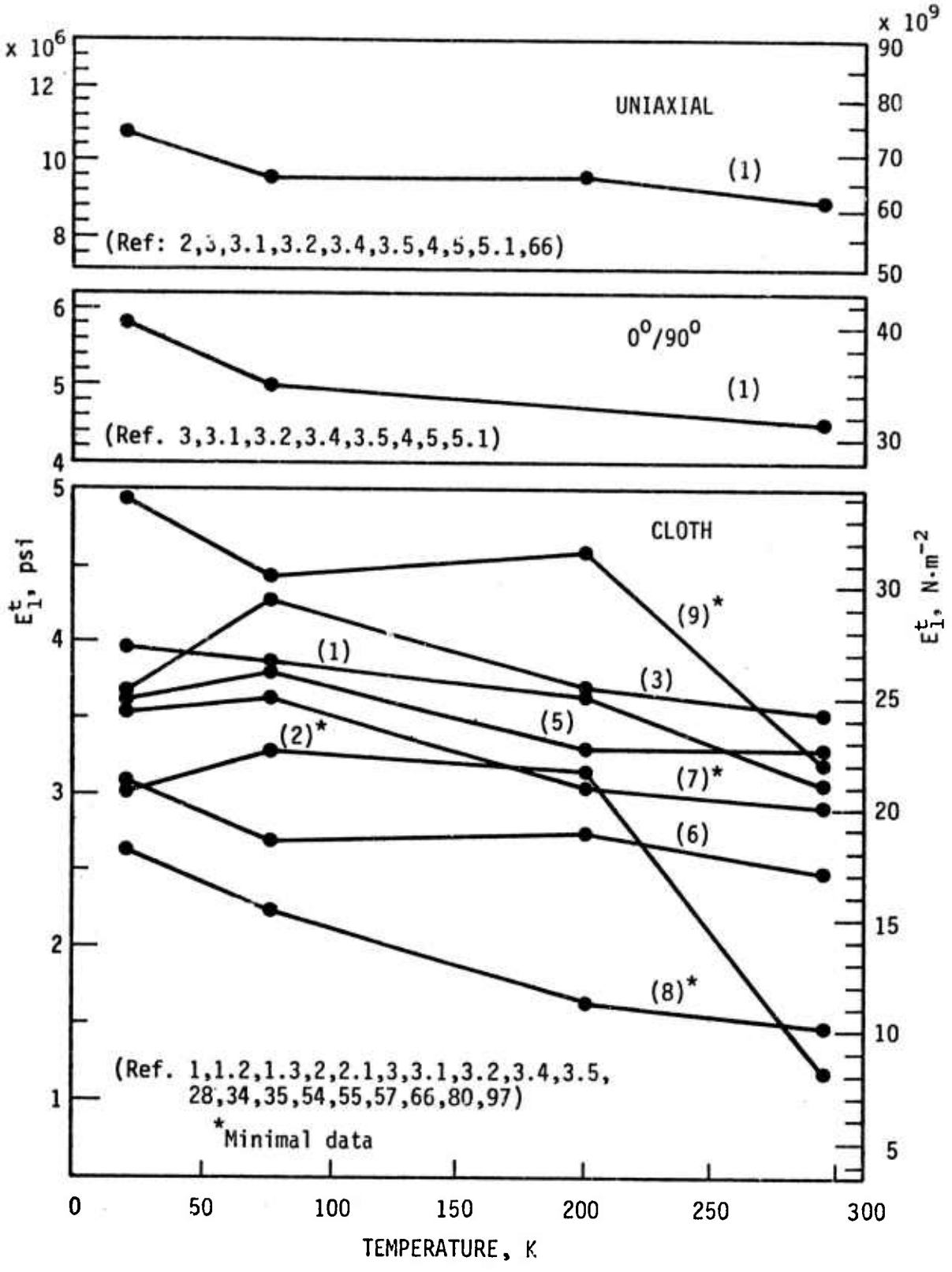

Fig. 2. Initial Tensile Modulus of Glass-Reinforced Composites.

(1) Epoxy	(4) Polyimide	(7) Phenyl Silane
(2) Polyurethane	(5) Polyester	(8) Teflon
(3) Phenolic	(6) Silicone	(9) Imidite

Although the average modulus of the glass cloth-phenolic composites was higher than that of the epoxies, literature values ranged from 3-4.7 x 10^6 psi which suggests that no significant difference in moduli should be expected for good composites made with either epoxy or phenolic matrices. A detailed look at the glass-cloth-polyester data, however, shows a relatively narrow modulus range of about 3.5-4 x 10^6 psi suggesting that the best composites made with this polymeric matrix are probably inferior in modulus to the best epoxies or phenolics by about 10^6 psi. In a similar way, the glass cloth-silicone matrix composites are still more inferior having moduli which vary from 2.5-2.9 x 10^6 psi at 77K. Somewhat fewer moduli data are available for Imidite-, silicone-, polyurethane- and phenyl silane-matrix composites, but that available suggests that the teflon matrix produces moduli of only 1.6-3 x 10^6 psi with 3.3 x 10^6 psi and 3.6 x 10^6 psi for the polyurethane and phenyl silane matrices, respectively. The Imidite data was obtained with a 181/Imidite composite[2] and is impressive not only for the high average value of 4.38 x 10^6 psi developed at 77K, but also for the indication of a substantial increase to 4.9 x 10^6 psi at 20K.

As with the tensile data, Figure 2 indicates erratic moduli below 77K. Reference to Figure 5(b) shows that with the exception of a few crossply data, the literature suggests that cooling from 295K to 77K will produce a modulus increase of about 0.3-1.2 x 10^6 psi with about 0.7-0.8 x 10^6 psi being most likely. There does not appear to be a strong dependence on layup. Results of further cooling to 20K are more difficult to interpret. In general, the data seem to cluster around a small increase in modulus up to 0.6 x 10^6 psi for cloth-reinforcement and suggests that a somewhat larger increase on the order of 0.6-1.3 x 10^6 psi could be expected for crossply and uniaxial composites. Nevertheless, the scatter from -0.8 x 10^6 psi to +3.2 x 10^6 psi modulus change is indicative of something erratic occurring below 77K.

Again, the only surprises in the 200K data of Figure 2 is the high value of the modulus of the flexible polyurethane Adiprene L-100 compared to the room temperature modulus and the almost equally large increase in the Imidite data.

Flexure Strength and Modulus - Figures 3 and 4

Flexural tests are frequently used for screening a large number of composites during development studies, as such tests are simple and relatively inexpensive compared to tensile testing. In this application, flexure tests have the added advantage of testing the matrix as well as the reinforcement fiber. Unfortunately, the state of stress is continuously changing throughout the flexure specimen as the test proceeds, which makes engineering interpretation of the data difficult. Consequently, data on flexural strength and moduli are generally considered valid only for establishing relative performance ranking.

Figure 3 shows the flexural strengths of the glass-epoxies to be higher than that observed in tension by approximately 100 KSI in the uniaxial specimens and by about 50 KSI in the 0°/90° or cloth layups. *

As in the tensile results, the data show the epoxy-matrix composites to be superior in flexural strength at all temperatures, although the Imidite-matrix composites are almost as good. Among the other matrix types, the agreement with the tensile data is less clear. For those composites for which there is a reasonable amount of data, e.g., the polyester-, phenolic-, and teflon-matrix types, the strength order is the same at 77K as it is in tension; however, the relative strength differences bear little relationship to the tensile data. The polymide and phenyl silane-matrix composites rank near the top in flexural strength, while appearing near the bottom in tension. Conversely, the polyurethane-matrix composite appears good in flexure but poor in tension. However, as the data on the latter two composites are based on only one or two references and on a comparison between composites of different authors, caution is necessary in interpreting the results. The polyurethane-matrix data does reflect the same composite tested both in tension and in flexure.[2]

---

* Verified by comparison of σ^{tu} and σ^{fu} data from the same authors testing the same composites.

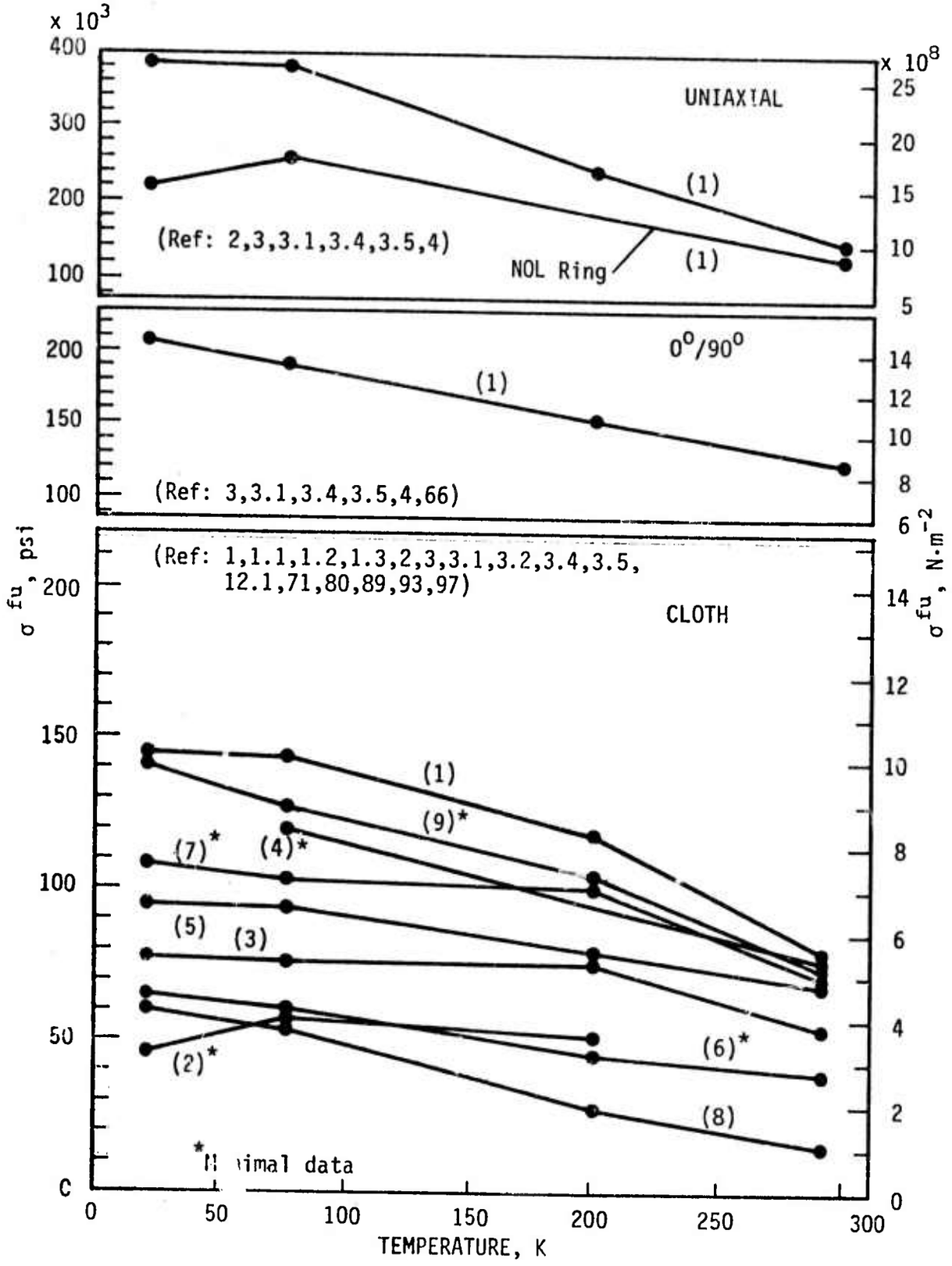

Fig. 3. Ultimate Flexural Strength of Glass-Reinforced Composites.

(1) Epoxy	(4) Polyimide	(7) Phenyl Silane
(2) Polyurethane	(5) Polyester	(8) Teflon
(3) Phenolic	(6) Silicone	(9) Imidite

Within the uniaxial data, a separation has been made between data generated from flat flexural specimens and that obtained from curved segments of NOL rings because flexural properties obtained from each type of specimen are distinctly different.

Examining the available flexural strength data in more detail, we find that the flat-specimen uniaxial strength of the glass-epoxies ranged from 325-470 KSI at 77K with the highest values reported for S-901/E-787.[3] The NOL specimen data was significantly lower, ranging 200-270 psi at 77K.[4] Flexural strengths varied among the 0°/90° epoxy data from 145-260 KSI at 77K with the highest values again reported in S-901 glass using either E-787 or an experimental epoxy formulation.[3] Data for the cloth-reinforced epoxies showed a spread of 95-175 KSI. The highest values were obtained with 1581/E-787,[3] almost as high values reported for 181 glass in a variation of Epon 826 resin.[2] These were the same composites which excelled in tensile testing.

The glass-phenolic composites ranged from 70-110 KSI at 77K. The highest values were reported for 181/CTL-91-LD.[1] Glass-Imidite data reflects only the average data with 181 glass reinforcement.[2] The glass-polyesters showed a slightly higher range, 80-127 KSI with the best value reported for 181/Hetron 31.[2] Reported flexural strengths of cloth-reinforced teflon-matrix composites varied from 30-70 KSI, the highest values being developed with 181/FEP.[2]

Following a pattern which is found to repeat itself in all strength properties of glass-polymeric composites, the flexural strengths all initially increased upon cooling from 295K to 77K; however, they then changed in erratic ways upon additional cooling to 20K. Changes in flexural strength during cooling as reported in the literature are summarized on Figure 5(c), which shows that the expected strength increase from 295K to 77K is about 50-80 KSI for crossply and woven-cloth layups. However, strength increases of up to 250 KSI have been reported for uniaxial composites, suggesting that the magnitude of the increase is layup-dependent

in flexural strength testing. A comparison of Figure 5(c) with that of 5(a) shows a much greater scatter in the flexural data as compared to the tensile data on cooling to 77K.

Upon cooling further to 20K, Figure 5(c) indicates that one may obtain strength changes varying from -50 KSI to +150 KSI with a higher probability of a decrease than an increase. The data does not appear to be layup sensitive at 20K.

The flexural modulus data, Figure 4, shows a value of about 8.5 x 10^6 psi for uniaxial glass-epoxy. This is lower than the average moduli in tension; however, this data reflects only data for a flat specimen of S-901/E-787.[3] A check of the data shows that this specific composite had an initial tensile modulus of only about 8.8 x 10^6 psi, which suggests that the two methods are giving about the same answers for the uniaxial case. The same is true for the 0°/90° case, about 5 x 10^6 psi being obtained in both the flexural and tensile modes of testing. The cloth-reinforced polymer flexural modulus data range of 2-3 x 10^6 psi to about 5 x 10^6 psi is also similar to that of tensile modulus.

Except for the teflon-matrix showing poorest performance, the silicone-matrix showing next poorest, and the Imidite matrix being one of the best, in both tests there appears to be little correlation between the relative modulus ranking in flexure and in tension for the same series of composite types. This is not a blanket condemnation of the flexural test - it may equally well indicate that average data from the literature cannot be used to predict tensile behavior from flexural data with any degree of reliability.

Examining the flexural modulus data in more detail, we find that the 0°/90° crossply glass-epoxy data ranged from 4.6-5.8 x 10^6 psi at 77K with the highest values for S-901/E-787.[3] Among the cloth-reinforced composites, the epoxy-matrix data varied from 2.6-5 x 10^6 psi with maximum values reported in 181/Epon 828[1] and in 181 glass with modified Epon 828 resin.[2]

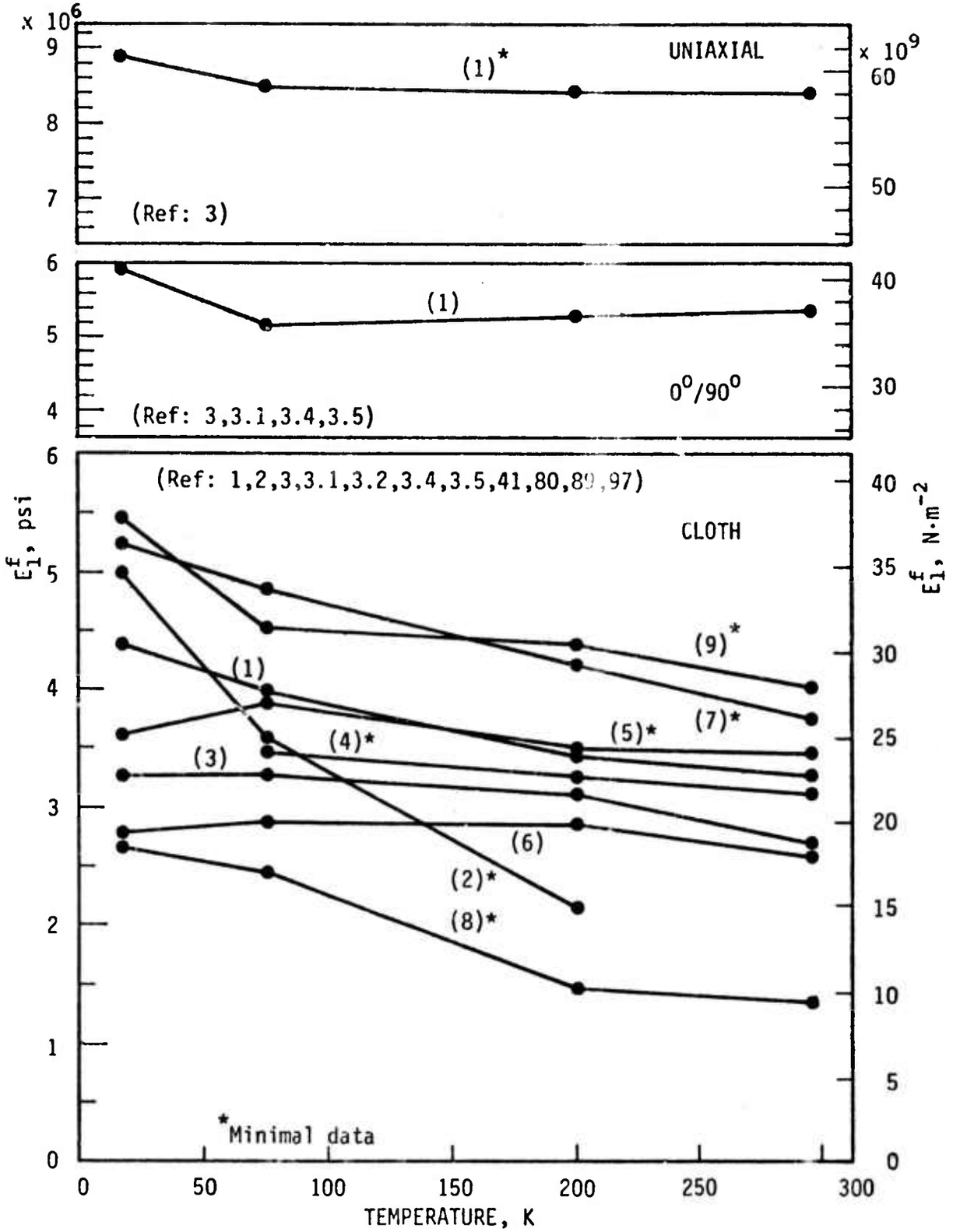

Fig. 4 Initial Tensile Modulus of Glass-Reinforced Composites.

(1) Epoxy	(4) Polyimide	(7) Phenyl Silane
(2) Polyurethane	(5) Polyester	(8) Teflon
(3) Phenolic	(6) Silicone	(9) Imidite

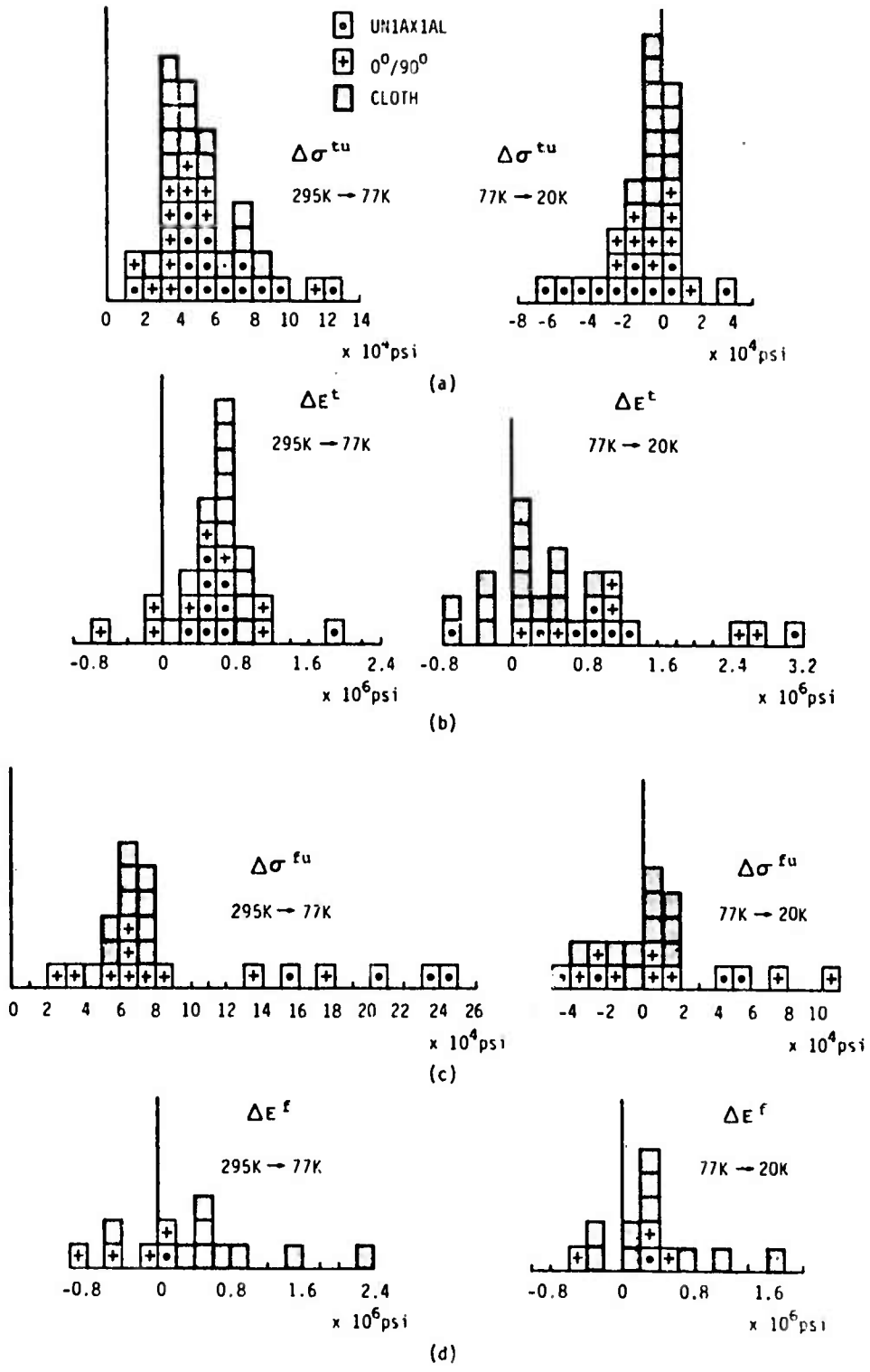

Fig. 5 Histogram Illustrating Changes in Tensile and Flexural Properties of Glass-Epoxy Composites Upon Cooling.

The phenolic-matrix data emcompassed 1.2-4.3 x 10^6 psi at 77K, the highest values being developed in Conolon 516.[41, 97] The silicone-matrix type composites showed a relatively small spread of 2.6-3.2 x 10^6 psi at 77K the highest value reported for 181 glass/Trevarno F-131.[2] Among the composites for which less data were available, the excellent showing of the phenyl silane-matrix composites in flexural modulus is somewhat of a surprise, but the data, coming from the work of Chamberlain, et al.,[2] on Narmco 534, appear to be valid. The data again shows excellent moduli at all temperatures for 181/Imidite composites.[2] The polyurethane- and polyimide-matrix flexural modulus data reflect only one reference each.[89, 2]

Again, cooling below 77K causes the data to become erratic. Figure 5(d) summarizes the glass-epoxy flexural modulus data and shows that, while on the average one would expect an increase of about 0.4 x 10^6 psi on cooling to 77K and a like increase in further cooling to 20K, one may find changes ranging from -0.8 to +2 x 10^6 psi. The data suggest that the crossply might be more adversely affected by cooling to 77K than the cloth-reinforced specimens; however, there are not sufficient data to verify this indication.

Compressive Strength and Modulus - Figure 6 and 7

The compressive strength data discussed herein was obtained by compressing in the fiber direction or, in the case of cloth-reinforced materials, in the plane of the cloth. As most composites are used in fairly thin sheet form, the major problem is one of avoiding failure by column buckling during the test. Problems are further accentuated in the uniaxial longitudinal case, where slight misorientation of the fibers can substantially reduce the compressive strength.

One observes from Figure 6 that the average of the data reported in the literature for the compressive strength of uniaxial glass-epoxy composites is less than half of the ultimate tensile strength average for the same type composites. Yet, the 0°/90° compressive strength is but slightly lower than its tensile strength, while the cloth-reinforced data span about the same

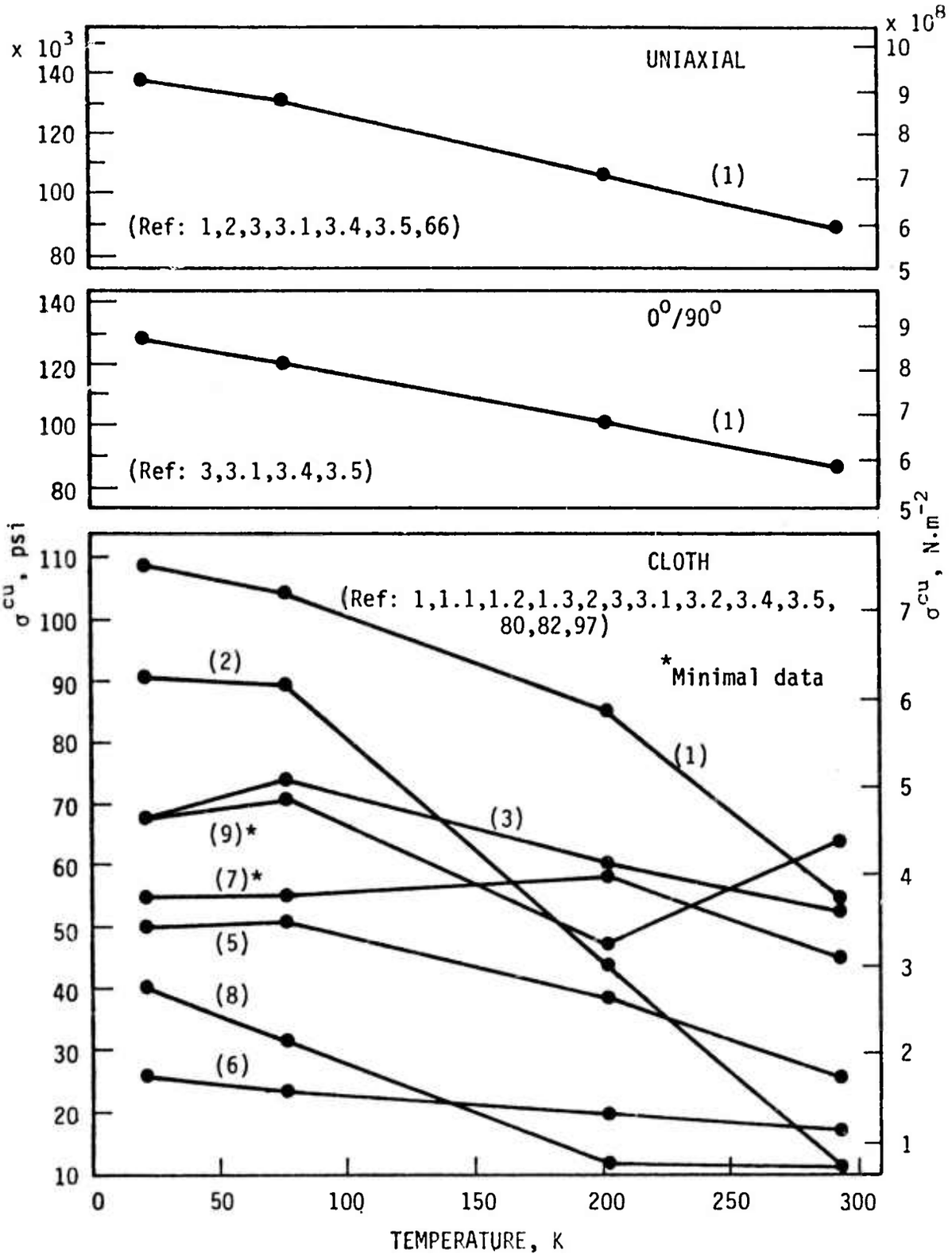

Fig. 6 Ultimate Compressive Strength of Glass-Reinforced Composites.

(1) Epoxy
(2) Polyurethane
(3) Phenolic
(4) Polyimide
(5) Polyester
(6) Silicone
(7) Phenyl Silane
(8) Teflon
(9) Imidite

range in compression and in tension. Consideration should thus be given to the possibility that the uniaxial data, and to a lesser extent the 0°/90° data, are lower than the true values due to testing problems.

Among the cloth-reinforced polymers, the epoxy-matrix composites continue to show superiority over all others. Once again, as in the tensile case, the polyurethane-matrix materials indicate a remarkable transformation from an extremely low strength at 295K to one of the strongest of the group at 77K. The glass-phenolics continue their reasonably good performance previously noted in the tensile results. The glass-Imidite appears to rank about average in compressive strength, similar to its performance in tension. The glass-phenyl silanes appear to rank somewhat better in compression than in tension, although few data are available. The glass-polyesters appear to have relatively poor compressive strength, although they were ranked among the top in tension. Finally, the teflon- and silicone-matrix composites display consistently the lowest compressive strengths of all materials surveyed.

Considering the uniaxial compressive strength data in more detail, we found the reported data at 77K to vary widely from 100-240 KSI with about equal scatter at the other temperatures. This is almost twice the percentage variation found in the uniaxial tensile data even though the latter data was much more extensive. This large scatter very likely reflects the aforementioned problems inherent in compression testing. The highest value reported at 77K for uniaxial compression was 237 KSI in S-901/E-787.[3]

The 0°/90° data showed much less scatter, ranging from 106-130 KSI at 77K, the highest value reported in biaxially filament-wound S-901 glass in DER 332 epoxy.[3]

Among the glass-reinforced composites, the epoxy-matrix data varied from 90-138 KSI at 77K with the highest value reported for a modified 181/Epon 828 composite.[2] Glass-phenolic properties covered a range of 60-100 KSI at 77K, distinctly inferior to the epoxies. The highest value was reported for 181/Narmco 506.[1] The polyester-matrix composites were another notch down in strength with a 35-68 KSI showing at 77K, the best

results being obtained in 181 glass with Hetron 31 or Narmco 527 resin.[2] The 19-40 KSI range of the glass-silicones and the 25-40 KSI range of the glass-teflons at 77K leave little doubt of the inferiority of the latter composite types in compression. The data for polyurethane-, Imidite-, and phenyl silane-matrix composites reflects the work of Chamberlain et al.[2]

As with tensile and flexural properties, cooling below 77K produces somewhat erratic results in compression. The 200K data appear to be in line except for the glass-teflon composite for which cooling to 200K had no apparent effect.

No uniaxial or 0°/90° data were available for compressive moduli. Average values among the cloth-reinforced polymers which appear in Figure 7 bear a striking resemblance to the tensile modulus data. Again, the phenolic-matrix composites were superior with the epoxy-matrix second. Teflon-matrices were clearly the poorest with the polyurethanes starting out equally low in modulus but again rapidly increasing its value to the middle of the group. The silicone-matrices were again on the low modulus side. The only significant change from the tensile modulus ranking is the somewhat poorer relative performance of the polyester and Imidite-matrix composites in compression.

The phenolic composites ranged from 4-8.4 x 10^6 psi in compression modulus at 77K, maximum value being reported for 181/CTL-91-LD.[1] The glass-epoxy data showed much less scatter at 77K ranging from 4-5.15 x 10^6 psi. The highest reported value for 181 glass/modified Epon 826 composite.[2] The phenyl silane and polyurethane data reflect only the values for Narmco 534 and 181/Adiprene L-100, respectively.[2] Somewhat more compressive modulus data were available for glass-polyester composites, values ranging from 2.5-4.3 x 10^6 psi at 77K the highest value obtained with 181/Polyester C.[1] The silicones not only averaged about like the polyesters but had about the same spread in 77K values at 2.3-4.6 x 10^6 psi. The data on glass-teflon and glass-Imidite composites were provided by Chamberlain et al.[2] It is of particular interest to note that the 181 glass/Imidite

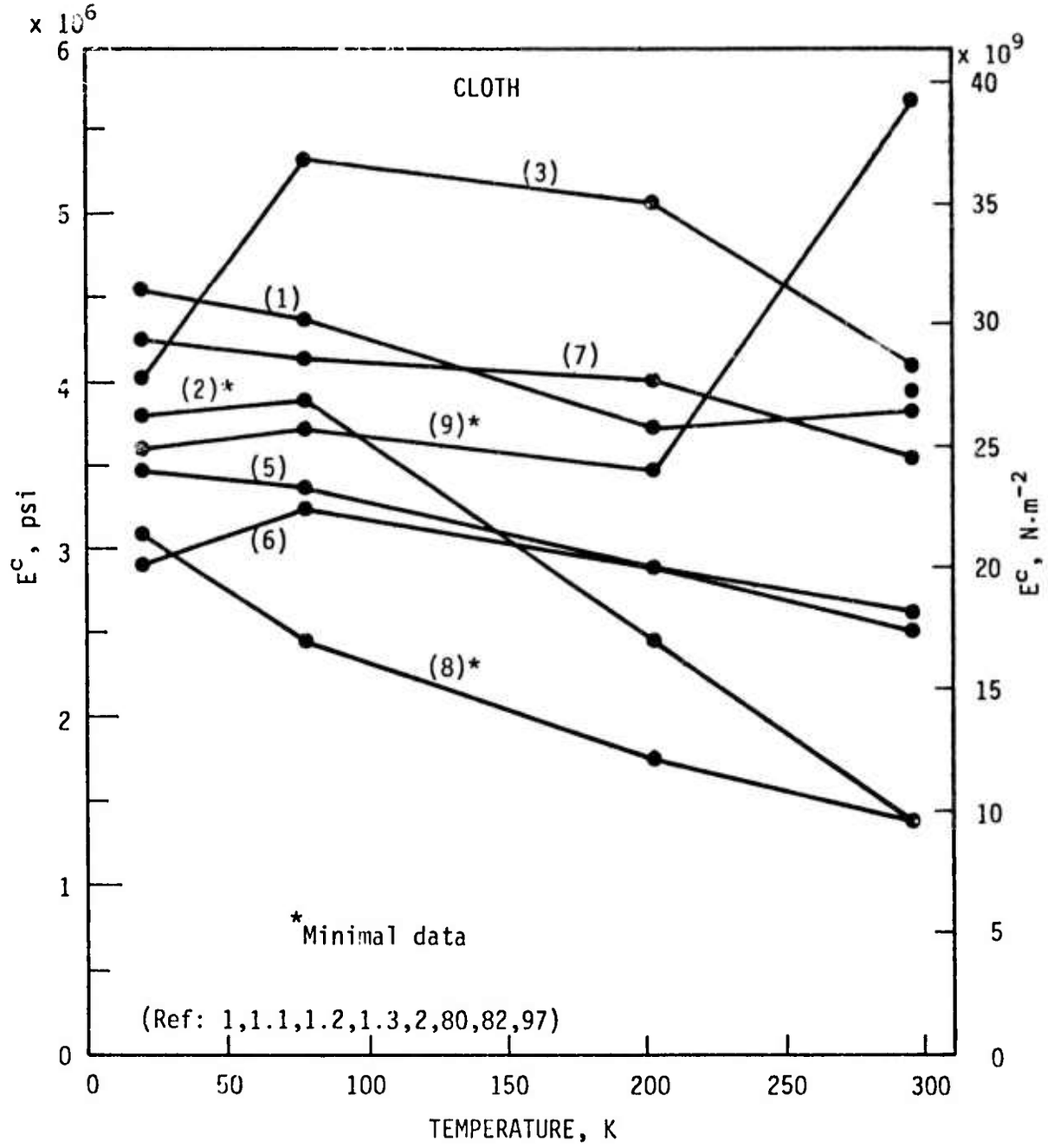

Fig. 7 Compressive Modulus of Glass-Reinforced Composites.

(1) Cpoxy	(4) Polyimide	(7) Phenyl Silane
(2) Polyurethane	(5) Polyester	(8) Teflon
(3) Phenolic	(6) Silicone	(9) Imidite

composite shows a sharp decline in both compressive strength and modulus on cooling from 295K to 77K, the only composite to show this behavior.

Interlaminar Shear Strength - Figure 8

Interlaminar shear strength is a property unique to composites. It is the resistance to shearing in the plane of the lamella defined by the fiber reinforcement. It is believed to strongly affect structural integrity, particularly in compression loading. Like the flexural test, the results of interlaminar shear tests evaluate several composite parameters, including resin strength, resin-fiber bond strength, filament distribution, and matrix porosity. As such, interlaminar shear joins the flexure test in being a valuable indication of overall composite quality but providing few data directly useful in engineering calculations. Its most valuable application may well be in quality control during composite manufacture.

Nevertheless, it is of interest to consider the published values for interlaminar shear, if for no other reason than to compare the results obtained with the different methods. Interlaminar shear is usually measured either by the guillotine method in which interlaminar shear is forced by the imposition of opposing but offset cuts in a flat tensile specimen or by a dimensional modification of the flat-specimen flexural specimen so as to force failure by shear on the central layers of the composite (short-beam shear). Of the two methods, the latter is most widely used. Unfortunately, the results obtained by the two methods are not comparable, the short-beam test usually yielding values higher than that of the guillotine. The overall situation is made still more complex by the understandable desire of some investigators to obtain interlaminar shear data from filament-wound composites prepared by the NOL ring method in which case the flexural method must be used with a short section of the ring. Because the specimen is not flat, the results are not comparable to either of the above methods. It is for this reason that the interlaminar data appearing on Figure 8 have been separated according to the various test methods.

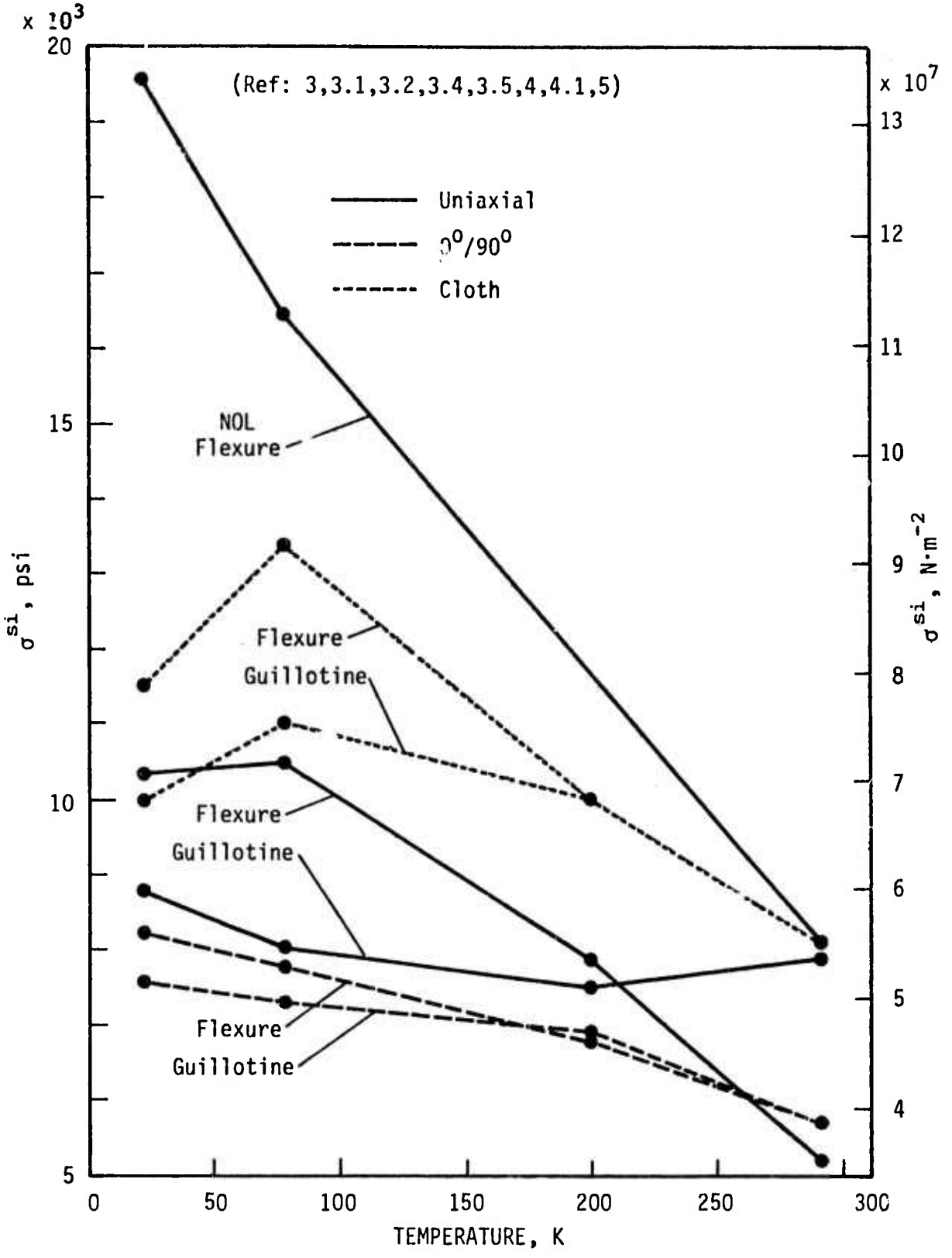

Fig. 8 Interlaminar Shear Strength of Glass-Epoxy Composites.

The largest discrepancy is observed for the uniaxial composites, the values obtained by the NOL short-beam method being much higher than those in conventional short-beam or guillotine methods. It is obvious from Figure 8 that one must be very cautious in comparing interlaminar shear values published in the literature. In interpreting these kind of data, it is also necessary to take into consideration that the very high values developed in the NOL short-beam test may also reflect the generally lower void content in filament-wound composites as compared to vacuum-bagged or autoclave-cured flat layups.

In the case of crossply or cloth laminates, only the conventional short-beam flexure test or the guillotine test may be used. Figure 8 shows that the results of these two test methods are in reasonably close agreement for the 0°/90° crossply layups, while the cloth-reinforced composites show lower values for the guillotine as compared to the short-beam test mode. The same is true for the uniaxial layups tested by these two methods.

The variety of test methods used and the variety of different epoxy matrices which have been evaluated make it almost an exercise in futility to attempt to identify composite types which are clearly superior in interlaminar shear. The S-901/E-787 composite reported by Toth et al.[3] at 14.7 KSI (77K) in short-beam flexure looks good as this value is almost as high as those reported for the NOL short-beam test. The same composite also looked comparatively good when tested by the same author in a 0°/90° biaxially-filament-wound layup. Other composites which appeared to be relatively superior among their group were S-901 glass in an experimental resin Epon 826/Empol 1040/Z-6077/DSA/BDMA[5] in NOL short-beam and a 0°/90° layup of Hi-Stren glass in Epon 828/LP-3/Cure agent D resin in conventional short-beam shear.[4]

Ignoring the NOL flexure data, one observes on Figure 8 that the interlaminar shear values are the highest for the cloth-reinforced composites and lowest for the 0°/90° crossplies with the uniaxial layups in between. The

relatively high values for the cloth composites probably reflect the added shear resistance provided by the convolutions in the woven glass cloth. By similar reasoning, the uniaxial composites may be superior to the 0°/90° crossplies simply because the former provides no distinct lamella along which shear can propagate.

Again, in a repetition bordering on monotonous, the interlaminar shear strength is found to become erratic upon cooling from 77K to 20K, while the 200K properties appear to be as expected.

Ultimate Tensile Strain - Figure 9

In view of the high strength of the glass-polymeric composites coupled with their relatively low modulus and absence of significant plastic flow at rupture, it might be expected that the strains accommodated at fracture would be somewhat larger than those of the higher-modulus advanced composites. This is substantiated by Figure 9 on which it is seen that ultimate tensile strains are in the 10^{-2} range for glass reinforcement while, as we shall see later in this review, similar data for the advanced composites are in the 10^{-6} range.

This relatively high fracture strain is, of course, a direct reflection of the high fracture strain of the glass reinforcement. This has some interesting consequences because while the fracture strain of some polymeric matrix materials may approach that of glass at 295K, the ductility of almost all polymers falls drastically upon cooling to cryogenic temperatures with the result that at low temperatures, fracturing of the matrix occurs well before fracture of the glass fibers.[6] A dramatic example of this phenomenon is found during proof testing of filament-wound pressure vessels where the cracking of the polymeric matrix is very audible. It is surprising that, at least in the case of hydrostatically loaded pressure vessels, such rupturing of the matrix does not decrease the overall rupture strength of the tanks and may even produce an increase. One must emphasize, however, that this does not imply that fracturing of the matrix is always acceptable or that it may be tolerated in other structures.

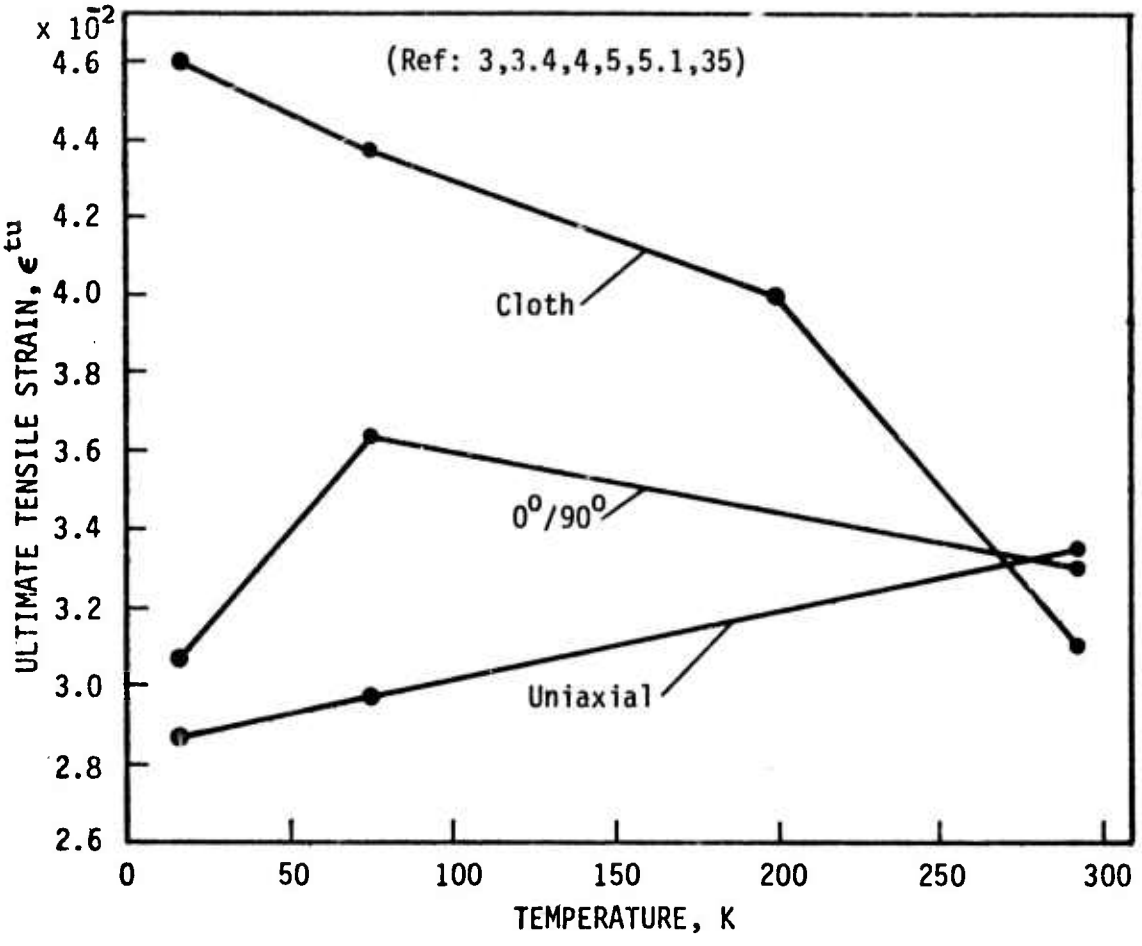

Fig. 9 Ultimate Tensile Strain of Glass-Epoxy Composites.

Figure 9 indicates that at 295K, the average fracture strain will be similar for uniaxial, 0°/90° and woven-cloth glass-epoxy composites, the strains being on the order of 3.2×10^{-2}. On cooling, however, marked differences develop between the layup types. Ultimate tensile strains in the uniaxial composites (tested in the longitudinal direction) decreased upon cooling to 77K while cooling the 0°/90° and cloth layups resulted in increased fracture strain. Detailed examination of the data shows this to be a true behavior, as five of the six composites forming the uniaxial data showed the decline (the exception being S-901/E-787[3]) while all eight of the 0°/90° and all three of the cloth composite types showed substantial increases upon cooling to 77K.

Again, considering 77K as a reference temperature, the uniaxial data were found to range from $1.9\text{-}5.3 \times 10^{-2}$, the highest being the previously noted work of Toth, et al.[3] Among the 0°/90° crossply data, values showed a relatively narrow spread of $3.2\text{-}4.5 \times 10^{-2}$, the S-901/E-787 composite again topping the list.[3] Cloth-reinforced data ranged from $3.5\text{-}5 \times 10^{-2}$, the highest ultimate tensile strain being reported for 1581/E-787.[3]

Data on strain to fracture at cryogenic temperatures are rare for other than the epoxy-matrix types. Kerlin, et al.[64, 65] have reported a fracture strain of 2.75×10^{-2} for a Mobaloy 81 AH7 glass-cloth phenolic composite at 77K and a value of 5.3×10^{-2} for a Selectron 5003 glass-cloth polyester composite at the same temperature. Also, Toth, et al.,[3] have reported 5.3×10^{-2} for a crossply glass-polyester composite Selectron 5003.

Static Fatigue

Under sustained room temperature loading, glass filaments have been found to deteriorate and fracture under applied stresses substantially below that of their normal ultimate tensile strength. As such, the failure is analogous to stress corrosion in metals. Some published data indicate that glass-filament-wound pressure vessels may undergo similar deterioration,[99] although some indication has also been obtained suggesting that static fatigue

of glass-reinforced composites may pose less of a problem at cryogenic temperatures than at 295K.[66] Static fatigue will be an important factor in any composite used in the rotating components of superconducting motors and generators, and in view of the minimal data presently available, further studies are needed to clarify the magnitude of the problem and to select formulations providing utmost resistance to such failure at cryogenic temperatures. T. T. Chiao of the Lawrence Livermore Laboratories is currently directing an extensive static fatigue program at room temperature on dead-weight loaded filaments coated with resin. As this latter method tests a basic structural element of the composite and permits many specimens to be run concomitantly, it should provide a useful and relatively inexpensive method of evaluating static fatigue at cryogenic temperatures.

Bearing Yield Strength - Figure 10

Bearing yield strength is a test designed to determine bearing stress as a function of the deformation of a hole through the composite. The load is applied by a pin inserted into the hole. The intent of the test is to provide information on the stress that may be sustained across riveted or bolted joints without loosening the joint. Bearing yield strength is defined as that stress on the stress-strain curve which corresponds to a distance of 4% of the bearing hole diameter when measured from the intersection of a line tangent to the stress-strain curve at this point and the zero load axis. (See insert, Figure 10.)

Bearing yield strengths for a series of epoxy-matrix composites have been reported by Toth et al.,[3] while Chamberlain et al.,[2] have provided data on silicone-, polyurethane-, and phenyl silane-matrix composites. These data are summarized on Figure 10.

The glass-epoxy composites developed bearing yield strengths which increased from about 50 KSI at 295K to 70-75 KSI at 77-20K. The uniaxial and 0°/90° data were very similar, while the cloth-reinforced epoxies were lower at 295K and at 200K but increased their strength to equal that of the others at 77K.

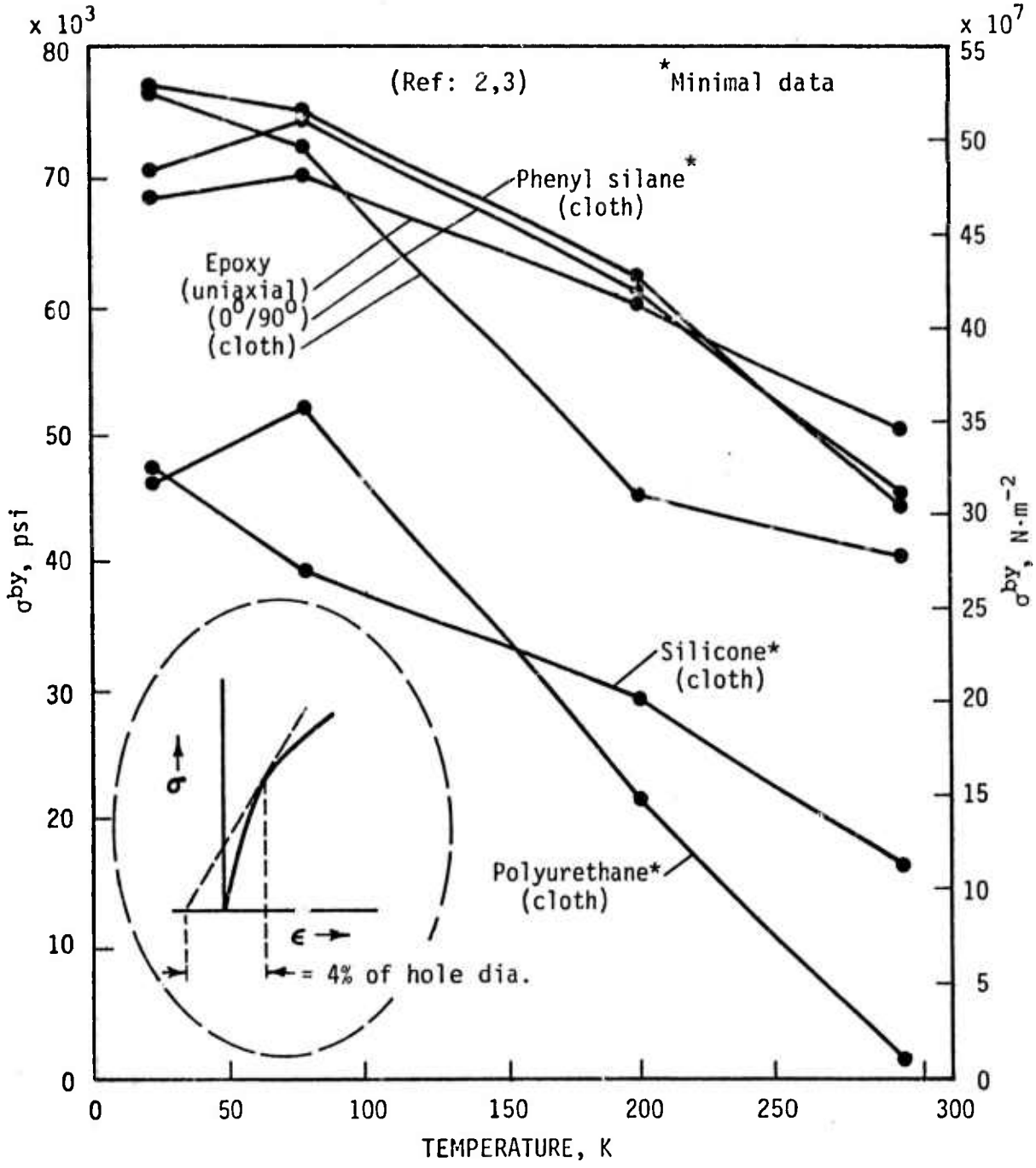

Fig. 10 Bearing Yield Strength of Glass-Reinforced Composites.

Data on the other matrix types were only available for cloth reinforcements. The phenyl silane composite developed a bearing strength equal to that of the epoxies, while the silicone- and polyurethane-matrix materials were distinctly inferior.

Again, there is indication of erratic behavior on cooling from 77K to 20K.

DYNAMIC MECHANICAL PROPERTIES

Cyclic Fatigue - Figure 11

Cyclic fatigue of glass-reinforced composites at cryogenic temperatures has been studied by Brink, et al.,[1] and by Chamberlain, et al.,[2] in tension, by Fontana, et al.,[34] by reciprocating beam, while Lavengood and Anderson[70] have contributed data on torsional fatigue. The data are not extensive, reflecting the very high cost of generating complete S-N curves at cryogenic temperatures. Yet, such testing is mandatory to provide assurance that composite components will fulfill their life expectance in such applications as rotating cryogenic machinery. Every effort must, therefore, be made to restrict such testing to composites which have the best chance of developing superior fatigue properties. The data reviewed herein provide some sense of direction; however, there remains an urgent need for some type of relatively inexpensive screening test which will permit relative ranking of composite cyclic fatigue performance at cryogenic temperatures.

In comparison to that of the advanced composites or to most conventional metals, the dynamic fatigue properties of glass-reinforced composites are not good. This is primarily due to the fatigue behavior of glass-polymeric materials being controlled by the properties of the matrix. Even at room temperature, the strain accommodation of the most epoxy resins is less than that of the glass reinforcement, and as it is the latter which controls the ultimate strength of the composite, cracking of the matrix will occur at ultimate loads far below the composite ultimate strength, allowing corrodents to attack the glass. In crossply layups, such cracking may occur at stress levels as low as 20% of the ultimate composite strength.

Lavengood has pointed out that since fatigue life of a glass-reinforced composite is related to the strain capability of the matrix, embrittling of the matrix due to lowering of the temperature should lower the fatigue life. However, this is not always experimentally verified. Based on an analysis of experimental torsional fatigue data, Lavengood concluded that fatigue life at cryogenic temperatures is strongly affected by the composite interfacial stress which arises due to differential thermal contractions of the filament and the matrix. Where fatigue strains serve to increase compressive interfacial stresses, the fatigue life may increase with lowering of temperature, the reverse being true when strains decrease the interacial stress.

The published tensile-fatigue data of Brink[1] and Chamberlain[2] and their coworkers were, with one exception, obtained on 181 cloth-reinforced composites. As an initial criteria, composites were screened by testing at 30% of their ultimate tensile strength developed at 295K and 77K. Those composites failing to achieve 10^6 cycles were dropped while those which were successful were further tested at 200K and 20K. The conventional polyester-matrix composites 181/Hetron 92, 181/Hetron H-31, 181/paraplex P-43, and 181/Narmco 527 were unsuccessful as was the silicone-matrix composite 181/Trevarno F-131.

It is beyond the scope of the present task to comprehensively review this data for which the reader may refer to the original references. However, in order to provide the reader with a sense of the fatigue performance of glass-polymeric composites, we have prepared Figure 11 from the data of Brink[1] and Chamberlain.[2] This Figure presents the fatigue strength of the various successful materials as a function of temperature after 10^6 fatigue cycles, the maximum studied in this work. It is also instructive to know the percent of the relevant ultimate strength retained by each composite type at each temperature after 10^6 cycles; consequently, these data also appear on Figure 11.

Figure 11 shows that the absolute magnitude of the stress required to induce fatigue failure at 10^6 cycles generally increases with decreasing

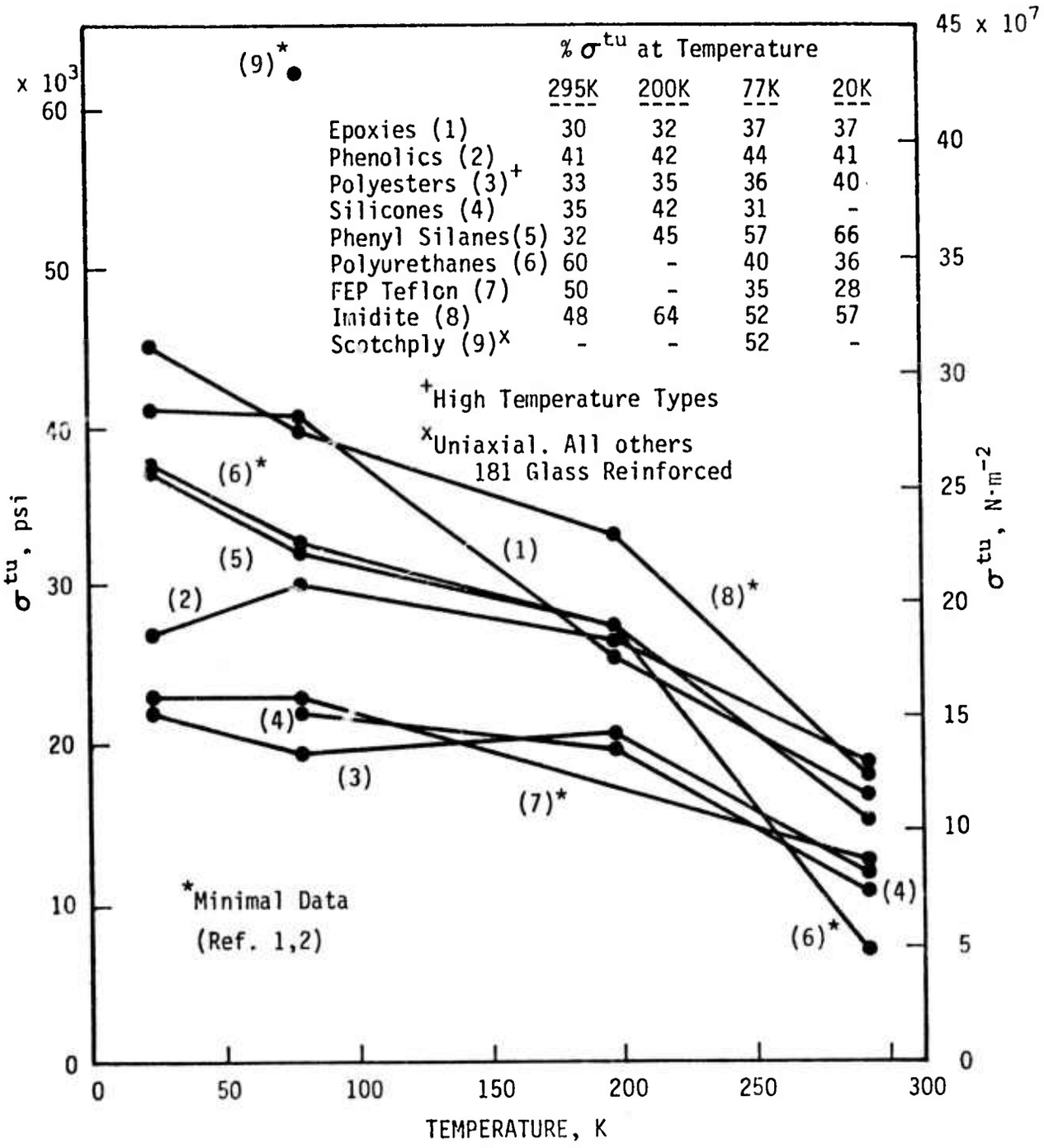

Fig. 11 Cyclic Tensile Fatigue Strength of Glass-Reinforced Composites After 10^6 Cycles.

temperature for all materials studied, only the high-temperature polyesters (Laminac 4232 and Vibrin 135) and perhaps the silicones (Narmco 513 and Trevarno F-130) not showing an appreciable increase below 200K. At all temperatures, the Imidite composite demonstrated superior fatigue performance both in terms of absolute retained tensile strength after 10^6 cycles and in the percentage of the original strength retained. The epoxies also looked good, but primarily because of the somewhat higher initial strength--their percentage retention of strength was among the lowest of the group. The best of the epoxies appeared to be Epon 828/DDS.[2] The polyurethane-, phenyl silane-, and phenolic-matrix composites appeared to group into an intermediate performance class while the polyester-, silicone-, and teflon-matrix composites showed distinctly inferior fatigue properties. Data at 77K only was available for a Scotchply 1002 uniaxial glass-epoxy composite,[2] which Figure 11 shows to have a much higher strength after 10^6 fatigue cycles at 77K than any of the cloth-reinforced types; nevertheless, even this composite showed retention of only about 52% of its original strength at that temperature.

Do the data indicate the existence of a stress limit below which fatigue life is essentially infinite? In most cases, testing was not carried out to a sufficiently large number of cycles to answer this question. However, judging from the shapes of the S-N curves developed with 181/Epon 1001 by Brink and his coworkers,[1] it appears that this glass-epoxy formulation may reach such a limit at about 30 KSI for temperatures below 77K (~30% UTS). Conversely, the S-N curve for the 181/Epon 828 composite showed no indication of flattening out at 10^6 cycles. With the possible exception of the silicone-resin composites, 181/Narmco 513 and 181/Trevarno F-130, there was no evidence that cooling the composites had any effect on establishment of a fatigue limit where none was evident in the room temperature data.

Again, one notices an apparent tendency for the data to become erratic when cooling from 77K to 20K.

Impact Strength and Fracture Toughness

Impact strength and its more sophisticated partner--fracture toughness--are measurements of the amount of energy that may be stored in a structure before the energy is released by fracture. As it is only in recent years that fracture mechanics has been put on solid theoretical grounds and exploited in homogeneous metals, it is not strange to find that application of parallel concepts to composites is still in its infancy. Furthermore, there is a major problem in applying basic principles of fracture mechanics to composites where, in most cases, multiple cracking occurs so that a unique "crack length" cannot be defined.

Measurement of the energy required to fracture specimens--the impact test--is the most simple method of obtaining data on relative material toughness. Such tests show the glass-reinforced composites to have much greater toughness than do the advanced composites, probably reflecting the much larger strain-accommodation of glass filaments in comparison to the advanced fiber reinforcements. Unfortunately, the literature contains few low temperature data even on this simple parameter, and that which is available is impossible to systematize due to differing test methods, specimen design, and filament orientation. Lewis and Bush[4] have evaluated a series of epoxies and modified epoxies reinforced with Hi-Stren glass using the Izod impact method. For unidirectional composites, they find the 295K impact strength to vary from 82-128 ft-lb in^{-1} of notch. On cooling to 77K, the measured values ranged from 67-162 ft-lb in^{-1}, some formulations showing 45% increase in impact strength while others showed as much as a 26% decline. A 0°/90° crossply test with the same composite formulations yielded room temperature impact strengths from 49-96 ft-lb in^{-1} and 77K values of 59-76 ft-lb in^{-1} with strength changes ranging from +36% to -26%, no consistent behavior being shown by any specific composite formulation. Data published by other authors,[71, 80, 103, 109, 110] are equally confusing. Perhaps part of the answer is provided by Levin[71] who followed the change in impact strength of glass-phenolic and glass-epoxy specimens at closely spaced intervals from 295K to 77K and found that the impact properties peaked

sharply at about -30°C followed by a rapid decline at lower temperatures. If the impact properties are indeed such a rapidly changing function of temperature, it might account for the lack of systematic change noted in data taken only at two or three temperatures. Clearly, this is an area which must be given much more attention in the future if composite behavior at cryogenic temperatures is to be well understood.

THERMAL PROPERTIES

Thermal Contraction - Figures 12 and 13

All of the glass-reinforced polymers contract when cooled. As we wish to review the behavior of such composites on cooling from 295K, the data have been plotted as thermal contraction, avoiding negative values of $\Delta L/L$.

Thermal contraction is very dependent on the type of composite layup as well as on the orientation of the composite. Figures 12 and 13, therefore, present data on values obtained normal to the fiber reinforcement for uniaxial, 0°/90° crossply and cloth layups. Other factors affecting thermal contraction are the specific resin used and the composite fiber density.

The thermal contraction is always found to be higher in a direction normal to the fibers than in the fiber plane, the difference increasing as the temperature is lowered. This reflects the much higher thermal contraction of the polymer as compared to the glass reinforcement. This is very evident in the data for uniaxial epoxy-matrix composites, where at 20K the thermal contraction normal to the fibers varies from about 2.5 to 5 times that in the fiber direction at 20K. An apparent anomaly appears in the 0°/90° crossply data, which shows a remarkably small difference in contraction between these two directions. This occurs because, in a filament-wound crossply composite, each layer of glass is in close proximity to the orthogonal layer next to it and thus provides resistance to dimensional change in the thickness direction. This effect is much less evident in the cloth layups because the

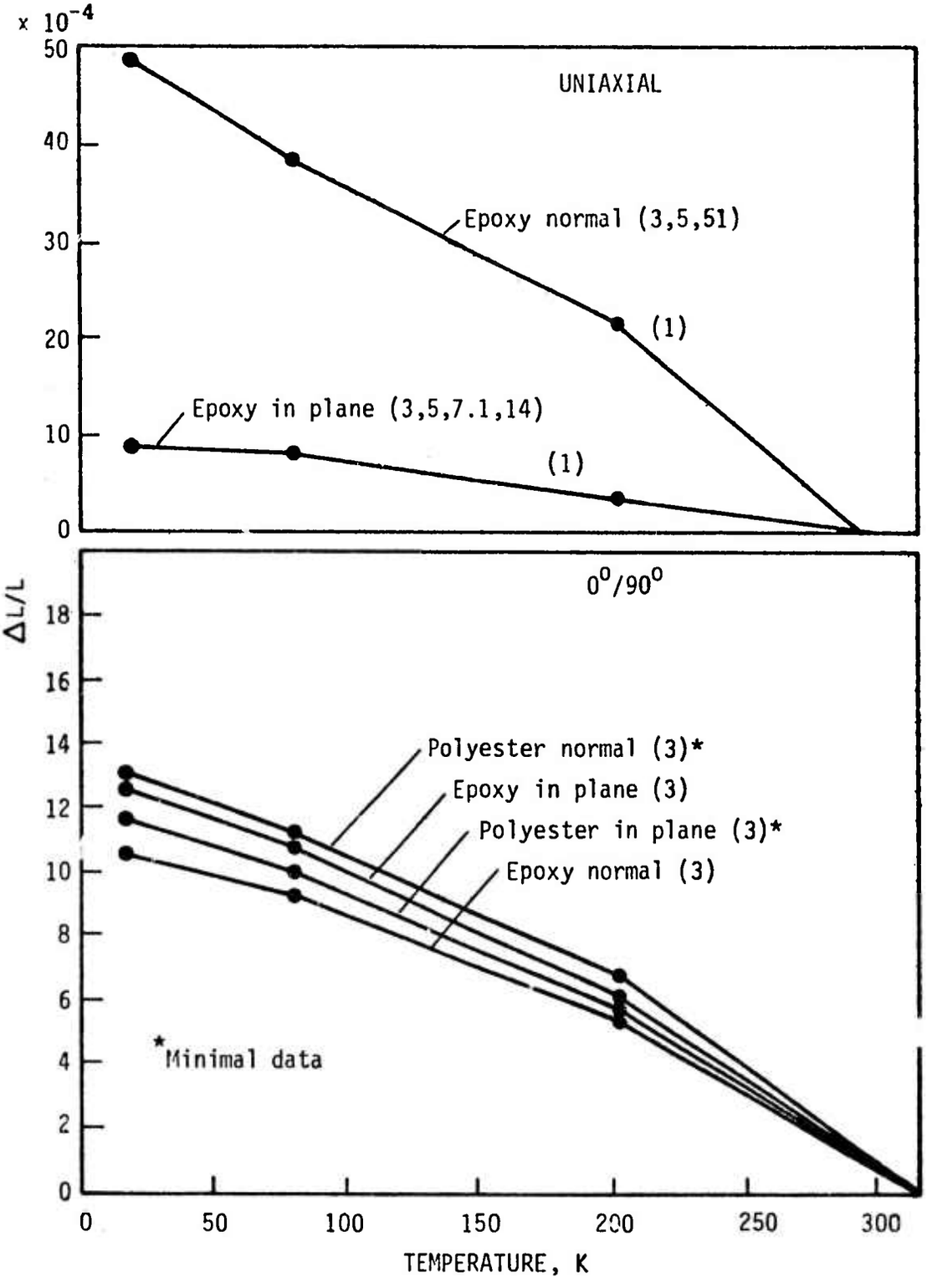

Fig. 12 Thermal Contraction of Glass-Fiber Reinforced Composites.

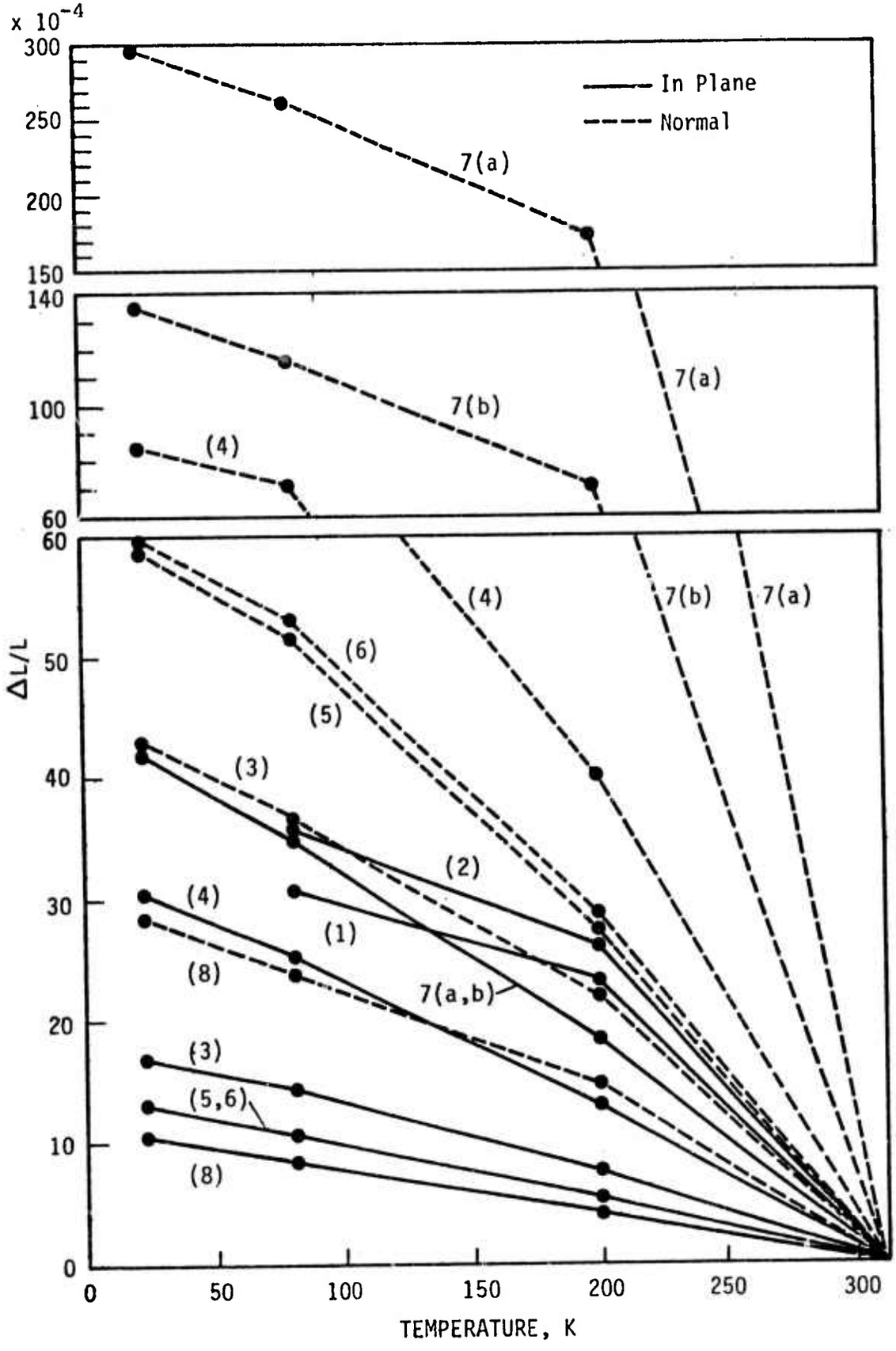

Fig. 13 Thermal Contraction of Glass-Cloth Reinforced Composites.

(1) Epoxy (Ref. 85, 101)
(2) Polyurethane (Ref. 85)
(3) Phenolic (Ref. 14)
(4) Polyester (Ref. 14)
(5) Silicone (Ref. 14)
(6) Phenyl Silane (Ref. 14)
7(a) Teflon TFE (Ref. 14)
7(b) Teflon FEP (Ref. 80)
(8) Imidite (Ref. 16)

262

latter are prepared from prepreg tape which results in a much lower filament density than is obtained in filament winding.

As the thermal contraction of the composite is dominated by the properties of the polymeric matrix on cooling, one might anticipate considerable variation in contraction even within a given matrix type, reflecting, for example, the effect of additives to epoxy resins. This is found to be true; for example, the $\Delta L/L$ data for epoxy matrix composites varied from 20-75 x 10^{-4} in the thickness direction and from 4.4-11.5 x 10^{-4} in the fiber direction. In the 0°/90° layups, the epoxy composites showed variations of 5.1-13.8 x 10^{-4} in thickness and 9.2-13 x 10^{-4} in the fiber direction. The polyester resins gave similar data spread in the 0°/90° layups.

A much greater variation is observed in the thermal contraction among cloth-reinforced composites, reflecting both the larger variety of matrix materials for which data are available and the greater variation in fabrication method. The glass-teflon composites have the highest thermal contractions of all the materials examined. Furthermore, the teflon matrix may be either of the TFE (polytetrafluoroethylene) or FEP (copolymer with hexafluoropropalene) type which have markedly differing thermal contraction characteristics. This difference does not appreciably affect contraction in the fiber plane due to the restraint provided by the fibers. However, the difference is marked in the direction normal to the fibers. As indicated by the dashed curves 7(a) and 7(b) on Figure 13, the TFE-matrix composites have twice the transverse thermal contraction of the FEP-matrix types.

The epoxy- and the polyurethane-matrix composites also have relatively high thermal contractions. Unfortunately, no data were available in the fiber normal directions for these composites. The data indicate that the polyester-matrix composites are next in decreasing order of thermal contraction, with the fiber normal data being approximately 2.8 times greater than in the fiber plane. Showing the least thermal expansion in the

fiber plane are the phenolic-, silicone-, phenyl silane-, and Imidite-matrix composites. Of these, the phenolic composite data appear to be abnormally high for the fiber normal case, since, if all else were equal, the order in the fiber normal direction should follow that in the fiber plane.

All of the polymeric matrices create compressive stresses in the glass reinforcement upon cooling to cryogenic temperatures, such stresses being added to those already existing from cooling from the cure temperature to room temperature. This is primarily manifested as shear stress at the resin-fiber interface, so that it might be expected that an effect would be seen on those strength properties which are sensitive to debonding of the matrix-glass interface. One such property is fatigue, and from Figure 11, it is noted that the fatigue properties of the teflon-matrix composites are poor, while that for the Imidite is good, consistent with the respectively high and low thermal expension of these two composite types. A similar relationship holds for the flexural strength, Figure 3. Interfacial residual stress is but one of the factors influencing fiber debonding, of course, others being the ability of the interface to sustain a shear load and the strength of the matrix itself.

Specific Heat - Figure 14

The specific heats of glass-reinforced composites show an almost linear dependence on temperature from 295K to 77K, and relatively small difference between matrix types. The specific heats are relatively high compared to most metals, being roughly comparable to that of aluminum but substantially higher than that of titanium, iron, or copper. Teflon- and polyester-matrix composites have the highest specific heat. The epoxy-, Imidite-, silicone-, and phenolic-matrix composites are bunched on the lower specific heat side of the group. The phenyl silane-matrix composite seems to have a slightly larger temperature dependence, starting out in the middle of the group at 295K, but showing the lowest specific heat at 77K.

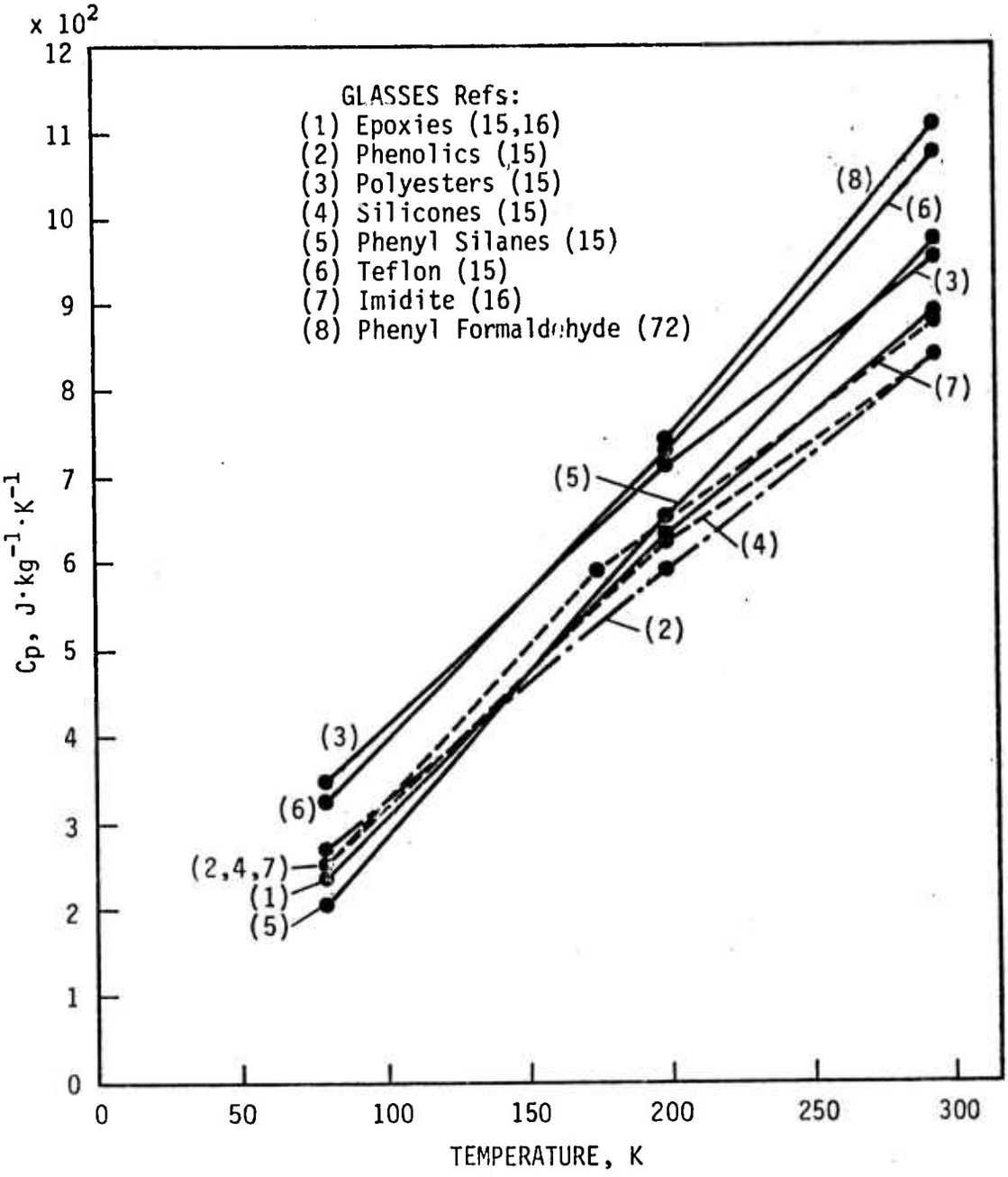

Fig. 14 Specific Heat of Glass-Reinforced Composites.

The data reflects the work of Campbell, et al., [15, 16] with the sole exception of the phenyl formaldehyde contribution of Luikov. [72] Except for the epoxies, data reflect only one composite for each type of matrix. The epoxy data reflect the average of three compositions: a unidirectional YM-31-A/DER-332 and a unidirectional S-994/E-787 composite. The spread in specific heat values for these three formulations at 295K, 200K, and 77K was 8.16-9.21, 6.07-6.7 and 2.09-2.72 x 10^{-2} J $Kg^{-1}K^{-1}$, respectively, with the highest value associated with the S-994/E-787 composite.

Thermal Conductivity - Figures 15 and 16

As with thermal contraction, the conductivity is dependent on the type of layup and on the orientation of the composite. Figures 15 and 16, therefore, present data on values obtained normal to the fiber reinforcement (thickness direction) and in the plane of the reinforcement for uniaxial, 0°/90° crossply and for woven-glass cloth layups. Also, as with contraction, the thermal conductivities are affected by the matrix resin and by the density of the reinforcement fiber. Continuity of the fiber is also a factor affecting in-plane conductivity.

Both the difference between the fiber normal and the in-plane conductivities for a given composite and the absolute spread of conductivity values among the various composite types is the widest at room temperature. However, these differences rapidly diminish as the temperature is lowered.

Figure 15 contains data for uniaxial and 0°/90° epoxy layups and for a 0°/90° silicone-matrix layup. The highest thermal conductivity was for the filament-wound uniaxial epoxy composite in the plane of the fiber. This is to be expected from the high density of continuous glass fibers in that direction. The conductivity in the fiber normal direction is 25-50% less, reflecting the lower thermal conductivity of the matrix. Thermal conductivity in the fiber plane of the 0°/90° epoxy layup is only about 80% of that for the uniaxial composite, reflecting the lower effective fiber density in the direction of the heat flow.

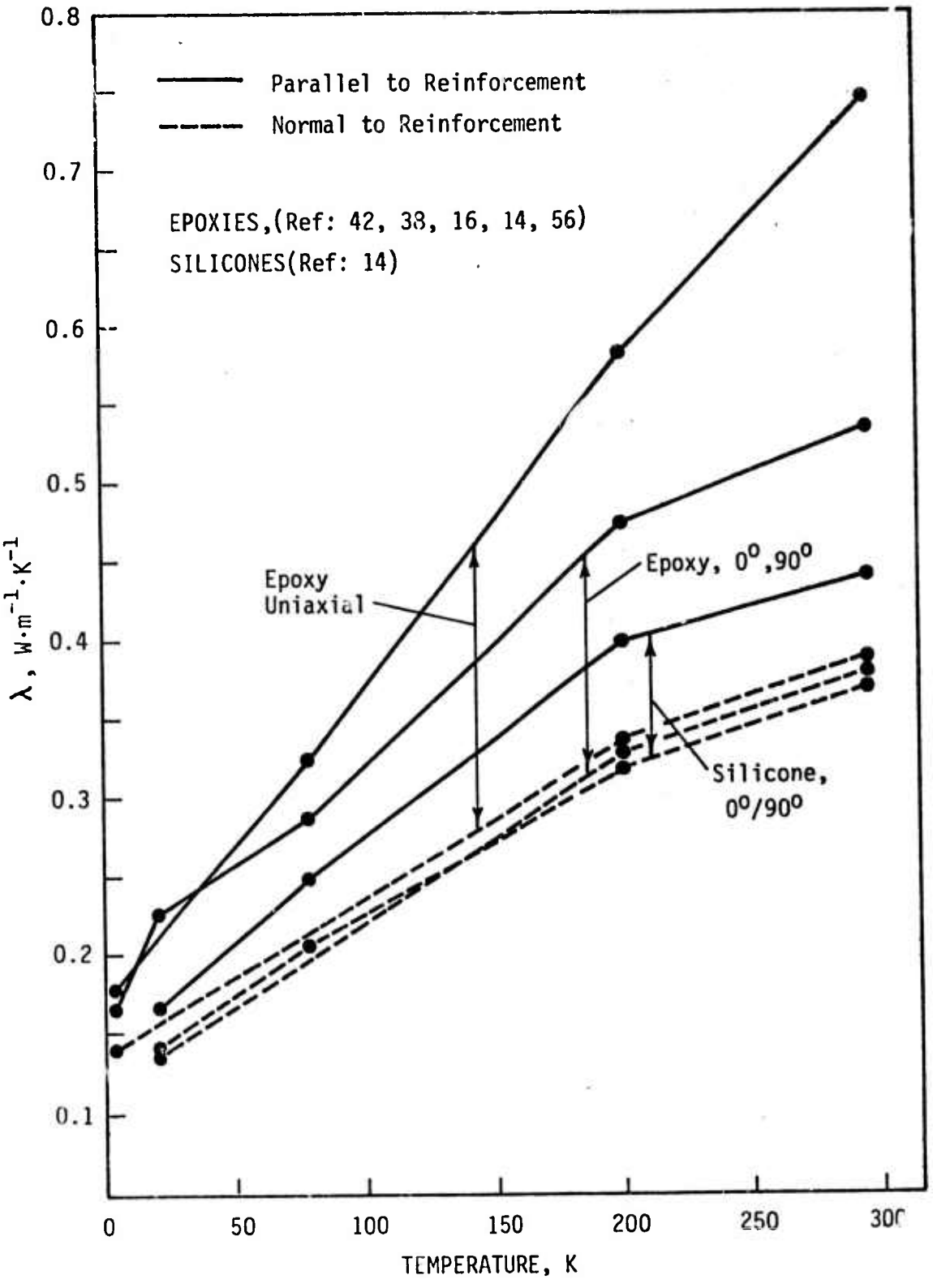

Fig. 15 Thermal Conductivity of Glass-Fiber Reinforced Composites.

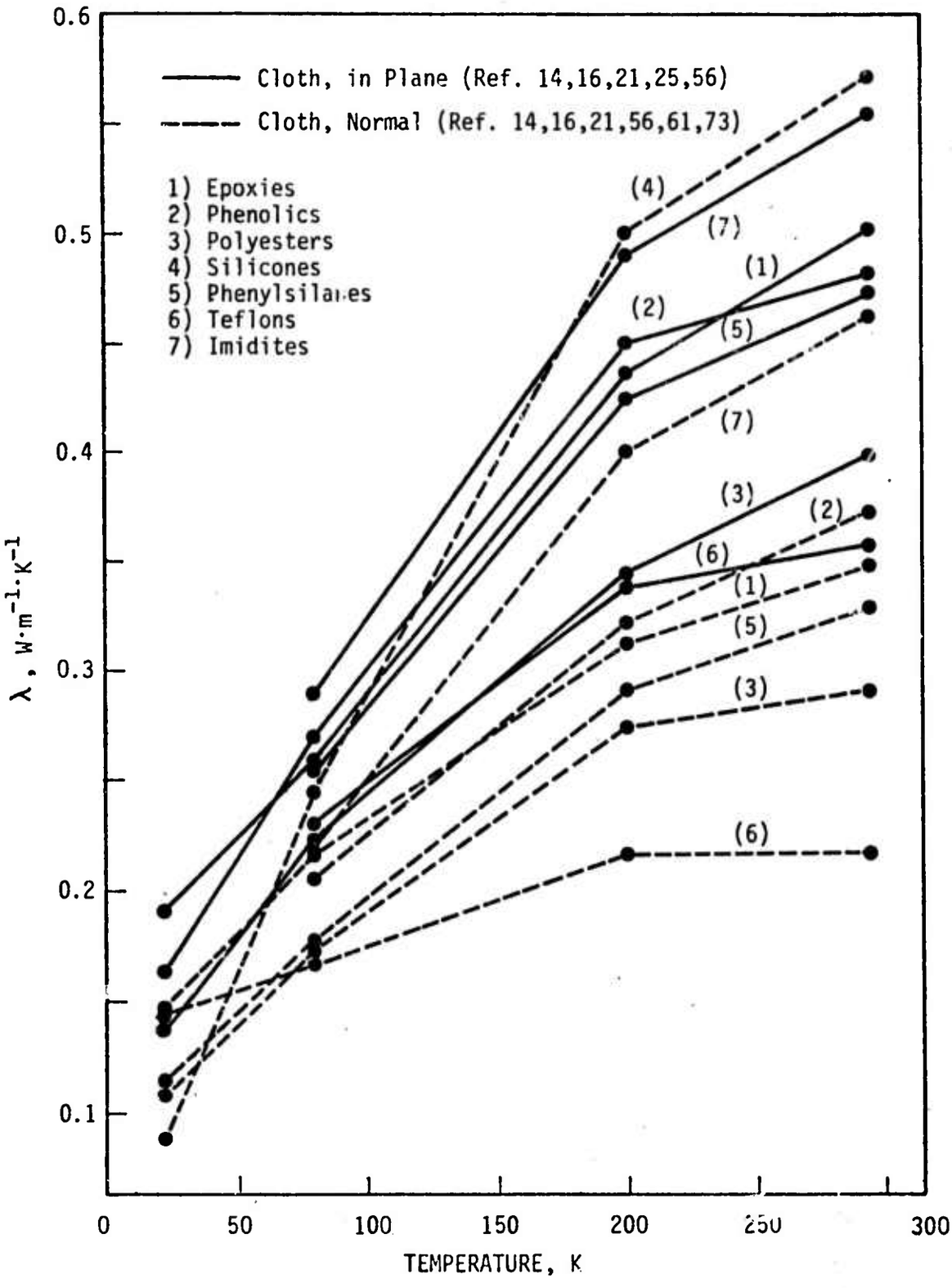

Fig. 16 Thermal Conductivity of Glass-Cloth Reinforced Composites.

Figure 15 shows the 0°/90° silicone-matrix composite to have a substantially lower in-plane conductivity than the 0°/90° epoxy layup. This does not imply that the conductivity of the silicone matrix is less than that of the epoxy; indeed, the marked similarity between the fiber normal data for both polymeric matrices indicates that the matrix conductivity is very similar in both materials. The difference reflects the relatively inferior heat transfer properties of glass roving which was used for the silicone-matrix composite as compared to the continuous filament used with the epoxy.

Among the cloth-reinforced composites, the highest thermal conductivity was found for the silicone-matrix composites. Only fiber normal data were available; however, even in this least conducting orientation, the conductivity exceeded that of all the other materials in their more favorable in-plane direction. The Imidite composite was next lowest, and in decreasing order were the epoxies, phenolics and phenyl silanes, all with approximately equal conductivities, both in-plane and plane normal. The lowest conductivities were evidenced by the polyesters and the teflons.

An interesting facet of these data is that, unlike the other thermal properties of composites, the thermal conductivity is affected by the ambient atmosphere in which the measurement is taken, i.e., it differs in helium, nitrogen or in vacuum. The values plotted in Figure 15 and 16 are averages of data obtained in the various atmospheres. However, a more detailed analysis of the literature data shows that, compared to values obtained in helium gas, data taken in nitrogen will average 7% lower, while in a vacuum the data will, on the average, be lowered by 20%.

The only composites for which there were more than one literature reference were the epoxies. For the latter, the data spread was found to be much greater for the in-plane conductivity than for the plane-normal, as would be expected in view of the relatively high conductivity of the fibers compared to the matrix. As an example, the data which averaged $0.50\ w \cdot m^{-1} \cdot K^{-1}$ for the 295K cloth-reinforced epoxy ranged from

0.30 to 0.65 $w \cdot m^{-1} \cdot K^{-1}$, while the plane normal data for the identical composites average 0.35 $w \cdot m^{-1} \cdot K^{-1}$ but ranged from 0.30 to 0.40 $w \cdot m^{-1} \cdot K^{-1}$. The scatter decreased significantly at lower temperatures.

COMMENTS ON GLASS-REINFORCED COMPOSITES

We have reviewed the properties of filamentary-glass reinforced composites at cryogenic temperatures in order to provide the reader with an overall feel for their behavior and the magnitude of the properties which may be expected. Having this information, for what applications should glass-reinforced composites be used? What composite formulation should be selected?

It would appear that glass-reinforced composites are most useful in applications requiring high tensile strength combined with high toughness and low thermal conductivity, but where stiffness is not required and where cyclic fatigue is not a major problem. In such applications, glass-reinforced composites have given and will continue to give excellent performance at relatively low cost. Filament-winding techniques should be used whenever possible in order to obtain the highest quality composites; in particularly the lowest void content.

The choice of composite will be dictated by the particular application, considering not only the final properties but considering equally the problems involved in working with a specific composite under production conditions. At the present time, the composite most widely used for cryogenic applications is S-901 glass filament-wound in an epoxy matrix known as Resin 2.[5] This resin, composed of Epon 828/DSA/Empol 1040/BDMA in proportions of 100/115.9/20/1 by weight, probably represents the current state-of-the-art for cryogenic applications.

An unexpected result of the present review is the surprisingly good overall performance of the glass-Imidite (polybenzimidazole) type. Presently available data indicate that at 77K, such a composite ranks second only to the epoxies in ultimate tensile strength and flexural strength while developing tensile and flexural moduli superior to the epoxies. Compressive properties

appear only average; however, in cyclic fatigue, the Imidite-matrix composite appears superior to all other matrix materials, particularly in percent of retained ultimate tensile strength. A key to its excellent fatigue properties may be the comparatively low thermal contraction of Imidite compared to the other polymers, resulting in comparatively low residual interfacial stress between the fiber and the matrix. It would seem that a second look at glass-Imidite composites is in order.

A pervasive characteristic of glass-polymeric composites is the erratic behavior of the mechanical properties on cooling from 77K to 20K. With few exceptions, the strength properties increase on cooling from 295K to 77K; however, on further cooling to 20K, the data indicate that such properties may either increase, decrease, or remain unchanged, the behavior being quite unpredictable, even among composites of the same matrix type. It is difficult to attribute this simply to the matrix becoming suddenly much more brittle between 77K and 20K, as cooling to 77K has already decreased the strain capability of the matrices to a level far below that of the glass reinforcement. The present task does not permit more than a cursory consideration of the possible factors involved in this phenomena; however, the author believes it relevant to call attention to recent studies on the low temperature properties of polymers which have provided convincing evidence that, in at least the linear polymers of the polycarbonate (PC) and polyethelene terepthalate (PET) types, the media in which the low temperature test is conducted can strongly affect the fracture mode and the resultant mechanical properties measured for the polymer.[125, 126] The experimental evidence indicates that the failure in such polymers in the cryogenic range is controlled by a crazing phenomena which, in turn, is related to the activity of the gas or liquid in contact with the polymer surface. Such studies have not been extended to the strongly cross-linked polymers; however, until proven otherwise, it must be considered a possibility that the mechanical properties of glass-polymeric composites may be influenced by the ambient media such that data obtained at 20K or 77K in liquid hydrogen or nitrogen may not be the same as those which would be obtained in a helium atmosphere.

This review suggests that the following work would be valuable in preparing glass-reinforced composites for use in critical components of superconducting machinery:

a) There are indications that static fatigue of glass-reinforced composites may not be a problem at cryogenic temperatures; however, data are minimal and should be expanded.

b) Data on cyclic fatigue of glass-reinforced composites at cryogenic temperatures, particularly high cycle fatigue, is minimal. That which is available does not clearly indicate the existence of a fatigue limit, although the available data does show the fatigue life for a given composite to be higher at cryogenic temperatures than at room temperature. It is evident that additional fatigue data will have to be obtained before glass-reinforced composites can be used with confidence under cyclic loading in superconducting machinery.

c) In view of the extremely high cost of conducting fatigue tests at 4K, an effort should be made to devise a screening test to correlate incipient damage with fatigue life so that full cycle fatigue testing will be restricted to those composite formulations showing the most promise.

d) No literature data were available on the resistance of glass-reinforced composites to thermal fatigue. As cycling through elevated temperatures has been shown to seriously degrade many types of composites, this parameter should be investigated for any composite likely to be subjected to thermal cycling in its application in superconducting machinery.

BIBLIOGRAPHY

CONTRACT BIBLIOGRAPHY

I - MECHANICAL PROPERTIES

Contract AF-33(616)-8289

Contractor: Directorate of Materials and Processes, Aeronautical Systems Division, Air Force Systems Command, Wright-Patterson Air Force Base, Ohio.

Research Facility: Narmco Research and Development, San Diego, California.

1.0 Brink, N. O., "Determination of the Performance of Plastic Laminates Under Cryogenic Temperatures", ASD-TDR-62-794, August 1962 (AD 288 944).

1.1 Ibid., "Mechanical Behavior of Reinforced Plastics at Cryogenic Temperatures", Technical Papers, 20th Annual Technical Conference, Society of Plastics Engineers, Vol. 10, Section XV-2, 1964, pp. 1-19.

1.2 Ibid., "Mechanical Behavior of Reinforced Plastics at Cryogenic Temperatures", Society of Plastics Engineers Journal, Vol. 20, 1964, pp. 1123-1131.

1.3 Ibid., "Mechanical Behavior of Reinforced Plastics at Cryogenic Temperatures", Narmco Research and Development Report, Code No. 105-4, 1964.

2.0 Chamberlain, D. W., Lloyd, B. R. and Tennant, R. L., "Determination of the Performance of Plastic Laminates at Cryogenic Temperatures", ASD-TDR-62-794, Part II, March 1964 (N64-24212).

2.1 Chamberlain, D. W., "Tensile Fatigue Testing at Temperatures Down to 20 K", Advances in Cryogenic Engineering, Vol. 9, 1964, pp. 131-138.

2.2 Ibid., "Mechanical Properties Testing of Plastic Laminate Materials Down to 20 K", Advances in Cryogenic Engineering, Vol. 10, 1965, pp. 117-125.

Contract NAS 8-11070

Contractor: National Aeronautics and Space Administration, George C. Marshall Space Flight Center, Huntsville, Alabama.

Research Facility: Goodyear Aerospace Corporation, Akron, Ohio.

3.0 Toth, L. W., Boller, T. J., Butcher, I. R., Kariotis, A. H. and Yoder, F. D., "Program for the Evaluation of Structural Reinforced Plastic Materials at Cryogenic Temperatures", NASA CR-80061 (Final), August 1966 (N67-12051).

3.1 Toth, L. W., "Properties Testing of Reinforced Plastic Laminates Through the 20 degree K Range", Technical Papers, 20th Annual Technical Conference, Society of the Plastics Industry, Section 7-C, 1965, pp. 1-10.

3.2 Toth, L. W. and Kariotis, A. H., "An Assessment of Test Specimens and Test Techniques Useful to the Evaluation of Structural Reinforced Plastic Materials at Cryogenic Temperatures", Advances in Cryogenic Engineering, Vol. 10, 1965, pp. 126-133.

3.3 Toth, L. W., "Properties of Glass-Reinforced Epoxy Through the 20 K Range", Modern Plastics, Vol. 42, August 1965, pp. 123-130.

3.4 Toth, L. W. and Burkley, R. A., "Mechanical Response at Cryogenic Temperatures of Selected Reinforced Plastic Composite Systems", Goodyear Aerospace Report GER-13169, Paper No. 16, Seventieth Annual Meeting of the American Society for Testing and Materials, June 1967.

3.5 Toth, L. W., Boller, T. J., Kariotis, A. H. and Yoder, F. D., "Program for the Evaluation of Structural Reinforced Plastic Materials at Cryogenic Temperatures", NASA CR-64005, June 1963 through June 1964 (N65-29724).

Contract NAS 3-6297

Contractor: National Aeronautics and Space Administration, Lewis Research Center, Cleveland, Ohio.

Research Facility: Aerojet General Corporation, Azuza, California.

4.0 Lewis, A. and Bush, G. E., "Improved Cryogenic Resin-Glass Filament Wound Composites", NASA CR-72163 (Final), March 1967 (N67-31856).

4.1 Lewis, A., Bush, G. E. and Creedon, J., "Improved Cryogenic Resin/Glass Filament-Wound Composites", NASA Interim Report CR-54867, May 1966 (N66-28040).

Contract NAS 6-6287

Contractor: National Aeronautics and Space Administration, Lewis Research Center, Cleveland, Ohio.

Research Facility: Aerojet General Corporation, Azuza, California.

5.0 Soffer, L. M. and Molho, R., "Cryogenic Resins for Glass Filament-Wound Composites", NASA CR-72114 (Final), January 1967 (N67-25076).

5.1 Ibid., "Mechanical Properties of Epoxy Resins and Glass/Epoxy Composites at Cryogenic Temperatures", Cryogenic Properties of Polymers, J. L. Koenig, Ed., Marcel Dekker, New York, 1968, pp. 87-117. (Identical to NASA CR-84451, 1967, (N67-27217).

Contract F04701-69-C-0059

Contractor: Space and Missiles Systems Organization, Air Force Systems Command, Los Angeles Air Force Station, Los Angeles, California.

Research Facility: The Aerospace Corporation, El Segundo, California.

6.0 Pepper, R. T., Rossi, R. E., Upp, U. W. and Riley, W. E., "Development of an Aluminum-Graphite Composite", SAMSO-TR-70-301, August 1970 (AD 718 409).

6.1 Pepper, R. T., Upp, J. W., Rossi, R. C. and Kendall, E. G., "Aluminum-Graphite Composites", SAMSO-TR-70-174, April 1970 (AD 706 883). (Identical to Metallurgical Transactions, Vol. 2, January 1971, pp. 117-120.)

6.2 Rossi, R. C., Pepper, R. T., Upp, J. W. and Riley, W. C., "Development of Aluminum-Graphite Composites", Ceramic Bulletin, Vol. 50, May 1971, pp. 484-487.

Contract NAS 8-11508

Contractor: National Aeronautics and Space Administration, George C. Marshall Space Flight Center, Huntsville, Alabama.

Research Facility: Harvey Engineering Laboratories, Torrance, California.

7.0 Sumner, E. V. and Davis, L. W., "Development of Ultrahigh Strength, Low Density Aluminum Sheet and Plate Composites", NASA CR-85863 (Final), July 1966 (N67-31181).

7.1 Davis, L. W., "Composites at Low Temperature", Paper No. 15, Seventieth Annual Meeting of the American Society for Testing Materials, June 1967.

Contract NASA DPR C 10360-B

Contractor: National Aeronautics and Space Administration, Lewis Research Center, Cleveland, Ohio.

Research Facility: Naval Ordnance Laboratory, Silver Springs, Maryland.

8.0 Simon, R. A. and Alfring, R., "Properties of Graphite Fiber Composites at Cryogenic Temperatures", NASA CR-72652 (NOLTR 69-183), May 1970, Tasks I and II (AD 746 885).

9.0 Larsen, J. V., "Properties of Graphite Fiber Composites at Cryogenic Temperatures -- Effect of Elastomeric Additions to Resin Systems", NASA CR-72804 (NOLTR 70-195), March 1971, Task III (AD 882 972).

10.0 Larsen, J. V. and Simon, R. A., "Carbon Fiber Composites for Cryogenic Filament-Wound Vessels", NASA CR-120899, (NOLTR 71-201), May 1972, Tasks IV, V and VI, (N73-11553).

10.1 Simon, R. A., "Graphite Fiber Composites at Cryogenic Temperatures", Technical Papers, 26th Annual Technical Conference, Society of the Plastics Industry, Section 10-D, 1971, pp. 1-4.

10.2 Larsen, J. W., "Fracture Energy of CBTN/Epoxy-Carbon Fiber Composites", Technical Papers, 26th Annual Technical Conference, Society of the Plastics Industry, Section 10-D, 1971, pp. 1-4.

Contract NAS 8-26198

Contractor: George C. Marshall Space Flight Center, Huntsville, Alabama.

Research Facility: General Dynamics/Convair, San Diego, California.

11.0 Scheck, W. G., "Development of Design Data for Graphite Reinforced Epoxy and Polyimide Composites", Report No. GDC-DBG70-005, General Dynamics Quarterly Report No. 1, 1970.

12.0 Maximovich, M. and Scheck, W. G., "Development of Design Data for Graphite Reinforced Epoxy and Polyimide Composites", Report No. GDC-DBG70-005, General Dynamics Quarterly Report No. 2, 1970.

12.1 Stuckey, J. M. and Scheck, W. G., "Development of Graphite/Polyimide Composites", National Technical Conference, Society of Aerospace Material and Process Engineers, Vol. 3, 1971, pp. 717-723.

Contract F33615-70-1442

Contractor: Air Force Materials Laboratory, Wright-Patterson Air Force Base, Ohio.

Research Facility: General Dynamics/Convair, San Diego, California.

13.0 Hertz, J., Christian, J. L. and Varlas, M., "Advanced Composite Applications for Spacecraft and Missiles, Phase I Final Report, Volume II: Material Development", AFML-TR 71-186, Vol. 2, March 1972 (AD 893 715L).

13.1 Forest, J. D., Fujimoto, A. F. and Foelsch, G. F., "Advanced Composite Applications for Spacecraft and Missiles, Phase I Final Report, Volume I: Structural Development", AFML-TR-71-186, Vol. 1, March 1972.

13.2 Forest, J. D. and Varlas, M., "Advanced Composite Applications for Spacecraft and Missiles, Final Report", AFML-TR-72-278, March 1973.

13.3 Christian, J. L. and Campbell, M. D., "Mechanical and Physical Properties of Several Advanced Metal-Matrix Composite Materials", Advances in Cryogenic Engineering, Vol. 18, 1973, pp. 175-183.

II - THERMOPHYSICAL PROPERTIES

Contract AF-33(657)-9160

Contractor: Air Force Materials Laboratory, Wright-Patterson Air Force Base, Ohio.

Research Facility: General Dynamics? Astronautics, San Diego, California

The following reports are in a series entitled "Thermophysical Properties of Plastic Materials and Composites to Liquid Hydrogen Temperature (-423°F)".

14.0 Haskins, J. F., Campbell, M. C., Hertz, J. and Percy, J. L., ML-TDR-64-33, Part I, June 1964 (AD 601 337).

15.0 Campbell, M. D., Hertz, J., O'Barr, H. L. and Haskins, J. F., ML-TDR-64-33, Part II, March 1965 (X65-18921).

16.0 Campbell, M. D., O'Barr, G. L., Haskins, J. F. and Hertz, J., ML-TDR-64-33, Part III, August 1965 (AD 468 155).

16.1 Hertz, J. and Haskins, J. F., "Thermal Conductivity of Reinforced Plastics at Cryogenic Temperatures", Advances in Cryogenic Engineering, Vol. 10, 1965, pp. 163-169.

16.2 Campbell, M. D., "Thermal Expansion Characteristics of Some Plastic Materials and Composites from Room Temperature to -253°C", Advances in Cryogenic Engineering, Vol. 10, 1965, pp. 154-162.

16.3 Campbell, M. D., Haskins, J. F., O'Barr, G. L. and Hertz, J. "Thermophysical Properties of Reinforced Plastics at Cryogenic Temperatures", Journal of Spacecraft, Vol. 3, April 1966, pp. 596-599.

(See also Ref. 13.0)

Contract F33615-72-C1388 (Work currently in progress)

Contractor: Air Force Materials Laboratory, Wright-Patterson Air Force Base, Ohio.

Research Facility: General Dynamics/Convair, San Diego, California.

17.0 Forest, J. D. and Schaeffer, W. H., "Advanced Composite Missile and Space Design Data", General Dynamics Report GDCA-CHB72-001-1, Progress Report No. 1, October 1972.

18.0 Forest, J. D., "Advanced Composite Missile and Space Design Data", General Dynamics Report GDCA-CHB72-001-2, Progress Report No. 2, January 1973.

III - GENERAL BIBLIOGRAPHY

19.0 Aleck, B., "Fiberglass-Overwrapped 2219-T87 Aluminum Alloy Low-Pressure Cryogenic Tankage", Society of Aerospace Material and Process Engineers National Technical Conference, Space Shuttle Materials, Vol. 3, 1971, pp. 131-134.

20.0 Alfring, R. J., Morris, E. E. and Landes, R. E., "Cycle-Testing of Boron Filament-Wound Tanks", NASA CR-72899, National Aeronautics and Space Administration, Lewis Research Center, August 1971 (N71-38023).

21.0 Barber, J. R., "Design and Fabrication of Shadow Shield Systems for Thermal Protection of Cryogenic Propellants", NASA CR-72595, National Aeronautics and Space Administration, Lewis Research Center, Cleveland, Ohio, November 1969 (N70-25098).

22.0 Baucom, R. M., "Tensile Behavior of Boron Filament-Reinforced Epoxy Rings and Belts", NASA TN D-5053, Langley Research Center, Hampton, Virginia, March 1969 (N69-19918).

23.0 Benton, W., Carr, R., Cohen, A., Gustafson, G., Lankton, C. and Zeldin, B., "Propellant Storability in Space", RPL-TDR-64-75 (Final), Air Force Systems Command, Edwards Air Force Base, California, June 1964 (AD 603 215).

24.0 Brechna, H., "Superconducting Magnets for High Energy Physics Applications", Proceedings 1st International Cryogenic Conference, Tokyo and Kyoto, Japan, April 1967, Heywood Temple Industrial Publishers, Ltd., London, 1968, pp. 119-129 (CFSCI N67-36009).

25.0 Bullard, B. R., "Cryogenic Tank Support Evaluation", NASA CR-72546, NASA Lewis Research Center, Cleveland, Ohio, December 1969 (N70-13085).

26.0 Campbell, M. D., "Development of Thermal Expansion Capabilities and the Investigation of Expansion Characteristics of Space Vehicle Materials", General Dynamics/Astronautics Report ERR-AN-251, 14 December 1962.

27.0 Campbell, M. D., "Development of the Thermal Expansion Capabilities and the Investigation of the Thermal Expansion Characteristics of Space Vehicle Materials (II)", General Dynamics/Astronautics Report ERR-AN-450, 26 December 1963.

28.0 Caren, R. P., Coston, R. M., Holmes, A. M. C. and Dubus, F., "Low-Temperature Tensile, Thermal Contraction, and Gaseous Hydrogen Permeability Data on Hydrogen-Vapor Barrier Materials", Advances in Cryogenic Engineering, Vol. 10, 1965, pp. 171-180.

29.0 Chiao, T. T. and Moore, R. L., "Tensile Properties of PRD-49 Fiber in Epoxy Matrix", Journal of Composite Materials, Vol. 6, October 1972, pp. 547-551.

30.0 Cooper, G.A. and Sillwood, J. M., "Multiple Fracture in a Steel Reinforced Epoxy Resin Composite", Journal of Materials Science, Vol. 7, 1972, pp. 325-333.

31.0 Darwish, F. and Tetelman, A. S., "Mechanical Behavior of SiO_2-Epoxy Composite", Conference Proceedings No. 63, Advisory Group for Aerospace Research and Development, Symposium on Composite Materials, Paper No. 9, Paris, April 1970 (Hartford House, London).

32.0 Davis, J. G. and Zender, G. W., "Mechanical Behavior of Carbon Fiber Reinforced-Epoxy Composites", 12th National Symposium, Society of Aerospace Material and Process Engineers, Vol. 12, 1967, Section AC-10.

33.0 Dervy, A. J., "Reinforced Plastics of High Strength/Weight Ratio for Space Applications", Technical Papers, 17th Annual Technical Conference, Society of the Plastics Industry, Section 7-D, 1962, pp. 1-10.

34.0 Fontana, M. G., Bishop, S. M. and Spretnak, J. W., "Investigation of Mechanical Properties and Physical Metallurgy of Aircraft Alloys at Very Low Temperatures, Part 5 - Mechanical Properties of Metals and a Plastic Laminate at Low Temperatures", AF Technical Report 5662, Part 5, Materials Laboratory, Wright-Patterson Air Force Base, Ohio, December 1953 (AD 27726).

35.0 Freeman, S. M., "Properties of Vapor Barriers, Adhesives and Foams at Cryogenic and Elevated Temperatures", Lockheed Aircraft Corporation Report ER-5687, April 1962.

36.0 Freeman, W. T. and Campbell, M. D., "Thermal Expansion Characteristics of Graphite Reinforced Composite Materials", Composite Materials: Testing and Design (Second Conference), ASTM STP 497, American Society for Testing and Materials, 1972, pp. 121-142.

279<

37.0 Funk, C. W. and Dixon, C. E., "Cryogenic Radiation Damage in Structural Polymers", Transactions of the American Nuclear Society, Vol. 9, 1966, pp. 406.

38.0 Gille, J. P., "Development of Advanced Materials for Integrated Tank Insulation System for the Long Term Storage of Cryogens in Space", NASA CR-102570 (Final), National Aeronautics and Space Administration, Huntsville, Alabama, September 1969 (N70-23348).

39.0 Gleich, D., "Development of a Filament-Overwrapped Cryoformed Metal Pressure Vessel", NASA CR-72753, National Aeronautics and Space Administration, Lewis Research Center, Cleveland, Ohio, January 1971 (N71-22401).

40.0 Gray, P. D., Cornelius, G. K., O'Donnell, J. D., and Howard, W. W., "Rockets in Space Environment, Volume 1: The Experimental Program", RTD-TDR-63-1050, Aerojet General Corporation, February 1963 (N63-20999).

41.0 Greer, F., "Flexural Properties of Conolon 506 at Room Temperature, -320°F and -423°F", Convair/Astronautics Report 55E 522, June 1961 (AD 677 565).

42.0 Hale, D. V., "Study of Thermal Conductivity Requirements: MSFC 20-Inch and 105-Inch Cryogenic Tank Analyses", NASA CR-61288, National Aeronautics and Space Administration, Marshall Space Flight Center, Alabama, June 1969 (N69-35811).

43.0 Hall, J., "Cryogenic Tensile Tests- Epoxy Fiberglas", Douglas Aircraft Company Report MP 1348, September 1961.

44.0 Hanson, M. P., "Effects of Temperature and Creep Characteristics of PRD-49 Fiber/Epoxy Composites", NASA TN D-7120, National Aeronautics and Space Administration, Lewis Research Center, Cleveland, Ohio, November 1972 (N73-12607).

45.0 Hanson, M. P., "Tensile and Cyclic Fatigue Properties of Graphite Filament-Wound Pressure Vessels at Ambient and Cryogenic Temperatures", NASA TN D-5354, National Aeronautics and Space Administration, Lewis Research Center, Cleveland, Ohio, July 1969 (N69-31300). (Identical to SAMPE Vol. 15, pp. 249-256).

46.0 Hanson, M. P., Richards, H. T. and Hickel, R. O., "Preliminary Investigation of Filament-Wound Glass-Reinforced Plastics and Liners for Cryogenic Pressure Vessels", NASA TN D-2741, National Aeronautics and Space Administration, Lewis Research Center, Cleveland, Ohio, March 1965.

280<

47.0 Hanson, M. P., "Glass-, Boron-, and Graphite-Filament-Wound Resin Composites and Liners for Cryogenic Pressure Vessels", NASA TN D-4412, National Aeronautics and Space Administration, Lewis Research Center, Cleveland, Ohio, February 1968. (Identical to NASA TM X-52350, 1967.)

48.0 Hanson, M. P., "Static and Dynamic Fatigue Behavior of Glass Filament-Wound Pressure Vessels at Ambient and Cryogenic Temperatures", NASA TN D-5807, National Aeronautics and Space Administration, Lewis Research Center, Cleveland, Ohio, May 1970 (CFSTI-CSCL-20K).

49.0 Haskins, J. F. and Hertz, J., "Thermal Conductivity Testing of Coast F-224-6 Phenolic-Fiberglass Laminate", General Dynamics/Convair Report No. AR-592-1-482, July 1963.

50.0 Haskins, J. F. and Hurlich, A., "Measured Values for the Coefficients of Linear Expansion of Plycel 420 and Conolon 506 at Low Temperatures", Convair/Astronautics Report MRG-154, May 1960.

51.0 Haylett, J. W., Rottmayer, E. and Butcher, I., "Advanced Composite Material Study for Millimeter Wavelength Antennas", Technical Report AFML-TR-71-205, Vol. 1, Air Force Materials Laboratory, Wright-Patterson Air Force Base, Ohio, October 1971 (AD 893 368).

52.0 Haylett, C. E., "Advanced Composite Material Study for Millimeter Wavelength Antennas, Volume II, Environmental Tests", AFML-TR-71-205-Vol. 2, Air Force Materials Laboratory, Wright-Patterson Air Force Base, Ohio, October 1971 (AD 893 358 L).

53.0 Herring, H. W., Baucom, R. M. and Pride, R. A., "Research on Boron Filaments and Boron Reinforced Composites", 10th National Symposium, Society of Aerospace Material and Process Engineers, Vol. 10, 1966, pp. B-21 to B-34.

54.0 Hertz, J., "Tensile Testing of Conolon 506 at Room and Sub-Zero Temperatures", Convair/Astronautics Report MRF-120, December 1959.

55.0 Hertz, J., "Tensile Testing of Adlock 851, Adlock PG-LA and Adlock EG-11A-81A from -423°F to 78°F", Convair/Astronautics Report MRG 237, June 1961.

56.0 Hertz, J., "Investigation of Potential Low Temperature Insulations", General Dynamics/Astronautics Report GS/A-ERR-AN-668, December 1964.

57.0 Hertz, J., "The Effect of Cryogenic Temperatures on the Mechanical Properties of Reinforced Plastic Laminates", General Dynamics Report AR-592-1-415, March 1963 (AD 405 170).

58.0 Hertz, J., "Investigation into the High-Temperature Strength Degradation of Fiber-Reinforced Resin Composite During Ambient Aging", General Dynamics/Convair Report No. GDCA-DBG73-005 (Final Contract NAS 8-27435), June 1973.

59.0 Hoggatt, J. T., "Development of Cryogenic PRD-49-1 Filament-Wound Tanks", NASA CR-120835, National Aeronautics and Space Administration, Lewis Research Center, Cleveland, Ohio, December 1971 (N72-24941).

60.0 Hoggatt, J. T., "High Performance Filament Wound Composites for Pressure Vessel Applications", Society of Aerospace Material and Process Engineers National Technical Conference, Space Shuttle Materials, Vol. 3, 1971, pp. 157-167.

61.0 Hust, J. G., "Thermal Conductivity of an Epoxy-Fiberglass Laminate", Unpublished data (1973).

62.0 Johnston, H. L. and Brooks, H. E., "Impact Strength of Various Metals at Temperatures down to 20° Absolute", Ohio State University Cryogenic Laboratory Report TR 264-17, May 1952.

63.0 Keller, C. W., "Fiberglass Supports for Cryogenic Tanks", NASA CR-120937 (Final), National Aeronautics and Space Administration, Lewis Research Center, Cleveland, Ohio, October 1972 (N72-33564).

64.0 Kerlin, E. E. and Smith, E. T., "Measured Effects of the Various Combinations of Nuclear Radiation, Vacuum and Cryotempteratures on Engineering Materials: Biennial Report", NASA CR-77772, National Aeronautics and Space Administration, George C. Marshall Space Flight Center, Huntsville, Alabama, July 1966 (N66-35963).

65.0 Kerlin, E. E. and Smith, E. T., "Measured Effects of the Various Combinations of Nuclear Radiation, Vacuum and Cryotemperatures on Engineering Materials: Annual Report", NASA CR-58830, National Aeronautics and Space Administration, George C. Marshall Space Flight Center, Huntsville, Alabama, May 1964 (N64-33043).

66.0 Keys, R. D., Kiefer, T. F. and Schwartzberg, F. R., "Cryogenic Properties of High-Strength Glass-Reinforced Plastics", Advances in Cryogenic Engineering, Vol. 11, 1966, pp. 470-477.

67.0 Krause, D. R., "Development of Lightweight Material Composites to Insulate Cryogenic Tanks for 30-Day Storage in Outer Space", NASA CR-123797, National Aeronautics and Space Administration, George C. Marshall Space Flight Center, Huntsville, Alabama, June 1972 (N72-30495).

68.0 Krause, D. R., Fredrickson, G. O. and Klevatt, P. L., "Effects of Cyclical Environments on High-Performance Multi-Layer Insulation Materials", Society of Aerospace Material and Process Engineers National Technical Conference, Space Shuttle Materials, Vol. 3, 1971, pp. 639-643.

69.0 Lantz, R. B., "Materials for Filament Wound Cryogenic Pressure Vessels", 6th National Symposium. Society of Aerospace Materials and Process Engineers, Vol. 2, Engineering Paper No. 1750.

70.0 Lavengood, R. E. and Anderson, R. M., "Matrix Properties Controlling Torsional Fatigue Life of Fiber Reinforced Composites", Technical Papers, 24th Annual Technical Conference, Society of the Plastics Industry, Section 11-E, 1969, pp. 1-7.

71.0 Levin, V. A., Naumenkov, P. G. and Shchitov, M. V., "Some Properties of Plastics at Low Temperatures", Plasticheskia Massy, Vol. 11, 1966, pp. 64-65.

72.0 Luikov, A. V., Vasiliev, L. L. and Shashkov, A. G., "A Method for the Simultaneous Determination of all Thermal Properties of Poor Heat Conductors Over the Temperature Range 80 to 500 K", Proceedings, Third American Society of Mechanical Engineers Symposium, Purdue University, March 1965, pp. 314-319.

73.0 Lyon, D. N. and Parrish, W. R., "Low Temperature Thermal Conductivities of Two High Compressive Strength Materials", Cryogenics, Vol. 7, No. 1, 1967.

74.0 Maher, L. E., "Some Problems Arising from the Use of Hydrogen-Fuelled Propulsion Systems", Journal of the Royal Aeronautical Society, Vol. 68, November 1964, pp. 765-771.

75.0 McKannon, E. C. and Gause, R. L., "Effects of Nuclear Radiation and Cryogenic Temperatures on Non-Metallic Engineering Materials", Journal of Spacecraft, Vol. 2, August 1965, pp. 558-564.

76.0 Morris, E. E., "Glass-Fiber-Reinforced Metallic Tanks for Cryogenic Service", 12th National Symposium, Society of Aerospace Materials and Process Engineers, Vol. 12, October 1967, Section AS-4. (Also NASA CR-72224.)

77.0 Morris, E. E., "The Performance of Glass-Filament-Wound Pressure Vessels with Metal Liners at Cryogenic Temperatures", Journal of Materials, Vol. 4, December 1969, pp. 970-1004.

78.0 Morris, E. E. and Alfring, R. J., "Cryogenic Boron-Filament-Wound Pressure Vessels", Composite Materials: Testing and Design, ASTM STP 460, American Society for Testing and Materials, 1969, pp. 430-443.

79.0 Morris, E. E. and Landes, R. E., "Cryogenic Glass-Filament-Wound Tank Evaluation", NASA CR-72948 (Final), National Aeronautics and Space Administration, NASA Lewis Research Center, Cleveland, Ohio, July 1971 (N72-14696).

80.0 Mowers, R. E., Leib, J. H. and Sherman, S., "Program of Testing Nonmetallic Materials at Cryogenic Temperatures", Rocketdyne Corporation Report R-3498, Rocket Propulsion Laboratories, Edwards, California, December 1962 (AD 294 772).

81.0 Nadler, M. A., Yoshino, S. Y. and Darms, F. J., "Boron/Epoxy Support Strut for Non-Integral Cryogenic Tankage", North American Rockwell Space Division Report SD 68-99501, February 25, 1969. (See also 15th National Symposium SAMPE April 1969 and North American Rockwell Report SD 995 2, 1968.)

82.0 Nelson, L. F., "Compressive Strength of Conolon 506 at +75°F and -320°F", Convair/Astronautics Report No. 27E 1336, January 1962.

83.0 Nelson, L. R., "Mechanical Properties of Adlock 851 at Room Temperature, 1000°, -320° and -423°F", Convair/Astronautics Report No. 55E 812, July 1961.

84.0 Nelson, P. T. and Archer, J. S., "Graphite Reinforced Plastic EHF Antenna", TRW Systems Group, Redondo Beach, California Report No. 99900-7128-RO-11, December 1969.

85.0 Patten, P. M., "Internal Insulation Liner Alteration", Douglas Aircraft Company Report No. SM 45975, August 1964.

86.0 Perkins-Elmer Optical Group, Norwalk, Connecticut, Work-In-Progress on Contract No. F33615-72-C-2033, Air Force Systems Command, Wright-Patterson Air Force Base, Ohio.

87.0 Pink, E. and Campbell, J. D., "The Effect of Strain Rate and Temperature on the Deformation Behavior of Reinforced and Unreinforced Epoxy Resin", Oxford University Department of Engineering Report No. 1040/72, Oxford, England, July 1972 (N73-10568).

88.0 Pirgon, O., Wostenholm, G. H. and Yates, B., "Thermal Expansion at Elevated Temperatures, IV. Carbon-Fibre Composites", Journal of Physics D: Applied Physics, Vol. 6, 1973, pp. 309-321.

89.0 Pride, R. A., Stein, B. A. and Schmidt, F. W., "Mechanical Properties of Polyimide-Resin/Glass-Fiber Laminates for Various Time, Temperature and Pressure Exposures", Technical Papers, 23rd Annual Reinforced Plastics Technical and Management Conference, Washington, DC, 1968, Section 17-c. pp. 1-8.

90.0 Ratcliffe, E. H., "Thermal Conductivities of Plastics with Glass, Asbestos and Cellulosic Fiber Reinforcements", Applied Material Research, Vol. 5, 1966, pp. 200-201.

91.0 Roseland, L. M., "Materials for Cryogenic Usage", Technical Papers, 21st Annual Technical Conference, Society of the Plastics Industry, 1966, Section 4-C, pp. 1-6.

92.0 Roseland, L. M., "Investigation of Structural Properties at Cryogenic Temperatures of Filament-Wound Pressure Vessels Containing Both Organic and Flass Filaments", Douglas Aircraft Corporation Report No. SM-48409, January 1966.

93.0 Ross, J. E., "Fiberglass Laminate- Ultimate Tensile and Flexural Strength Tests at Room Temperature, -100°F and -320°F", Convair Astronautics Report No. 7E 1687, June 1959 (AD 830 230).

94.0 Sanders, R. H. and Weleff, W., "Final Report on GTR-17 Effects of Radiation on Organic Materials Irradiated in Liquid Hydrogen", Aerojet-General Corporation Report No. RN-S-0327, March 1967.

95.0 Sanger, M. J., Molho, R. and Howard, W. W., "Exploratory Evaluation of Filament-Wound Composites for Tankage of Rocket Oxidizers and Fuels", AFML-TR-65-381, Air Force Materials Laboratory, Wright-Patterson Air Force Base, Ohio, January 1966 (AD 477 455).

96.0 Sanger, M. J. and Reinhart, T. J., "Development of Filament-Wound Tankage for Rocket Oxidizers and Fuels", Technical Papers, 12th National Symposium, Society of Aerospace Material and Process Engineers, 1967, Section AS-7.

97.0 Sewell, J. J. and Kuno, J. K., "Aerospace Use of Plastic Hardware and Thermal Insulation", Technical Papers, 17th Annual Technical Conference, Society of the Plastics Industry, 1962, Section 7-A, pp. 1-14.

98.0 Shriver, C. B., "Design and Fabrication of an Internally Insulated Filament Wound Liquid Hydrogen Propellant Tank", NASA CR-127, National Aeronautics and Space Administration, Washington, DC, November 1964 (N65-10775).

99.0 Soltysiak, D. J. and Toth, J. M., "Static Fatigue of Fiber Glass Pressure Vessels from Ambient to Cryogenic Temperatures", Technical Papers, 22nd Annual Technical Conference, Society of the Plastics Industry, 1967, Section 14-E, pp. 1-14.

100.0 Speare, J. C., "Preliminary Sizing of Filament-Wound RNS Tanks", Report No. TOR-0066 (5759-07)-13, Space and Missile Systems Organization, Air Force Systems Command, Los Angeles Air Force Station, Los Angeles, California, June 1970 (AD 872 626).

101.0 Steinhauer, R. A., "Linear Thermal Expansion of 828CL 181 Cloth Laminate", Douglas Aircraft Company Report No. MP 11,979, August 1961.

102.0 Stinnett, W. D., "Cryogenic Tensile Properties of Selected Materials", NASA CR-71751, AEC-NASA Space Nuclear Propulsion Office, Report No. 2712, January 1964 (N66-22816).

103.0 Suezawa, Y., Hojo, H. and Nakamura, K., "Impact Characteristics of Fiberglass Reinforced Plastics at Low Temperatures", Kagaku Kogaku (Chemical Engineering, Japan), Vol. 33, 1969, pp. 1051-1059.

104.0 Toth, J. M., "Barrier Films for Filament-Wound Fiberglass Cryogenic Vessels", Advances in Cryogenic Engineering, Vol. 1, 1964, pp. 537-544.

105.0 Toth, J. M. and Soltysiak, D. J., "Investigation of Smooth-Bonded Metal Liners for Flass Fiber Filament-Wound Pressure Vessels", NASA CR-72165 (Final), National Aeronautics and Space Administration, Lewis Research Center, Cleveland, Ohio, May 1967 (N67-25070).

106.0 Toth, J. M., Sherman, W. C. and Soltysiak, D. J., "Investigation of Smooth-Bonded Metal Liners for Glass Fiber Filament-Wound Pressure Vessels", Douglas Missile and Space Systems Division Report No. SM-49384, Quarterly Report No. 3, Contract No. NAS 3 6293, NASA Lewis Research Center, Cleveland, Ohio, April 1966.

107.0 Toth, J. M., Sherman, W. C. and Soltysiak, D. J., "Investigation of Structural Properties of Fiber-Glass Filament-Wound Pressure Vessels at Cryogenic Temperatures", NASA CR-54393, National Aeronautics and Space Administration, Lewis Research Center, Cleveland, Ohio, 1965 (N65-35392).

108.0 Toth, J. M. and Barber, J. R., "Structural Properties of Glass-Fiber Filament-Wound Cryogenic Pressure Vessels", Advances in Cryogenic Engineering, Vol. 10, 1965, pp. 134-144.

109.0 Voloshenko-Klimovitskii, Yu. Ya., Belyaev, Yu. A., L'vof, B. S. and Schpakovskaya, E. I., "Strength of Cold-Hardening GRPs Based on PN-1 Resin Under Impact Tension at Normal (20°C) and Low (-196°C) Temperatures", Plasticheski Massy, Vol. 6, 1964, pp. 39-40.

110.0 Voloshenko-Klimovitskii, Yu. Ya., Belyaev, Yu. A. and Korenkov, Yu. A., "Impact Tensile Tests on Glass-Fibre Reinforced Plastics at Normal and Low Temperatures", Plasticheski Massy, No. 5, 1963, pp. 51-54.

111.0 Watson, J. F., Christian, J. L. and Hertz, J., "Selection of Materials for Cryogenic Applications in Missiles and Aerospace Vehicles", Convair/Astronautics Report No. MRG 132-1, February, 1960.

112.0 Weleff, W., "Effect of Nuclear Radiation and Liquid Hydrogen on Mechanical Properties of Three Phenolic Materials", Advances in Cryogenic Engineering, Vol. 11, 1966, pp. 486-491.

113.0 Weleff, W., "Final Report, GTR-16 Radiation Effects Test on Structural Materials at -423°F", Aerojet-General Corporation Report No. RN-S-0290, November 1966.

IV - HANDBOOKS AND REVIEWS

114.0 Coston, R. M., "Handbook of Thermal Design Data for Multilayer Insulation Systems", LMSC-A847882, Vol. II (Final), George C. Marshall Space Flight Center, Huntsville, Alabama, June 1967 (N67-34910).

115.0 Hertz, J., "The Effect of Cryogenic Temperatures on the Mechanical Properties of Reinforced Plastic Laminates", Society of Plastics Engineers Journal, Vol. , February 1965, pp. 181-189.

116.0 Hertz, J. and Knowles, D., "Survey of Thermal Properties of Selected Materials", General Dynamics/Convair Report AAL-65-008 (AR-504-1-553), February 1965 (N65-31775).

117.0 Jurevic, W. G. and Rittenhouse, J. B., "Structural Applications Handbook", AFML TR-67-332, Air Force Materials Laboratory, Wright-Patterson Air Force Base, Ohio. August 1968 (AD 804 585).

118.0 Lackman, L. M., Arvin, G. H., et al., "Advanced Composite Design Guide, Third Edition, Volume IV: Materials", Air Force Materials Laboratory, Wright-Patterson Air Force Base, Ohio, January 1973.

119.0 Landrock, A. H., "Properties of Plastics and Related Materials at Cryogenic Temperatures", Plastec Report No. 20, Plastics Technical Evaluation Center, Picatinny Arsenal, Dover, New Jersey, July 1965 (AD 469 126).

120.0 Maximovich, M. and Scheck, W. G., "Data Summary and Reference File for Graphite and Boron Reinforced Composite Materials", General Dynamics/Convair Report No. GDCA-DBG71-006, 1971 (Contract NAS 8-26198, George C. Marshall Space Flight Center, Huntsville, Alabama).

121.0 Nored, D. L., Hennings, G., Sinclair, D. H., Smith, G. T., Smolak, G. R. and Stofan, A. J., "Storage and Handling of Cryogenic Fluids", NASA Special Publication SP-5053, Proceedings of Conference on Selected Technology for the Petroleum Industry, Lewis Research Center, Cleveland, Ohio, December 1965 (N66-33674).

122.0 "Plastics for Aerospace Vehicles, Part 1. Reinforced Plastics", MIL-HDBK-17A, Department of Defense, Washington, DC, January 1971.

123.0 Rittenhouse, J. B. and Singletary, J. B., "Space Materials Handbook", Third Edition, NASA Special Publication SP-3051, National Aeronautics and Space Administration, Washington, DC, 1969 (Limited publication as AFML-TR-68-205).

124.0 Schwartzberg, F. R., Hertzog, R. G., Osgood, S. H., et al., "Cryogenic Materials Data Handbook (Revised), Volume II", AFML-TDR-64-280-Vol. II (Revised), Air Force Materials Laboratory, Wright-Patterson Air Force Base, Ohio, July 1970 (AD 713 620).

V. MISCELLANEOUS REFERENCES

125.0 Kastelic, J. R., Hiltner, A. and Baer, E., "Crazing, Yielding and Fracture in Polycarbonate and Polyethelene Terephthalate at Low Temperatures", Journal of Macromolecular Science-Physics, B7(4). 1973. pp. 679-703.

126.0 Relationships Between Structure and Mechanical Behavior in Polymeric Solids. ASM Materials Science Seminar. Chicago. Ill., 1973 (in preparation).

BIBLIOGRAPHIC CROSS-REFERENCE

Property	Glass Epoxy	Glass Polyester	Glass Phenolic	Glass Teflon	Glass Silicone	Glass Polyurethane	Glass Phenyl Silane	Glass Imidite
σ^{tu}	1-1.3, 2-2.2, 3-3.5, 4, 5, 5.1, 22, 24, 28, 33, 35, 40, 43, 46, 47, 52, 54, 55, 57, 66, 71, 87	1-1.3, 2-2.2, 3-3.2, 3.4, 3.5, 34, 40, 55, 57, 63, 64, 66, 75, 109	1-1.3, 2-2.2, 40, 54, 55, 57, 64-66, 71, 75, 83, 93, 97, 111, 112	2-2.2, 37, 67, 68, 80, 94, 102, 113	1-1.3, 2-2.2, 24, 40, 57, 64, 66, 68, 97	2-2.2, 85	2-2.2, 57, 66	2-2.2
E_1^t	1-1.3, 2-2.2, 3-3.5, 4.5, 5, 5.1, 24, 28, 35, 55, 56, 57, 66, 87	1-1.3, 2-2.2, 3, 34, 55, 57,	1-1.3, 2-2.2, 54, 55, 57, 97, 111	2-2.2, 80	1-1.3, 2-2.2, 24, 57	2-2.2	2-2.2, 57, 66	2-2.2, 24
E_2^t	1-1.3, 2, 3-3.5, 20, 55, 56, 57	1-1.3, 2, 55, 57	1-1.3, 55, 57		1-1.3, 2, 57	2	2, 57	2
ε^t	3-3.5, 4, 5, 5.1, 35, 64 85	3-3.5, 64	64, 65, 112	80, 89, 102	64	85		
σ^{fu}	1-1.3, 2-2.2, 3-3.5, 4, 40, 57, 66, 71	1-1.3, 2-2.2, 3-3.3, 3.5, 40, 57, 66	1-1.3, 2-2.2, 40, 41, 57, 71, 83, 93, 97	2-2.2, 80	1-1.3, 2-2.2, 40, 57, 97	2-2.2	2-2.2	2-2.2
E_1^f	1-1.3,2, 3-3.2, 3.4, 3.5, 57	1-1.3, 2, 2.2, 57	1-1.3, 2-2.2, 57, 83, 93, 97	2-2.2, 80	1-1.3, 2-2.2, 57	2-2.2	2-2.2	2-2.2
E_2^f	1-1.3, 2	1-1.3, 2	1-1.3, 2		1-1.3, 2	2	2	
σ^{cu}	1-1.3. 2, 2.2, 3-3.2, 3.4, 3.5, 24, 57, 66	1-1.3, 2, 2.2, 3-3.5, 34, 57	1-1.3, 2-2.2, 57, 82, 97	2-2.2, 80	1-1.3, 2-2.2, 24, 57	2-2.2	2-2.2, 57	2-2.2, 24
E^c	1, 1.2, 1.3, 2, 2.2, 57	1-1.3, 2, 2.2, 57, 66	1-1.3, 2-2.2, 57, 82, 97	2-2.2, 80	1-1.3, 2-2.2, 57	2-2.2	2-2.2	2-2.2
σ^{si}	3-3.2, 3.4, 3.5, 4, 4.1, 5, 5.1, 22, 47, 71	3-3.5	71					
η^t	1, 1.3, 2, 2.1, 2.2, 22, 66, 70, 99	1-1.3, 2-2.2, 34, 70	1-1.3, 2-2.2		1-1.3, 2	2	2	2
σ^{by}	2-2.2, 3-3.2, 3.4, 3.5				2	2	2	2
σ^{Ik}	4, 71, 103	62, 109	71, 97	80				
λ	3, 4.1, 14, 16-16.3, 21, 23-25, 38, 42, 56, 61, 63, 90, 114	3, 14, 16-16.3 90	14, 16-16.3, 49	14, 16-16.3	14, 16-16.3, 24, 73, 90		14, 16-16.3	16, 24
$\Delta L/L$	3, 5, 14, 16, 16.2, 16.3, 28, 69, 85, 91, 100, 101, 104, 114	3, 14, 16-16.3	14, 16-16.3, 26, 27, 50, 111	14, 16-16.3, 80	14, 16-16.3, 67	5, 85, 91	14, 16-16.3	16, 16.2
C_p	15, 16, 16.2, 16.3, 24, 114	15, 16-16.3	15, 16-16.3, 64	15, 16-16.3	15, 16-16.3, 24		15, 16-16.3	16-16.3, 24

*Includes fracture toughness

Property	Graphite Epoxy	Boron Epoxy	Boron Aluminum	PRD-49 Epoxy
σ^{tu}	8, 9, 10, 10.2, 13, 13.2, 32, 47, 51, 58	13, 20, 22, 47, 53, 58, 81	13, 13.3	29, 44, 59, 60
E^t_l	8, 9, 10, 10.1, 13, 51	13, 81	13, 13.3	44, 59, 60
ε^t	13	20	13	
σ^{fu}	8, 10, 10.1, 11, 12, 13, 13.2, 58	58		
E^f	8, 10.1			
σ^{cu}	13		13, 13.3	
E^c	13	13, 81	13, 13.3	
σ^{si}	8, 9. 10, 10.1, 10.2, 12, 13, 13.2, 47, 58	13, 22, 47, 58, 81	13, 13.3	59, 60
n^t	45	20, 22		
σ^{by}			13, 13.3	
σ^{I*}	9, 10.2	81		
λ	13, 17, 18, 38	13, 38, 63, 81		
L/L	10, 13, 13.2, 17, 18, 36, 51, 52, 84, 88	13	13, 13.3	59, 60
C_p	13	13	13, 13.3	

*includes fracture toughness

MISCELLANEOUS COMPOSITES

Glass-Polyimide σ^{tu}(24, 67, 68), σ^{fu}(89), σ^{si}(12.1, 89) $\Delta L/L$(67)

Glass-Melamine σ^{tu}(65), ε^t(65), λ(90)

Glass-Viton σ^{tu}(68)

Glass-Phenyl Formaldehyde σ^{I}(110), λ(72), C_p(72)

SiO_2-Epoxy σ^{tu}(31), $\Delta L/L$(28)

Graphite-Aluminum σ^{tu}(thermal cycling effects 6-6.2)

Graphite-Polyimide σ^{tu}(13), σ^{fu}(11, 12.1, 13), σ^{si}(13), L/L(36)

Graphite-Phenolic λ(14, 16-16.3), $\Delta L/L$(14, 16-16.3)

Steel-Aluminum σ^{tu}(7, 7.1), ε^t(7.1), σ^{I}(7, 7.1)

Steel-Epoxy σ^{tu}(2, 30), E^t(2, 30), σ^{fu}(2), E^f(2), σ^{cu}(2), E^c(2), n^t(2)

Boron/Steel-Aluminum, Boron/Titanium-Aluminum σ^{tu}, E^t, σ^{cu}, E^c, σ^{by}, $\Delta L/L$, C_p, (13, 13.3), σ^{si}, ε^t, n^t (13)

Potassium Titanate-Epoxy λ(16), C_p(16)

MISCELLANEOUS PROPERTIES

Notch Tensile Strength Glass-Epoxy (3-3.2, 3.4, 3.5, 43, 46)

Vapor Permeability Glass-Epoxy (28)

Modulus of Rigidity Glass-Epoxy (53), Glass-Teflon (80), Boron-Epoxy (53)

Poissons Ratio Glass-Epoxy (53), Boron-Epoxy (53)

Proportional Limit in Tension Glass-Epoxy (55, 56), Glass-Polyester (1-1.3, 55, 56)

Static Fatigue Glass-Epoxy (66, 99), PRD 49-Epoxy (44)

Environmental Effects Glass-Epoxy (4-4.1), Graphite-Epoxy (13, 13.2, 17, 58) Boron-Epoxy (13, 58), Boron-Aluminum (13, 36), PRD 49-Epoxy (44)

Electrical Resistivity Graphite-Epoxy (13), Boron-Epoxy (13)

Thermo-Optical Effects Graphite-Epoxy (13, 84), Boron-Epoxy (13)

Density Glass-Epoxy, Polyester, Phenolic, Silicone, Phenyl Silane (14, 57), Glass-Teflon (14), Glass-Imidite (16), Graphite-Epoxy (9, 13), Graphite-Phenolic (14), Graphite-Polyimide (12.1)

Radiation Effects (13.2, 33, 37, 40, 51, 52, 64, 65, 75, 94, 112, 113)

Cryogen Compatability (33)

PRESSURE VESSEL APPLICATIONS

Glass-Filament
(19, 20, 39, 42, 46-48, 53, 67, 69, 76, 77, 91, 92, 95, 96, 98-100, 104-108, 113)

Graphite-Filament
(8, 10, 10.1, 45, 47, 100)

Boron-Filament
(20, 47, 53, 78)

PRD 49-Filament
(59, 60)

COMPOSITE TESTING PROGRAM

PROCEDURES

The objective of the present effort in the composite testing program is to make an initial evaluation of the tensile properties of current state-of-the-art (commercial production) boron/epoxy, boron/aluminum and graphite/epoxy composites over the 295K to 4K temperature range. The procedure is as follows:

a) design and construct a tensile cryostat capable of testing composite specimens of the required length,

b) obtain the required test materials,

c) conduct initial tests at 295K to check out specimen instrumentation,

d) conduct initial tests at 77K to work out any problems related to specimen gripping or any other problems adversely affecting test results at cryogenic temperatures, and

e) evaluate the tensile properties of the commercial composites at temperatures of 295K, 77K and 4K. Test data shall include tensile properties in the uniaxial longitudinal and uniaxial transverse modes including poissons ratio values.

These procedures will lay the groundwork for future work, the direction of which shall be determined by the results of the work at NRS (both the literature survey and the experimental work) and by the results of the experimental composite screening program currently being conducted by General Electric under ARPA sponsorship. It is anticipated that future efforts will involve fabrication and testing of experimental composites optimized for cryogenic service, following the same procedures as for the commercial products. A comparison of results will dictate the choice of materials for inclusion in a test program aimed at producing design allowable data.

CRYOSTAT CONSTRUCTION

The tensile cryostat has been completed. Figure 17 shows the unit in cross-section. The design is similar to that previously developed in our laboratory and successfully used for many years. It differs only in the incorporation of a thermal short designed to minimize helium loss by cooling the aluminum face plate to which the cryostat barrel is attached. The use of a fiberglass adapter plate between the face plate and the crosshead of the tensile machine also provides a thermal barrier.

In operation, the instrumented specimen is carefully aligned in the grips and hung from the upper pull rod. Instrumentation leads are then passed out of the instrumentation port. The cryostat barrel is then hung onto its pin supports, the end cap is attached, and the nut loosely attached to the lower pull rod. The inner dewar is then attached and filled with liquid nitrogen to precool the fixture. The nitrogen is removed from the inner dewar both dewars are attached and the outer dewar is filled with liquid nitrogen. Liquid helium is then transferred into the inner dewar through the vacuum-jacketed transfer tube. Liquid height is monitored through clear sections of the dewars. The test is then begun.

The present system allows for self-alignment of the specimen in the cryostat. Where needed, the specimen can be forced into alignment by means of a self-centering, tapered fixture in the bottom cap of the cryostat.

The cryostat is designed to take the full 20,000 pound capability of the tensile frame with which it is to be used. However, the present composite study will utilize only a small amount of this capability.

Figure 18 shows the unit attached to the tensile frame before installation of the dewars. Figure 19 shows the unit with both dewars installed.

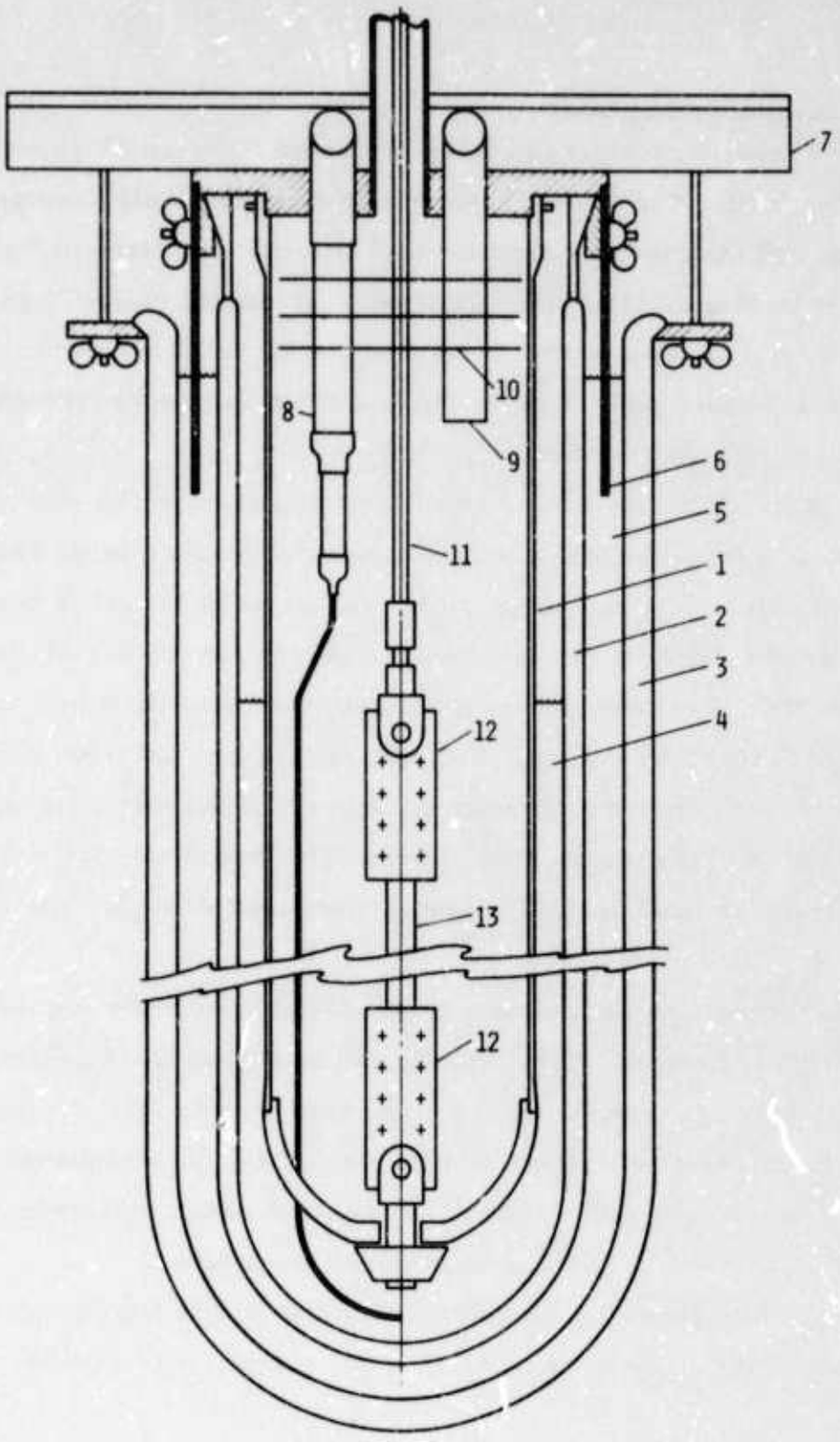

Fig. 17 Cross-Section of Tensile Cryostat

1. Cryostat Barrel
2. Helium Dewar
3. Nitrogen Dewar
4. Liquid Helium
5. Liquid Nitrogen
6. Thermal Short
7. Fiberglass Baseplate
8. Helium Transfer Line
9. Instrumentation Port
10. Radiation Shields
11. Titanium Pull Rod
12. Specimen Grips
13. Specimen

SELECTION OF MATERIALS

The following materials are being donated by two cooperating commercial composite fabricators. All materials are unidirectional.

	Supplier	Plies		
5.6 mil Boron-Epoxy	A	4	longitudinal	on hand
5.6 mil Boron-Epoxy	A	11	transverse	on hand
Graphite-Epoxy	A	6	longitudinal	on hand
Graphite-Epoxy	A	16	transverse	on hand
5.6 mil Boron-Epoxy	B	6	longitudinal	on hand
5.6 mil Boron-Epoxy	B	(12)	transverse	(committed)
5.6 mil Boron-Aluminum	B	(6)	longitudinal transverse	(committed)

Longitudinal and transverse tests will include ultimate tensile strength, tensile modulus, and poissons ratio data. Sufficient material is being obtained to prepare a minimum of 15 specimens of each composite type and thickness, permitting five tests to be performed with each material at 295K, 7K, and 4K.

A sufficient amount of each of the above materials shall be sent to the General Electric Research Laboratory for inclusion in their flexural test program, enabling a comparison to be made between materials representative of current commercial production and the experimental composites being evaluated at that laboratory in their current year's research effort.

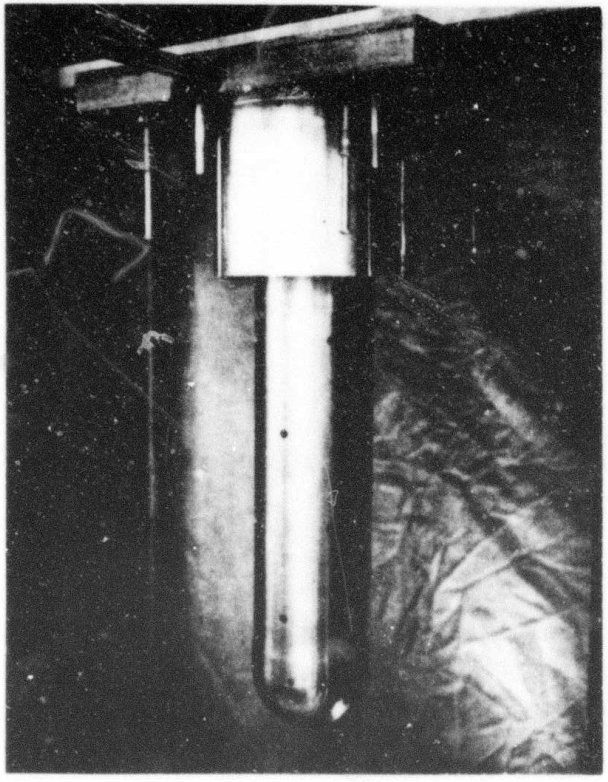

Fig. 18- Installed Tensile Cryostat Without Dewars.

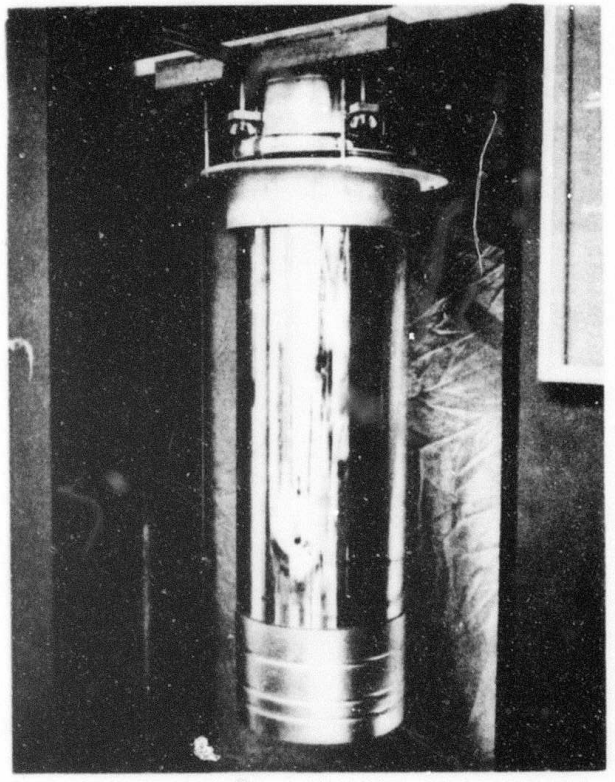

Fig. 19- Tensile Cryostat With Dewars Installed.

SEMI-ANNUAL REPORT ON MATERIALS RESEARCH IN SUPPORT OF SUPERCONDUCTING MACHINERY

FATIGUE AND FRACTURE TOUGHNESS TESTING AT CRYOGENIC TEMPERATURES

Semi-Annual Report

March 1974

by

R. L. Tobler, R. P. Mikesell, R. L. Durcholz,
C. W. Fowlkes, and R. P. Reed

Cryogenic Division
NBS - Institute for Basic Standards
Boulder, Colorado

SUMMARY

I. The fatigue crack growth rates for Ti-6Al-4V, AISI 304 and AISI 316 alloys were essentially independent of temperature over the interval 298-76-4 K.

II. The fatigue crack growth rate of A-286 alloy was significantly lower at 4 K as compared to room temperature.

III. At room temperature, the plane strain fracture toughness of Ti-5Al-2.5Sn (K_{IC} = 66.9 ksi$\sqrt{in}$) exceeded that of Ti-6Al-4V. The value of K_{IC} for Ti-6Al-4V decreased from 44 ksi$\sqrt{in}$ at 298 K to 35 ksi$\sqrt{in}$ at 4 K.

IV. The fracture toughness of alloys AISI 304 and 316 was higher at 4 K than at room temperature. These stainless steels exhibited very tough fracture behavior and preliminary K_{IC} values were obtained by J integral tests.

V. Valid J-integral tests on A-286 alloy revealed that K_{IC} decreased from 117 ksi$\sqrt{in}$ at 298 K to a value of 95 ksi$\sqrt{in}$ at 4 K.

TABLE OF CONTENTS

LIST OF FIGURES

LIST OF FIGURES (continued)

LIST OF FIGURES (continued)

LIST OF FIGURES (continued)

LIST OF TABLES

INTRODUCTION

The phenomenon of superconductivity is currently being exploited in the design and construction of motors and generators. Superconducting components are normally cooled with liquid helium, and since some structural parts must operate at 4K, there is a need for property data in this environment. Existing mechanical property data on structural alloys at 4K are limited to tensile properties. Few fracture data have been reported at this temperature. Therefore, it was decided to characterize the fracture behavior of various structural materials immersed in liquid helium.

This report presents the fatigue crack growth rate and fracture toughness data of the alloys AISI 304, AISI 316, A-286, Ti-6Al-4V, and Ti-5Al-2.5Sn. Both the growth rate and fracture toughness were determined at 298, 76, and 4K. The stainless steels were chosen because they are austenitic and, hence, very tough at low temperatures; the titanium alloys and the A-286 were selected because of their high yield strengths.

Tensile tests were also conducted on the same material used with the fracture tests in order to describe the material in terms of flow stress, ductility, and work hardening behavior.

Work on the Ti-6Al-4V, the AISI 304, and the AISI 316 was previously reported to the Naval Ship Research and Development Center.[1] The present report includes a more involved study of these alloys as well as presentation of data on the Ti-5Al-2.5Sn, the AISI 310, and the A-286 alloy.

Fracture Toughness

Fracture tests are conducted to characterize the strength of materials in the presence of sharp flaws. Fatigue cracks are a very common type of

flaw induced in structural components subjected to fluctuating loads. A fatigue crack may reduce the strength of a structure to a value far below the strength predicted by normal continuum failure criteria. The unexpected and catastrophic fracture of a number of ships, storage tanks, steam turbines, missiles and aircraft have underlined the importance of relatively small cracks on strength. The problem is usually more severe at low temperatures. The fact that the yield strength increases and ductility decreases for most structural materials as temperature is lowered increases the likelihood of brittle fracture.

Research into the mechanics of crack propagation or fracture has resulted in the identification of parameters which describe the fracture toughness and growth of fatigue cracks in materials. In this report, two techniques have been applied to characterize fracture behavior:

1) linear elastic fracture mechanics, and

2) J-integral analysis.

Linear Elastic Fracture Mechanics

In cases where a material exhibits insignificant plastic deformation prior to fracture, the techniques of linear elastic fracture mechanics apply. The theory of linear elastic fracture mechanics is discussed in references 2-4. The approach utilizes the stress intensity factor "K" to describe fracture behavior. The parameter K characterizes the elastic stress field near the crack tip which governs fracture behavior. For a specimen of a given geometry, K is calculated from load, crack length, and specimen dimensions. The stress intensity factor is the fundamental parameter of interest because it relates all of these variables with a single term.

Many normally ductile materials may fail in a relatively brittle manner in the presence of a crack and under conditions of plane strain. Consequently, a wide range of structural materials may be characterized by linear elastic fracture mechanics. Plane strain conditions prevail for "thick" specimens where the plastic zone at the crack tip is constrained by the surrounding bulk of elastically loaded material. Under these conditions, materials which are loaded in the mode of crack opening exhibit a critical stress intensity, K_{IC}, at which the crack propagates catastrophically without significant plastic deformation.

The fracture toughness parameter K_{IC} is a material property and a useful design criterion. Provided that size requirements are met, K_{IC} may easily be determined from fracture tests on specimens of standard geometry. However, specimens which are too thin to establish a state of plane strain do not render valid K_{IC} data. Thin specimens are subject to conditions of plane stress or a mixed mode of plane strain and plane stress. The fracture toughness (K_Q) measured on undersized specimens is therefore less meaningful, varying with thickness and usually higher than K_{IC}.

The ASTM guideline[5] for assuring valid K_{IC} is that specimen thickness, B, (and the crack length, a,) should be greater than or equal to $2.5 (K_{IC}/\sigma_y)^2$. It is apparent from this equation that the specimen size required to achieve valid tests is prohibitively large for low yield strength, tough materials. For a stainless steel with a yield stress of 40,000 psi (2.8×10^7 Nm^{-2}) and K_{IC} estimated at 200 ksi in (220×10^6 $Nm^{-2} \times m^{1/2}$), the required specimen would be about 62 inches (158 cm) thick. A specimen this size

is obviously impractical, which means that direct measurement of K_{IC} for this category of materials is impossible within the framework of linear elastic fracture mechanics.

J-integral Fracture Criterion

The concept of stress intensity loses its significance in the case of "thin" specimens which do not provide sufficient constraint at the crack tip. A different fracture criterion is needed to account for the effects of large scale plasticity, i.e., the case where linear elastic fracture mechanics is not applicable.

The recently developed J-integral technique is a valuable tool in the treatment of thin, ductile materials. The theory of the J-integral was originated by Rice[6]. Experimental verification of J as a fracture criterion for "elastic-plastic" materials has been established primarily by Begley and Landes[7-8], and others[9-11]. The approach is based on the premise that fracture behavior in elastic-plastic materials is governed locally by conditions at the crack tip. J is the parameter characterizing crack tip conditions; its role is analogous in some respects to the role of K in linear elastic fracture mechanics.

J may be understood as the potential energy difference between two identically loaded specimens of slightly different crack sizes. J is represented as[7]

$$J = \frac{du}{da} \qquad (1)$$

where "u" is potential energy and "a" is the crack length. The parameter J is also derived from the area under the load versus deflection curve of a pre-cracked sample pulled in tension. The value of J just prior to crack initiation is the critical value J_{IC}, assuming that measurements are made on samples of sufficient size.

The J-integral criterion has been successfully applied to cases of large scale yielding, but only with plane strain conditions predominating. The applicability of J to cases of plane stress has not been demonstrated. Nevertheless, size requirements for J_{IC} tests are not the same as those required by ASTM for K_{IC} testing.

The rationale for using the J-integral as a fracture criterion is that J_{IC} may be converted to K_{IC} by means of the relation[8,9]:

$$J_{IC} = \frac{1-\nu^2}{E} K_{IC}^2 \qquad (2)$$

where E is Young's modulus and ν is Poissons ratio. J_{IC} yields the design parameter K_{IC} if the test specimen size and design are adequate. Therefore, K_{IC} may be determined for non-linear elastic materials from specimens which are significantly smaller than those required for direct K_{IC} measurements.

MATERIALS

The materials tested in this study were Ti-6Al-4V, Ti-5Al-2.5Sn, AISI types 304, 310 and 316 stainless steels, and the iron base alloy ASTM A-286. These materials were obtained in various forms as given by Table 1. With the exception of A-286, the materials were tested in the as-received condition. Specimens of A-286 were machined from stock and subsequently heat treated in two steps as follows:

(1) solution treat at 1650°F for 2 hrs, oil quench

(2) age at 1350°F for 16 hrs, air cool.

The chemical analyses of all materials are given in Table 2. Note that two different heats of AISI 316 were used. Except for three samples, all of the 316 specimens were machined from the same plate, designated as "heat 1". Three samples were machined from the material designated "heat 2", which was of slightly higher hardness. The hardnesses of all materials tested are listed in Table 3.

Table 1. Original Condition

Material	Form	Condition as Received
Ti-6Al-4V	1" x 2" bar	Commercially annealed (1300°F 2 hrs), air cooled, descaled
Ti-5Al-2.5Sn	4-3/4" square bar	Commercially annealed
AISI 304	1.5" plate	Commercially annealed, descaled
AISI 310	1.5" plate	Commercially annealed, descaled
AISI 316, heat 1	1.5" x 4" bar	Commercially annealed, descaled
AISI 316, heat 2	1.5" plate	Commercially annealed, descaled
A-286	4-1/2" square bar forging	Forged and annealed

Note: 1 in = 2.54 cm

310<

Table 2. Chemical Analysis of Materials Tested (wt%)

	Al	V	Fe	Sn	C	N	O	H
Ti-6Al-4V	6.24	4.18	0.174	---	0.035	0.011	0.155	14 ppm
Ti-5Al-2.5Sn	5.28	---	0.327	2.46	0.01	0.010	0.174	40 ppm

	C	Mn	P	S	Si	Cr	Ni	Mo	Co	Cu	Ti	B	V	Al
AISI 304	0.052	1.60	0.028	0.015	0.75	18.33	9.82	0.20	---	0.13	---	---	---	---
AISI 310	0.038	1.41	0.023	0.016	0.72	24.65	20.40	0.13	---	0.14	---	---	---	---
AISI 316 (heat 1)	0.040	1.72	0.019	0.019	0.51	17.80	13.10	2.18	---	---	---	---	---	---
AISI 316 (heat 2)	0.051	1.55	0.026	0.014	0.68	17.34	12.17	2.16	0.19	0.34	---	---	---	---
A-286	0.05	1.52	0.016	0.007	0.54	13.96	24.97	1.30	---	---	2.23	0.004	0.30	0.19

Table 3. Hardness of Materials Tested

Material	Hardness
Ti-6Al-4V	R_C 37.0
Ti-5Al-2.5Sn	R_C 33.8
AISI 304	R_B 86.2
AISI 310	R_B 80.1
AISI 316, Heat 1	R_B 84.1
AISI 316, Heat 2	R_B 85.7
A-286	R_C 30.8

EXPERIMENTAL PROCEDURES

Tensile Tests

Uniaxial tensile tests were performed with a 10,000 lb (4,500 kg) Instron Universal testing machine. Tests were made with a stainless steel cryostat, as previously described by Reed[12]. Testing in liquid nitrogen (76 K) was accomplished by immersion of specimen and cryostat in a single metal dewar containing the cryogen. Testing in liquid helium (4 K) was accomplished with a double glass dewar arrangement, the outer dewar containing liquid nitrogen.

Load was monitored with a 10,000 lb (4,500 kg) commercial load cell. An X-Y recorder was used to obtain load versus displacement curves in the conventional manner.

Specimen extension was measured with a commercial clip-on extensometer calibrated with a dial micrometer at each temperature. There was little decrease in sensitivity with temperature: at 298 K, a strain increment of 3.2×10^{-4} was recorded for every small division of chart paper; at 76 K, the sensitivity was 3.4×10^{-4} strain per division; and at 4 K, the sensitivity was 3.65×10^{-4} strain change per division. The extensometer monitored strain to about 25%. Strain to fracture was monitored according to a constant chart and crosshead speed. With Ti-6Al-4V, strain at 298 K was measured with a clip-on Baldwin extensometer. This extensometer monitored a strain change of 1.2×10^{-4} per chart division.

With the exception of the alloy Ti-6Al-4V, all tensile samples were machined according to ASTM specifications[13] as shown in figure 1. Ti-6Al-4V specimens had a reduced section that was 1-1/8 inch long, due to limitations in the width of stock. The Ti-6Al-4V specimens were tested in

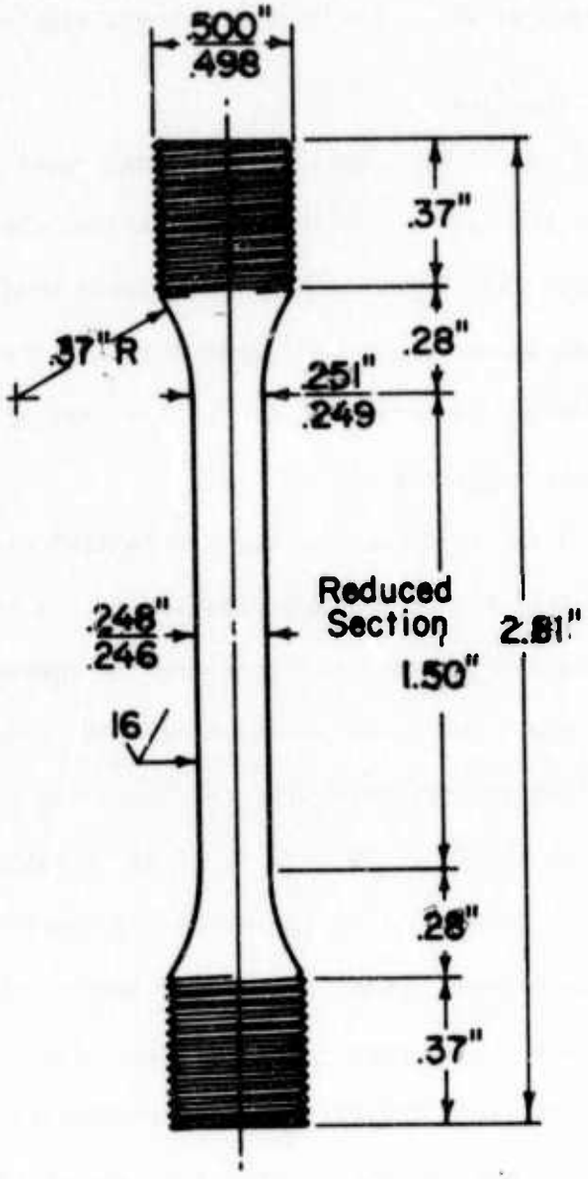

Figure 1. Tensile Sample (1 in. =2. 54 cm.)

both the longitudinal and transverse orientations. All other materials were tested in the transverse orientation so that the plane of fracture would be in the rolling direction. This orientation of the fracture plane was the same as for a fracture toughness sample.

Low Temperature Fatigue

A 20,000 lb (9,000 kg) cryostat was constructed primarily for fatigue testing and some fracture tests in liquid helium. To minimize the consumption of costly liquid helium over relatively long term (4 hr.) fatigue test periods, the steady state heat gain into the system had to be minimized. This was accomplished by efficient use of low thermal conductivity, non-metallic composite materials.

Figures 2, 3 and 4 illustrate the 4 K fatigue cryostat and associated apparatus. The load carrying frame consists of two tubular stand-off compression members which were designed for low thermal conductivity and buckling resistance. The lower sections of these columns are AISI 304, 0.125 inch (0.3 cm) in wall thickness; the upper sections are fiberglass reinforced plastic (FRP), 0.250 inch (0.6 cm) in wall thickness. The bridge linking the lower ends of the stand-off members is a maraging steel. The lower specimen grip is inserted into the center of the bridge and pinned in place. The upper specimen grip, also of maraging steel, is threaded and attached directly to a titanium alloy pull rod.

A double dewar arrangement is used for fatigue and fracture tests in liquid helium. Conventional glass dewars were rejected for fracture testing applications on the basis of fragility. Instead, an inner helium

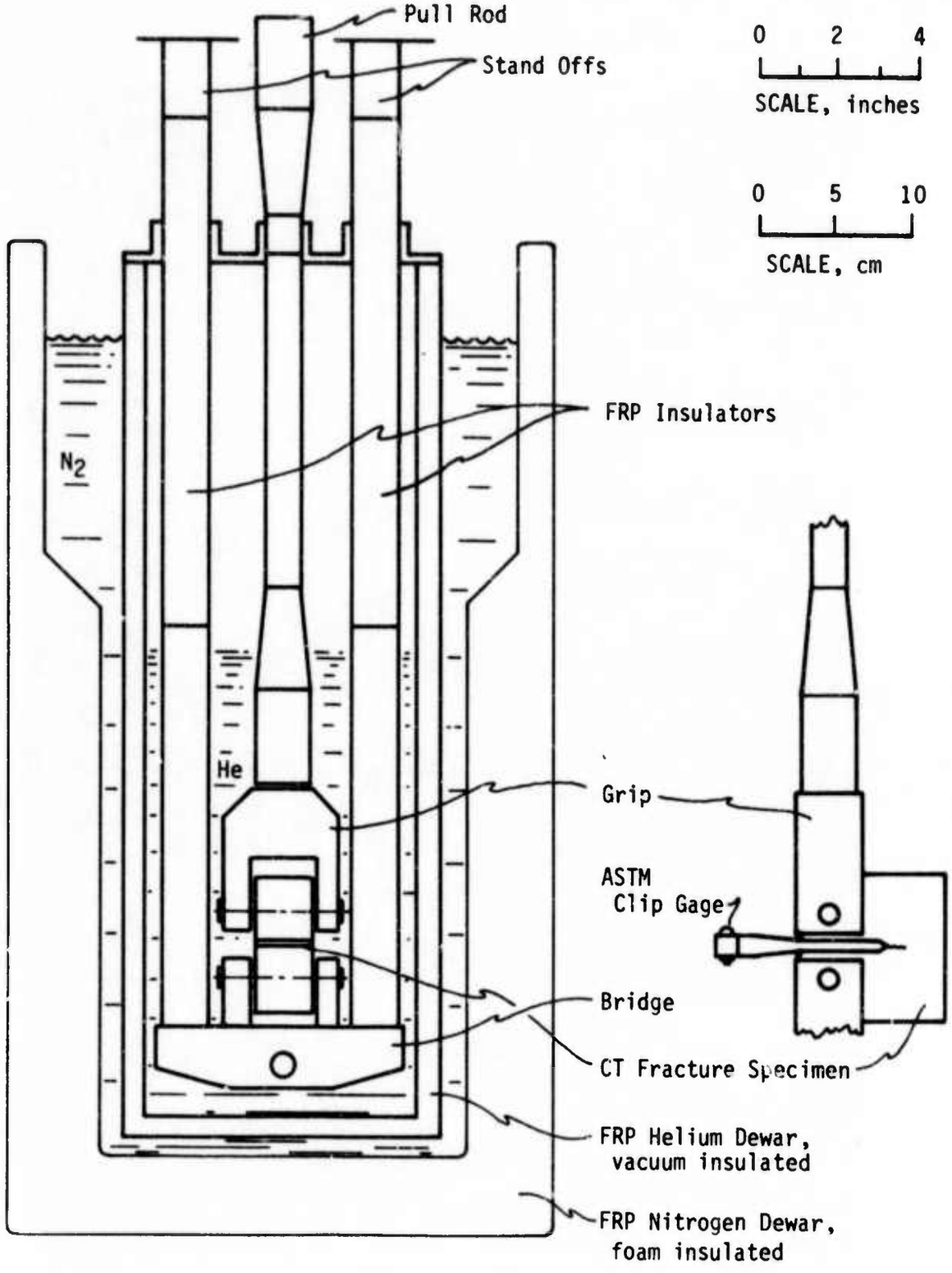

Figure 2. Helium Fatigue and Fracture Cryostat

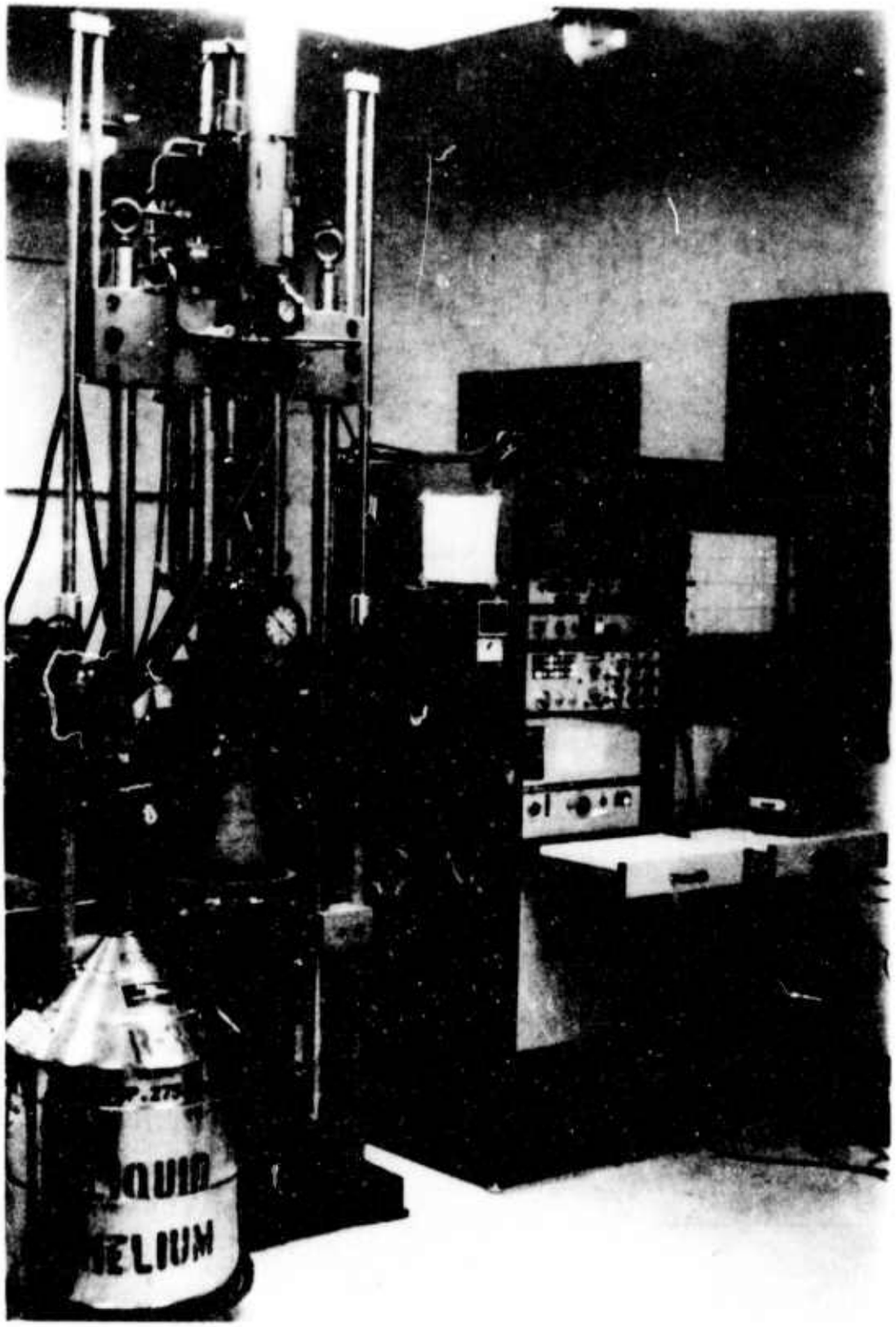

Figure 3. Cryogenic Fatigue Testing Apparatus

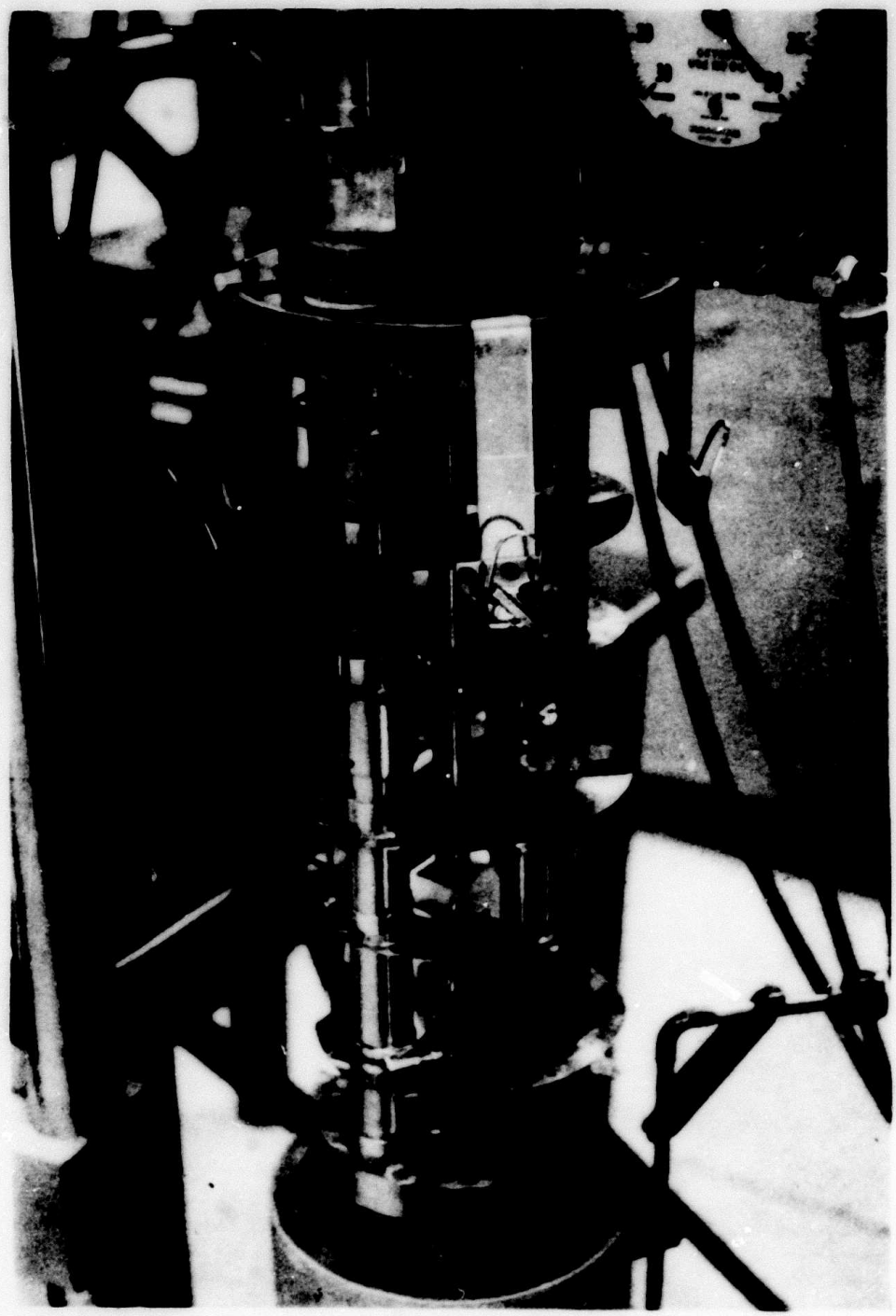

Figure 4. Helium Fatigue Cryostat

dewar was fabricated from fiberglass reinforced plastic. The two concentric cylindrical walls of this dewar are each 0.1 inch (0.25 cm) thick. A vacuum is maintained in the space between the walls by periodic mechanical pumping, and five layers of aluminized mylar are located in the vacuum space for added insulation. During 4 K tests, an outer dewar of liquid nitrogen surrounds the inner dewar of liquid helium. This outer nitrogen dewar was fabricated from fiberglass and epoxy. The space between the walls of the outer dewar contains polyurethane foam and several layers of aluminized mylar.

Thin copper baffles may be attached with hose clamps at locations along the stand-off columns of the cryostat frame as shown in figure 5. These baffles are intended to direct the flow of cold gas resulting from boil off during transfer of liquid helium. They also serve as radiation shields. Other features of the cryostat include two vents, a carbon resistor liquid level indicator, a connection for gas pressurization, and a lead-through for clip gage wiring.

Liquid nitrogen is used to precool the cryostat. Liquid helium is transferred into the precooled inner dewar through a vacuum jacketed fill tube. Under static load conditions, there was only a loss of 0.05-0.10 liter of liquid helium per hour. The loss of helium is higher under dynamic conditions. For fatigue loads up to 4,000 lbs (1,800 kg) the rate of helium loss increases to 0.5 liter/hr (five times the rate for static conditions). For fatigue tests at loads greater than 10,000 lbs (4,500 kg), cryogen loss is such that liquid helium is continuously transferred into the dewar at a slow rate. The increased loss of cryogen

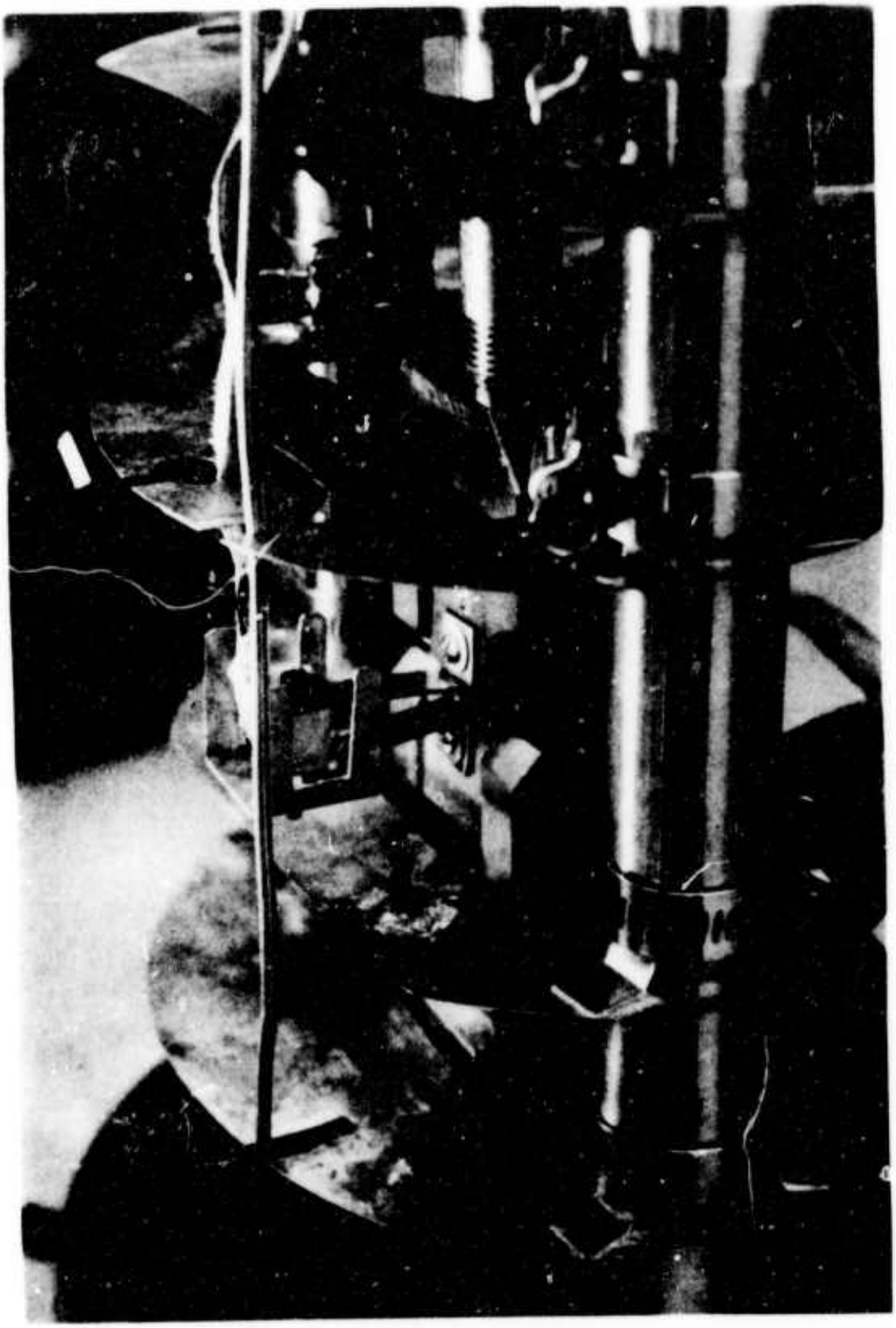

Figure 5. Specimen and Clip Guage Positioned in Fatigue Cryostat

during fatigue is attributed primarily to heat generated by the work done on the cryostat frame. The total helium consumption for this cryostat has varied between 11 and 35 liters per test, depending on the amount of reserve fluid added above the specimen, the efficiency of helium transfer, and the applied fatigue load.

Compact tensile specimens were employed in all fatigue and fracture tests. The geometry and dimensional tolerances for this specimen design are described in ASTM standard E-399[5]. As shown in figure 6, the Ti-6Al-4V specimens were 1 inch (2.54 cm) thick. Ti-5Al-2.5Sn alloy specimens were 1.5 inch (3.81 cm) thick. For both titanium alloys, deflections were measured between attachable knife edges located on opposite sides of the crack mouth at the specimen edge.

AISI 304, AISI 316, and A-286 alloy specimens were 1.5 inch (3.81 cm) thick. J-integral fracture tests were to be performed on these materials subsequent to fatigue crack growth tests. A modification in notch configuration was therefore introduced to enable measurement of loadline deflection. Integral knife edges were machined at the loadline as shown in figure 7.

All alloys were oriented with the machined notch in the rolling direction. The depth of the machined notch was such that $a_m/W = 0.3$ for the majority of specimens. Some specimens were machined to notch depths of $a_{m/W} = 0.46 - 0.475$ to facilitate precracking. The notch root radius was 0.005 inches (0.013 cm).

Fatigue crack growth tests were conducted at 298 K, 76 K, and 4 K, using a 20,000 lb (9,000 kg) MTS servo-hydraulic test machine in the mode of load control. The load was varied sinusoidally and the ratio of minimum

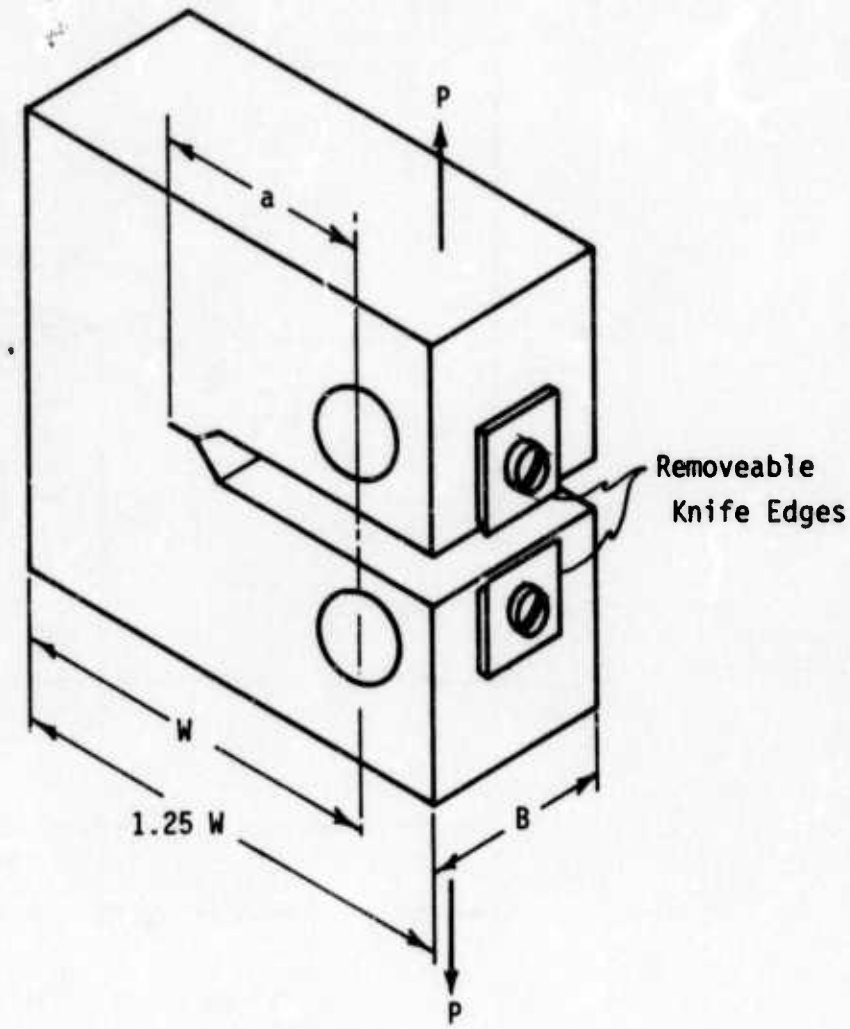

B = 1.00 inch

W = 2.00 inch

Figure 6. Compact Tensile Fracture Specimen used for Ti-6Al-4V (1 in = 2.54 cm).

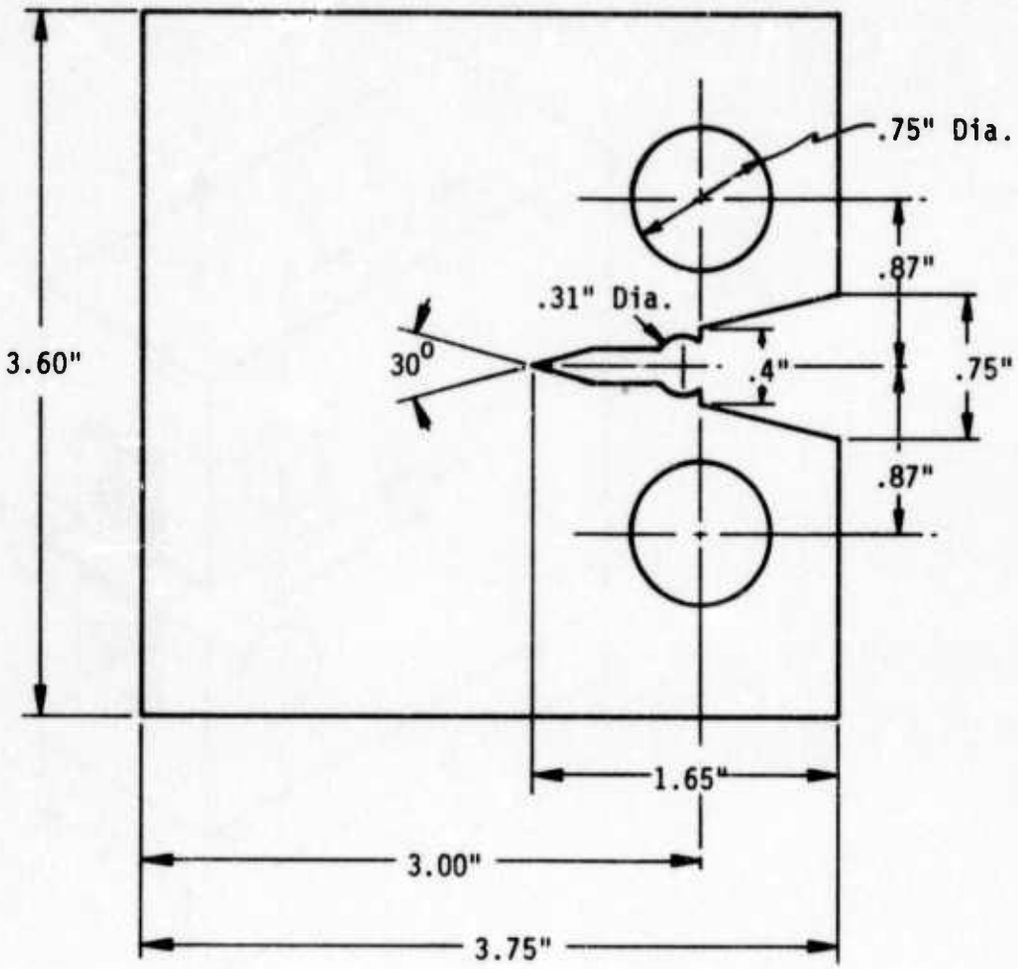

Thickness (B) = 1.50"

Figure 7. Compact Tensile Specimen Used for AISI 304, AISI 316, and A-286 Alloys (1 in. = 2.54 cm).

to maximum load (stress ratio) was maintained at R = 0.1. The loads were measured to within 1% during dynamic testing by means of a peak recording oscilloscope.

A conventional ASTM clip gage (figure 5) with a useful operating range of 0.17 - 0.37 inches (0.4 - 0.9 cm) was used to measure deflection in all fatigue tests. An extensometer calibrator was used to ascertain that clip gage linearity met ASTM requirements[5] for K_{IC} testing.

Changes in crack length were detected by means of compliance measurements. The compliance technique[14] is based on the fact that, for a given load, specimen deflection increases with increasing crack length. Experimental crack length-compliance correlations were determined for each material and temperature. The experimental correlations were not always in agreement with the theoretical solution as given by Roberts[15]. Discrepancies were attributed to differences in degree of crack front uniformity. Crack fronts in actual test specimens always exhibit some non-uniformity (crack front curvature). The experimentally determined compliance was correlated to an averaged crack length (a), measured according to ASTM standard E-399[5].

Testing consisted of cooling the specimen and cryostat to the desired temperature, initiating a crack, and propagating the crack at various levels of stress intensity. For titanium alloy and A-286 alloy specimens, cracks were always initiated at the temperature of testing. For stainless steels, cracks were always initiated at room temperature. It is known that crack growth rates may be temporarily retarded in going from a higher to a lower temperature, or from a higher to a lower applied load. Therefore,

whenever such a change was made, the crack growth rate was allowed to stabilize before data was accepted as valid.

The procedure for determining crack growth rates involved plotting compliance on an X-Y recorder at intervals during a fatigue test. The total number (N) of fatigue cycles sustained by the specimen was also noted. The crack growth rate, da/dN, was obtained by graphical differentiation of the a versus N curve.

The loads applied in fatigue varied from 3000 lbs (1350 kg) to 12,000 lbs (5400 kg), depending on the material and starting notch depth.

Fatigue cycling was usually conducted at rates of 20-26 Hz and no variation in crack growth rates was detected as a result of frequency variations in this range. A few high stress intensity fatigue tests were conducted at frequencies no greater than 10 Hz.

Three to four specimens were used to generate data at each temperature. The majority of specimens were intended for subsequent fracture tests, so that fatigue stress intensity was limited to 0.6 K_Q. A few specimens were tested solely for fatigue crack growth data; these were subjected to stress intensities approaching K_Q, and cracks were extended to maximum depth of a/W = 0.7.

For specimens employed in subsequent J-integral tests, the stress intensity factor was no greater than 35 ksi$\sqrt{\text{in}}$ during the final 3% of crack growth. Fatigue loads were reduced to increase the sharpness of terminated cracks. When this was done on AISI 304 and 316 stainless steel alloys, the degree of crack front curvature increased significantly. Pronounced crack front curvature invalidates the crack length-compliance

relationship; however, the fatigue crack growth rate data were not significantly affected since data were not recorded during the terminal stages of fatigue cracking. The degree of crack front curvature did not increase for high crack growth rate tests where stress intensity was not reduced.

Fracture Toughness

Fracture toughness tests were carried out on titanium alloys using the 20,000 lb (9,000 kg) MTS servo hydraulic test machine in the mode of stroke control. K_{IC} tests were conducted according to ASTM standards[5]. Fracture tests were performed with the helium fatigue apparatus, subsequent to crack growth tests.

J-integral fracture toughness tests on precracked specimens of AISI 304, AISI 316, and A-286 required loads in excess of 20,000 lbs (9,000 kg). Fracture tests were performed on these alloys using a 60,000 lb (27,000 kg) controlled hydraulic tensile machine. A 60,000 lb (27,000 kg) cryostat was designed similarly to the helium fatigue cryostat, except that composites were not employed in the stand-off columns. The frame is shown in figure 8 (left view). The stand-off columns are AISI 321 stainless steel tubes, 1.5 inch O.D. by 0.875 inch I.D. (3.7 x 2.2 cm). This design provides rigidity and greater load capacity. The higher rate of steady state heat gain is not a vital consideration since the cryostat is intended for short term tests. About 11-15 liters of liquid helium are consumed per test.

Load was monitored with a commercial load cell. A clip gage with a useful operating range of 0.17-0.75 inches (0.4-2.5 cm) was used to

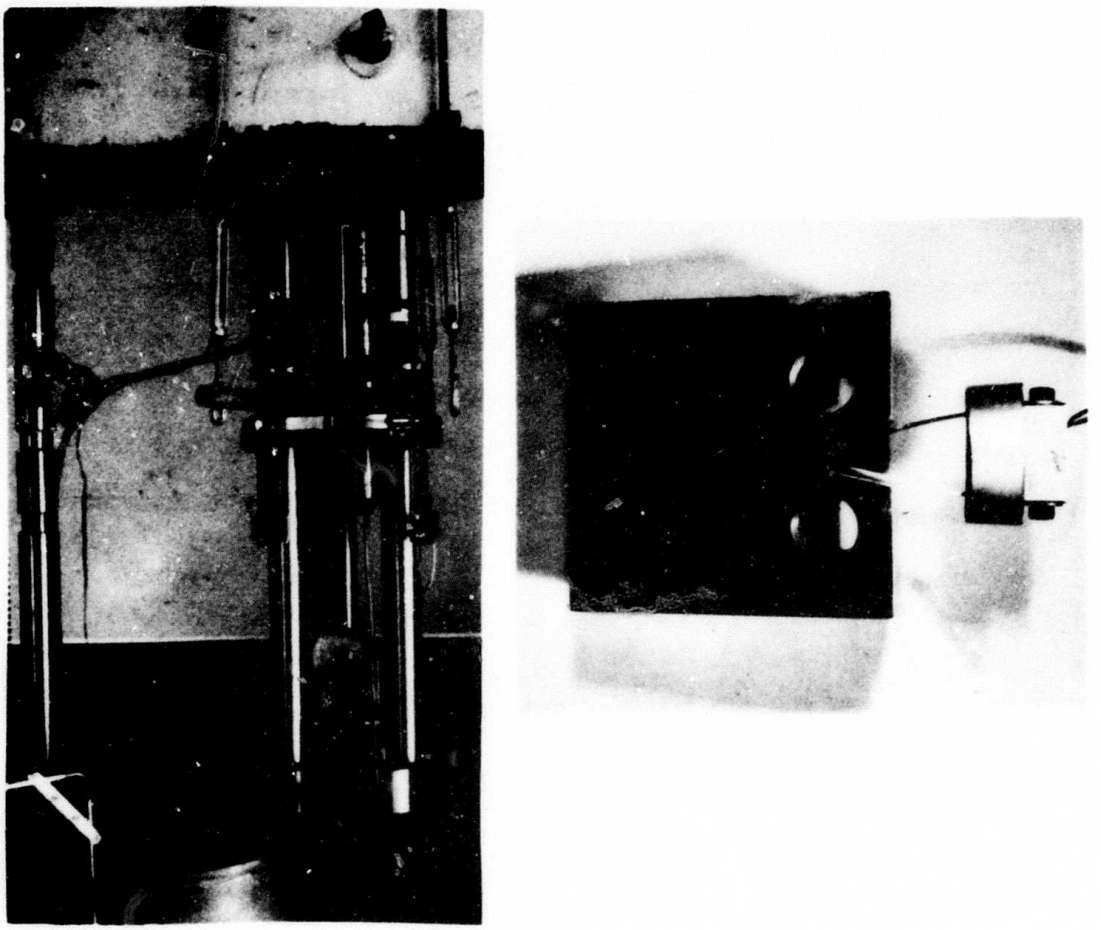

Figure 8. Fracture Cryostat and Sample with 60,000 lb. (27,200 kg.) Machine

to measure deflection in all J-integral tests. The clip gage is shown in figure 8 (right view). This clip gage was evaluated using an extensometer calibrator; precision corresponds to a maximum deviation of + 0.003 inches (0.007 cm) from linearity over the useful operating range. The calibration was performed at each testing temperature. Other equipment such as specimen grips and dewars were identical to the apparatus described previously for fatigue testing.

J-integral tests were performed similarly to a procedure outlined by Landes and Begley[16]. According to this method, three or four nearly identical specimens (having equivalent average crack lengths) are tested at each temperature. The specimens are loaded to various increments of stable crack extension and the tests interrupted. Specimens were pulled apart for analysis after a heat tinting treatment oxidized the exposed surfaces. Each value of J, as derived from the area under the load-displacement curve, is plotted as a function of the measured crack extension, Δa. The critical J integral, J_{IC} is obtained by extrapolation of the J versus Δa plot to the vertical "stretch zone" line. The stretch zone is the transition region ahead of the fatigue precrack zone where the material deforms under load prior to crack extension. The measured crack extension, Δa, includes an increment contributed by the stretch zone.

For the compact tensile specimens described in this report, J was calculated from the relation[9,16]:

$$J = \frac{2A}{Bb} ,$$

where A is the area under the load-displacement curve to a particular value of extension, B is specimen thickness, and b is the length of ligament or the uncracked portion of the precracked sample. The area A was measured using a planimeter.

Crack extension was measured in several different ways: the value taken at the specimen centerline (Δa, cent), the value taken as an average of measurements at the center and edges or midpoints (Δa, ave), and a "true" average determined by measuring the extension area with a planimeter and dividing by specimen thickness. Results are presented for the AISI 304 and AISI 316 using the true average. The A-286 results are reported in terms of "Δa, center" and Δ a, average (of center and the midpoints).

Values of K_Q and K_{max} were obtained from the secant value of the sample load and the ultimate load, respectively. The secant value was determined according to ASTM designation E 399-70T[9]: the level in question is the intersection with the load-displacement curve of a line that has 5% less slope than the tangent. Both K_Q and K_{max} are obtained from the relation

$$K = \frac{P}{BW^{1/2}} \; f\,(a/W),$$

where P is the load, B is the thickness, W is the length from the hole centerline to the sample back, and "a" is the fracture crack length measured from the hole centerline. The "a" value used was an average of three measurements: one taken at the center and the other two taken midway between the center and outside.

RESULTS

Tensile Tests

The tensile strengths and yield strengths measured at 0.2 percent offset for the titanium alloys are shown in Table 4. Ductility of the titanium alloys is shown in Table 5. Only a limited number of tests were conducted since both the alloys had been thoroughly tested to 4 K. Some testing was performed in both orientations at 298 K in order to predict the mechanical behavior at low temperatures for samples oriented in the transverse direction.

Figures 9 and 10 show the temperature dependence of strength for Ti-6Al-4V[17-19] and annealed Ti-5Al-2.5Sn[17,19,20], respectively. Tests done by other investigators are included. With the exception of Ti-5Al-2.5Sn at 76 K, the yield strengths are close to the values of the tensile strengths. The data of this report can be extrapolated to the lower temperatures on noting the temperature trend of the other tests.

Table 6 shows the yield and tensile strengths of AISI 304, 310 and AISI 316. The strengths of A-286 are shown in Table 7. Ductility of AISI 304, 310 and 316, and A-286 is shown in Table 8. The A-286 samples reported by Warren are essentially the same hardness as the samples of this report; thus, using Warren's data, the low temperature yield and tensile strengths of A-286 for the transverse orientation can be approximated. Figure 11 shows the strength of AISI 304[21-25] and AISI 316. Note that there is a maximum in the AISI 304 of Guntner and Reed[22], the strength dropping between 20 and 4 K.

Table 4. Strengths of Titanium Alloys

Alloy	Temp. (K)	Orientation	0.2% Yield* Strength (psi)	Tensile Strength* (psi)
Ti 6Al-4V	298	longitudinal	134,900	145,900
			134,300	143,600
		Av =	134,600	144,750
	298	transverse	145,300	152,700
			145,100	152,200
		Av =	145,200	152,450
Ti 5Al-2.5 Sn	298	transverse	124,600	132,000
			118,650	126,850
		Av =	121,625	129,425

* 1 ksi = 0.689×10^{7} Nm^{-2}

Table 5. Ductility of Titanium Alloys (Annealed)

Alloy	Author	Temp. (K)	Orientation	Elongation (%)	Reduction of Area (%)
Ti-6Al-4V	Warren[20](1963)	298	Longitudinal	16.6 (4D)	47.4
		76	Longitudinal	10.2 (4D)	40.6
		20	Longitudinal	6.7 (4D)	31.0
	Nachtigall[17](1974)	298	Longitudinal	---	45.
		76	Longitudinal	---	36.
		4	Longitudinal	---	13.5
Ti-5Al-2.5Sn	This report	298	Transverse	15.2 (4D)	32.4
	Warren[20](1963)	298	Longitudinal	19.0 (4D)	43.6
		76	Longitudinal	13.8 (4D)	29.5
		20	Longitudinal	11.5 (4D)	18.3
	Nachtigall[17](1974)	298	Longitudinal	---	45.
		76	Longitudinal	---	34.
		4	Longitudinal	---	30.

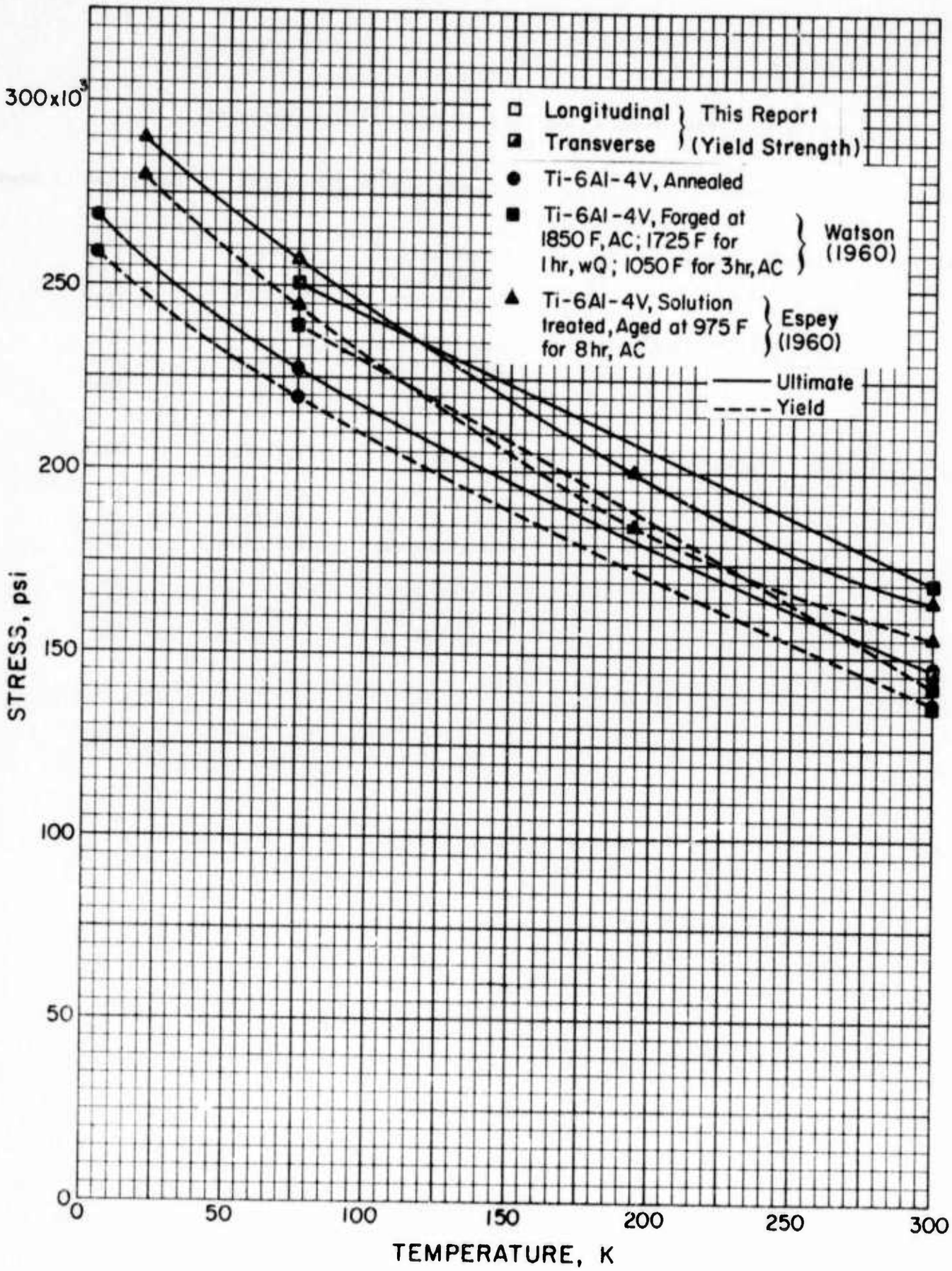

Figure 9. Strength of Ti-6Al-4V as a Function of Temperature (1 psi. = 6.895 x 10^3 N/m^2)

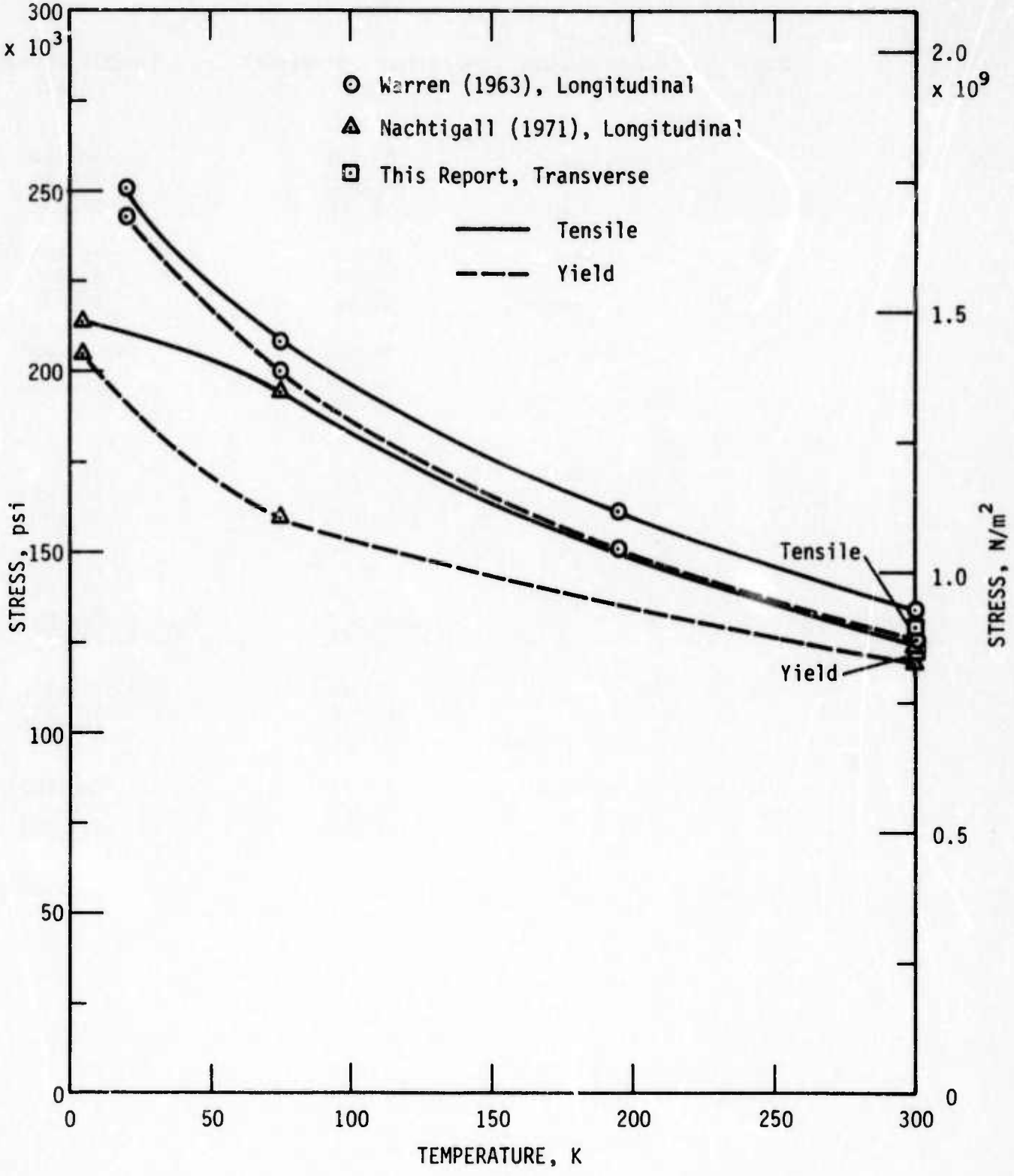

Figure 10. Strength of Ti-5Al-2.5Sn as a Function of Temperature

Table 6. Strengths of AISI 304, AISI 310, and AISI 316

Alloy	Temp. (K)	Orientation	0.2% Yield Strength* (psi)	Tensile Strength* (psi)
AISI 304	298	Longitudinal	39,800	90,500
			36,600	86,400
		Av =	38,200	88,450
	298	Transverse	36,900	86,100
			36,900	86,900
		Av =	36,900	86,500
	76	Transverse	62,600	207,000
			62,600	--
		Av =	62,600	207,000
AISI 310	298	Transverse	35,200	78,950
			34,200	78,700
		Av =	34,700	78,800
AISI 316	298	Transverse	35,800	77,400
			35,100	78,700
		Av =	35,450	78,050
	76	Transverse	75,300	172,200
			68,500	170,500
		Av =	71,900	171,350
	4	Transverse	78,600	193,000
			79,600	--
		Av =	79,100	193,000

* 1 ksi = 0.689 x 10^7 Nm^{-2}

Table 7. Strengths of A-286

Author	Condition	Temp.	Orientation	0.2% Yield* Strength (psi)	Tensile* Strength (psi)
This Report	1650°F 2 h-O.Q., Aged 1325°F-16 h-AC	298 K	Transverse	93,300	156,100
				83,100	144,850
			Av =	88,200	150,475
Warren[20] (1963) (Average Values)	1800°F-1-1/2 h-O.Q, Aged 1350°F-16 h-AC	298	Longitudinal	111,100	160,000
		195	Longitudinal	120,300	175,800
		76	Longitudinal	135,400	209,400
		20	Longitudinal	150,200	235,300
		4	Longitudinal	155,000(est.)	245,000(est.)

* 1 ksi = 0.689×10^{7} Nm^{-2}

Table 8. Ductility of Stainless Steels

Alloy	Author	Temp. (K)	Orientation	Elongation (%)	Reduction of Area (%)
AISI 304	Guntner[22](1962)	298	Longitudinal	84 (1"GL)	84
	Annealed	76	Longitudinal	47 (1"GL)	69
		4	Longitudinal	44 (1"GL)	57
AISI 310	This report, Annealed	298	Transverse	46.9 (4D)	70.7
	Guntner[22](1962),	298	Longitudinal	59 (4D)	71
	Annealed	76	Longitudinal	68 (4D)	50
		4	Longitudinal	50 (4D)	41
AISI 316	This report, Annealed	298	Transverse	75 (4D)	73.2
	Desisto[25](1960),	298	Longitudinal	46.5	76.5
	Annealed	76	Longitudinal	59	74.7
		4	Longitudinal	50.5	58
A-286	Warren[20](1963),	298	Longitudinal	25.4 (4D)	49.3
	Solution Treated	76	Longitudinal	35.8 (4D)	49.2
	1800°F, aged	20	Longitudinal	36.2 (4D)	42.8
	at 1350°F, R_c 30				

337<

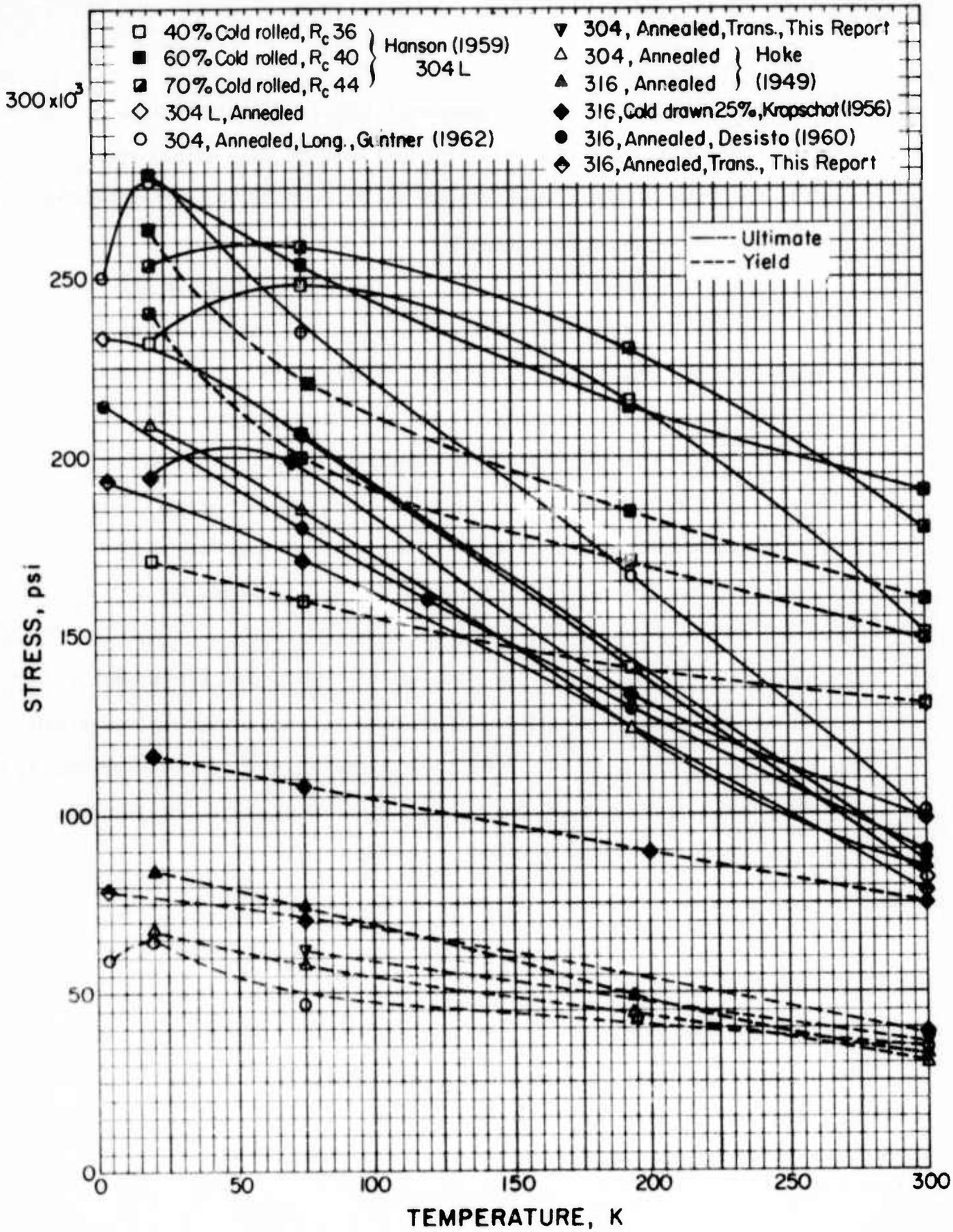

Figure 11. Strength of AISI 304 and AISI 316 as a Function of Temperature (1 psi=6.895 x 10^3 N/m^2)

Stress-strain curves for the titanium alloys is shown in figures 12 and 13. Typically, there is little work hardening of these alloys even to the lowest temperatures. Note the discontinuous yielding of Ti-5Al-2.5Sn alloy at 4 K, as reported by Nachtigall.

Stress-strain curves for AISI 304, 310, and 316 are shown in figures 14, 15, and 16. The three stainless steel alloys work harden at a much higher rate with temperature than do the titanium alloys. In particular, the AISI 304 work hardens extremely at the lower temperatures. The discontinuous yielding observed with the stainless steels at 4 K is a result of localized heating and is dependent on the rate of strain. This rate dependence is also observed at 20 K with AISI 310 (see figure 15). Explanation of the discontinuous phenomenon has been presented by Basinski[26].

Table 9 and figures 17 and 18 shows the work hardening coefficients of Ti-6Al-4V, AISI 304, and AISI 316 as determined from the stress or load-strain curves. The strain values were taken from the third, or temperature dependent, stage of work hardening, i.e., the latter part of the curve to the ultimate. The coefficients are derived from the empirical relation

$$\sigma_t = K \epsilon_t^n ,$$

where σ_t is the true stress, ϵ_t is the true strain, n is the work hardening coefficient, and K is the strength coefficient. Taking the logarithm of both sides of the above equation,

$$\log \sigma_t = \log K + n \log \epsilon_t .$$

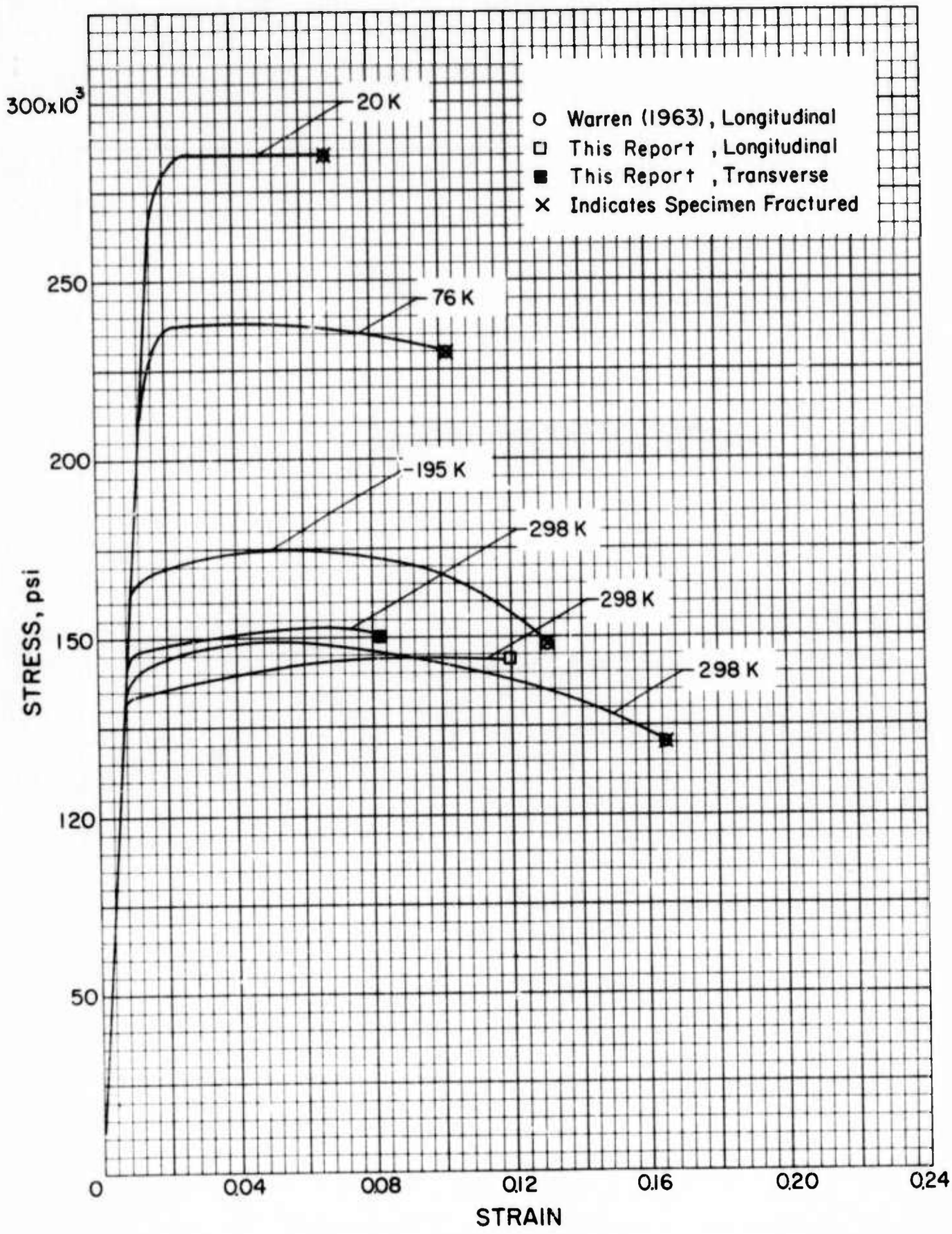

Figure 12. Stress-Strain Curves of Ti-6Al-4V
(1 psi. = 6.895 x 10^3 N/m^2)

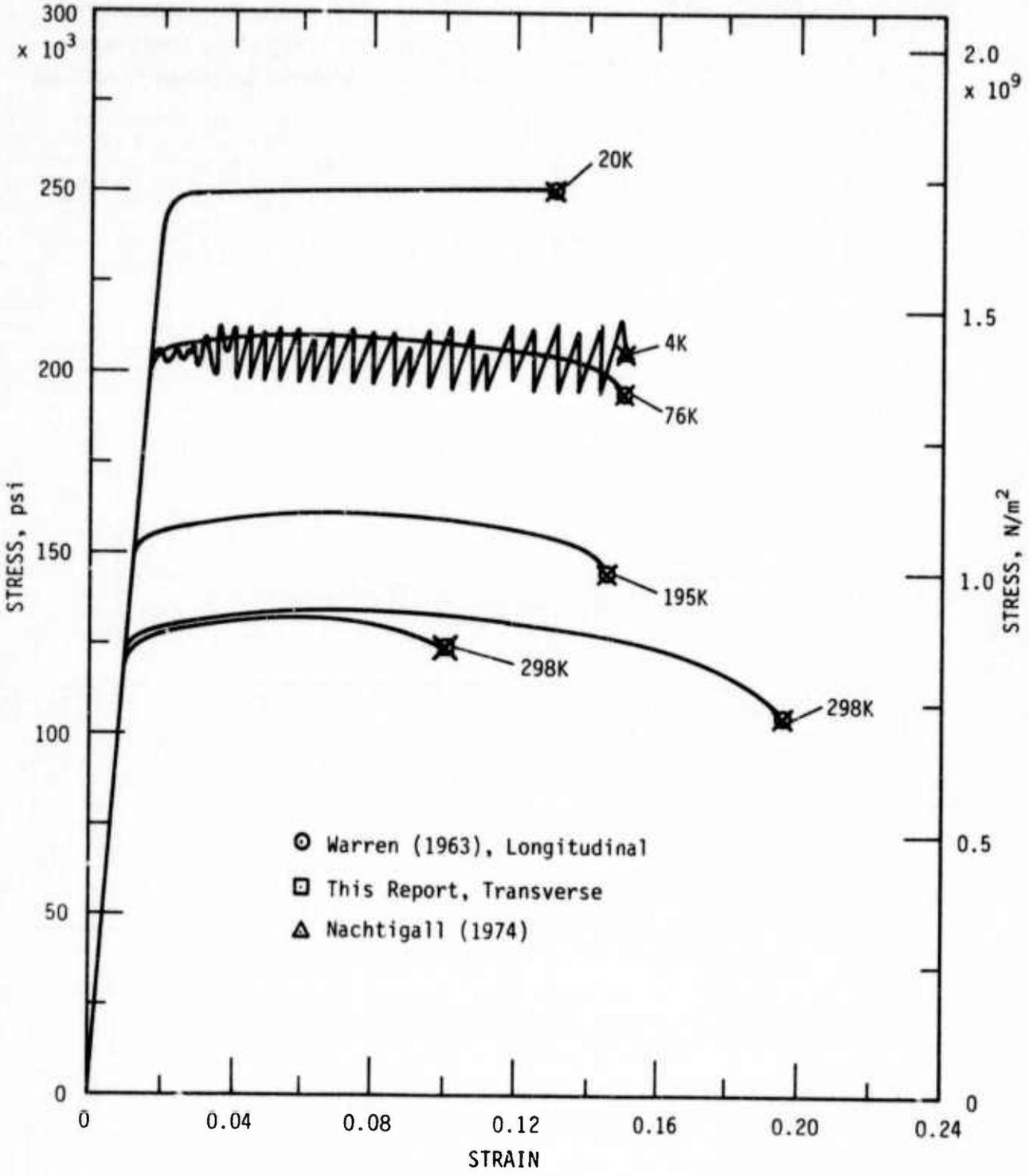

Figure 13. Stress-Strain Curves of Ti-5Al-2.5Sn

341<

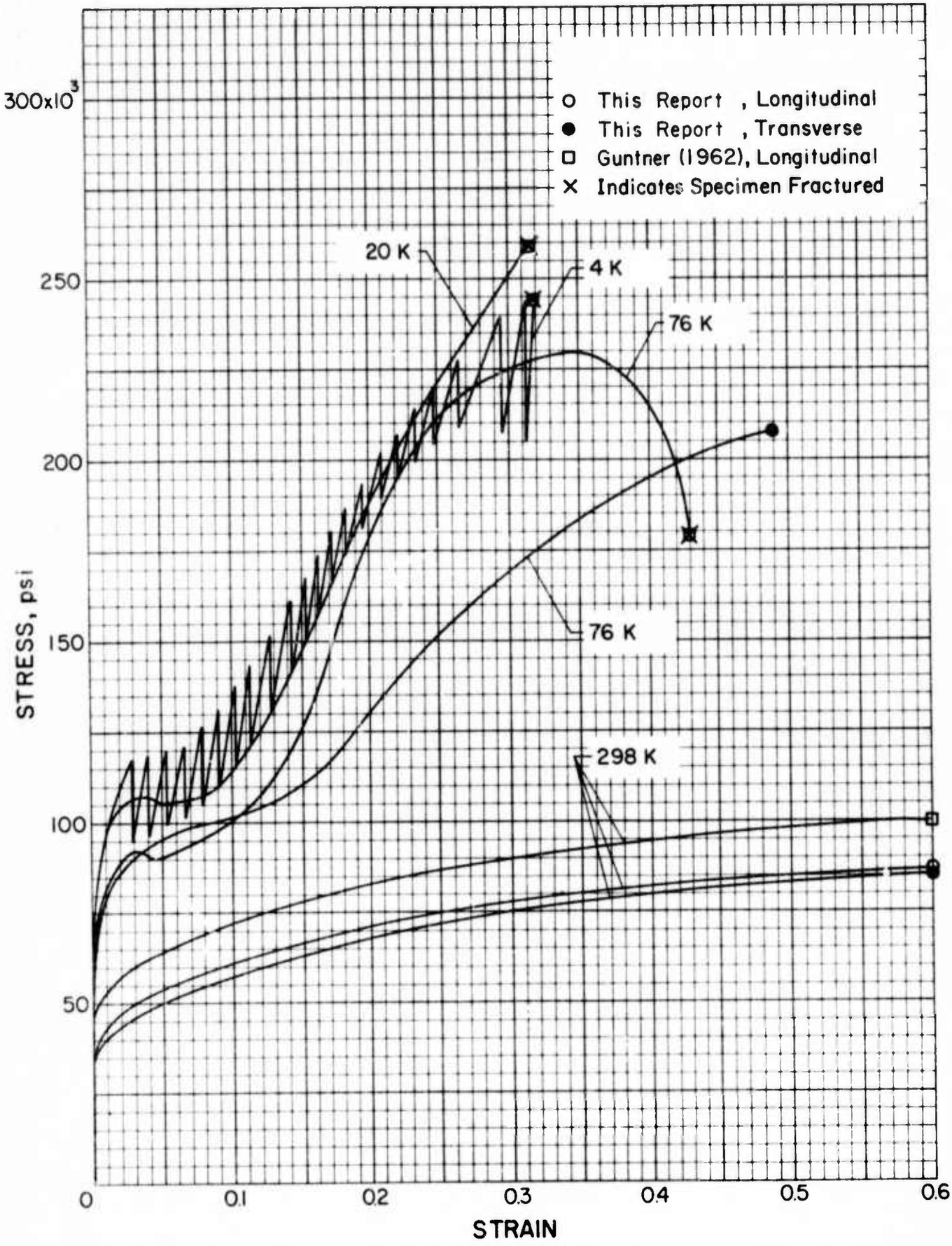

Figure 14. Stress-Strain Curves of AISI 304
(1 psi. = 6.895 x 10^3 N/m^2)

342<

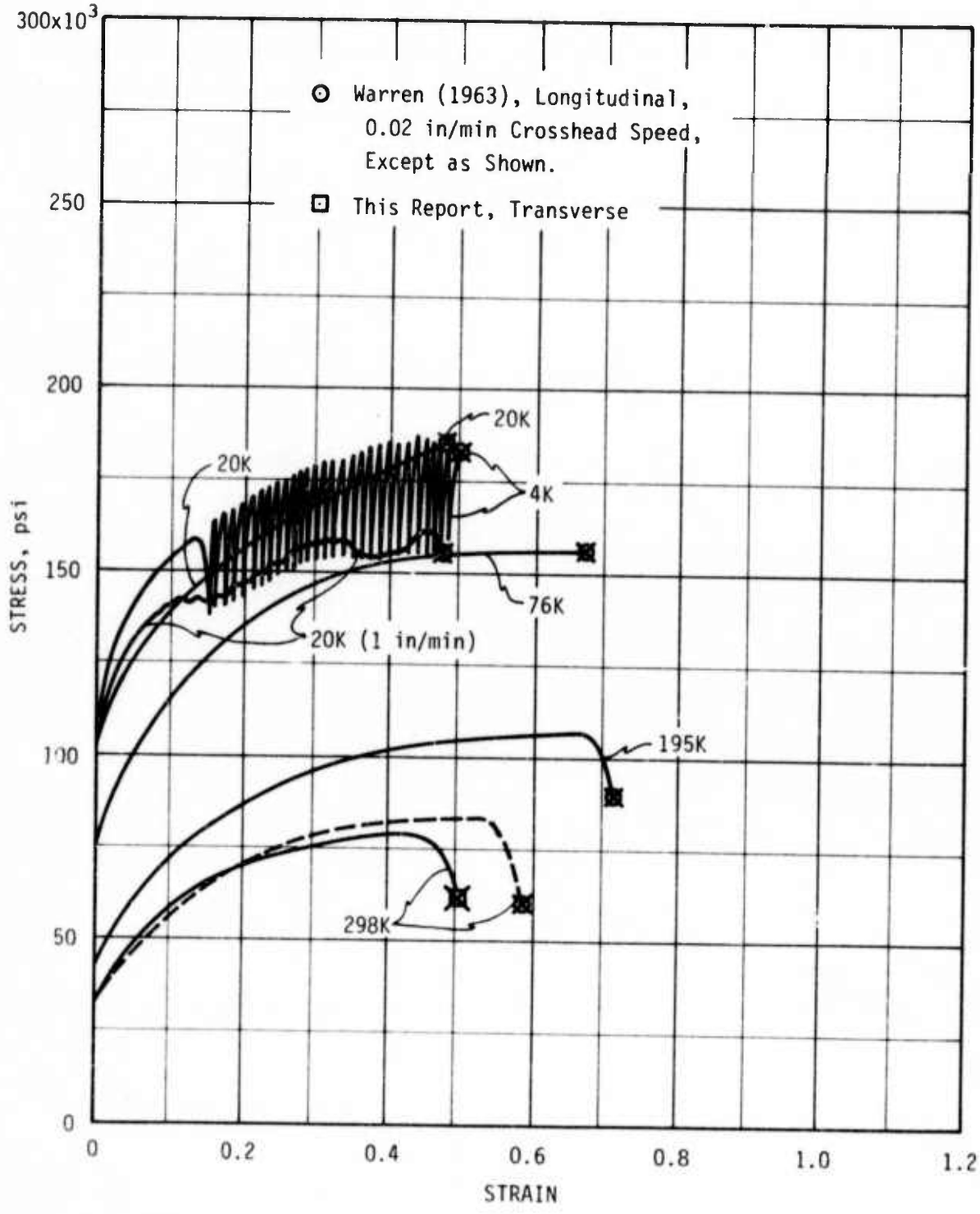

Figure 15. Stress-Strain Curves of AISI 310
(1 psi.=6.895 x 10^3 N/m^2)

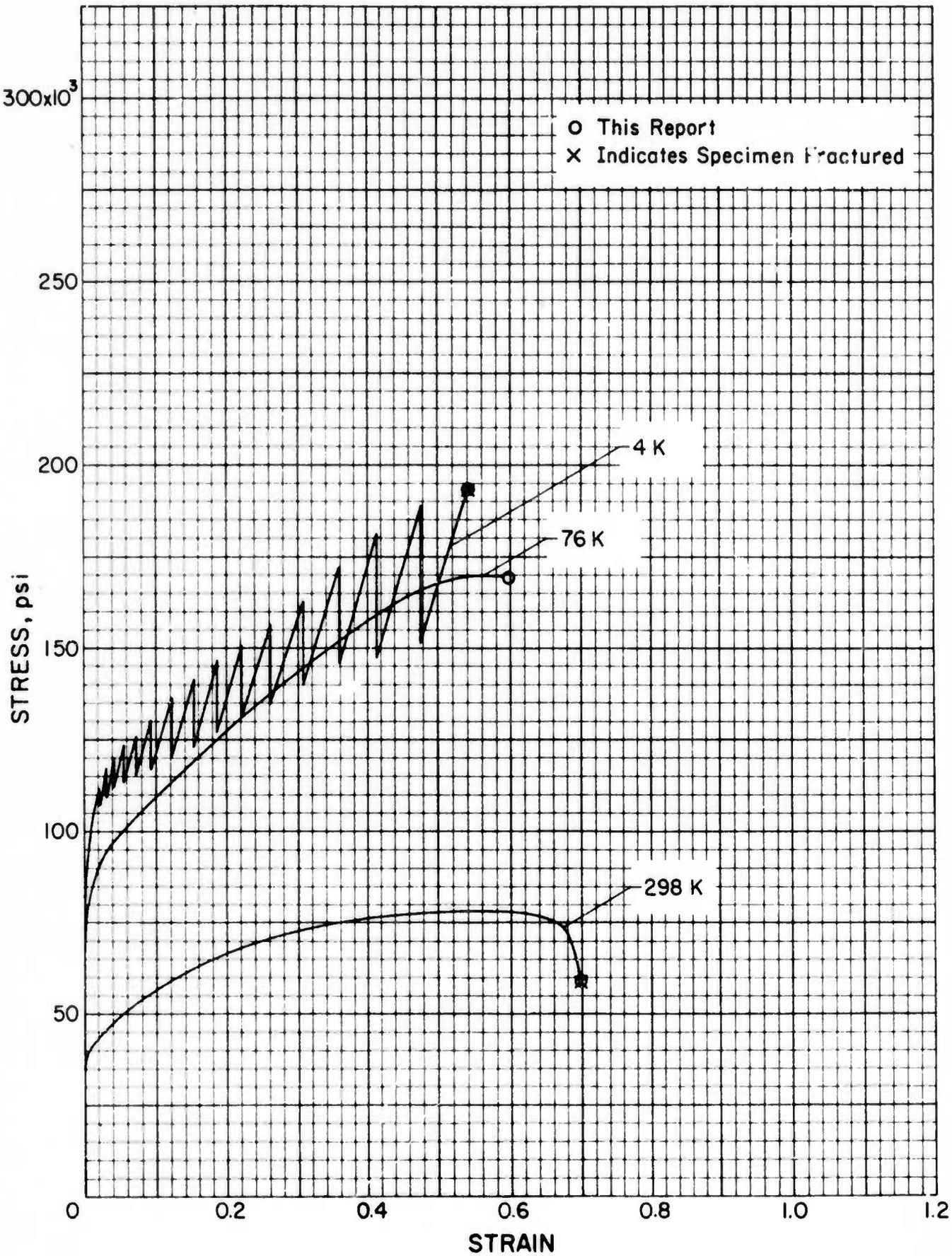

Figure 16. Stress-Strain Curves of AISI 316
(1 psi. =6.895 x 10^3 N/m^2)

Table 9. Work Hardening Coefficients of the Alloys

Alloy	Temperature	Orientation	n	Ave. Deviation, Log True Stress
Ti-6Al-4V	298 K	longitudinal	0.071	0.01%
(Warren[20])	195		0.062	0.01
	76		0.080	0.09
	20		0.118	0.05
Ti-6Al-4V	298	longitudinal	0.068	0.09
(this report)		transverse	0.057	0.04
304	298	longitudinal	0.333	0.39
(Guntner, Reed[22])	76		0.875	0.27
	20		< 1(1.04)	0.06
	4		0.654	0.08
304	298	longitudinal	0.392	0.53
(this report)	298	transverse	0.403	0.44
	76	transverse	0.897	0.10
316	298	transverse	0.383	0.34
(this report)	76		0.649	0.04
	4		0.585	0.12

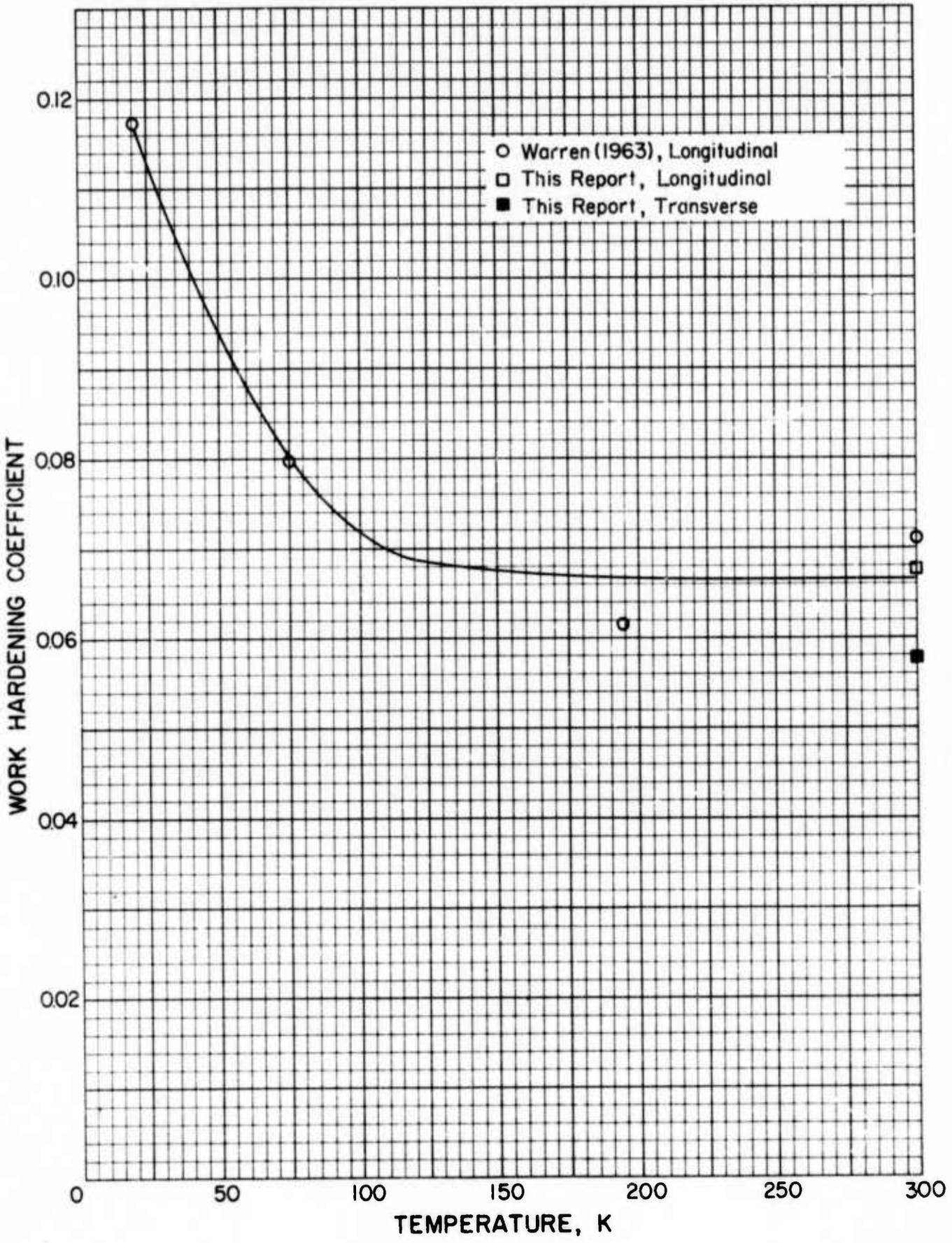

Figure 17. Work Hardening Coefficient of Ti-6Al-4V as a Function of Temperature

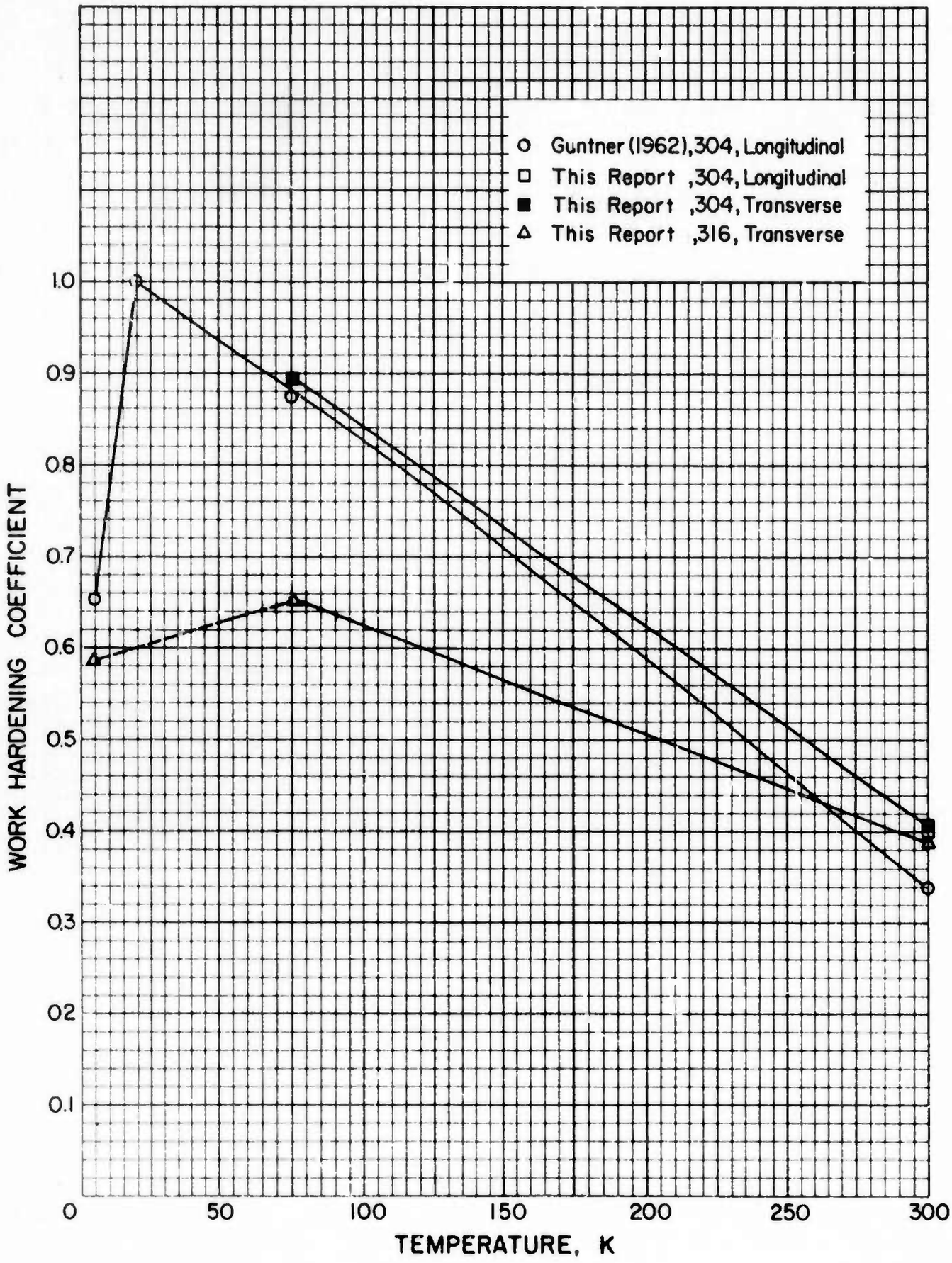

Figure 18. Work Hardening Coefficient of AISI 304 and AISI 316 as a Function of Temperature

Thus, if the points are plotted on log-log paper, "n" is the linear slope of a straight line. A computer program was developed that enables the coefficient to be determined through these steps. The straight line plot is established by a linear least squares fit. The straight line data fit is indicated by the numbers in the right hand column of Table 9. These values represent the difference between a single number and the straight line. The coefficients were also determined as a function of orientation; there was a possibility that hardening due to dislocation pile-up would vary with inclusion direction. For the AISI 304 at 20 K (Guntner), the coefficient calculated to be 1.04. Since obviously this is wrong, the coefficient is reported to be a number less than 1. A discussion relating the rate of work hardening to fracture toughness will be presented in the last section.

Fatigue Crack Growth Rate

Ti-6Al-4V

The results obtained at room temperature are presented in figure 19, and data obtained at 76 K and 4 K are shown together in figure 20. The data are described in terms of the equation

$$da/dN = C(\Delta K)^n$$

where "a" is crack length, N is number of cycles and C and n are empirical constants. This equation was originated by Paris[27] and applies to all materials tested in this program.

Superimposed on the data is a band which represents the room temperature data appearing in the Damage Tolerant Design Handbook[28]. The room temperature results are in good agreement with this reference; they fit within the band of currently accepted data.

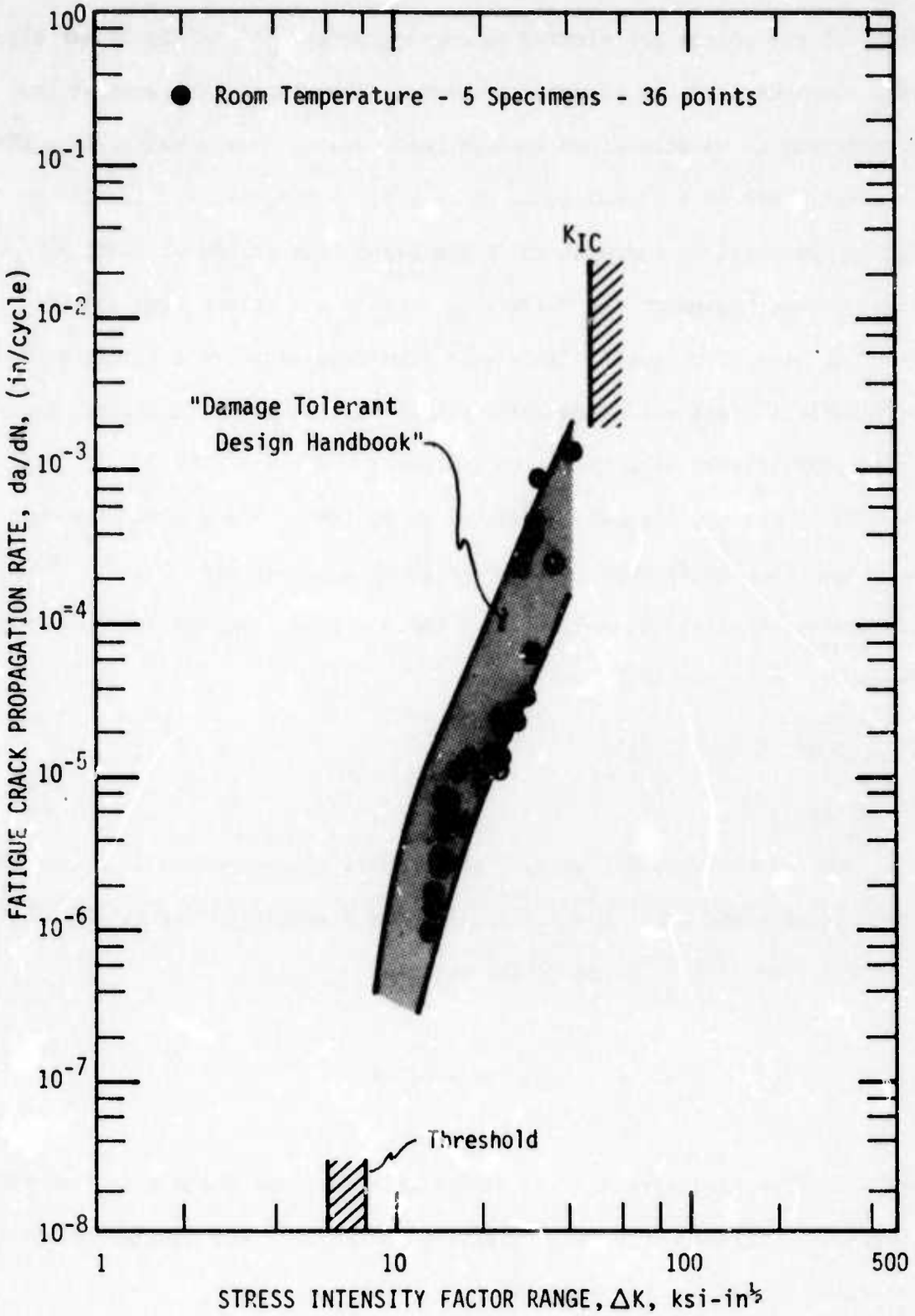

Figure 19. Crack Growth Rate Data of Ti-6Al-4V at 298 K. (1 ksi.$\sqrt{\text{in}}$=1.093 x 10^{6} N/m^{2} x m$^{1/2}$ and 1 in. = 2.54 cm.)

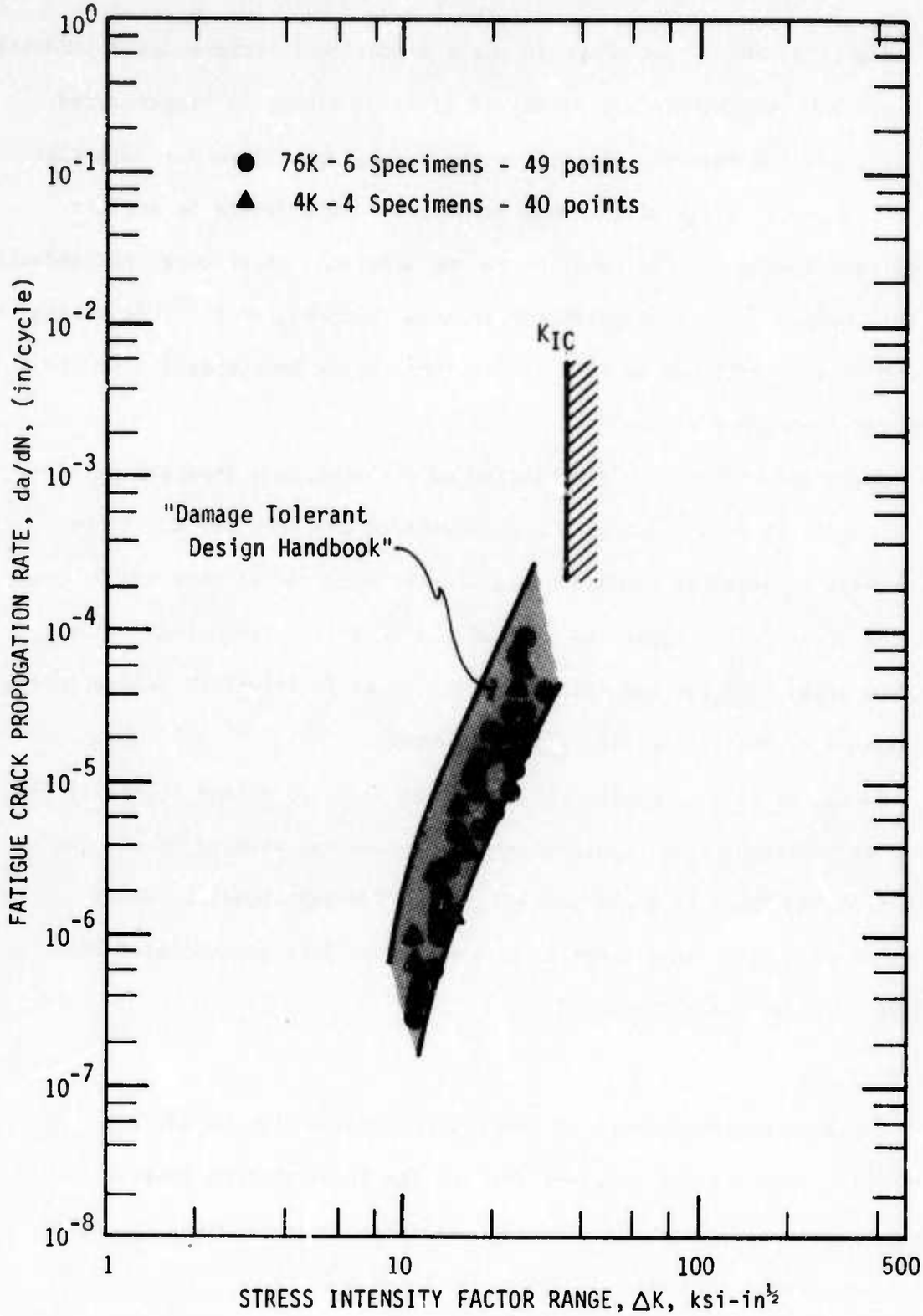

Figure 20. Crack Growth Rate Data of Ti-6Al-4V at 76 and 4 K. (1 ksi. $\sqrt{in.}$ =1.093 x 10^{6} N/m^{2} x $m^{1/2}$ and 1 in. =2.54 cm.)

Figure 20 shows that there is not a significant temperature dependence of the crack growth rate for Ti-6Al-4V alloy at cryogenic temperatures. The 76 K and 4 K data are plotted on the same graph, since any variation due to temperature was of the same magnitude as the degree of scatter among test specimens. In relation to the apparent temperature independence of this property, it is significant to note that Wei, et al[29], found the crack growth rate of a Ti-6Al-4V alloy to be temperature independent over the interval from 298 K to 563 K.

Crack growth tests were conducted on two specimens immersed in a solid-liquid mixture of alcohol and granulated dry ice, 195 K. These tests were regarded as invalid because compliance curves were non-linear and the crack fronts exhibited irregularities (crack branching). These results imply that fatigue cracking behavior of Ti-6Al-4V is deleteriously influenced by the alcohol-dry ice environment.

Bucci, et al[30], measured the threshold value of stress intensity (the value at which the rate of crack growth becomes vanishingly small) for Ti-6Al-4V and found it to be 6-8 ksi$\sqrt{\text{in.}}$. This experimental result compares well with the present room temperature data extrapolated one decade lower in da/dN (figure 19).

Ti-5Al-2.5Sn

Crack growth rate tests of the alloy Ti-5Al-2.5Sn are not yet completed. The results obtained for two specimens at room temperature are presented in figure 21. Testing is currently in progress to expand the crack growth rate data at 298 K, 76 K and 4 K.

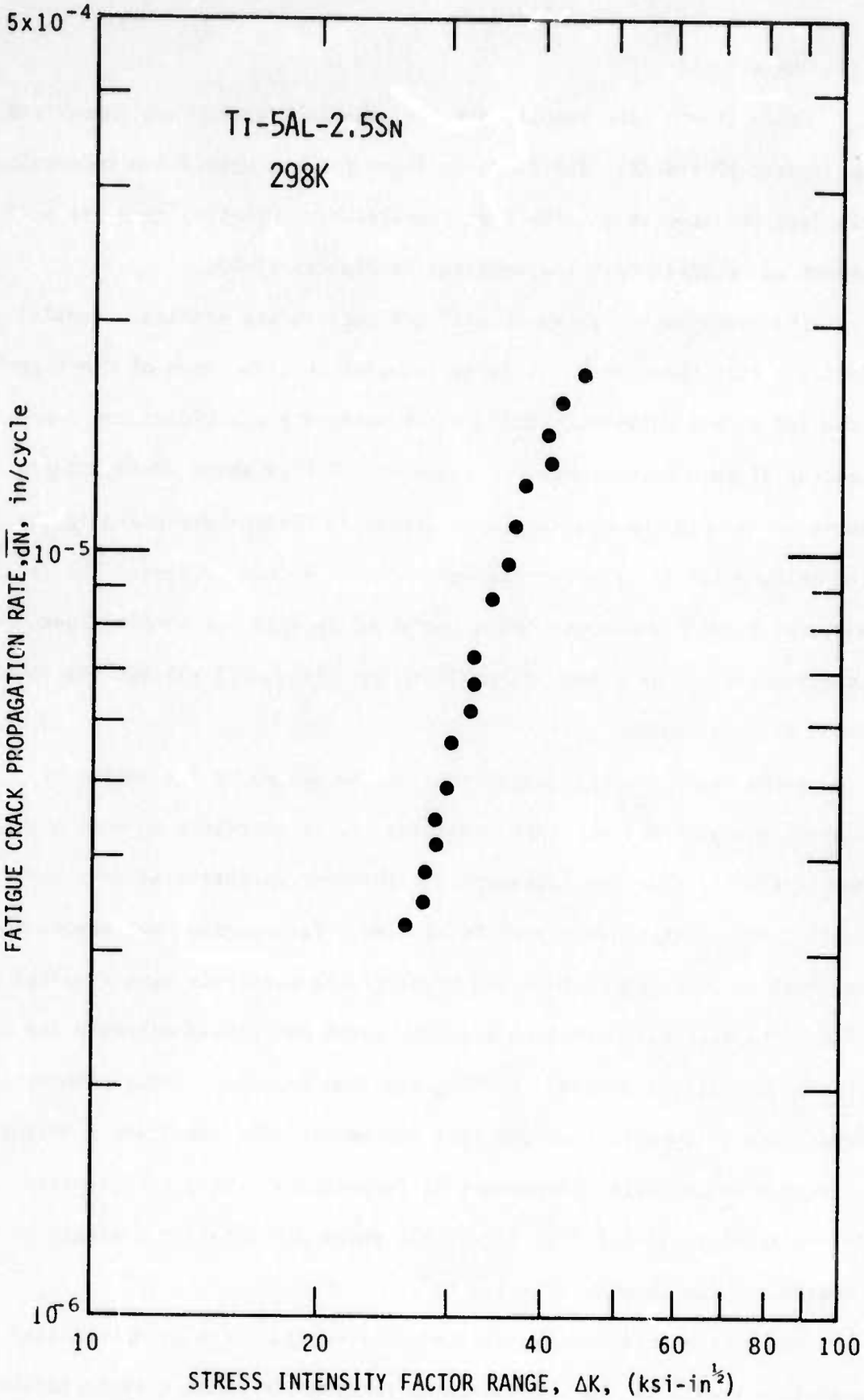

Figure 21. Crack Growth Rate of Ti-5Al-2.5Sn at 298 K.
(1 ksi $\sqrt{in}$ = 1.093 x 10^6 N/m^2 x $m^{1/2}$ and 1 in. = 2.54 cm.)

AISI 304 and 316

Crack growth rate results for the stainless steels are summarized in figures 22 and 23. The bands in these figures were drawn to envelop all data obtained at a given test temperature. Original data are presented at specific test temperatures in figures 24-29.

The crack growth rates of AISI 304 and 316 are similar. Results indicate that there is not a large temperature dependence of crack growth rate for either material. The scatter bands are coincident and independent of temperature over the range of ΔK from about 20-40 ksi$\sqrt{in}$. Above 40 ksi$\sqrt{in}$ the scatter bands appear to diverge depending on the temperature but it is uncertain whether this effect is real. The data above 40 ksi$\sqrt{in}$ represent tests performed on only one specimen per temperature. It is likely that additional tests will enlarge the scatter bands in this region.

Since small temperature effects may be masked by the degree of scatter among individual test specimens, it is revealing to test a single sample at more than one temperature. This was investigated in a test on AISI 304. Figure 30 shows the results. The specimen was precracked as usual at room temperature and crack growth rate data were obtained at 76 K. The test was halted at a midway point and liquid nitrogen was replaced with liquid helium. Testing was then continued under identical conditions of dynamic load and test frequency. The resulting a versus N curve was essentially independent of temperature. This is reflected in the results presented in Figure 31, where all data fit a single equation of the form $da/dN = C(\Delta K)^n$.

One of the interesting aspects of cryogenic tests on austenitic stainless steels is the phenomenon of martensitic phase transformations.

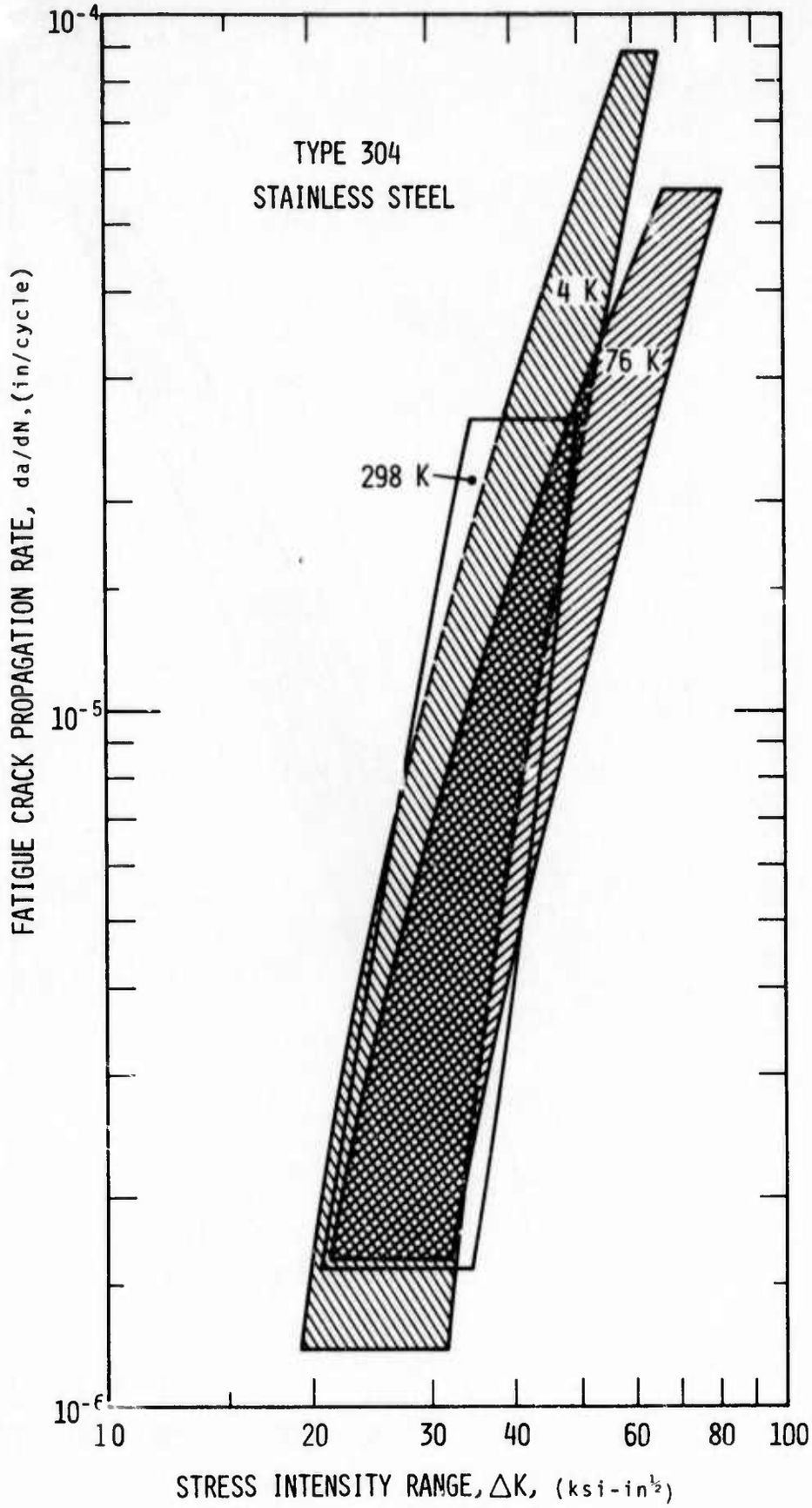

Figure 22. Crack Growth Rate Data of AISI 304 at 298 K, 76 K and 4 K. (1 ksi $\sqrt{in}$ =1.093 x 10^6 N/m^2 x $m^{1/2}$ and 1 in. =2.54 cm.)

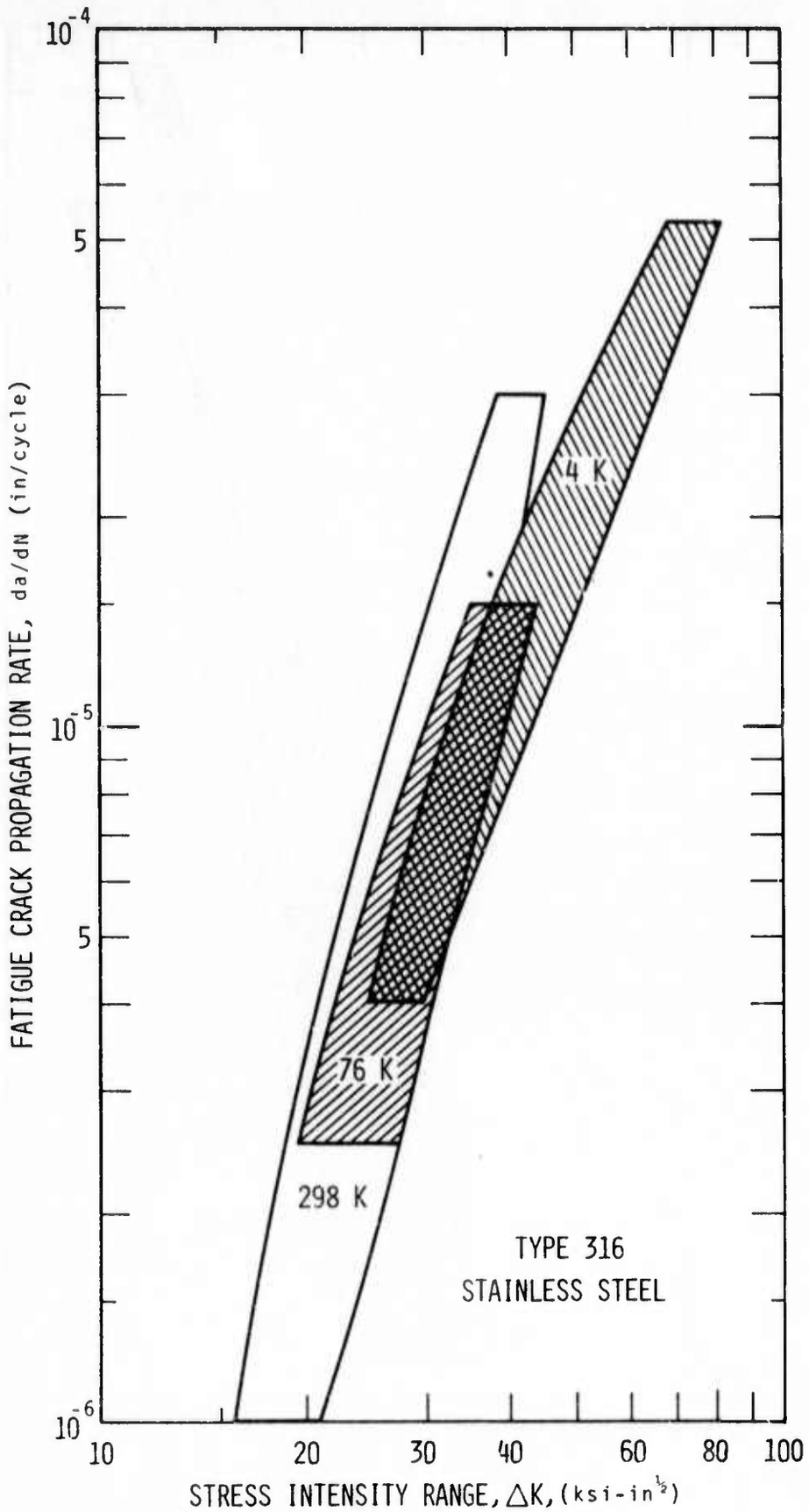

Figure 23. Crack Growth Rate Data of AISI 316 at 298 K, 76 K, and 4 K. (1 ksi $\sqrt{\text{in}}$=1.093 x 10^6 N/m^2 x m$^{1/2}$ and 1 in. =2.54 cm.)

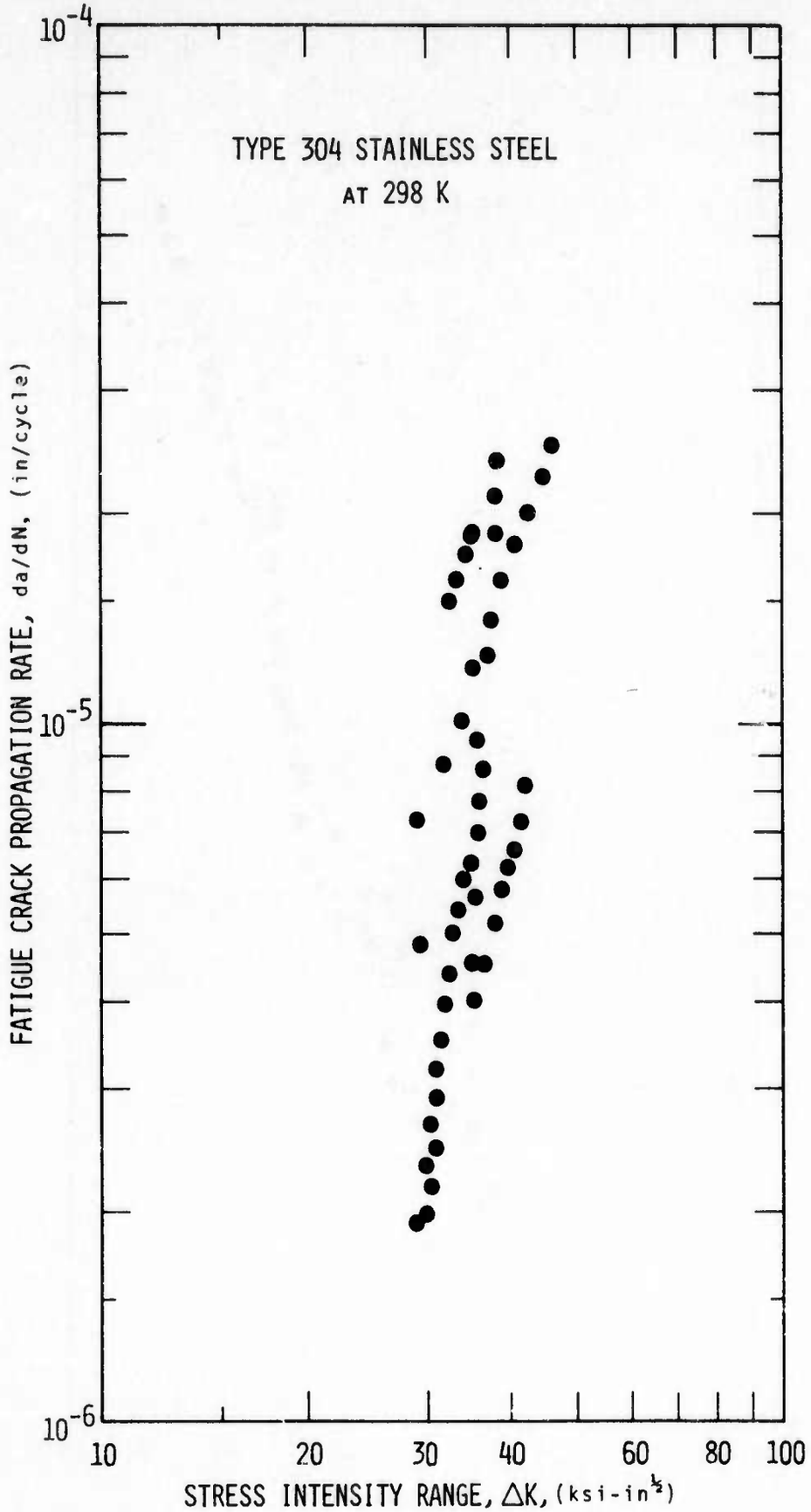

Figure 24. Crack Growth Rate Data of AISI 304 at 298 K.
(1 ksi $\sqrt{in}$=1.093 x 10^6 N/m^2 x m$^{1/2}$ and 1 in.=2.54 cm.)

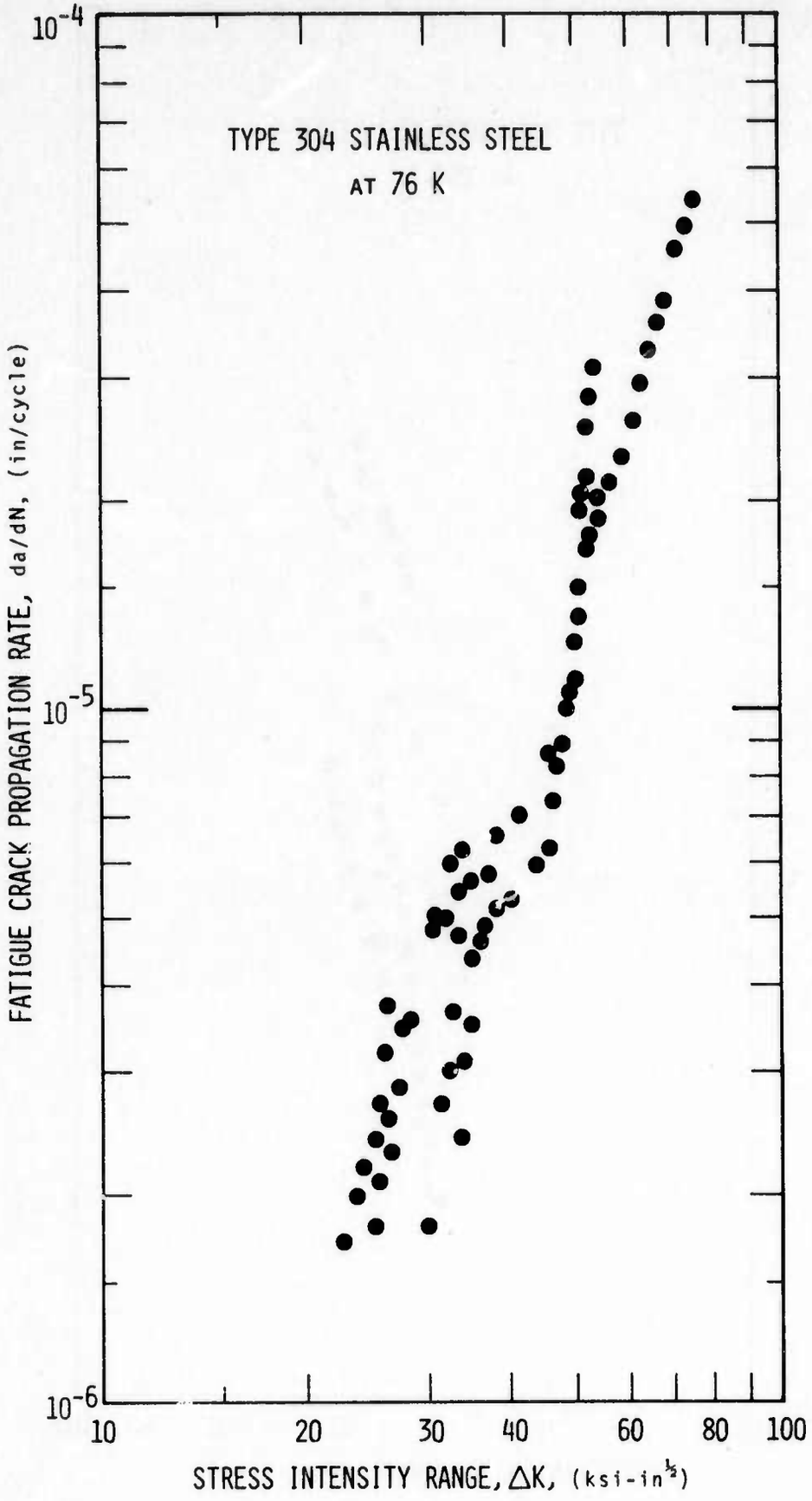

Figure 25. Crack Growth Rate Data of AISI 304 at 76 K.
(1 ksi $\sqrt{in}$=1.093 x 10^6 N/m^2 x $m^{1/2}$ and 1 in.=2.54 cm.)

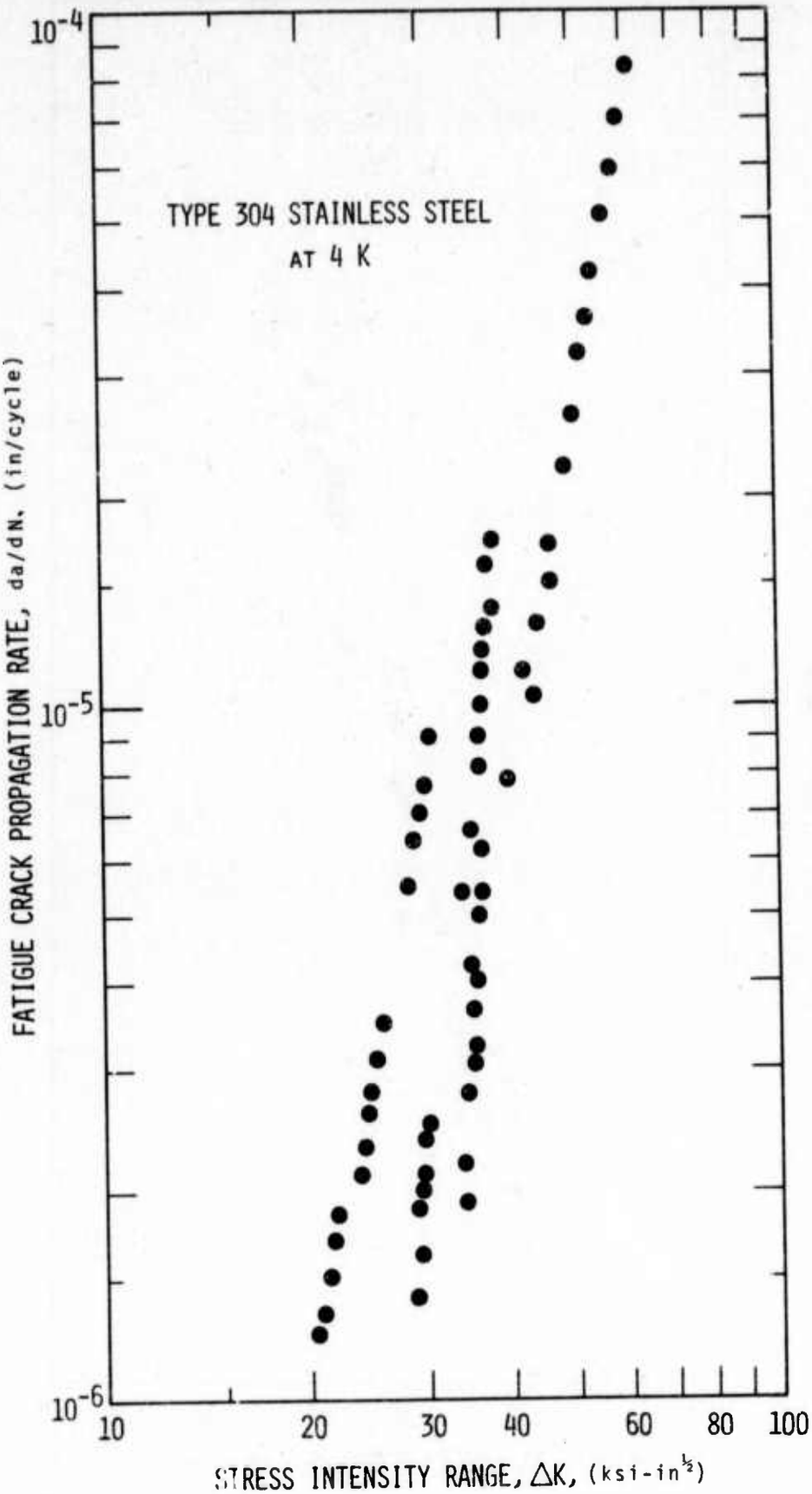

Figure 26. Crack Growth Rate Data of AISI 304 at 4 K.
(1 ksi $\sqrt{\text{in}}$=1.093 x 10^6 N/m^2 x m$^{1/2}$ and 1 in.=2.54 cm.)

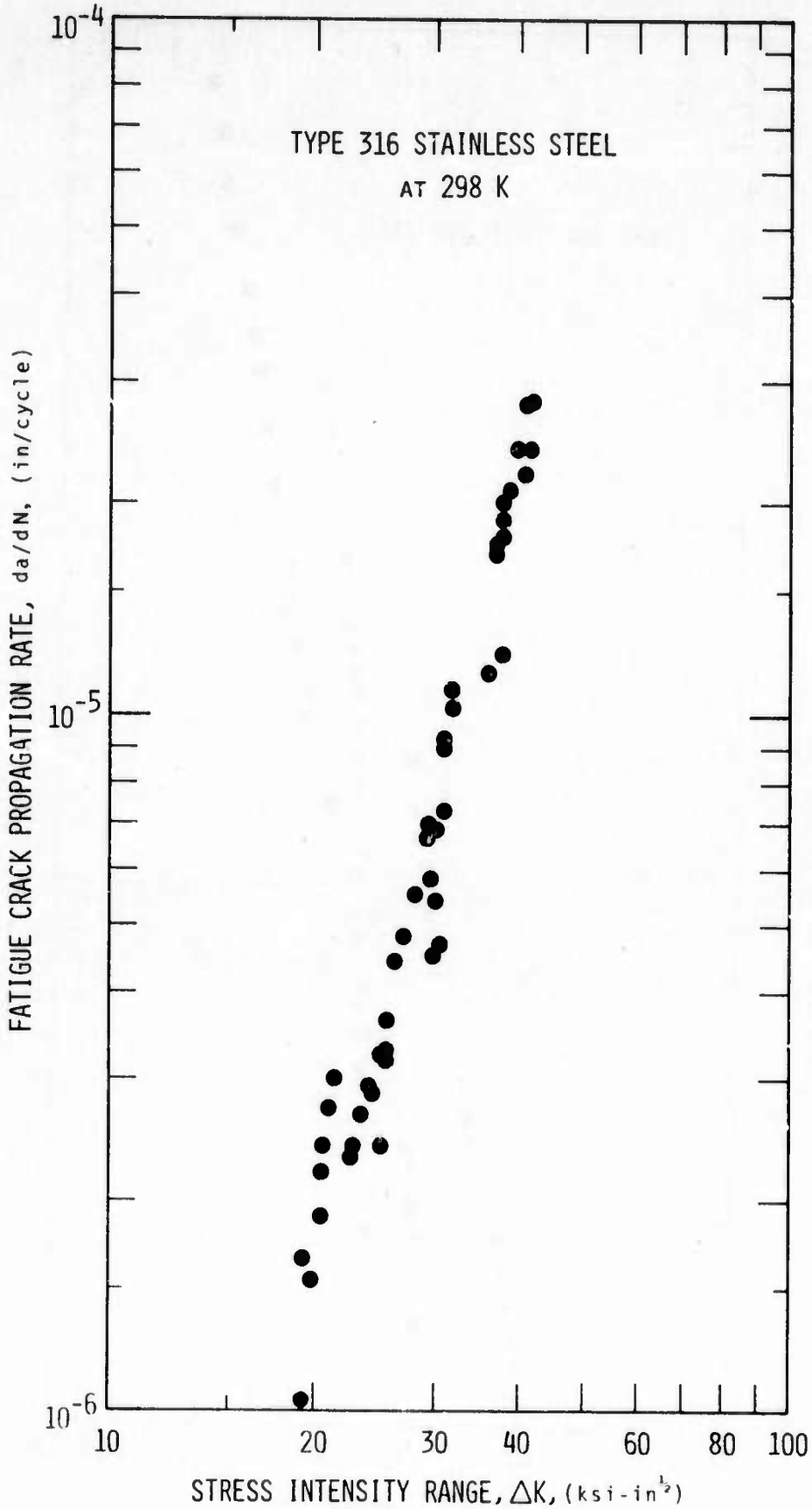

Figure 27. Crack Growth Rate Data of AISI 316 at 298 K.
(1 ksi $\sqrt{\text{in}}$=1.093 x 10^{6} N/m^{2} x $m^{1/2}$ and 1 in. = 2.54 cm.)

359<

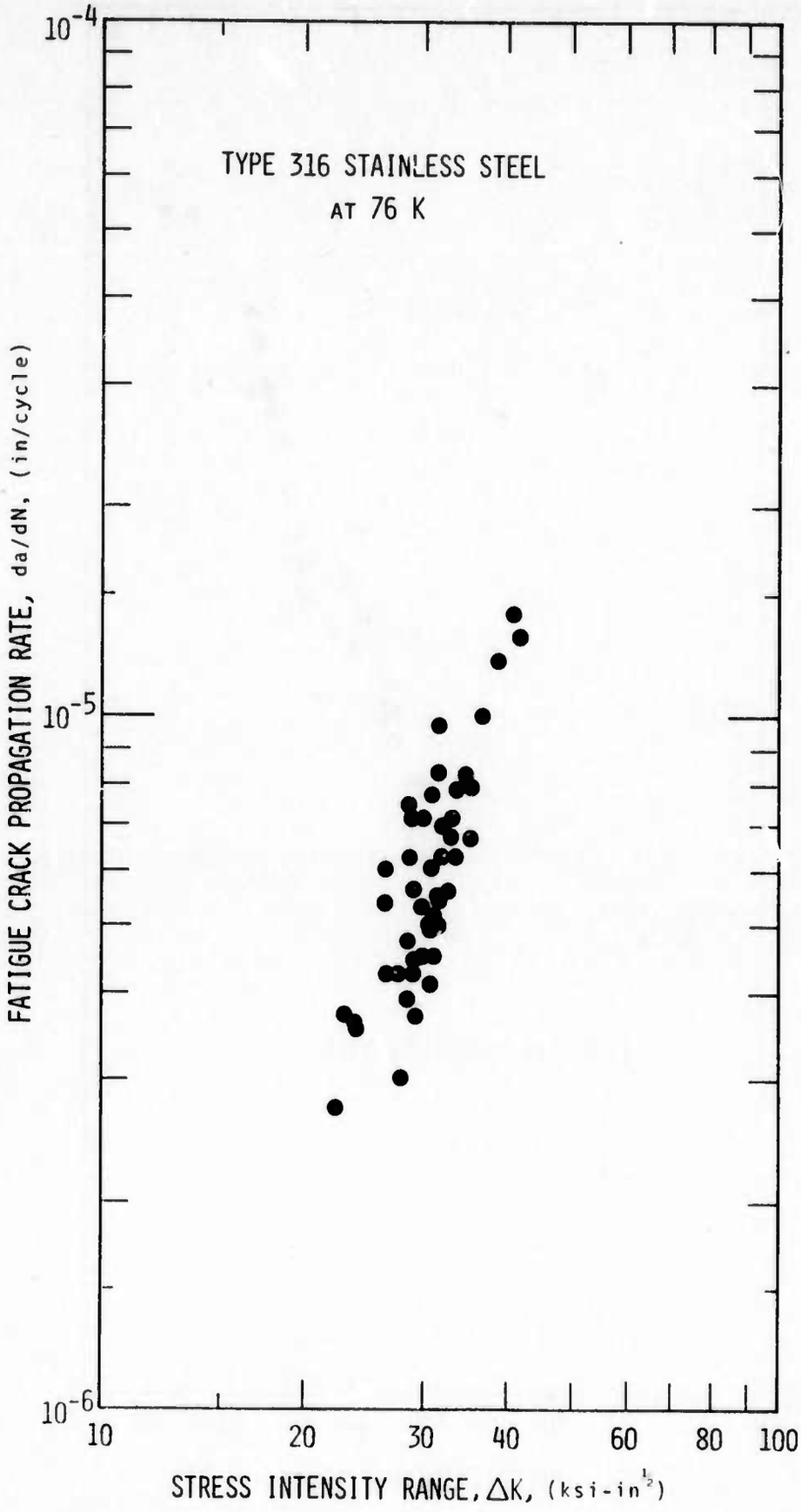

Figure 28. Crack Growth Rate Data of AISI 316 at 76 K.
(1 ksi $\sqrt{\text{in}}$=1.093 x 10^{3} N/m^{3} x $m^{1/2}$ and 1 in. = 2.54 cm.)

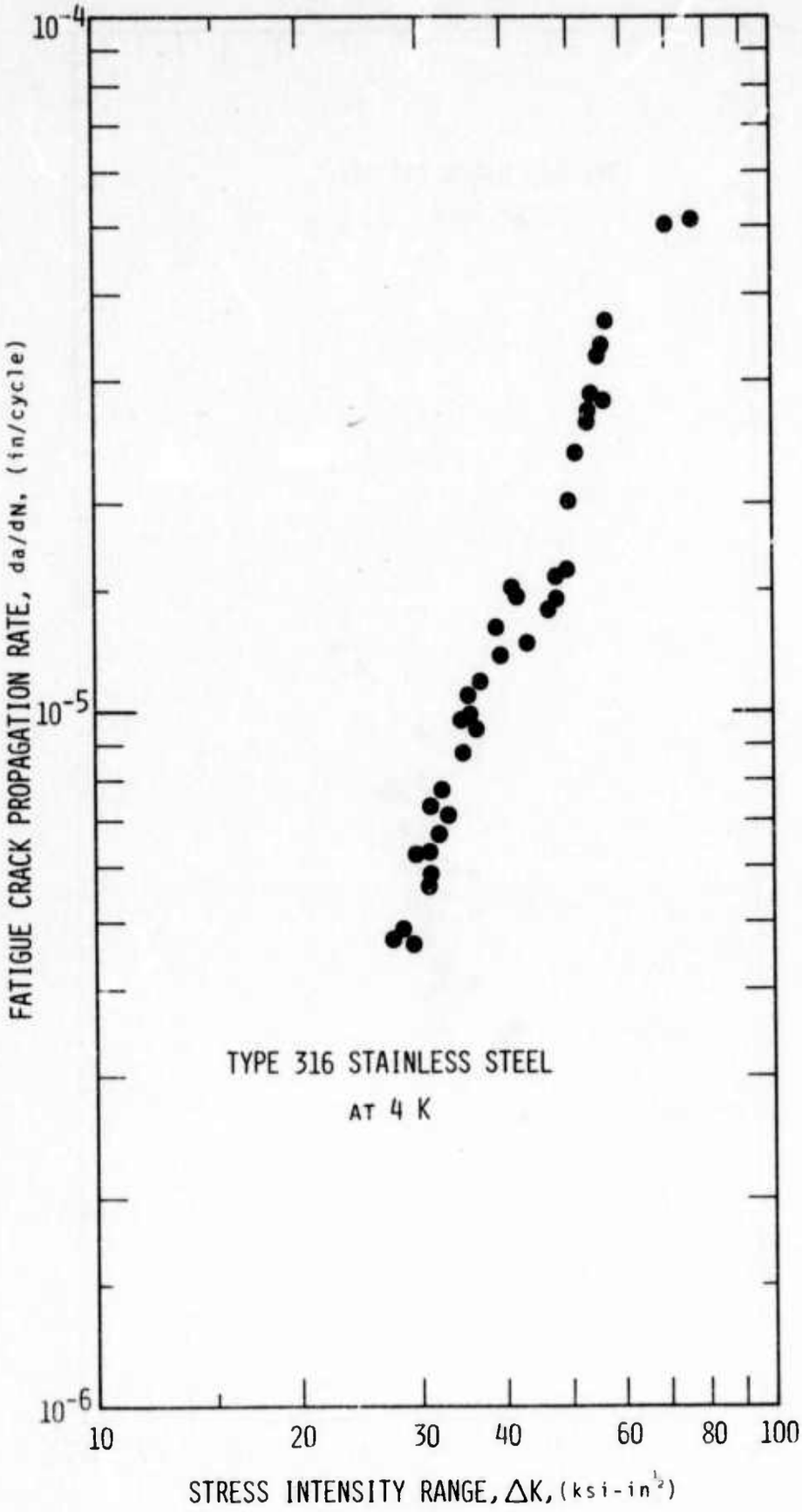

Figure 29. Crack Growth Rate Data of AISI 316 at 4 K.
(1 ksi $\sqrt{\text{in}}$=1.093 x 10^{6} N/$m^{3/2}$ x $m^{1/2}$ and 1 in. = 2.54 cm.)

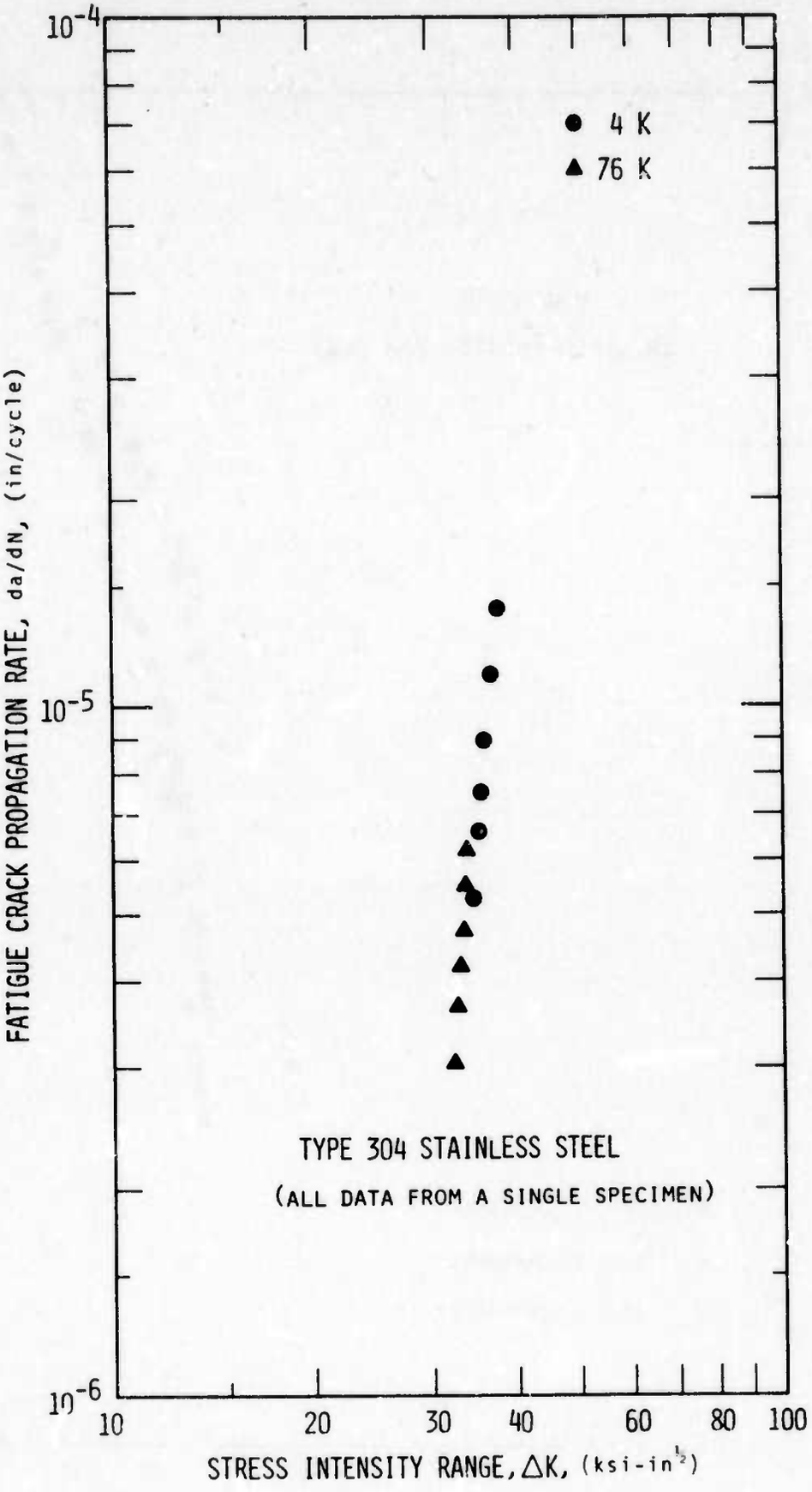

Figure 30. Temperature Independence of Crack Growth Rate of AISI 304 (1 ksi $\sqrt{in}$=1.093 x 10^6 N/m^2 x $m^{1/2}$ and 1 in. =2.54 cm.)

362<

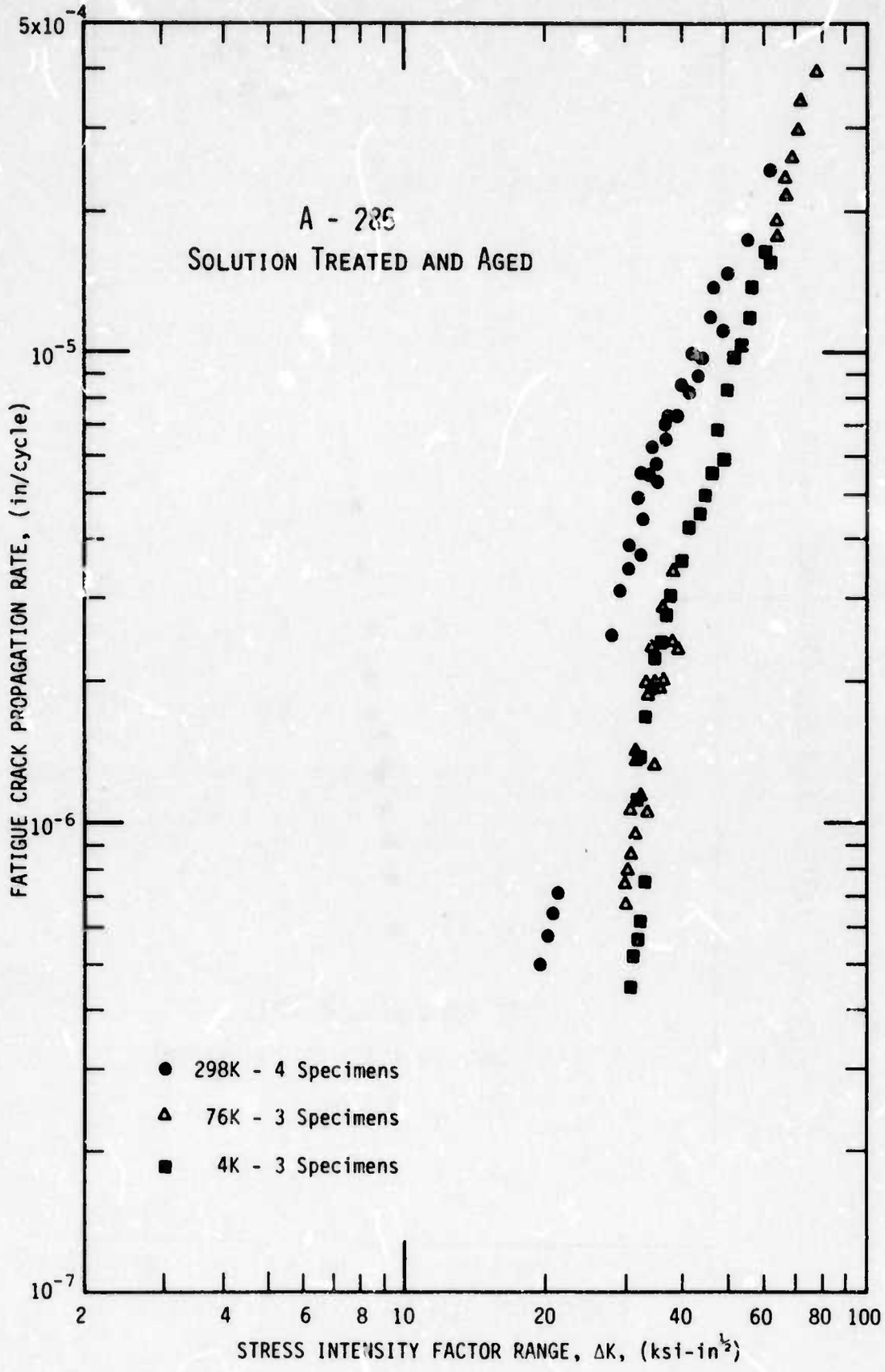

Figure 31. Crack Growth Rate Data of A-286 at 298, 76, and 4K. (1 ksi $\sqrt{in.}$ = 1.093 x 10^6 N/m^2 x $m^{1/2}$ and 1 in. = 2.54 cm).

An austenite-to-martensite transformation occurs as a result of plastic deformation at low temperatures[22]. It is clear that martensite formed during fatigue tests. This was most obvious in the case of AISI 304 stainless steel tested at 4 K. Austenite is paramagnetic while martensite is ferromagnetic, allowing qualitative detection by a magnetic device. These magnetic measurements indicate appreciable martensitic transformation occurred when the stress intensity had reached approximately 50 ksi$\sqrt{in}$ at 4 K.

A-286

The crack growth rate results for alloy A-286 are presented in figure 31. This was the only alloy tested which exhibited a temperature dependence of crack growth rate.

Figure 31 shows that the crack growth rate is significantly lower at cryogenic temperatures as compared to room temperature. However, comparison of data obtained at 76 K and 4 K show no significant difference.

Fracture Toughness

Ti-6Al-4V

One inch thick specimens of Ti-6Al-4V amply satisfied the ASTM thickness criterion (Table 10). Valid plane strain fracture toughness tests have been performed at 298 K, 76 K, and 4 K.

A typical load-displacement record for a specimen at 4 K is shown in figure 32. There is a slight departure from linearity during the last 5% of the curve. The specimen failed spontaneously from the maximum load.

Table 10. Dimensional Criteria for Valid K_{IC}: Titanium Alloys

Alloy	Temp. (K)	a (in)	B (in)	0.2% Yield Strength (psi)	K_{IC} (ksi$\sqrt{in}$)	$2.5\left(\frac{K_{IC}}{ys}\right)^2$ (in)
Ti-6Al-4V	298	1.12	1.0	145,200	43.65	0.22
	76	1.12	1.0	237,325	35.32	0.06
	4	1.12	1.0	278,300	35.03	0.04
Ti-5Al-2.5Sn	298	1.62	1.5	121,625	66.9	0.76

Notes: 1 in = 2.54 cm

1 ksi = 0.689×10^7 Nm^{-2}

1 ksi $\sqrt{in}$ = 1.093×10^6 $\frac{N}{m^2} - m^{1/2}$

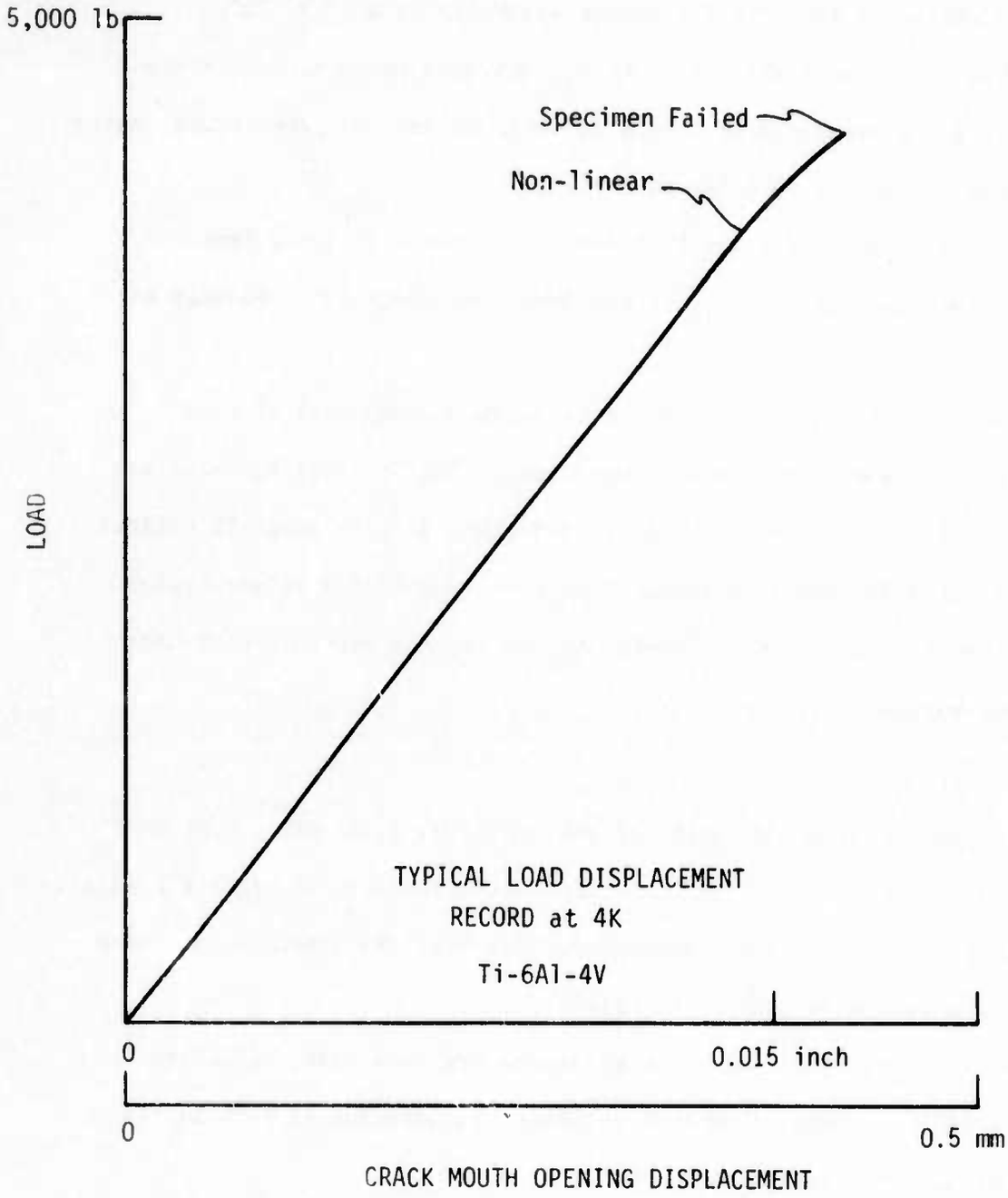

Figure 32. Typical Load-Displacement Record at 4 K for Ti-6Al-4V (1 lb. =0.454 kg)

The room temperature tests revealed a more noticeable pop-in behavior prior to catastrophic crack propagation. The load-displacement records at 298 K resembled the Type III record described in ASTM E-399[5].

Table 11 presents the values of K_{IC} obtained at each temperature. The results are presented in figure 33 as a function of temperature, along with results obtained by other authors.

There is a 20% reduction in fracture toughness in going from 298 K to 4 K. This reduction in K_{IC} is monotonic and there is no anomaly at 4 K.

Figure 34 illustrates the fracture surface appearance of four specimens -- one tested at each temperature. The fracture surfaces are predominantly flat. Room temperature specimens display about 2% oblique fracture; this decreases to about 1% at 4 K. The flat fracture region is relatively rough at room temperature and becomes smoother with decreasing temperature.

Ti-5Al-2.5Sn

Cryogenic fracture toughness tests on Ti-5Al-2.5Sn alloy specimens are currently in progress, but low temperature results are not yet available. Preliminary results at room temperature show that the fracture toughness of this alloy exceeds that of Ti-6Al-4V.

The 1.5 inch (3.81 cm) thick specimens are more than sufficient to assure valid K_{IC} tests. The ASTM thickness requirement is 0.76 inches (1.93 cm) as indicated in Table 10.

Two tests at room temperature have yielded K_{IC} of 62.15 ksi$\sqrt{in}$ and 71.72 ksi$\sqrt{in}$. The average K_{IC} is 66.9 ksi$\sqrt{in}$. These results are in good agreement with the values reported by Witzell[39] for a similar Ti-5Al-2.5Sn alloy at 298 K.

Table 11. Fracture Toughness of Ti-6Al-4V

Specimen No.	Test Temp.	K_{IC}, ksi$\sqrt{in}$ ‡
A 12	298 K	43.09
A 15	"	42.71
A 16	"	45.00 †
A 18	"	43.80
A 13	195 K	38.45*
A 14	"	36.21*
A 6	77 K	34.33
A 7	"	34.64
A 8	"	37.13
A 9	"	35.19
A 10	4 K	35.51
A 11	"	34.79
A 21	"	34.80

† Fatigue stress intensity exceeded 0.6 K_{IC}

* Invalid, irregular crack front

‡ 1 ksi$\sqrt{in}$ = 1.093×10^6 Nm^{-2} $m^{1/2}$

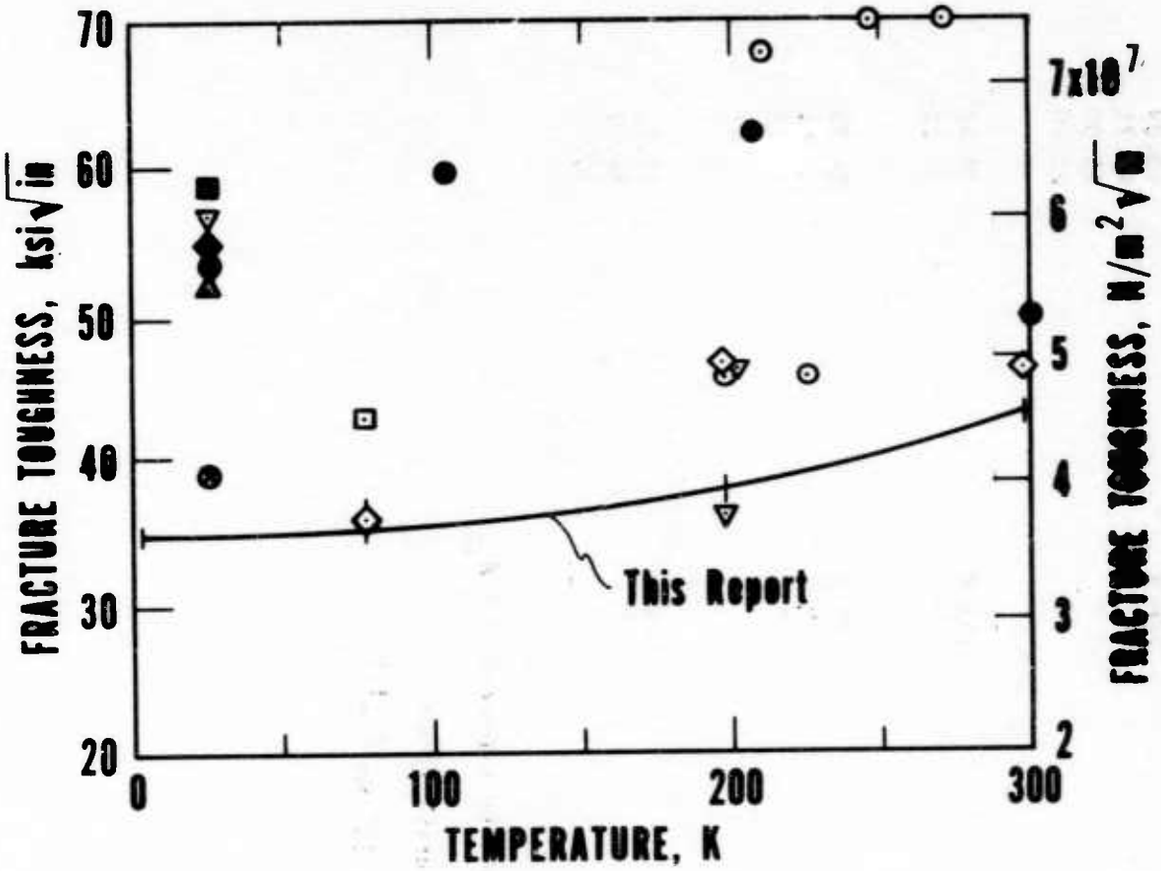

Figure 33. Temperature Dependence of K_{IC} for Ti-6Al-4V. Each Type of Symbol Represents a Particular Investigator: Reference 31 (■), Reference 32 (▽), Reference 33 (◆), Reference 34 (△), Reference 35 (⊗), Reference 36 (⊡), Reference 37 (◇), Reference 38 (○), Reference 39 (●).

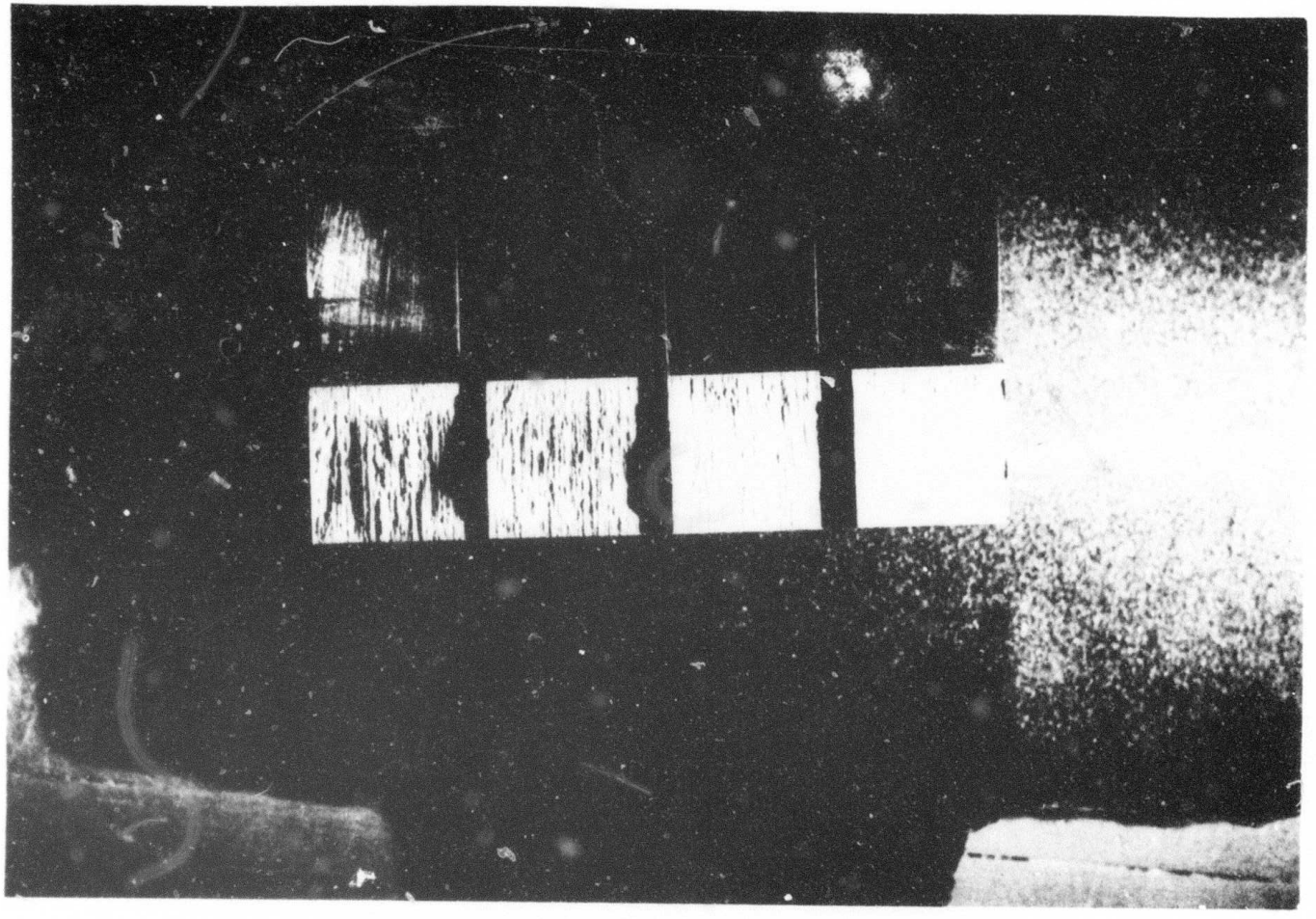

Figure 34. Fracture Surface Appearance of Ti-6Al-4V Specimens

The load-displacement records of Ti-5Al-2.5Sn fracture specimens were similar qualitatively to those of Ti-6Al-4V specimens at 298 K. Slight non-linearity occurred during the final 5% of deflection. A single pop-in occurred prior to catastrophic crack extension.

The fracture surface appearance of a Ti-5Al-2.5Sn specimen is presented in figure 35. The region of oblique fracture (shear lip) amounts to no more than 3% of specimen thickness.

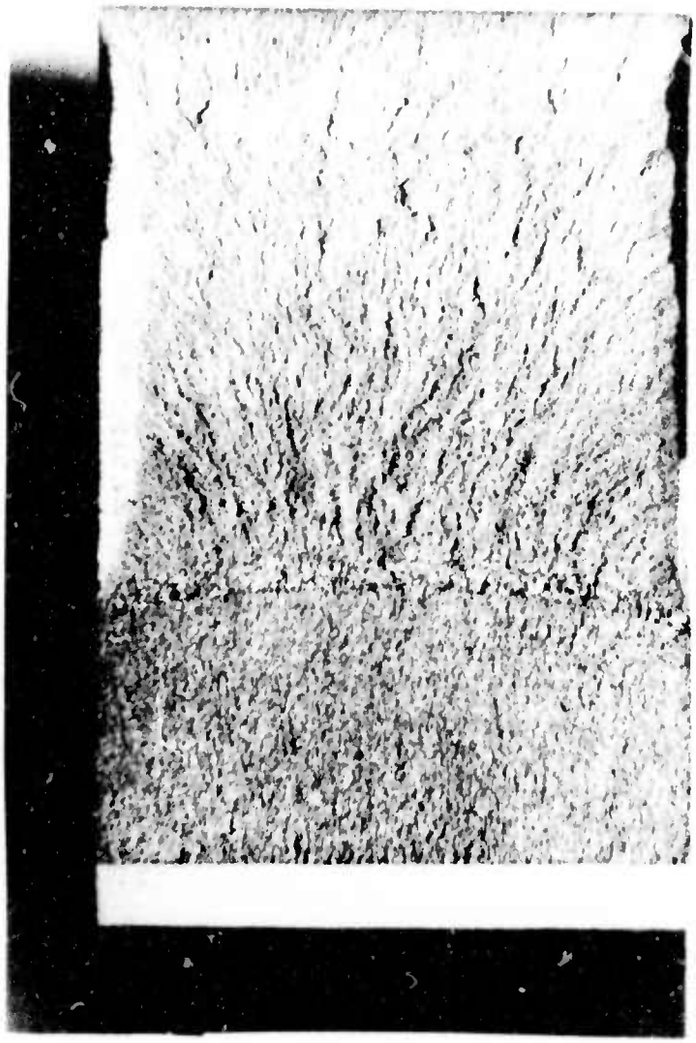

Figure 55. Fracture Surface Appearance of Ti-5Al-2.5Sn at 298 K.

AISI 304 and 316

As was stated in the section on experimental procedure, the J integral is determined from the load displacement curve. Typical curves for AISI 304 are shown in figures 36-38; curves for AISI 316 are shown in figures 39-41. As with the tensile tests, discontinuous yielding with both steels was observed at 4 K. Although the phenomenon is rate dependent, it does exist even to a crosshead rate of 0.005 inch per minute. A rate of 0.02 inch was maintained at 4 K for the curves shown. For the most part, the rate was held steadily throughout each test except at 4 K. At this temperature, the rate increased rapidly with each drop in load but could be maintained steadily on the rise in load. The arrow marked "P_c" on each curve indicates the load at which the crack begins to extend. This particular load is derived from the critical value of the J-integral; derivation of the critical load will be discussed later. The load P_c shows a temperature dependence with both steels: as the temperature is lowered, the critical load level increases from 298 to 76 K and then decreases slightly from 76 to 4 K.

Figure 42 is a plot of the J integral for AISI 304 as a function of the crack extension. Values of J_{IC} are derived from the intersection of the J versus Δa lines with the vertical stretch zone lines. The zone lines are plotted at an average value of the stretch zones measured from each specimen. This derivation of J_{IC} is somewhat of a departure from the method of Landes and Begley[16] who use a "flow" curve instead of a zone line. They show that J values for very slightly extended cracks fall on the flow curve. However, data of this report, such as the lower

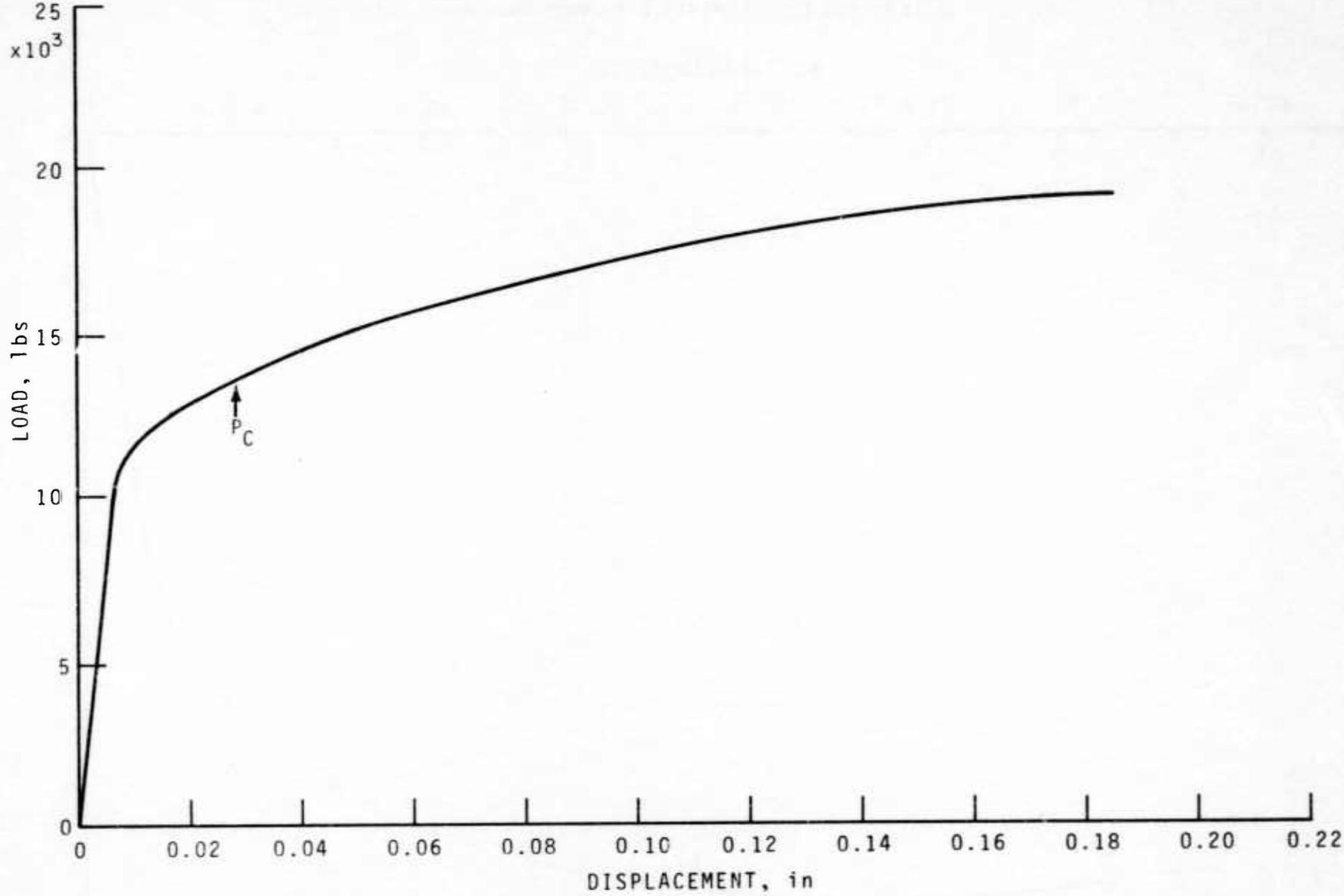

Figure 36. Load-Displacement Curve of AISI 304 at 298 K
(1 lb. =0.454 kg. and 1 in. =2.54cm.)

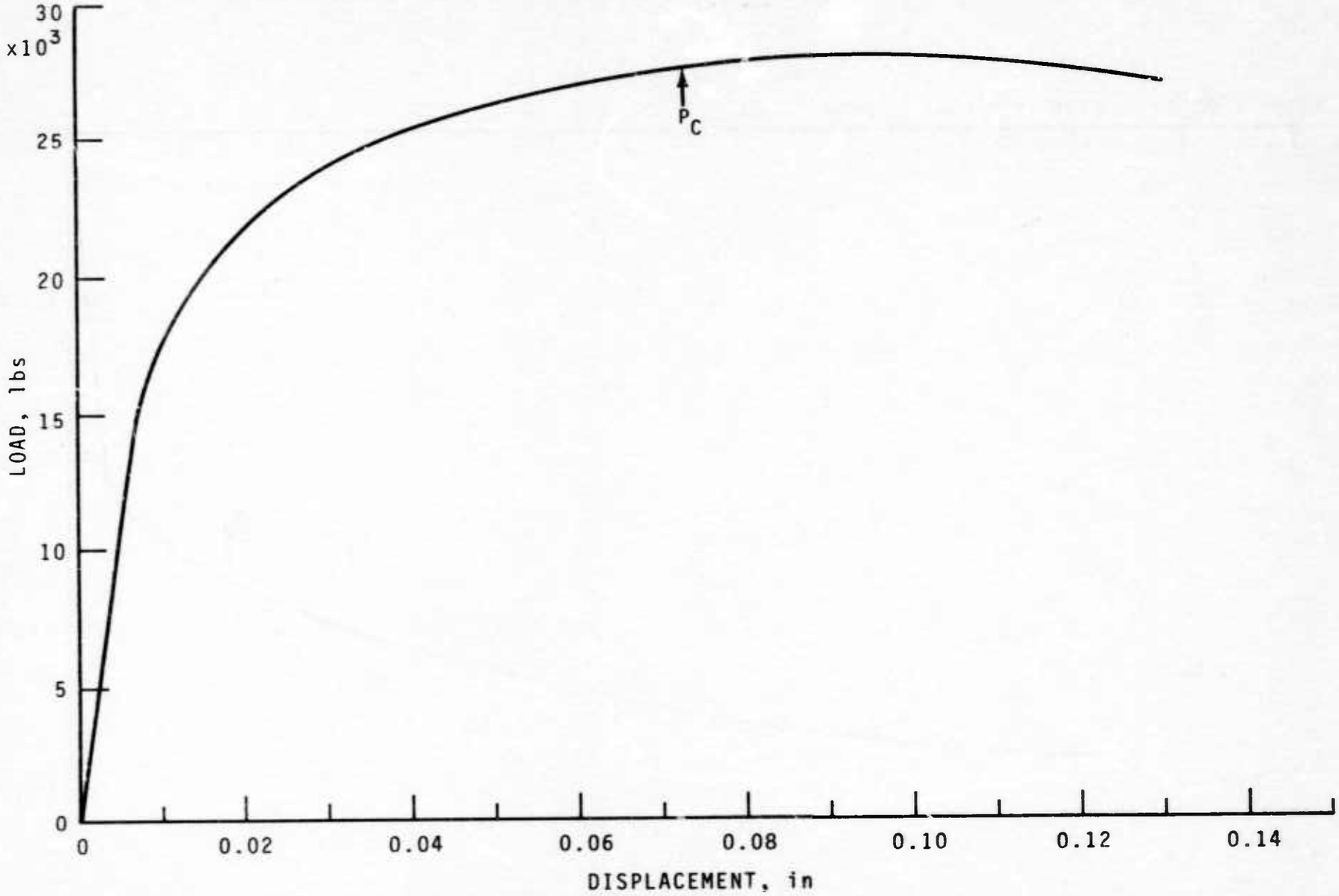

Figure 37. Load-Displacement Curve of AISI 304 at 76 K
(1 lb. =0.454 kg. and 1 in. =2.54 cm.)

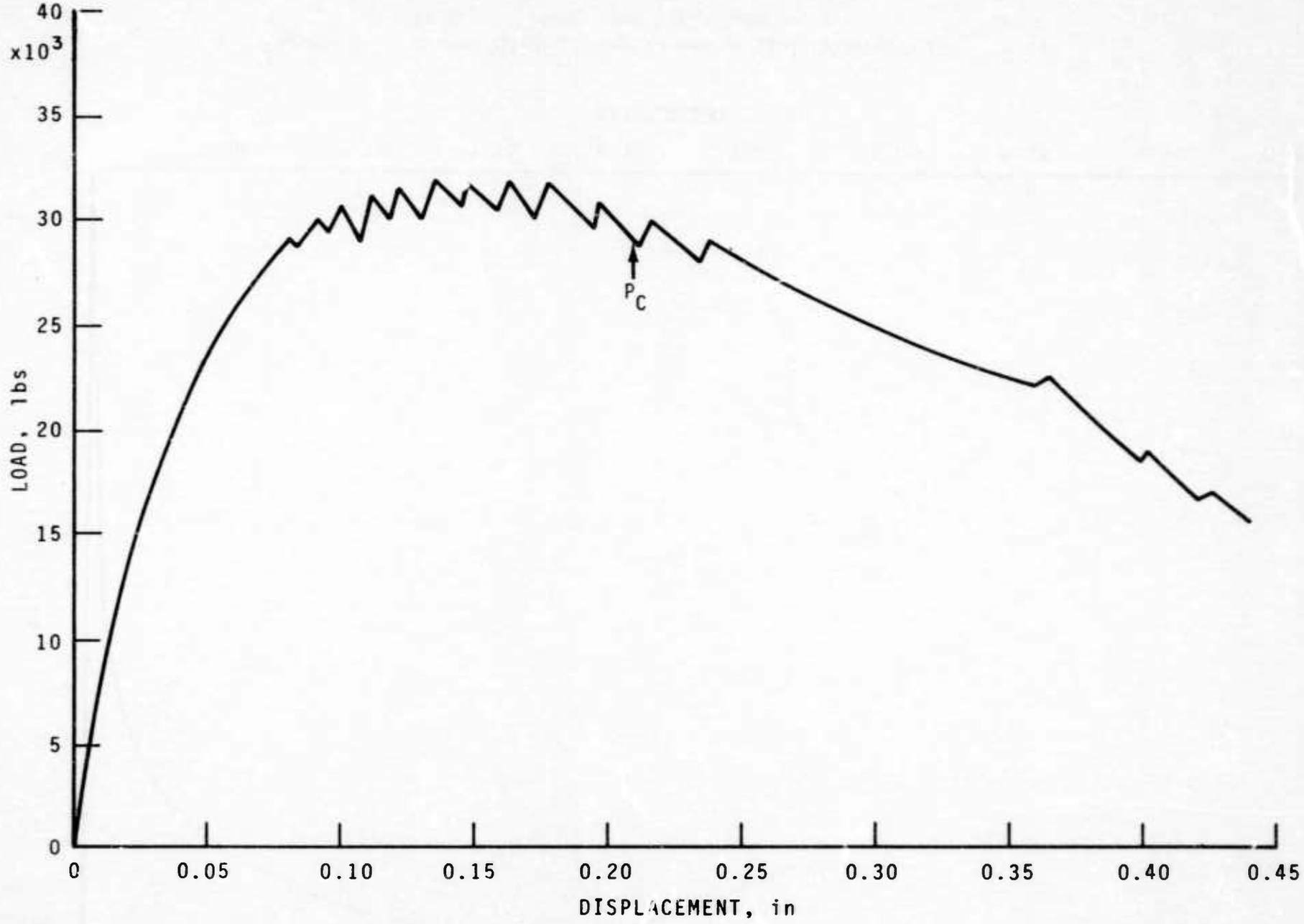

Figure 38. Load-Displacement Curve of AISI 304 at 4 K
(1 lb. =0.454 kg. and 1 in. =2.54 cm.)

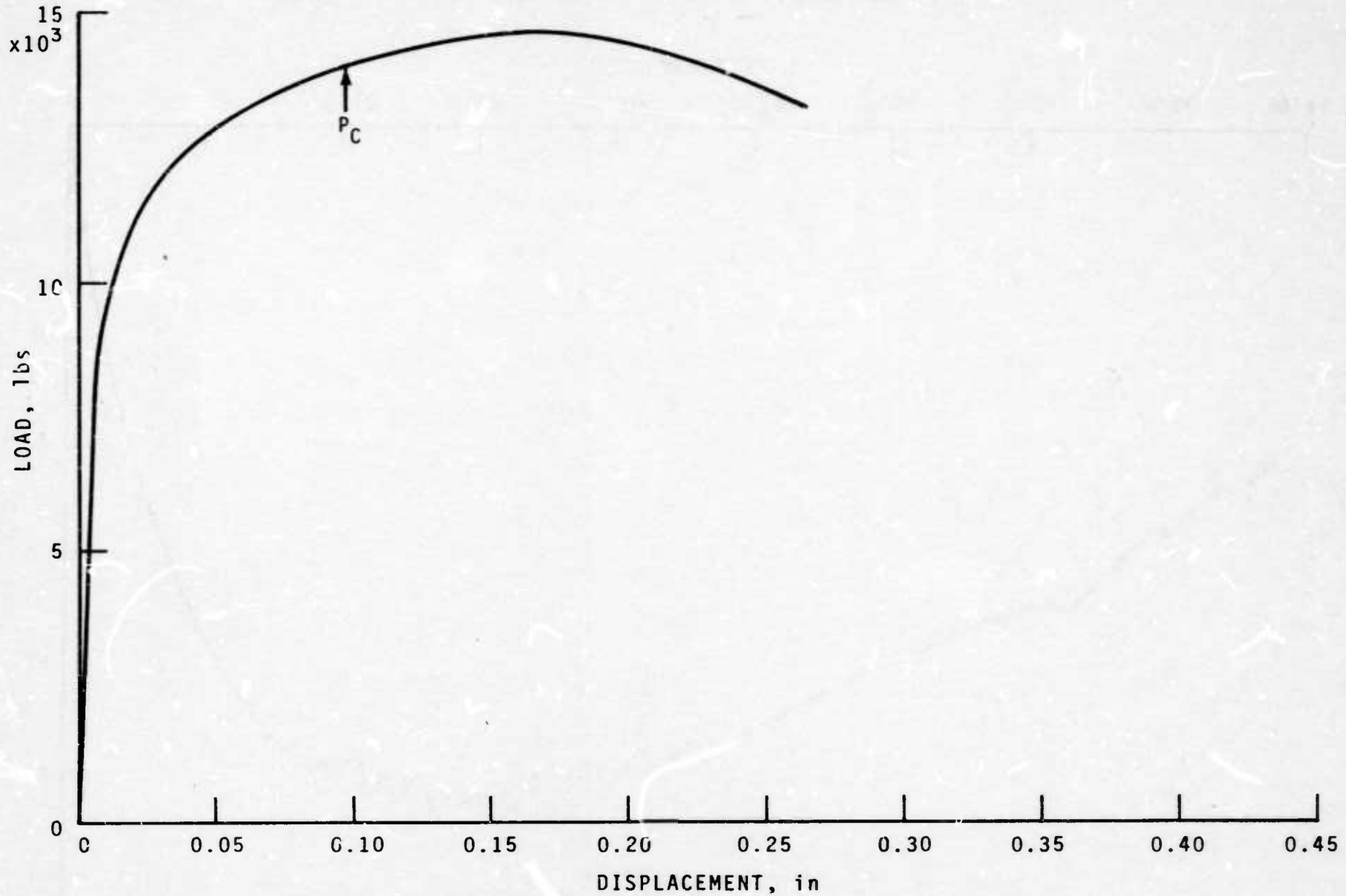

Figure 39. Load-Displacement Curve of AISI 316 at 298 K
(1 lb. =0.454 kg. and 1 in. =2.54 cm.)

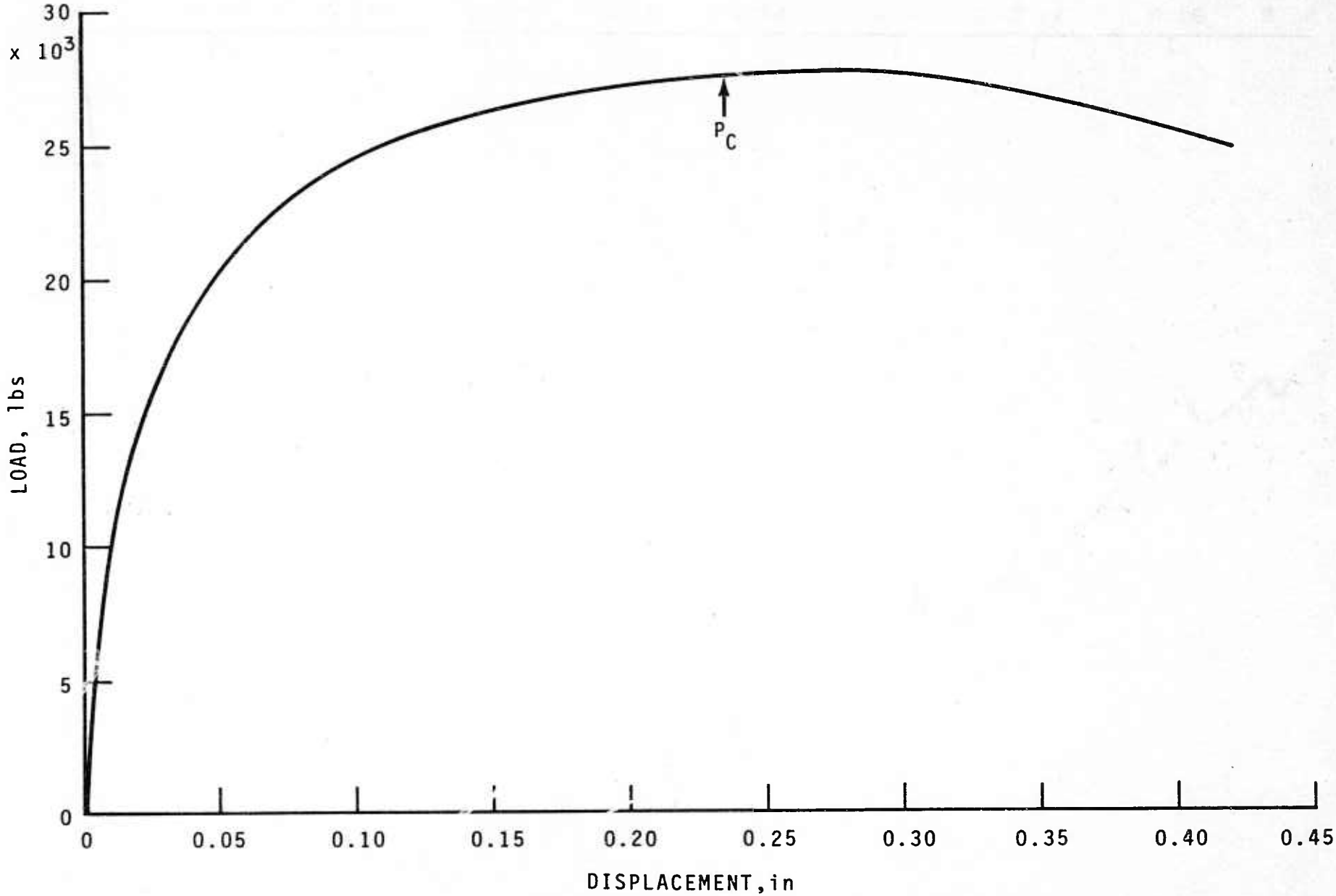

Figure 40. Load-Displacement Curve of AISI 316 at 76 K
(1 lb. =0.454 kg. and 1 in. =2.54 cm.)

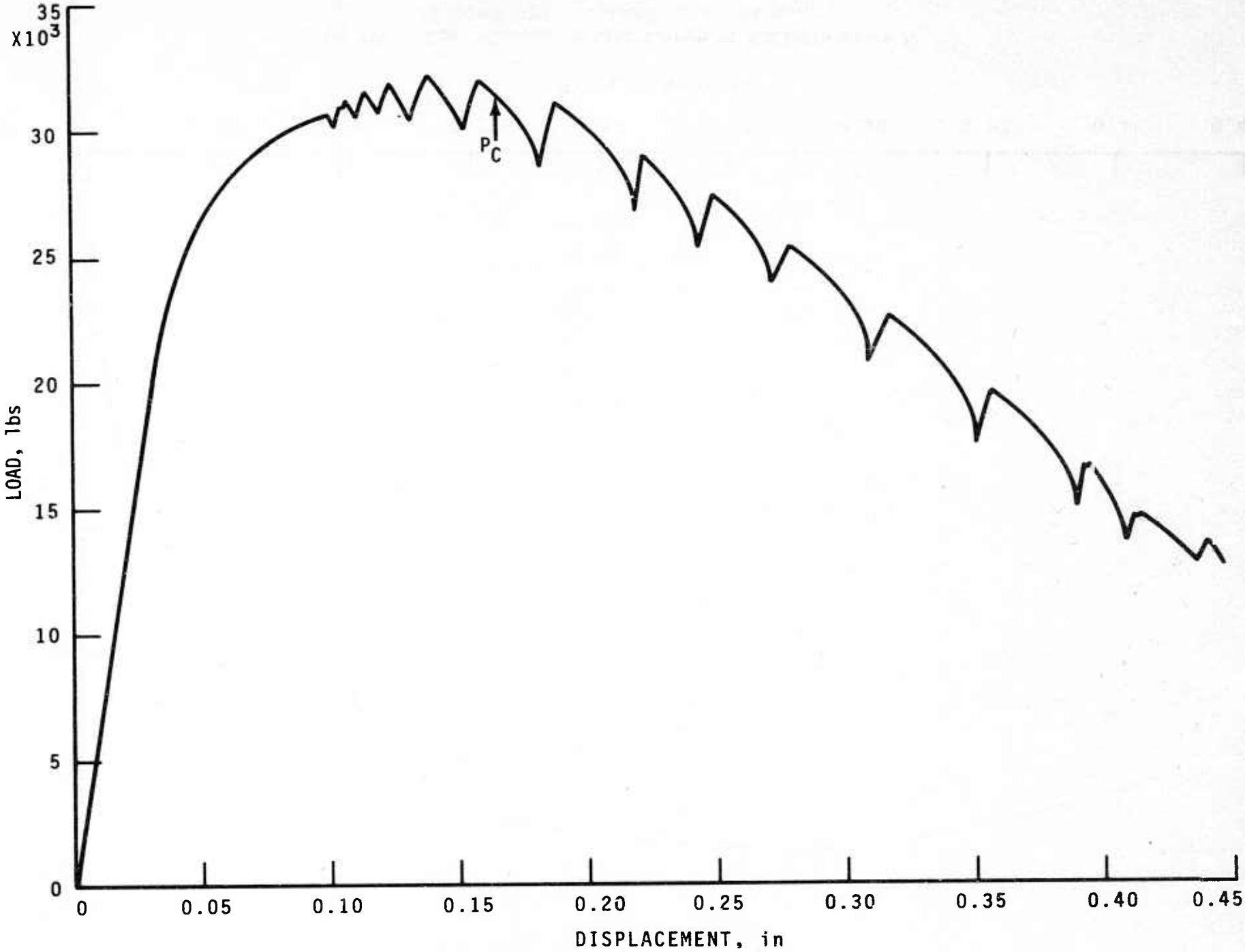

Figure 41. Load-Disp;acement Curve of AISI 316 at 4 K
(1 lb. =0.454 kg. and 1 in. =2.54 cm.)

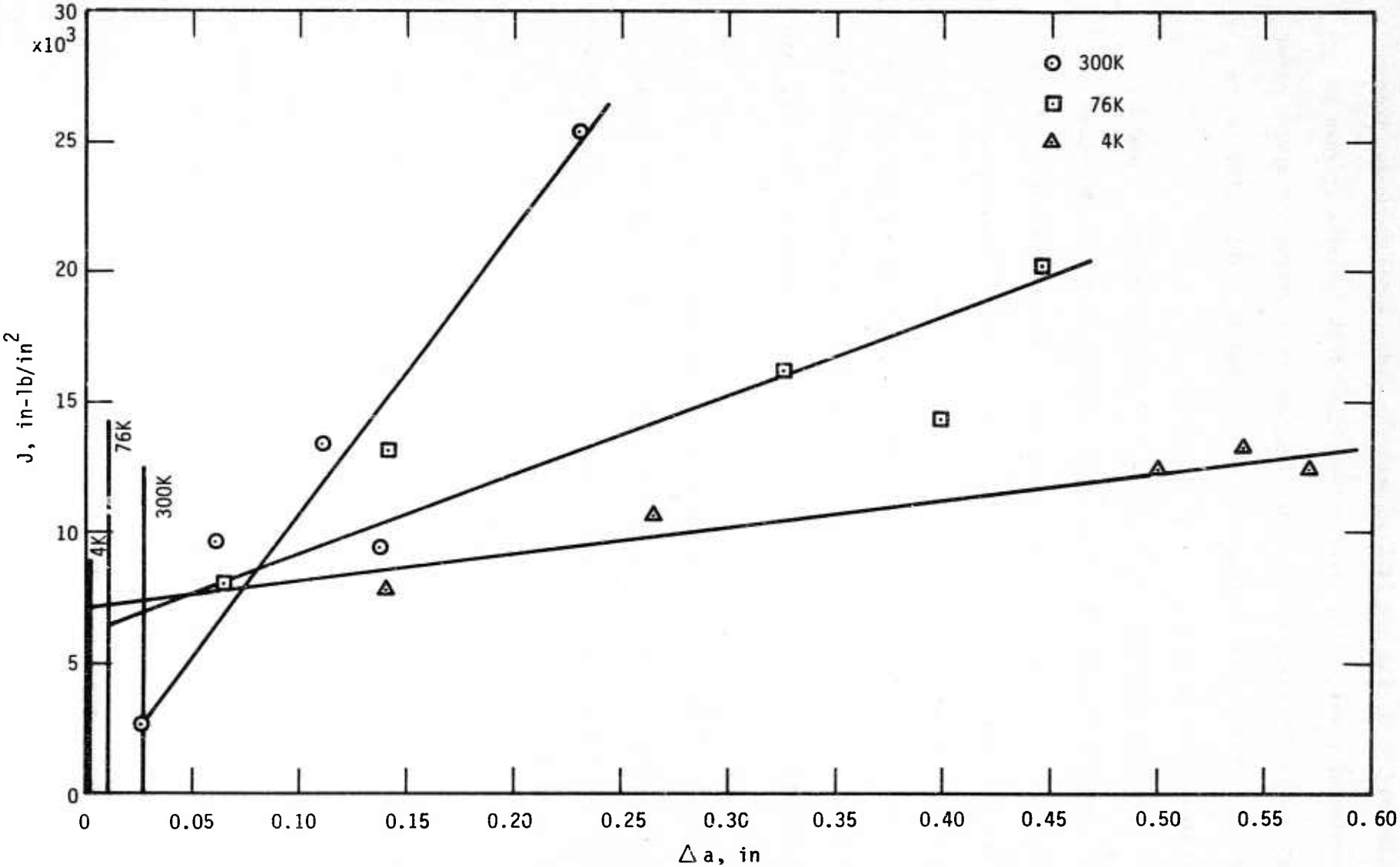

Figure 42. The J-Integral as a Function of Crack Extension for AISI 304 at 298 K, 76 K and 4 K (1 in. -lb./in.^{2} = 1.75 x 10^2 m-N/m^2 and 1 in. = 2.54 cm.)

point at 298 K, did not fall on such a curve. The J value for this particular point at the stretch zone line is of interest because it represents the quantity of energy required to initiate the crack, after having "stretched" the material a maximum amount. This point is the critical value of J, J_{IC}.

Fracture surfaces for increasing extensions at 298, 76 and 4 K are shown in figures 43 and 44. The depicted loads are the values at which the particular tests were terminated. Notice the nature of the crack profiles which developed quite differently at low temperatures, particularly 4 K.

Results of the tests to determine the J integral of AISI 304 are given in table 12. Three different extensions, as defined under "Experimental Procedures", are tabulated. The plot of figure 42 uses Δa, true average.

Each of the critical values given can be considered to be a valid J_{IC} according to a tentative criterion proposed by Begley and Landes[7]. Their criterion, based on limited experimental results of a few materials, is the following:

$$a,\ B,\ b \geq \alpha\ \frac{J_{IC}}{\sigma_{flow}}\ ,$$

where α is between 25 and 50, σ_{flow} is the average of the yield and ultimate strengths, a is the crack length, B is the sample thickness, and b is the ligament or uncracked lengt In other words, for the critical value of J to actually be J_{IC}, the above ratio should be equal to or less than the particular dimensions. According to table 13,

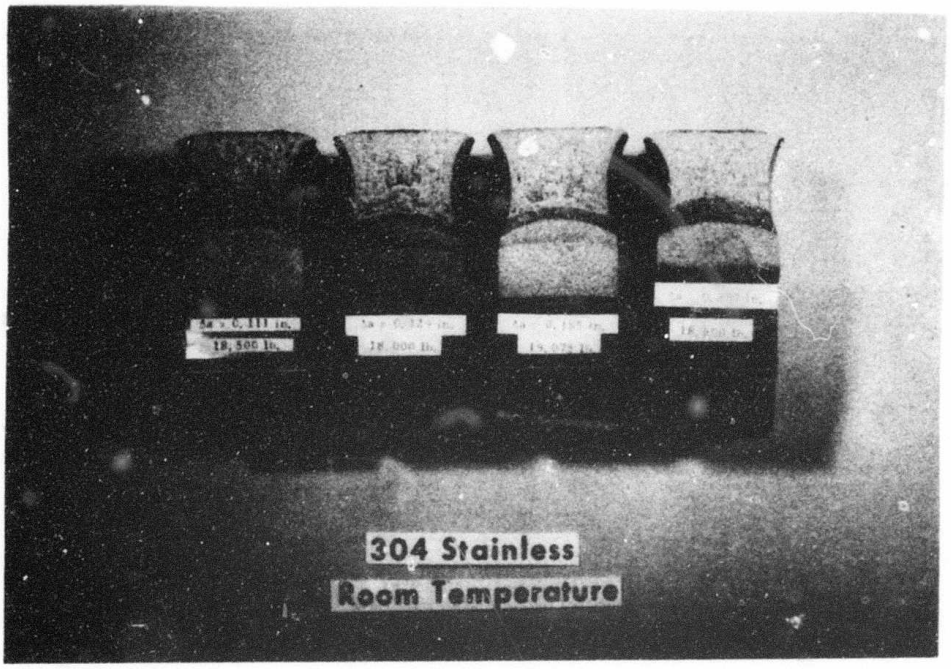

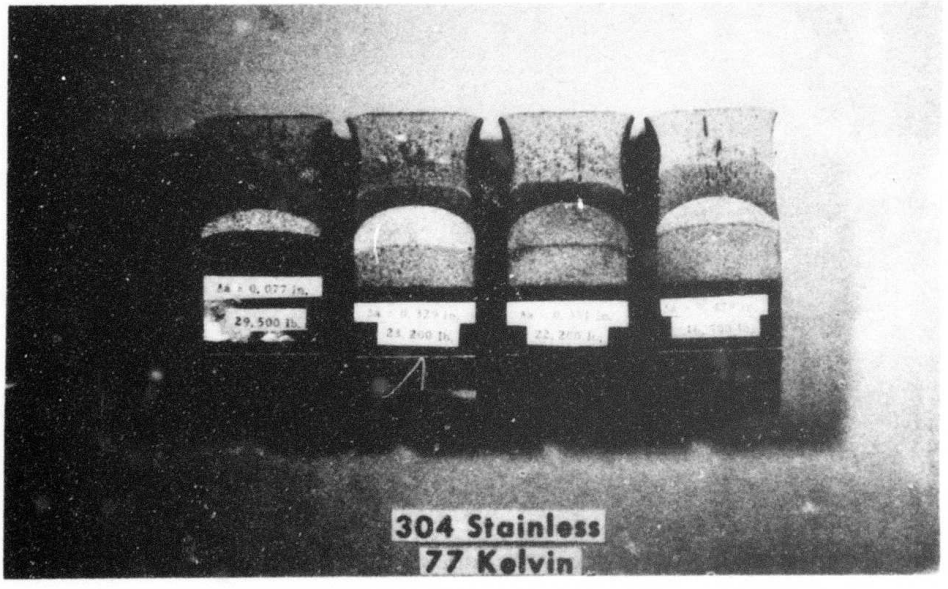

Figure 43. Fracture Surfaces of AISI 304 at 298 and 77 K.

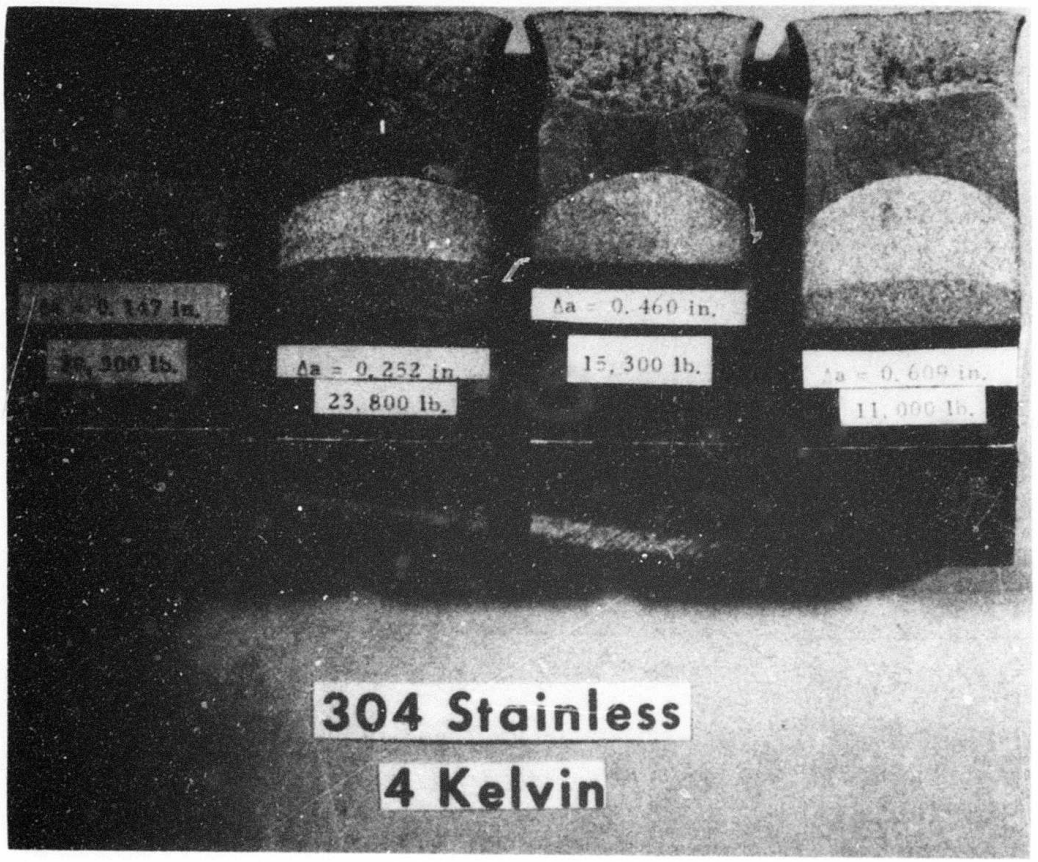

Figure 44. Fracture Surfaces of AISI 304 at 4 K

Table 12. Results for J Integral of AISI 304

Temp. (K)	Spec.	Cr hd. Rate, in/min	J ($\frac{in\text{-}lb}{in^2}$)	Δa center (in)	Δa out/cent (in)	Δa true av (in)	Stretch Zone (in)	J_{IC} ($\frac{in\text{-}lb}{in^2}$)
298	5	0.02	9.37×10^3	0.074	0.129	0.137	0.025	2.7×10^3
298	4	0.02	9.63	0.080	0.111	0.061	0.032	
298	3	0.02	2.74	0.029	0.021	---	0.026	
298	2	0.02	13.38	0.151	0.185	0.109	0.031	
298	18	0.02	25.40	0.299	0.207	0.232	0.022	
						Av =	0.027	
76	14	0.02	16.3×10^3	0.252	0.351	0.326	0.015	6.5×10^3
76	15	0.02	20.2	0.410	0.479	0.446	0.017	
76	12	0.02	14.4	0.251	0.329	0.399	0.012	
76	20	0.02	13.1	0.130	0.214	0.142	0.009	
76	19	0.02	8.04	0.061	0.077	0.065	0.010	
						Av =	0.013	
4	17	0.02	12.37×10^3	0.389	0.460	0.500	0.0028	7.1×10^3
4	7	0.005	12.25	0.424	0.540	0.570	0.0014	
4	13	0.02	13.17	0.733	0.609	0.540	0.0028	
4	10	0.02	10.6	0.245	0.252	0.267	0.0016	
4	16	0.02	7.8	0.138	0.147	0.140	0.003	
						Av =	0.002	

Notes: 1 in = 2.54 cm

$$1 \frac{in\text{-}lb}{in^2} = 1.75 \times 10^2 \frac{m\text{-}N}{m^2}$$

Table 13. Dimensional Criteria for Valid J_{IC}: Stainless Steel Samples

Steel	Temp. (K)	a (in)	B (in)	b (in)	σ_{flow} (psi)	J_Q (in-lb/in^2)	$\frac{25\ J_Q}{\sigma_{flow}}$ (in)	$\frac{50\ J_Q}{\sigma_{flow}}$ (in)
AISI 304	298	1.89	1.50	1.11	61,700	2.7×10^3	1.094	2.188
	76	1.93	1.50	1.07	134,800	6.5	1.20	2.41
	4	1.94	1.50	1.06	151,000	7.1	1.18	2.35
AISI 316	298	1.90	1.50	1.10	56,750	3.41×10^3	1.50	3.00
	76	1.88	1.50	1.12	121,625	7.20	1.48	2.96
	4	1.89	1.50	1.11	136,050	5.0	0.92	1.84
A-286	298	1.62	1.49	1.38	119,350	4.5×10^2	0.095	0.19
	76	1.65	1.50	1.35	152,225	3.54	0.06	0.12
	4	1.65	1.50	1.35	176,725	2.90	0.04	0.08

Notes: 1 in = 2.54 cm

1 ksi = 0.689 Nm^{-2}

$1\ \frac{\text{in-lb}}{\text{in}^2} = 1.75 \times 10^2\ \frac{\text{m-N}}{\text{m}^2}$

AISI 304 does meet the Begley-Landes requirement for the most part if α is chosen to be 25. Thus, considering the critical value of J to be J_{IC}, the latter can be converted to K_{IC} through the relation[7,8]

$$K_{IC} = J_{IC}\sqrt{\frac{E}{1-\nu^2}} \quad ,$$

where E is Youngs modulus and ν is Poissons ratio.

Table 14 tabulates the values of K_{IC} for AISI 304 as well as other toughness parameters. The load required for crack initiation is derived from the load displacement curve knowing the value of J_{IC}. The parameter J_Q is determined from the relation

$$J_Q = \frac{2A}{Bb} \quad ,$$

where A is the area under the load-displacement curve to the ultimate load. This particular parameter is convenient to measure since only one test per temperature is required. The value of J_Q decreases with decreasing temperature, as opposed to the manner in which J_{IC} and K_{IC} change with temperature. This temperature decrease of J_Q is due to the fact that the load reaches the ultimate value more rapidly the lower the temperature.

Figure 45 is a temperature plot of the load parameters P_{max}, P_c, and P_Q for AISI 304. The critical load approaches the ultimate load level at 76 K, and then at 4 K, P_c has "moved" beyond the ultimate. Figure 46 is a plot of the toughness parameters as a function of temperature.

Table 14. Toughness Parameters of AISI 304

Temp. (K)	Spec.	Load for Crack Initiation (lb)	K_{IC} (ksi$\sqrt{in}$)	P_Q (lb)	K_Q (ksi$\sqrt{in}$)	P_{max} (lb)	K_{max} (ksi$\sqrt{in}$)	J_Q ($\frac{in\text{-}lb}{in^2}$)
298	5	13,850	285	7,900	48.	---	---	---
298	4			9,550	54.5	---	---	---
298	3			8,100	49.5	---	---	---
298	2			10,400	60.	19,075	110.	13.38×10^3
298	18			8,200	46.5	20,100	114.	20.19
				Av =	51.		112.	16.78
76	14	27,200	457.1	13,000	81.	27,700	174.	8.30×10^3
76	15			12,500	77.5	27,400	173.	---
76	12			12,100	76.	27,500	174.	8.05
76	20			10,200	63.	28,100	174.	9.45
76	19			12,000	67.5	---	---	---
				Av =	75.		174.	8.60
4	17	28,600	476.4	19,600	122.	31,900	199.	4.9×10^3
4	7			16,600	112.	28,600	197.	---
4	13			17,200	109.	30,550	190.5	---
4	10			21,550	127.	32,400	194.	4.81
4	16			17,500	93.	33,400	195.	5.2
				Av =	113.		194.	4.97

Notes: 1 lb = 4.448 Newtons

1 ksi $\sqrt{in}$ = 1.093×10^6 $N/m^2\text{-}m^{1/2}$

$1 \frac{in\text{-}lb}{in^2} = 1.75 \times 10^2 \frac{m\text{-}N}{m^2}$

287<

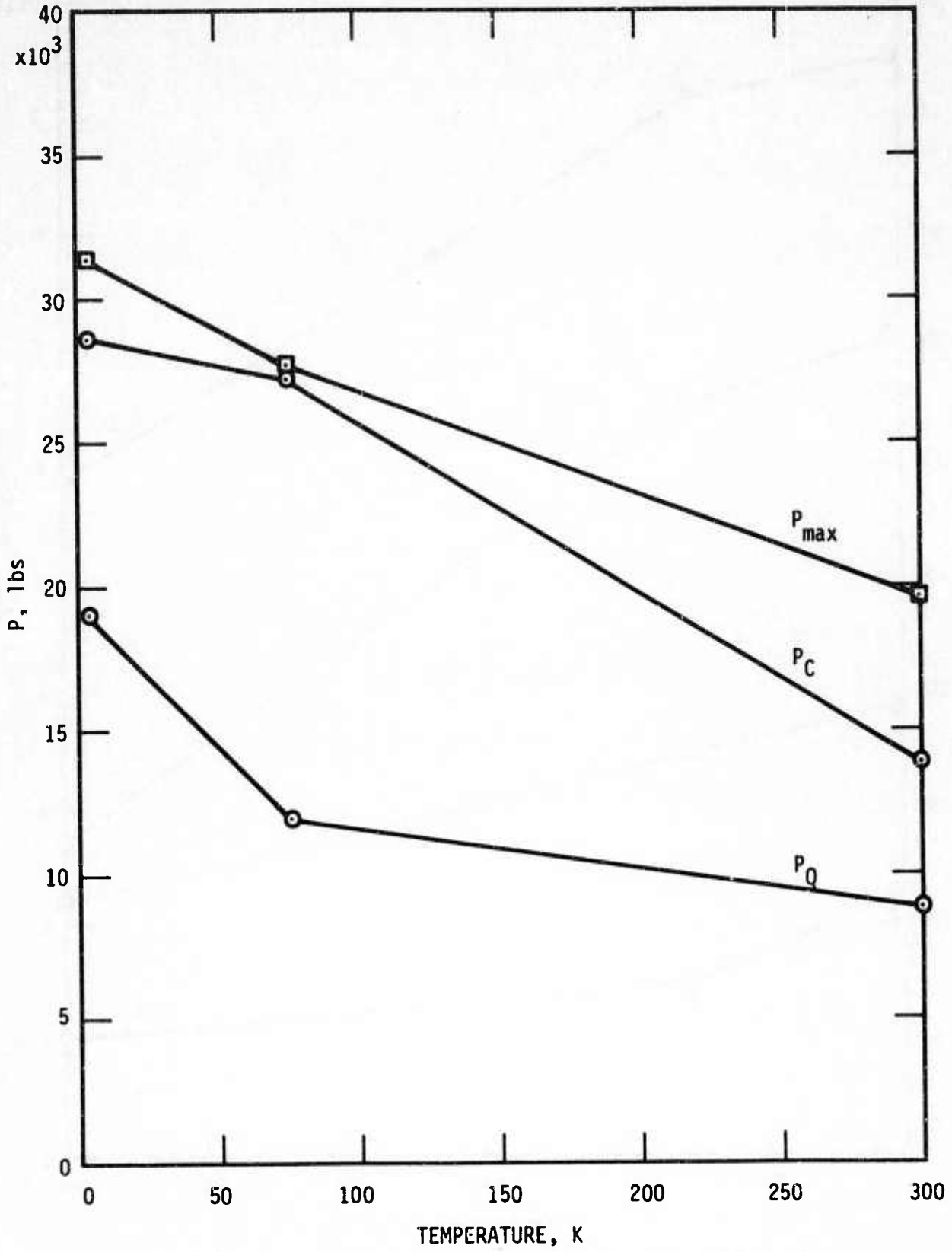

Figure 45. Load Parameters of AISI 304 as a Function of Temperature (1 lb. = 0.454 kg.)

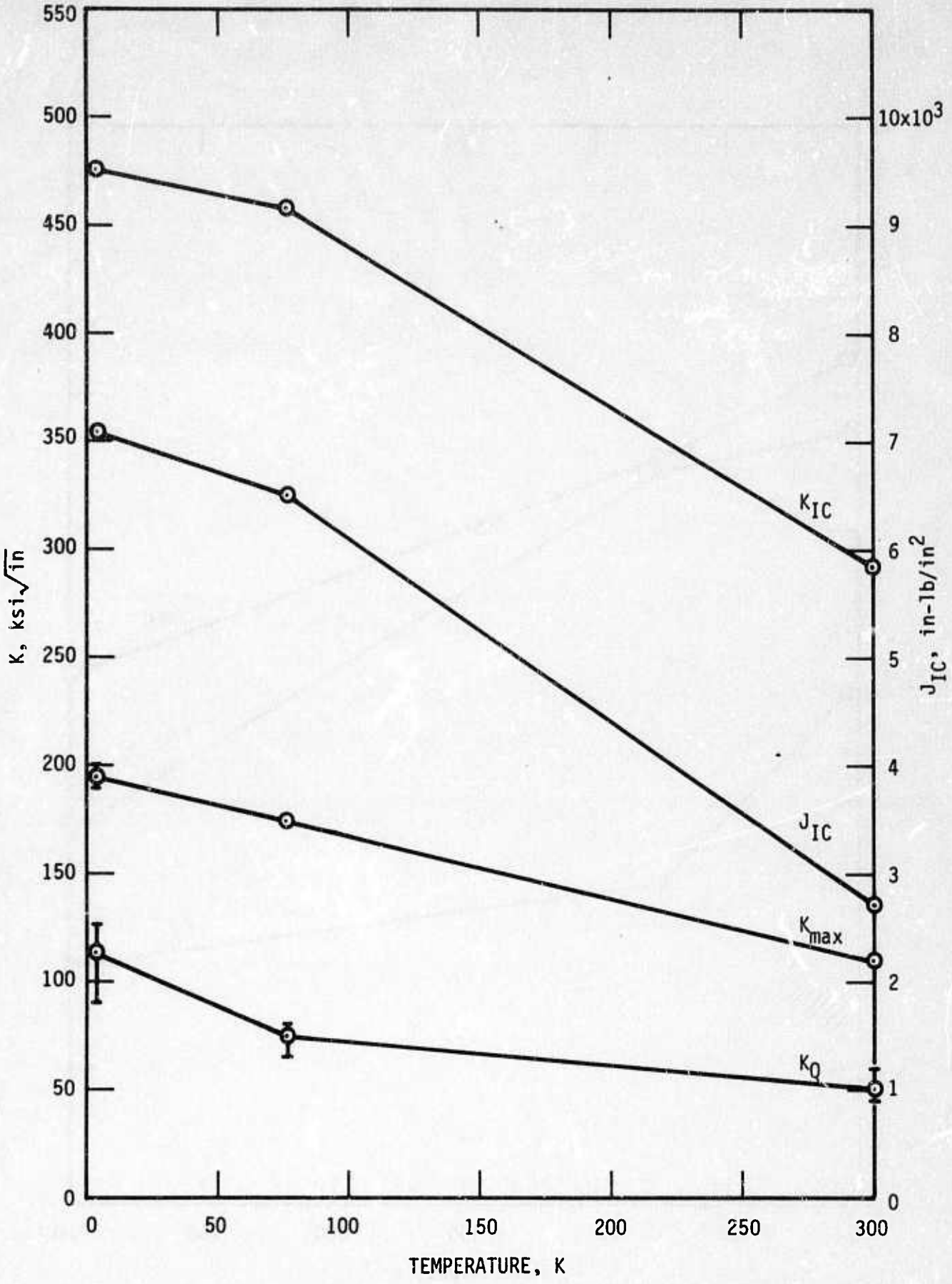

Figure 46. Fracture Toughness Parameters of AISI 304 as a Function of Temperature.
(1 ksi $\sqrt{in}$=1.093 x 10^6 N/m^2-$\sqrt{m}$ and 1 in-lb/in^2 = 1.75 x 10^2 m-N/m^2

389<

The graph of the J integral versus crack extension for AISI 316 at 300 and 76 K is presented in Figure 47. Two heats were tested at 300 K. In heat 2, although only 3 data points were obtained, one specimen represents a point just after crack opening initiated. Since there are no points for heat 1 near the stretch line and since heat 1 data points do exhibit considerable scatter, the J_{IC} value obtained from heat 2 data is considered more reliable.

The fracture surfaces of AISI 316 at 300 and 76 K are shown in Figure 48; the surface of a 4 K specimen is presented in Figure 49. The heat tinting of the 4 K specimen left well-defined ridges very apparent. The number of these ridges exactly correspond to the number of major load drops obtained from the load-deflection curve (see Figure 41). Presumably these ridges, defined by differing heat tint coloring, result from varying martensite concentrations along the fracture surface. These sudden, repeated crack advances are thought to result from internal, localized adiabatic heating, leading to reduced flow stresses at the higher temperatures and sudden shearing with a concomitant drop in load. Therefore, by measurement of crack extension to each ridge and of J values to each associated load drop, it is possible to obtain a series of J- Δa points from one specimen.

Figure 50 shows the J plots for three specimens of AISI 316 at 4 K. Each ordinate data point represents the J value for the integrated area to the bottom of a particular load drop. The corresponding Δa is that extension measured from the end of the fatigue crack at the center to the particular ridge, as shown in Figure 49. The point corresponding to the maximum extension (i.e., at the interface between the heat tint area and the remaining part of the fracture), falls in line with the points illustrated.

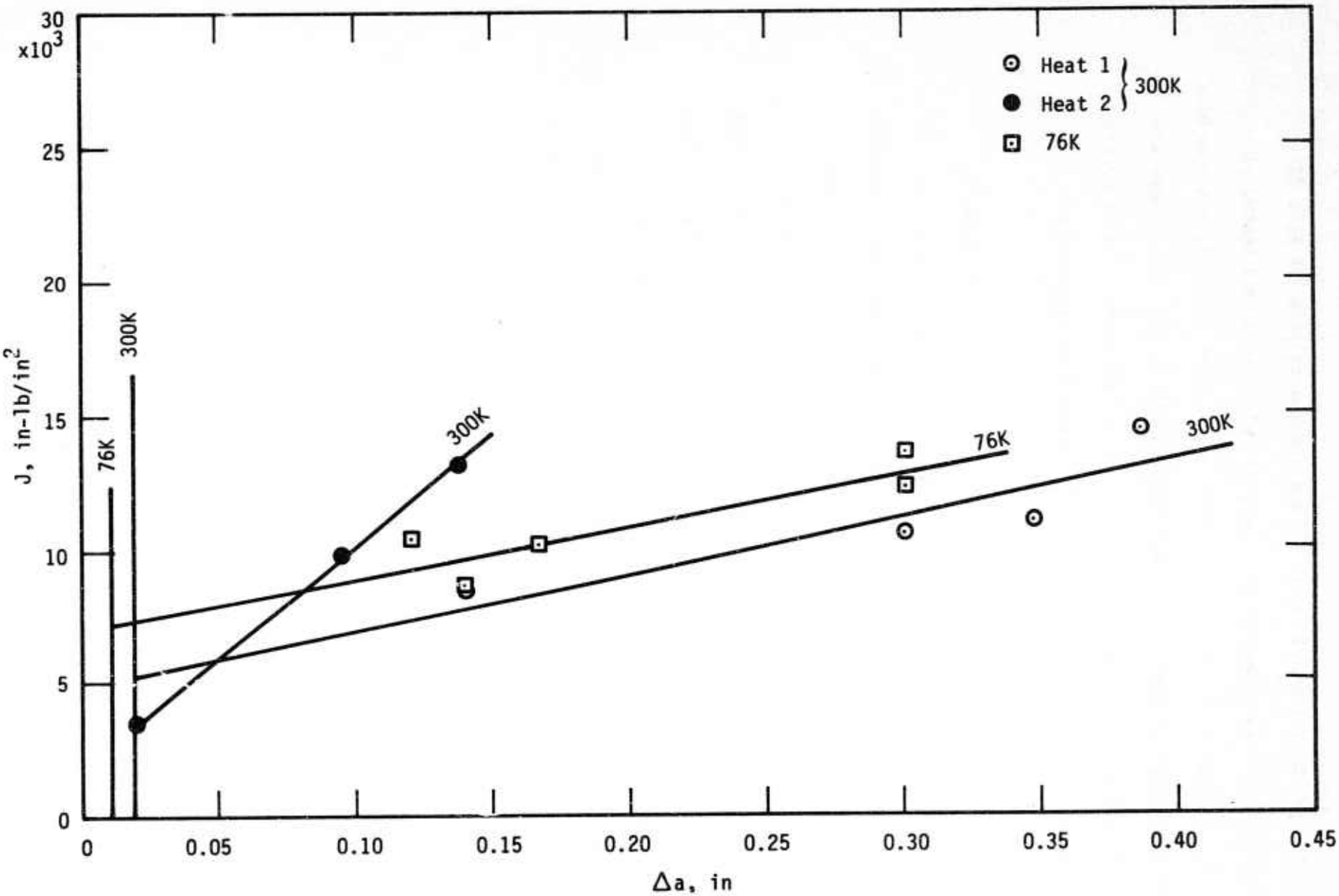

Figure 47. The J-Integral as a Function of Crack Extension of AISI 316 at 300 and 76 K (1 in-lb/in^2= 1.75 x 10^2 m-N/m^2 and 1 in. =2.54 cm.)

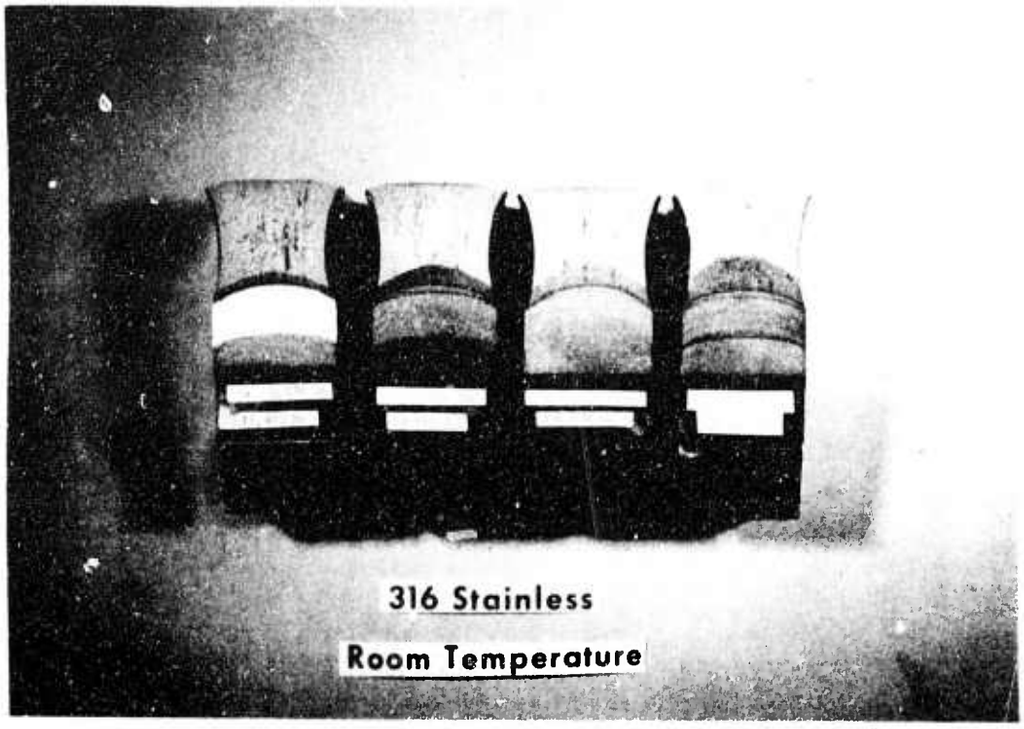

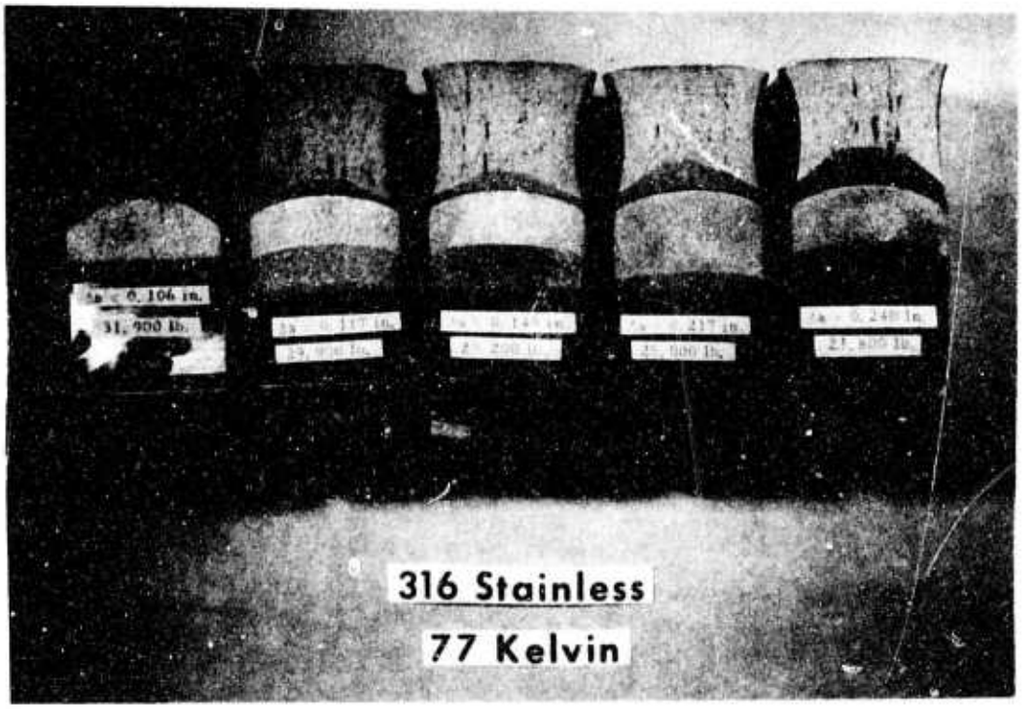

Figure 48. Fracture Surfaces of AISI 316 at 298 and 77 K

Figure 49. Fracture Surfaces of AISI 316 at 4 K

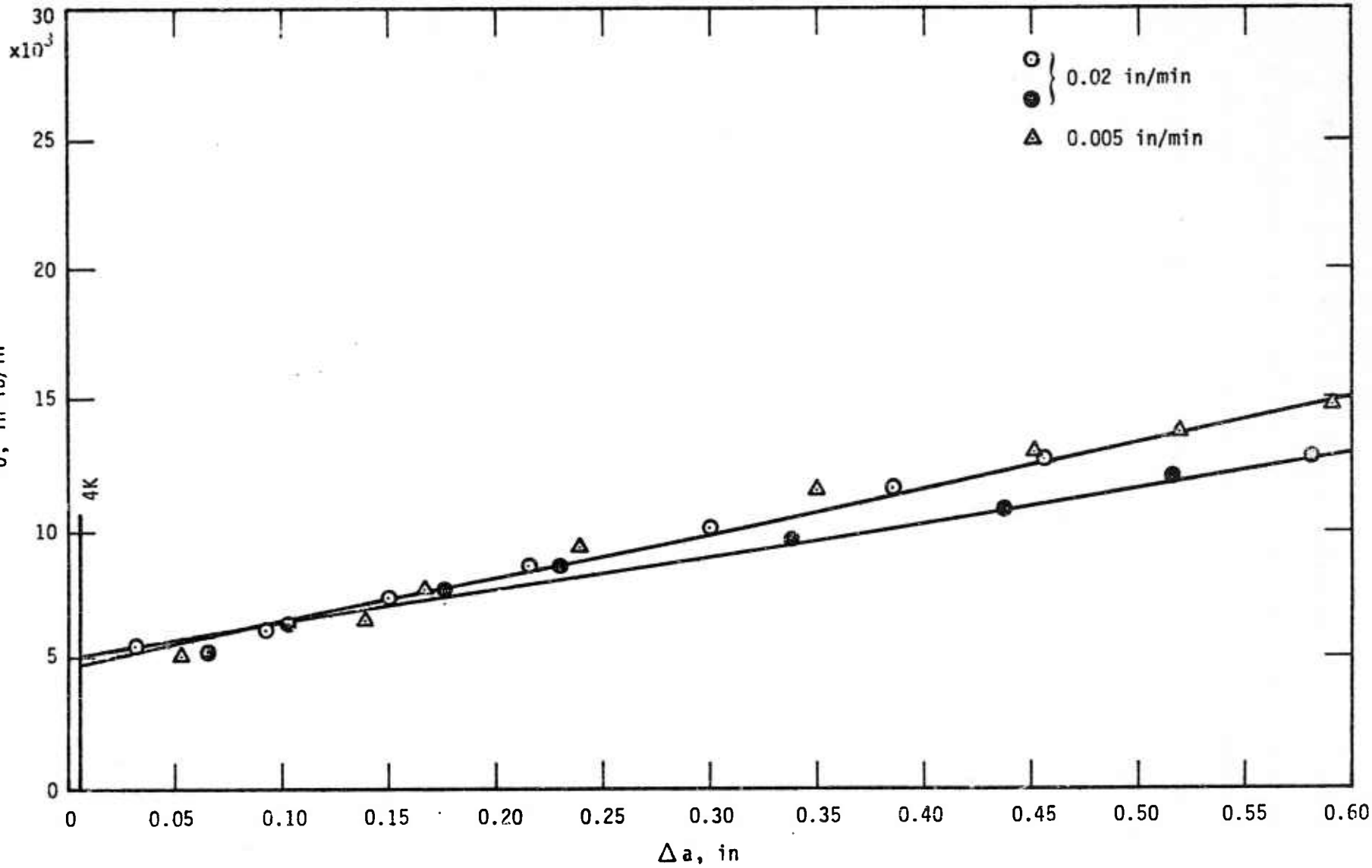

Figure 50. The J-Integral as a Function of Crack Extension of AISI 316 at 4 K

(1 in-lb/in^2 = 1.75 x 10^2 m-N/m^2 and 1 in. = 2.54 cm)

Results for the J-integral of AISI 316 are shown in table 15. Intermediate J values for AISI 316 at 4 K, each point corresponding to the particular load drop, are shown in table 16. In spite of the steel not conforming completely to the dimensional criterion (see table 13), the J_{IC} values were converted to K_{IC}. Table 17 tabulates the values of K_{IC} as well as the other toughness parameters.

A temperature plot of the load parameters of AISI 316 is shown in figure 51. The toughness parameters as a function of temperature are plotted in figure 52. The P_c and P_{max} curves are nearly parallel. Notice that the J_{IC} and K_{IC} values decrease between 76 and 4 K, as opposed to the behavior of AISI 304.

A-286

The alloy A-286 was found to be less tough than AISI 304 and 316. In fact, the alloy exhibited "pop-in" at 76 and 4 K.

Figure 53 shows the load displacement curves for A-286 at 298, 76, and 4 K. Since it was desirable to obtain J-values for very small extensions, most tests were terminated shortly after the load-displacement curve would flatten out. At 76 K, the first drop in load was accompanied by a fairly low sounding "pop"; the load then continued at nearly the same level until complete fracture occurred with a very loud sounding "pop". The other two tests at 76 K were terminated before pop-in occurred. At 4 K, slight extension occurred with 2 tests before termination; very low pops were heard. A louder, more definite pop occurred with a third test at 4 K; a relatively larger extension accompanied the pop-in.

Table 15. Results for J Integral of AISI 316

Temp. (K)	Spec.	Cr hd. Rate, in/min and Cond.	J ($\frac{in\text{-}lb}{in^2}$)	Δa center (in)	Δa out/cent (in)	Δa true av (in)	Stretch Zone (in)	J_{IC} ($\frac{in\text{-}lb}{in^2}$)
298	1	0.02, Heat 1	11.12×10^3	0.263	0.264	0.347	0.013	3.41×10^3
298	10	"	10.68	0.237	0.240	0.30	0.013	
298	3	"	14.6	0.407	0.381	0.386	0.020	
298	11	"	8.45	0.140	0.136	0.107	0.015	
298	14	0.02, Heat 2	13.1	0.078	0.137	0.10	0.030	
298	15	"	9.8	0.068	0.097	0.094	0.027	
298	17	"	3.41	0.024	---	---	0.024	
						Av =	0.020	
76	12	0.02, Heat 1	10.2×10^3	0.184	0.148	0.167	0.010	7.2×10^3
76	2	"	13.65	0.358	0.240	0.30	0.008	
76	4	"	12.32	0.277	0.217	0.30	0.011	
76	8	"	8.53	0.155	0.117	0.139	0.014	
76	13	"	10.47	0.115	0.106	0.120	0.013	
						Av =	0.011	
4	5	0.02, Heat 1	14.8×10^3	0.709	0.578	---	0.004	5.0×10^3
4	6	"	12.66	0.475	0.309	---	0.002	
4	7	0.005, Heat 1	15.16	0.643	0.492	---	0.007	
						Av =	0.004	

Notes: 1 in = 2.54 cm

$$1 \frac{in\text{-}lb}{in^2} = 1.75 \times 10^2 \frac{m\text{-}N}{m^2}$$

Table 16. Intermediate J integral values of AISI 316 at 4 K

Specimen No.	Load Drop No.	J, in-lb/in^2*	Δ a, in*
5	1	5.10	0.065
	2	6.23	0.120
	3	7.62	0.176
	4	8.59	0.229
	5	9.65	0.336
	6	10.8	0.433
	7	12.04	0.516
	8	12.95	0.581
	9	13.6	0.646
	10	14.4	0.671
6	1	5.39	0.032
	2	6.09	0.092
	3	7.31	0.150
	4	8.65	0.214
	5	10.10	0.299
	6	11.59	0.374
	7	12.66	0.454
7	1	5.07	0.053
	2	6.48	0.141
	3	7.75	0.168
	4	9.44	0.238
	5	11.5	0.350
	6	12.88	0.452
	7	13.69	0.520
	8	14.76	0.589

* 1 inch = 2.54 cm, $\frac{1 \text{ in-lb}}{\text{in}^2} = 1.75 \times 10^2 \frac{\text{m-N}}{\text{m}^2}$

Table 17. Toughness Parameters of AISI 316

Temp. (K)	Spec.	Load for Crack Initiation (lb)	K_{IC} (ksi$\sqrt{in}$)	P_Q (lb)	K_Q (ksi$\sqrt{in}$)	P_{max} (lb)	K_{max} (ksi$\sqrt{in}$)	J_Q ($\frac{in\text{-}lb}{in^2}$)
298	1	14,400	343.1	9,080	55.5	14,600	90.	7.14×10^3
298	10			6,800	40.	15,200	89.	6.95
298	3			8,580	48.	15,150	89.	---
298	11			7,075	40.5	---	---	8.45
298	14			7,550	46.	---	---	---
298	15			6,250	36.5	---	---	---
298	17			7,600	44.5	---	---	---
			Av (Heat 1) =		46.		89.	7.51
			Av (Heat 2) =		42.3			
76	12	29,200	515.6	17,050	93.	30,250	164.	7.09×10^3
76	2			---	---	29,400	166.	---
76	4			15,000	89.	27,800	166.	7.94
76	8			17,100	91.5	30,050	159.	6.43
76	13			18,150	108.	---	---	---
				Av =	95.4		164.	7.15
4	5	31,600	430.	16,700	89.5	32,200	173.	4.41×10^3
4	6			16,000	89.5	32,550	183.	4.62
4	7			17,600	100.	33,400	190.	4.02
				Av =	89.5		178.	4.52
				for 0.02 in/min (see table 15)				

Notes: 1 lb = 4.448 Newtons

1 ksi$\sqrt{in}$ = 1.093×10^6 $N/m^2\text{-}m^{1/2}$

1 in-lb/in^2 = 1.75×10^2 $\frac{m\text{-}N}{m^2}$

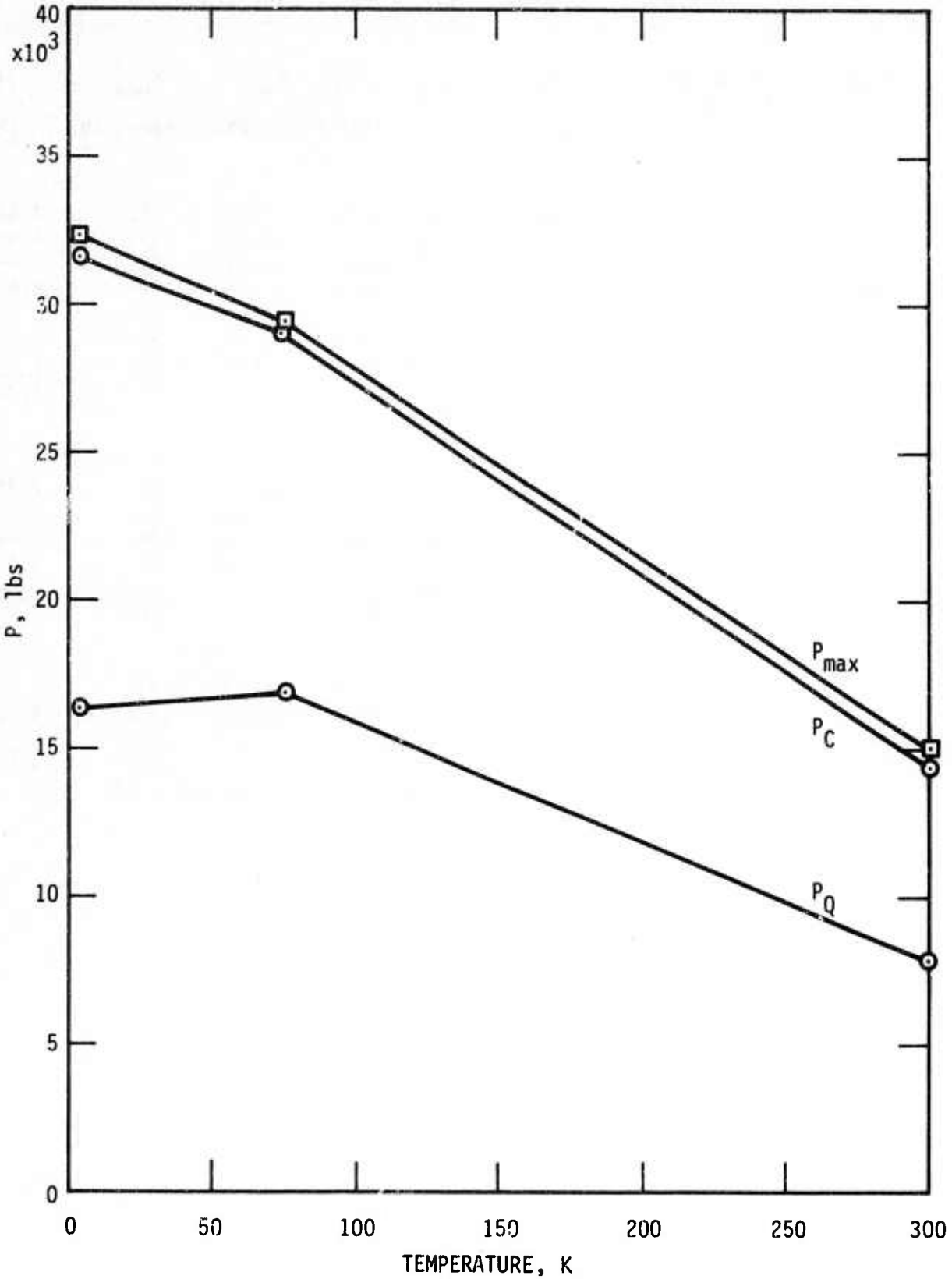

Figure 51. Load Parameters of AISI 316 as a Function of Temperature (1 lb. = 0.454 kg.)

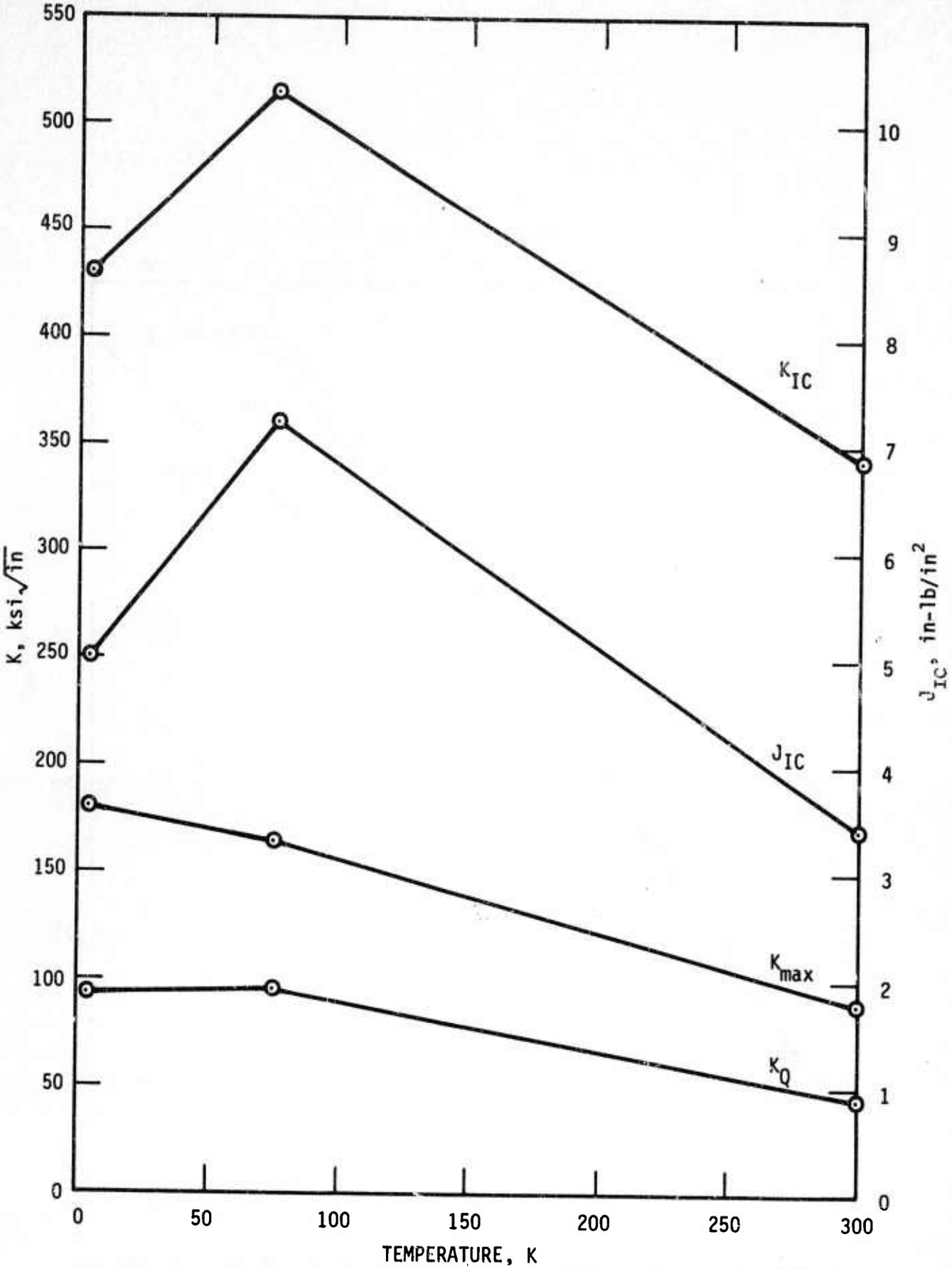

Figure 52. Fracture Toughness Parameters of AISI 316 as a Function of Temperature (1 ksi $\sqrt{in}$=1.093 x 10^6 N/m^2 x m$^{1/2}$ and 1 in-lb/in^2=1.75 x 10^2 m-N/m^2)

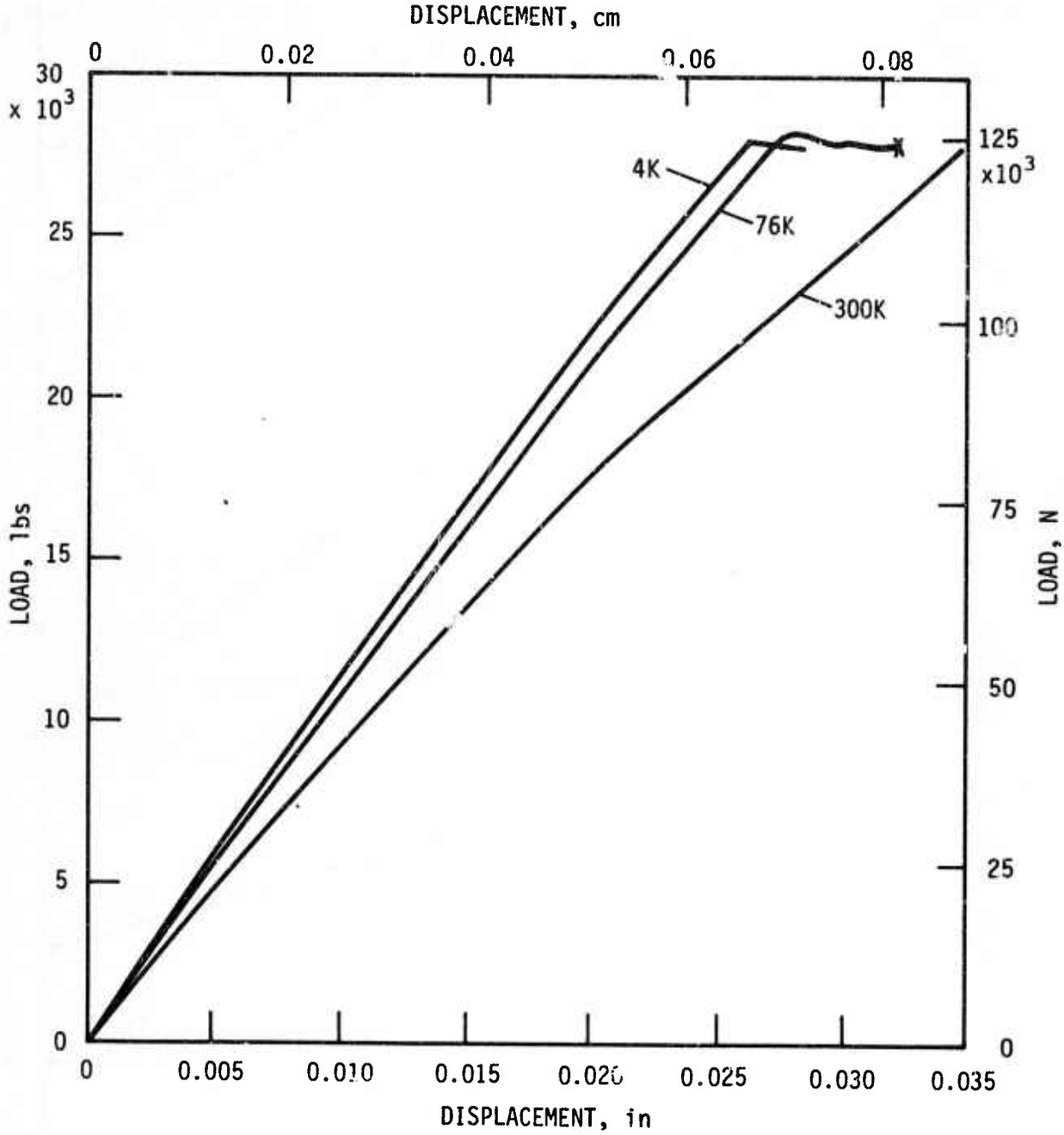

Figure 53. Load-Displacement Curves of A-286 at 300, 76, and 4K.

Figures 54 and 55 are plots of the J-integral of A-286 as a function of extension. The J_{IC} values are obtained from the zero value of extension, i.e., there is essentially no stretch zone with this alloy. Notice that there are extremely small extensions at 76 K.

Fracture surfaces of A-286 tested at 298, 76, and 4 K are shown in figures 56, 57, and 58, respectively. Observe the very small extensions with most of the samples.

Test results of A-286 are shown in table 18. The K_{IC} values are obtained from J_{IC} through the relation involving Youngs modulus and Poissons ratio. What is called "K_{pop}" is derived directly from the load at pop-in. It is interesting to note that the K_{pop} values are higher than the K_{IC} values. Figure 59 is a plot of the toughness parameters as a function of temperature. As opposed to the AISI 304 and 316, the J_{IC} and K_{IC} decrease with a decrease in temperature.

Referring back to table 13, it is seen that A-286 easily meets the requirements for a valid J_{IC}. However, the alloy does not comply with the requirements for a valid K_{IC} (see table 19) according to ASTM specification E-399 that states

$$a, B \geq 2.5 \left(\frac{K_{IC}}{\sigma_{ys}} \right)^2 .$$

The K_{IC} is close to being valid at 4 K. It is possible that the flow stress is higher than estimated at 4 K, thus giving a valid K_{IC} at this temperature.

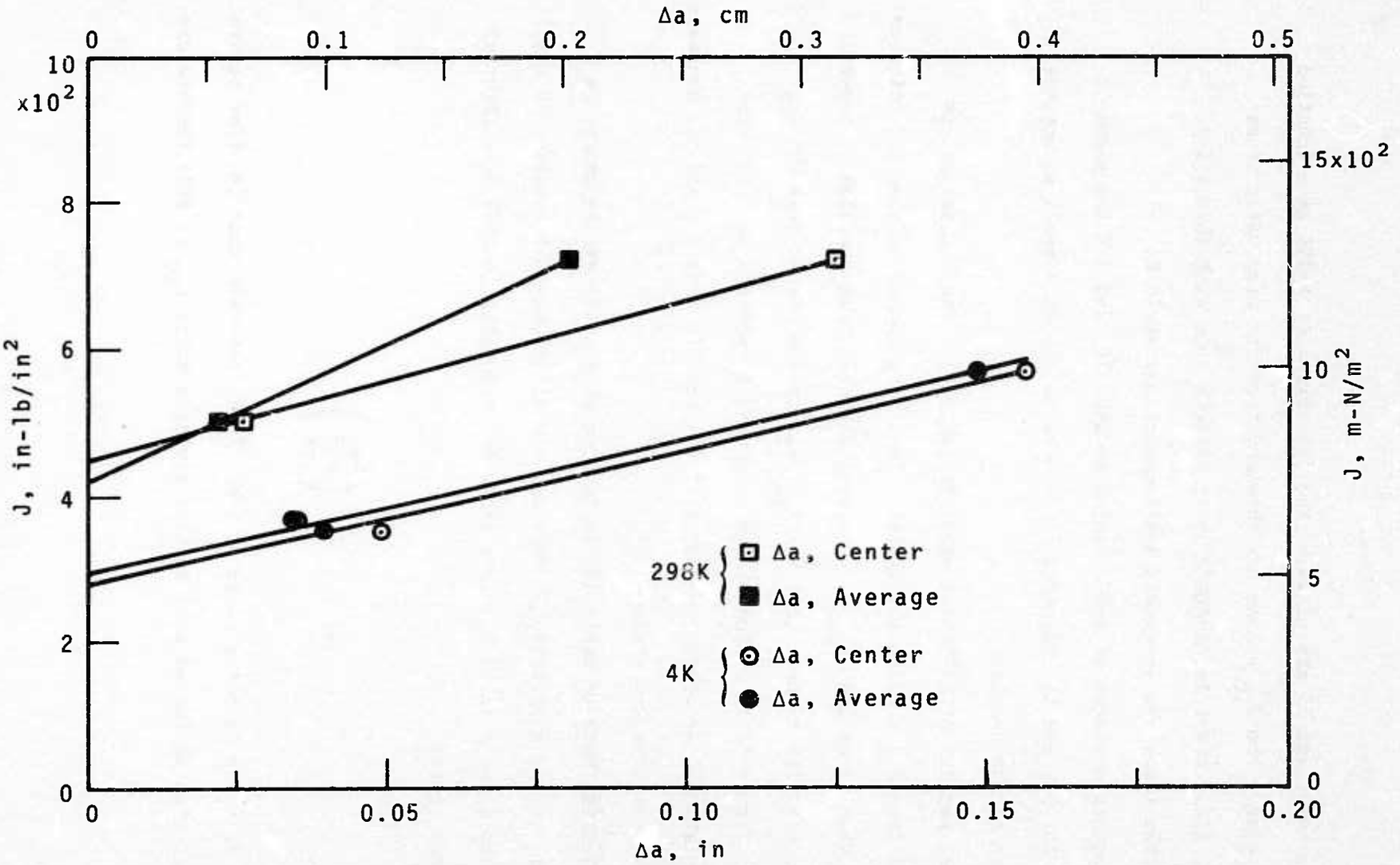

Figure 54. The J-Integral as a Function of Crack Extension of A-286 at 298 and 4K.

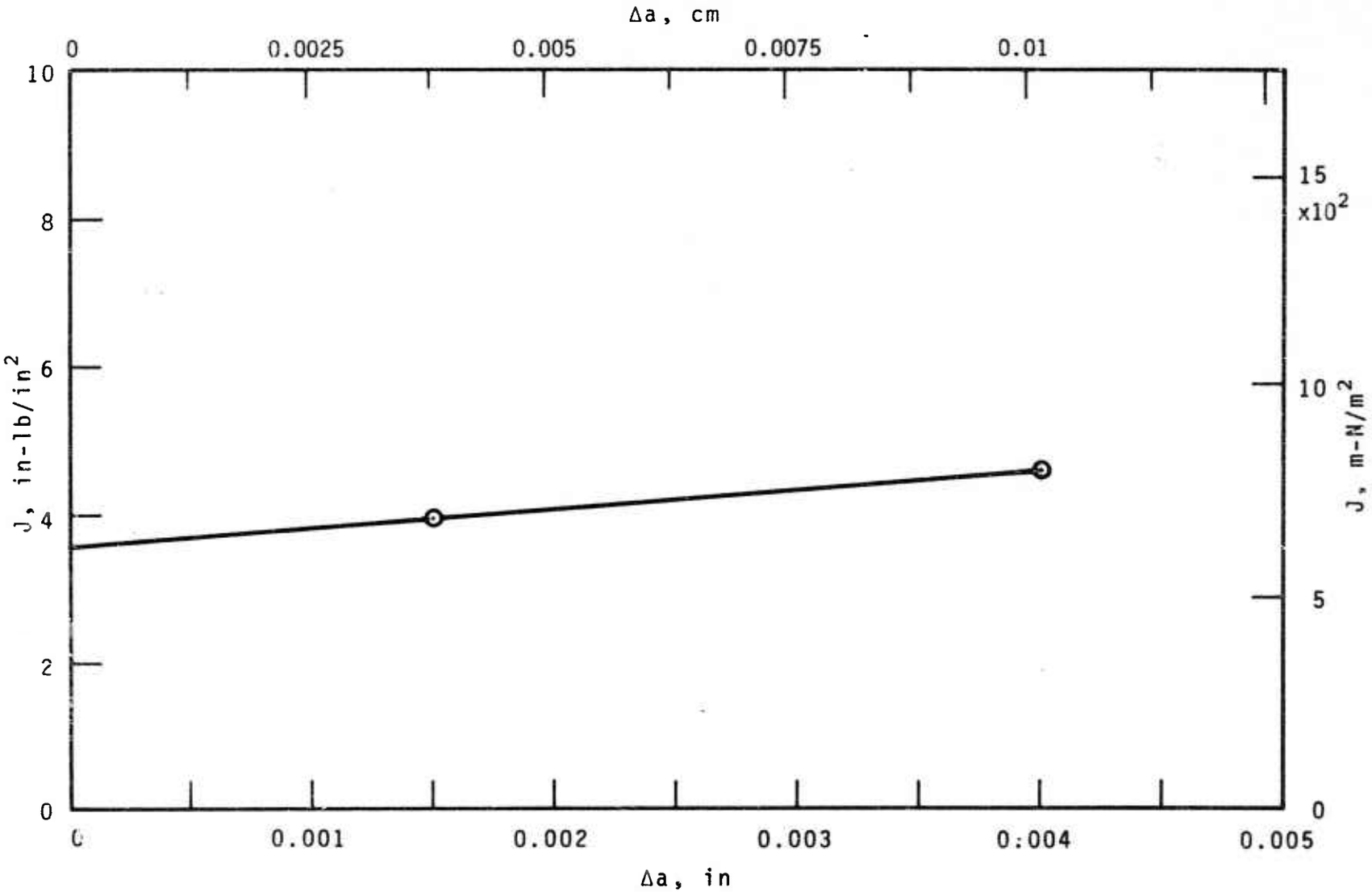

Figure 55. The J-Integral as a Function of Crack Extension of A-286 at 76K.

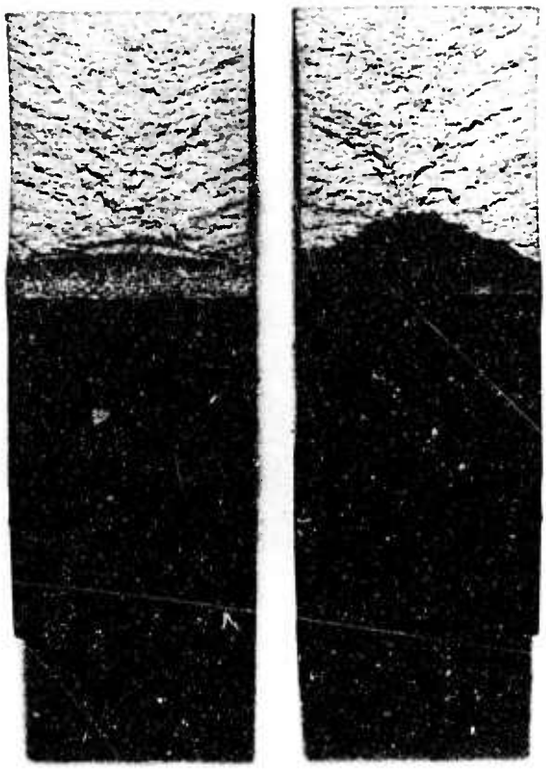

Figure 56. Fracture Surfaces of ASTM A-286 at 298 K

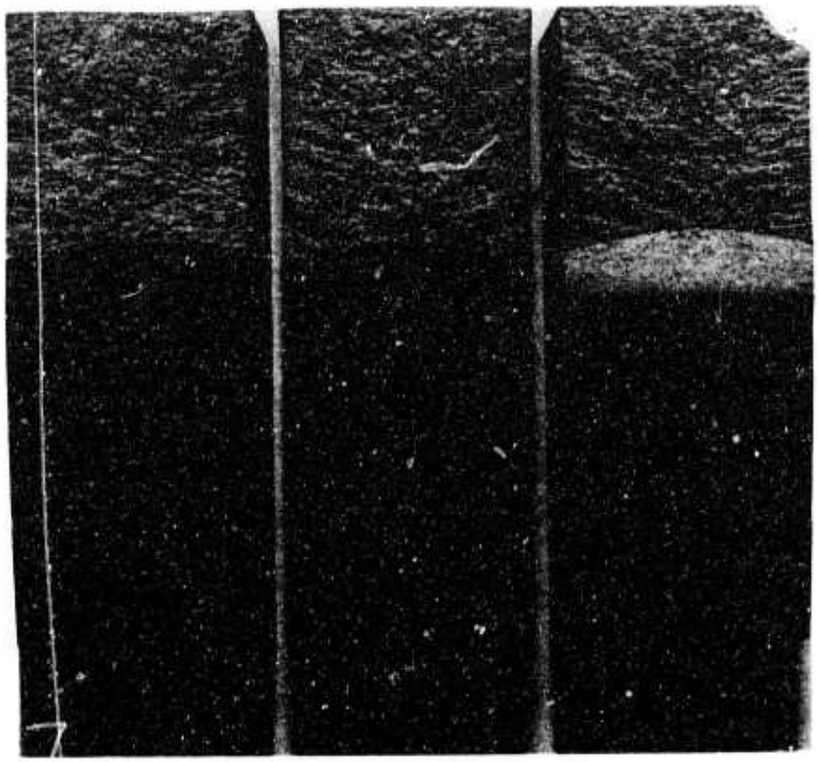

Figure 57. Fracture Surfaces of ASTM A-286 at 76 K

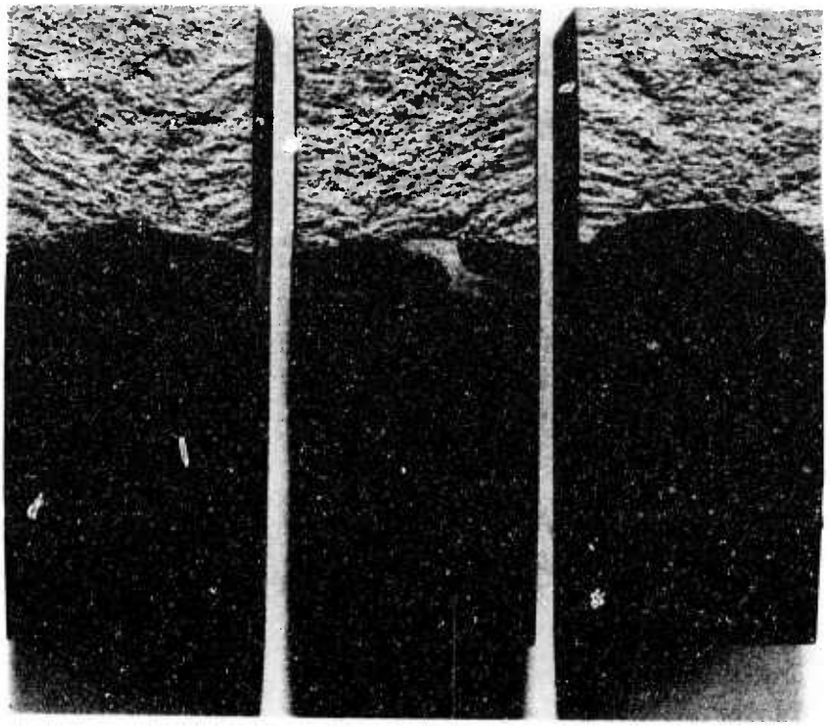

Figure 58. Fracture Surfaces of ASTM A-286 at 4 K

Table 18. Test Results of A-286

Temp. (K)	Spec.	P_Q (lb)	K_Q (ksi$\sqrt{in}$)	J ($\frac{in\text{-}lb}{in^2}$)	Δa center (in)	Δa av (in)	J_{IC} ($\frac{in\text{-}lb}{in^2}$)	K_{IC} (ksi$\sqrt{in}$)	P_{pop} (lb)	K_{pop} (ksi$\sqrt{in}$)
298	5	25,000	105.	5.07×10^2	0.026	0.022	4.50×10^2 for Δa/center	120.9	---	---
298	2	18,370	78.	7.25	0.124	0.080			---	---
298	1	18,500	80.	4.08	0.079	0.048	4.25×10^2 for Δa/av	117.5	---	---
		Av =	87.7				Av =	119.2		
76	13	---	---	4.62×10^2	0.004	---	3.54×10^2	107.2	---	---
76	9	27,150	122.	---	---	---			29,420	133.2
76	6	27,900	117.	3.96	0.0015	---			---	---
		Av =	119.5				Av =	107.2		133.2
4	7	26,220	114.	5.71×10^2	0.156	0.148	2.78×10^2 for Δa/center	95.05	28,280	123.
4	0	Same as P_{pop}	120.	3.51	0.049	0.039	2.90×10^2 for Δa/av		27,650	120.
4	10	"	117.	3.73	0.035	0.034		97.08	26,980	117.
		Av =	117.				Av =	96.06		120.

Notes: 1 lb = 4.448 Newtons

1 ksi$\sqrt{in}$ = 1.093×10^6 $N/m^2 - m^{1/2}$

1 $\frac{in\text{-}lb}{in^2}$ = 1.75×10^2 $\frac{m\text{-}N}{m^2}$

1 in = 2.54 cm

1 $\frac{in\text{-}lb}{in^2}$ = 1.75×10^2 $\frac{m\text{-}N}{m^2}$

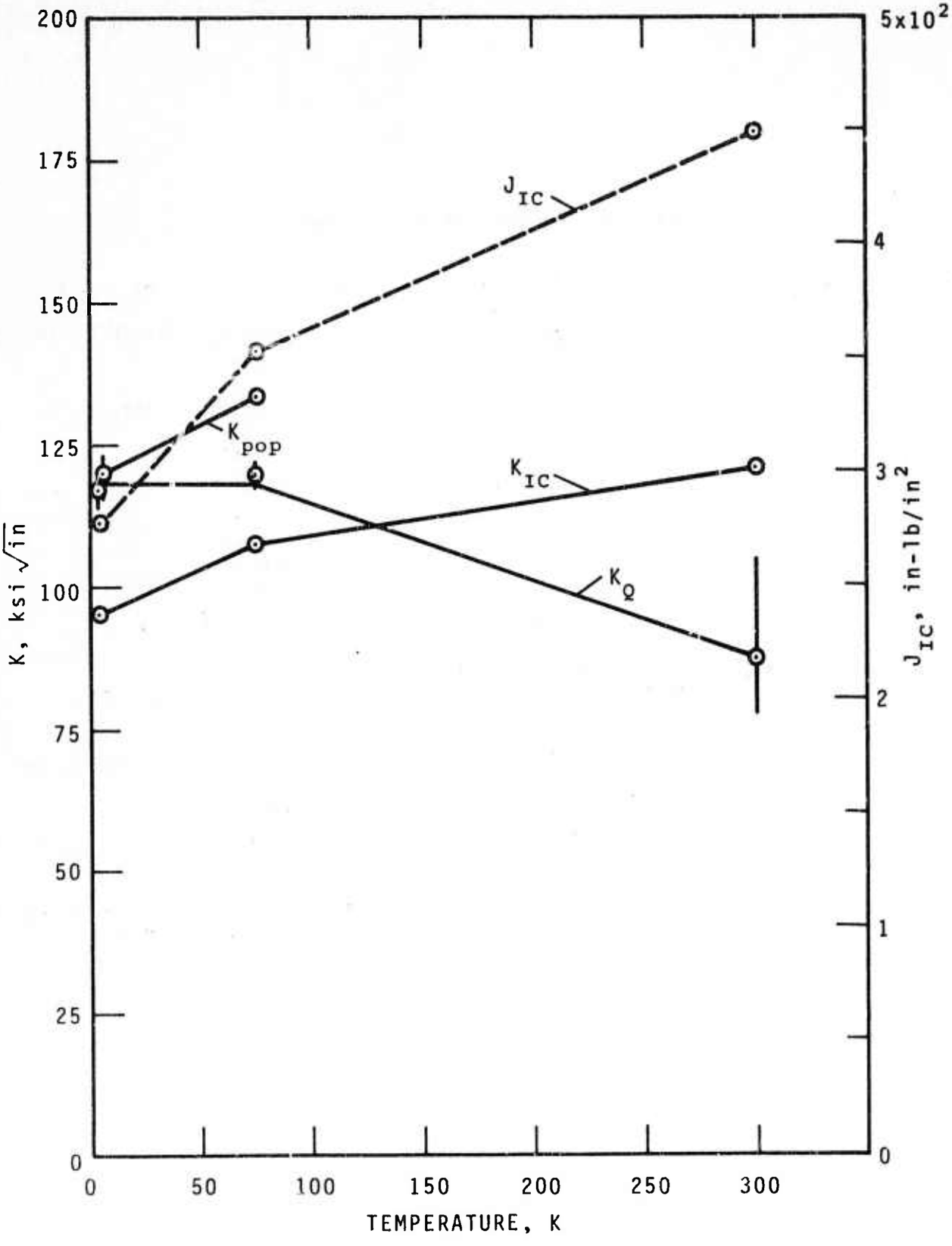

Figure 59. Fracture Toughness Parameters of A-286 as a Function of Temperature

Table 19. Dimensional Criteria for Valid K_{IC}: A-286

Temp. (K)	a (in)	B (in)	0.2% Yield Strength (psi)	K_{IC} (ksi$\sqrt{in}$)	$2.5\left(\frac{K_{IC}}{\sigma_{ys}}\right)^2$ (in)	K_{pop} (ksi$\sqrt{in}$)	$2.5\left(\frac{K_{pop}}{\sigma_{ys}}\right)^2$ (in)
298	1.62	1.49	88,200	120.9	4.69	---	---
76	1.65	1.50	107,500	107.2	2.49	133.2	3.84
4	1.65	1.50	123,050	97.08	1.55	120.	2.38

notes: 1 in = 2.54 cm

1 ksi = 0.689 Nm^{-2}

1 ksi$\sqrt{in}$ = 1.093 x 10^6 N/m^2 - $m^{1/2}$

DISCUSSION

The discontinuous yielding observed with AISI 304 and 316 at 4 K in both tensile and fracture toughness tests has been attributed to a combination of highly localized heating and the temperature dependence of the flow stress[22,26]. The most acceptable explanation of this phenomenon may be described as follows: at 4 K the specific heat and thermal conductivity of alloys are very low; therefore, any heat generated internally cannot easily escape and local warming occurs. Temperature rises in tensile specimens as high as 40 K have been measured[40]. In some alloys the temperature dependence of the flow stress at low temperatures is quite large, insuring that, if local temperature rises do occur, plastic deformation occurs more easily. In tensile specimens the local temperature rises and associated plastic deformation surges do occur at intervals along the reduced specimen length, much in the same manner that Luders bands propagate along the specimen length (see figures 14-16). These effects are a function of the strain rate[40]. Observation of figures 38 and 41 indicate that the same phenomena occur in fracture toughness tests of austenitic stainless steels. Testing a few specimens at reduced load rates revealed that, again, the magnitude of the load drops (higher load rates producing higher load drops) was influenced by load rate. The surprising evidence was that, at least in AISI 316, very distinct crack front ridges could be directly associated with these load drops. This indicates that the crack front propagated discontinuously, influenced considerably by local specimen temperature.

Another possible indication of local temperature effects is the nature of the crack front geometry after partial propagation in J integral tests (see figures 49 and 50). The unusual tendency of reduced propagation rate in the specimen center and increased crack propagation tendencies nearer the surfaces are very apparent. Now, if local heating did occur, the interior would be expected to be warmer than the exterior (due to reduced specimen thermal conductivity and lower heat capacity near 4 K). If the propagation rates were temperature dependent (in the temperature range 4 to about 50 K), then crack fronts such as observed could be rationalized. Another explanation, of course, is that loading conditions, after crack growth to achieve an $a/w = 0.8 - 0.9$, tend to produce such a crack front.

The da/dN fatigue results do not portray a marked temperature dependence. More experiments are required to sort out the possible temperature dependence exhibited by fracture toughness tests, opposed to the apparent temperature independence portrayed by fatigue results.

The martensitic transformation does not seem to significantly influence this discontinuous yielding phenomena. The transformation can best be considered as an after-effect, i.e., the sudden strains cause the transformation. In regions of large plastic deformation there will be more martensite. Toughness testing of AISI 310, which has no martensite transformation, yet has similar chemical composition (thus similar thermal conductivity and specific heat) should considerably assist in describing the role of phase transformations on low temperature discontinuous yielding of austenitic stainless steels. It is interesting to note that this discontinuous yielding occurs in tensile testing AISI 310 (see figure 15). Of course, the transformation does influence the work hardening rates and, therefore, should influence the absolute value of the fracture toughness.

Divergent suggestions have been made to relate the temperature dependence of the toughness behavior to the change in the rate of work hardening. The theoretical paper of Rice and Rosengren[41] suggests that there will be a decrease in toughness of steel with an increase in the work hardening coefficient due mainly to a rapid rise in stress triaxiality at the crack root. On the other hand, Krafft[42] argues that the plane strain toughness, K_{IC}, is directly proportional to the work hardening coefficient; fracture performance is favored by a relatively high rate of work hardening. The relation of Krafft is supported by his experimental values on selected steels.

Plots of K_{IC} as a function of the work hardening coefficient for Ti-6Al-4V and AISI 304 and 316 are shown in figures 60 and 61. Our data are, at first glance, conflicting. The titanium alloy data support the suggestions of Rice and Rosengren[41]; i.e., as the work hardening coefficient increases (figure 23), the fracture toughness decreases (figure 36). The stainless steel data support Krafft[42]; for these alloys, to a rough approximation, K_{IC} (calculated from J_{IC}) is proportional to the work hardening coefficient. It may be significant that in the case of the Ti alloy plane strain fracture conditions existed, while the stainless steels exhibited extensive plastic deformation.

The decreased work hardening rates of AISI 304 and 316 at 4 K may be attributed to two factors: (1) Adiabatic heating insures a higher specimen temperature than 4 K and (2) below 60 K, the isothermal shear modulus is lower. Since the interaction force between dislocations is directly proportional to the shear modulus, which decreases between 76 and 4 K, it is expected that the work hardening rate would decrease between these two temperatures.

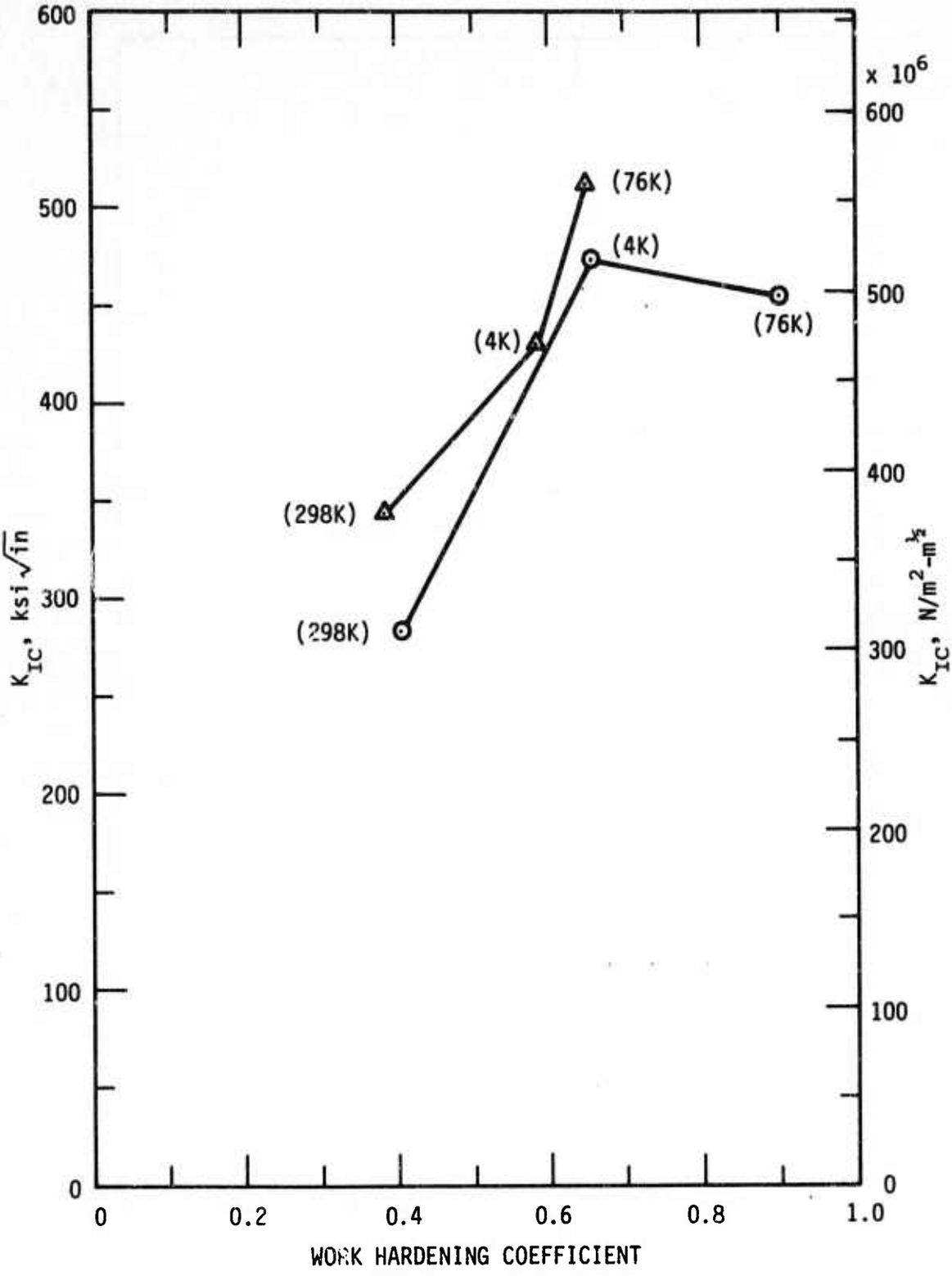

Figure 60. Critical Stress Intensity Factor as a Function of the Work Hardening Coefficient of AISI 304 and AISI 316

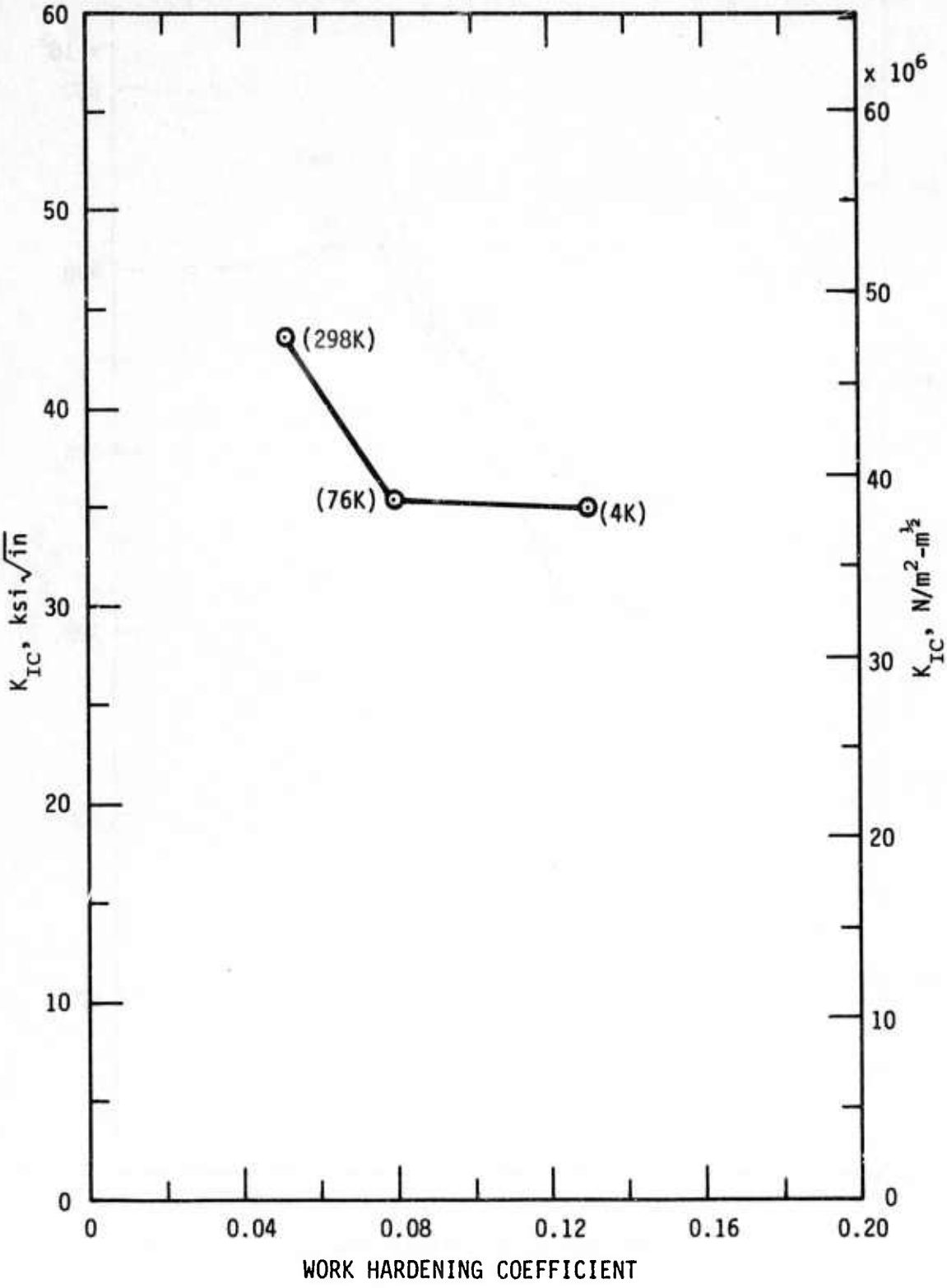

Figure 61. Critical Stress Intensity Factor as a Function of the Work Hardening Coefficient of Ti-6Al-4V

The critical load of AISI 304 and 316, P_c, cannot be clearly related to either P_Q or P_{max}. For example, at room temperature the critical loads for both steels were nearly the same; however, 304 supported a higher maximum load than 316. Nor was there a direct correlation between P_c and P_Q. In 316 stainless steel, P_c increased from 76 K to 4 K, but P_Q slightly decreased in the same temperature interval.

The fracture parameters K_Q and J_{IC} (J integral) were determined for AISI 304 and 316 at 298, 76, and 4 K. The newly developed J integral approach was used since plane strain conditions were not possible to achieve using compact tensile specimens up to 1.5 inches (3.0 cm) thick. These stainless steels are extremely tough; the estimated K_{IC} values from J integral tests is about 300 ksi$\sqrt{in}$ at room temperature and about 450 ksi$\sqrt{in}$ at 4 K. The values of K_Q at 300 K average 50 ksi$\sqrt{in}$ and at 4 K average about 100 ksi$\sqrt{in}$. Therefore, caution must be exercised in using the absolute K_{IC} values derived from J_{IC} tests, as they are considerably higher than the K_Q and K_{max} values obtained for each specimen. Careful consideration and additional testing must be applied Two conclusions can be reached: (1) AISI 304 and 316 are tougher at 4 K than at 300 K; all fracture toughness parameters are higher at 4 K than at 300 K; (2) both alloys have about the same toughness.

Additional discussion on these J integral results seem in order. The parameter K_{max} has little practical meaning since the concept of stress intensity loses its significance in the presence of plastic deformation. The parameter K_Q retains significance as the value of stress intensity at which plastic deformation first initiates.

Intuitively one expects the critical plane strain value, K_{IC}, to have a value between K_Q and K_{max}. That the K_{IC} value is considerably higher than both K_Q and K_{max} is not out of line, if one considers that K_Q and K_{max} increase with sample thickness. The larger thickness leads to a greater constraint which, in turn, raises the flow curve. Thus, at a thickness considerably larger than the 1-1/2 inch (3.8 cm) dimension of these experiments, the K_{max} should approach and perhaps exceed the value of K_{IC}.

It is clear that these calculated values of K_{IC} could not be used for design purposes for 1.5 inch (3.8 cm) thick material since failure would occur at lower stress intensities (K_Q - K_{max}). This result implies that

1) 1.5 TCT specimens were too thin to yield valid J integral results, and/or that

2) K_Q and the load-deflection record in general must increase considerably with thickness.

If the test specimen is too small, J will not accurately characterize the crack tip field. Specimens of insufficient thickness yield values of J which are higher than the true value of J_{IC}. Thus, for small specimens the value of K_{IC} is overestimated. The state-of-the-art of J integral testing is such that rigorous size requirements for valid testing have not been ascertained. The size criterion suggested by Begley and Landes, as previously described, is tentative and will undoubtedly be subject to

revision in the future as more results are made known. In view of present uncertainty as to the size requirement, the values of J_{IC} and K_{IC} derived for stainless steels in this study must be regarded as tentative.

Again referring to the thickness effect, toughness measurements on invalid specimen sizes show a decrease with increasing thickness until a limiting minimum value K_{IC} is reached. However, it is possible for invalid toughness parameters to increase with thickness in cases where the plastic zone size R_p is of the order of specimen thickness. For stainless steels, calculations indicate that this occurs for thicknesses of 1.5 inch. The large lateral contractions displayed in fractured stainless steel specimens is an effect of insufficient constraint. Thicknesses over 1.5 inch would lend greater constraint in the thickness direction and prevent early yielding. The stress intensity K_Q would then be higher for thicker material, and this was indicated by a single isolated test performed on 1 inch thick AISI 316 stainless steel at 4 K.

There is some further evidence to support the above ideas. Nelson et al,[43] found a continuous increase in K_Q as a function of thickness in tests on the aluminum alloy 6061-T651. K_Q increased as much as 100% before reaching K_{IC} which was not a "lower limiting value" of fracture toughness. There is no comparable published literature to relate the present results obtained for stainless steels.

The alloy A-286 exhibits much less plasticity than does the AISI 304 or 316. The alloy would approach true plane strain conditions with a somewhat larger increase in thickness.

Results of other investigations of Ti-6Al-4V at cryogenic temperatures were shown in figure 33. Previous authors have not reported data at 4 K. The data of this report are in accord only with the results of Vishnevsky and Steigerwald[37], who obtained valid K_{IC} data to 76 K. Their specimens were equivalent in thickness to those tested in this report (one inch), and this size largely accounts for the agreement in results.

With the exception of Vishnevsky and Steigerwald[37], the bulk of data from other investigators are in rather poor agreement. In general, their results are too high. Direct comparison is complicated because of variations in heat treatment, purity and specimen design. Variation in heat treatment affects the morphology and relative proportion of phases in the microstructure, while minute differences in interstitial impurity content (the elements C, O, N, and H) should influence fracture toughness of titanium significantly. Nevertheless, the major cause of high K_{IC} values must be attributed to specimen size effects. The "surface flawed" specimens tested by Hall[33] (t = 0.375") and Tiffany, et al,[31] (t = 0.25") nominally satisfy the present ASTM thickness requirement, but the specimens of other authors referred to in figure 33 clearly do not. In addition, recent results by Golda and Munz[44] indicate that the ASTM thickness requirement should be doubled in the case of the Ti-6Al-4V alloy. Jones and Brown[45] have also indicated that the present ASTM size requirement should be doubled for some materials. This possibility casts doubt on the results of Hall[33] and Tiffany et al[31]. so that the results of Vishnevsky and Steigerwald[37] and the current NBS data appear to be the most reliable.

REFERENCES

1. Tobler, R. L., Mikesell, R. P., Durcholz, R. L., Fowlkes, C. W., Reed, R. P., Ledbetter, H. M., Naimon, E. R., and Weston, W. F., "Fatigue and Fracture Toughness Testing at Cryogenic Temperatures," Report to Naval Ship Research and Development Center, Annapolis, Maryland, Work Request 3-0852 (Nov. 7, 1972).

2. "Fracture Toughness Testing and its Applications", ASTM STP 381, American Society for Testing and Materials, (1965).

3. Brown, W. F., Jr., and Shrawley, J. E., "Plane Strain Crack Toughness Testing of High Strength Metallic Materials," ASTM STP 410, American Society for Testing and Materials, (1966).

4. "Review of Developments in Plane Strain Fracture Toughness Testing," ASTM STP 463, American Society for Testing and Materials and NASA (W. F. Brown, Jr., Editor 1970).

5. "Standard Method of Tests for Plane Strain Fracture Toughness of Metallic Materials," E-399, Annual Book of ASTM Standards, Part 31 (1973).

6. Rice, J. R., "A Path Independent Integral and the Approximate Analysis of Strain Concentration by Notches and Cracks," J. Appl. Mechs., Trans. of Am. Soc. of Mech. Engrs., p. 379, June 1968.

7. Begley, J. A., and Landes, J. D., "The J Integral as a Fracture Criterion," Fracture Toughness, Proc. of the 1971 National Symposium on Fracture Mechanics, Part II, ASTM STP 514 (1972), pp. 1-20.

8. Landes, J. D., and Begley, J. A., "The Effect of Specimen Geometry on J_{IC}," Fracture Toughness, Proc. of the 1971 National Symposium on Fracture Mechanics, Part II, ASTM STP 514 (1972), pp. 24-39.

9. Rice, J. R., Paris, P. C., and Merkle, J. G., "Some Further Results on J Integral and Estimates," Progress in Flaw Growth and Fracture Toughness Testing, ASTM STP 536, (1973).

10. Yoder, G. R., and Griffis, C. A., "J-integral and the Initiation of Crack Extension in a Titanium Alloy," NRL Report 7662 Naval Res. Lab., Washington, D.C. (1973).

11. Kobayashi, A. S., Chiu, S. T., and Beeuwkes, R., Engrg. Fract. Mech. 5, pp. 298-305 (1973).

12. Reed, R. P., "A Cryostat for Tensile Tests in the Temperature Range 300° to 4°K," Advances in Cryogenic Engineering, Volume 7 (Published by Plenum Press, Inc., New York, Edited by K. D. Timmerhaus, 1962), p. 448.

13. "Standard Methods of Tension Testing of Metallic Materials," E8. Annual Book of ASTM Standards, Part 31 (1973).

14. Bubsey, R. T., Fisher, D. M., Jones, M. H., and Srawley, J. E., "Compliance Measurements," Experimental Techniques in Fracture Mechanics (A. S. Kobayashi, Editor, Society Experimental Stress Analysis and Iowa State Univ. Press), 1973.

15. Roberts, E., Jr., "Elastic Crack-Edge Displacements for the Compact Tension Specimen," Materials Res. & Standards, 9, 27 (1969).

16. Landes, J. D., and Begley, J. A., "Test Results from J Integral Studies - An Attempt to Establish a J_{IC} Testing Procedure," Private Communication from J. A. Begley to R. P. Reed, Cryogenics Division, NBS, Boulder, Colorado (1973).

17. Nachtigall, A. J., "Strain-Cycling Fatigue Behavior of Ten Structural Metals Tested in Liquid Helium (4 K), in Liquid Nitrogen (78 K) and in Ambient Air (300 K)," NASA TN D-7532 National Aeronautics and Space Administration, Washington, D.C. (1974).

18. Watson, J. F., Christian, J. L., and Hertz, J., "Selection of Materials for Cryogenic Applications in Missiles and Aerospace Vehicles," Rep. MRG-132-1, Convair Astronautics, San Diego, Calif. (1960).

19. Espey, G. B., Jones, M. H., and Brown, W. F., Jr., "Sharp-Edge-Notch Tensile Characteristics of Several High Strength Titanium-Sheet Alloys at Room and Cryogenic Temperatures," Amer. Soc. Testing Materials (ASTM) Spec. Tech. Pub. 287 (1960).

20. Warren, K. A., and Reed, R. P., "Tensile and Impact Properties of Selected Materials from 20 to 300°K," National Bureau of Standards Monograph 63 (June 28, 1963).

21. Hanson, M. P., Lewis Research Center, NASA, Cleveland, Ohio, private communication to T. F. Durham, National Bureau of Standards, Cryogenic Engineering Lab. (Div. 275.03), Boulder, Colorado (1959).

22. Guntner, C. J., and Reed, R. P., "The Effect of Experimental Variables Including the Martensitic Transformation on the Low-Temperature Mechanical Properties of Austenitic Stainless Steels," ASM Transactions Quarterly 55, 399-419 (1962).

23. Hoke, J. H., Mabus, P. G., and Goller, G. N., "Mechanical Properties of Stainless Steels at Subzero Temperatures," Metal Progress, 55, 643 (1949).

24. Kropschot, R. H., and Graham, W. F., "Mechanical Properties of the Austenitic Stainless Steels at Low Temperatures," National Bureau of Standards Technical Memorandum No. 39 (1956).

25. Desisto, T. S., and Carr, F. L., "Low Temperature Mechanical Properties of 300 Series Stainless Steel and Titanium," AD609909 (Watertown Arsenal Laboratories), (August 1960).

26. Basinski, Z. S., Proc. Roy. Soc. London, A240, 229 (1957).

27. Paris, P. C., and Erdogan, F., Journal of Basic Eng., Trans. of ASME Series D, 85, 528-534 (1963).

28. "Damage Tolerant Design Handbook" (A Compilation of Fracture and Crack-Growth Data for High-Strength Alloys), compiled by Metals and Ceramics Information Center, Battelle Memorial Institute, Columbus, Ohio (Dec. 1972).

29. Wei, R. P., and Ritter, D. L., N72-26435, NASA-CR-127042 (1972).

30. Bucci, R. J., Paris, P. C., Hertzberg, R. W., Schmidt, R. A., and Anderson, A. F., American Soc. Testing Materials (ASTM) Spec. Tech. Pub. 513 (1972), pp. 125-140.

31. Tiffany, C. F., and Lorenz, P. M., "An Investigation of Low Cycle Fatigue Failure using Applied Fracture Mechanics," Tech. Doc. Report No. ML-TDR-64-53, The Boeing Co., (May 1964).

32. Unpublished data from Boeing Co., Seattle, Washington.

33. Hall, L. R., "Plane-Strain Cyclic Flaw Growth, 2014-T62 Aluminum and 6Al-4V Titanium," N69-20265, NASA-CR-72396, Boeing Co. (Nov. 1968).

34. Witzell, W. E., "Fracture Data for Materials at Cryogenic Temperatures," AD 825264, General Dynamics/Convair (Nov. 1967).

35. Martin-Marietta Co., Denver, Colo. (Unpublished data).

36. Bixler, W. D., "Comparison of Flaw Growth Characteristics under Cryogenic Proof and Ambient Test Conditions for Apollo Titanium Pressure Vessels," N70-18309, Boeing Co. (Jan. 1970).

37. Vishnevsky, C., and Steigerwald, E. A., "Plane Strain Fracture Toughness of Some Cryogenic Materials at Room and Subzero Temperatures," Amer. Soc. Testing Materials Spec. Tech. Pub. 496 (1971), pp. 3-26.

38. Wessel, E. T., Clark, W. G., and Wilson, W. K., "Engineering Methods for the Design and Selection of Materials Against Fracture," AD 801500, Westinghouse Research Labs. (June 1966).

39. Witzell, W. E., "Fracture Mechanics - Plane Strain Characteristics of Several Materials," General Dynamics/Convair (Dec. 1967), AD 854 611 L.

40. Reed, R. P., Unreported data, NBS Cryogenic Engineering Division (1973).

41. Rice, I. R., and Rosengren, G. F., "Plane Strain Deformation Near a Crack Tip in a Power-Low Hardening Material," J. Mech. Phys. Solids, 16, 1-12 (1968).

42. Krafft, J. M., "Correlation of Plane Strain Crack Toughness with Strain-Hardening Characteristics of a Low, a Medium, and a High Strength Steel," Applied Materials Research, 3, 88-1011 (1964).

43. Nelson, F. G., Schilling, P. E., and Kaufman, J. G., "The Effect of Specimen Size on the Results of Plane Strain Fracture Toughness Tests," Engrg. Fracture Mechanics, 4, 33-50 (1972).

44. Golda, K. H., and Munz, D., "Effect of Specimen Thickness on Fracture Toughness of Ti-6Al-4V," Intn. J. of Fracture Mechanics, 8, 472 (1972).

45. Jones, M. H., and Brown, W. F., Jr., "The Influence of Crack Length and Thickness in Plane Strain Fracture Toughness Tests," Review of Developments in Plane Strain Fracture Toughness Testing, ASTM STP 463, (1970), p. 97.

Research Report 74-9D4-CRYMT-R1
Westinghouse Program 9D43-CRYMT
NBS Contract No. CST-8304

STRUCTURAL MATERIALS FOR CRYOGENIC APPLICATIONS

(First Semi-Annual Progress Report)

G. G. Lessmann, W. A. Logsdon, R. Kossowski,
M. P. Mathur and J. M. Wells

Westinghouse Electric Corporation
Research and Development Center
Pittsburgh, Pennsylvania 15235

March 1, 1974

This research was supported by the Advanced Research Projects Agency of the Department of Defense and was monitored by the Cryogenics Div., NBS, Boulder, CO under Contract No. CST-8304, Contract Amount $157K

Sponsored by Advanced Research Projects Agency ARPA Order No. 2569, Program Code No. 4D10

TITLE: Structural Materials for Cryogenic Applications
(First Semi-Annual Progress Report - March 1, 1974)

CONTRACTOR: Westinghouse Electric Corporation
Research and Development Center
Pittsburgh, Pennsylvania 15235

Westinghouse Program Manager: G. G. Lessmann (412) 256-3412

Westinghouse Principal Investigators:

Mr. W. A. Logsdon	(412) 256-3652
Dr. R. Kossowsky	(412) 256-3684
Dr. M. P. Mathur	(412) 256-3289
Dr. J. M. Wells	(412) 256-3633

Contract Start Date: September 10, 1973

Contract Expiration Date: September 9, 1974

TABLE OF CONTENTS

TABLE OF CONTENTS (CONTINUED)

LIST OF FIGURES

LIST OF FIGURES (CONTINUED)

LIST OF FIGURES (CONTINUED)

LIST OF FIGURES (CONTINUED)

LIST OF FIGURES (CONTINUED)

LIST OF TABLES

1.0 ABSTRACT

Progress in the first semi-annual period on NBS-Boulder Contract CST 8304 is reported. Results include preliminary data on the low temperature mechanical and magnetic performance of structural materials of interest in first generation rotating and stationary cryogenic hardware. A variety of common metallurgical conditions of these materials are included in this evaluation. This will assure that mechanical performance can be predicted and that structural reliability analyses can be extrapolated to advanced fabricated structures.

The materials being evaluated include OFHC copper and three austenitic alloys - AISI 310 stainless steel, Inconel X750 and Kromarc 58. Metallurgical-Structural variables include the wrought and heat treated forms resulting from cold work, stress relief, solution annealing, quenching, aging and sensitization to which these respective systems are exposed in routine processing for fabricated hardware.

Ingot consolidation practice is also being evaluated to provide flexibility in process selection and property control. Three melting practices are used singularly or in series including vacuum induction melting, arc melting and vacuum arc remelting. Conversion from powder to wrought structure by hot isostatic pressing is being evaluated as an alternative to casting.

Structural fabrication requirements are being screened by evaluating basic joining techniques. These are: gas tungsten arc welding, electron beam welding, soldering, brazing, shielded metal arc welding and gas metal arc welding.

The primary screening and alloy assessment technique is mechanical. Current fracture mechanics technology coupled with special low temperature test techniques and advanced analytic capabilities are

being exploited to provide the basis for optimized structural reliability in designing and building cryogenic structures. This systematic evaluation includes testing at RT, -320°F, and -452°F for tensile, notched tensile, fracture toughness - K_{IC}, J_{IC}, and fatigue crack growth rate behavior. This information will be used to demonstrate the principles, and technique for reliability analyses, and to predict future data base requirements for successful cryogenic design. A complete structural characterization of test materials is included for pre and post test evaluation. Hence, an assessment of structural effects on mechanical performance, and potential for improved metallurgical control of low temperature materials properties is being provided. A magnetic properties screening study is integrated into this analysis to assure that the austenitic alloys maintain their desirable magnetic and structural stability at low temperatures.

2.0 INTRODUCTION

Work described in this report represents the Westinghouse Electric Corporation contribution to the Advanced Research Project Agency program for Low Temperature Properties of Structural Materials. Program management is the responsibility of the Cryogenics Division of the National Bureau of Standards. Dr. Edward C. van Reuth is the ARPA sponsor while Dr. Richard P. Reed, NBS-Boulder, is overall program manager and Dr. Alan F. Clark, NBS-Boulder, is contract monitor.

The total program is divided into the general categories of mechanical properties, thermal properties, composites, data compilation and evaluation, and specialized structures. The program will continue for three years with annual reevaluation regarding program scope and participation. Table 2-1 indicates the first year's program, the research organizations doing the work and a brief description of each effort.

From a glance at the table it is obvious that the initial major effort is to provide low temperature fatigue and fracture data which are needed for current design. The effects of size, processing, and fabrication are also being pursued. Thermal properties are being measured early in the program for design data. The properties and potential applications of composite materials are being investigated as well as the effects of the dynamic loading of magnet materials. The accumulation and compilation of all this data are an essential part of the effort.

The output of the program is expected to take four forms: (1) Semiannual technical reports will be distributed to all the contractors as well as to ARPA and the various "user" groups in the agencies, (2) it is hoped that most data will be published in the open literature, (3) data

will be incorporated into the Handbook in the year subsequent to its generation, and (4) possibly a reference book, complementary to the Handbook, will be composed by contributions from each laboratory and edited by NBS.

The Westinghouse Electric Corporation responsibilities in the current year's effort are divided into three tasks:

Task I	Characterization of Current Cryogenic Structural Materials
Task II	Processing Effects on Properties of Structural Cryogenic Materials
Task III	Evaluation of Joints in Structural Cryogenic Materials

This progress report presents initial results of these three tasks based on the functional areas of investigation: materials, fracture mechanics, microstructural analysis, and magnetic properties. In addition to semi-annual progress reports, a tentative list of topical reports which are planned for release all or in part under this contract include the following:

- Materials Considerations for Structural Cryogenic Applications
- Low Temperature Mechanical Properties of Austenitic Alloys
- Low Temperature Mechanical Behavior of Joints in Austenitic Alloys
- Fracture Mechanics Reliability Analysis Relative to the 5 mVA - 12,000 rpm Generator, Reference Contract USAF, F33615-71-C-1591

TABLE 2-1

ARPA - Low Temperature Properties of Structural Materials

First Year Program (FY 74)

Program Area	Program Description
Mechanical Properties	
1. Fracture and Fatigue	
a. Materials Group (NBS-Cryogenics)	Fracture toughness, fatigue crack growth rate, fatigue, sustained load crack growth rate tests from 4-300 K on structural alloys.
b. Materials Group (Westinghouse)	Mechanical, magnetic, electrical loss characterization of alloys currently in use by Westinghouse in DOD sponsored programs. Mechanical tests include tensile, fracture toughness, fatigue.
c. High Load-Large Specimens (Martin-Denver)	Fracture toughness, fatigue crack growth rate data on very selected tough alloys requiring loads in excess of 30,000 lbs to fracture.
2. Effects	
a. Processing (Westinghouse)	Identification of effects of fabrication and processing techniques on mechanical properties of selected alloys. Variables include industrial melting practices, powder metallurgy techniques, and cold working.
b. Joining (Westinghouse)	Mechanical properties of fabricated metal joints, including welding (GTAW, EB, GMAW) brazing, and soldering from 4-300 K. Properties include tensile, notched tensile, fracture toughness, and fatigue crack growth rate.
3. Elastic Moduli, Tensile (NBS-Cryogenics)	Tensile and dynamic elastic (Young's, shear, bulk moduli) measurements on structural alloys from 4-300 K.
Thermal Properties	
4. Thermal Expansion, Specific Heat (Battelle)	Thermal expansion and specific heat measurements on selected insulations and structural alloys.
5. Thermal-Magnetothermal Conductivity (NBS-Cryogenics)	Thermal conductivity and thermal conductivity in magnetic fields up to 50 kilogauss from 4-300 K of structural alloys.
Composites	
6. Evaluation of Advanced Composites (NBS-Cryogenics)	Screening tests (tensile, fatigue at 4 K) on selected candidate metal and non-metal base composites, including B-epoxy, C-epoxy and polyimide, PRD 49-epoxy, borsic-Al, Steel-Al.

TABLE 2-1 (Continued)

Program Area	Program Description
7. Screening for Shield Materials (General Electric)	Screening study of composites for torque tube and electromagnetic shield applications.
Data Compilation and Evaluation	
8. Handbook (Battelle)	Publication of Handbook containing recommended best value data and complete set of references for 39 selected materials (structural alloys, superconductors). Data presented in graphical and tabular formats; mechanical, thermal, magnetic properties from 0-300 K.
Specialized Structures	
9. Effects on Magnet Materials (Argonne)	Characterization of change of electrical and mechanical properties of magnet materials as a function of fatigue and temperature.

3.0 SUMMARY

A test status summary for this entire program is shown in Table 3-1. This chart integrates the entire project into one test matrix showing both the anticipated level of testing in each catagory and the degree of completion. These are shown as fractions: one complete of two planned (1/2), none of 3 (/3), one of one (1/1) etc.

Essentially all materials are on hand although some still require special processing such as HIP consolidation of X-750 powder and drawing of Kromarc-58 wire for GTA welding. Otherwise the major portion of the metallurgical processing, including welding is complete.

Base metal mechanical behavior testing has been essentially completed to liquid helium temperatures, -452°F, for copper, 310S stainless steel, and X-750. A significant amount of weld testing is also complete. The processing variable tests and Kromarc-58 tests will be the last to be completed because of special handling requirements.

Using notched tensile test criteria, i.e. notched strength to tensile yield strength ratio, all three base metal materials exhibited ratios well in excess of 1.0 regardless of heat treatments with a minimum value of 1.6. All should be reasonably resistant to catastrophic fracture in service.

Copper proved to be extremely ductile throughout the temperature range. Hence, valid fracture toughness tests using either linear elastic or elastic plastic criteria could not be obtained. No further fracture toughness tests or copper base metal are necessary for 1/2 inch section size.

One inch compact tension specimens at -320°F and one-half inch specimens at -452°F yielded valid fracture toughness results for only one case in base metal tests of X-750 and 310 stainless steel. Hence, K_{IC}

values were obtained from elastic-plastic mechanics from crack growth initiation estimates or utilizing the J-integral resistance technique.

X-750 fracture toughness does not have much temperature sensitivity between -320°F and -452°F. The higher strength of the double aged material is achieved at some sacrifice in toughness relative to solution treated material.

The fracture toughness of 310S stainless steel base metal demonstrates a significant temperature dependence between -320°F and -452°F. Also, sensitization compromises fracture toughness.

Fatigue crack growth rate tests were completed for both conditions of X-750 and also solution treated 310S stainless steel base metal. Standard relationships were developed for fatigue crack growth as a function of stress intensity factor range at both room temperature and -452°F. No structural effect was noted for the different X-750 heat treatments.

Tensile and notch tensile properties of welds in X-750 and 310 stainless steel were determined from -452°F to room temperature. All 310 stainless steel specimens were tested as shielded metal arc welded whereas X-750 was tested with two pretreatments and one post weld heat treatment for both GTA and EB welds. Properties appear favorable but are more complicated to interpret than base metal tests. Weld evaluation and analysis will require supportive microstructural examination which is in progress.

Microstructural analysis of all tested materials are in progress. A systematic grain size influence has been identified for X-750 tensile specimens in which an inadvertant increase in size occurred for decreased test temperature. This resulted from specimen location in cutting blanks from the forging billet. This factor will be integrated into an analysis of overall results. The X-750 material deforms by homogeneous slip and fails by intergranular cracking at room temperature and below. Room temperature fatigue crack growth proceeds by crystallographic shear. At low temperatures, cleavage and intergranular cracking associated with carbide

precipitates has been observed. Significant differences in 310S stainless steel fracture mode accompanies sensitization with significantly increased intergranular fracture.

Preliminary results on magnitization measurements for X-750 and Kromarc-58 have been obtained. The Inconel X-750 samples are ferromagnetic while the Kromarc-58 samples remain either paramagnetic or are weakly ferromagnetic at 70 kOe and -452°F.

TABLE 3-1—SUMMARY PROJECT TEST MATRIX FOR STRUCTURAL MATERIALS FOR CRYOGENIC APPLICATIONS

Overall Program Status As Of March 1, 1974

Material Code	Condition	Chem. Analy.	Metallography (1)	Metallography (2)	Physical Prop. Mag.	Physical Prop. Res.	Processing	Joining	Tensile R	Tensile N	Tensile H	Notched Tensile R	Notched Tensile N	Notched Tensile H	K1C R	K1C N	K1C H	J_{IC} (3) R	J_{IC} (3) H	FCGR R	FCGR N	FCGR H	Fractography (4) R	Fractography (4) N	Fractography (4) H
OFHC-Cu																									
10XX	AR	/1	/1	1					1/1	1/1	1/1	1/1	1/1	1/1		1/2	1/2				/2	/3	1/1	3/3	3/3
11XX	SR		/1	1			1/1		1/1	1/1	1/1	1/1	1/1	1/1		/2	/2				/2	/3			3/3
12XX	GMAW		/2					/2	/2	/2	/2	/1	/2	/2		/2	/2					/2	/1	/1	/3
13XX	B		/2					/2	/2	/2	/2	/1	/2	/2		/2	/2						/1	/1	/2
14XX	S		/2					/2	/2	/2	/2	/1	/2	/2		/2	/2						/1	/1	/2
A1S1 310S																									
20XX	STQ	□/1	2/2	1	/2	/2	1/1		1/1	3/2	4/2	1/1	1/2	1/2	•/1	2/2	2/3			1	/2	2/3	1/2	1/3	1/3
21XX	STFC		1/1	1			1/1		1/1	1/2	2/2	1/1	1/2	1/2	•/1	2/2	2/3			/1	/2	/3	1/2	1/3	1/3
22XX	SMW		2/2		/1	/1	2/2	/2	2/1	2/2	2/2	2/1	2/2	2/2		/2	/3				/2	/2	/1	/3	/3
Inconel X750																									
30XX	ST	1/1	2/2	2	1/2	/2	2/2		1/1	2/2	2/2	1/1	2/2	2/2	•/1	4/2	2/3	4		2/2	/2	4/3	2/2	2/3	2/4
31XX	STDA		2/2	2	1/1	/1	2/2		1/1	2/2	2/2	1/1	2/2	2/2	•/1	4/2	2/3	5		2/2	/2	4/3	2/2	2/3	2/3
32XX	ST/EBW		2/3	1			3/3	3/3	1/1	1/2	1/2	1/1	1/2	1/2		/2	/2				1	2	1/1	1/2	1/2
33XX	STDA/EBW		2/3	1			3/3	3/3	1/1	1/2	1/2	1/1	1/2	1/2		/2	/2				/1	/2			1/2
34XX	EBW/STDA		2/3				3/3	3/3	1/1	1/2	1/2	1/1	1/2	1/2		/2	/2				1/2	2/2			/2
35XX	ST/GTW		3/3	1			3/3	3/3	1/1	1/2	1/2	1/1	1/2	1/2		/2	/2				1/2	2/2			1/2
36XX	STDA/GTW		3/3	1			3/3	3/3	1/1	1/2	1/2	1/1	1/2	1/2		/2	/2				1/2	2/2			1/2
37XX	GTW/STDA		3/3				3/3	3/3	1/1	1/2	1/2	1/1	1/2	1/2		/2	/2				1/2	2/2			/2
38XX	B		/2					/2	/2	/2	/2	/1	/2	/2		/2	/2							/2	/2
40XX	MP 2/STDA	■/1	/2				/3		/1	/2	/2	/1	/2	/2		/2	/2								/2
50XX	MP 3/STDA	■/1	/2				/3		/1	/2	/2	/1	/2	/2		/2	/2								/2
60XX ◊	HIP	1/2	1/2				1/2		/1	/2	/2	/1	/2	/2		/2	/2				/2	/2	/1	/2	/2
61XX ◊	HIP/STDA		/2				1/2		/1	/2	/2	/1	/2	/2		/2	/2				/2	/2			/2
Kromarc 58																									
80XX	STQ	1/2	1/2		1/1	/1	1/2		/1	/2	/2	/1	/2	/2		/2	/3			/2	/2	/3	/2	/3	/3
81XX	CW		1/2		1/1	/1	1/2		/1	/2	/2	/1	/2	/2		/2	/3			/2	/2	/3	/2	/3	/3
82XX ••	GTW	1/1	/2				/2	/2	/1	/2	/2	/1	/2	/2		/2	/3				/2	/2	/1	/3	/3
83XX	CW/GTW		/2				/1	/1	/1	/2	/2	/1	/2	/2		/2	/3								/2
84XX	GTW/CW		/2				/1	/1	/1	/2	/2	/1	/2	/2		/2	/2								/2
85XX	GTW/CW/AN		/2				/1	/1	/1	/2	/2	/1	/2	/2		/2	/2								/2

Notes: 1 Optical Microscopy

2 Replicate and Transmission Electron Microscopy, X-Ray Dispersive and Microprobe Analysis to be Incorporated as Required

3 Elastic-Plastic (J_{IC}) Testing and Analysis Techniques to be Incorporated Where Linear-Elastic (K_{IC}) Data Is Non-Valid

4 Macro-and Microfractographic (SEM) Examination Schedule to be Adjusted In Response to Exhibition of Unusual Material Behavior

• Available Specimen Size Invalid for Meaningful K_{IC} Interpretation - Test Eliminated

□ Certified Chem. Analysis Available from Supplier

■ Ditto-Additional Interstitial Analysis Completed at

◊ X750 Powder on Hand & Characterized, Two Initial Hip Tests Conducted, Specimens Being Evaluated

•• K58 Filler Wire Processing Revised, in Progress

4.0 PROJECT DESCRIPTION

This project represents the active participation of the Research Laboratories of the Westinghouse Electric Corporation in the Advance Research Projects Agency Program for Low Temperature Properties of Structural Materials.

The main objective of the first year program is to define and conduct a logical and well focused characterization and evaluation of materials in current use, including processing and fabrication considerations.

The application area for cryogenic structural materials requiring immediate attention is superconducting electrical machinery as typified by the two recent 5 MVA S.C. prototypes generators developed by Westinghouse. The first year's programs key-off typical materials requirements for these machines. Other cryogenic structural materials requirements which must be considered as this project progresses include electrical transmission lines, structures for superconducting magnet support for Controlled Thermonuclear Reactor (CTR) projects, and materials for more advanced rotating machinery designs.

The overall outline for the current Westinghouse portion of the NBS-ARPA program is shown schematically in Fig. 4-1. The principal personnel involved are listed in Fig. 4-2 according to respective functional project areas. This project is broken down into three tasks as follows:

Task I — Characterization of four materials currently being considered for superconducting machinery applications. These materials include OFHC Copper (102), 310 S Stainless Steel, Inconel X-750 Superalloy and Kromarc-58 Stainless Steel. An operational flow chart of Task I is shown in Fig. 4-3, while the test matrix is shown in Table 4-1.

Task II Evaluation of selected processing effects on the structure and properties of two representative structural materials being considered for cryogenic applications. These processing considerations include three different commercial melting practices of Inconel X-750, hot isostatically pressed (HIP) compaction of powder Inconel X-750, and the combined effects of cold working and welding in Kromarc-58 stainless steel alloy. An operational flow chart of Task II is shown as Fig. 4-4 and the test matrix in Table 4-2.

Task III Evaluation of selective joint fabrication methods in four materials for cryogenic applications. Joining techniques include shielded metal arc (SMA), gas metal arc (GMA), gas tungsten arc (GTA), vacuum electron beam (EB) welding, brazing and soldering. An operational flow chart of Task III is shown as Fig. 4-5 and the test matrix in Table 4-3.

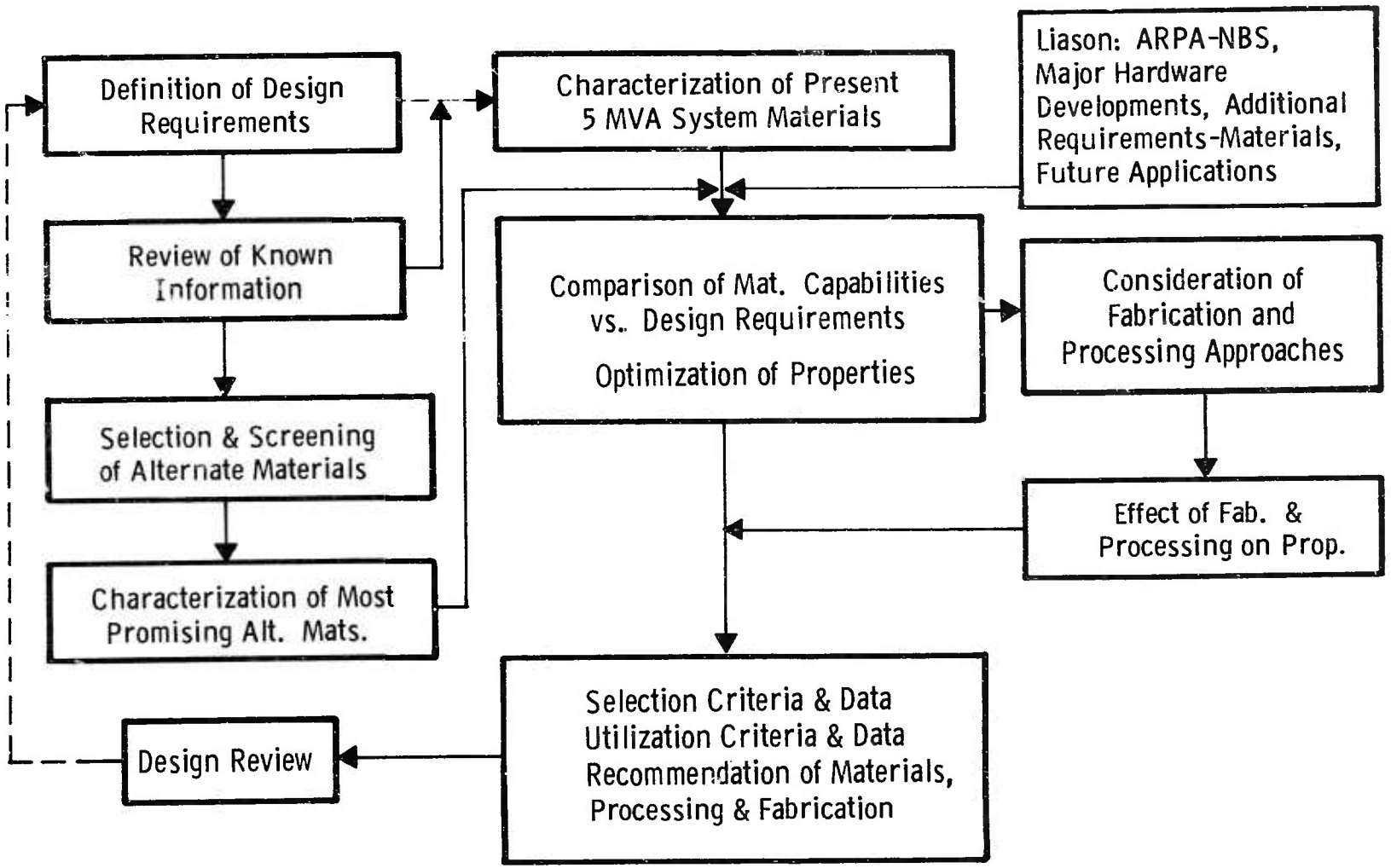

Fig. 4-1 Program Outline – Structural Materials for Cryogenic Applications

EVALUATION OF CRYOGENIC STRUCTURAL MATERIALS, NBS CONTRACT 8304

Functions	Task I Basic Characterization	Task II Processing Effects	Task III Joint Behavior
Metallurgy, Processing, Joining	•	•	•
Fracture Mechanics	•	•	•
Fractographic & Micro-Structural Analysis	•	•	•
Magnetic Properties	•		

Westinghouse Project Organization

Management	Principal Investigators
Project Manager - G. G. Lessmann Fracture Mechanics - E. T. Wessel	Materials, Fabrication, Processing - J. M. Wells Fracture Mechanics - W. A. Logsdon Microstructural Analysis - R. Kossowsky Magnetic Properties - M. P. Mathur

Fig. 4-2 Westinghouse Project Organization

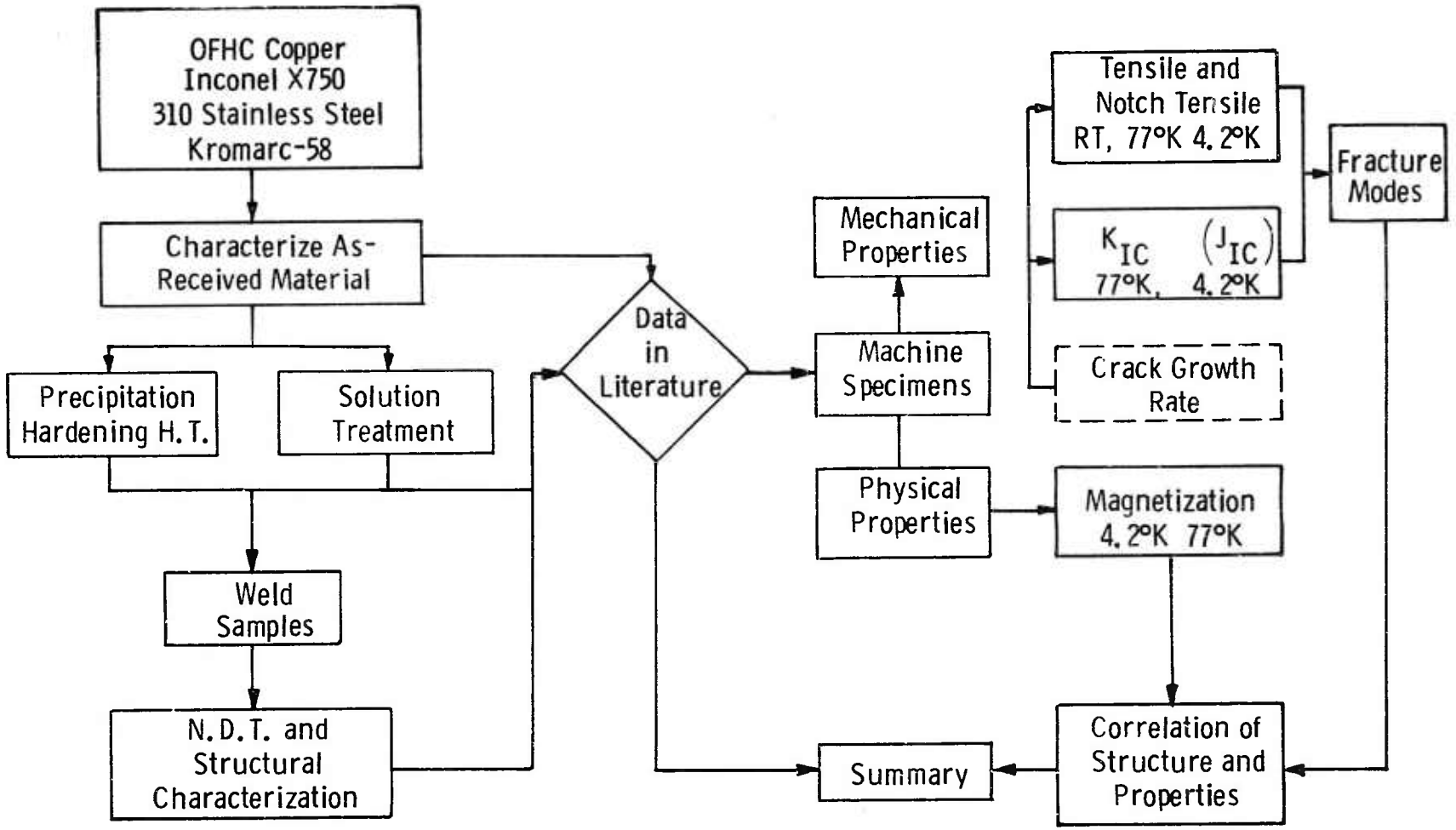

FIG. 4-3 TASK I—CHARACTERIZATION OF CURRENT CRYOGENIC STRUCTURAL MATERIALS.

Dwg. 7258194

TABLE 4-1 TASK I TEST MATRIX FOR MATERIALS CHARACTERIZATION

Material and Conditions		Mechanical and Fracture Mechanics Properties												Physical Properties		Structural Properties			
		Standard Tensile			Notched Tensile			Fracture Toughness			Crack Growth Rate			A-C Losses	Magnetization	Optical	Fractographic	Grain Size	Phase Stability
Material	Condition	75°F	−320°F	−452°F	75°F	−320°F	−452°F	75°F	−320°F	−452°F	75°F	−320°F	−452°F	4.2 − 77°K	4.2 − 77°K				
OFHC Copper	As-received	1	1	1	1	1	1		2	2		2	3	–	–	✓	✓	✓	✓
	Stress Relieved	1	1	1	1	1	1		2	2		2	3	–	–	✓	✓	✓	✓
310 Stainless Steel	Solution Treated and Water Quenched	1	3	2	1	3	3	1	2	3	1	2	3	2	2	✓	✓	✓	✓
	Sensitized	1	3	2	1	3	3	1	5	7	1	2	3	1	1	✓	✓	✓	✓
SMA	Weld ST-WQ/W	1	1	1	1	3	3			7									
Inconel X750	Solution Treat	1	2	2	1	2	2	1	2	3	2	2	3	2	2	✓	✓	✓	✓
	Solution Treat and Double Age	1	2	2	1	2	2	1	2	4	2	2	3	1	1	✓	✓	✓	✓
	GTA Weld St/W	1	1	1	1	3	3			6				–	–	✓	✓	✓	✓
	GTA Weld St-DA/W	1	1	1	1	3	3			6				–	–	✓	✓	✓	✓
	Electron Beam ST-DA/W	1	1	1	1	3	3			2				–	–	✓	✓	✓	✓
	Electron Beam W/ST-DA	1	1	1	1	3	3			2				–	–	✓	✓	✓	✓
Kromarc 58	Annealed	1	2	2	1	2	2		2	3	2	2	3	1	1	✓	✓	✓	✓
	Cold Worked	1	2	2	1	2	2		2	3	2	2	3	1	1	✓	✓	✓	✓
	AN/GTA Weld	1	1	1	1	2	2			3				–	–	✓	✓	✓	✓
	CW/GTA Weld	1	1	1	1	2	2			3				–	–	✓	✓	✓	✓

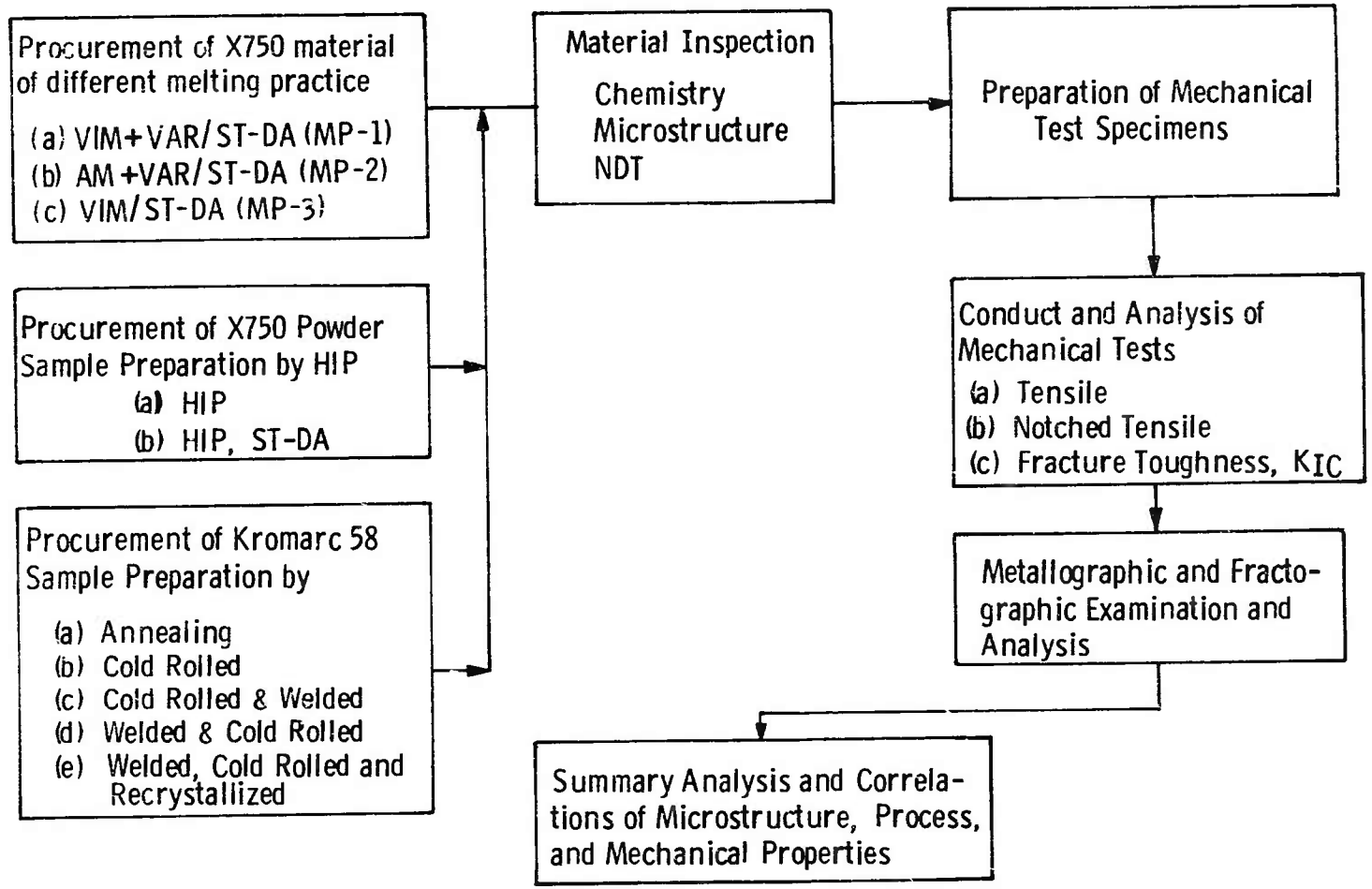

FIG. 4-4 TASK II–PROCESSING EFFECTS ON PROPERTIES OF STRUCTURAL CRYOGENIC MATERIALS.

Dwg. 7258193

TABLE 4-2 TASK II TEST MATRIX FOR PROCESSING EFFECTS ON MECHANICAL PROPERTIES TO 4.2°K

Material	Processing	Treatment	Tensile			Notch Tensile			K_{IC}	
			RT	77°K	4.2°K	RT	77°K	4.2°K	77°K	4.2°K
Inconel X750	VIM +VAR	ST-DA	1	2	2	1	2	2	2	2
	AM +VAR	ST-DA	1	2	2	1	2	2	2	2
	VIM	ST-DA	1	2	2	1	2	2	2	2
	HIP	As HIP	1	2	2	1	2	2	2	2
	HIP	ST-DA	1	2	2	1	2	2	2	2
Kromarc 58	Hot Rolled		1	2	2	1	2	2	2	2
	Cold Rolled (30%)		1	2	2	1	2	2	2	2
	Cold Rolled and Welded		1	2	2	1	2	2	2	2
	Welded and Cold Rolled Recrystallized		1	2	2	1	2	2	2	2

Note: VIM — Vacuum Induction Melted

AM +VAR — Air Melted and Vacuum Arc Remelted

VIM +VAR — Vacuum Induction Melted and Vacuum Arc Remelted

ST-DA — Solution Treated-Double Aged

Dwg. 7258081

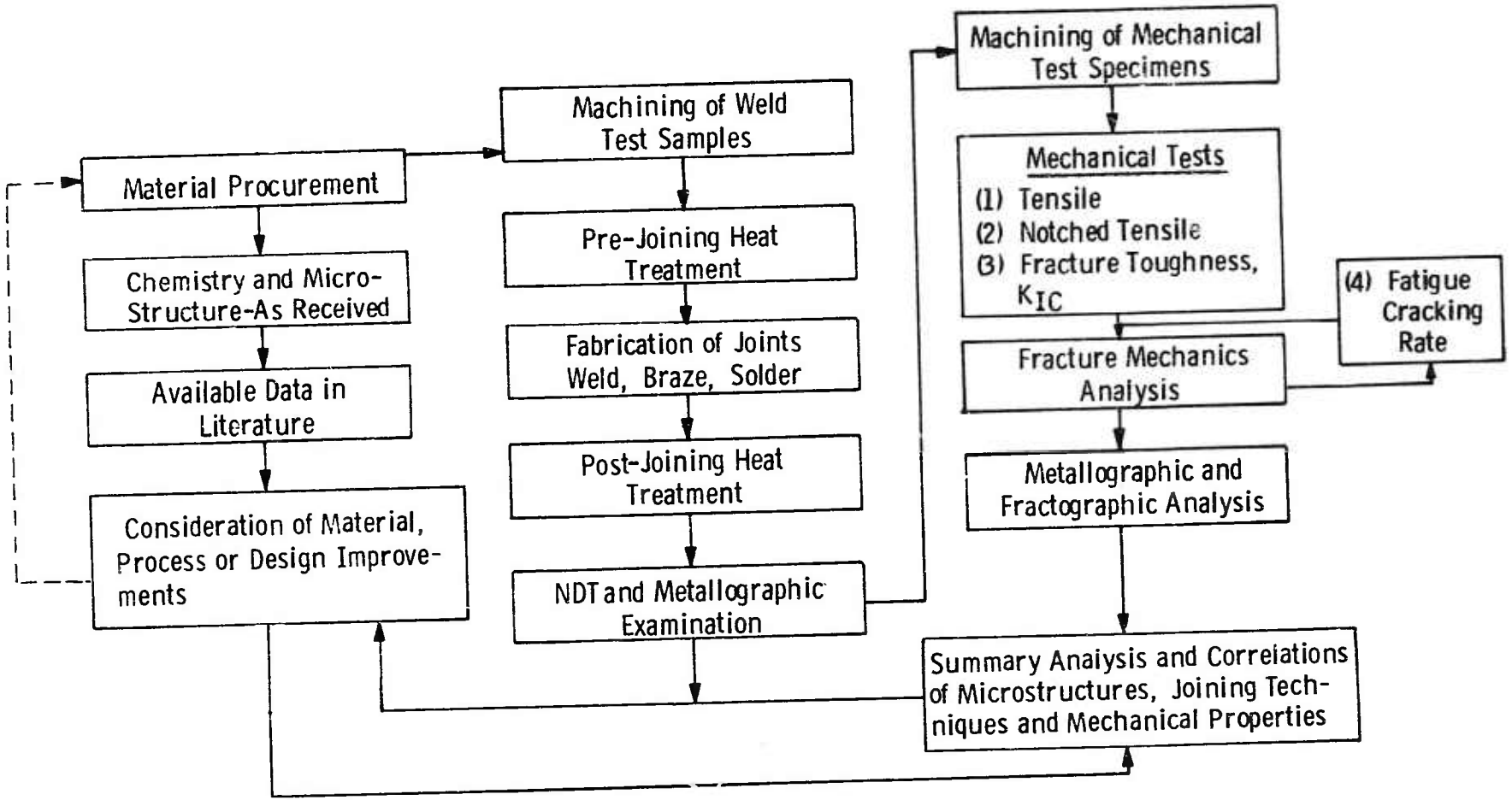

FIG. 4-5 TASK III—EVALUATION OF JOINTS IN STRUCTURAL CRYOGENIC MATERIALS

Dwg. 725B192

TABLE 4-3 TASK III TEST MATRIX FOR EVALUATION OF FABRICATED JOINTS TO 4.2°K

Materiai	Joint Condition	Treatment	Tensile			Notched Tensile			K_{IC}		FCGR	
			RT	77°K	4.2°K	RT	77°K	4.2°K	77°K	4.2°K	77°K	4.2°K
Inconel X750	GTA Weld (69F)	ST/W	1	2	2	1	2	2	2	2	2	2
		ST-DA/W	1	2	2	1	2	2	2	2	2	2
		W/ST-DA	1	2	2	1	2	2	2	2	2	2
	EB Weld	ST-DA/W	1	2	2	1	2	2	2	2	2	2
		W/ST-DA	1	2	2	1	2	2	2	2	2	2
	CU(102) Braze	ST/B	2	2	2	1	2	2	2	2		
AISI 310 S. S.	SMAW (E 310-16)	ST/W	1	2	2	1	2	2	2	2	2	2
Kromarc 58	GTAW (K58)	ST/W	1	2	2	1	2	2	2	2	2	2
OFHC Cu (102)	GMAW (RCu)	W/SR	2	2	2	1	2	2	—	2	—	2
	Braze	B	2	2	2	1	2	2	2	2	—	—
	Solder	S	2	2	2	1	2	2	2	2	—	—

Note: a. Numbers indicate minimum no. of samples per condition and test indicated for this program.

b. Treatment code ST = Solution treatment
ST-DA = ST + double age
W = Welded
B = Brazed
S = Soldered
SR = Stress Relief

c. FCGR—Fatigue Crack Growth Rate

5.0 GENERAL CRYOGENIC STRUCTURAL MATERIALS CONSIDERATIONS

Two primary catagories of cryogenic structural materials applications have been identified as:

- Rotating Machinery Components - generally high speed and highly stressed, such as the 5 MVA Superconducting Generator Rotor prototype built by Westinghouse for the USAF to operate at 4.2°K and 12,000 rpm (See Fig. 5-1)
- Static Support and/or Containment Structures - nominally low to moderately stressed, used as static S.C. magnet supports, cryogenic electrical transmission structures, and structural components of large S.C. magnetic field particle accelerators or nuclear fusion test assemblies.

A specific cryogenic structural application often requires unique design constraints on materials. It does not appear that all the cryogenic materials information required by designers will be readily available in the near future. However, the need for such information becomes appreciably more evident as cryogenic or superconducting devices are more frequently being considered as viable approaches to difficult engineering tasks. In addition to identifying, generating, cataloging and disseminating such cryogenic materials information, a concerted effort is required to introduce and maintain an effective information feedback loop. This loop once established with cryogenic system designers and fabricators, ensures the cryogenic materials data available is timely, relevant and sufficiently detailed to achieve the ultimate objective of failure-safe performance.

Considerable information is available (1-12) concerning general mechanical and physical properties of materials at cryogenic temperatures. However, most materials of present and future interest are

still inadequately characterized for full confidence in selection and utilization in potentially high risk cryogenic application areas where failure-safe performance is required, such as high speed rotating equipment and high radiation level controlled thermonuclear reactor systems. Some areas in which much of the existing cryogenic materials data presently available is found lacking are the following:

- Many materials of interest to this program were developed for high temperature applications and have had little if any cryogenic property data available.
- Of the materials which have been somewhat catagorized, only limited data is available of direct engineering applicability in areas of fracture toughness and fatigue crack initiation and propagation rates at room temperature; such data was virtually non-existant for extreme cryogenic temperatures.
- Available cryogenic data for many materials pertains to thin sheet material and is not necessarily representative of larger structural components.
- Available cryogenic materials property data often do not extend to liquid hydrogen (20°K) or to liquid helium (4.2°K) temperatures. Assumptions or extrapolations to these temperatures are not always justified.
- Effects of various yet specific materials processing techniques (both those in common commercial practice as well as new developmental approaches) generally have not been evaluated with respect to cryogenic properties.
- Effect of fabrication and joining processes (again both those in common commercial practice as well as newer advanced fabrication and joining approaches) has been a similarly neglected area.

- Effect of special enviornmental considerations such as accumulated radation damage on cryogenic structural materials properties is likewise an inadequately documented area.
- Materials other than metals such as ceramics, metal and epoxy matrix composites, fiberglass, plastics and superconducting elements themselves, are all inadequately characterized for structural applications at extreme cryogenic temperatures.

5.1 Materials Selection

5.1.1 Establishment of Selection and Utilization Criteria

Criteria for selection and utilization of structural materials for cryogenic applications will depend on both the primary application catagory and the specific design requirements of a particular device. The main objective in establishing selection and utilization criteria is to define minimum acceptable materials properties achievable in the final product upon which specific designs can be based and cryogenic equipment performance predicted with maximum confidence. With cryogenic devices of a significant level of sophistication, a failure safe design criterion (13-18) is generally necessary to ensure an economical and logical engineering approach to produce a safe, reliable structure or device with predictable performance to minimize downtime and repairs.

The traditional mechanical properties of materials such as yield and ultimate tensile strengths, % elongation and % R.A., notched tensile strength and charpy impact strength, are, of course, useful in screening materials for selection and monitoring process and fabrication effectiveness. However, such mechanical properties do not provide the designer with sufficiently quantitative capability of assessing damage tolerance, i.e. the impact of a given defect in a selected material on structural performance under operating conditions. Consequently, a need has evolved for the employment of Fracture Mechanics Technology in evaluating the fracture toughness and fatigue crack growth rate properties of materials for cryogenic structures. Combined with advanced metals

fabrication and processing techniques and non-destructive testing techniques to evaluate existing defects in such materials or structures, fracture mechanics should assist in establishment and evaluation of better design/materials criteria.

Physical properties as well will play a significant role in establishing materials criteria. Low thermal conducting materials are required to minimize undesirable thermal leaks into cryogenic systems, whereas high thermal conductivity materials may be required for specific thermal equilibration applications. Specification of electrical conductivity, specific heat, thermal expansion and magnetic permeability and magnetic saturation levels may also be required.

Structural stability to the lowest cryogenic temperatures in terms of dimensional stability, mechanical strength and magnetic stability may likewise be critical in some applications. Other factors which one should consider in selecting or utilizing cryogenic materials include formability, weldability, machinability, cost, shape and size availability and material variability between suppliers or between heats from a given supplier.

Therefore, materials selection and utilization criteria must encompass all of the above considerations, with the appropriate weighing or priority factor assigned for the particular component requirements in a given structural design. Also, alternative materials should be identified in the event the optimum designated material is not available for sundry reasons.

5.1.2 Candidate Materials for Structural Cryogenic Applications

An initial list of candidate materials for structural cryogenic applications is enclosed as Table 5-1. The major metals classifications addressed are:

- Austenitic Stainless Steels
- Iron Base Superalloys
- Nickel Base Superalloys
- Other Superalloys

- Low Expansion Alloys
- Titanium Alloys
- Aluminum Alloys
- Copper and Copper Alloys

One consideration in establishing this tentative listing was to initially avoid materials known to experience a ductile to brittle transition at temperatures near or above that of liquid nitrogen (77°K). Consequently, conventional ferromagnetic alloy steels (19), high strength maraging steels (20-21), and up to 9% nickel alloy steels (22-24) were not included in Table 5-1. Certain cryogenic applications may nevertheless exist, where these alloys might prove suitable, as for example, where localized and/or shaped magnetic flux concentrations are desirable or where stress levels are sufficiently low to preclude the occurrance of brittle fracture.

Austenitic stainless steels appear attractive as candidate cryogenic structural alloys (25-32) in that they generally retain good ductility and toughness to extreme cryogenic temperatures. The yield strength level of these alloys is generally low to moderate at room temperature and increases markedly with decreasing temperature. Many austenitic alloys are reported to be either structurally and/or magnetically unstable at very low temperatures which may present significant problems. Reed and Mikesell (27) have shown a paramagnetic austenite to ferromagnetic α' martensite transition at low temperature for 304 stainless steel. Nachtigal (28) has also shown, for example, that 304L stainless steel does not remain fully austenitic, but undergoes an austenite transformation to α' martensite at liquid helium temperature whereas 310S stainless steel with approximately twice the yield strength and elongation of 304L, was found to remain fully austenitic, i.e. structurally stable. Larbalestier and King (29-31) also have shown that 304 becomes structurally unstable at low temperatures and furthermore that 310S stainless, although apparently structurally stable even after deformation to rupture at 4.2°K, is associated with a paramagnetic-ferromagnetic transition which occurs within the austenite phase.

Interestingly, these latter authors found that Kromarc 55 experienced neither a structural instability after deformation to fracture at 4.2°K nor a magnetic transition to ferromagnetic behavior. Kromarc 58, a wrought version of the Kromarc 55 cast alloy, developed by Westinghouse (32), therefore, offers the potential of being a unique stainless alloy possessing both complete structural and magentic stability to liquid helium temperature.

While Iron, Nickel and Cobalt base superalloys were developed for high temperature applications beyond the useful range of stainless steels, consideration has been previously given to using some austenitic superalloys as cryogenic structural materials (33-38). These alloys have considerably higher strength levels than the austenitic stainless steels and yet remain relatively ductile at low temperatures.

Low expansion alloys (39-42) have definite potential for certain cryogenic structural applications. Normal Invar type alloys (Fe-36Ni) have controlled low thermal expansion characteristics and are magnetic below their curie temperature (530°F) but have moderately low room temperature yield strengths (40,000 psi) and are non-hardenable by standard heat treatments. At least two age hardenable low expansion alloys have been developed by Inco which may be extremely useful for cryogenic application.

(1) Incoloy Alloy 903 (40-41) - a precipitation-hardenable nickel-iron-cobalt alloy has coefficient of thermal expansion of approximately 4×10^{-6} in./in./°F and is hardenable to a room temperature yield strength of 160,000 psi.

(2) An Unnamed Inco Alloy (42) - an age hardenable low expansion alloy developed specifically for cryogenic applications. This alloy has a coefficient of thermal expansion of about 1.7×10^{-6} in./in./°F and is hardenable to a room temperature yield strength of 140,000 psi.

Various titanium alloys have been explored for cryogenic applications and indicate considerable potential (43-46). However, while Goode et al. (46-54) have already considered titanium alloys for fail-safe design in structural applications using fracture toughness characterization, this effort needs to be extended to extreme cryogenic temperatures and to include fatigue crack growth rate data to be more effective.

Considerable interest has also been shown in evaluating aluminum alloys for cryogenic structural applications (47-55). One particular aluminum alloy, Reynolds X2048, has recently been announced (51,52) to have markedly improved fracture toughness (approximately 50% greater than 2024). Containment vessels for LNG transport and storage systems is one of several high interest areas at present. Once again, Goode et al. (53,54) have already considered various aluminum alloys for failure-safe design in structural applications using fracture toughness characterization, but with emphasis other than at cryogenic temperatures and with fatigue crack growth rate considerations.

Copper and copper alloys have been investigated by Reed and Mikesell (55) for low temperature mechanical properties and found in general, to improve with decreasing temperature. Little cryogenic property data, however, is available on high conductivity, high strength, heat treatable or dispersion strengthened copper alloys such as those shown in Table 5-1.

Finally, various non-metallic materials such as selected polymers (57) and glass fiber reinforced polymer materials (58-61) have been considered for cryogenic applications. Although not included in the tentative materials listing in Table 5-1, these materials may be very useful in certain cryogenic applications.

5.1.3 Initial Program Materials Selection

The materials selected for inclusion in this FY 74 Westinghouse portion of the ARPA Program are:

(a) OFHC Copper (CDA No. 102)

(b) 310S Stainless Steel

(c) Inconel X750 Nickel Base Superalloy

(d) Kromarc 58 Stainless Steel

The first three of these wrought alloys have been employed extensively in the cryogenic machinery hardware components of two Westinghouse prototype 5 MVA Superconducting Generators. The Kromarc 58 is a wrought version of the cast Kromarc 55 stainless steel used extensively in large bubble chambers.

Because of the exigent nature of the earlier S.C. machinery prototyping effort, the selection of the above initial structural materials, as well as the associated processing and fabrication techniques, was made on a conservative and best-information-available basis. It should be clearly noted that these initial candidate materials were not established as the optimum structural materials for that application. At present, it can only be asserted that these materials did prove to be satisfactory, as demonstrated by actual proof tests of specific S.C. machine prototype designs under dynamic loading and cryogenic operating conditions.

The additional and more detailed information on the alloys resulting from this program should assist in establishing a more complete baseline status for materials selection and utilization criteria for cryogenic structural materials for discrete applications. This baseline status provides a basis upon which further improvements will be made to allow identification and effective design exploitation of optimum cryogenic structural materials. The test specimen identification system established for this program is described in Table 5-2.

The chemical composition of the initial candidate materials presently being evaluated in this program are shown in Table 5-3. Further materials documentation information is provided in Table 5-4.

5.2 Materials Processing Considerations

The characterization and evaluation of materials for cryogenic structural applications is sometimes conducted on material samples unjustifiably assumed to be fully representative of finished material components or structures. To be fully justified in attributing materials properties obtained from laboratory test data to actual structural components, the effects of various primary and secondary processing and fabrication steps either in current practice or those being considered by rationale of performance or cost improvements, must be adequately evaluated. A "full" evaluation can readily extrapolate to an almost infinite number of parametric combinations and often, depending upon the extent of the application and the level of acceptable risks, cannot be economically justified. Nevertheless, the concept of a failure-safe design may prove meaningless without adequate definition and evaluation of those process and fabrication effects which may indeed significantly alter the performance of structural components in cryogenic service to an unacceptable level beyond that predicted. Therefore, one key approach to this situation is to conduct an exploratory, yet well focused evaluation of basic processing and fabrication techniques to determine their effects on the cryogenic behavior of selected candidate materials. The results from such an evaluation thus provide a more comprehensive and logical basis for selecting and utilizing processing and fabrication technology as well as materials.

Three metals processing areas have initially been identified as warranting investigation as to their possible deleterious or beneficial effects on the mechanical behavior of strucutral components at cryogenic temperatures. These areas include:

- Contemporary melting practices of Inconel X-750
- Hot Isostatic Pressing (HIP) of Inconel X-750 powder
- Cold Working of Kromarc 58 stainless steel

5.2.1 Contemporary Melting Practices of Inconel X-750

Consideration of various combinations of contemporary melting practices is required if control of starting material quality is to be exercised. Differences in trace element (solid) impurity concentration, distribution and configuration as well as residual gas content may be encountered from different melting practices and may exert substantial effects on subsequent processing steps as well as on final material component service performance.

In this program, a single material Inconel X-750 was selected with which to evaluate various commercial melting practices. Melting practices for superalloy materials were recently reviewed by Cremisio (62). The materials available and obtained for this program selection are as follows:

- MP-1 Vacuum Induction Melted followed by Vacuum Arc Remelt (VIM-VAR)
- MP-2 Air Arc Melted (Electric Furnace) followed by Vacuum Arc Remelt (AAM-VAR)
- MP-3 Vacuum Induction Melted Only (VIM)

The chemical compositions and other documentation data for these materials are included in Tables 5-3 to 5-6. All Inconel X-750 data contained in this report other than that explicitly labeled MP-2 or MP-3, pertains to the MP-1 (VIM-VAR) Inconel X-750. Only one heat treatment (STDA) is considered for MP-2 and MP-3, whereas MP-1 is being evaluated in several heat treatment and welded conditions. An additional melting practice for Inconel X-750 of interest to this program but not readily available when the above alloys were procured, is Electroslag-Remelted material (ESR or EFM).

5.2.2 Hot Isostatic Pressing of IN X-750 Powder

Conventional IN X-750 billet material in large section sizes is often found to contain a significant grain size distribution (See Section 7.3). This material, being an austenitic superalloy, does not

undergo grain refinement through simple thermal treatment alone but rather requires plastic deformation and subsequent recrystallization. Such mechanical-thermal treatments are possible, of course, but may be impractical for some component configurations. Consequently, consolidation of IN X-750 powder through Hot Isostatic Pressing (HIP) is being investigated as another means of providing a fine, uniform grained microstructure in this material. It is quite probable that such fine grained material is advantageous in cryogenic mechanical behavior. Additional advantages to HIP processing may include: (1) Minimum scrap generation with high cost materials, (2) reduction of additional processing costs such as rough machining by initially arriving at close to finish machined component sizes, and (3) minimizing segregation and residual stress gradients.

A quantity of Inconel X-750 Powder was manufactured with the inert gas atomizing process by Federal Mogul. The starting material was IN X-750 MP-1 billet stock. Characterization data for the as-received powder is listed in Table 5-7. Scanning electron micrographs of the as-received powder are shown in Fig. 5-2. Two initial processing (HIP) conditions of the powder were selected as follows:

1. HX-1 1120°C and 10,000 psi (Argon)
2. HX-2 1200°C and 10,000 psi (Argon)

Samples consisting of powder in evacuated and backfilled 1/2" diameter 304 Stainless Steel tubes were seal welded and hipped at these selected conditions. Segments from these samples were given the standard X-750 STDA heat treatment. Microstructures of these initial hipped samples are shown in Fig. 5-3. Further examination of these samples with SEM is planned to evaluate these microstructures for evidence of microporosity or poor interface bonding. Upon satisfactory evaluation of hipped microstructures, sample plates approximately 4" x 12" x 5/8" thick will be hipped at the best selected HIP conditions for further materials property characterization.

5.2.3 Cold Working of Kromarc 58 Stainless Steel

Cold working, i.e. plastic deformation well below the normal recrystallization temperature, is one practical way of modifying the microstructure and strength of both parent base material and weldments. Kromarc 58, being a fully austenitic stainless steel, is not hardenable by thermal treatment and consequently is an excellent material with which to evaluate the effects of cold working on strength and fracture toughness at cryogenic temperatures.

Samples of Kromarc 58 from Westinghouse R&D Stock were cold reduced in thickness by 30% to significantly work harden this material at room temperature. Microstructures of the starting material, solution treated and quenched (STQ), and 30% cold worked K-58 material (both longitudinal and transverse sections) are shown in Fig. 5-4. Additional samples are to be welded, both prior to and following cold working, and will also be further characterized for low temperature mechanical behavior.

5.3 Materials Fabrication Considerations

Superconducting generators apparently introduce more severe low temperature dynamic service requirements than are encountered in most other cryogenic structural applications. In particular, the various structural components of the cryogenic rotor assembly are highly stressed components rotating at 3600 to 12,000 rpm and subjected to 4.2°K. Materials for such components in the final fabricated assembly must possess reliable and predictable cryogenic properties to attain the design objective of failure safe service performance. Unfortunately, relatively little is known concerning the mechanical behavior of dynamically loaded fabricated joints at 4.2°K. Mechanical property degradation of materials evidenced by reduced strength, ductility, fracture toughness and fatigue crack growth rate can occur through microstructural alterations associated with a cast weld fusion zone and the associated heat affected zones. In addition, discrete joint discontinuities or defects may be introduced such as incomplete fusion or bonding, macro-cracking, microfisuring, and porosity as well as significant residual stress levels.

5.3.1 Fusion Welding

A good description of fusion welding considerations with stainless steels is available (63-69). Two major considerations with austenitic stainless steels is the avoidance of hot cracking (or microfisuring) and avoidance of grain boundary sensitization.

One approach to avoid or control microfisuring is to ensure a minimum weldment ferrite level of approximately 3% (66). However, this approach is not acceptable for applications where fully nonmagnetic properties are desired or required. Another approach is to maintain the sulphur and phosphorous impurity content, to say below .015% for fully austenitic Type ER 310 Weld metal (67). A third approach to minimizing microfisuring is to use an alloy with major composition modification such as Kromarc 55 or 58 (68) where addition of elements such as manganese and molybdenum reduces the tendency for hot cracking. The superior resistance of Kromarc 55 to hot cracking was a major selection criteria in the bubble chamber application (69).

Methods available to minimize grain boundary sensitization in austenitic stainless steel nominally employ either the use of carbide stabilizing elements such as Niobium (Columbium) or the use of low carbon versions (310S) of conventional stainless alloys. In either case, it is desirable to employ a welding technique, such as minimizing heat input, to cool rapidly through the intergranular carbide precipitation temperature range of 800 to 1600°F. The Kromarc 58 alloy employed in this program has a low carbon concentration of .03% and the K-58 weld filler metal has an order of magnitude lower carbon content. At present the Kromarc 58 weldments of this program have not been completed. The macro-and micro-structure of a typical SMA weldment in 310S are shown in Fig. 5-5.

Nickel Superalloy fusion welding considerations have been well reviewed in the literature (70-74). Strain-age cracking in precipitation-hardenable, nickel-base alloys is a form of intergranular fracturing

which sometimes occurs with components containing residual stresses when post-weld heated through the precipitation reaction thermal range. This problem can generally be eliminated by either avoiding a thermal exposure of the material to the aging temperature or by preceeding any subsequent thermal aging exposure with a full solution treatment which provides an effective stress relief. Consequently, strain-age cracking has not been experienced in the fabrication of the prototype cryogenic machinery.

Microfisuring, a second problem typical of these nickel base superalloys has been experienced in this program to date, however. A microfisure is basically a small intergranular crack usually extending only one or two grains in extent and localized in the heat-affected zone (HAZ) immediately adjacent to the weld fusion zone. Such microfisures are attributed to partially liquated grain boundaries and have been extensively reported in alloy 718 (71, 73).

Examples of microfisures experienced with the Vacuum EB weldments of Inconel X-750 in this program are shown in Fig. 5-6. The major liability of such microfisures is whether they will propagate under fatigue loading conditions in cryogenic service. Such information is being sought in the K_{IC} and FCGR tests of X-750 weldments in this program. The general microstructures of a typical weldment fusion zone, heat affected zone and base metal of Vacuum Electron Beam and Gas Tungsten Arc weldments in IN X-750 are shown in Figs. 5-7 and 5-8, respectively.

There is apparently little information available (75) concerning the mechanical property behavior of copper and copper alloy weldments at cryogenic temperature. Although the base metal OFHC copper is quite ductile and tough, no cryogenic fracture toughness data is known available concerning a weldment for this material. Such a weldment is being prepared and the evaluation of this material will be reported later.

5.3.2 Brazing and Soldering

Little information appears available concerning the mechanical behavior of brazed joints under cryogenic service conditions. Several references (76-82) have, however, been located and reviewed concerning the mechanical behavior of commercial solder materials at cryogenic temperatures. In general, soldered joints behave in a manner similar to the solder base metals, i.e. increasing tensile and shear strength with decreasing ductility is experienced with decreasing temperature. Thin brazed or soldered joints may experience a restriction in reduction of area or elongation through a triaxial tensile stress condition and consequently attain a higher fracture stress than indicated by simple base solder or braze metal tension tests. However, the reliability of property data for brazed or soldered joints is often considerably less than that for parent braze or solder metal due to the many fabrication variables introduced into making a specific joint. Consequently, while the information found available is quite helpful, direct testing of solder joints for particular base metal-solder joint configurations fabricated under specific procedures should be conducted for assurance of compliance with specific critical design requirements.

Overall, the following aspects of cryogenic behavior of solder materials are summarized:

- Many solders are apparently quite sensitive to strain rate, more so at room temperature than at cryogenic temperatures (81, 82). Tensile and shear strength of commercial solders vary appreciably with chemical composition as well as with temperature. Strength of tin-lead solders increases with increasing tin and solders containing appreciable amounts of Ag, Bi, Cd, In and Sb are stronger yet than Sn-Pb solders (81, 82).

- Ductility (elongation and reduction of area) of solders is also quite dependent on strain rate, chemical composition and temperature. A commonly used 60 Sn-40 Pb solder, although quite strong (19,800 psi UTS) at -423°F was found (81) to have zero ductility at this temperature. Other solders, such as 10Sn-90Pb and 1Sn-97.5Pb-1.5Ag, although lower in tensile strength (11,300 and 13,300 psi, respectively), had a measured elongation of 14% and a reduction of area of about 40%. Consequently, these latter two

solders appear more suitable for extreme cryogenic temperature applications where brittle fractures are to be avoided.

- Allotropic phase transformations at low temperatures are generally undesirable, both from the standpoint of introduction of brittle phases and of introducing large strain energies through specific volume changes. A phase transition is reported in tin (83) which may transform from the Beta or white phase (A5-body centered tetragonal) to the Alpha or grey phase (A4-diamond cubic structure). This transformation in pure tin occurs at a maximum rate at about -40°C by a nucleation and growth mechanism which involves a diffusional incubation period that would be considerably lengthened at 4.2°K. This transformation is retarded by soluble impurities such as lead, bismuth, antimony and thallium, enhanced by elements of diamond structure such as germanium and silicon and also enhanced by plastic deformation at low temperatures. An important point to be made is that although much concern has been expressed with this transformation in high tin solders, no evidence of this transformation has been found with commercially available solders (78, 80). Of greater practical concern is the large intrinsic loss of ductility with decreasing temperature of high tin containing solders which have <u>not</u> experienced the Beta to Alpha transition.

- Toughness, defined by Christian (81), as the ability of solders to resist brittle fracture has received some, but inadequate, attention. Ductility measurements on base solder metals have received the most emphasis and was discussed above. The application of linear elastic or elastic-plastic fracture mechanics techniques on soldered joints should be thoroughly evaluated. The only published attempt at using this technique known to the author was reported by Reichenecker (79). This brief exploratory effort was limited to room temperature conditions and should be extruded to 4.2°K.

- Thermal cycling of soldered joints form 78 to -320°F with only 2 to 8 cycles was found (81) to result in a significant decrease of tensile strength and increase in scatter for 50Sn-50Pb soldered joints, but not for 35Sn-65Pb or 25In-75 (Sn+Pb). Loss of interface adhesion on thermal expansion and contraction possibly through fatigue may be a contributing failure mechanism to be addressed for cryogenic applications.

References

1. Anon., "Mechanical Properties of Metals at Low Temperatures," NBS Circular 520, U.S. Dept. of Commerce, 1952.

2. R. M. McClintock, and H. P. Gibbons, "Mechanical Properties of Structural Materials at Low Temperatures,", NBS Monograph 13, U.S. Dept. of Commerce, 1960.

3. H. Hamilton, and M. Katcher, "Which Metals for Cryogenic Applications," Materials in Design Engineering, May, 1964, p. 83.

4. Anon., "Low Temperature Mechanical Properties of Various Alloys," NASA SP-5921 (01), 1970.

5. H. L. Martin, et al, "Effects of Low Temperatures on the Mechanical Properties of Structural Metals," NASA SP-5012 (01), 1968.

6. C. Perry, and R. Irving, "Aerospace Alloys March into New Markets," Iron Age, Jan. 13, 1972, p. 49.

7. F. R. Schwartzberg, R. D. Keys, and T. F. Kiefer, "Cryogenic Alloy Screening," NASA CR-72733, Nov. 1970.

8. F. R. Schwartzberg, et al, "Cryogenic Materials Data Handbook, ML-TDR-64-280, (AD 609562), Aug. 1964.

9. J. F. Watson, "Properties of Engineering Materials at Extreme Sub-zero Temperatures with Supplementary Information on Liquid Hydrogen," General Dynamics, Astronautics Div. Report ENG-44, Dec. 8, 1958.

10. E. T. Wessel, "Some Basic and Engineering Considerations Regarding the Fracture of Metals at Cryogenic Temperatures," ASTM STP 387, Am. Soc. Testing Mats., 1966, p. 32.

11. E. T. Wessel, "The Relationship of the Low Temperature Behavior of Metals to the Structural and Mechanical Effects of Repeated Cooling," Westinghouse Scientific Paper 8-0103-P9, Nov. 1958.

12. C. Vishnevsky, and E. A. Steigerwald, "Plain Strain Fracture Toughness of Some Cryogenic Materials at Room and Subzero Temperatures," ASTM STP 496, (1971), p. 3-26.

13. W. S. Pellini, "Principles of Fracture-Safe Design - Part I," Welding Journal, Vol. 50, No. 3, March 1971, p. 91-S.

14. W. S. Pellini, "Principles of Fracture-Safe Design - Part II," Welding Journal, Vol. 50, No. 4, April 1971, p. 147-S.

15. F. M. Burdekin, "The Practical Application of Fracture Tests to Prevent Service Failures," Welding Journal, Vol. 47, No. 3, March 1968, p. 129-S.

16. W. S. Pellini, "Design Options for Selection of Fracture Control Procedures in the Modernization of Codes, Rules, and Standards", and "Analytical Design Procedures for Metals of Elastic-Plastic Fracture Properties," WRC Bulletin No. 186, August 1973.

17. W. G. Clark, Jr., "Fatigue Crack Initiation and Growth Properties as Materials Selection and Design Criteria," Westinghouse Scientific Paper 73-1E7-MSLRA-P2, November 1973.

18. E. T. Wessel, et al, "Engineering Methods for the Design and Selection of Materials Against Fracture," Westinghouse Report 66-9B4-315-R1, June 1966.

19. W. S. Pellini, and F. J. Loss, "Integration of Metallurgical and Fracture Mechanics Concepts of Transition Temperature Factors Relating to Fracture-Safe Design for Structural Steels," WRC Bulletin No. 141, June 1969.

471<

20. A. M. Hall, and C. J. Slunder, "The Metallurgy, Behavior, and Application of the 18-Percent Nickel Maraging Steels", NASA SP-5051, (1968).

21. D. L. Corn, "Cryogenic Properties of 18Ni-9Co-5Mo and 18Ni-7Co-5Mo Maraging Steel Sheet," Adv. in Cry. Engrg, V. 12, (1967), p. 532.

22. N. J. Huettich, A. W. Pense, and R. D. Stout, "The Toughness of 2-1/4% and 3-1/4% Nickel Steels at Cryogenic Temperatures," WRC Bulletin No. 165, Sept. 1971.

23. Anon., "9% Nickel Steel for Low Temperature Service," Int. Nickel Co. Publication No. 3749, (1973).

24. A. W. Pense, "The Static and Dynamic Fracture Toughness of 5% and 9% Nickel Steel," Lehigh Univ. Quarterly Report No. 5, Jan. 15, 1973.

25. K. G. Brickner, "Stainless Steels for Cryogenic Applications," Preprint for presentation at ASM Symposium on Stainless Steels at Cleveland, OH, dated 1969.

26. Anon., "Mechanical and Physical Properties of the Austenitic Chromium-Nickel Stainless Steels at Subzero Temperatures," Int. Nickel Co. Brochure No. 3846 (4), dated 1963.

27. R. P. Reed, and R. P. Mikesell, "The Stability of Austenitic Stainless Steels at Low Temperatures as Determined by Magnetic Measurements", Advances in Cryogenic Engineering, Vol. 4, (1960), p. 84.

28. A. J. Nachtigal, "Comparison of Tensile Properties of 304L and 310S Stainless Steels in Liquid Helium," NASA Tech. Memo TM-X-52703, Oct. 1969.

29. D. C. Larbalestier, and H. W. King, "Prediction of the Low Temperature Stability of Type 304 Stainless Steel From a Room Temperature Deformation Test," Reprint from the Proc. of the 4th Int. Cryogenic Engineering Conference (Undated).

30. D. C. Larbalestier, and H. W. King, "Non-Magnetic Stainless Steels for Cryogenic Purposes," Rutherford Laboratory Report RHEL/R217, Jan. 1971.

31. D. C. Larbalestier, and H. W. King, "Austenitic Stainless Steels at Cryogenic Temperatures, I - Structural Stability and Magnetic Properties," CRYOGENICS, V. 13, No. 3, March 1973, p. 160.

32. F. C. Hull, and E. W. Johnson, "Kromarc-58 For Large Cryogenic Structures," Westinghouse Research Memo 64-1B4-191-M1, Dec. 7, 1964.

33. C. Perry, and R. Irving, "Aerospace Alloys March into New Markets," Iron Age, Jan. 13, 1972, p. 49.

34. A. J. Nachtigal, S. J. Klima, and J. C. Freche, "Fatigue Behavior of Rocket Engine Materials to -452°F (4°K)," Journal of Materials, JMLSA, Vol. 3, No. 2, June 1968, p. 425.

35. J. E. Campbell, Low Temperature Properties of Metals, Review of Recent Developments, DMIC.

36. W. Weleff, et al, "Cryogenic Properties of Selected Aerospace Materials," Adv. in Cry. Engrg, Vol. 10, (1965), p. 14

37. J. L. Christian, "Mechanical Properties of Several Nickel-Base Alloys at Room and Cryogenic Temperatures," Adv. in Cry. Engrg., V. 12, (1967), p. 520.

38. C. O. Malin, "Low Temperature Properties of Large Inconel 718 Forgings," Rocketdyne Div. of North American Rockwell Corp., Report MFS-18244, Aug. 1968.

39. Anon., "Iron-Nickel and Related Alloys of the Invar and Elvinar Types," Int. Nickel Co. Bulletin 2758, (1962).

40. Anon., "Incoloy Alloy 903," Huntington Alloys Div. of Inco, Bulletin S-51, (1973).

41. Anon., "New Ni-Fe-Co Alloy Combats Stresses," Metals Progress, p. 7, Oct. 1973.

42. H. L. Eiselstein, "An Age Hardenable, Low Expansion Alloy for Cryogenic Service," Adv. in Cry. Engrg., V. 12, (1967), p. 508.

43. R. J. Davis, and E. J. Prance, "Cryogenic Tensile Properties of Ti-6Al-4V Forgings," NASA Industrial Applications Flash Sheet M-FS-2533, March 1967.

44. J. A. Halchak, "Low Temperature Properties of Forgings of Ti-5Al-2.5Sn Alloy (ELI)," NASA MFS-18245F, (1968).

45. J. L. Christian, and A. Hurlich, "Mechanical Properties of Titanium Alloys at Cryogenic Temperatures," Adv. in Cry. Engrg., V. 13, (1968), p. 318.

46. R. J. Goode, R. W. Judy, and R. W. Huber, "Procedures for Fracture Toughness Characterization and Interpretations to Failure-Safe Design for Structural Titanium Alloys," WRC Bulletin No. 134, October 1968.

47. J. G. Waufman, and M. Holt, "Evaluation of Fracture Characteristics of Aluminum Alloys at Cryogenic Temperatures," Adv. in Cry. Engrg., V. 10, (1965), p. 77.

48. J. G. Kaufman, et al, "Tensile Properties and Notch Toughness of Aluminum Alloys at -452°F in Liquid Helium," Adv. in Cry. Engrg., V. 13, (1968), p. 294.

49. F. R. Schwartzberg, et al, "Fatigue Behavior of Aluminum and Titanium Sheet Material Down to -423°F," Adv. in Cry. Engrg., V. 10, (1965), p. 1.

50. J. W. Coursen, et al, "Notch Toughness of Some Aluminum Alloy Castings at Cryogenic Temperatures," Adv. in Cry. Engrg., V. 12, (1967), p. 473.

51. Anon., "New Alloy Developed for Supersonic Service," Metals Progress, June 1973, p. 7.

52. S. A. Levy, "X2048 Alloy, A High Strength, High Toughness Alloy," Reynolds Aluminum Aerospace Review, (1974).

53. R. W. Judy, R. J. Goode, and C. N. Freed, "Fracture Toughness Characterization Procedures and Interpretations to Fracture - Safe Design for Structural Aluminum Alloys," WRC Bulletin No. 140, May 1969.

54. R. J. Goode, and R. W. Judy, Jr., "Application of Principles for Fracture Safe Design for Aluminum and Titanium Alloys," Welding Journal, Vol. 53, No. 3, March 1974, p. 135-S.

55. F. G. Nelson, and J. G. Kaufman, "Plain Strain Fracture Toughness of Aluminum Alloys at Room and Subzero Temperatures," ASTM STP 496, (1971), p. 27-39.

56. R. P. Reed, and R. P. Mikesell, "Low-Temperature (295 to 4°K) Mechanical Properties of Selected Copper Alloys," Journal of Materials, Vol. 2, No. 2, June 1967, p. 370.

57. R. P. Reed, R. E. Schramm and A. F. Clark, "Mechanical, Thermal and Electrical Properties of Selected Polymers," Cryogenics, Vol. 13, No. 2, February 1973, p. 67.

58. E. E. Morris, "Glass-Fiber Reinforced Metallic Tanks for Cryogenic Service," Adv. in Structural Composites, 12th National SAMPE Symposium, AS-4, (1967).

59. R. D. Keys, T. F. Kiefer, and F. R. Schwartzberg, "Cryogenic Properties of High Strength Glass Reinforced Plastics," Adv. in Cry. Engrg., Vol. 11, (1966), p. 470.

60. D. P. Kendall, "Crack Growth Resistance in Laminated, Glass Epoxy Sheet," Journal of Materials, JMLSA, Vol. 7, No. 3, September 1972, p. 430.

61. R. W. Hertzberg, "Fatigue Crack Propagation Characteristics in Polymeric Materials," Closed Loop Mag. (MTS), (1973), p. 12.

62. R. C. Cremisio, "Chapter 13 - Melting," The Superalloys, Ed. by C. T. Sims and W. C. Hagel, J. Wiley & Sons, NY, (1972), p. 373.

63. G. E. Linnert, "Welding Characteristics of Stainless Steels," ASM, Metals Engineering Quarterly, November 1967, p. 1.

64. R. P. Sullivan, "Fusion Welding of Stainless Steel," ASM, Metals Engineering Quarterly, November, 1967, p. 16.

65. S. Asakura, et al, "The Effect of Welding Conditions on the Crack Sensitivity of Austenitic Stainless Steel Weld Metals," Welding Research Abroad, Vol. XX, No. 1, January 1974, p. 34.

66. H. F. Reid and W. T. DeLong, "Making Sense Out of Ferrite Requirements in Welding Stainless Steels," Metals Progress, June 1973, p. 73.

67. A. Bernstein, et al, "Influence of Phosphouous and Sulphur on the Properties of the Weld Metal in Certain Austenitic Stainless Steels," Welding Journal, Vol. 44, November 1965, p. 504-S.

68. F. C. Hull, "Effects of Alloying Additions on Hot Cracking of Austenitic-Chromium Nickel Stainless Steels," ASTM Paper No. 78, 1960 Annual Meeting.

69. C. L. Goodzeit, "Evaluation of Stainless Steel Casting Alloys for Cryogenic Service in the 80-inch Liquid-Hydrogen Bubble Chamber," Adv. in Cry. Engrg., V. 10, (1965), p. 26.

70. W. Yeniscavich, "Chapter 18 - Joining," The Superalloys, Ed. by C. T. Sims and W. C. Hagel, J. Wiley & Sons, NY, (1972), p. 509.

71. M. Prager and C. S. Shira, "Welding of Precipitation Hardening Nickel Base Alloys," WRC Bulletin No. 128, February 1968.

72. Anon., "Joining the Huntington Alloys," International Nickel Company, Inc., Technical Bulletin T-2, (1972).

73. B. M. MacPherson, Ed, "Effects of Minor Elements on the Weldability of HIgh Nickel Alloys," Proceedings of a Symposium Sponsored by the Welding Research Council, July 1969.

74. J. Heuschkel, "Weld Metals in Nickel Base Alloys," Welding Journal, Vol. 39, June 1960, p. 236-S.

75. R. P. Reed, "Low Temperature Mechanical Properties of Welded and Brazed Copper," Adv. in Cry. Engrg., Vol. 14, (1969), p. 83.

76. R. I. Jaffee, et al, "Low Temperature Properties of Lead-Base Solders and Soldered Joints," Metals Progress, Dec. 1948, p. 843.

77. A. B. Kaufman, "Selecting Solders for Low Temperature Service," Materials in Design Engineering, Nov. 1958, p. 114.

78. R. M. MacIntosh, "Tin in Cold Service," Tin and Its Uses, V. 76, 1968, p. 7.

79. W. J. Reichenecker, "Development of HIghly Reliable Soldered Joints for Printed Circuit Boards," Westinghouse Report 69-8D4-SOLDR-R1.

80. H. S. Kalish, and F. J. Dunkerley, "The Low Temperature Properties of Tin and Tin-Lead Alloys," TAIME 180, 1949, p. 637.

81. J. L. Christian, "Design Criteria for Solders in Cryogenic Environments," Electro-Technology, 71, June 1963, p. 109.

82. J. L. Christian, and J. F. Watson, "Tensile and Shear Properties of Several Solders at Cryogenic Temperatures," SAE, Oct. 1962, p. 1.

83. C. S. Barrett, and T. B. Massalski, "Structure of Metals," 3rd Edition, McGraw-Hill, NY, 1966, p. 490.

477<

TABLE 5-1

CANDIDATE MATERIALS FOR STRUCTURAL CRYOGENIC APPLICATIONS

AUSTENITIC STAINLESS STEELS

* AISI 310S
* KROMARC 58
ARMCO 21-6-9
ARMCO 21-13-5
CARPENTER 20Cb-3

IRON BASE SUPERALLOYS

A-286
W-545
PYROMET 860
DISCALOY

NICKEL BASE SUPERALLOYS

INCONEL 625
INCONEL 718 (706)
* INCONEL X-750 (751)
HASTELLOY C-276
PYROMET 680
PYROMET 102
UNITEMP-HX

OTHER SUPERALLOYS

HAYNES 188
MULTIPHASE MP35N

LOW EXPANSION ALLOYS

INCOLOY 903
INCO (UN-NAMED)

TITANIUM ALLOYS

Ti-6Al-4V (ELI)
Ti-5Al--2.5Sn (ELI)

ALUMINUM ALLOYS

2014
2219
5083
X2048

COPPER AND COPPER ALLOYS

* OFHC-Cu
AMZIRC-Cu (CW/HT)
GLIDCOP (Al_2O_3 - D.S.)
PD-135 (Cu-Cr-Cd/PHT)

* Materials presently being characterized in Westinghouse FY 1974 Program, NBS Contract CST-8034.

TABLE 5-2

TEST SPECIMEN IDENTIFICATION SYSTEM

Material	Condition	Code
OFHC Cu	As Received, AR	10XX-X
	Stress Relieved, SR	11XX-X
	GTAW	12XX-X
	Braze, B	13XX-X
	Solder, S	14XX-X
AISI 310S	Sol'n. treated and quenched, STQ	20XX-X
	Sensitized (STFC)	21XX-X
	SMAW	22XX-X
Inconel X-750 (VIM-VAR) MP-1	Sol'n. treated, ST	30XX-X
	STDA	31XX-X
	ST/EBW	32XX-X
	STDA/EBW	33XX-X
	EBW/STDA	34XX-X
	ST/GTAW	35XX-X
	STDA/GTAW	36XX-X
	GTAW/STDA	37XX-X
	Brazed	38XX-X
X-750 (AAM-VAR), MP-2	STDA	40XX-X
(VIM), MP-3	STDA	50XX-X
X-750	HIP	60XX-X
	HIP/STDA	61XX-X

Specimen ID System

4 digets + Dash No.

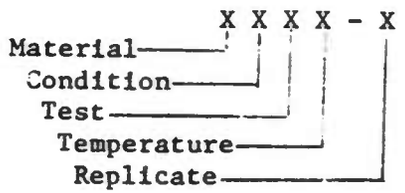

TABLE 5-2 (CONTINUED)

TEST SPECIMEN IDENTIFICATION SYSTEM

Material	Condition	Code
Kromarc-58	STQ	80XX-X
	CW	81XX-X
	GTAW	82XX-X
	CW/GTAW	83XX-X
	GTAW/CW	84XX-X
	GTAW/CW/AN	85XX-X

Test (3rd Diget)	Code		
Tensile	XX1X-X	or	XXTX-X
Notched Tensile	XX2X-X		XXNX-X
K_{IC}	XX3X-X		XXKX-X
J_{IC}	XX4X-X		XXJX-X
FCGR	XX5X-X		XXFX-X

Test Temp. (4th Diget)	
+70°F Rm Temp.	XXX1-X
-320°F Liq. Nit.	XXX2-X
-452°F Liq. He	XXX3-X

Sample Replicate (Dash + No.)	
	XXXX-1
	XXXX-2
	XXXX-3
	etc.

TABLE 5-3

CHEMICAL COMPOSITION OF (W) PROGRAM MATERIALS (FY 74)

Material	
OFHC Copper (102)	Analysis not completed to date

310S Stainless	C	P	S	Si	Mn	Ni	Cr	Mo	Cu
Base Material	.064	.017	.009	.74	1.70	19.66	24.40	.17	.15
Weld Plate	.053	.027	.001	.48	1.70	20.80	25.00	.21	.14

X-750 Superalloy	C	P	S	Si	Mn	Ni	Cr	(Nb+Ta)	Cu	Fe	Al	Ti	Co	O	N	H
MP-1 (VIM-VAR)	.04	.003	<.001	.11	.089	73.0	15.2	.90	.022	6.47	.92	2.40	.017	.0016	.004	.0006
MP-2 (AAM-VAR)	.02	.004	.007	.24	.12	74.82	14.19	.95	.06	6.22	.73	2.62	.051	.0006	.004	.00007
MP-3 (VIM)	.04	.004	.003	.27	.13	73.02	15.40	.89	.04	6.87	.68	2.64	.009	.0006	.007	.00010

		O	N	H	Ar
Powder (Pre-HIP)	(Starting Mat. MP-1)	.0105	.0038	.0005	<.0007
Powder (Post-HIP)	To be analyzed				

Kromarc-58 Stainless	C	P	S	Si	Mn	Ni	Cr	Mo	Al	Zr	B	V	O	N	H
K-58 Base Mat. and Weld Plate	.030	.005	.005	.05	9.3	23.0	15.5	2.2	.02	.008	.016	.16	--	.17	--
K-58 Weld Filler Mat.	.003	.001	.004	.09	11.5	21.4	15.3	2.18	--	<.002	.010	.20	--	.15	--

TABLE 5-4

MATERIAL DOCUMENTATION DATA

Material	Source	Heat No.	Form
OFHC Copper (102)	Ⓦ R&D Stock	Unknown	1/2" and 5/8" thick plate
310S Stainless			
Base Plate	McInnes Steel Co.	500096	Forging Billet - Annealed
Weld Plate	Rolled Alloys, Inc.	20880	5/8" thick Plate, HRAP
E310-16	Arcos Corp.	(a) 3A17B-M9	1/8" dia. SMAW Electrode
		(b) 2N10B-M16A	5/32" dia. SMAW Electrode
		(c) 2N8B-M16	5/32" dia. SMAW Electrode
Inconel X-750			
MP1	Inco-Huntington Div.	HT56C1XY	10" dia. round HFFQ (VIM-VAR)
MP2	Inco-Huntington Div.	HT1250XV	4" dia. round HFFQ (AAM-VAR)
MP3	Inco-Huntington Div.	HT57F8XS	2" dia. round HF (VIM)
Powder for HIP	Federal-Mogul Corp.	HT56C1XY	-60 mesh powder from MP1
Inco Weld Filler 69	Inco-Huntington Div.	HT21C8X	.093" dia. GTAW Filler Wire
		HT00F7XS	.062" dia. GTAW Filler Wire
		HT21C8X	.062" dia. GTAW Filler Wire
Kromarc-58 Stainless			
Base and Weld Plate	Ⓦ R&D Stock	HT-D8339	1" thick plate
Weld Filler Wire	Ⓦ R&D Stock	HT-3736	0.287" dia. wire draw stock

TABLE 5-5

PROCESSING AND HEAT TREATMENT SCHEDULES COMPLETED

Material	Code	Condition	
310S	20XX	STQ	2000°F - 1 hr - Water Quenched
	21XX	STFC	2000°F - 1 hr - Furnace Cool to 800°F min; then Air Cool
	22XX	SMAW	STQ, then SMA Weld with E310-16 Electrodes
IN X-750	30XX	ST	1800°F - 1 hr - Air Cool
	31XX	STDA	ST, then age at 1350°F - 8 hrs, F.C. to 1150°F hold 8 hrs and A.C.
	32XX	ST/EBW	ST, then Vacuum Electron Beam Weld
	33XX	STDA/EBW	STDA, then VEB Weld
	34XX	EBW/STDA	Vacuum EB Weld, then STDA
	35XX	ST/GTW	ST, then Gas Tungsten Arc Weld with Inco 69 Filler
	36XX	STDA/GTW	STDA, then GTA Weld with IN69 Filler
	37XX	GTW/STDA	GTA Weld (F69), then STDA
	60XX	HIP	Hot Isostatic Press
		HX-1	1st Trial - 1120°C and 10,000 psi - 2 hrs
		HX-2	2nd Trial - 1200°C and 10,000 psi - 2 hrs
		HIP/STDA	HIP, then Standard STDA Heat Treatment
K-58	80XX	STQ	1800°F - 1 hr - Water Quench
	81XX	CW	Cold Work ∿ 30% Reduction in Thickness
	82XX	GTW	Gas Tungsten Arc Welding of STQ Material (presently processing redraw rod to make K-58 filler wire)

TABLE 5-6

MATERIAL HARDNESS AND GRAIN SIZE MEASUREMENTS COMPLETED

Material	Code	Condition	Hardness	Grain Size (ASTM No.)
310S(1)	20XX	STQ	73 Rb	8
	21XX	STFC	67.3 Rb	5
IN X-750	----	MP-1 As Received	29.3 Rc	3.5*
	30XX	ST	30.8 Rc	3.5*
	31XX	STDA	28.5 Rc	3.5*
	40XX	MP2/As Received	35.3 Rc	6.5
	50XX	MP3/As Received	35.3 Rc	9
	60XX	HIP (HX-1)	36.3 Rc	9
		(HX-2)	35.0 Rc	8
	61XX	HIP/STDA (HX-1)	41.7 Rc	11
		(HX-2)	41.0 Rc	8
Kromarc 58	80XX	STQ	88 R_B	5.5
	81XX	CW (30%)	33 Rc	9.5
	----	As Received	93 R_B	9

(1) Weld Plate Material

* Grain Size VAriation in 10" dia. billet, see Section 7.3

TABLE 5-7

CHARACTERIZATION DATA FOR INCONEL X-750 POWDER

STARTING MATERIAL: Inconel X-750, MP-1 (VIM-VAR)

POWDER MANUFACTURE METHOD: Vacuum Melted and Atomized in high purity Argon Gas (FM)

Certified Sieve Analysis		Westinghouse Sieve Analysis	
Mesh	%	Mesh	%
+ 60	-	-	-
+ 80	1.8	+ 80	3.65
+ 100	4.5	+ 100	6.45
+ 120	5.2	-	-
+ 140	6.8	+ 140	13.11
+ 170	8.4	-	-
+ 230	16.0	+ 200	17.34
+ 270	7.8		
+ 325	7.9	+ 325	22.66
+ 500	25.6		
- 500	16.0	Pan	36.19
Total	100.0	Total	99.40

FLOW RATE (MPIF Std. No. 3-45) 15.2 Sec. (50 gm sample)

APPARENT DENSITY (MPIF Std. No. 04) 4.23 gm/cc (25 cc sample Std. Cup)

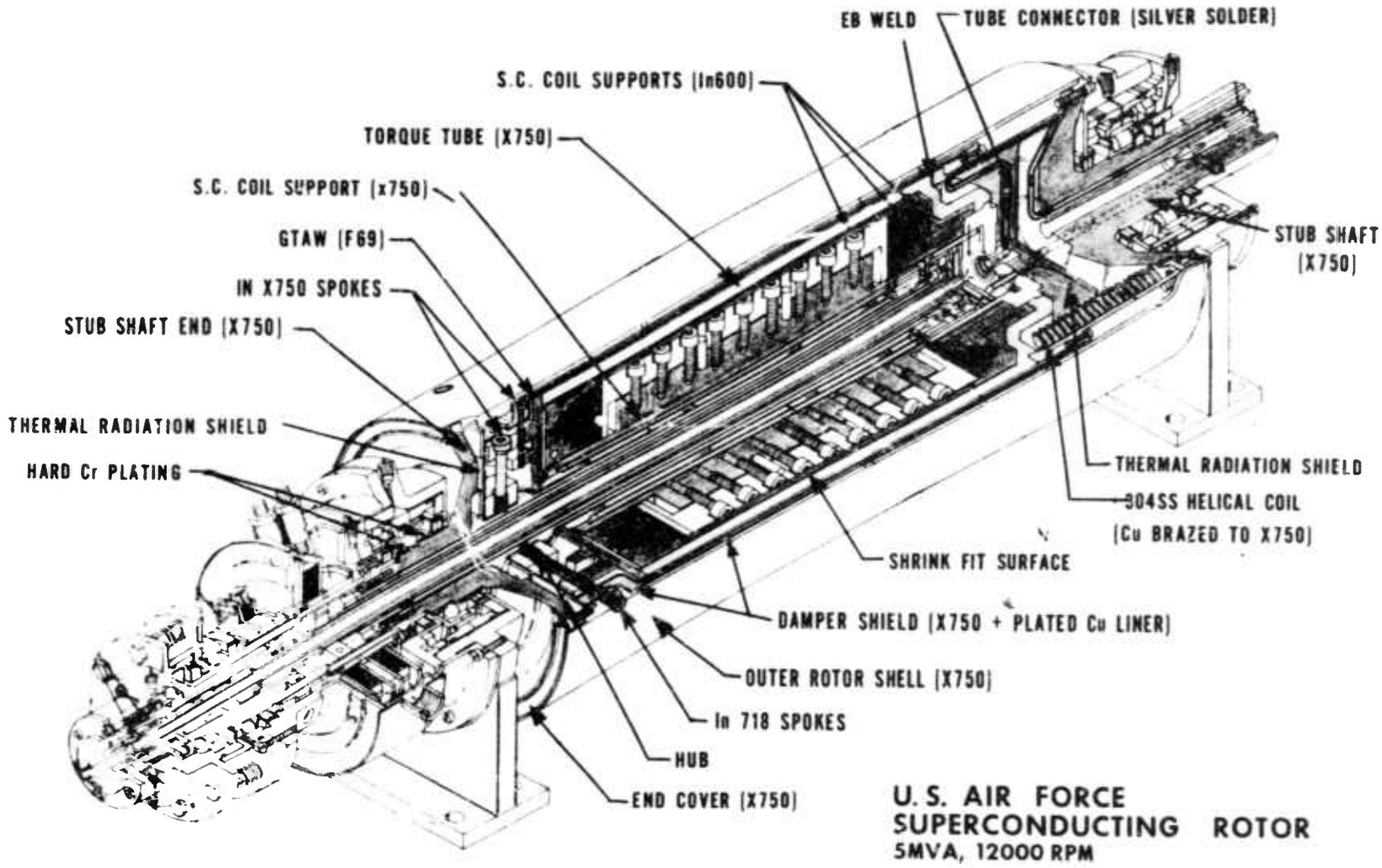

Fig. 5-1 Prototype superconducting generator rotor assembly indicating structural materials utilization and design/fabrication complexity.

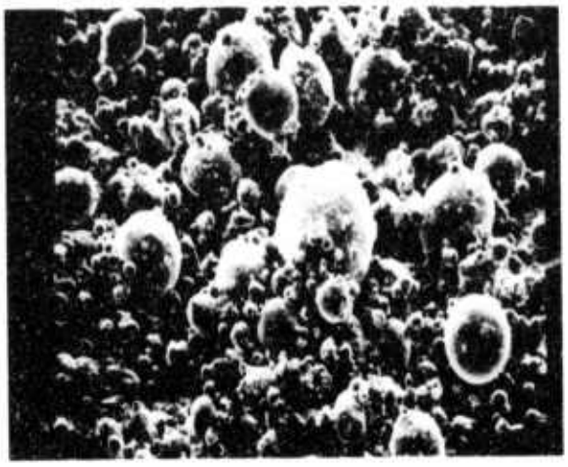

(a) Area One (X100)

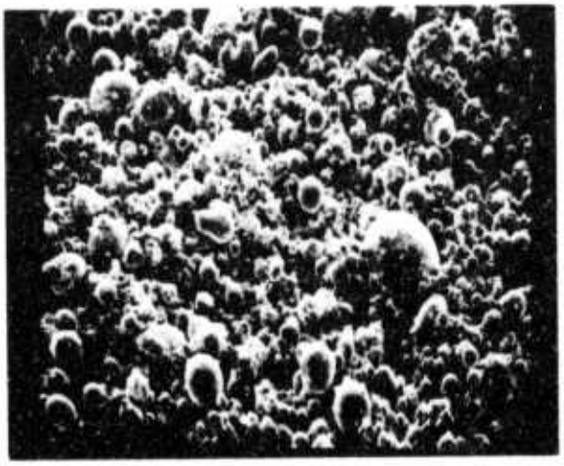

(b) Area Two (X100)

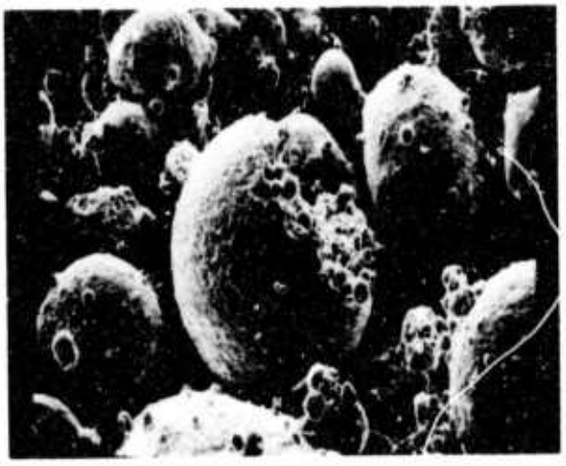

(c) Area Three (X200)

Fig. 5-2 Scanning electron micrographs of Inconel X750 powder made from MP - 1 starting material (VIM-VAR)

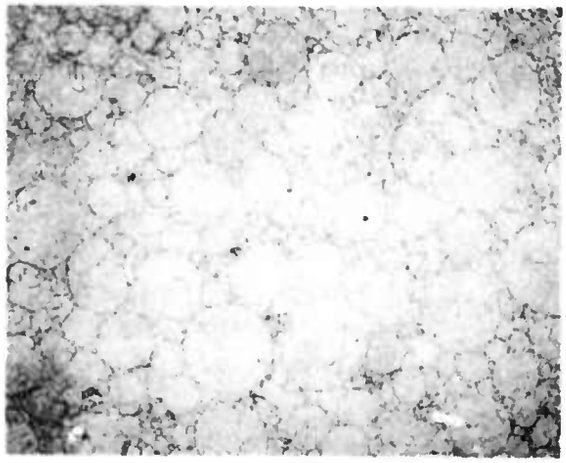

(a) HX-1 As Hipped

(b) HX-1 HIP + STDA

(c) HX-2 As Hipped

(d) HX-2 HIP + STDA

Fig. 5-3 Microstructures of initial hot isostatic pressed (HIP) X750 powder samples. (X100) HX1 - Hipped at 1120 ° C & 10,000 psi (60XX) HX2 - Hipped at 1200 ° C & 10,000 psi (60XX) STDA - Solution treat (1800 ° F for 1 hr and air cooled, aged at 1350 ° F for 8 hrs, furnace cooled to 1150 ° F, hold 8 hrs and air cool (61XX)

I

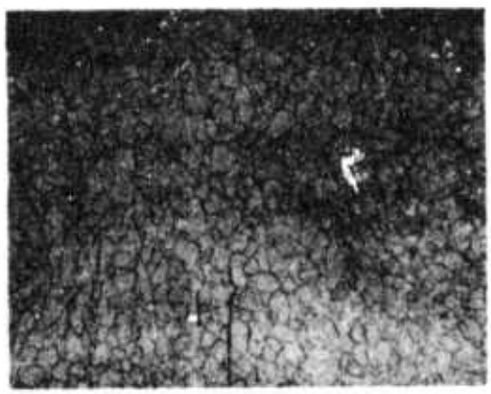

(a) AR Longitudinal (200X)

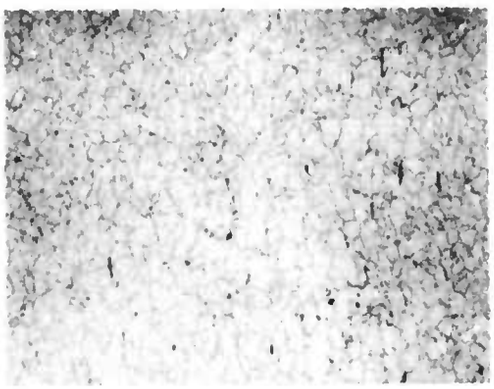

(b) AR Transverse (200X)

II

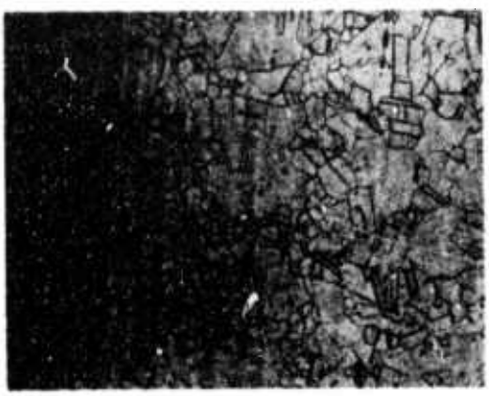

(a) STQ, Longitudinal (200X)

(b) STQ, Transverse (200X)

III

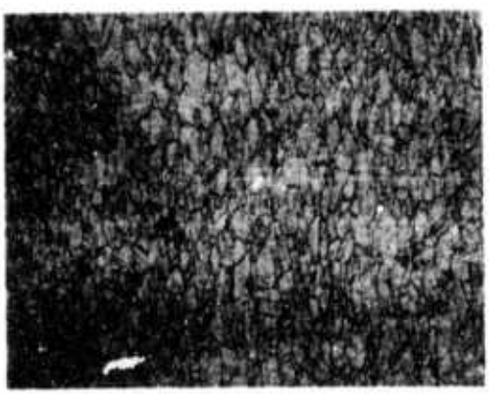

(a) CW, Longitudinal (200X)

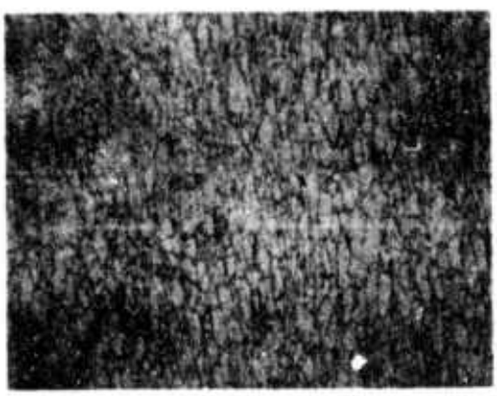

(b) CW, Transverse (200X)

Fig. 5-4 Kromarc 58 stainless steel microstructure. Condition I-As received, II-STQ (80XX) and III- cold worked, 30% reduction in thickness (81XX)

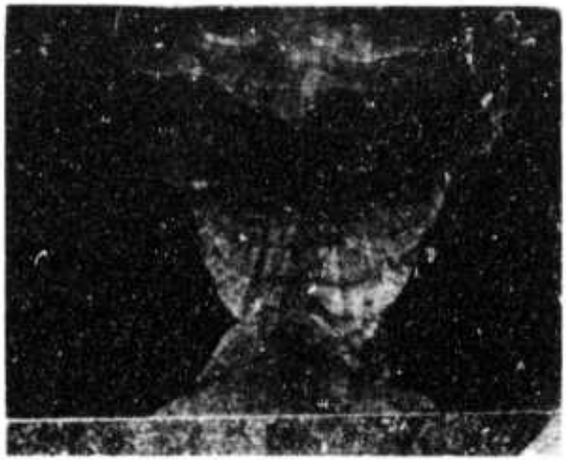

(a) Macro Weld Profile (X5)

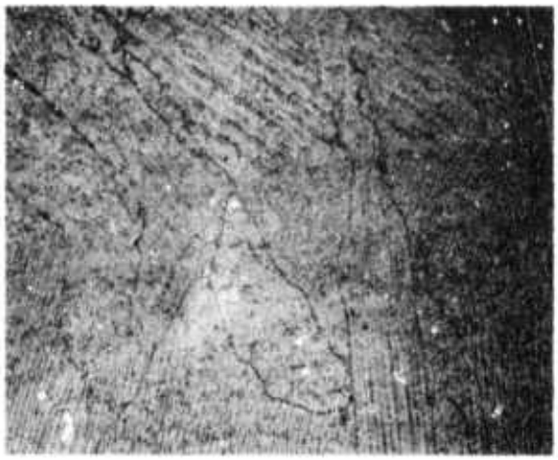

(b) Micro Weld Fusion Zone (X200)

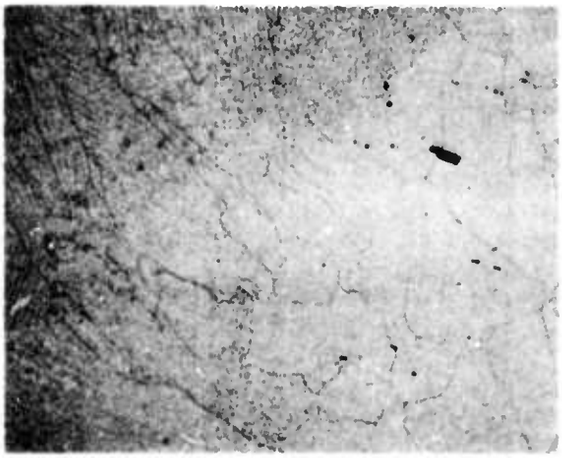

(c) Micro Weld FZ-HAZ Transition (X200)

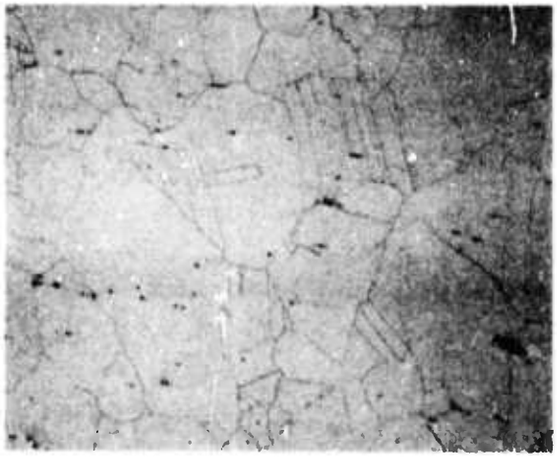

(d) Micro-Base Metal Structure (X200)

Fig. 5-5 Macro (a) and microstructure (b, c, & d) of 310S stainless steel base metal and typical SMA weldment (5/8" thick) using E310-16 covered electrode. (22XX)

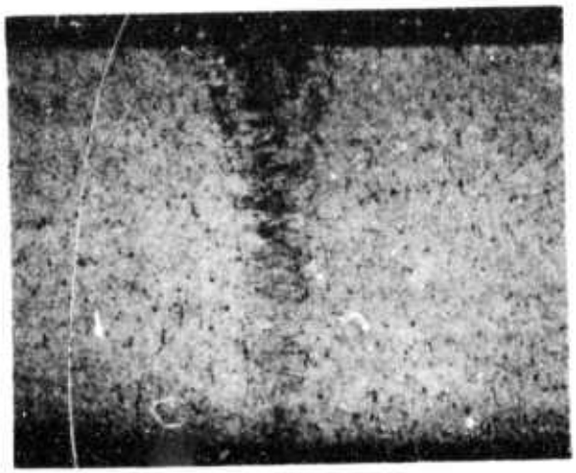

(a) Electron Beam Weld in Inconel X750 (X8)

(b)

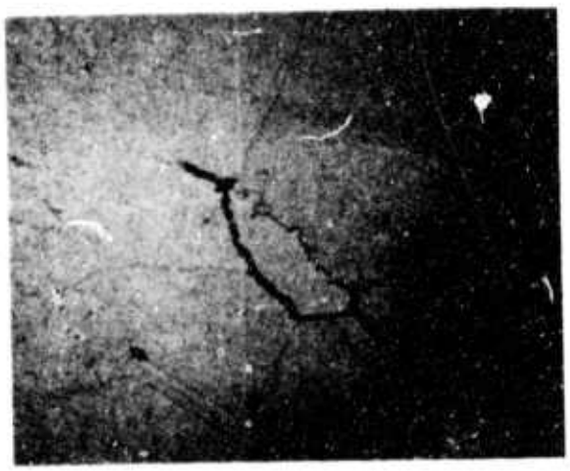

(c)

Microfissures in HAZ Adjacent to E. B. Welds in Inconel X750 (X200)

Fig. 5-6 Typical electron beam weldment profile (a) and base metal microfissuring (b) in Inconel X750.

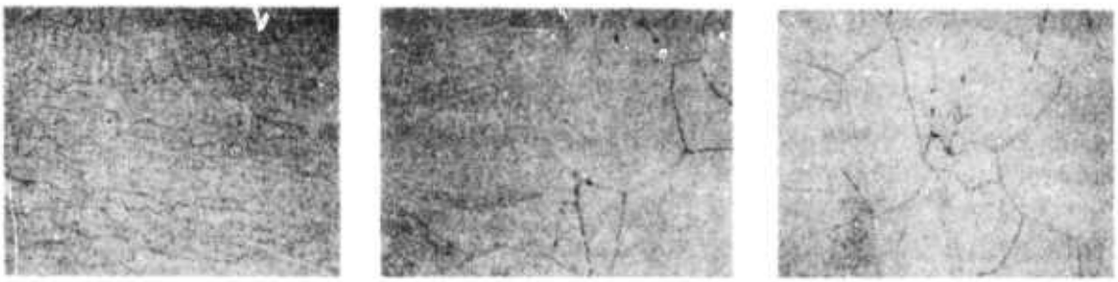

(a) Fusion Zone (32XX) (b) FZ-HAZ Transition (32XX) (c) Base Metal (32XX)

(a) Fusion Zone (33XX) (b) FZ-HAZ Transition (33XX) (c) Base Metal (33XX)

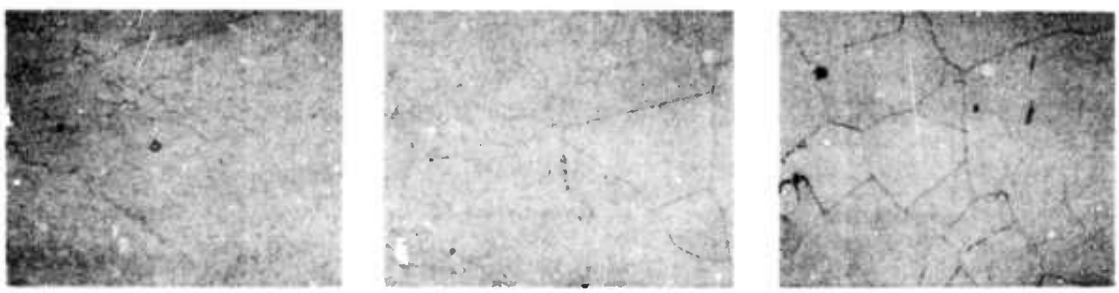

(a) Fusion Zone (34XX) (b) FZ-HAZ Transition (34XX) (c) Base Metal (34XX)

Fig. 5-7 Microstructure of Inconel X750 vacuum electron beam weldments (5/8" thick), Condition I-ST/EBW (32XX), Condition II-STDA/EBW (33XX), and Condition III-EBW/STDA (34XX) (X200)

(a) Macro-GTAW Profile (35XX) (X5)

I

(a) Fusion Zone (35XX)

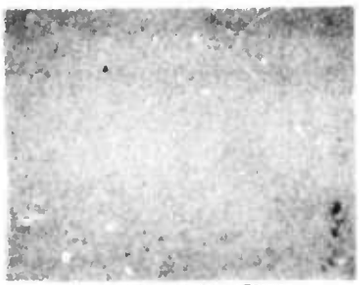

(b) FZ-HAZ Transition (35XX)

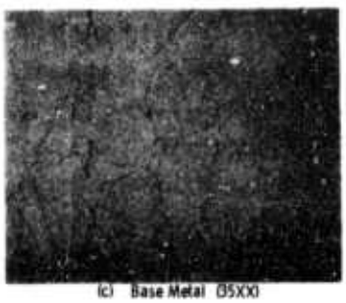

(c) Base Metal (35XX)

II

(a) Fusion Zone (36XX)

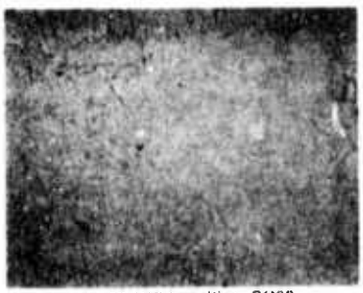

(b) FZ-HAZ Transition (36XX)

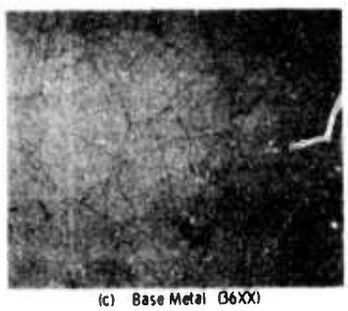

(c) Base Metal (36XX)

III

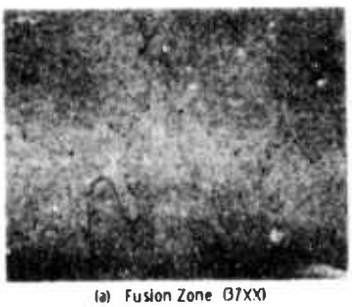

(a) Fusion Zone (37XX)

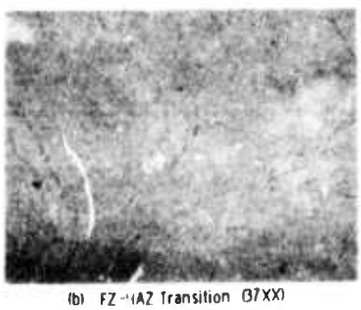

(b) FZ-HAZ Transition (37XX)

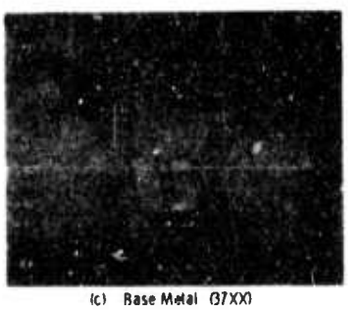

(c) Base Metal (37XX)

Fig. 5-8 Macrostructure (a) and microstructure of Inconel X750 gas tungsten arc (GTA) weldments (5/8" thick) Condition I-ST/GTAW (35XX), Condition II-STDA/GTAW (36XX), and Condition III-GTAW/STDA (37XX) (X200)

6.0 FRACTURE MECHANICS

Introduction

The linear-elastic fracture mechanics approach to design against failure of structural materials is basically a stress intensity consideration in which criteria are established for fracture instability in the presence of a crack.[1-4] The essence of the approach is to relate the stress field developed in the crack vicinity to the applied nominal stress on the structure, the material properties, and to the geometry and size of defect necessary to initiate failure.

Therefore, successful use of fracture mechanics technology as a tool for design against failure requires basic information in three areas of concern: material properties, stress analysis and defect characterization. In addition, an appropriate expression (generally referred to as the stress intensity expression or K-calibration) which describes the relationship between these factors for the structural configuration of interest must be available.[5] Providing our fracture mechanics material properties include data for both the rapid propagation (K_{IC} fracture toughness) and slow growth (crack growth rate) phases of fracture, we can evaluate the fracture potential of components in various situtations. Specifically, it is possible to:

a. select materials to provide the desired reliability against fracture;

b. develop a quantitative evaluation of the fracture potential of components in specific situations;

c. predict the useful life expectancy of components under sustained and/or cyclic loading conditions;

d. establish realistic acceptance and nondestructive inspection specifications that will assure the desired degree of immunity from failure for the required life of the structure.

The purpose of this section of the progress report is to present the tensile, notched tensile, fracture toughness and fatigue crack growth rate data generated to date on Inconel X750, 310 S stainless steel and OFHC copper relative to performing a fracture mechanics analysis on cryogenic structural components manufactured from these materials. Obviously, further testing is required (welds, heat affected zones, etc.) before a confident, overall fracture mechanics analysis can be performed. This testing is currently underway.

6.1 Base Metal Results

6.1.1 Tensile Tests

The base metal tensile properties of Inconel X-750, 310 S stainless steel and OFHC copper are illustrated in Figs. 6-1 through 6-3 respectively. Standard 0.2 in. diameter button head specimens were utilized for all base metal tensile tests. Observing Fig. 6-1, note the yield strength of solution treated and double aged Inconel X-750 exceeds that of the solution treated Inconel X-750 throughout the entire test temperature range. Also, the yield strength of both heat treatments is essentially constant with temperature. The reduction in area and percent elongation properties of solution treated Inconel X-750 surpass those of solution treated and double aged Inconel X-750 throughout the entire test temperature range.

Concerning the tensile properties of 310 S stainless steel (Fig.6-2), the yield and ultimate strength properties of solution treated and water quenched 310 S stainless steel are slightly higher at all three test temperatures than the corresponding properties of sensitized 310 S stainless steel. Also unlike Inconel X-750, the yield and ultimate strengths of both heat treatments of 310 S stainless steel are not constant but increase significantly with decreasing temperature. Reduction in area and percent elongation values are substantial, even at -452°F, indicating good ductility.

The tensile properties of OFHC copper are illustrated in Fig. 6-3.Stress relieving the OFHC copper did not influence the tensile properties. Also, the yield strength remained constant with temperature whereas the ultimate strength increased with decreasing temperature. In addition, the reduction in area was quite high and demonstrated only a slight reduction with decreasing temperatures. Test specimen elongation was also sufficient and increased with decreasing temperature.

6.1.2 Notched Tensile Tests

The purpose of notched tensile tests is to determine the comparison parameter defined as the ratio of notched tensile fracture strength to the tensile yield strength of a particular material for a specific notch acuity. Increasing values of the ratio above 1.0 are considered to indicate increasing ability of the material for plastic deformation at the notch tip. Stated alternatively, increasing values of the ratio above 1.0 can be utilized as a measure of the material's resistance to catastropic brittle fracture.

The specimen configuration employed was a 0.20 in. diameter button head specimen notched to a 0.140 in. diameter test section. The root radius at the bottom of the sharp V-notch equaled 0.0005 in. This yielded a stress concentration factor (K_t) equivalent to 10. It should be pointed out that the notched tensile fracture strength was calculated by dividing the maximum load experienced by a test specimen by its original as opposed to final cross sectional area. This was largely due to the great difficulty in accurately measuring the extremely small change in test section diameter (hence cross sectional area) experienced by the test specimens.

The base metal notched tensile properties of Inconel X-750, 310 S stainless steel and OFHC copper are illustrated in Figs. 6-4 through 6-6, respectively. Note for each material regardless of heat treatment or test temperature, the ratio of notched tensile fracture strength to tensile yield strength is always greater than one, the minimum value equaling 1.6.

6.1.3 Fracture Toughness Tests

Half inch and one inch thick compact tension specimens (note Fig. 6-7) were used to generate the fracture toughness properties of Inconel X750, 310 S stainless steel and OFHC copper. The OFHC copper specimens were simply removed from a plate while the Inconel X750 and 310 S stainless steel fracture toughness specimens were removed from cylindrical forging quality round stock with their crack directions oriented as near radial as possible.

Prior to conducting the fracture toughness tests, the compact tension specimen starter notches were extended to fatigue crack severity. In order to avoid introducing any bias to the fracture toughness test results, the amount of crack-tip placticity created during fatigue precracking was limited to amounts less than those anticipated in the subsequent fracture toughness tests.

After precracking, the compact tension specimens were fracture toughness tested. Fracture toughness tests (also referred to as rising load tests) were conducted at two temperatures (-320°F and -452°F). A linear variable differential transformer (LVDT) attached to the specimen face (note Fig. 6-8), enabled an X-Y recorder to register autographically the load versus displacement occurring across the notch at the specimen edge. These load-deflection records were interpreted according to the ASTM standard requirements for obtaining valid plane-strain fracture toughness data.[6] This procedure for evaluation of load-deflection records permits direct determination of the nominal stress intensities, K_Q. The relationship between stress intensity factor, applied load and crack length which determined the nominal stress intensities for the compact tension specimens is given by the expression:

$$K_Q = Y \frac{P_Q \sqrt{a}}{BW}$$

where P_Q is the applied load determined from the load-deflection curve, W is the specimen width, B is the specimen thickness, "a" is the crack length measured from the centerline of loading and Y is a compliance constant dependent upon crack length.[4] K_{IC} is the plane-strain critical

stress intensity factor representative of the inherent material toughness. K_Q becomes a valid measure of K_{IC} when

$$\text{"a" and } B \geq 2.5 \left(\frac{K_Q}{\sigma_{ys}}\right)^2$$

where σ_{ys} is the material's yield strength at the particular fracture toughness test temperature.

The fracture toughness properties of Inconel X-750 and 310 S stainless steel are illustrated in Figs. 6-7 and 6-10, respectively. Note that only the one-inch thick compact tension specimens of solution treated and double aged Inconel X-750 tested at -320°F yielded valid K_{IC} fracture toughness results based on the above ASTM size requirement. Based on this same size criteria, all other fracture toughness tests at both -320°F and -452°F on both Inconel X-750 and 310 S stainless steel did not yield valid plane strain fracture toughness results. To obtain K_{IC} fracture toughness values, it was first necessary to estimate the points on the load-displacement records where crack growth first occurred (pop-in, discontinuity, etc.). By obtaining the area under the load-displacement record to this point, an elastic plastic fracture toughness value (J) was calculated utilizing the formula:[7]

$$J = \frac{4a + b}{4(c+a) + b} \quad \frac{2A}{Bb} \qquad \text{for displacements measured at LVDT location}$$

where A is the area under the load displacement record in lb. in., c is the distance from the specimen centerline of loading to the LVDT centerline and b is the remaining ligament, or

$$b = w - a$$

where w is the specimen width and "a" is the crack length measured from the specimen centerline of loading prior to the destructive fracture

toughness test. The value of linear elastic fracture toughness (K) was finally calculated by employing the relationship between linear elastic fracture mechanics parameters and elastic plastic fracture toughness (J) as follows:[8,9]

$$J = \frac{1 - \nu^2}{E} K^2$$

where ν is Poisson's ratio and E is the modulus of elasticity.

In addition to the above test procedures, a newly developed "resistance curve" technique was employed to obtain the critical value of elastic plastic fracture toughness, termed J_{IC}, for Inconel X-750 at a temperature of -452°F (note Fig. 6-9).[10] Essentially, the prime advantage of this method is that it gives the exact point of crack initiation, thus eliminating the uncertainty of estimating the point of first crack growth from a load-displacement record.

A thorough description of this test method can be found in Ref. 10. The only variation in test procedure is that we measured specimen crack opening displacement utilizing a linear variable differential transformer (LVDT) attached to the specimen front face as opposed to employing a modified test specimen which permits displacement measurements at the test specimen centerline of loading. Briefly, the testing procedure is to,(1) load each half inch thick compact tension specimen to different displacement valves, (2) unload each specimen and mark the crack (heat tinting was used in this case (1200°F, 6 hrs), (3) pull the specimen apart and measure crack extension. A resistance curve is then constructed by plotting J for each specimen versus its corresponding crack extension. The critical value of J (J_{IC}) is obtained by extrapolating this resistance curve backward to the point of zero crack extension due to actual material separation.

The resistance curves obtained for each heat treatment of Inconel X-750 are illustrated in Figs. 6-11 and 6-12. The resistance curve for the solution treated Inconel X-750 is ideal. The resistance curve

for the solution treated and double aged Inconel X-750, however, is poor since stable crack growth without catastrophic failure occurred in only three specimens. In addition, the crack growth which occurred in the solution treated and double aged Inconel X-750 test specimens was very difficult to observe and measure. Due to the very flat nature exhibited by both resistance curves, however, crack extension measurements need not be extremely accurate and we feel confident in extrapolating the solution treated and double aged Inconel X-750 resistance curve to zero actual material separation crack extension with a simple straight line.

Returning again to the fracture toughness temperature curves, Figs. 6-9 and 6-10, note the fracture toughness of solution treated Inconel X-750 significantly exceeds that of the solution treated and double aged Inconel X-750. In addition, for both heat treatments of Inconel X-750 the fracture toughness is quite similar regardless of test temperature (-320°F or -452°F).

Observing Fig. 6-10, note the fracture toughness of solution treated and water quenched 310 S stainless steel substantially exceeds that of the sensitized 310 S stainless steel. Also,the fracture toughness of both heat treatments of 310 S stainless steel increases with temperature from -452°F to -320°F.

Concerning the fracture toughness tests of OFHC copper, two tests were conducted on both the stress relieved and as received conditions. The OFHC copper proved extremely ductile even at -452°F in the half-inch thick section size, however, and did not satisfy the previously mentioned ASTM size requirement for valid plane strain fracture toughness tests.[6] In fact, the half inch thick compact tension specimens (maximum test specimen size which mounts in the cryostat) also did not satisfy the size requirement for a valid elastic plastic J_{IC} fracture toughness test[10]

$$a,\ b,\ B,\ \geq\ 50\ \frac{J_Q}{\sigma_f}$$

where σ_f is a flow stress usually taken as a stress midway between the material's yield and ultimate stresses. Therefore, no additional fracture toughness tests (either linear elastic or elastic plastic) on OFHC copper in the half-inch thick section size will be performed.

6.1.4 Crack Growth Rate Tests

Fatigue crack growth rate tests were conducted on the half and one-inch thick wedge open loading (WOL) specimens illustrated in Fig. 6-7. The Inconel X-750 WOL specimens were removed from cylindrical forging quality round stock with their crack directions oriented as near radial as possible. The 310 S stainless steel WOL specimens were removed from plate stock, not the cylindrical forging quality round stock utilized for the fracture toughness specimens. All WOL specimens were precracked in air at an alternating load less than that employed for the actual crack growth rate test.

Fatigue crack growth rate testing was conducted on a constant load universal hydraulic fatigue machine under sinusoidal tension loading (0 to maximum load). The maximum alternating load (ΔP) was maintained constant throughout each individual test. Test frequency equalled 10 Hertz.

The room temperature, air environment fatigue crack growth rate properties of Inconel X-750 in both the solution treated and solution treated and double aged condition are presented in Fig. 6-13. The extent of fatigue crack growth encountered during room temperature, air environment cyclic loading was measured and recorded with an ultrasonic nondestructive testing crack growth monitor developed specifically for use with the WOL specimen.[11] The test procedure exhibits a crack length measurement sensitivity of ± 0.010 in. and provides a continuous record of crack length (a) versus number of elapsed cycles (N). This raw test data was subsequently translated into the crack growth rate ($\frac{da}{dN}$) versus stress intensity factor range (ΔK) data required to conduct a fracture mechanics failure prevention analysis.

These room temperature air environment and all succeeding crack growth rates were established by means of a computerized curve-fitting analysis of the crack length versus number of elapsed cycles data

obtained directly from the fatigue crack growth rate experiments.[12] The ΔK value associated with a specific crack growth rate was determined from the following expression:

$$\Delta K = K_{max} - K_{min} = Y \frac{P_{max}\sqrt{a}}{BW} - Y \frac{P_{min}\sqrt{a}}{BW}$$

where P_{max} and P_{min} are the maximum and minimum values of the alternating load, respectively.

The nearly linear relationship between log $\frac{da}{dN}$ and log ΔK shown in Fig. 6-13 is typical of most fatigue crack growth rate data. Since this linear relationship exists, the crack growth rate data can be expressed in terms of the generalized fatigue crack growth rate law developed by Paris.[13] This crack growth rate law is expressed as:

$$\frac{da}{dN} = Co\ \Delta K^n$$

where $\frac{da}{dN}$ is the rate of crack growth, Co is an intercept constant determined from the log $\frac{da}{dN}$ versus log ΔK plot, n is the slope of the log-log plot and ΔK is the stress intensity factor range. Since the upper scatterband data represent a conservative estimate of the material's crack growth rate properties, the generalized crack growth rate expression describing this line is normally reported as the material's crack growth rate properties. For the case of Inconel X-750 exposed to a room temperature, air environment, the crack growth rate expression is

$$\frac{da}{dN} = 4.83 \times 10^{-16}\ \Delta K^{7.0} \qquad \text{(inches/cycle, ksi } \sqrt{\text{in.}}\text{)}.$$

This crack growth rate expression should be employed when making fatigue life predictions or calculating initial allowable flaw sizes applicable to Inconel X-750 structures subjected to a room temperature, air environment. Finally, heat treatment (solution treated versus solution treated

and double aged) had no apparent influence on the crack growth rate properties of Inconel X-750 in a room temperature, air environment (note Fig. 6-13).

The fatigue crack growth rate properties of solution treated plus solution treated and double aged Inconel X-750 and solution treated and water quenched 310 S stainless steel all in a -452°F helium environment are illustrated in Figs. 6-14 through 6-16, respectively. In these helium environment tests, the previously described procedures were utilized to transform the crack growth versus elapsed cycles data into crack growth rate versus change in stress intensity factor range data. The methods employed to obtain the crack length versus elapsed cycles data, however, were quite different. Essentially, the primary difference between the room temperature and cryogenic temperature test methods is the procedure employed to measure crack length. Where crack length was previously measured by utilizing an ultrasonic transducer, the crack growth test method for very low temperatures rules out ultrasonics primarily due to crystal interface problems. At these cryogenic temperatures, crack length was determined by first measuring test specimen crack opening displacement by utilizing a linear variable differential transformer (LVDT) attached to the specimen front face and finally transforming this crack opening displacement value via specimen compliance into crack length. Figures 6-8 and 6-17 show the LVDT in position and the overall crack growth test setup, respectively. The LVDT had 0.100 in. total travel and was hermetically sealed. Linear output was guaranteed even at -452°F in a helium environment. Test specimen compliance was determined by utilizing a procedure originally developed by Novak and Rolfe.[14]

Returning again to Figs. 6-14 and 6-15, note the crack growth rate expression for solution treated plus solution treated and double aged Inconel X-750 in a -452°F helium environment is

$$\frac{da}{dN} = 2.04 \times 10^{-18} \Delta K^{8.0} \quad \text{(inches/cycle, ksi } \sqrt{\text{in.}}\text{)}$$

Therefore, the above crack growth rate expression should be employed when making fatigue life predictions or calculating initial allowable flaw sizes applicable to Inconel X-750 (comparable heat treatments) structures subjected to a -452°F helium environment. Also, note as was the case in a room temperature air environment, heat treatment had no apparent influence on the crack growth rate properties of Inconel X-750 in a -452°F helium environment.

The crack growth rate properties of solution treated and water quenched 310 S stainless steel in a -452°F helium environment are given by the expression

$$\frac{da}{dN} = 1.29 \times 10^{-13} \Delta K^{4.85} \qquad \text{(inches/cycle, ksi } \sqrt{\text{in.}}\text{)}$$

Therefore, the above crack growth rate expression should be employed when making fatigue life predictions or calculating initial allowable flaw sizes applicable to 310 S stainless steel (comparable heat treatment) structures subjected to a -452°F helium environment.

Figure 6-18 summarizes the crack growth rate expressions generated for Inconel X-750 and 310 S stainless steel. Note the greater rate of crack growth occurs in Inconel X-750 subjected to a room temperature air environment.

6.2 Weld Metal Results

6.2.1 Tensile Tests

Standard 0.357 in. diameter button head specimens were utilized for all weld metal tensile tests. In all cases the weld was centered in the gauge length of the tensile specimen with the specimen's longitudinal axis perpendicular to the weld bead direction.

The Inconel X-750 electron beam and gas tungsten arc weld metal tensile properties (0.2% yield strength, ultimate strength, reduction in area and percent elongation) are illustrated in Figs. 6-19

through 6-22, respectively. Each of the Inconel X-750 weld metal tensile specimens were given one of three heat treatments. These heat treatments are described as follows:

(i) solution treated/welded
(ii) solution treated and double aged/welded
(iii) solution treated/welded/solution treated and double aged

Regardless of which type weld is considered, the highest yield strength values were associated with specimens which were solution treated and double aged after welding (note Fig. 6-19). Also, note for each of the three heat treatments described above, the yield strengths of the gas tungsten arc welds always exceed those of the corresponding electron beam welds regardless of test temperature. It should be mentioned that all the Inconel X-750 electron beam and gas tungsten arc weld metal specimens fractured in the base metal or heat affected zone. Additional details on fracture locations and any corresponding correlations are presented in the microstructural analysis section of this report. As a result, the yield strengths of either electron beam or gas tungsten arc welds solution treated and double aged after welding are very similar to the correspondingly heat treated Inconel X-750 base metal tensile yield strengths (note Fig. 6-1). Finally, the electron beam and gas tungsten are welds which were solution treated prior to welding (no post weld heat treatment) for the most part exhibited the greatest reduction in area and percent elongation.

The tensile properties of 310 S stainless steel shielded metal arc welds are illustrated in Figs. 6-23 and 6-24. Since these 310 S stainless steel weld tensile specimens were removed from flat plate stock, not the cylindrical forging quality round stock utilized for the original base metal tensile specimens, additional base metal tensile results from specimens removed from the flat plate stock are also illustrated in Figs. 6-23 and 6-24. Note that all this material was solution treated and water quenched before welding.

As was the case for the Inconel X-750 weld tensile specimens, none of the 310 S stainless steel shielded metal arc weld tensile specimens fractured in the welds. Again, more details on specimen fracture locations are contained in the microstructural analysis section of this report. Yield strengths of the shielded metal arc welds are slightly higher than those previously reported for 310 S stainless steel base metal (note Fig. 6-2).

6.2.2 Notched Tensile Tests

As previously indicated, the purpose of notched tensile tests is to determine the comparison parameter defined as the ratio of notched tensile fracture strength to the tensile yield strength of a particular material for a specific notch acuity. Increasing values of the ratios above 1.0 are considered to indicate increasing ability of the material for plastic deformation at the notch tip.

The specimen configuration employed was a 0.357 in. diameter button head specimen notched to a 0.252 in. diameter test section. The root radius at the bottom of the sharp V-notch equalled 0.0009 in. This yielded a stress concentration factor (K_t) equivalent to 10.8. In all cases the specimens were etched before final machining to ensure notch placement in the center of the weld. As was the case for the base metal notched tensile tests, the notched tensile fracture strength was calculated by dividing the maximum load experienced by a test specimen by its original as opposed to final cross sectional area.

The Inconel X-750 electron beam and gas tungsten arc plus 310 S stainless steel shielded metal arc weld metal notched tensile properties are illustrated in Figs. 6-25 through 6-27, respectively. Keep in mind that the yield strengths shown in Figs. 6-25 through 6-27 resulted from the unnotched weld metal specimens, none of which actually fractured in a weld. Therefore, the comparison parameter for the weld tests is actually the notched tensile fracture strength of a particular weld metal divided by the tensile yield strength of the corresponding base metal or possibly heat affected zone material. Note for each material regardless of heat treatment or test temperature, however, the ratio of notched tensile fracture strength to tensile yield strength is always greater than one, the minimum value equalling 1.6.

REFERENCES - SECTION 6

1. G. R. Irwin, "Fracture Mechanics," Structural Mechanics, Pergamon Press, New York City and London (1960).

2. G. R. Irwin, J. M. Krafft, P. C. Paris and A. A. Wells, "Basic Aspects of Crack Growth and Fracture," NRL Report 6598, November 1967.

3. C. F. Tiffany, J. N. Masters, "Applied Fracture Mechanics," Fracture Toughness Testing and Its Applications, ASTM STP 381, April 1965.

4. W. F. Brown, Jr. and J. E. Srawley, "Plane Strain Crack Toughness Testing of High Strength Metallic Materials," ASTM STP 410, American Society for Testing and Materials, January 1967.

5. W. G. Clark, Jr. and E. T. Wessel, "Application of Fracture Mechanics Technology to Medium Strength Steels," Review of Developments in Plane Strain Fracture Toughness Testing, ASTM STP 463, American Society for Testing and Materials, 1970, p. 160.

6. "Standard Method of Test for Plane-Strain Fracture Toughness of Metallic Materials," E399-72, ASTM Standards, Part 31, July 1972.

7. J. R. Rice, P. C. Paris and J. G. Merkle, "Some Further Results of J-Integral Analysis and Estimates," Progress in Flaw Growth and Fracture Toughness Testing, ASTM STP 536, American Society for Testing and Materials, 1973, pp. 231-245.

8. J. A. Begley and J. D. Landes, "The J Integral as a Fracture Criterion," Fracture Toughness, Proceedings of the 1971 National Symposium on Fracture Mechanics, Part II, ASTM STP 514, American Society for Testing and Materials, 1972, pp. 1-20.

9. J. A. Begley, J. D. Landes, and E. T. Wessel, "Fracture Mechanics, A Practical Tool for Preventing Failures," Presented at the Third International Conference on Fracture, Munich, Germany, April 1973.

10. J. D. Landes and J. A. Begley, "Test Results from J Integral Studies - An Attempt to Establish a J_{IC} Testing Procedure," Presented at the Seventh National Symposium on Fracture Mechanics, College Park, Maryland, August 1973.

11. W. G. Clark, Jr. and L. J. Ceschini, "An Ultrasonic Crack Growth Monitor," Materials Evaluation, August 1969, p. 180.

12. A. J. Federowicz and B. A. Powell, "A Computer Program to Obtain a Min-Max Regression Model by Linear Programming," Unpublished Westinghouse Research data.

13. P. C. Paris, "The Fracture Mechanics Approach to Fatigue," Proc. Tenth Sagamore Army Materials Research Conference, August 1963, Syracuse University Press, 1964.

14. S. R. Novak and S. T. Rolfe, "Modified WOL Specimen for K_{Iscc} Environmental Testing," Journal of Materials, JMLSA, Vol. 4, No. 3, September 1969, pp. 701-728.

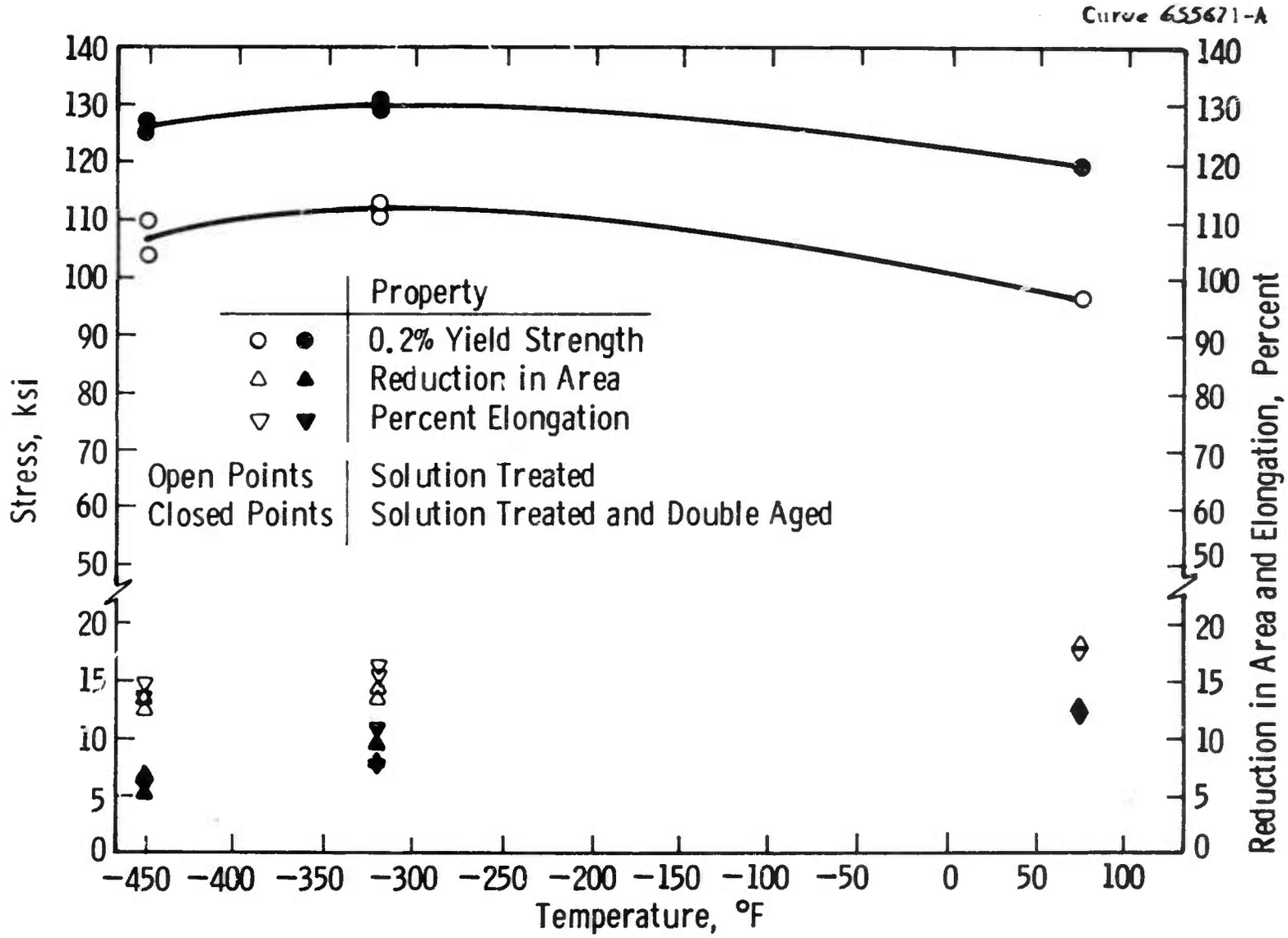

Fig.6-1—Tensile properties of Inconel X750

Curve 655675-A

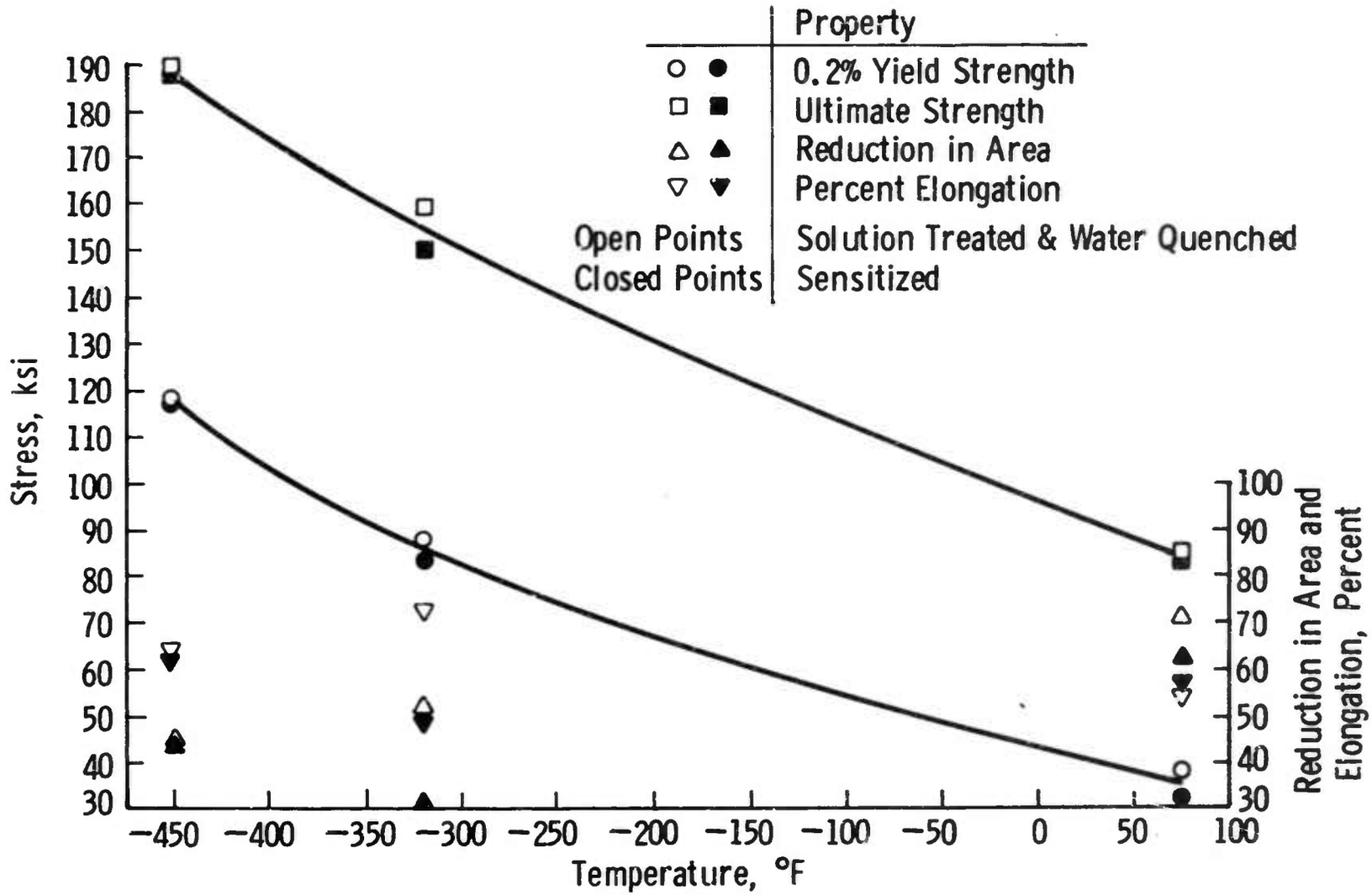

Fig.6-2—Tensile properties of 310 S stainless steel

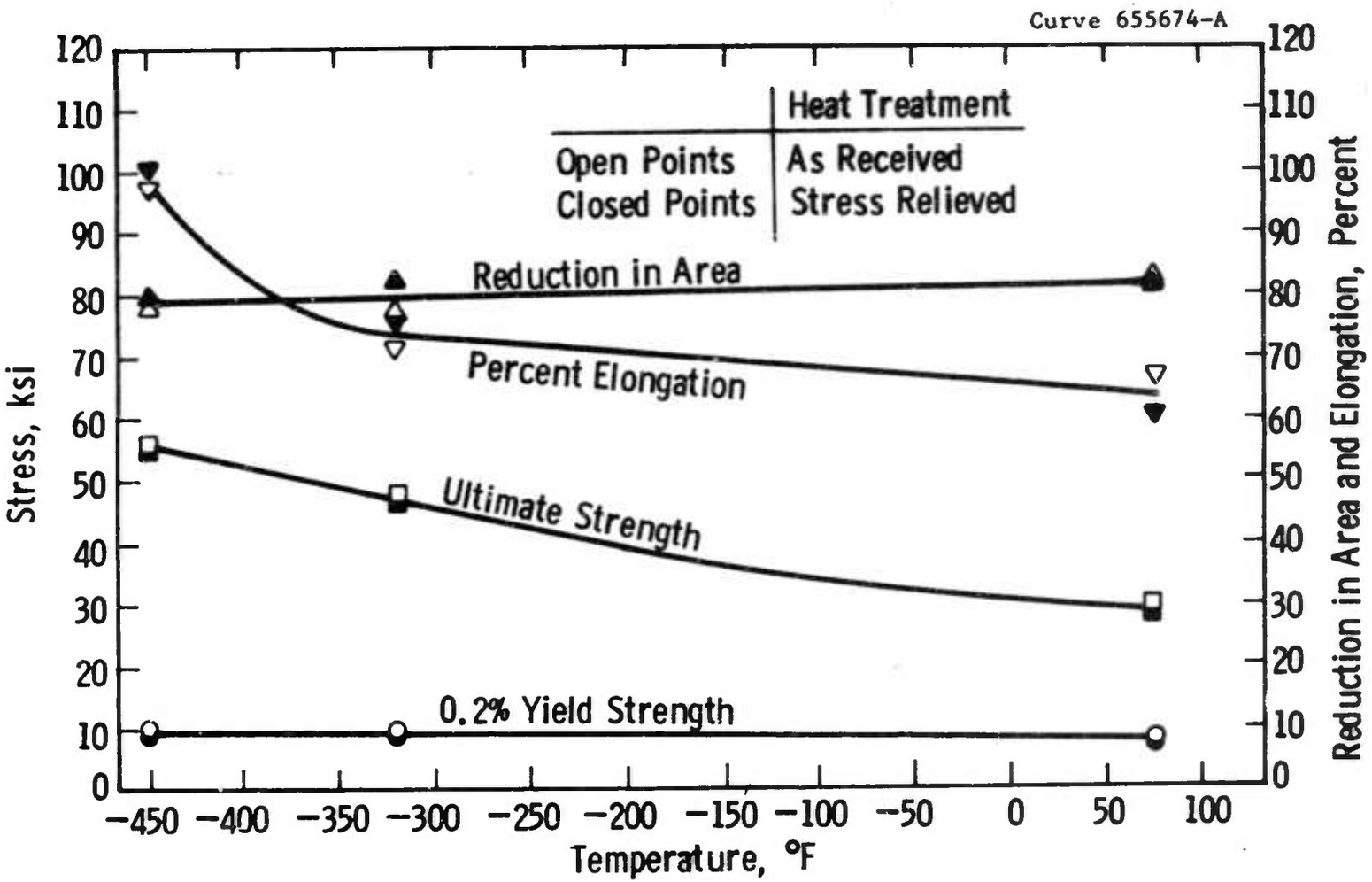

Fig.6-3— Tensile properties of OFHC copper

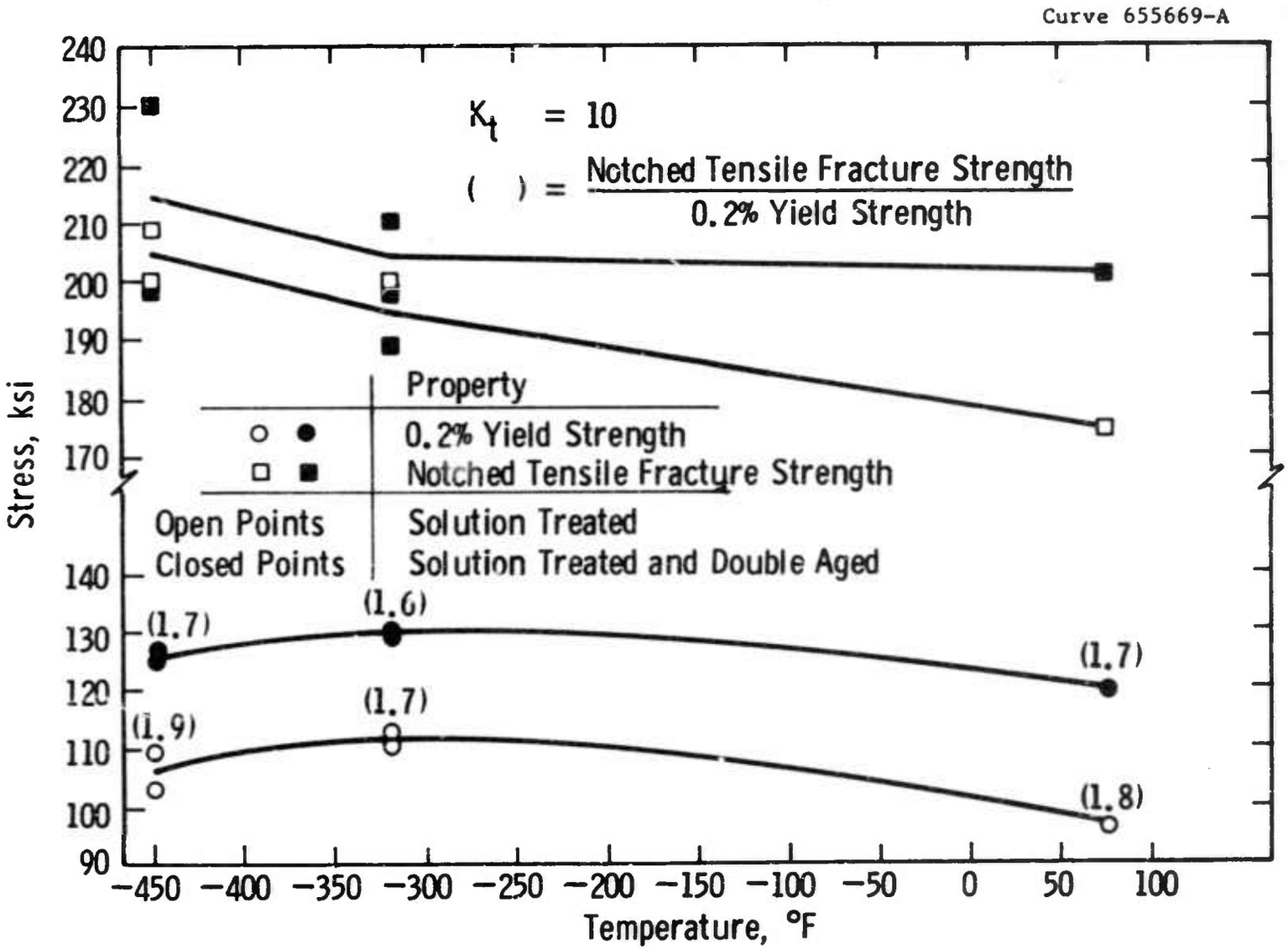

Fig. 6-4— Yield strength and notched tensile fracture strength of Inconel X750

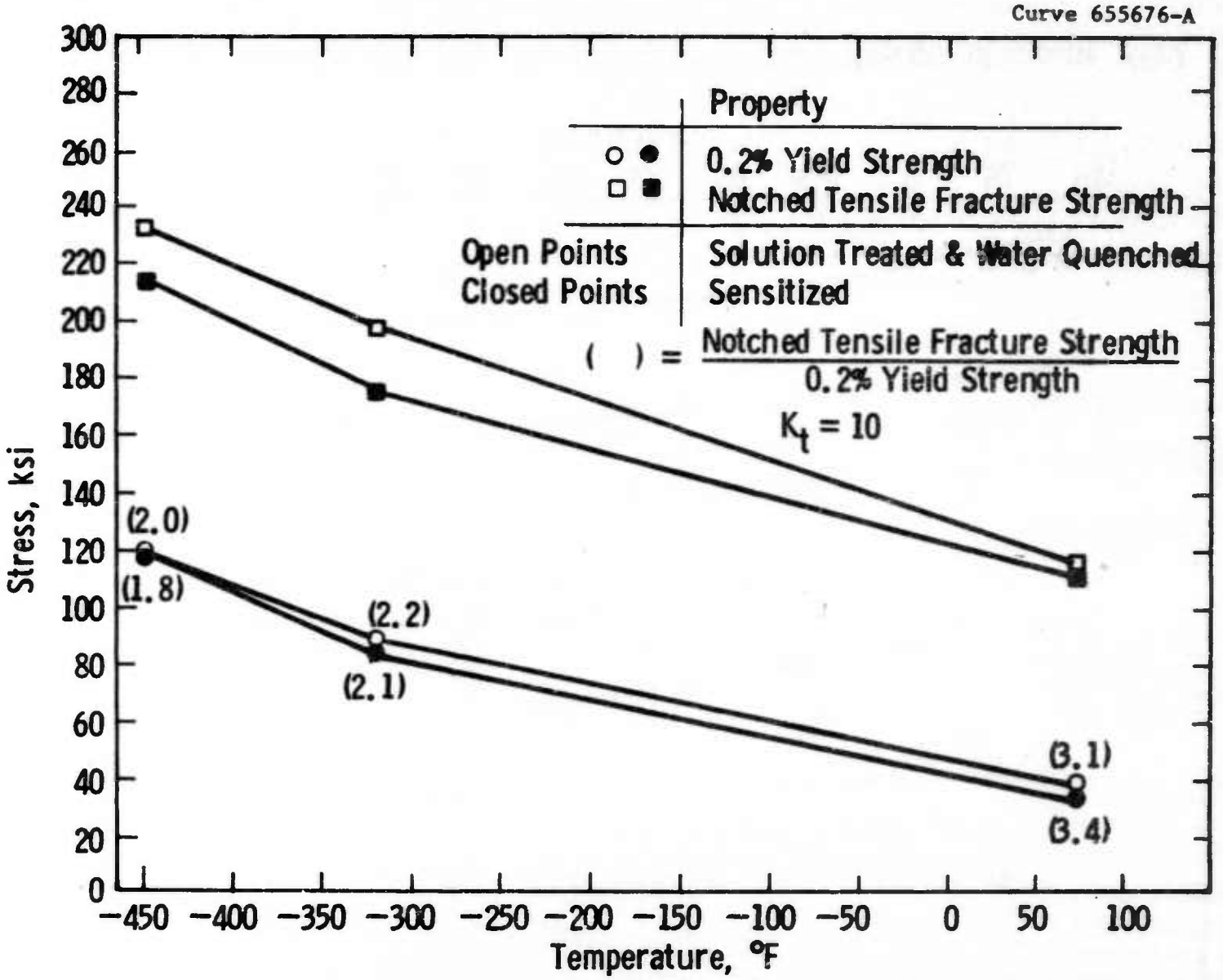

Fig.6-5—Yield strength and notched tensile fracture strength of 310 S stainless steel

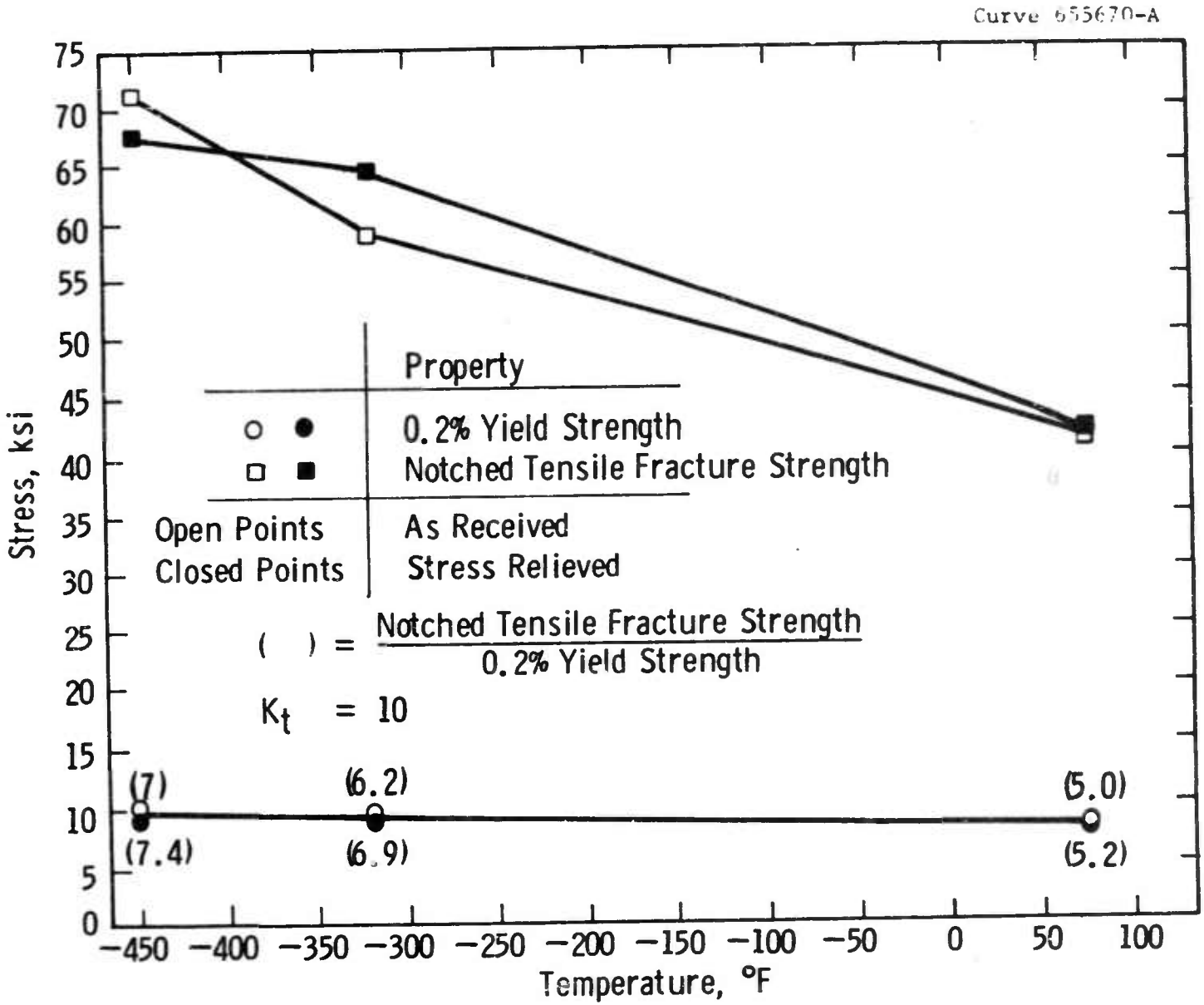

Fig.6-6— Yield strength and notched tensile fracture strength of OFHC copper

Dwg. 856A449

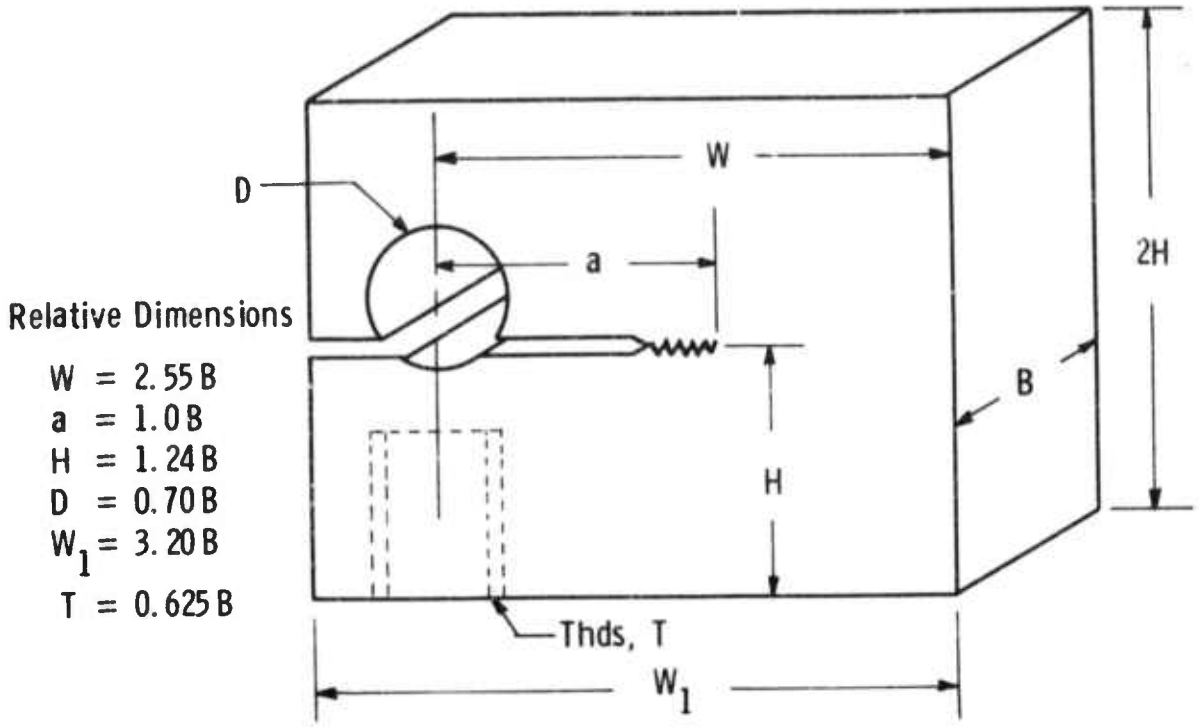

"T" Type WOL Specimen

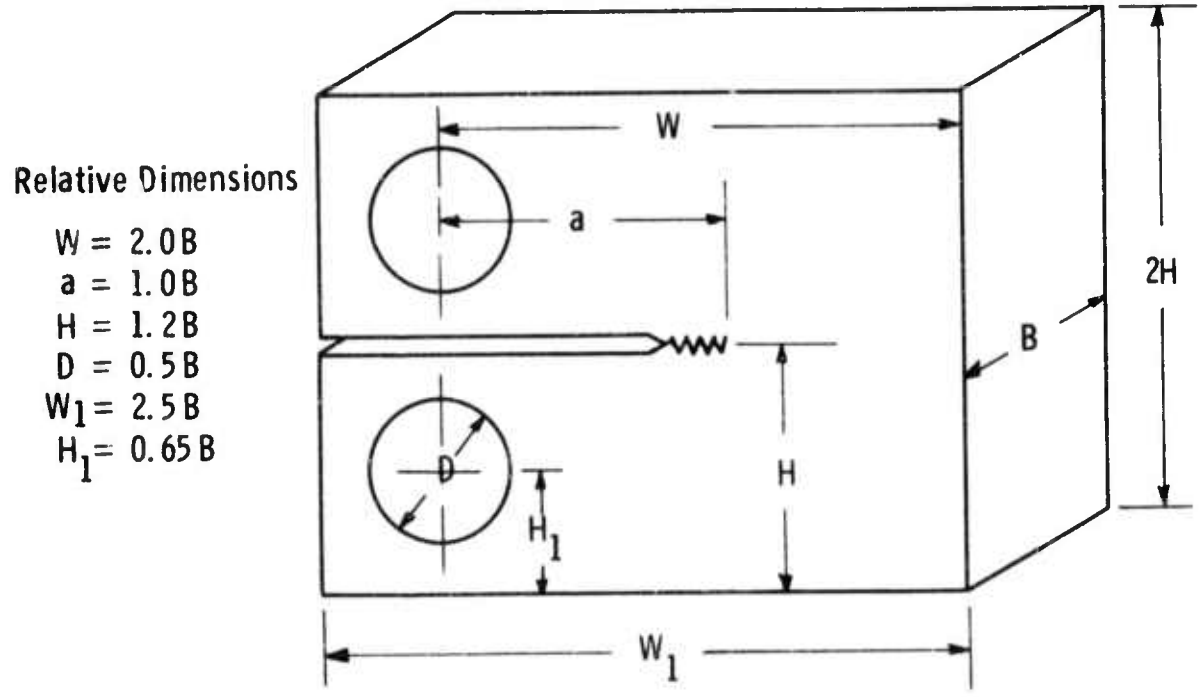

Compact K_{IC} Specimen

Fig. 6-7—Compact fracture toughness specimens (relative dimensions in terms of thickness, B)

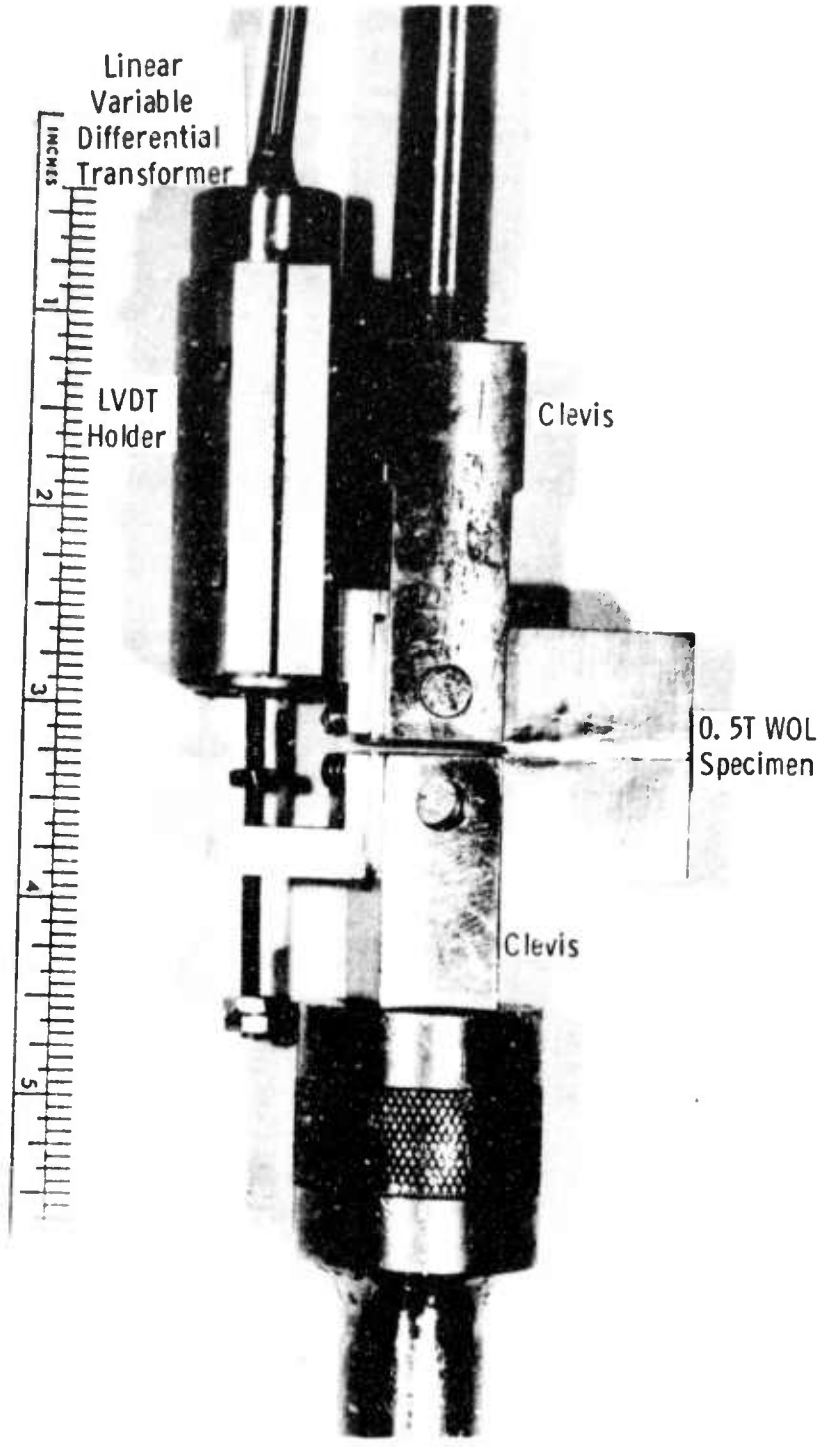

Fig. 6-8—Test setup for fracture toughness and crack growth rate tests

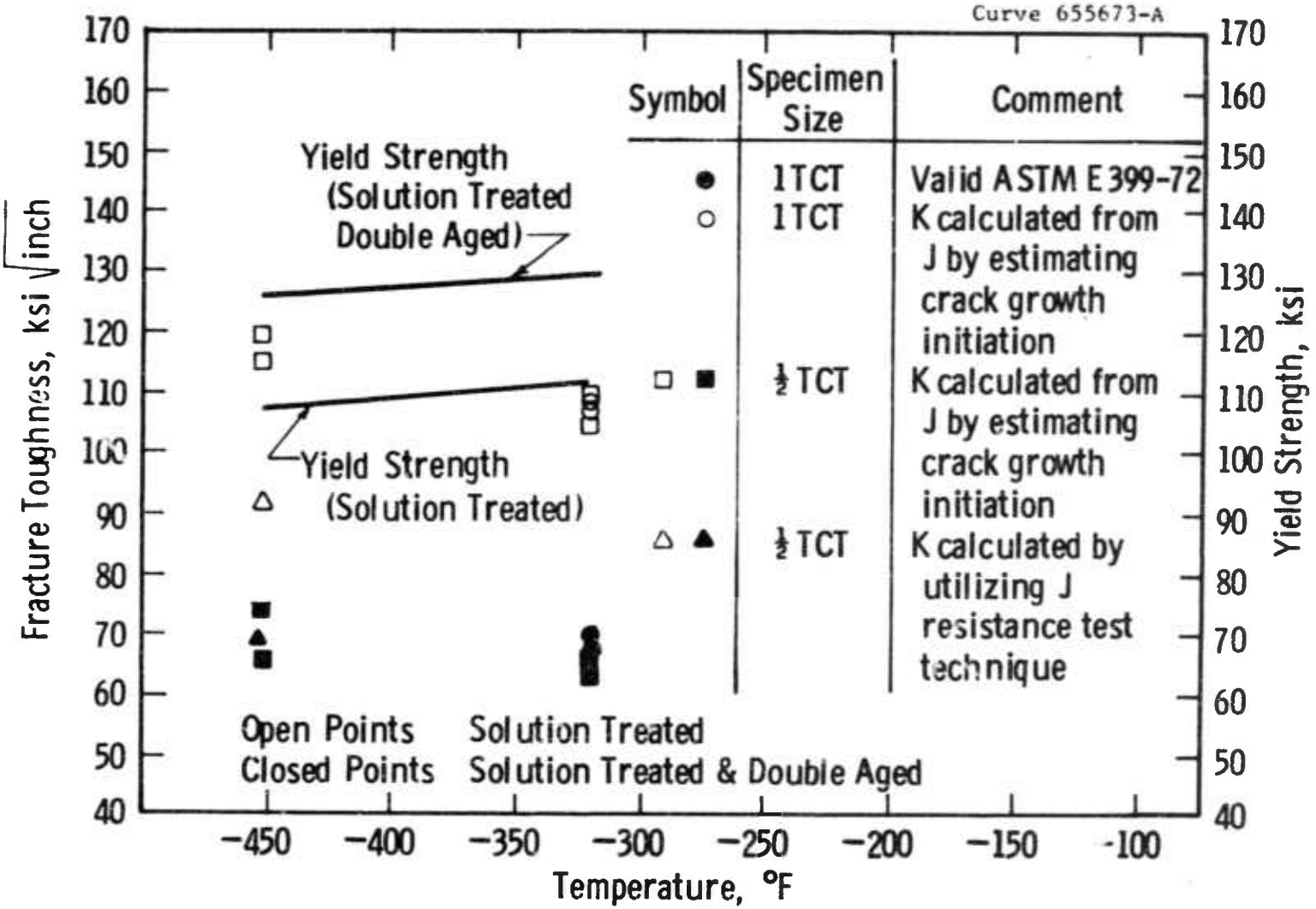

Fig.6-9—Temperature dependence of yield strength and fracture toughness for Inconel X750

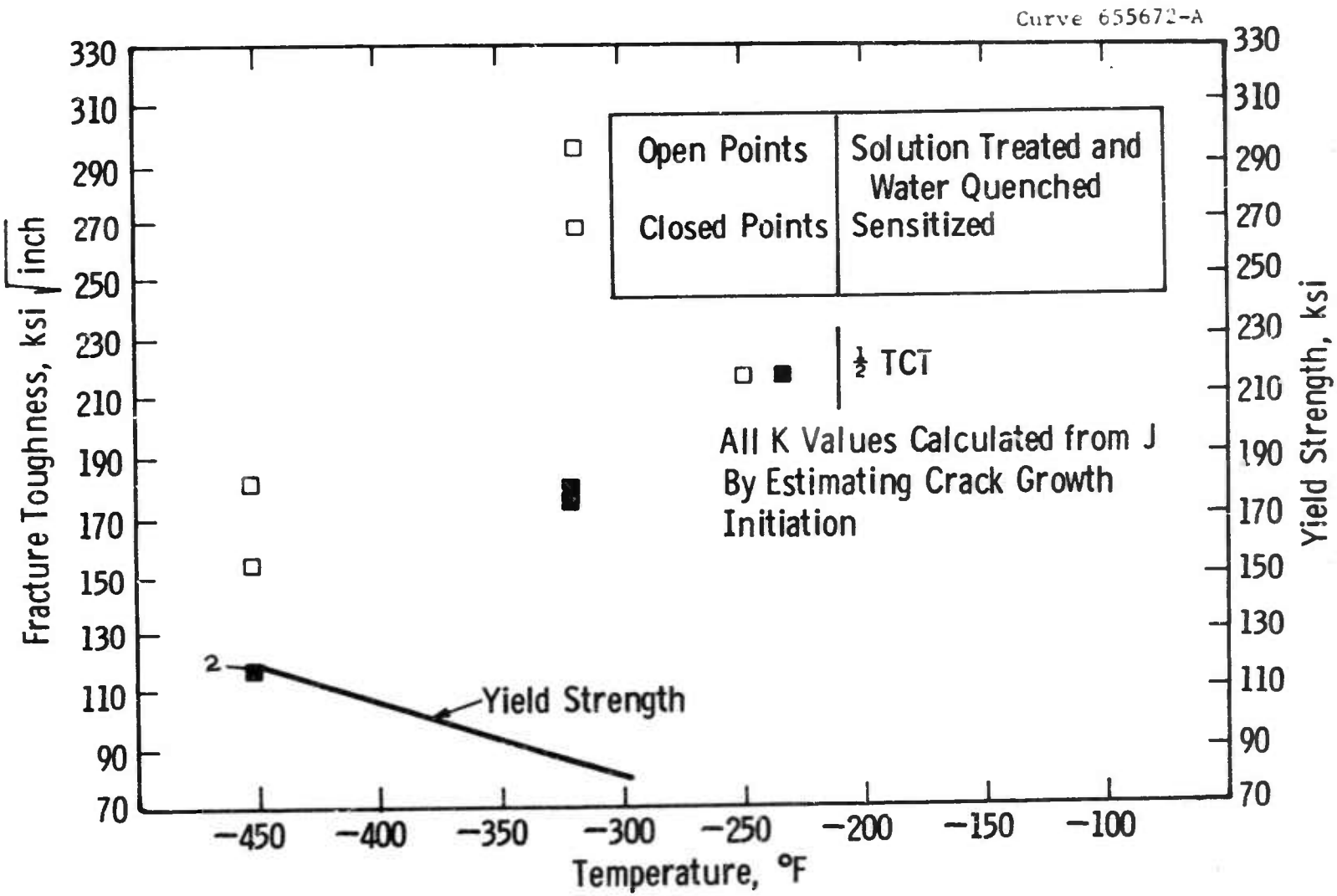

Fig.6-10-Temperature dependence of yield strength and fracture toughness for 310 S stainless steel

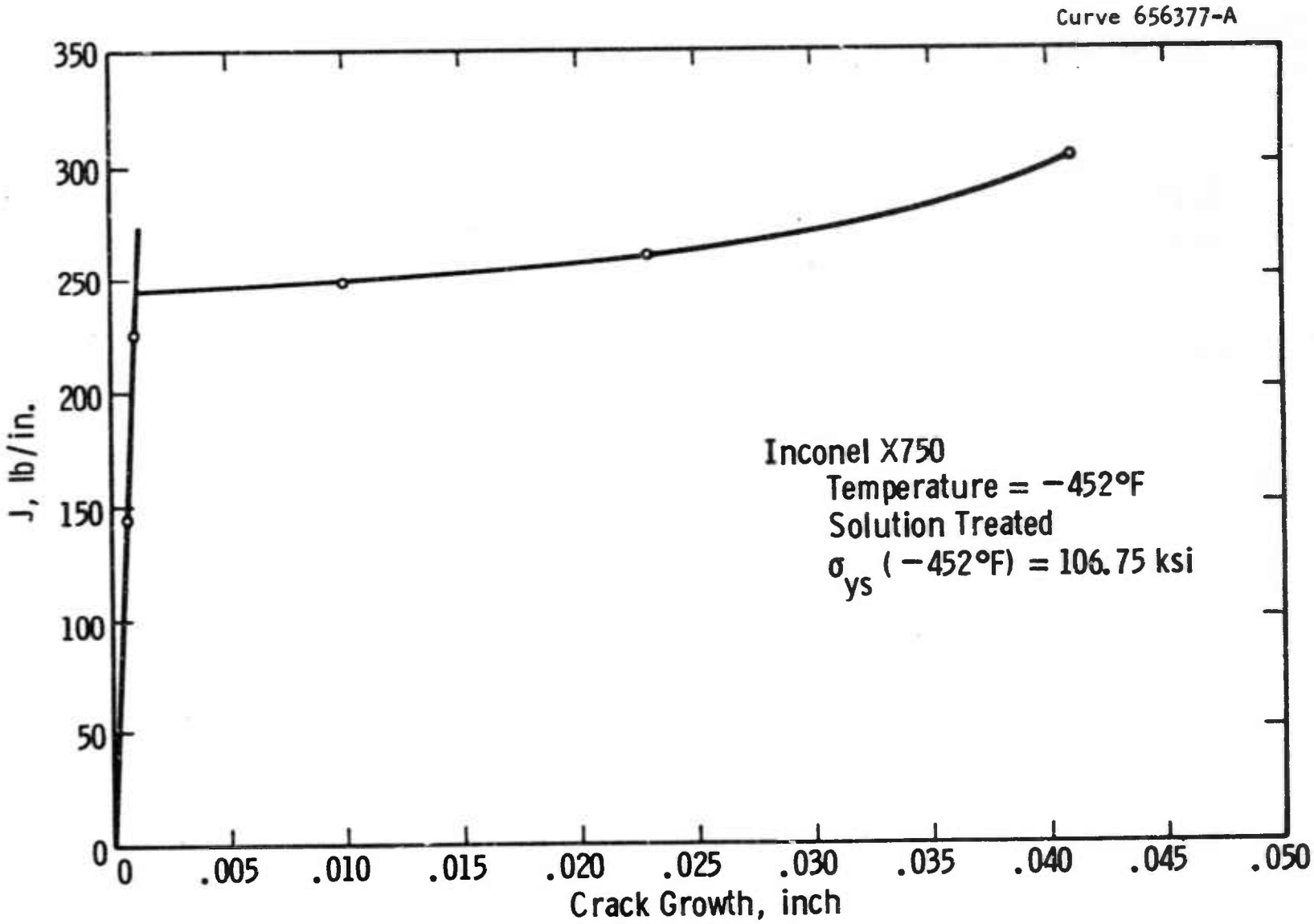

Fig. 6-11 —J resistance curve for solution treated Inconel X750 at a temperature of −452°F

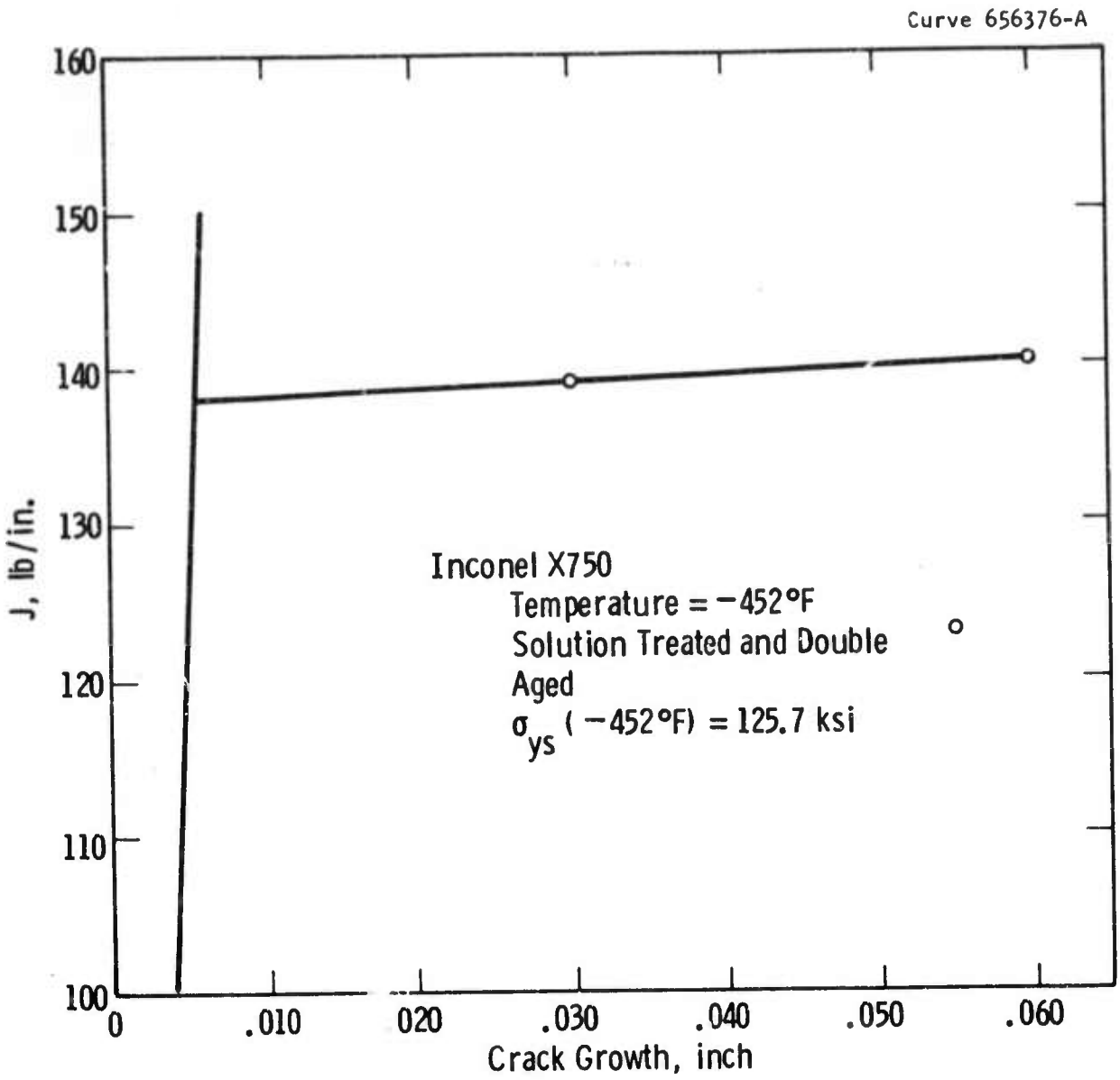

Fig. 6-12 −J resistance curve for solution treated and double aged Inconel X750 at a temperature of −452°F

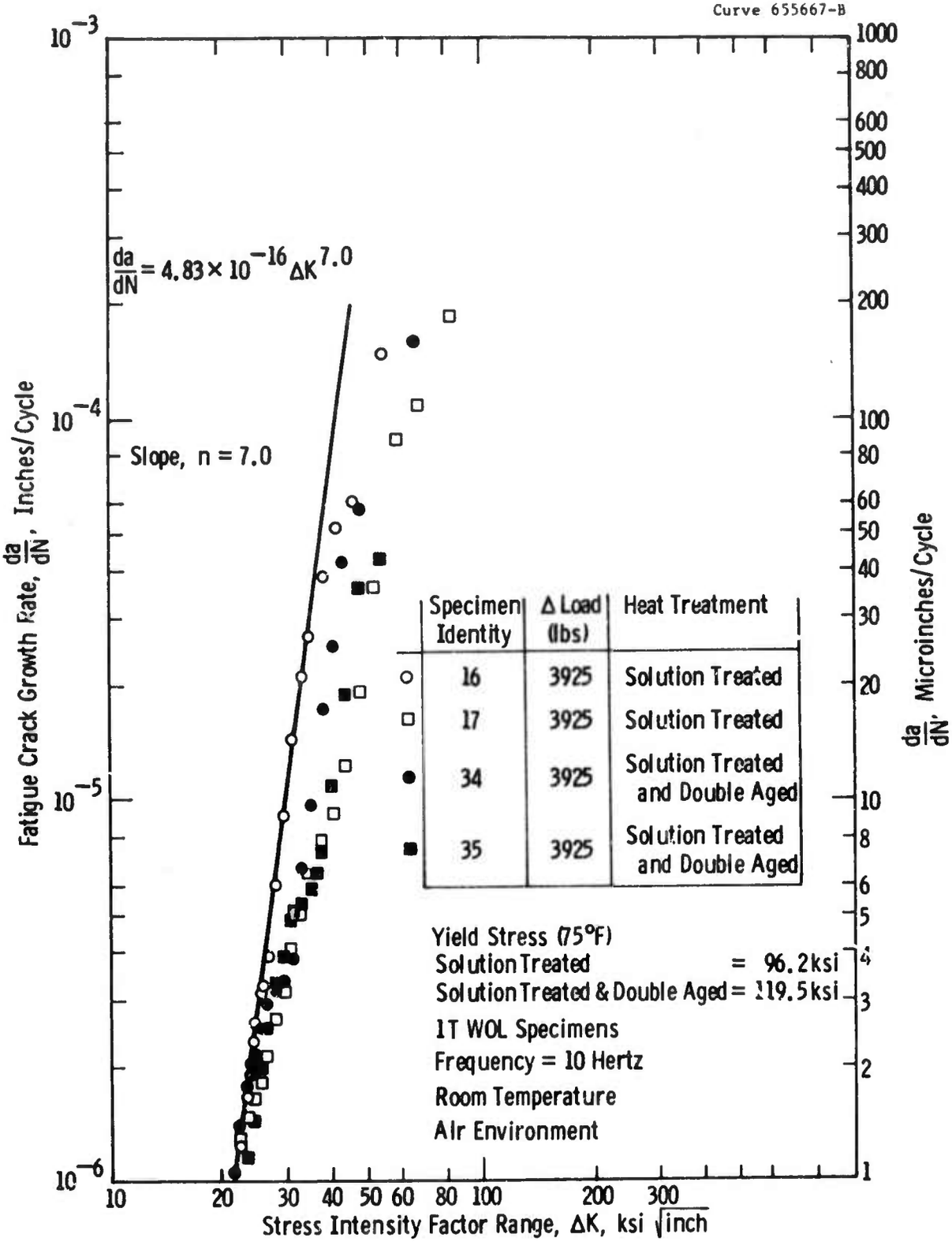

Fig.6-13-Fatigue crack growth rate properties of Inconel X750 in a room temperature air environment

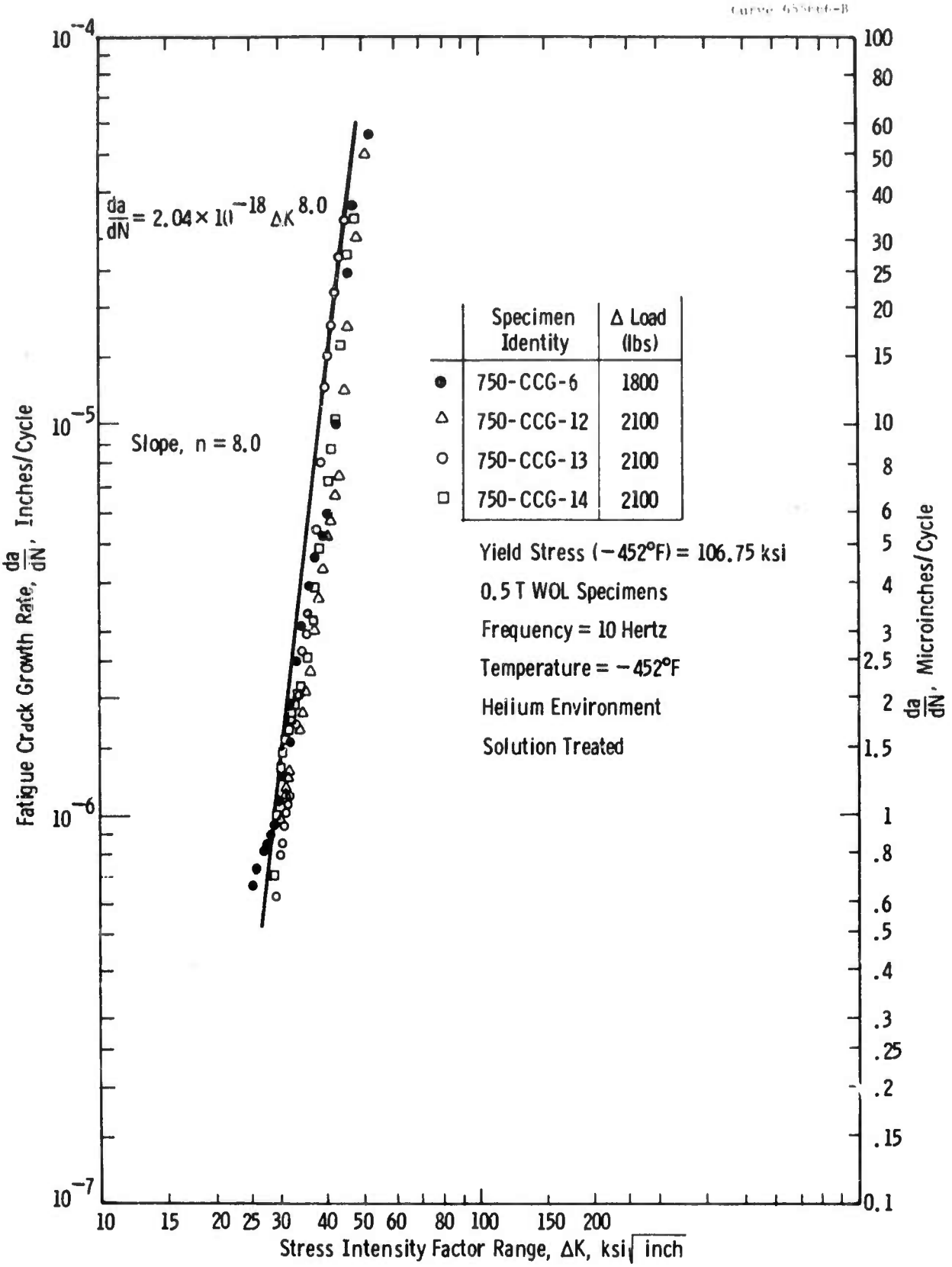

Fig.6-14-Fatigue crack growth rate properties of Inconel X750 (solution treated) in a −452°F helium environment

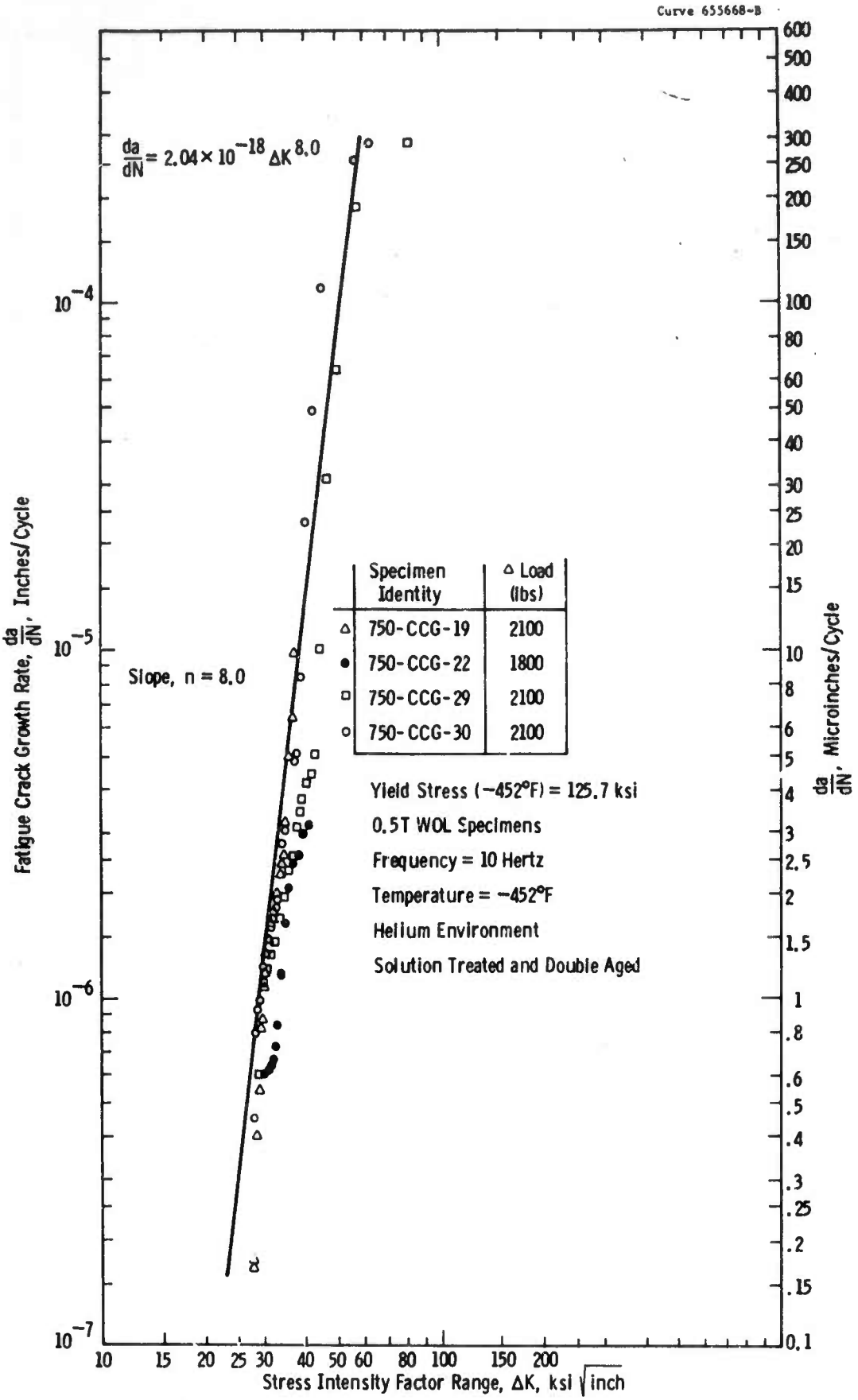

Fig.6-15-Fatigue crack growth rate properties of Inconel X750 (solution treated and double aged) in a −452°F helium environment

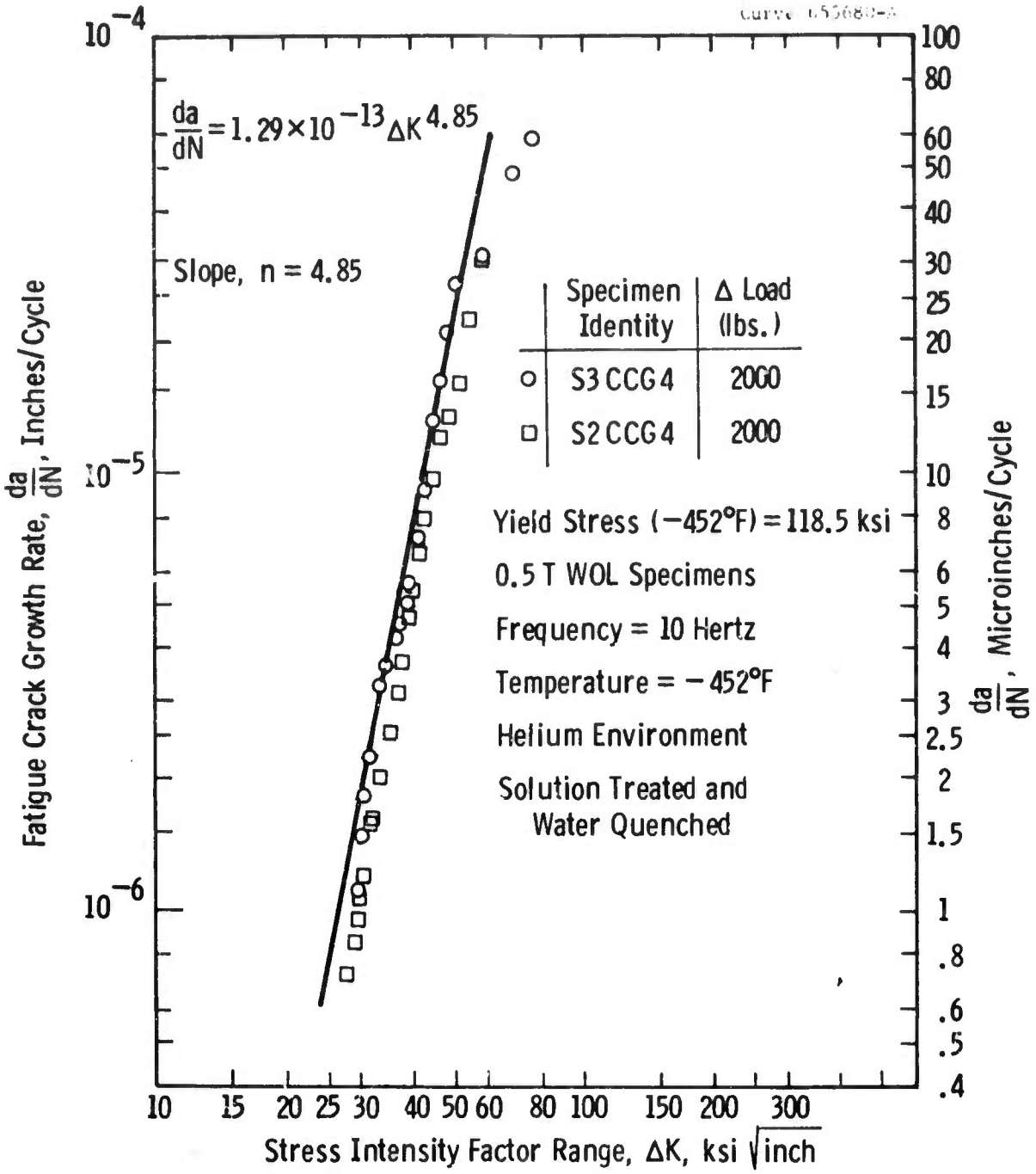

Fig.6-16-Fatigue crack growth rate properties of 310 S stainless steel (solution treated and water quenched) in a −452°F helium environment

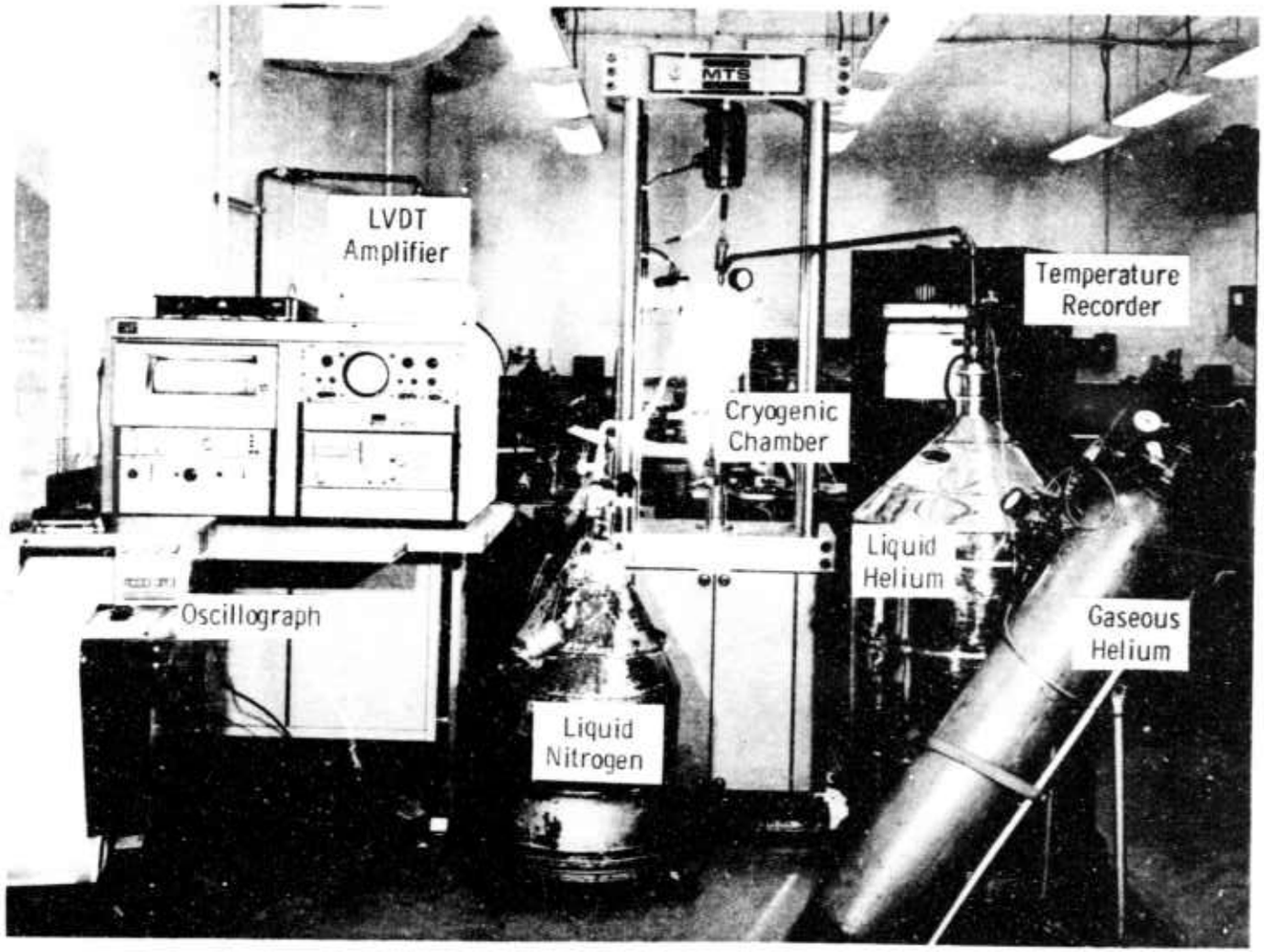

Fig. 6-17—Test equipment employed for cryogenic fatigue crack growth rate tests

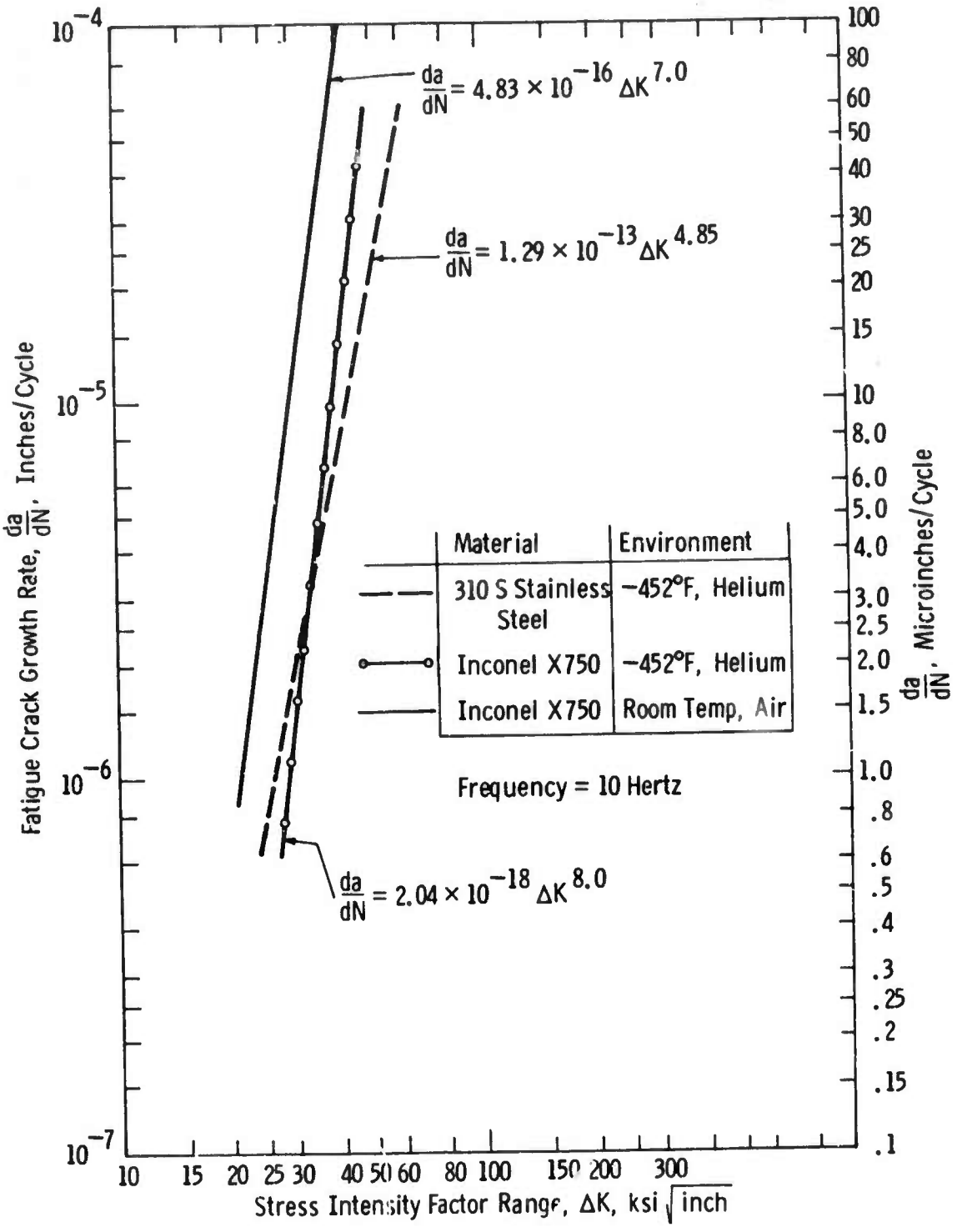

Fig.6-18-Comparison of the fatigue crack growth rate data generated for Inconel X750 and 310 S stainless steel

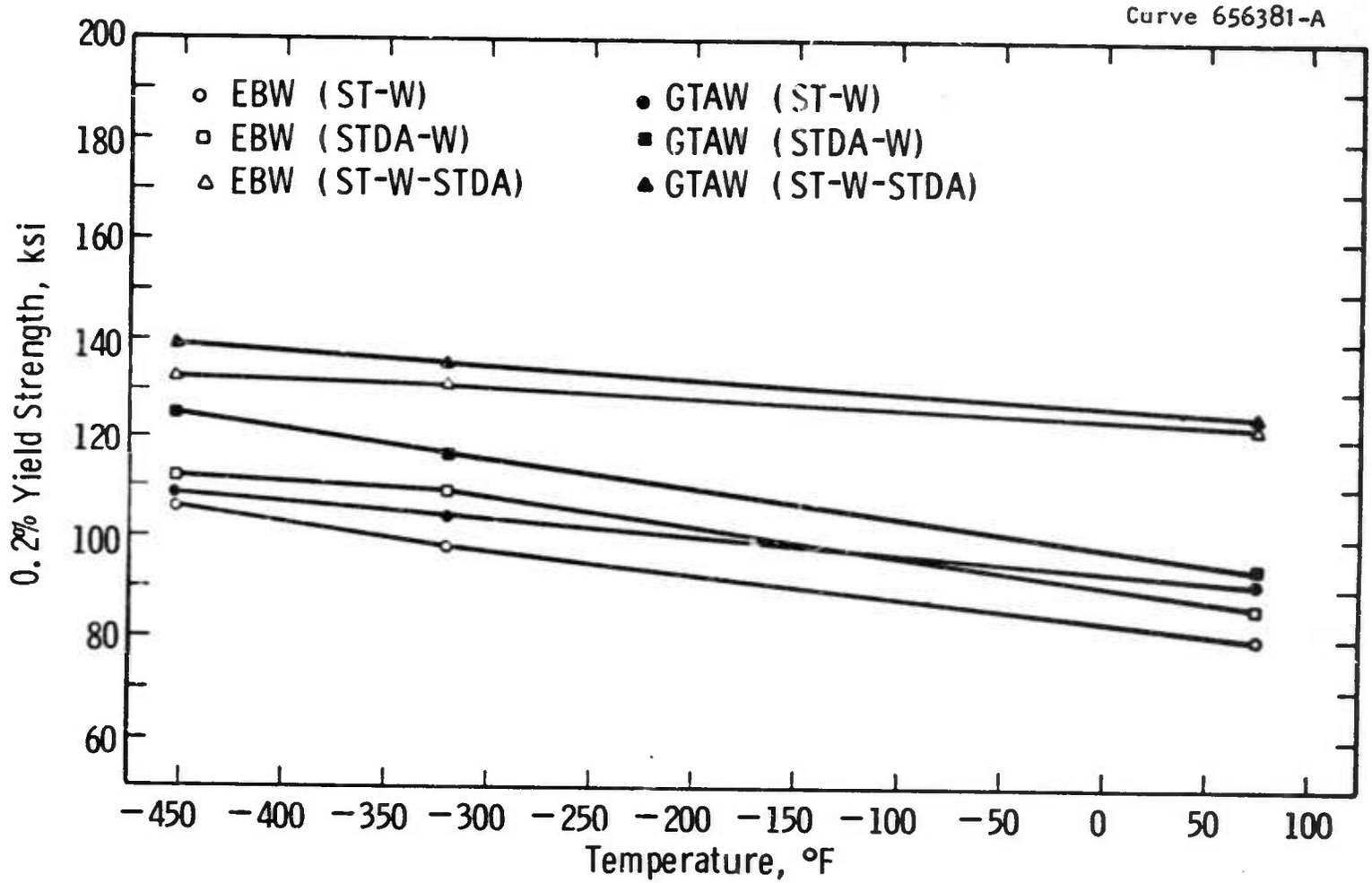

Fig. 6-19 —Yield strengths of Inconel X750 electron beam and gas tungsten arc welds

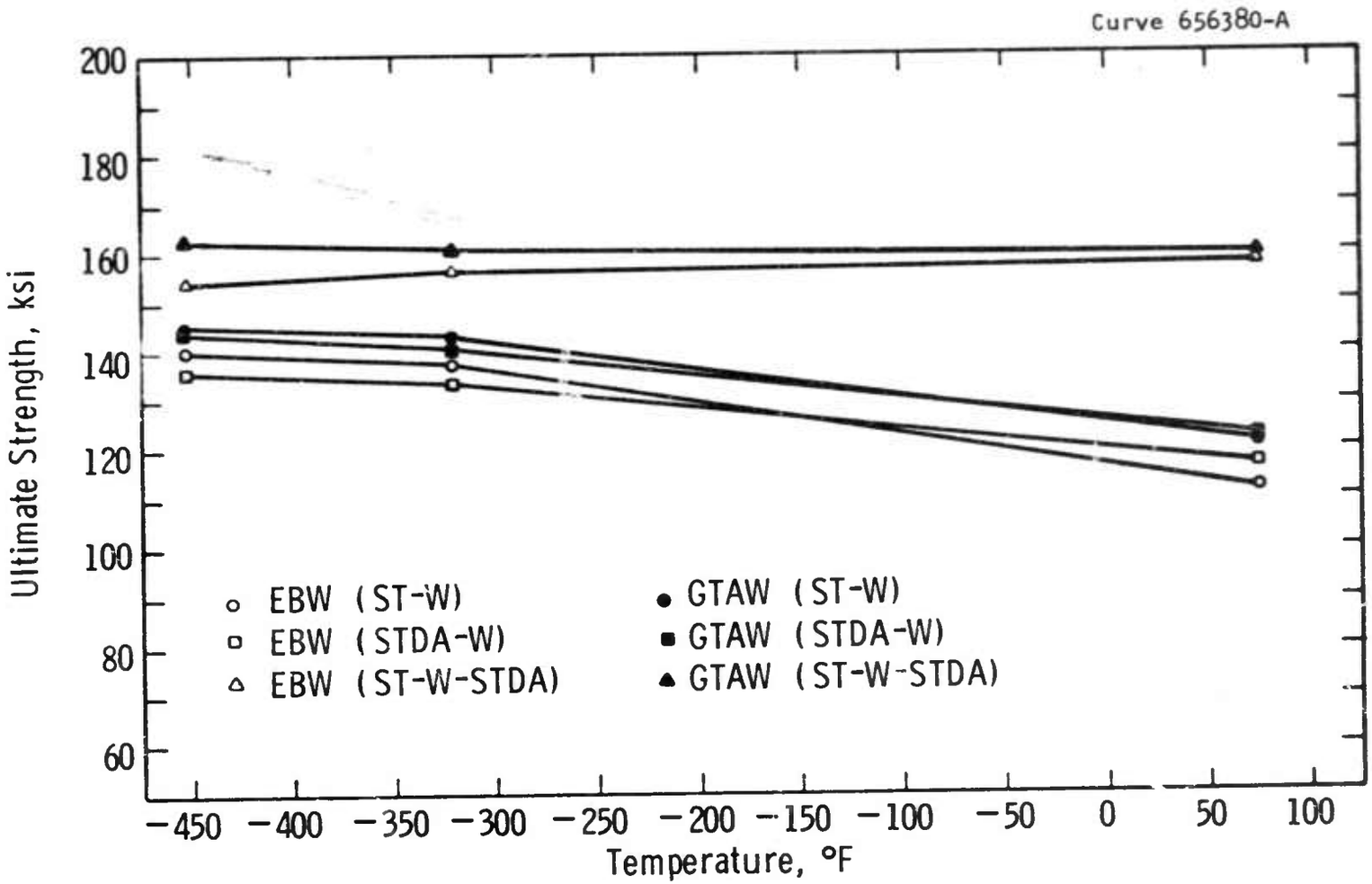

Fig. 6-20 —Ultimate strengths of Inconel X750 electron beam and gas tungsten arc welds

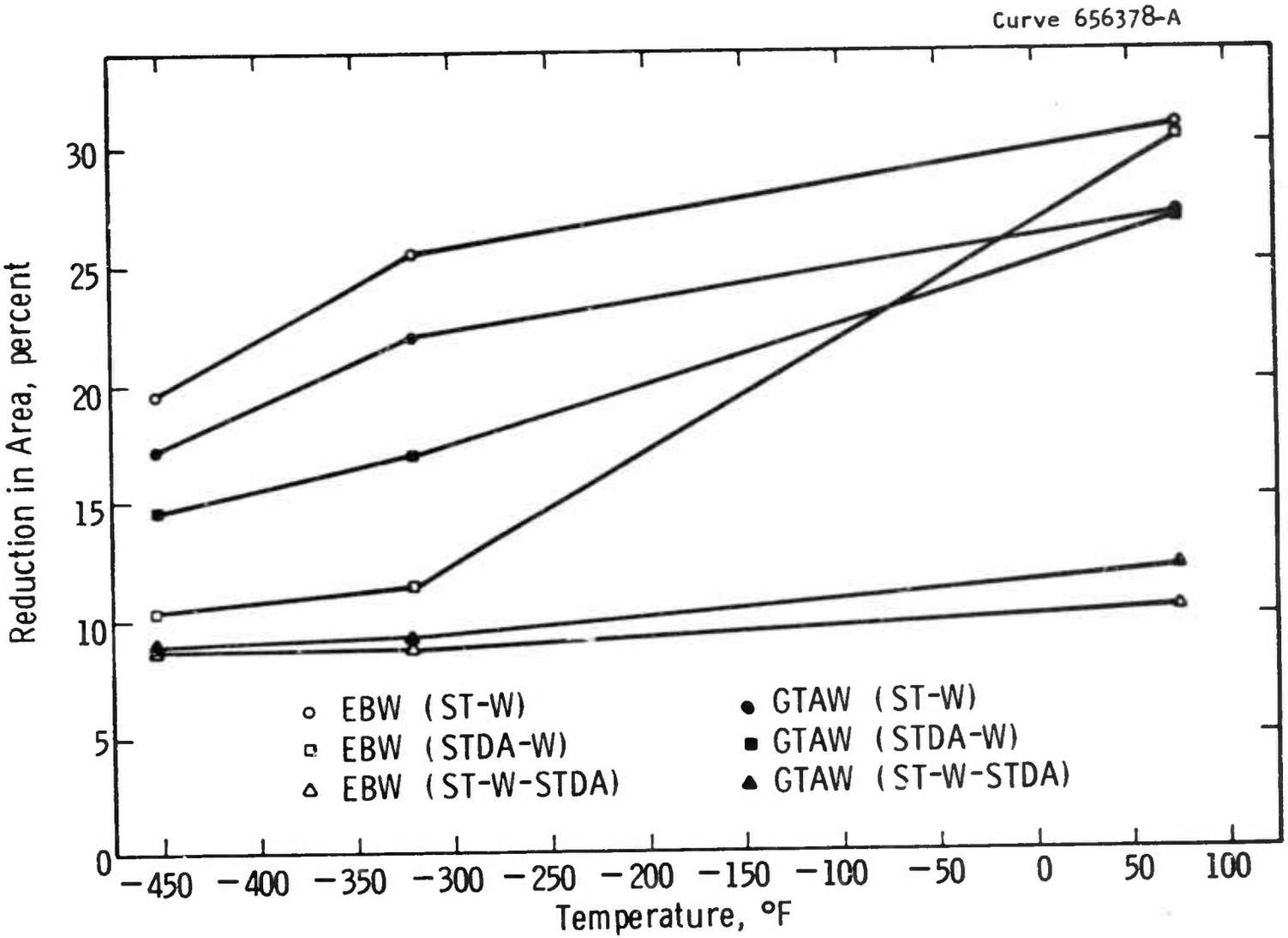

Fig. 6-21—Reductions in area of Inconel X750 electron beam and gas tungsten arc welds

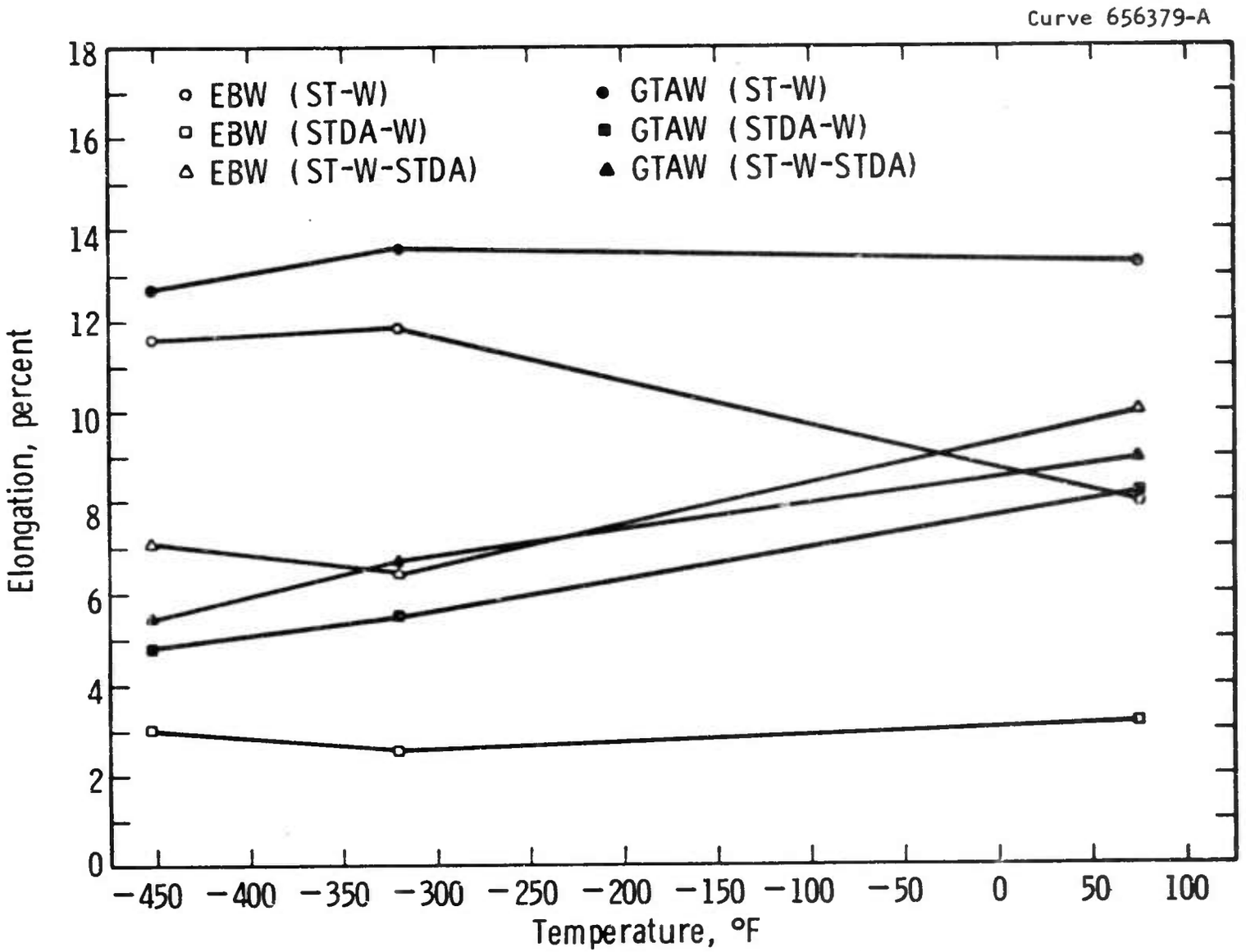

Fig. 6-22 —Elongations of Inconel X750 electron beam and gas tungsten arc welds

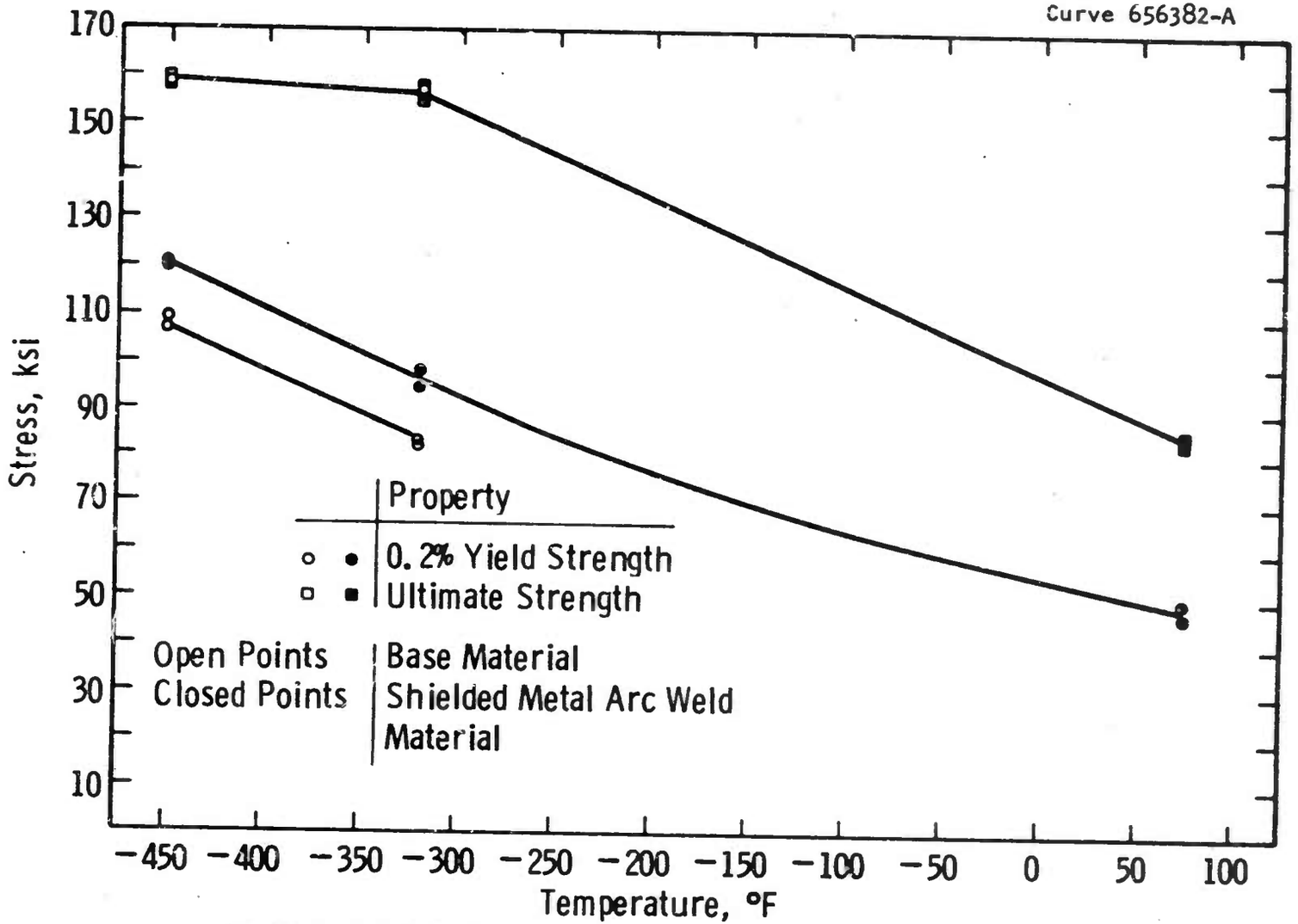

All Material Solution Treated and Water Quenched Before Welding
Weld Specimens Fractured in Base Material

Fig. 6-23—Tensile properties of 310 S stainless steel shielded metal arc welds

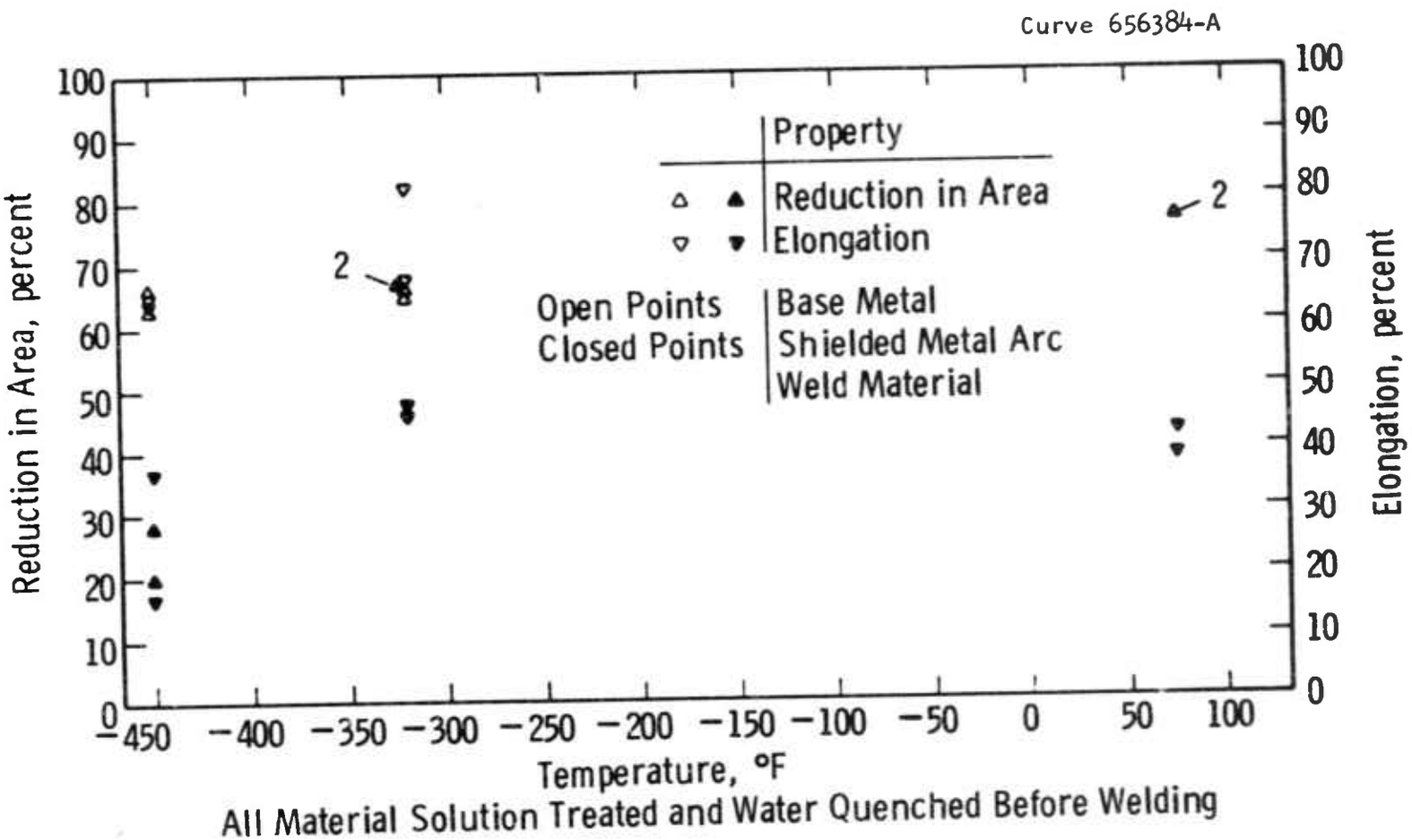

All Material Solution Treated and Water Quenched Before Welding

Fig. 6-24—Tensile properties of 310 S stainless steel shielded metal arc welds

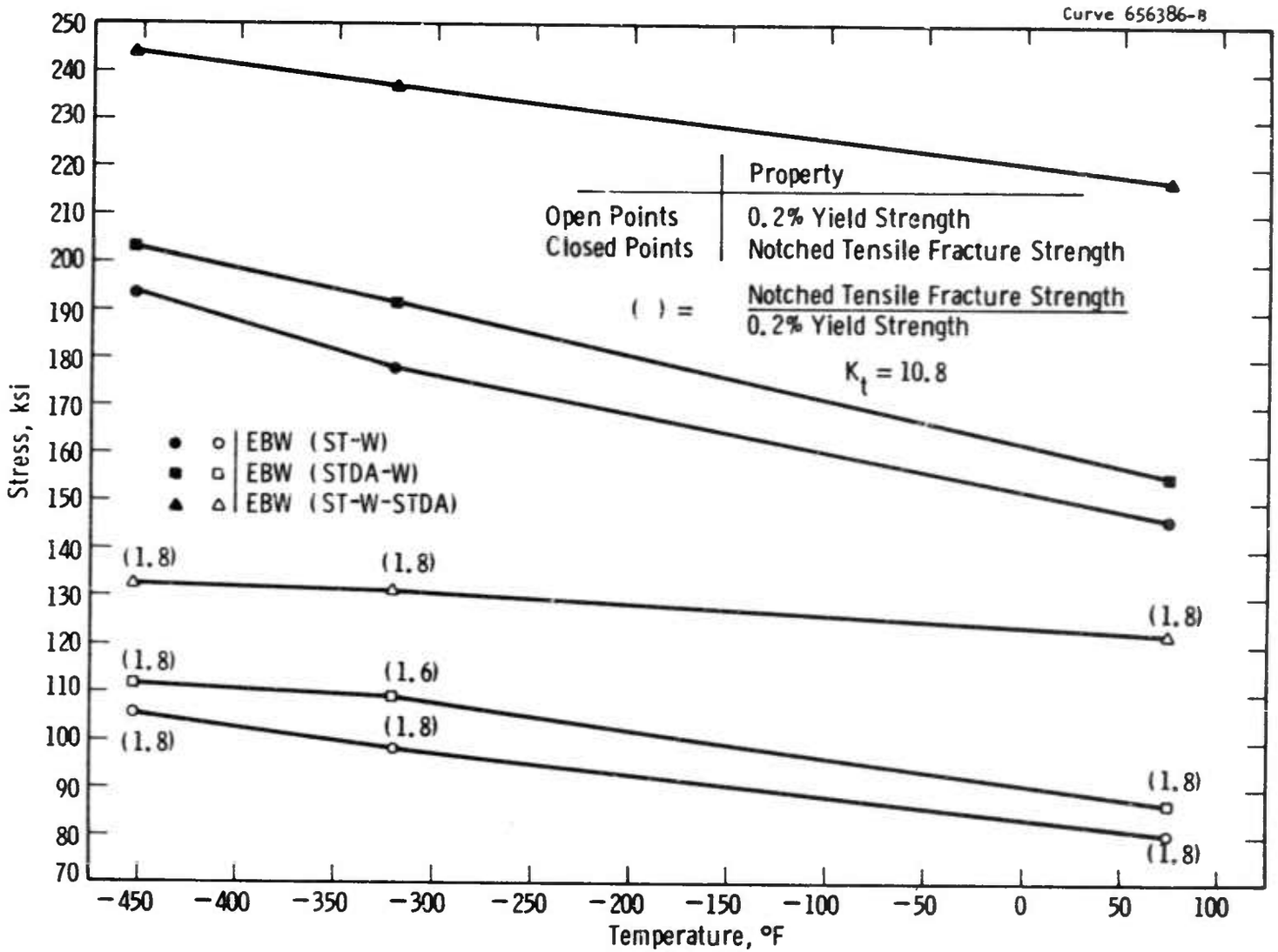

Fig. 6-25 —Yield strength and notched tensile fracture strength of Inconel X750 electron beam welds

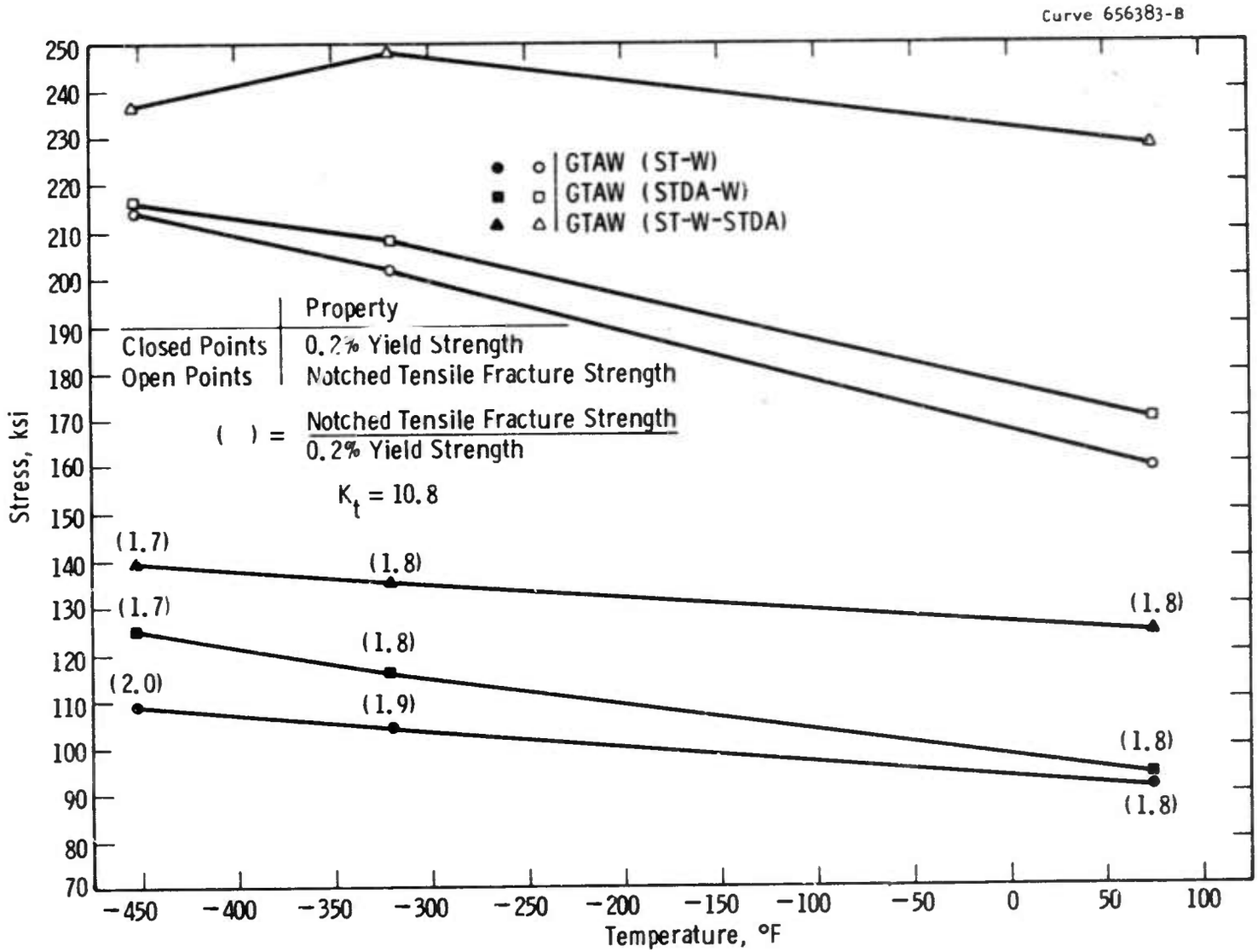

Fig. 6-26—Yield strength and notched tensile fracture strength of Inconel X750 gas tungsten arc welds

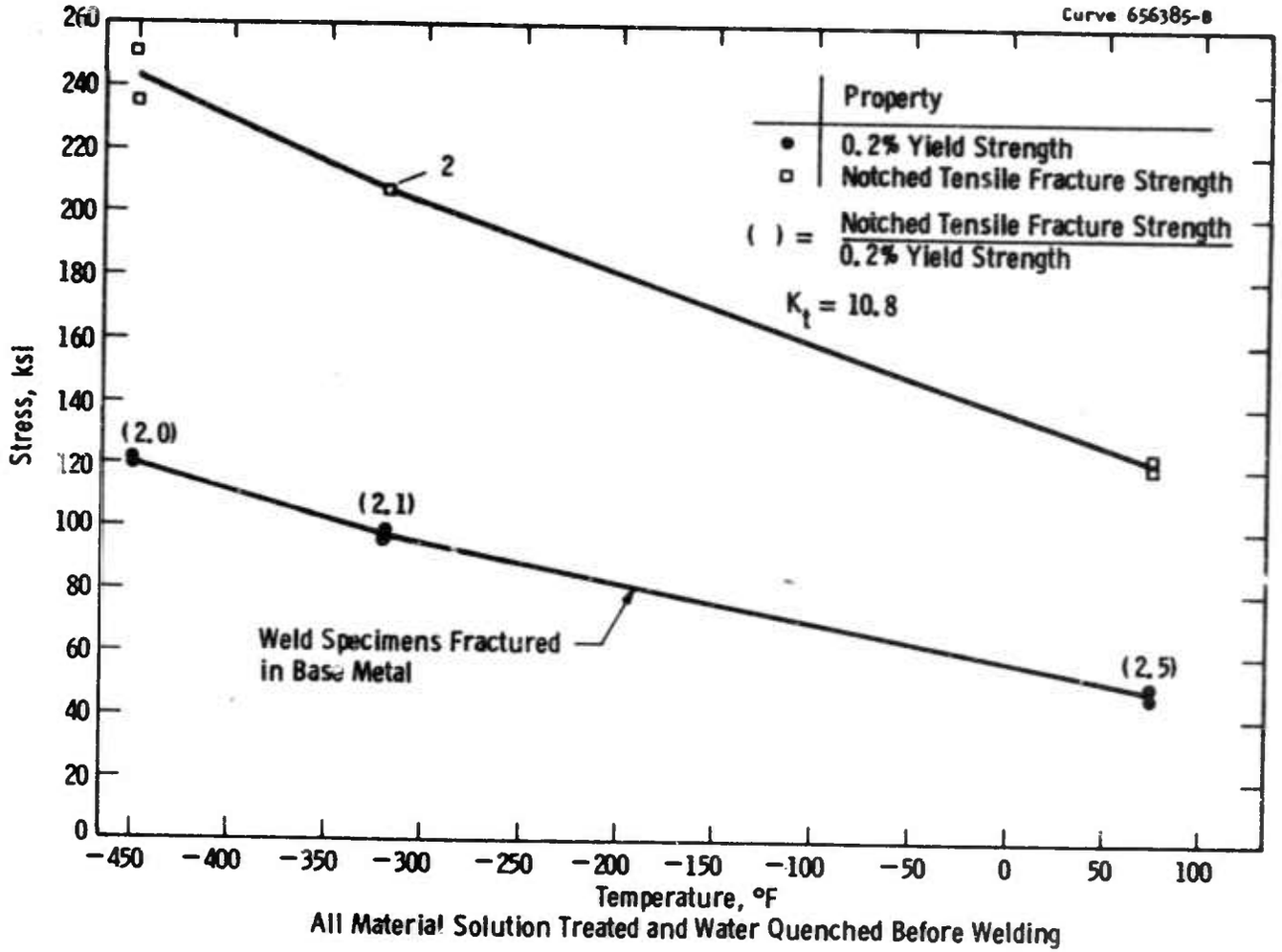

Fig. 6-27—Yield strength and notched tensile fracture strength of 310 S stainless steel shielded metal arc welds

7.0 MICROSTRUCTURAL ANALYSIS

The purpose of this phase of the work is twofold. (a) Examine the microstructure of tested specimens to determine cause and mode of failure and (b) Correlate the microstructural features with mechanical test data to establish failure mechanism and effects of processing variables. With this knowledge in hand, one is able to identify critical areas in processing or end use and suggest modification for an optimization of processing, material use, and performance realization. Three materials were examined during the period of this report. OFHC Cu, 310S stainless steel and Inconel X-750. The thermal and mechanical treatments given to each group of these materials is discussed in Section 5. Each material was first examined in the as received condition to determine the general microstructural features of the starting stock. Following that, fracture surface and other microstructural details were examined and defined on three groups of test specimens, i.e., tensile, fracture toughness, and crack-growth-rate specimens. An operational flow chart of this functional area is shown in Fig. 7-1, while the corresponding test matrix is shown in Table 7-1.

7.1 OFHC Copper

The examination of OFHC Cu was limited to a few specimens only because the material is very ductile and no particular difficulties were encountered in tests down to -452°F.

Figure 7-2 shows a light micrograph of a longitudinal section from specimen 11T3-1 and SEM micrograph of the fracture surface of specimen 11T2-1. The former was tested at 4°K (-452°F) while the latter was tested at 77°K (-320°F). Figure 7-2a indicates that a substantial amount of deformation has occurred, as is indeed shown by

the test results, Section 6. The ductile nature of the fracture is indicated in Fig. 7-2b. The deep holes are typical of a severe necking process typified by a uniform grain deformation with only a limited indication of intergranular failure. Fracture surfaces from a fracture toughness specimen tested at -452°F are shown in Fig. 7-3. Figure 7-3a shows the surface of the fatigue pre-crack produced at ambient temperature. Figure 7-3b shows the fracture surface following the -452°F test. This fracture surface is very similar to the one shown in Fig. 7-2b. This is to be expected since the fracture toughness specimen is tested in the first mode (I), or tensile mode. It will be shown later, that for the three materials studied there is a close similarity between the features of fracture surfaces in tensile and mode I fracture toughness specimens.

Although fatigue deformation is not the subject of this report, the mode of fatigue crack growth is of interest. Figure 7-3a indicates a combination of stage I crystallographic fatigue crack propagation and a ductile tearing failure modes. Since Cu exhibited high ductility to -452°F, crack-growth-rate experiemnts were not carried out with this material. In fact, the few fracture toughness tests conducted have indicated ample ductility so that accurate determination of K_{IC} was not possible. Tests were then discontinued beyond the few that have been described.

7.2 310S Stainless Steel

Test specimens were subjected to two heat treatments: (a) 1 hr at 2000°F followed by water quench, (STQ), and (b) 1 hr at 2000°F followed by furnace cool to 800°F, then air cooled (STFC). The second heat treatment is a "sensitization" treatment.

A light micrograph of a sensitized specimen is shown in Fig. 7-4. Matrix and grain boundary carbides can be seen in addition to a fair amount of annealing twins. Twin density was much lower in the solution treated and water quenched structure.

Cross sections taken near the broken edge of two tensile specimens are depicted in the light micrographs of Fig. 7-5. There is a heavy agglomaration of grain boundary precipitates, mostly $Cr_{23}C_6$ type carbides. There is no evidence of deformation twinning; slip lines indicate heavy deformation through the entire grain volume, including pre-existing twins. The effect of furnace cooling (sensitizing) upon the mode of fracture in 310S is illustrated in Figs. 7-6 through 7-8. The room temperature fatigue-precracked surface, the transition to low temperature fracture, and the fracture surface of a fracture toughness specimen solution treated and water quenched and tested at -452°F are shown in Fig. 7-6 . The ductile, mostly cross-granular mode of fracture is quite obvious. The particles on the low temperature fracture surface are probably undissolved, or partially precipitated, carbides.

In contrast to Fig. 7-6, the intergranular mode of fracture following furnace cooling is seen in Fig. 7-7. The crystallographic, stage I, fatigue deformation is shown in Fig. 7-7a and a substantial grain boundary cracking is seen in Fig. 7-7c. The transition from room temperature fatigue to low temperature opening mode fracture is shown in Fig. 7-7b. A higher magnification micrograph of a low temperature fracture of a sensitized specimen (Fig. 7-8) shows carbide precipitates associated with intergranular cracks (arrows). Previously shown tensile data, indicated a sensitization effect at room temperature and -320°F of a 10% decrease in strength. A deterioriation in ductility is observed for both low temperature tests. The proportional limit, indicating the lowest resolvable yielding, is independent of heat treatment, while the decrease in 0.2% yield with sensitization is confined to RT and -320°F tests. This indicates that the sensitization treatment has no effect on the intrinsic strength of the material; the precipitates forming in the boundary do not affect the solution hardening function of Cr, and do not enter the yielding phenomenon. However, work hardening rate increases due to the presence of the carbides in the

boundary. Thus, the ultimate strength, which reflects the intrinsic metal strength, is the same for both treatments. This, in turn, causes a lower ductility for the sensitized specimens.

In summary, therefore, the test results with 310S indicate an embrittlement effect of slow cooling due to precipitation of grain boundary carbides. Although the change in tensile properties is not substantial, the grain boundary embrittlement may manifest itself in fatigue and crack growth rate tests. This will have to be watched for during subsequent tests. It seems further possible that the problem of sensitization will appear in welded structures, where the rate of cooling of the heat affected zone may be slow enough to produce a carbide precipitation. Test results of welded specimens will be discussed in subsequent reports.

7.3 Inconel X-750 Alloy

General grain morphologies of X-750 materials are shown in Fig. 7-9. Two heat treatments were studied, i.e., solution treated for one hour at 1800°F followed by air cool and a double age treatment consisting of a solution treatment as above, furnace cooling to 1350°F with an 8 hour hold, followed by furnace cool to 1150°F, followed by another 8 hour hold and air cool. The double aging is designed to precipitate a fine, closly packed structure of γ' and transform MC carbides into grain boundary, discontinuous, $M_{23}C_6$ precipitates.

The light micrograph in Fig. 7-9 do not reveal the microstructural changes occurring upon aging. At this magnification and resolution, a typical austenitic structure is revealed, namely, an equiaxed structure with occasional annealing twins present. Some of the dark spots seen in the micrographs are artifacts; others may be due to a pulled out carbide during polishing followed by overetching effect at the cavity (arrows). One should note, however, the difference in grain size. This is not due to heat treatment but rather to the distribution of grain sizes in the 10" dia. forging billet from which samples and test specimens were machined. The variation in grain sizes among the tensile specimen is shown in Table 7-1.

TABLE I -- GRAIN SIZES IN X-750 TENSILE SPECIMENS

Spec. desig. (ST + AC)	Test Temp.	Avg. Intercept mm	Spec. desig. (ST + DA)	Test Temp.	Avg. Intercept mm
30T1-1	75°F	0.070	31T1	75°F	0.080
30T2-1	-320	0.071	31T2-1	-320	0.069
30T3-2	-320	0.085	31T2-2	-320	0.052
30T3-1	-452	0.133	31T3-1	-452	0.125
30T3-2	-452	0.148	31T3-2	-452	0.134

Figure 7-10 is an extraction replica taken off a solution treated and aged specimen. Very fine, (∿ 100° A dia.) uniform distribution of spherical γ' precipitates are seen. The larger black spots are probably due to extracted MC carbides.

Two stage carbon replicas of polished and overetched surfaces of an aged structure are shown in Fig. 7-11. A few significant features can be noted. (a) Denuded grain boundary zone. This is a typical aging phenomenon in Ni-Cr superalloys. The precipitation of $M_{23}C_6$ carbides in the boundary depletes the adjacent matrix of chromium. This in turn increases the solubility of γ' in the Ni-Cr matrix resulting in precipitation free zones along the grain boundaries. These zones are clearly marked by etching facets. (b) The γ' precipitates in the grain cause a wavy etching pattern. (c) The $M_{23}C_6$ discontinuous precipitates deliniate grain boundary lines. In some grains, the denuded zones seem to extend somewhat beyond the narrow band around the grain boundary. This may be significant as far as occurrance of weak spots within the structure.

The deep etching method can be used to scan large areas for γ' distribution since the extractive replica method is tedious and does not lend itself to observation of large, continuous areas. Figure 7-11c provides support for the above suggestion. Indeed, an overetched structure of a solution treated specimen, where there is no γ' precipitation, shows the faceted structure which is typical of the γ' denuded zones around the boundary in aged specimens (Fig. 7-11a,b).

Longitudinal sections of three tensile specimens tested at low temperatures are shown in Fig. 7-12. All three micrographs exhibit similar general features. There is a fair amount of uniform deformation in the grains as evidenced by the slip lines. All three specimens failed by intergranular fracture. In Fig. 7-12c there is a clear evidence that grain boundary cracking is associated with carbide precipitates (arrows). The fine, "pepper" like particles are from contaminants present in the as received material. It can be concluded from Fig. 7-12 that the macroscopic features of deformation and fracture are similar for the solution treated and solution treated and aged specimens. However, tensile test data, indicate a 25% increase in strength at all three temperatures in the aged specimen over the unaged specimens. This is accompanied by a 50% reduction in ductility, due both to increased rate of work hardening of the grain and increased notch sensitivity due to the presence of carbides in the grain boundaries. The increased notch sensitivity is better manifested in the fracture toughness data which show a decrease in K_{IC} from about 110 KSI $\sqrt{in.}$ for the unaged specimens to 70 KSI $\sqrt{in.}$ for the aged specimens.

Further, there is an apparent decrease in tensile strength at -452°F compared to -325°F test. With the limited amount of data available to date it is difficult to draw definite conclusions. It is well known that the strength of γ', which governs the strength of the aged structures, decreases with decreasing temperature. However, the decrease in strength is the same for both the aged and unaged specimens. An examination of Table 7-1 reveals that all specimens tested at -452°F had a grain

size about twice as large as those tested at higher temperatures. It is, therefore, probable that the apparent decrease in strength at -452°F is coincidental with the larger grain size. It is also apparent that more work is needed to establish the effect of grain size on strength.

Occasionally, unusual defects were found associated with the fracture surface as shown, for example, in Fig. 7-13. A low melting phase was found in the grain boundaries. Figure 7-13b, which is a cross section of the tensile specimen about 1 mm below the fracture shown in Fig. 7-13a, indicates that the boundary phase was confined to the fracture area only. From X-ray energy dispersive analysis it is concluded that the molten phase is rich in Al and contains also Si and Zr. The origin of the defect is not known at present. It might be associated with faults in the melting practice or some localized temperature excursion during heat treatment.

Typical fracture surfaces of crack growth rate specimens are shown in Fig. 7-14. We selected this specimen for illustration because the room temperature pre-cracked surface (Fig. 7-14a) is essentially the same as for the fracture toughness specimens. The final tensile mode fracture at low temperature (Fig. 7-14c) is again similar to the appearance of the fracture surfaces in fracture toughness and tensile specimens.

The room temperature fatigue surface (Fig. 7-14a) indicates stage I crystallographic fatigue crack propagation, similar to the observation on 310S stainless steel (Fig. 7-7). At low temperatures, (Fig. 7-14b) crack growth is typified by a combination of slip (A), cleavage (B), and intergranular crack branching (C). Carbides associated with the fracture propagation are clearly visible (arrows). The tensile fracture (Fig. 7-14c) shows the already mentioned combination of grain deformation and intergranular cracking.

7.4 Summary

The microstructural analysis of tensile and fracture toughness test specimens has shown and confirmed that:

(a) OFHC Cu exhibits high enough ductility. Further examination of this material will be confined to joined structures.

(b) 310S stainless steel shows a potential of deterioration of properties in sensitized structures. This is apparently due to intergranular cracking caused by precipitation of carbides in the grain boundaries.

(c) X-750 material deforms by homogeneous slip and fails by intergranular cracking at room temperature and below.

(d) There is an apparent grain size effect which is manifested in a decrease of strength with increasing grain size in X-750. The effect of processing on grain size and uniformity of size distribution has to be established.

(e) Occasional melting practice defects were observed. The source of these defects has to be established.

(f) Room temperature fatigue crack growth procedes by crystallographic shear. At low temperatures, cleavage and intergranular cracking associated with carbide precipitates has been observed.

TABLE 7-1 OPERATIONAL TEST MATRIX FOR MICROSTRUCTURAL ANALYSIS

Dwg. 2566432

Material Code	Condition	Microstructural Analysis of Specimens																		
		SEM + XEDA, Light Micros									Replica, Microprobe						In Depth Analysis of Defects & Failure			
		Tensile			K_{IC}			CGR			Tensile			K_{IC}			CGR			Tensile			CGR		
		R	N	H	R	N	H	R	N	H	R	N	H	R	N	H	R	N	H	R	N	H	R	N	H
OFHC-Cu	AR	1	1	1	1	1	1		—		2	2	2	2	2	2	4	2	2	3	4	3	4	4	3
	SR	1	1	1	1	1	1	3	3	3	2	2	2	2	2	2	4	2	2	3	4	3	4	4	3
	GMAW	1	1	1	1	1	1	3	3	3															
	B	1	1	1	3	3	2	3	2	2		4			4			4			5			5	
	S	1	1	1	3	3	2	3	2	2		4			4			4			5			5	
310 SS	STQ	1	1	1	2	2	2	1	1	1	2	2	2	3	3	3	4	3	3		5			5	
	STFC	1	1	1	2	2	2	1	1	1	2	2	2	3	3	3	4	3	3		5			5	
	SMW	1	1	1	2	2	2	1	1	1	2	2	2	3	3	3	4	3	3		5			5	
X-750	ST	1	1	1	2	2	2	1	1	1	2	2	2	3	3	3	3	3	2						
	STDA	1	1	1	2	2	2	1	1	1	2	2	2	3	3	3	3	3	2		4			4	
	ST/EBW	1	1	1	2	2	2	1	1	1		3			3			3			4			4	
	STDA/EBW	1	1	1	2	2	2	1	1	1	2	2	2	3	3	3	2	2	2		4			4	
	EBW/STDA	1	1	1	2	2	2	1	1	1	2	2	2	3	3	3	2	2	2		4			4	
	ST/GTW	1	1	1	2	2	2	1	1	1		3			3			3			4			4	
	STDA/GTW	1	1	1	2	2	2	1	1	1		3			3			3			4			4	
	GTW/STDA	1	1	1	2	2	2	1	1	1		3			3			3			4			4	
	B	1	1	1	3	3	3	3	2	2		3			4			4			5			5	
	MP2/STDA	1	1	1	2	2	2	1	1	1		3			4			3			5			5	
	MP3/STDA	1	1	1	2	2	2	1	1	1		3			4			3			5			5	
	H1P	1	1	1	2	2	2	1	1	1	2	2	2		3			3			4			4	
	H1P/STDA	1	1	1	2	2	2	1	1	1		3			3			3			4			4	
Kromarc 58	STQ	1	1	1	2	2	2	1	1	1	3	3	3	3	3	3	2	2	2		4			4	
	CW	1	1	1	2	2	2	1	1	1	3	3	3	3	3	3	2	2	2		4			4	
	GTW	1	1	1	2	2	2	1	1	1	3	3	3	3	3	3	2	2	2		4			4	
	CW/GTW	1	1	1	2	2	2	2	2	2	3	2	2		3		3	2	2		4			4	
	GTW/CW	1	1	1	2	2	2	2	2	2	3	2	2		3		3	2	2		4			4	
	GTW/CW/AN	1	1	1	2	2	2	2	1	1	3	2	2		3		3	2	2		4			4	

Step 1: Immediate 1 Specimen per Condition

Step 2: Selective, Follows 1

Step 3: Selective Depends on Findings in 1 and 2

Steps 4, 5: Optional, Indepth Solution of Identified Critical Problem Areas

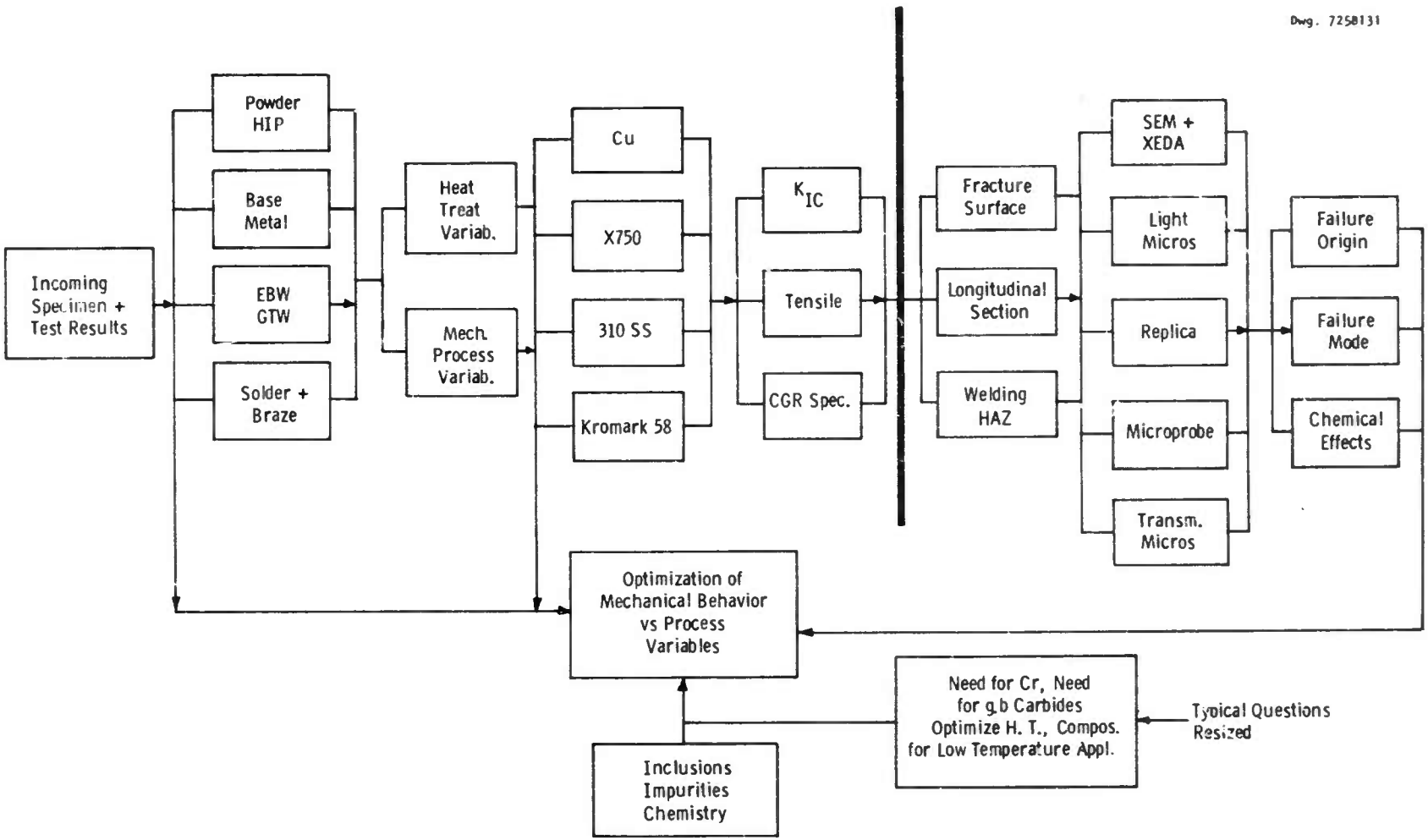

Fig. 7-1 Operational flow chart for microstructural analysis

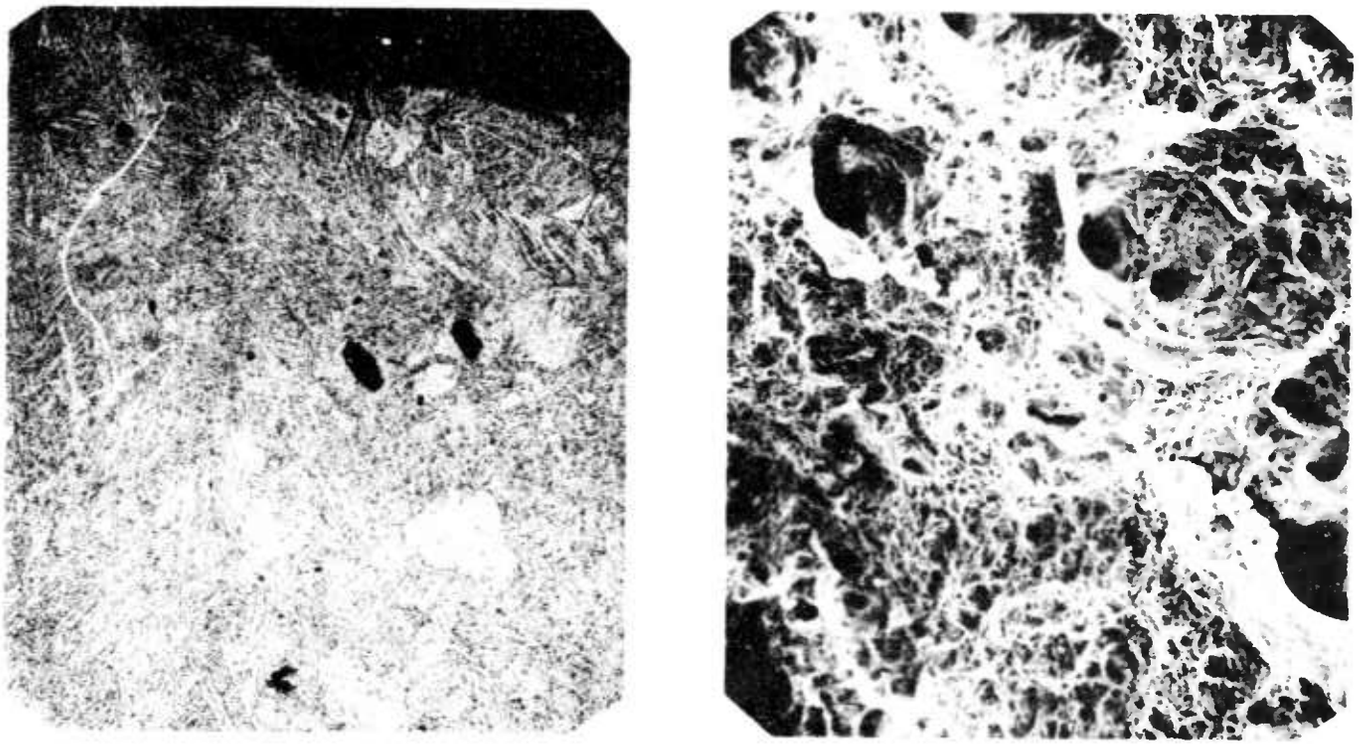

a

b

Fig. 7-2 OFHC Cu, stress-releived condition a: longitudinal section, near the fracture surface of tensile specimen 11T3-1 tested at −452°F. (X100) b: Fracture surface, tensiie specimen 11T2-1 tested at −320°F. (X500)

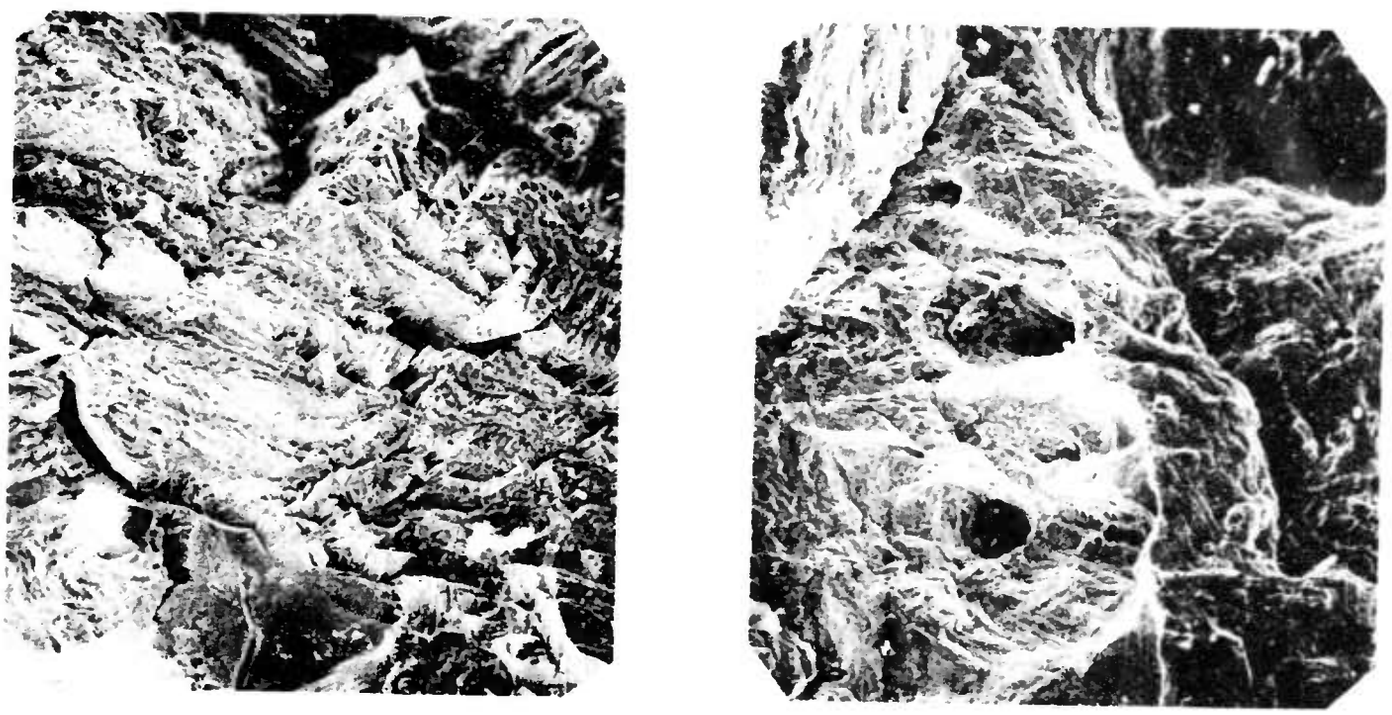

a b

Fig. 7-3 OFHC Cu, code 10K3-1, fracture toughness specimen. a: RT pre-crack fatigue surface b: −452°F fracture surface (X320)

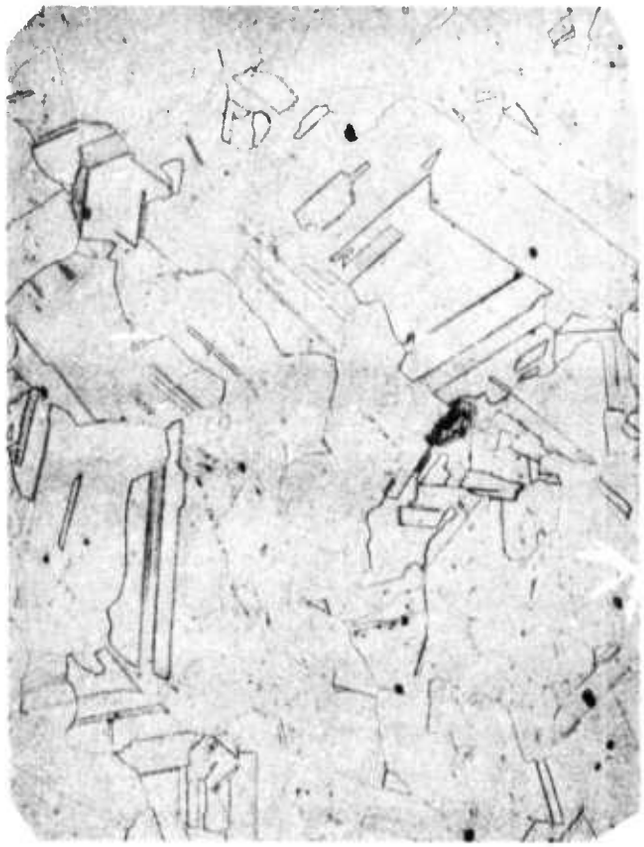

Fig. 7-4 310S Stainless steel base metal, sensitized (21XX) (X150) Aqua Regia etch

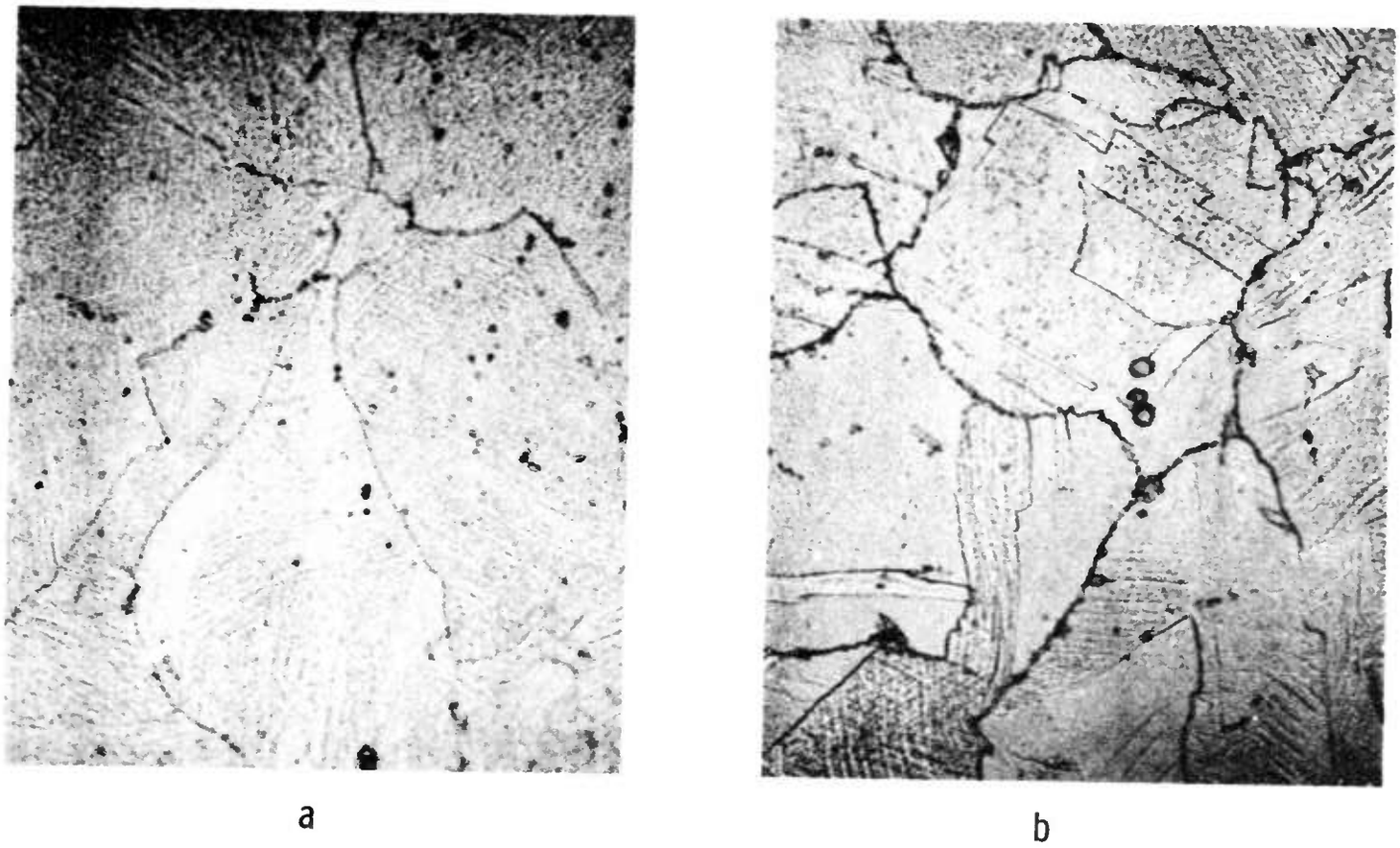

a b

Fig. 7-5 310S Stainless steel longitudinal polished and etched section of tensile specimens, near fractured edge (X500) a: specimen 20T4 b: specimen 21T11

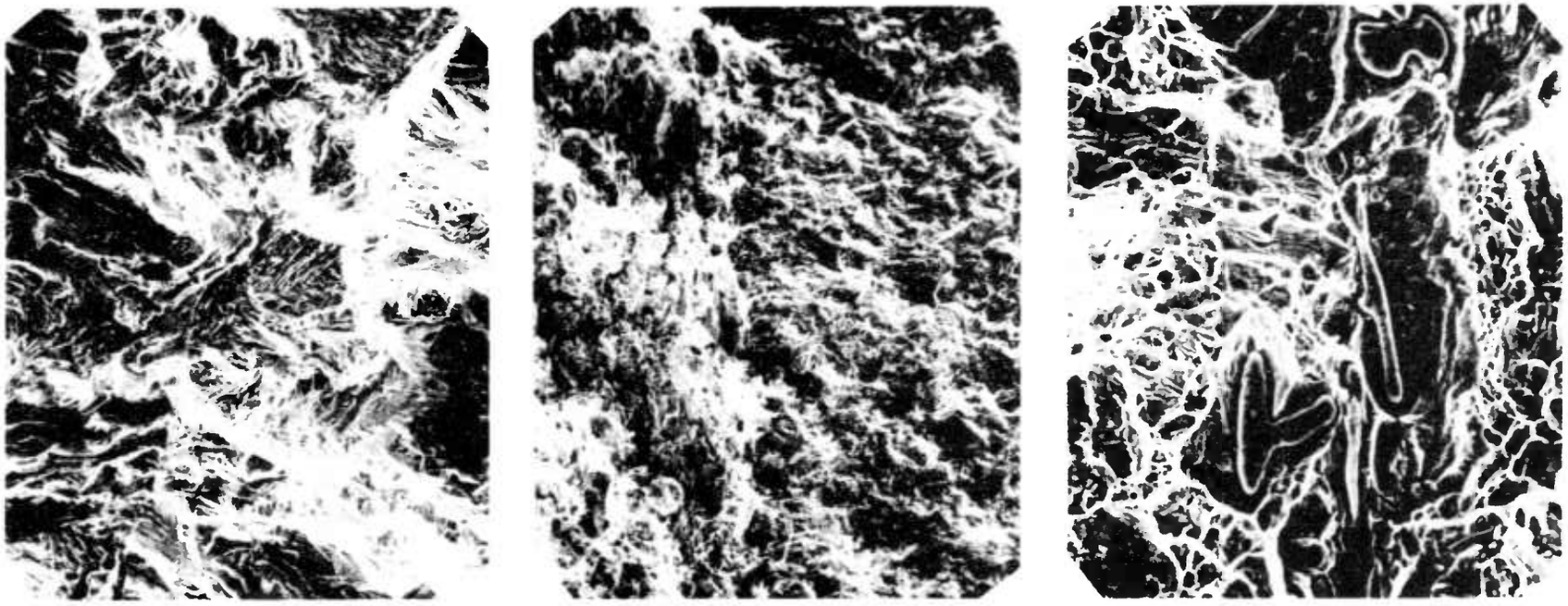

a b c

Fig. 7-6 310S fracture toughness specimen, group 20XX, solution treated water quenched. a: RT pre-crack fatigue surface (X280) b: transition pre-crack to L.T. fracture (X27) c: −452°F fracture surface (X680)

a b c

Fig. 7-7 310S fracture toughness specimen, condition 21XX, solution treated, furnace cooled. a: RT pre-crack fatigue surface, (X1300) b: transition, pre-crack to fracture (arrows) (X130) c: −320°F fracture surface, (X130)

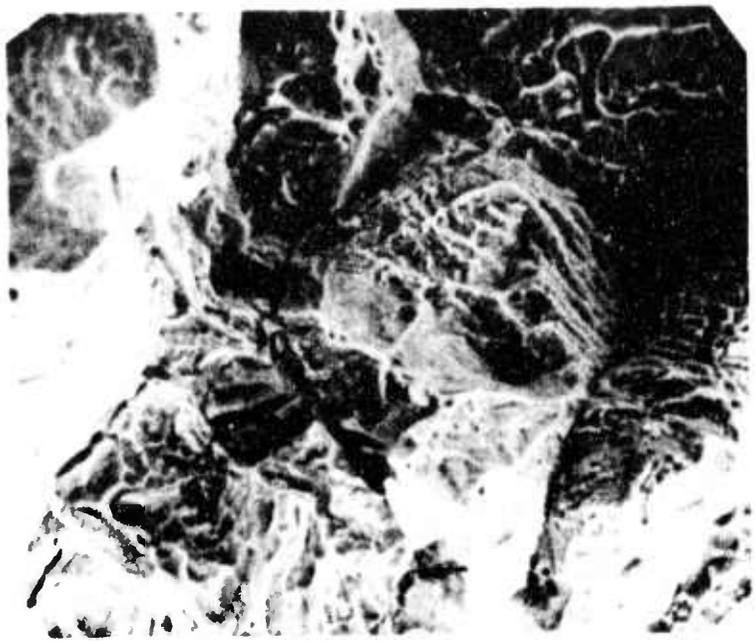

Fig. 7-8 310S Fracture toughness specimen, −320 °F fracture surface. Treatment 1 hour 2000 °F, furnace cooled (21XX group) (X650)

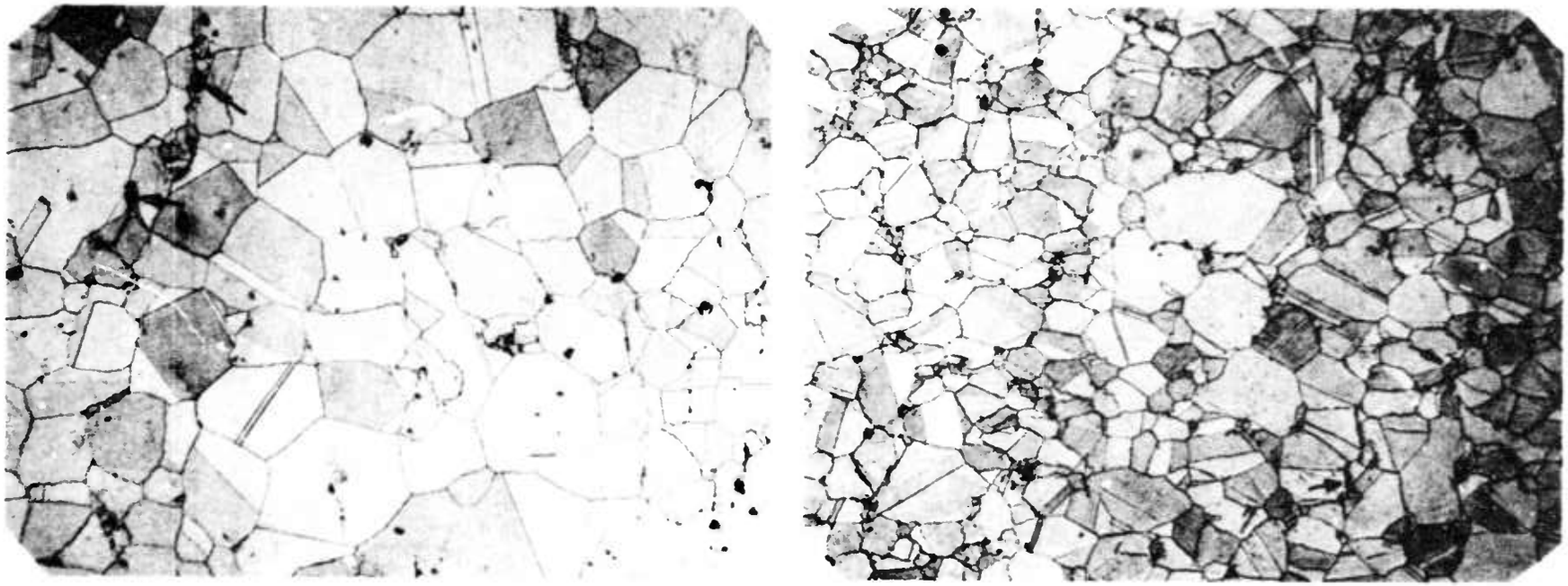

a b

Fig. 7-9 Light micrograph of Inconel X750 base metal. Grain size variation due to location of specimen in original 10" dia forging billet a: ST and double age (31XX group) b: ST and air cool (30XX group) (X50)

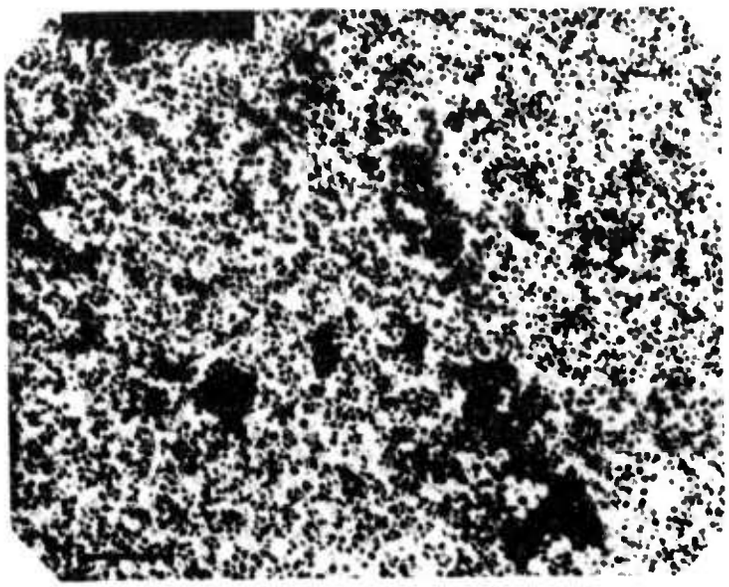

Fig. 7-10 Transmission electron micrograph, extraction replica of In X750 ST + double aged. (31XX group) γ' and MC carbides. 0.1μm scale bar

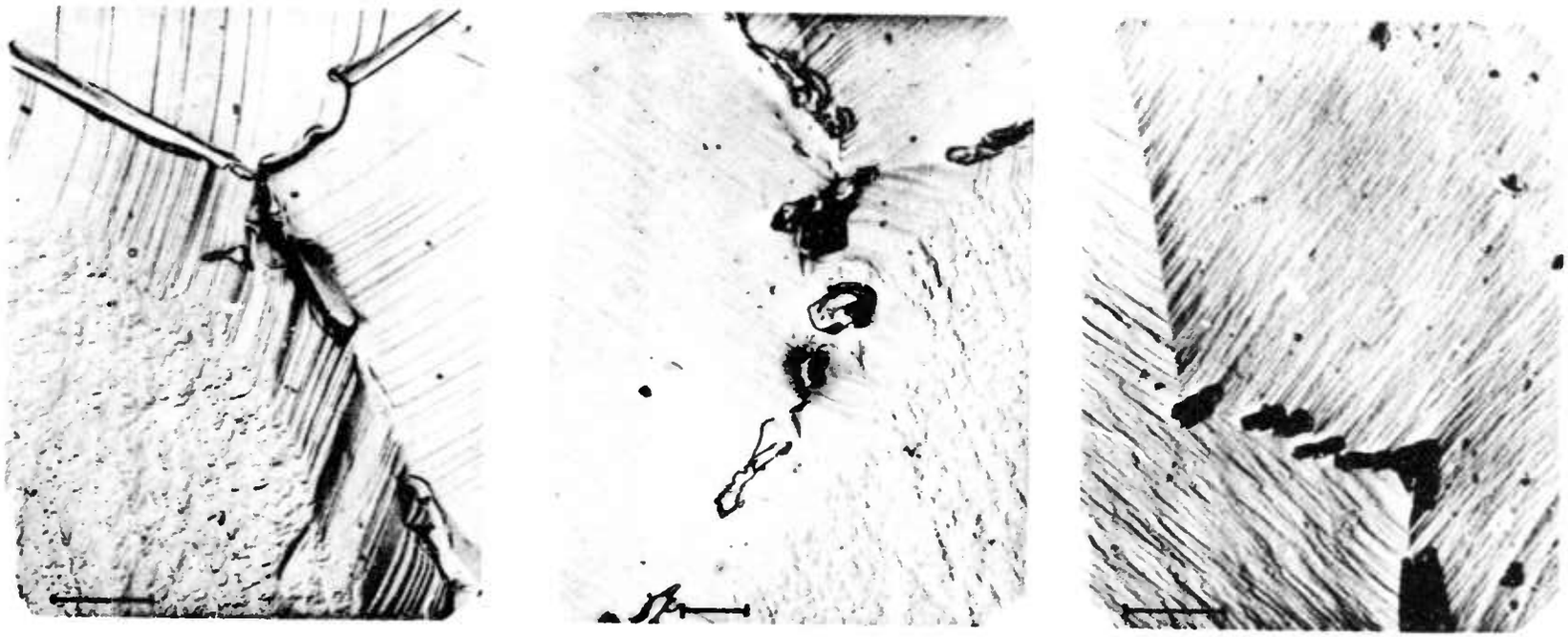

a b c

Fig. 7-11 Two stage carbon replica of polished and heavily etched surfaces (H_2O_2 + HCl) X750. a,b: ST and double aged specimen (31XX group) c: ST specimen (30XX group) 1μm scale bars.

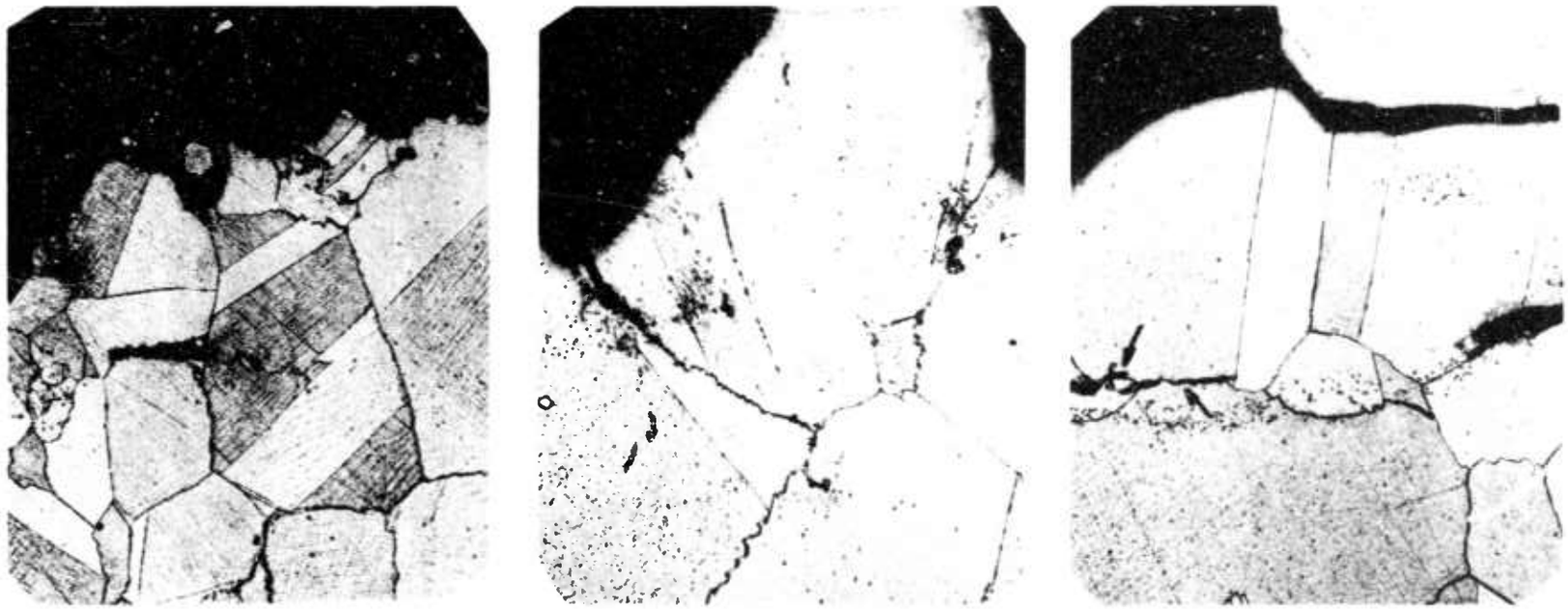

a b c

Fig. 7-12 Longitudinal sections near fractured surface In X750 tensile specimens, (X200) a: ST (specimen 30T2-1) tested at −320°F b: ST (specimen 30T2-1) tested at −452°F c: ST + double age (specimen 31T3-1) tested at −452°F

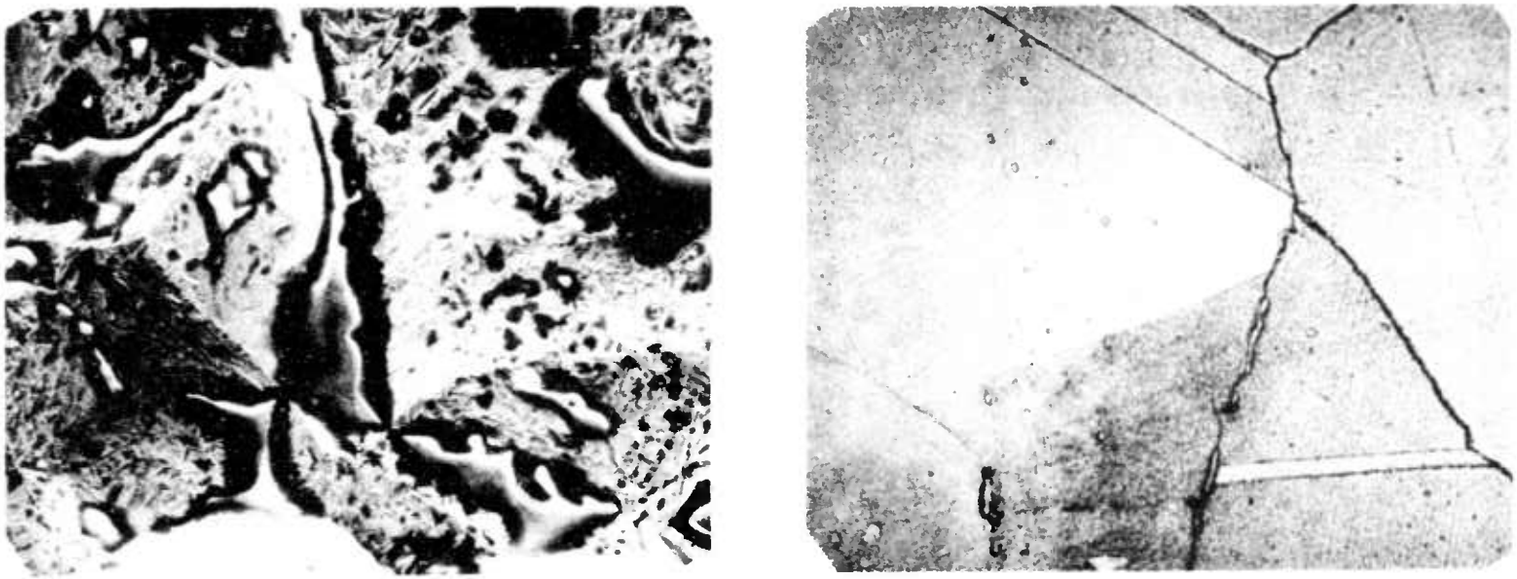

a b

Fig. 7-13 Tensile specimen tested at −452°F. In X750 material, specimen 31T3-2, ST + double age a: SEM of fracture surface showing a low melting phase in grain boundaries (X160) b: Light micrograph, cross section 1mm below fracture surface. (X500)

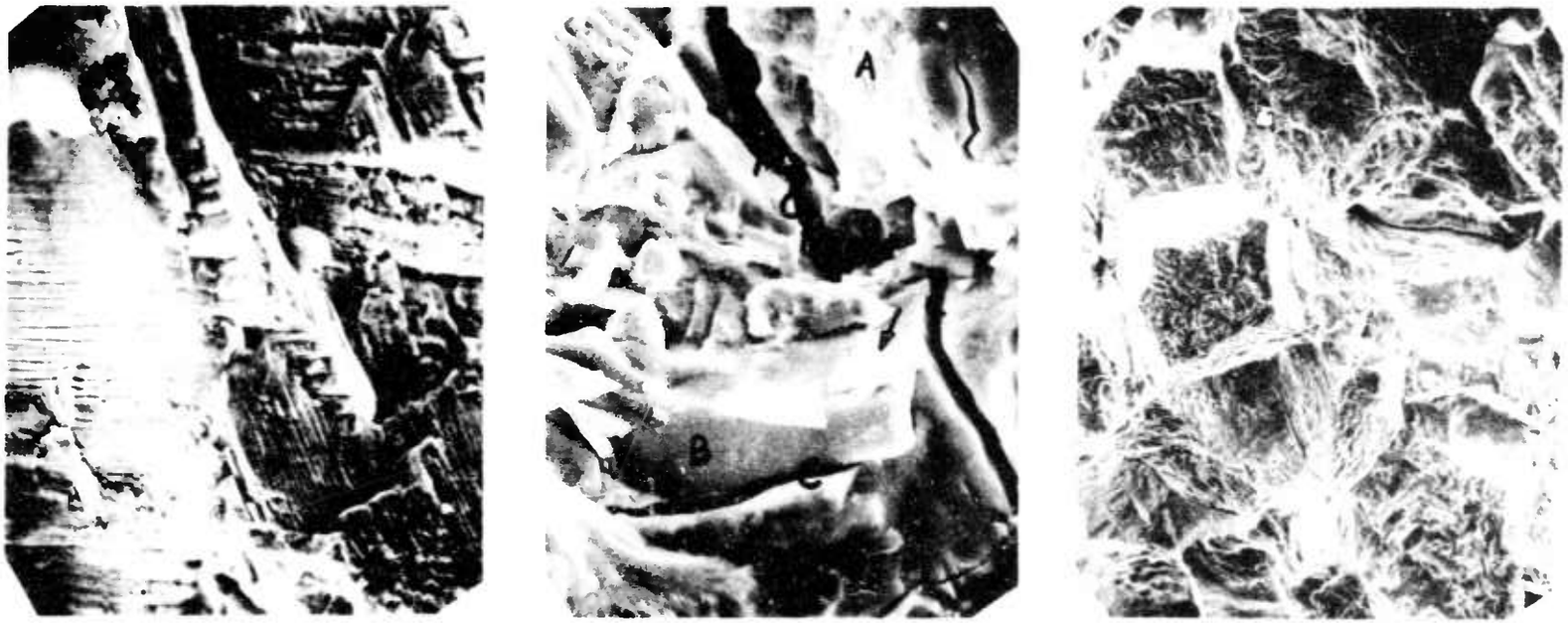

a b c

Fig. 7-14 Crack-growth-rate specimen In X750, ST + double age treatment (group31XX) a: Room temperature pre-crack fatigue surface (X1500) b: −452°F crack growth surface (X3000) c: −452°F fast Mode I fracture surface (X150)

8.0 MAGNETIC PROPERTIES

The austenite stability of structural materials as required for cryogenic applications is related to their chemical composition and is particularly influenced by the quantity of carbide present. Mn, Cr, and Ni have a strong effect in increasing austenite stability at low temperatures, Mn being the most potent of these elements. However, austenitic materials[1] can be subject to structural transformation at low temperatures which result in degradation and compromise of their useful engineering properties. Transformations may occur during cooling to some low temperature or be induced at higher temperatures by mechanical deformation. Low temperature deformation is even more potent in promoting such a transformation. The transformation is usually from austenitic phase which is either paramagnetic or antiferromagnetic. Thus, the study of the magnetic properties of these alloys at cryogenic temperatures provides an important tool for evaluation of their structural stability as well.

With this view in mind a systematic study of the structural stability of two alloys Inconel X-750 and Kromarc-58 was initiated. The compositions and selected metallurgical conditions being evaluated are given in Table 8-1. The samples for this study were cut from previously tested tensile specimens, away from the deformed region.

Magnetisation measurements as a function of the applied field and sample temperature are being made, using a vibrating sample magnetometer in conjunction with a 70 kOersted, NbTi superconducting magnet. The magnetometer measures the total magnetic moment of the sample using a sophisticated phase sensitive detection technique that enables changes as small as 5×10^{-5} emu in magnetic moment to be measured over a temperature span from 4.2°K to 125°K.

A gallium Arsenide diode is used as the sensing element. The sensor is small, stable, and is practically unaffected by strong magnetic fields. The sensor is located very near to the sample in a He-exchange gas enclosure. It has been previously calibrated and is used in conjunction with P.A.R. Model 156 cryogenic thermometer, which gives a direct read out of the sample temperature from 4.2°K to 125°K. It's resolution is 0.1°K and has an accuracy of ±0.2°K. The sample temperature is stabilized by balancing the heat from the sample neater (located near GaAs diode) and pumping the He-jacket surrounding the sample enclosure.

Direct M(H) curves at different temperature are obtained on the X-Y recorder connected to the magnetometer and the magnet power supply. These data are being analyzed. The preliminary results show that the Inconel X-750 samples are ferromagnetic while the Kromarc 58 samples remain either paramagnetic or become very weakly ferromagnetic at 70 kOe and at 4.2°K. Additional analytic work to confirm and rationalize these results is in progress.

TABLE 8-1

Samples	State	Composition								
		Ni	Cr	Ti	Fe	Mn	C	Si	S	P
Inconel X-750	S.T. S.T.D.A.	73	15	2.5	7	0.7	-	-	-	-
Kromarc-58	As recd. 30% C.R.	23	15.5	-	-	9.3	.03	.05	.005	.005

References

1. D. C. Larbalestier and H. W. King, Cryogenics: March (1973), p. 160.

ACKNOWLEDGMENTS

The authors wish to acknowledge the following personnel for their contributions and cooperation in the conduct of this work:

Dr. J. H. Parker, Jr.
Dr. F. C. Hull
Dr. E. W. Johnson
J. L. McCabria
D. C. Litz
C. S. Cook
W. R. Lovic
E. T. Wessel
W. H. Pryle
D. R. Young
R. R. Hovan
A. R. Petrush
W. R. Kuba
R. L. Berrier
M. J. Larkin

Special acknowledgment is extended to Huntington Alloy Product Division of the International Nickel Company, Inc. for providing samples of the Inconel X-750 (MP-2 and MP-3) material and their helpful comments regarding commercial melting practices for this alloy.